PACIFIC EARTHQUAKE ENGINEERING
RESEARCH CENTER

U.S. - Japan Workshop on Performance-Based Earthquake Engineering Methodology for Reinforced Concrete Building Structures

13 September 1999

Maui, Hawaii

Sponsors

Japan Ministry of Education, Science, Sports, and Culture
Pacific Earthquake Engineering Research Center
U.S. National Science Foundation

PEER 1999/10
DECEMBER 1999

U.S.-Japan Workshop on Performance-Based Earthquake Engineering Methodology for Reinforced Concrete Building Structures

13 September 1999

Maui, Hawaii

Organizers

Toshimi Kabeyasawa
Earthquake Engineering Research Institute
University of Tokyo

Jack P. Moehle
Pacific Earthquake Engineering Research Center
University of California, Berkeley

Sponsors

Japan Ministry of Education, Science, Sports, and Culture
Pacific Earthquake Engineering Research Center
U.S. National Science Foundation

PEER Report 1999/10
Pacific Earthquake Engineering Research Center
College of Engineering
University of California, Berkeley

December 1999

PREFACE

U.S.-Japan Workshop on Performance-Based Earthquake Engineering Methodology for Reinforced Concrete Building Structures

BACKGROUND

Considerable research is under way throughout the world to establish performance-based assessment and design methodology for buildings. Japan and the United States are at the forefront of this research effort, as well as efforts to implement the research results. The US-Japan Cooperative Research In Urban Earthquake Disaster Mitigation, sponsored in Japan by the Ministry of Education, Science, Sports, and Culture, and in the U.S. by the National Science Foundation, is funding collaborative research in Japan and the U.S. The Pacific Earthquake Engineering Research Center in the U.S. has established the development of performance-based earthquake engineering methodology as its primary mission. Because of the importance of this topic, it is timely for researchers and practitioners from the U.S. and Japan to meet to exchange technical data and ideas as well as to identify issues of mutual concern and opportunities for cooperative study.

The Workshop on Performance-Based Earthquake Engineering Methodology for Reinforced Concrete Building Structures was organized to meet the needs and opportunities of for research and practice in performance-based earthquake engineering. The objectives of the workshop were threefold: (1) to discuss different perspectives on performance-based earthquake engineering as it is applied to new and existing concrete buildings in Japan and the United States; (2) to exchange the latest findings related to the same subject; and (3) to enhance communications and promote opportunities for new and continuing collaborations.

The Workshop was held 13 September 1999 on Maui, Hawaii. It was attended by 13 Japanese and 16 U.S. participants. The participants are identified below.

JAPAN SIDE	U.S. SIDE
Tsuneo Okada, SIT	Wilfred Iwan, Caltech
Hiroshi Kuramoto, BRI	Anil Chopra, UCB
Taizo Matsumori, UT	Sashi Kunnath, U C Florida
Toshikatsu Ichinose, NIT	Filip Filippou, UCB
Fumio Watanabe, KU	James Wight, U Michigan
Akira Tasai, OIT	Vitelmo Bertero, UCB
Masaki Maeda, YNU	John Hooper, Skilling-Ward-Magnussen
Daisuke Kato, NU	Jack Moehle, UCB
Akira Wada, TIT	John Stanton, U Washington
Yuuki Sakai, UT	Sharon Wood, U Texas
Shigeru Fujii, KY	Helmut Krawinkler, Stanford
Koichi Kusunoki, UT	William Holmes, Rutherford & Chekene
Masaomi Teshigawara	Jon Heintz, Degenkolb
	James Jirsa, U Texas
	Allin Cornell, Stanford
	JoAnn Browning, U Kansas

HOST ORGANIZATIONS AND SPONSORS

The workshop was organized under the auspices of the US-Japan Cooperative Research In Urban Earthquake Disaster Mitigation, with funding by the Ministry of Education, Science, Sports, and Culture in Japan and the National Science Foundation in the U.S., and the Pacific Earthquake Engineering Research Center, with funding from the US National Science Foundation and the State of California.

The technical program was developed by Professor Toshimi Kabeyasawa, Professor in Disaster Mitigation Science, Earthquake Research Institute, University of Tokyo, and Professor Jack P. Moehle, Professor and Director, Pacific Earthquake Engineering Research Center, University of California, Berkeley. Special thanks are offered to Dr. S. C. Liu, U.S. National Science Foundation, for his support of the workshop, and Professor Toshikatsu Ichinose, Nagoya Institute of Technology, who chaired the meeting for the Japan side.

The efforts of Darlene Wright, Janet Cooks, and Barbara Mauk of the Pacific Earthquake Engineering Research Center to make local arrangements and finalize the program administrative details are especially appreciated. Janine Hannel organized the submission of manuscripts and finalized the publication of this special workshop proceedings.

ACKNOWLEDGMENTS

This work was supported in part by the Pacific Earthquake Engineering Research Center through the Earthquake Engineering Research Centers Program of the National Science Foundation under Award number EEC-9701568.

CONTENTS

SESSION 9: GENERAL DISCUSSION AND RESOLUTIONS ♦ Chaired by Toshimi Kabeyasawa and Jack Moehle

SESSION 1: WELCOME, INTRODUCTIONS, OBJECTIVES

Chaired by

♦ Toshimi Kabeyasawa and Jack Moehle ♦

AN OUTLINE OF THE US-JAPAN COOPERATIVE RESEARCH PROJECTS ON URBAN EARTHQUAKE DISASTER MITIGATION

Tsuneo OKADA[1] and Toshimi KABEYASAWA[2]

ABSTRACT

Process was reviewed from the experiences of the 1994 Northridge Earthquake and the 1995 Hyogo-ken-Nanbu Earthquake until the action plan of the US-Japan cooperative research project. The Japan side started the project in 1998, which was reorganized into a five-year project under a new budget source of Grant-in-Aid for Scientific Research on Priority Area (Category B), Monbusho, from April 1999 until March 2003. Research topics and investigator groups on the Japan side are outlined, which have been planned under the common theme of "US-Japan Cooperative Research in Urban Earthquake Disaster Mitigation." Out of the Japanese ten research topics, the theme (2-1) "Development of Performance-based Design Methodologies," is described in detail, which covers the main subject of the first US-Japan workshop with PEER group.

1. INTRODUCTION

Disasters from the 1994 Northridge Earthquake and the 1995 Hyogo-ken-Nanbu Earthquake exemplified the fact, commonly in US and Japan, that a near-source earthquake of Magnitude around seven could cause very serious damages to modern urban areas. Engineers, government officials as well as clients and users in both countries, recognized the necessity of research and practice for the mitigation of such urban disasters.

This paper reports on the process until the realization of the US-Japan cooperative research project from the experiences of the earthquakes and outlines the research projects of the Japan side, which have been planned under the common theme of "US-Japan Cooperative Research in Urban Earthquake Disaster Mitigation." Out of the Japanese ten topics, the theme (2-1)

[1] *Department of Architecture and Building Engineering, Shibaura Institute of Technology, Tokyo, Japan*
Email: okada@sic.shibaura-it.ac.jp

[2] *Earthquake Research Institute, University of Tokyo, Tokyo, Japan*
Email: kabe@eri.u-tokyo.ac.jp

"Development of Performance-based Design Methodologies," is described in detail, which covers the main subject of the workshop.

2. PLANNING OF THE US-JAPAN COOPERATIVE RESEARCH

A summit meeting between US government and Japanese government was held in Tokyo on April 1996, where the item, which emphasized the importance and necessity of research for the urban disaster mitigation against earthquakes, was adopted as one of the items on the agenda of the meeting. The urban disaster mitigation was regarded as a common political issue after the similar experiences on the damages caused by the 1994 Northridge Earthquake and the 1995 Hyogo-ken-Nanbu Earthquake.

To bring the above item into action plan, the sub-cabinet meeting on June 1996, decided the following nine items as the themes of US-Japan cooperative project for earthquake disaster mitigation:

(1) Quantitative evaluation of earthquake potential
(2) Estimation method for loss due to earthquake disaster
(3) Verification of fundamental theory on source process
(4) Near-source motion, site effect and response of structures
(5) Mitigation of seismic hazard, especially on steel structures
(6) Seismic performance evaluation and retrofit of existing structures and facilities
(7) Development of performance-based design methodologies
(8) Development of real-time earthquake information system
(9) Control of fire due to earthquake

These meetings were followed by US-Japan policy conference on earthquake, which was held at US National Academy of Science on September 1996. Representatives of US Agencies and Japanese Ministries related to the earthquake disaster mitigation, including Japanese Minster of Land Safety and US Secretary of FEMA, discussed on the political measures to realize the

common items from the summit meetings. Monbusho, Ministry of Education, proposed a cooperative research program between US universities and Japanese universities during the conference.

In parallel with the activities between US and Japanese governments, the discussion and coordination to realize the cooperative research was carried out among researchers in both countries. "The First US-Japan Workshop on Cooperative Research for Urban Earthquake Disaster Mitigation" was held on December 1995 in Maui, Hawaii and the second from February 27 to March 1, 1997 in Tokyo, under the grant aids of Monbusho and National Science Foundation. An appropriate and practical mechanism was planned in order to bring the common theme "Cooperative project for the mitigation of earthquake disaster" into action plan. Research items of high priority were selected based on the discussion by four sub-committees during the workshop. Also it was agreed that the relationships between governmental institutes and universities should be reorganized and that domestic coordinating committees should be established on both sides to promote the US-Japan cooperative research.

Based on the above agreement, a five-year research project "US-Japan Cooperative Research in Urban Earthquake Disaster Mitigation" was started on US side with a yearly budget of one and half million dollars from October 1998. On the other hand, corresponding to the plan on US side, the coordinating committee established in DPRI of Kyoto University started a three-year project under a normal grant-in-aid of Monbusho, from April 1998. The project offered public subscription, in which collaboration with the US proposals was supposed to be coordinated. The committee adopted several tens of individual proposals in total for the first year. However, actual tight collaboration was found to be difficult in some cases, because time for coordination was limited and only the proposal on either US side or Japan side was adopted as a result.

Because the amount of the budget was limited in above project on Japan side, the budget source mechanism was changed into a new one on April 1999, which was one of Grant-in-aid for Scientific Research on Priority Area (Category B), Monbusho. The new project, a five-year research project from 1999 to 2003 fiscal years, was started under the same theme of "US-Japan Cooperative Research for Urban Earthquake Disaster Mitigation." The yearly budget is around

fifty million yen for the first year and will be hundred million yen for the next four years.

The following five main research fields were selected on Japan side:

(1) Strong motion and geotechnical hazard assessment
(2) Enhancement of structural response performance
(3) Advanced technologies for improvement of seismic performance of urban structures
(4) High performance infrastructure systems for destructive urban earthquakes
(5) Comparative study on urban earthquake disaster management

Above five fields, consisting of ten research topics, are listed with principal investigators in Table 1. Due to the change of the budget source mechanism, the executive board can not offer the public subscription. The number of official research members is also limited to two for each topic. Instead, the executive board and the principal investigators can select additional cooperative investigators reflecting the research needs in each field.

To coordinate possible new collaboration based on the currently adopted topics and members, the first grantees meeting was held at Sonoma, CA, sponsored by Monbusho and The National Science Foundation, on March 19, 1999, where principal investigators in US and Japan projects introduced their research topics, objectives, plans and co-investigators. Collaboration for each research topic or individual research theme was coordinated, so that the research group on the topic (2-1) on Japan side(PI: Toshimi Kabeyasawa) and PEER group(PI: Jack Moehle) agreed at the meeting to promote cooperative research on the development of performance-based design methodologies and to plan the first workshop in Hawaii during August or September 1999.

Table 1 US-Japan cooperative research in urban earthquake disaster mitigation - Research themes and investigators on Japan side -

1. Executive Board

Project PI **Hiroyuki Kameda**, Disaster Prevention Research Institute, Kyoto University
E-mail: kameda@imdr.dpri.kyoto-u.ac.jp

Coordination Committee Chair: **Shunsuke Otani**, Graduate School of Engineering, University of Tokyo
E-mail: otani@sake.t.u-tokyo.ac.jp

Advisors: **Tsuneo Okada**, Shibaura Institute of Technology
E-mail: okada@sic.shibaura-it.ac.jp

Kenzo Toki, Graduate School of Engineering, Kyoto University
E-mail: toki@quake.kuciv.kyoto-u.ac.jp

Secretary General: **Tadanobu Sato**, Disaster Prevention Research Institute, Kyoto University
E-mail: sato@catfish.dpri.kyoto-u.ac.jp

Secretary: **Masayoshi Nakashima**, Disaster Prevention Research Institute, Kyoto University
E-mail: nakashima@archi.kyoto-u.ac.jp

(plus ten Topic PI's and several Evaluation Panels)

2. Research Teams

Section 1 Strong Motion and Geotechnical Hazard Assessment

Topic 1-1 Prediction of Strong Ground Motions in Urban Regions

PI **Tomotaka Iwata**, Disaster Prevention Research Institute, Kyoto University
E-mail: iwata@egmdpri01.dpri.kyoto-u.ac.jp

Topic 1-2 Protection of Underground Structures against Strong ground Motion and Liquefaction

PI **Masanori Hamada**, School of Science and Technology, Waseda University
E-mail: hamada@mn.waseda.ac.jp

Section 2 Enhancement of Structural Response Performance

Topic 2-1 Development of Performance-based Design Methodologies

PI **Toshimi Kabeyasawa**, Earthquake Research Institute, University of Tokyo
E-mail kabe@eri.u-tokyo.ac.jp:

Topic 2-2 Preventing Brittle Structural Failure and Ductility Enhancement

PI **Kazuo Inoue**, Graduate School of Engineering, Kyoto University
E-mail: inoue@archi.kyoto-u.ac.jp

Section 3 Advanced Technologies for Improvement of Seismic Performance of Urban Structures

Topic 3-1 Seismic Enhancement of Urban Infrastructures Using New Technologies and Smart Materials

PI **Kazuhiko Kawashima**, Department of Civil Engineering, Tokyo Institute of Technology
E-mail: kawasima@cv.titech.ac.jp

Topic 3-2 Development of Structural Monitoring and Damage Detection Systems

PI **Yoshiyuki Suzuki**, Disaster Prevention Research Institute, Kyoto University
E-mail: suzuki@zeisei.dpri.kyoto-u.ac.jp

Section 4 High Performance Infrastructure Systems for Destructive Urban Earthquakes

Topic 4-1 Criteria for Performance-based Design and Management of Infrastructure Systems

PI **Norio Okada**, Disaster Prevention Research Institute, Kyoto University
E-mail: okada@imdr.dpri.kyoto-u.ac.jp

Topic 4-2 Risk Analysis and Advanced Technologies for Infrastructures

PI **Takashi Okimura**, Research Center for Urban Safety and Security, Kobe University
E-mail: okimura@kobe-u.ac.jp

Section 5 Comparative Study on Urban Earthquake Disaster Management

Topic 5-1 Urban Earthquake Disaster Process Modeling and Real Loss Estimation

PI **Yoshiaki Kawata**, Disaster Prevention Research Institute, Kyoto University
E-mail: kawata@drs.dpri.kyoto-u.ac.jp

Topic 5-2 Assessment of Post-event Management Processes Using Multi-media Disaster Simulation

PI **Ken Sudo**, International Center for Disaster Mitigation Engineering, University of Tokyo
E-mail: sudo@incede.iis.u-tokyo.ac.jp

3. THEME (2-1): DEVELOPMENT OF PERFORMANCE-BASED DESIGN METHODOLOGIES

3.1 Background and objective

One of the important lessons learned from the damages to buildings caused by the Hyogo-ken-nanbu Earthquake, 1995 was that life safety is not enough as the design performance objective of seismic design, even after a very rarely severe earthquake. Instead, it was proved from the earthquake damages that whether most of the structures were economically repairable or not will be a fatal performance criteria for quick recovery of the city. It was also pointed out that accountability on actual structural performance under severe earthquake was not enough in the current building standards, building officials and structural designers. It should have been clearly explained to and understood by the clients that their buildings, even designed by satisfying the latest building standard, might suffer severe damages exceeding the economically repairable limit by the major earthquake.

Frameworks for performance-based seismic design have been under consideration worldwide, such as Japan and US, in which performance objectives are to be clearly prescribed instead of traditional specifications. In the design objectives of the performance-based design code, estimated damages shall clearly be related to the expected design motions with adequate reliability.

The Building Standard Law (BSL) of Japan was revised in May 1998 at the first time after about 50 years of its establishment, by which the statement was to be expressed in a performance-based style. However, the style, especially on the structural requirements, has not been so much changed in the BSL level. Building Standard Order, other lower level requirements and design guidelines are now under revision in accordance with the performance-based design philosophy.

On the other hand, Architectural Institute of Japan published a seismic design guidelines for reinforced concrete building structures, which is based on inelastic displacement concept in 1997[1]. This was at first planned as a revised edition of the former guidelines in 1990 and

English version in 1994[2] based on the ultimate strength concept. However, the style of the guidelines was changed a lot using inelastic displacement concept towards a future performance-based code. To extend the guidelines into a perfectly performance-based style, the new committee is active, by which the new guidelines will be published in a few years.

Considering the necessity and importance of the development of the performance-based seismic design philosophy, the coordinating committee selected one of the ten topics as theme (2-1): development of performance-based design methodologies.

The objective of this project at the proposal is to compile backup database, which will be necessary for structural design practice done by performance-based design concept. The main research theme will be the development of seismic design methodology for reinforced concrete building structures using displacement criteria. Practical calculation methods for response and limit states will be developed and verified through tests, analyses, theory, observation and literature survey.

3.2 Research items

The investigators and their individual research items are selected based on the adopted individual proposals, which were reorganized by the organizing committee into the common theme (2-1): Development of performance-based design methodologies. The coordinator, Toshimi Kabeyasawa, Earthquake Research Institute(UT), and members, Toshikazu Ichinose(NIT), Hitoshi Shiohara(UT) are also nominated by the coordinating committee. The cooperative members at the applications were Shunsuke Otani(UT), Manabu Yoshimura(TMU), Daisuke Kato(NU), Yoshiaki Nakano(UT), Kazuhiro Kitayama(TMU), Akira Wada(TIT), Jun Kanda(UT). Several cooperative investigators were added when adopted.

Individual research themes proposed by the cooperative members of the group may be classified into the following research items at the time of application to express the common research interest on performance-based design methodologies:

A. Development and verification of structural analysis

(A-1) Soil-structure interaction:

Analytical model for nonlinear soil-structure interaction will be verified through observation data at test site. Effects of the interaction on the earthquake motion input to the structure will be evaluated.

(A-2) Standard design analytical tool:

Capacity spectrum methods and push-over analysis for estimation of displacement responses will be sophisticated and verified with theoretical backgrounds.

(A-3) Dynamic analysis:

General purpose computer program with reliable models for nonlinear dynamic analysis will be developed for design practice.

B. Evaluation of seismic performance of structures and members and development of new design procedure

(B-1) Structural performance evaluation:

Methods to evaluate (a) yield and ultimate deformations, (b) crack widths, (c) residual deformations, (d) hysteretic energy dissipation capacity, will be developed based on mechanical models and experimental data, especially for limit states for serviceability and restorability.

(B-2) System for performance assurance:

Procedure will be presented in order to design such structure that evaluation of its performance is easy, stable and accurate. Capacity design procedure to ensure the selected hinge regions is an example.

(B-3) Hybrid structures:

A method will be developed to evaluate seismic performance of structures consisting of elements with different properties, i.e., stiffness, strength, deformability, and hysteretic damping, including retrofitted structures.

C. Draft of performance-based design requirements and criteria

(C-1) A design guidelines and performance indices:

A Performance-based code framework and a design guidelines will be drafted. A new index expressing the grade of seismic performance synthetically will be proposed.

(C-2) Life cycle cost based performance criteria:
Common method to determine performance criteria will be presented.

3.3 Members and individual research themes

The members or cooperative investigators of the theme (2-1) listed in the first of the following items of (1) through (9) planned their corresponding individual research topics at the time of application as follows. Topics added for this workshop are also included. The others joined in the related items of the project as planned or for this workshop as additional cooperative investigators. Investigators listed in the items (10) and (11) are invited to the workshop, who have been involved in the past US-Japan cooperative research projects related to reinforced concrete structures, and their current research topics are very close or indispensable to the theme of the workshop. The item (10) is the members for the theme (2-2) "Preventing Brittle Structural Failure and Ductility Enhancement" of the whole projects. The item (11) is the members of Building Research Institute, who have been leading the intensive task on the revision of Building Standards of Japan. Possible US counterpart, being in contact at the time of application, is also listed, regardless of whether funded or not by US-Japan program at this stage. New collaboration may be coordinated at the workshop.

(1) **Kabeyasawa, Toshimi**, Professor, Earthquake Research Institute, The University of Tokyo and **Sakai, Yuuki**, Research Associate, Earthquake Research Institute, The University of Tokyo
US counterpart: Jack Moehle, EERC, UC Berkeley
US counterpart: Yahya C. Kurama, B.F. Spencer, Univ. of Notre Dame
(1-a) Use of seismographs in the structure for performance evaluation and monitoring(related item: A-1)
(1-b) Dynamic test and analysis of irregular structures(A-2, A-3, B-1)
(1-c) Correlation of nonlinear response with basic characteristics of earthquake motions(A-2)
(1-d) Strong ground motions in performance-based seismic design(A-2, C-1)
(2) **Ichinose, Toshikatsu**, Professor, Faculty of Engineering, Nagoya Institute of Technology
US counterpart: John Bolander, UC Davis
(2-a) Bond splitting model for reinforced concrete beams and columns(B-1)

(3) **Shiohara, Hitoshi**, Associate Professor, Graduate School of Engineering, The University of Tokyo, and **Otani, Shunsuke**, Professor and **Matsumori, Taizo**, Research Associate, Graduate School of Engineering, The University of Tokyo

US Counterpart: Jack Moehle, EERC, UC Berkeley

(3-a) Shear resistance model and limit states for reinforced concrete beam-column joints(B-1)

(3-b) Development of structural system and design procedure for performance assurance(B-2)

(3-c) Response analysis, performance criteria, code framework(C-1)

(4) **Yoshimura, Manabu**, Professor, Graduate School of Engineering, Tokyo Metropolitan University

US counterpart: Helmut Krawinkler, Stanford University

US counterpart: Yahya C. Kurama, B.F. Spencer, Univ. of Notre Dame

(4-a) Dynamic analysis of irregular structures(A-3)

(4-b) Response control for displacement concentration(A-2, A-3)

(5) **Kato, Daisuke**, Professor, Faculty of Engineering, Niigata University

and **Tasai, Akira**, Associate Professor, Faculty of Engineering, Osaka Institute Technology

(5-a) Models of walls for stiffness, strength and deformation capacity(B-1)

(5-b) Ultimate state of columns under high axial load(B-1)

(5-c) Dynamic analysis of wall-frame structures(A-3)

(6) **Nakano, Yoshiaki**, Associate Professor, Institute of Industrial Science, The University of Tokyo and **Kusunoki, Koichi**, Research Associate, Institute of Industrial Science, The University of Tokyo

US Counterpart: Riyad S. Aboutaha, Assistant Professor, Georgia Institute of Technology

(6-a) Dynamic analysis of hybrid or retrofitted structures (B-3, A-3))

(6-b) Design of members with low stiffness and high strength (B-3)

(7) **Kitayama, Kazuhiro**, Associate Professor, Graduate School of Engineering, Tokyo Metropolitan University, and **Maeda, Masaki**, Associate Professor, Faculty of Engineering,

Yokohama National University

(7-a) Shear behavior of R/C columns and beam-column joints subjected to varying axial load from tension to compression (B-1)

(7-b) Yield deformation and hysteresis models in beams and columns(B-1)

(7-c) Calculation of maximum and residual crack widths (B-1)

(8) **Wada, Akira**, Professor, Structural Engineering Research Center, Tokyo Institute of Technology

and **Kasai, Kazuhiko**, Professor, Structural Engineering Research Center, Tokyo Institute of Technology

US Counterpart: Anil K. Chopra, University of California at Berkeley

(8-a) Practical application of dynamic analysis to performance based seismic design

(9) **Kanda, Jun**, Professor, Graduate School of Engineering, The University of Tokyo

and **Takada, Tsuyoshi**, Associate Professor, Graduate School of Engineering, The University of Tokyo

US Counterpart: Y. K. WEN, University of Illinois

(9-a) Lifecycle cost based performance criteria for evaluation and design

(10) **Watanabe, Fumio**, Professor, Graduate School of Engineering, Kyoto University,

Fujii, Sigeru and **Nishiyama, Minehiro,** Associate Professors, and **Kohno, Susumu,** Research Associate, Graduate School of Engineering, Kyoto University

US Counterpart: Riyad S. Aboutaha, Associate Professor, Syracuse Univ.

US Counterpart: Michael E. Kreger, Professor, Univ. of Texas at Austin and

US Counterpart: Robert J. Frosch, Assistant Professor, Purdue Univ.

(10-a) Analytical method for predicting the response of tied concrete columns to seismic loading

(10-b) New requirements on bond, anchorage and lap splices in AIJ Standard for Structural Calculation of Reinforced Concrete Structures

(10-c) Performance Evaluation of Beam-Column Joints in Reinforced Concrete Frames under Bi-Directional Seismic Loadings

(11) **Teshigawara, Masaomi,** Building Research Institute, Ministry of Construction, **Kuramoto, Horoshi,** and **Hiraishi Hisahiro,** Building Research Institute, Ministry of Construction

(11-a) Development of seismic performance evaluation procedure in Building Code of Japan

(11-b) Prediction of earthquake response of buildings using equivalent single degree of freedom system

(11-c) Dynamic test and analysis of irregular structures (A-2, A-3, B-1)

5. CONCLUSIONS

Process was reviewed until the action plan of the US-Japan cooperative research project. The research topics and investigator groups on the Japan side are outlined. Out of the Japanese ten research topics, the theme (2-1) "Development of Performance-based Design Methodologies," is described in detail, which covers the main subject of the first US-Japan workshop with PEER group. It is recommended that new individual research collaboration will be established through the workshop.

REFERENCES

1. Architectural Institute of Japan(1997), "*AIJ structural design guidelines for reinforced concrete buildings based on inelastic displacement concept (Draft, in Japanese)*," Architectural Institute of Japan, Tokyo.

2. Architectural Institute of Japan(1994), "*AIJ structural design guidelines for reinforced concrete buildings based on ultimate strength concept (in English)*," Architectural Institute of Japan, Tokyo.

SESSION 2: EARTHQUAKE AND RESPONSES

Chaired by

♦ Toshikatsu Ichinose and Sharon Wood ♦

IMPLICATIONS OF NEAR-FAULT GROUND MOTION FOR STRUCTURAL DESIGN

W. D. IWAN[1]

ABSTRACT

Idealized structural models are used to indicate important features of the response of inelastic structures to near-fault ground motions. The applicability of the capacity spectrum method (CSM) of analysis for cases of near-fault ground motions is investigated. It is shown that serious restrictions need to be placed on the use of equivalent viscous damping and static pushover when pulse-like near-fault ground motions are considered.

1.0 INTRODUCTION

Near-fault, or near-field, ground motions contain distinct velocity and displacement pulses. These pulses can cause high levels of interstory drift in structural systems. Such ground motions were recorded in both the Northridge, California, and Kobe, Japan, earthquakes, and most recently in the Kocaeli, Turkey, earthquake. Recent concern about the damage potential of near-field ground motions has led to considerable interest in the nature of these motions and their impact on structural performance. This paper investigates the response of inelastic structures to near-fault ground motions by using recently proposed performance-based analysis procedures. The results presented in this paper are discussed more fully in an upcoming paper in the *Proceedings* of the 12th World Conference on Earthquake Engineering, to be held in New Zealand. (Iwan et al. 2000).

2.0 EXAMPLES OF NEAR-FAULT GROUND MOTION

A suite of near-fault ground motion records was used in this study (Iwan et al. 1999). Representative of this suite is the Rinaldi Receiving Station (RRS), S33W record from the Northridge earthquake shown in figure 1. Figure 2 shows the ground motion from the Yarimca Petrokimya Tesisleri Station (YPT), N26W record from the Kocaeli, Turkey, earthquake of August 17, 1999. It is seen that these ground motions are characterized by well defined, discrete pulses as opposed

[1] *Department of Civil Engineering, California Institute of Technology, Pasadena, California, USA.*

to the generally broadband random appearance of far-field earthquake ground motions. The effect of these pulses on structural response is the focus of this paper.

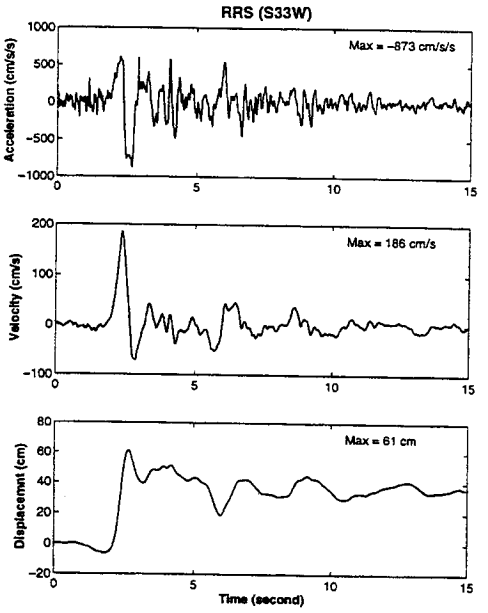

Figure 1. Rinaldi Receiving Station Ground Motion, Northridge Earthquake (S33W)

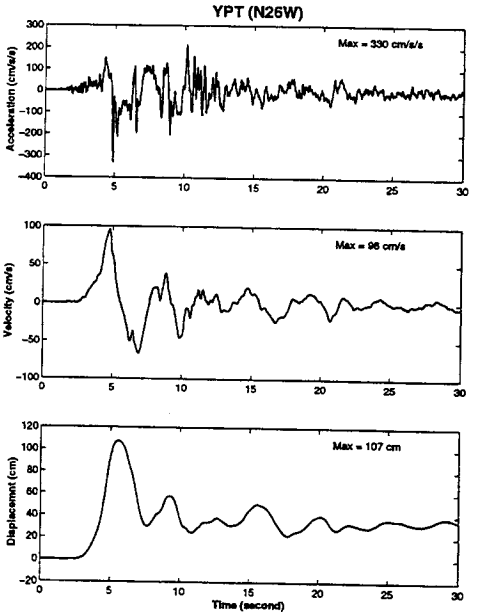

Figure 2. YPT Station Ground Motion, Kocaeli earthquake (N26W)

3.0 IMPLICATIONS FOR PERFORMANCE-BASED ANALYSIS

The Applied Technology Council has recently proposed a performance-based design/analysis methodology (ATC-40 1997) in which the traditional design spectrum is reduced to an inelastic demand spectrum and combined with a static pushover curve in what is usually referred to as a capacity spectrum method (CSM). This produces a performance point that predicts the maximum building response during an earthquake. In the CSM, the inelastic demand spectrum is derived from an elastic design spectrum using the concept of equivalent viscous damping. The result is an overall reduction in both acceleration and displacement demand. The effective viscous damping coefficient is generally based on some sort of equal energy dissipation rule in which the energy dissipated during one hysteretic cycle is equated to that from one cycle of elastic response with equivalent viscous damping.

In this paper, the results of the CSM are compared with the results of a nonlinear time history analysis for both single-degree-of-freedom (SDOF) and multidegree-of-freedom (MDOF) bilinear hysteretic systems subjected to near-fault ground motions. This study uses the Newmark-Hall spectral reduction factors SR_A and SR_V to perform global spectral reduction on the damped elastic response spectrum. Whether SR_A or SR_V is used is based upon a comparison

of the control period and the elastic period of the SDOF analytical model. Other forms of equivalent viscous damping could also have been used without significantly affecting the results.

3.1 Loci of Performance Points for SDOF Systems

For a SDOF system, a uniquely defined capacity spectrum curve is obtained using the CSM because there is no need to specify a pushover load profile. Consider a bilinear hysteretic system with a 5% linear viscous damping coefficient. This system is completely defined by its natural period, T, and the ratio of the postyielding stiffness to the initial stiffness, α.

The locus of performance points (LPP) may be defined as the continuous trace of performance points with a prescribed elastic period and varying ductility plotted in acceleration displacement response spectrum (ADRS) format. The LPP given by the equivalent viscous damping approach employed in the usual CSM formulation is herein compared to the locus of inelastic response (LIR) generated by time history analysis. The results for the case of a bilinear hysteretic system with $\alpha = 10\%$ subjected to the RRS ground motion are shown in figures 3 and 4. In these figures, the elastic and the $\mu = 8$ inelastic response spectra are both plotted to illustrate the global shape of the demand spectrum.

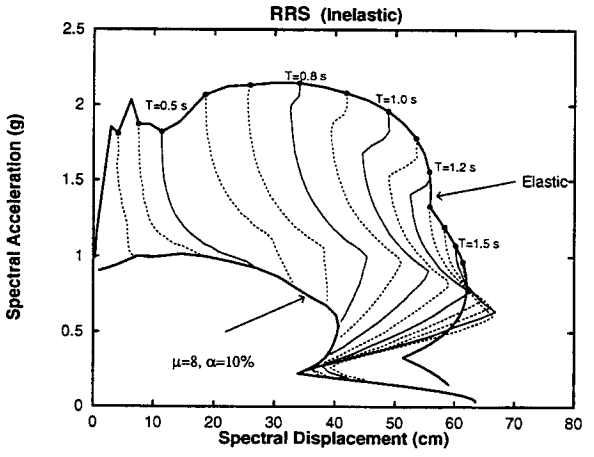

Figure 3. Loci of Inelastic Response, Time History Analysis, RRS

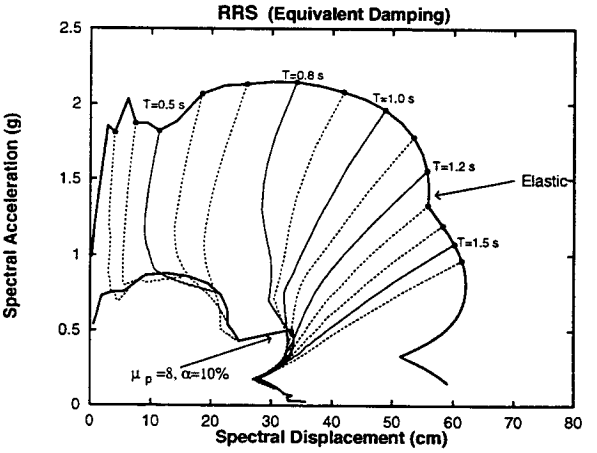

Figure 4. Loci of Performance Points, Equivalent Viscous Damping Analysis, RRS

The detailed shape of the demand spectrum and locus of performance points differ somewhat for different earthquake ground motions. However, the following general observations may be

1. The equivalent viscous damping approach yields satisfactory performance results only for a very limited structural period range where resonance build-up type of response occurs. This structural period range is generally near the predominant pulse period of the ground motion.

2. For near-fault ground motions, the locus of performance points obtained using equivalent viscous damping generally underestimates the true locus of inelastic response of SDOF systems with periods shorter than the predominant period of the ground motion pulse.

3.2 Displacement Demand Ratio for SDOF Systems

The displacement demand ratio (DDR) may be defined as the ratio of maximum inelastic spectral displacement resulting from the time history analysis to the spectral displacement calculated from the CSM approach using equivalent viscous damping. This ratio may be used as another indicator of the validity of the equivalent viscous damping assumption for near-fault ground motions.

DDR results for a bilinear hysteretic system with α = 10% subjected to the Takatori Station (TAK), N49W ground motion recorded during the Hyogoken Nanbu earthquake are shown in figure 5 for μ = 1, 1.5, 2, 4 and 6. This figure reinforces the observations made above. The equivalent viscous damping assumption works fairly well for structural periods near the predominant ground pulse period, but is quite nonconservative for structural periods significantly shorter than the predominant ground pulse period, especially for higher values of ductility. Equivalent viscous damping is also somewhat nonconservative for longer structural periods.

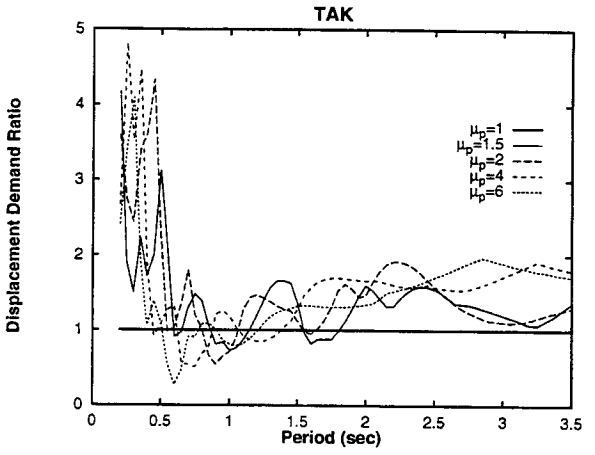

Figure 5. Displacement Demand Ratio for TAK Based on Equivalent Viscous Damping Model of RRS 5% Damped Elastic Spectrum

A primary reason for the failure of equivalent viscous damping for short period structures subjected to near-fault ground motions is that the response tends to become very one-sided. Therefore, the major hysteresis loops do not close. The result is much lower energy dissipation than is assumed by the usual equivalent viscous damping techniques. An example, figure 6, shows the response of a structure with a 1.4 second period subjected to the Lucerne Valley

(LUC), N80W ground motion recorded during the 1992 Landers, California, earthquake. The predominant ground pulse period for this case is about 4 seconds, so the structural period is short compared to the pulse period.

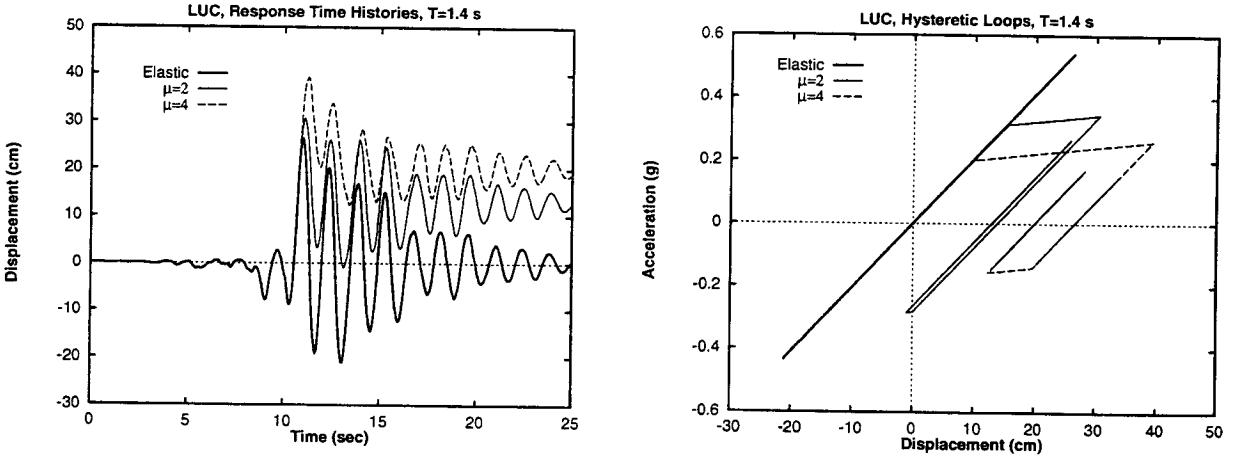

Figure 6. Displacement Time History and Hysteretic Loops for LUC, T = 1.4 second

3.3 Spatial Distribution of Shear and Drift Demand—MDOF Systems

The major response of MDOF systems excited by far-field earthquake ground motions is usually in the fundamental mode. The static pushover technique employed in the CSM approach makes use of this fact by using a lateral load profile resembling the fundamental mode of the structure. Thus, predictions of areas of yielding in the structure are based upon a response shape that is similar to the first mode shape. However, near-fault ground motions containing distinct pulses can cause the response of taller buildings to have greater participation in the higher modes.

In this paper, a nonuniform shear-building model is used to examine building response to near-fault ground motions. An equal mass distribution is assumed except for the top floor, for which the mass is half of the other masses. A bilinear hysteretic model is used to characterize the interstory shear force-deformation characteristics. The postyielding ratio, α, is assumed to be 5%, and the yielding interstory shear force is assumed to be proportional to the story shear stiffness. Rayleigh damping of 5% in the first two modes is assumed. Given the fundamental period of the structure, T, the height of the structure, L (in meters), is determined using the UBC formula $T = 0.0863\ L^{3/4}$. The number of stories is estimated using 3 meters per story height. The story shear stiffness distribution (or equivalently the story yielding shear) is chosen to give a straight-line deformation shape under the UBC lateral load distribution.

The spatial distributions of the shear and drift demands for structures with a fundamental period of 0.7 and 2.5 seconds subjected to the TAK ground motion are shown in figures 7 and 8. Based on the results shown in these figures, and results for the suite of other near-fault ground motions, the following observations are made:

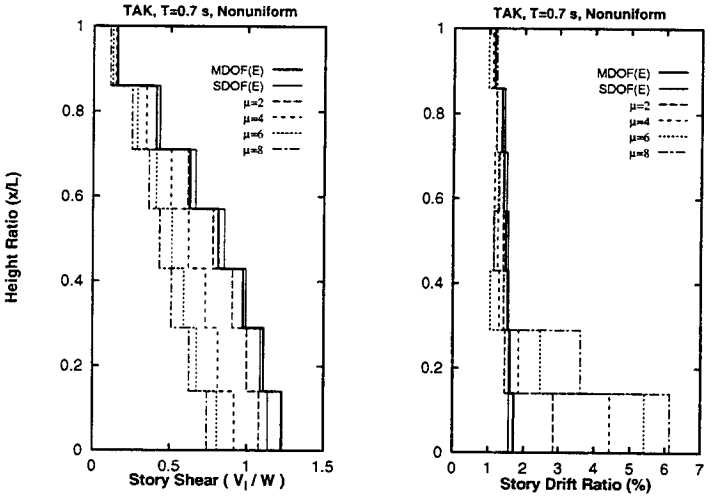

Figure 7. Spatial Distribution of Story Shear and Drift Demands, T = 0.7 second, TAK Input

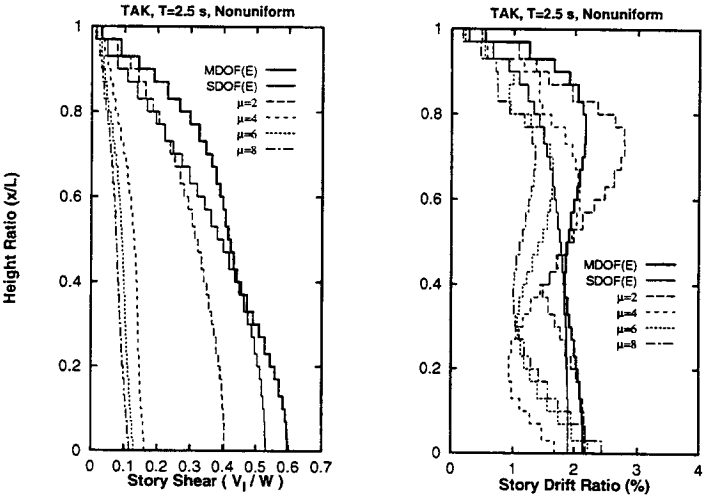

Figure 8. Spatial Distribution of Story Shear and Drift Demands, T = 2.5 second, TAK Input

1. The maximum story drift generally occurs at the base level except for a few cases where the maximum drift is located in the upper stories.

2. For structural periods shorter than the ground pulse duration, there is generally good correlation between elastic SDOF analysis and elastic MDOF analysis.

3. For longer period structures, an elastic SDOF analysis and an elastic MDOF analysis give very different results in both shape and magnitude.

4. An increase in ductility generally amplifies the base level drift ratio and sometimes decreases the upper-story drift ratios.

From analysis of the time histories of response for the suite of near-fault ground motions considered, it is observed that for longer period structures the maximum story drift often occurs at a different time than the maximum roof displacement. This is a clear indication that a single mode will not give an adequate representation of the spatial distribution of the response.

3.4 Limitations of Static Pushover Analysis

When the pushover procedure is performed on a MDOF system, the response prediction will be dependent upon many factors. Since the capacity becomes dependent upon the load patterns and detailed procedures used in the pushover analysis, there is no unique representation for the capacity of the structure. One important potential source of error will be the difference between the inelastic deformation shape assumed in the pushover analysis and that observed in an actual event. Additionally, as indicated above, the maximum story drift may not correlate in time with the maximum global response.

In order to examine only the effects of static pushover in a CSM type of analysis, equivalent viscous damping should not used. In this way, errors in demand estimation will be minimized. The procedure used herein for determining the effects of static pushover is as follows:

1. A static pushover analysis is performed in accordance with the Level 4 pushover procedure described in ATC-40.

2. The capacity spectrum is derived from the static pushover analysis of step 1.

3. A SDOF bilinear hysterestic system is constructed to represent the MDOF based on the capacity spectrum developed in step 2.

4. The displacement response of the equivalent SDOF system is determined using a full nonlinear time history analysis.

5. The maximum response of the physical MDOF system is estimated using the calculated maximum SDOF displacement response obtained in step 3.

A representative result is presented in figure 9 for the case of a 2.5 second period building subjected to the RRS ground motion. Shown are the spatial distribution of the maximum displacement and maximum interstory drift ratio based on the simplified CSM approach and a full MDOF inelastic time-history analysis

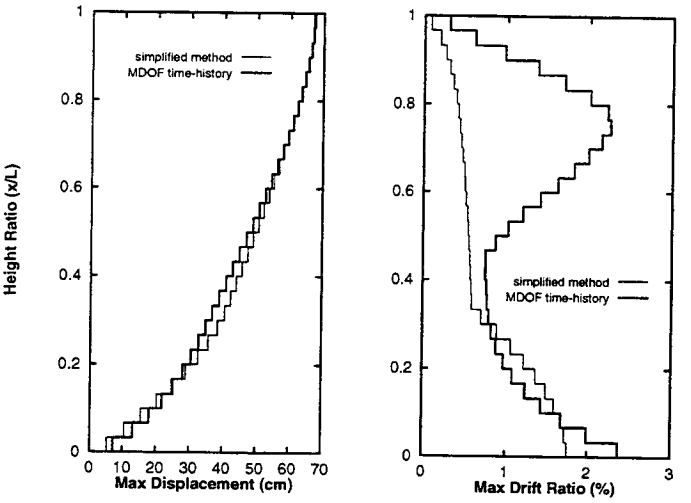

Figure 9: Comparison of Solutions Obtained by CSM (Simplified Method) and Full Nonlinear Time-History Analysis for Structure S8 (T = 2.5 second, μ = 4)

Based on the results shown in figure 9 and those for the suite of near-fault ground motions, the following observations are made:

1. The CSM approach provides a reasonable prediction of the maximum roof displacement for all cases considered regardless of building period, level of nonlinearity, or stiffness distribution.

2. For taller buildings, a simplified CSM analysis gives unsatisfactory predictions for maximum interstory drift response, particularly in upper stories. In some cases, it was observed that the actual drift demand was more than four times that predicted by the simplified method.

4.0 CONCLUSIONS

Based on the results of this study, the following conclusions are drawn:

1. The use of an equivalent viscous damping factor to account for inelastic behavior in a capacity spectrum method type of analysis is not generally valid for near-fault ground motions. This is particularly true for shorter period structures.

2. Use of a response deformation shape that is determined from a static pushover or an elastic response analysis may not accurately predict local structural deformations. This is particularly true for longer period structures. Inelastic deformations tend to accumulate at particular levels of a structure and increase with increasing ductility.

5.0 ACKNOWLEDGMENT

The results presented in this paper were obtained from research conducted with the financial support of the Pacific Earthquake Engineering Research (PEER) Center and the National Science Foundation. The author expresses his gratitude for this support. The opinions expressed are those of the author and do not necessarily reflect those of the sponsoring organizations.

6.0 REFERENCES

Comartin, Craig D. 1996. *Seismic evaluation and retrofit of concrete buildings*. Report No. SSC 96-01, Volumes 1 & 2. Prepared by ATC. [Sacramento, Calif.:] California Seismic Safety Commission.

Iwan, W. D., C.-T. Huang, and A. Guyader. 2000. *Proceedings 12WCEE*, Auckland, NZ. (Forthcoming.)

Iwan, W. D., C-T. Huang, and A. C. Guyader. 1999. *Earthquake Engineering Research Laboratory Report No. 99-01* Pasadena, Calif.: California Institute of Technology.

CORRELATION OF DISPLACEMENT RESPONSES WITH BASIC CHARACTERISTICS OF EARTHQUAKE MOTION

Toshimi KABEYASAWA[1] and Yukiko NAKAMURA[2]

ABSTRACT

Linear and nonlinear displacement responses of linear and nonlinear systems are correlated with basic characteristics of earthquake motion, which are supposed to be given as the amplitudes and the phases of Fourier spectrum. If the phase difference spectrum in Fourier transform is idealized as a normal probability curve, the standard deviation correlates to the duration of the earthquake. Expected values of time-history responses to the earthquake with the basic characteristics can be formulated mathematically by assuming constant Fourier amplitudes. The effect of damping on the linear response spectrum can be obtained based on this formula in relation to the duration of earthquake. Nonlinear displacement responses to earthquakes can be quantified based on instantaneous balance of input energy and dissipated energy. The input energy can be approximated from linear response spectrum, whereas the energy dissipation capacity and the equivalent period of vibration depend on the hysteretic path of responses. The peak displacement ratios, which are the ratios of previous peak displacement to the maximum displacement in nonlinear hysteresis, are defined to represent the hysteretic path. The ratios can also be related to the phase difference spectrum. A method of improving the linearization in capacity-demand diagram is presented using the peak displacement ratios approximated from the duration of motion.

1. INTRODUCTION

In the evaluation of seismic performance, the earthquake intensity is not specified as one level definitely but supposed as variable levels corresponding to the limit states. In the verification of safety, for example, the intensity level of the earthquake is supposed to be designated that would induce the near collapse of the structure. And the response of the structure is verified to be less than the ultimate deformation capacity under the varied intensity of earthquake. The instantaneous balance of energy is useful to evaluate maximum inelastic response to the earthquake. The ratio of the instantaneous energy input to the total energy is relatively high in case of the near-field

[1] *Department of Civil Engineering and Architecture, Niigata University, Niigata, Japan*
Email: nakamura@eng.niigata-u.ac.jp
[2] *Earthquake Research Institute, University of Tokyo, Tokyo, Japan*
Email: kabe@eri.u-tokyo.ac.jp

earthquake. To develop a rational performance-based design method, general correlation must be derived between the inelastic response and characteristics of the earthquake.

Here, the basic characteristics are supposed to be given as the amplitudes and the phases of Fourier spectrum of the earthquake. Fourier amplitudes correspond to the total input energy to the undamped system in terms of velocity . On the other hand, the phase angles have been assumed in practical design to be random or peculiar to the recorded motion. The distribution of the phase difference spectrum, which is defined as the difference between the phase angles of the two adjacent components in the Fourier decomposition, has been verified theoretically to be similar to the shape of the time-history of the original acceleration wave. In other words, the standard deviation of the phase difference spectrum corresponds to the duration of the earthquake motion.

The purpose of the study is to analyze the time-history responses based on the characteristics of the earthquake motion. A mathematical formula is given to calculate the expected value of the time-history response of the linear damped system to the earthquake motion, the characteristics of which are given by the phase difference spectrum of the Fourier components. The results can be applied to the theoretical formulation of the effect of damping on the response spectrum, or the maximum displacement amplitude ratio for the estimation of nonlinear responses.

2. CHARACTERISTICS OF INPUT EARTHQUAKE MOTIONS

Earthquake motions used in this study are listed in Table 1. Non-stationary waves can be expressed using the Fourier transform as Fourier amplitudes and phase difference spectrum. It has been pointed out theoretically that the phase difference spectrum is in good correlation with the time-history of the acceleration waveform. Therefore, the deviation of the spectrum may be used to express the duration of the earthquake. Here, the duration time t_0 is defined from 5% to 95% of the time history of the square of the acceleration, called frequency ensemble work, which corresponds to the work done to the system integrated in the domain of frequency. The duration times calculated for the earthquakes are shown in Table 1, with moment magnitudes of the source for the earthquakes after 1981 or the surface wave magnitudes before 1980. The time-history accelerations are shown in Figure 1.

The relations between the duration and the magnitudes were plotted in Figure 2. Simple empirical equations for the relations [Dobry, 1978][Trifunac, 1975] gives fair approximates for the defined duration. The Fourier angles of the two adjacent components in the Fourier decomposition, are idealized as normal distribution curves. Figure 3 shows examples of the correlation between the phase difference spectrum and the acceleration amplitude has been investigated so far, whereas the effect of the phase on the response has not been studied much. In the following study, the phase different spectrum, which is defined as the difference between the phase waveform for fkin30w and newrc1. The normal distributions fitted by the least square method are also shown in the figure. The standard deviation of the normal distribution is larger for the earthquake with the longer duration. The distribution of the phase difference spectrum has been verified theoretically to be similar to the envelope shape of the time-history of the original acceleration wave[Ohsaki, 1978]. In other words, the standard deviation of the phase difference spectrum corresponds to the duration of the earthquake motion. As shown in Figure 4, the duration corresponds to the four times of the standard deviation of the idealized normal distribution for the phase difference spectrum.

Table 1: List of Earthquake Motions.

Abbreviation	Earthquake	Site	Component	Date of occurrence	Magnitude	Amax(gal)	Duration (s)
elcns	Imperial valley earthquake	El Centro	NS	May 18,1940	7.1	341.7	24.4
taftse69	California earthquake	Kern county	S69E	Jul 21,1952	7.8	175.9	28.9
hacew	Tokachi-Oki	Hachinihe Harbor	EW	May 16,1968	8.2	182.9	24.4
pacs74w	San Fernando earthquake	Pacoima Dam	S74W	Feb 9,1971	6.6	1054.	7.28
tohns	Miyagi-ken-Oki	Tohoku University	NS	Jun 12,1978	7.6	258.2	19.5
sctew	Mexico	SCT1	EW	Sep 19,1985	8.0	167.9	38.9
ksrew	Kushiro-Oki	Kushiro Meteorological Observatory	EW	Jan 15,1993	7.6	711.4	19.3
sylew	Northrige earthquake	Sylmar county hosp.	EW	Jan 17,1994	6.7	826.7	5.34
kobns	Hyogo-ken-Nambu	Kobe Meteorological Obsevatory	NS	Jan 17,1995	6.9	820.6	8.38
fkin30w	Hyogo-ken-Nambu	Ohsaka Gas Fukiai Station	N30W	Jan 17,1995	6.9	802.0	6.76
newrc1	NewRC Artificial	--	--	--	--	394.6	29.6
newrc2	NewRC Artificial	--	--	--	--	407.2	78.5

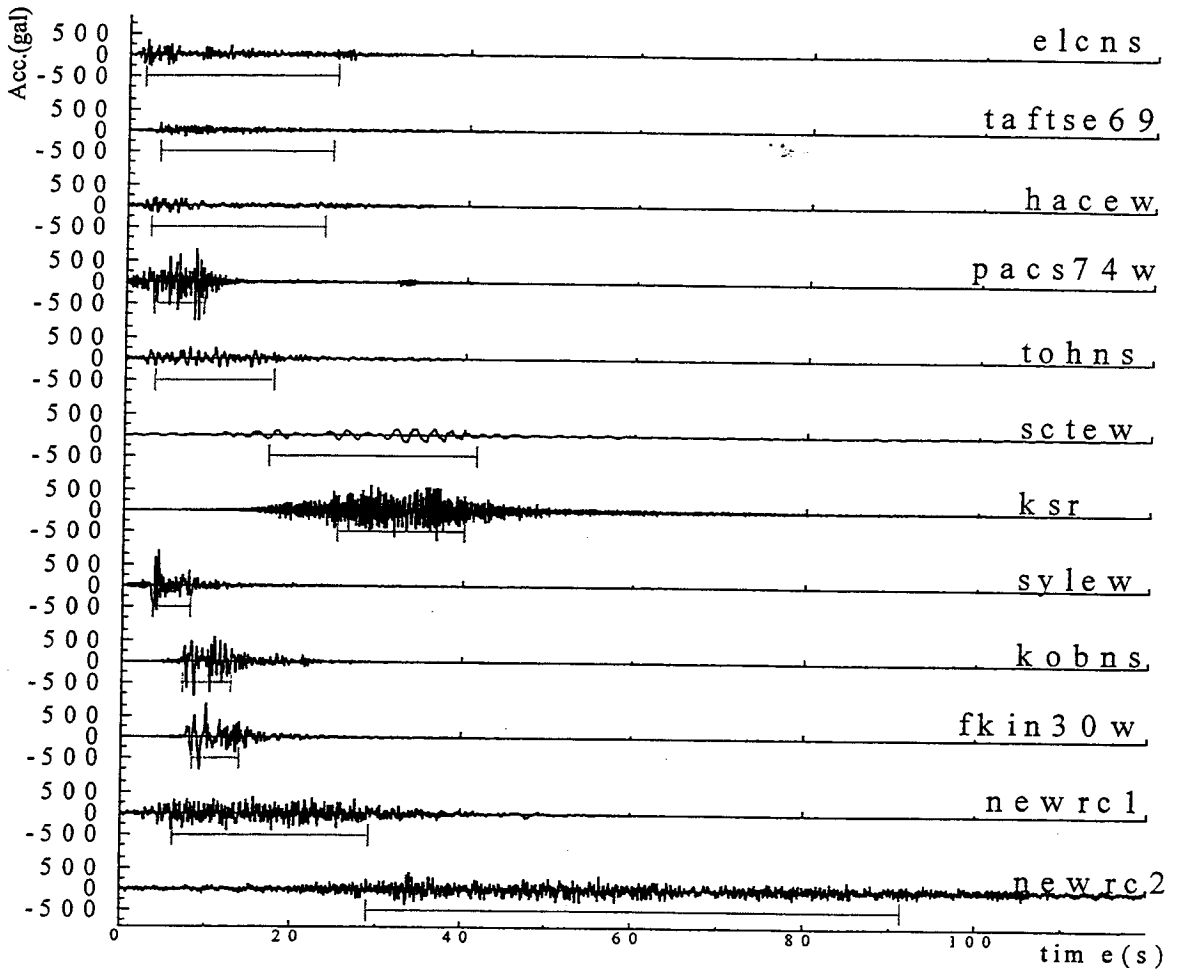

Figure 1: Time-history of the earthquake accelerations

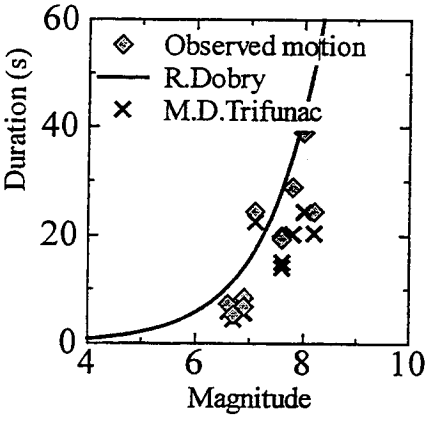

Figure 2: Duration and magnitudes

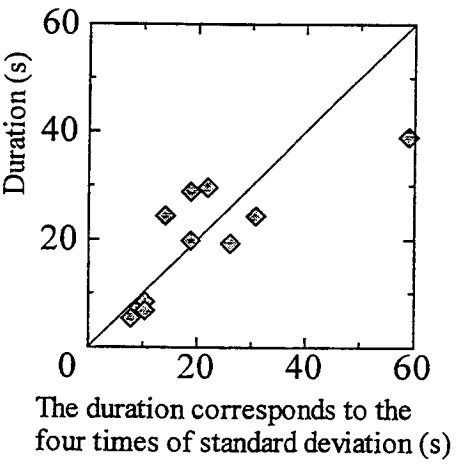

Figure 4: Duration and deviation of the phase difference spectrum

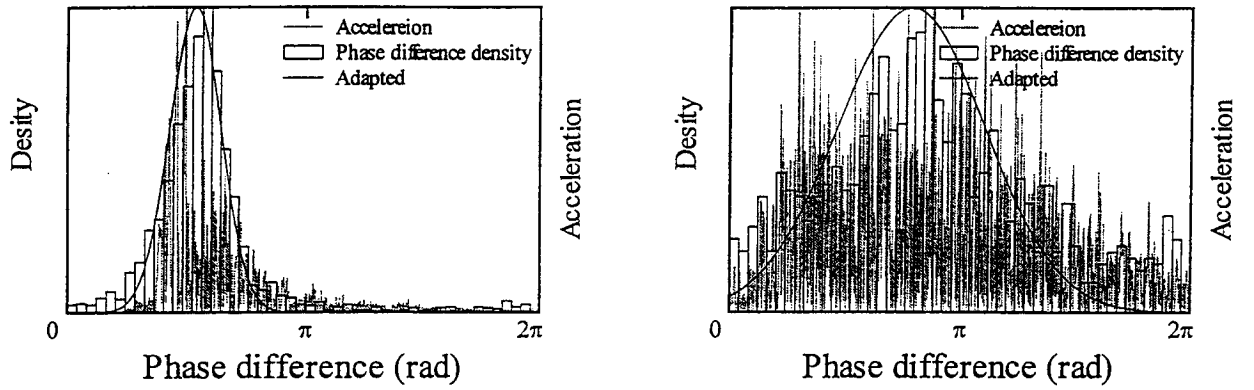

(a) fkin30w **(b) newrc1**

Figure 3: Probability density of the phase difference spectrum, idealized normal distribution and acceleration wave

3. EXPECTATION OF RESPONSE TIME-HISTORY FROM PHASE DIFFERENCE SPECTRUM

Expected value of the responses of the linear system with viscous damping was formulated as the superposition of the theoretical transient responses to the decomposed Fourier sinusoidal waves as follows. Earthquake acceleration is decomposed into the Fourier formula as the sum of cosine waves of Nf=N/2+1 as equation(1).

$$\ddot{y}_0(t) = \sum_{k=1}^{Nf} a_k \cos(\omega_k t + \phi_k) \tag{1}$$

$$p(\Delta\phi) = \frac{1}{\sqrt{2\pi\sigma}} \exp\left(-\frac{(\Delta\phi - \mu)^2}{2\sigma^2}\right) \tag{2}$$

where $\phi_k = \sum_{j=1}^{k} \Delta\phi_j$, φ_k : phase angle of the k-th component, $\Delta\varphi_k$: k-th phase difference ($=\varphi_k - \varphi_{k-1}$), $\ddot{y}_0(t)$: acceleartion of the motion, $\omega_k \left(= \sqrt{\frac{2\pi k}{N\Delta t}}\right)$: frequency of k-th component in the Fourier transform, N : total number of earthquake data, Δ□ : time increment of earthquake data, and $p(\Delta\phi)$: probability density function of the phase difference spectrum.

It is assumed here that the Fourier amplitudes of the acceleration ak are invariant and unity to investigate only the effect of phase difference spectrum. Also in the range out of 0 through 2_π, the

density spectrum is assumed to be negligibly small. Then the input acceleration of k-th component is expressed as equation (3).

$$\ddot{y}_{0k}(t) = \cos(\omega_k t + \phi_k) \tag{3}$$

Therefore, the transient response of the system with fundamental frequency ω and damping coefficient h to above component can be formulated as equation (4):

$$\dot{y}_k(t,h) = \Re\left[A_0\left\{i\Delta\omega k e^{\Delta\omega k p t} + e^{-h\omega t}(C_1 e^{i\sqrt{1-h^2}\omega t} C_2 e^{-i\sqrt{1-h^2}\omega t})\right\}e^{i\phi_k}\right] \tag{4}$$

where, $A_0 = \frac{-(\omega^2{\omega_k}^2 - 2ih\omega\omega_k)}{(\omega^2{\omega_k}^2)^2 + (2ih\omega\omega_k)^2}$, $C_1 = \frac{1}{2\sqrt{1-h^2}}\left(h\omega_k - \omega - i\omega_k\sqrt{1-h^2}\right)$, $C_2 = \frac{1}{2\sqrt{1-h^2}}\left(h\omega_k - \omega + i\omega_k\sqrt{1-h^2}\right)$, h is viscous damping coefficient of the system, ω is fundamental frequancy of the system. The response to the acceleration $\ddot{y}_0(t)$ can be expressed as equation (5) as the sum of all the components from 1st to Nf-th:

$$\dot{y}(t,h) = \sum_{k=1}^{Nf} \dot{y}_k(t,h) \tag{5}$$

Expected value of the average of the time-history response considering desnsity function of the phase spectrum can be expressed as equation (6):

$$E[\dot{y}(t,h)] = \int_{-\infty}^{\infty}\cdots\int_{-\infty}^{\infty}\{\dot{y}(t,h)\}\prod_{s=1}^{Nf} p(\Delta\phi_s)d\Delta\phi_1\cdots d\Delta\phi_{Nf} \tag{6}$$

And, the variance of the response is in the following equation(7), from which the envelope curve of the response can be derived as its square root:

$$Var[\dot{y}(t,h)] = \int_{-\infty}^{\infty}\cdots\int_{-\infty}^{\infty}\{\dot{y}(t,h)\}^2\prod_{s=1}^{Nf} p(\Delta\phi_s)d\Delta\phi_1\cdots d\Delta\phi_{Nf} - E[\dot{y}(t,h)]^2 \tag{7}$$

Calculated envelope curves for the systems with damping coefficients of 5, 10, 15 and 20 percent of critical are shown in Figure 5. The values of the standard deviation of the phase difference spectrum are $0.34\ \pi$and 1.01π for Fukiai and NewRC1 respectively.

4. EFFECT OF DAMPING ON RESPONSE SPECTRUM

The effect of damping on the response has been approximated empirically in practice and research, so that the basic characteristics, for example the phase spectrum, are not reflected in the

approximation. However, the effect of damping on the response is apparently different, for example, in the cases of far-field and near-field earthquakes. The relationship between the fundamental frequency of the system and the duration of the earthquake need be investigated.

The effect of damping can be formulated based on the power spectrum if the input wave is assumed as a white noise, which is basically determined by the duration of the input wave. Expected constant stable response to the white noise of the duration t_1 is expressed as equation (8), from which the effect of damping on the response is formulated as equation (9):

$$\sigma_y^2 = \frac{S_0}{4h\omega_0^2}\left[1-e^{-2h\omega_0 t_1}\right] \quad (h \neq 0) \qquad \sigma_y^2 = \frac{S_0 t_1}{2h\omega_0^2} \quad (h=0) \tag{8}$$

$$D_h(h) = \frac{S_V(h)}{S_V(h=0.0)} = \sqrt{\frac{1-e^{-2h\omega_0 t_1}}{2h\omega_0 t_1}} \tag{9}$$

where, σ_y^2 : expected square average of response displacement, S_0 : power spectrum density, t_1 : duration of the white noise, h : damping coefficient, ω_0 : fundamental frequency. The duration of earthquake t_0 must be converted into the equivalent duration in above formula. The equivalent duration t_1 for above equation (9) is derived as $t_1=t_0/4$ empirically so that the reduction from the equation (9) roughly agrees with the calculated responses of the damped system. Examples are shown in Figure 6.

Although above formula is simple and practical, the equivalent duration was determined empirically without theoretical background. The time-history response derived from the phase difference spectrum in the previous section can be used to correlate the effect of damping with the duration of the earthquake. The effect of damping can be formulated as equation (10), only by idealizing the phase difference spectrum as a normal distribution curve:

$$D_h(h) = \frac{S_V(h)}{S_V(h=0.0)} = \frac{Var\left[\dot{y}(t,h)\right]_{max}}{Var\left[\dot{y}(t,0)\right]_{max}} \tag{10}$$

The effect of damping on the response derived from above formula as response expectations is shown in Figure 7 for Fukiai and NewRC motions. As shown in the figure, good estimates can be derived theoretically based on the phase difference spectrum or the duration of the earthquake. The reduction of response estimated from above equation is apparently greater than the reduction estimated based on white noise (equation(9)) assuming the equivalent duration of $t_0/4$. Therefore, the equivalent duration longer than $t_0/4$ may be assumed to fit above theory. The response under the

actual earthquake is scattering because the phase difference spectrum is not normal distribution and Fourier amplitude is not constant through frequency. The method gives theoretical and smoothed expectation, although it takes a lot of computation time, which may be a theoretical background to the equivalent duration empirically determined based on the white noise.

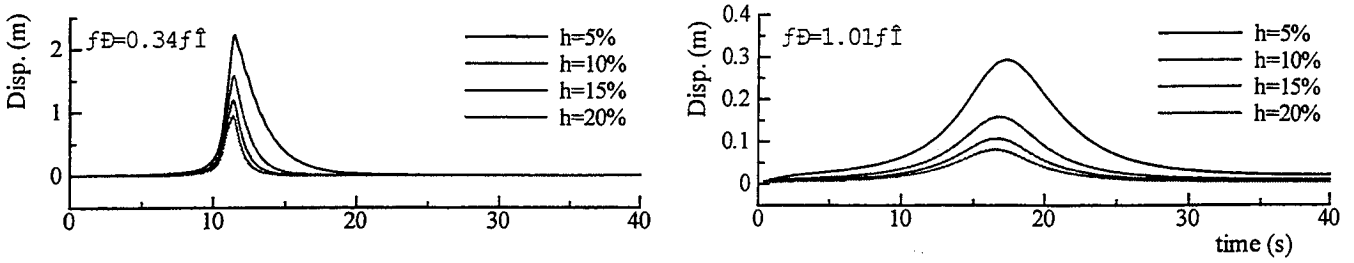

(a) fkin30w **(b) newrc1**

Figure 5: Expected envelope of response time-history

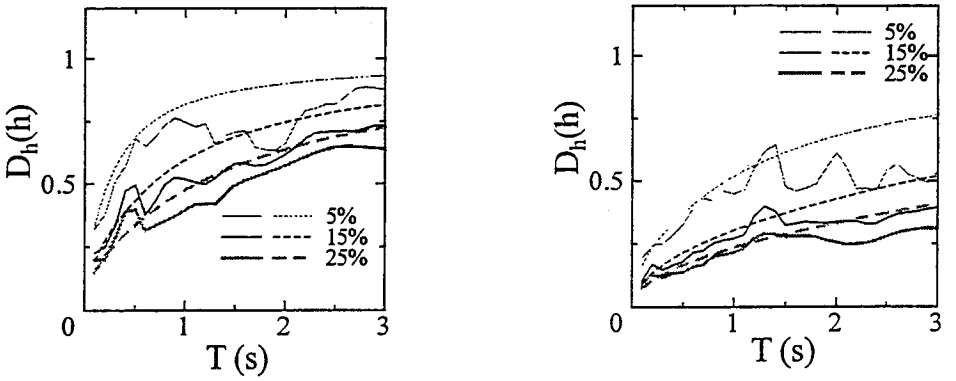

(a) fkin30w **(b) newrc1**

Figure 6: Reduction ratio of damped response to undamped response and estimation from equivalent white noise

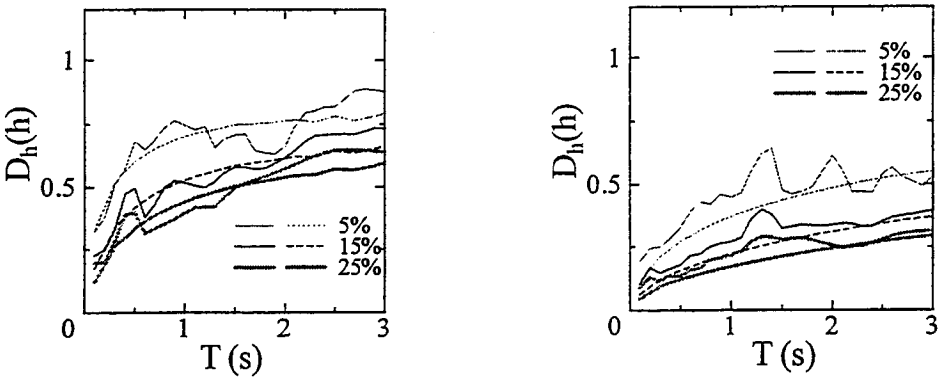

(a) fkin30w **(b) newrc1**

Figure 7: Reduction ratio of damped response to undamped response and estimation from the phase difference spectrum

5. PEAK DISPLACEMENT RATIO

Input and dissipated energy in the hysteretic damping system is balanced during the response to earthquake motions. In the past studies[Nakamura and Kabeyasawa, 1996], maximum response displacement of hysteretic damping system can fairly be correlated to the instantaneous input energy during the unit time in proportion to the equivalent period of inelastic system. Input energy can be evaluated relatively stable and constant, although it depends on the equivalent period. Also, the input energy to the inelastic system can be correlated to the linear response spectrum. On the other hand, the energy dissipation capacity depends on the hysteretic relations of the system, especially at the latest moment when the maximum displacement occurs.

For example, it is clearly different in the cases that the amplitude increases symmetrically and gradually with cyclic vibration and that the inelastic displacement increases rapidly in one direction. Figure 8 shows the hysteretic response of an inelastic system under NewRC and Fukiai motions. As shown in Figure 8(a) under Fukiai motion, i.e., a near-field motion, the displacement response increases rapidly up to maximum displacement in one cycle, whereas under NewRC motion in Figure 8(b), the response gradually increases with cyclic excitations. To differentiate these types of responses, the index of peak displacement ratio is proposed which is defined as the ratio of the peak displacement in the previous half- or one-cycle to the maximum displacement as follows:

$$\gamma_{1/2} = D_{\min} / D_{\max} \qquad (11)$$

$$\gamma_1 = D_{pre} / D_{\max}$$

where, $D_{\max}$: maximum response displacement, $D_{\min}$: half-cycle previous peak displacement in the opposite direction, D_{pre}: one-cycle previous peak displacement in the same direction

Figure 9 shows the peak displacement ratios $\gamma_1 \square \gamma_{1/2}$, calculated from responses of various nonlinear systems under NewRC and Fukiai motions. The ratios are plotted in relation to the equivalent period in horizontal axis, which is calculated from the secant stiffness from the origin to the maximum response displacement. The hysteresis rule of the systems is Takeda model, the yield strength of which is selected under each motion so that the nonlinear maximum response displacement of the systems attains the ductility factor of 2, 4, or 9. The peak displacement ratios are apparently different between the responses under the two motions. They depends on the equivalent period of the system:

the ratios are higher under NewRC motion with long duration and lower under Fukiai motion with short duration, which reduce with the elongation of the equivalent period.

The peak displacement ratios can also be derived theoretically from the expectations of time-history response. The ratios calculated from the expectations are plotted in Figure 9 with dotted lines, which conform to the observed relations that the ratios becomes lower with the elongation of the equivalent period and under the motion with short duration. The method gives a theoretical background for the peak displacement ratios. However, it requires too heavy calculations. Therefore, the ratios are formulated by simplifying the time-history of the input energy, as shown in Figure 10, using the duration, on the assumption that:

(1) Instantaneous input energy is the maximum at the middle point of the defined duration of motion.

(2) The maximum instantaneous energy is four times the average energy (two times in terms of velocity), which is defined as the total energy divided by the duration of the motion[Nakamura and Kabeyasawa, 1998].

(3) The maximum displacement occurs at the maximum instantaneous energy.

(4) The peak displacement ratios is in proportion to the maximum input energy, from which □ is given by the following equation, using the duration t_0 and the equivalent period Te,

$$\gamma = \frac{t_0/2 - T_e}{t_0/2 + T_e} = \frac{t_0 - 2T_e}{t_0 + 2T_e} \tag{12}$$

where, t_0 is the duration of motion, T_e is equivalent period

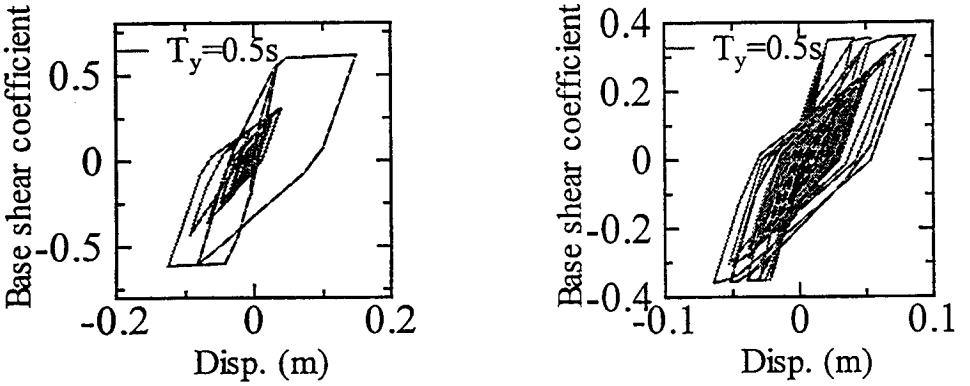

(a) fkin30w **(b) newrc1**

Figure 8: Examples of hysteretic responses

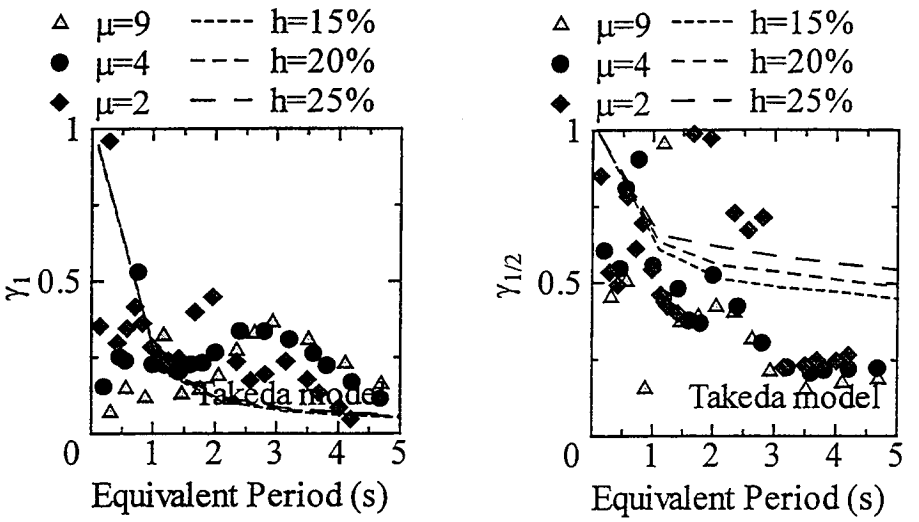

(a) fkin30w

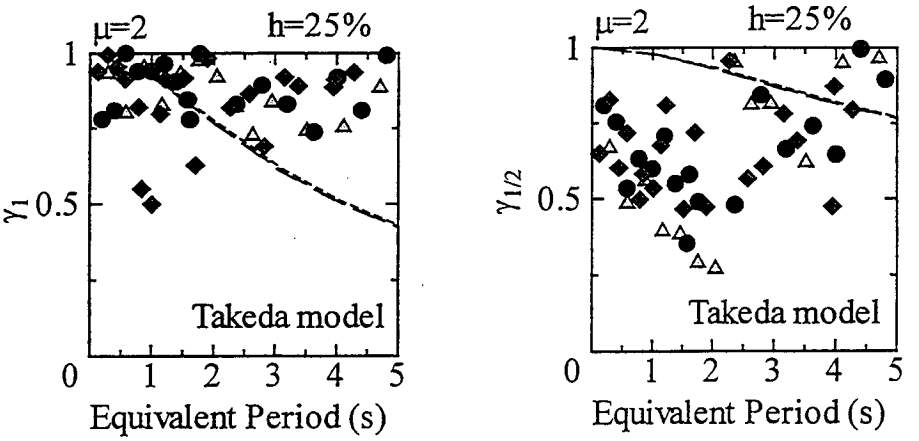

(b) newrc1

Figure 9: Peak displacement ratios

6. ESTIMATION OF NONLINEAR DISPLACEMENT RESPONSE

To estimate nonlinear and dynamic response to earthquake motions, a simple equivalent linearization is practical using pushover analysis and capacity-demand diagram. As shown in Figure 11, equivalent load-deformation curve of reduced single-degree-of-freedom system from the pushover analysis is plotted on S_A-S_D diagram, namely acceleration-displacement diagram. Then, the nonlinear dynamic response can be estimated to be the crossing point of the capacity curve and the demand curve, where the substitute damping of the hysteretic system is equal to that of the demand curve, i.e., the elastic response spectrum of the motion. It should be noted that the equivalent

fundamental period of the hysteretic system is simply and implicitly assumed to correspond to the secant stiffness starting from the origin to the estimated maximum inelastic response.

The accuracy of above method diagram is investigated for the responses of the nonlinear systems with hysteresis rules of Takeda-model, Takeda-Slip model and Bilinear model as shown in Figure 12. The marks of rectangle, triangle or circle are the responses calculated from inelastic system, which attain ductility levels of 2, 4, and 9, which are plotted at the corresponding strength(S_A) and response displacement(S_D). If the estimation method is appropriate, these responses are plotted on the demand curves with the corresponding damping coefficient. A fair correlation is observed only in the case of Takeda model under the artificial design motion of NewRC as shown in Figure 12 (a), in which stationary responses are dominant. In the other cases under recorded motions, the estimation is much worse in general, an example of which is shown in Figure 12 (b) under Fukiai Staion record (N30W) during 1995 Hyogoken-Nanbu Earthquake. The estimated responses by capacity-demand diagram as the crossing points are compared with the calculated under NewRC and Fukiai motions, as shown in Figure 13. The accuracy is not satisfactory. For example, when the inelastic displacement increases rapidly under near-field earthquake motion, the estimation could be smaller than the calculated.

If the displacement increases symmetrically and gradually with cyclic vibration, then the hysteretic damping in stationary behavior and the secant stiffness to the maximum displacement can be assumed in the estimation. On the other hand, if the inelastic displacement increase rapidly in one direction under relatively short earthquake motion, in other words, the peak displacement ratio is small, then the equivalent fundamental period should be assumed shorter and the energy dissipation capacity should be corrected considering the hysteresis path. In such case, the equivalent stiffness is defined here from the half-cycle previous peak to the maximum peak displacement, as shown in Figure 14. Equivalent viscous damping factor is also defined as the hysteretic damping for the half cycle as shown in the figure. The capacity-demand diagram method was modified using above equivalent period and damping on the assumption that the peak displacement ratio was given by equation (12) based on the duration of the earthquake. The estimated displacement and maximum response displacement under NewRC and Fukiai motion are shown in Figure 15, which give better estimation than those by the simple capacity-demand diagram method.

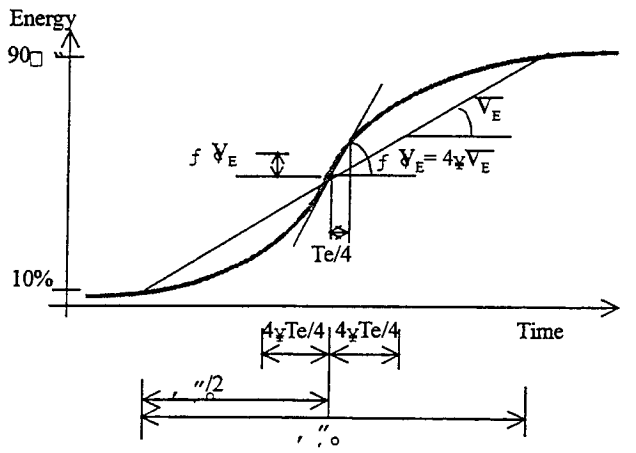

Figure 10: Simplified energy input time-history

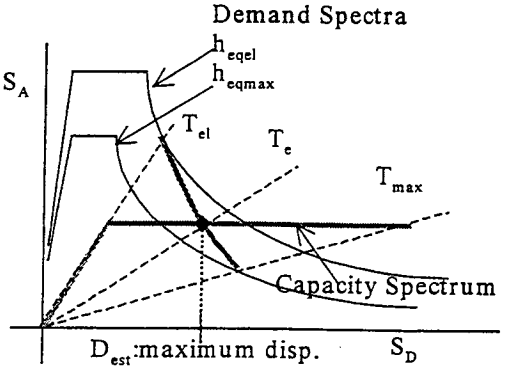

Figure 11: Capacity-demand diagram method

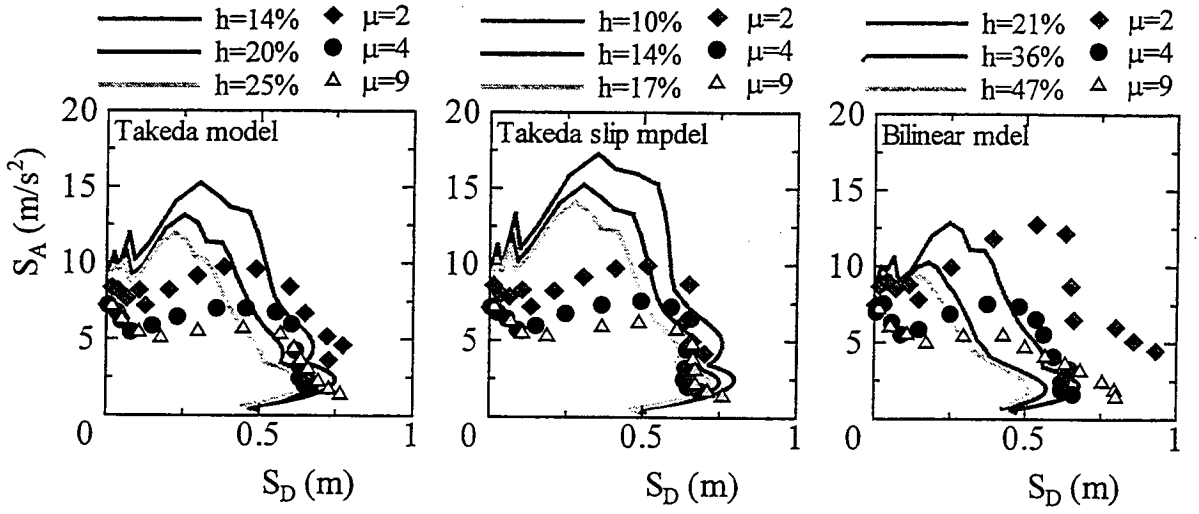

(a) fkin30w

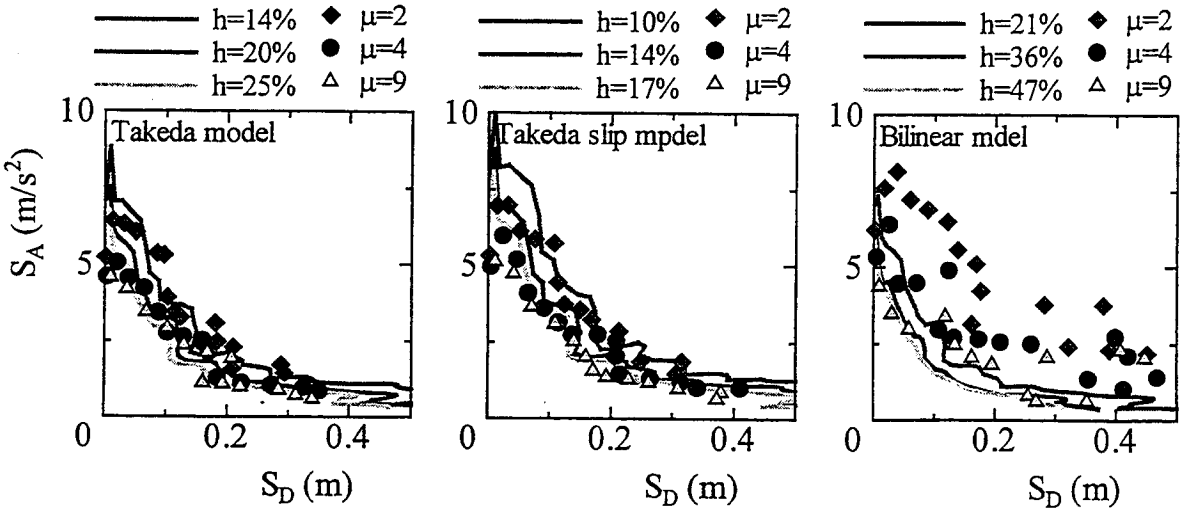

(b) newrc1

Figure 12: Responses of nonlinear system and demand curves in S_A-S_D format

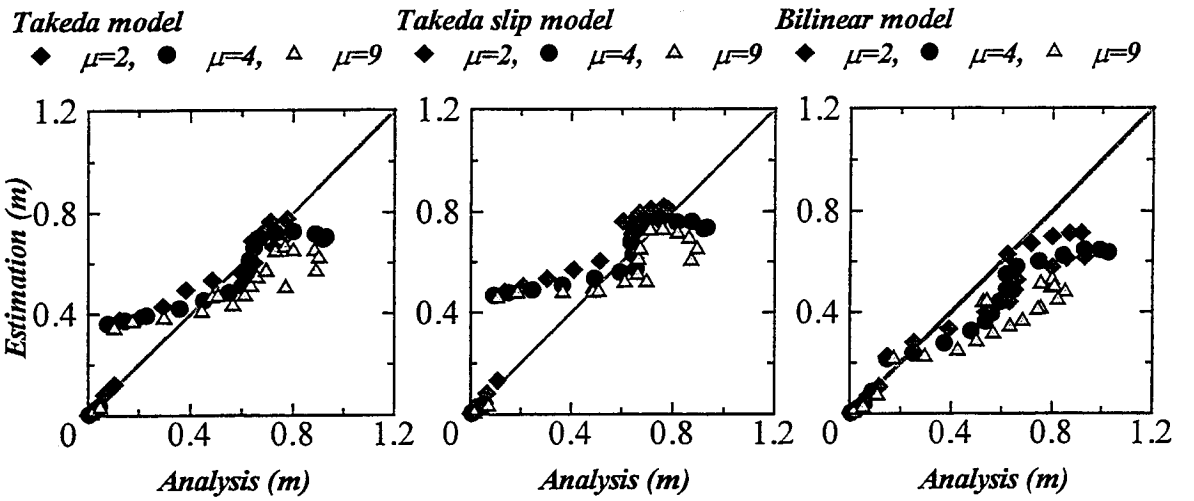

Figure 13: Estimation by capacity-demand diagram with calculated nonlinear responses to fkin30w

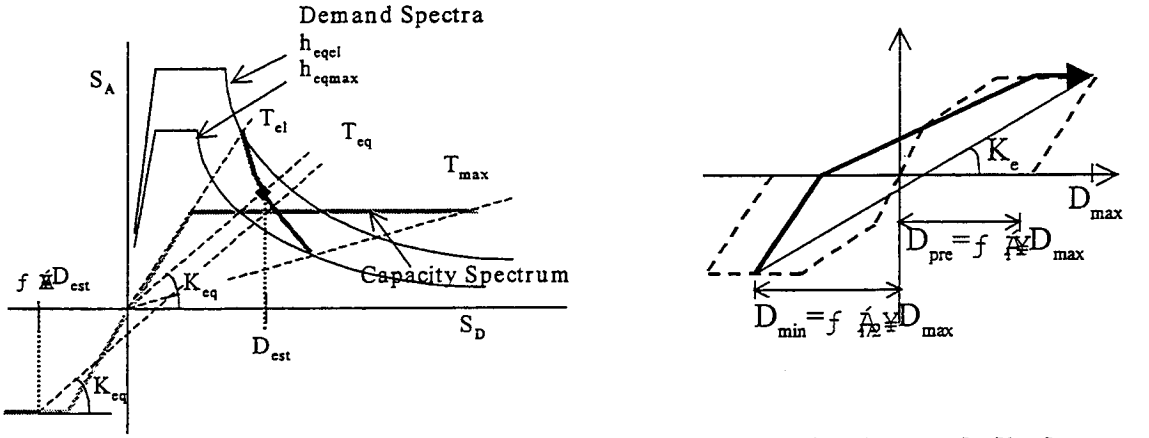

Figure 14: Modified capacity-demand diagram method using peak displacement ratios

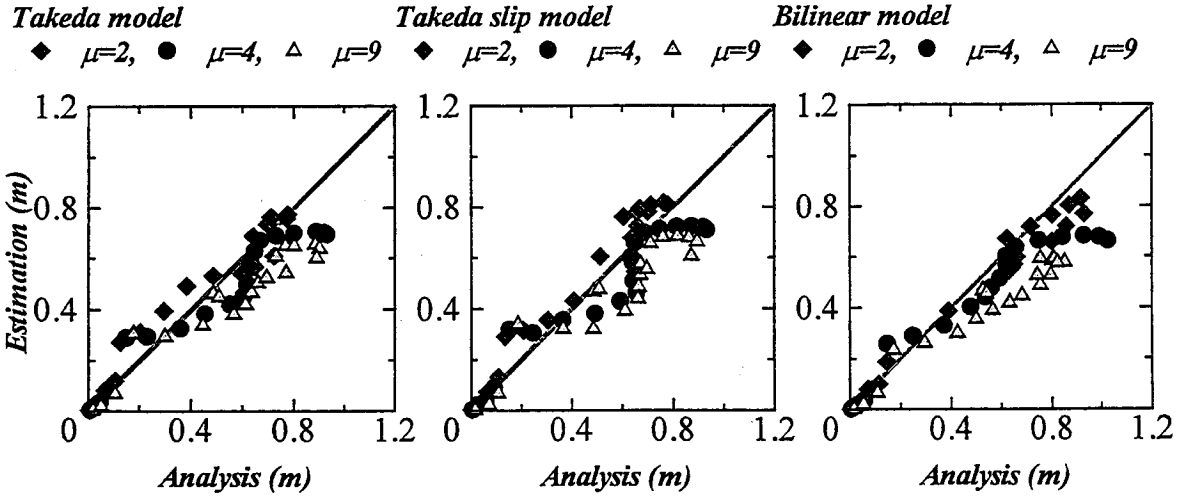

Figure 15: Modified estimation with calculated nonlinear responses

6. CONCLUSIONS

Expected value of time-history response can be formulated by assuming the phase difference spectrum in Fourier transform of earthquake waves as a normal probability curve. The effect of damping on the linear response spectrum can be obtained based on this formula, which should be correlated to the duration of earthquake in demand spectrum. The peak displacement ratios, which are the ratio of maximum displacement to previous peak displacement during nonlinear response, can also be calculated theoretically based on above formula from the phase difference spectrum. Estimation of the nonlinear response from an equivalent linear system in capacity-demand diagram can be improved using the peak displacement ratios approximated from the duration of motion.

REFERENCES

Dobry, R. Idriss, I. M. and E. Ng, (1978), "Duration chracteristics of horizontal components of strong-motion earthquake records", *Bulletin of Seismological Society of America*, Vol.68, No.5, pp1487-1520.

Nakamura, Y. and Kabeyasawa, T., (1996), "Estimation of Maximum Displacement Response of Reinforced Concrete Structures Based on Energy Input Rate Spectrum", *Transactions of the Japan Concrete Institute*, Vol. 18, pp205-212.

Nakamura, Y. and Kabeyasawa, T., (1998), "Estimation of Maximum Displacement Response of Reinforced Concrete Structures", *Proceedings of the Tenth Japan Earthquake Engineering Symposium*,

Ohsaki, Y., Iwasaki, R., Ohkawa, I. and Masao, T., (1978), "A study phase characteristics of earthquake motions and its application", *Proceedings of the Fifth Japan Earthquake Engineering Symposium*, pp201-208

Trifunac, M. D. and Brady, A. G. (1975), "A study on the strong earthquake ground motion", *Bulletin of Seismological Society of America,* Vol.65, No.3, pp581-626.

CAPACITY-DEMAND DIAGRAM METHODS BASED ON INELASTIC DESIGN SPECTRUM[1]

Anil K. CHOPRA[2] and Rakesh K. GOEL[3]

SUMMARY

An improved capacity-demand-diagram method that uses the well-known constant-ductility design spectrum for the demand diagram is developed and illustrated by examples. This method estimates the deformation of inelastic SDF systems consistent with the selected inelastic design spectrum, while retaining the attraction of graphical implementation of the ATC-40 *Nonlinear Static Procedure*. The improved procedure differs from ATC-40 procedures in one important sense. The demand diagram used is different: the constant-ductility demand diagram for inelastic systems in the improved procedure versus the elastic demand diagram in ATC-40 for equivalent linear systems.

INTRODUCTION

The *Nonlinear Static Procedure* in ATC-40 and FEMA-274 documents is based on the capacity spectrum method (Freeman et al., 1975) which is used to determine the seismic deformation of an SDF system derived from the pushover curve. This method is based on the belief that the earthquake-induced deformation of an inelastic SDF system can be estimated satisfactorily by an iterative method requiring analysis of a sequence of equivalent linear SDF systems, thus avoiding the dynamic analysis of the inelastic SDF system.

The principal objective of this investigation is to develop improved simplified analysis procedures, based on capacity and demand diagrams, to estimate the peak deformation of inelastic SDF systems. These improved procedures use the well-established inelastic response (or design) spectrum. The idea of using the inelastic design spectrum in this context was suggested by Bertero (1995), and introduced by Reinhorn (1997) and Fajfar (1999).

EVALUATION OF NONLINEAR STATIC PROCEDURE

The excitation is characterized by the elastic design spectrum of Fig. 1 which is the median-plus-one-standard-deviation spectrum constructed by the procedures of Newmark and Hall (1982), as described in Chopra (1995; Section 6.9). The yield strength of each bilinear hysteretic system analyzed was chosen corresponding to an allowable ductility μ:

$$f_y = (A_y/g)w \tag{1}$$

where w is the weight of the system and A_y is the pseudo-acceleration corresponding to the allowable ductility and the vibration properties — natural period T_n and damping ratio ζ — of the system in its linear range of vibration. Given the properties T_n, ζ, and f_y and the elastic design spectrum, the earthquake-induced deformation of the system can be determined as described in Chopra (1995: Section 7.6). Utilized in such a procedure is a T_n-dependent relation between yield strength reduction factor R_y and μ.

---

[1] This paper will also appear in the *Proceedings* of the 12th World Conference on Earthquake Engineering to be held in New Zealand, January 29–February 5, 2000.

[2] Dept. of Civil and Environmental Engineering, University of California, Berkeley, CA 94720.

[3] Dept. of Civil and Environmental Engineering, California Polytechnic State University, San Luis Obispo, CA 93407.

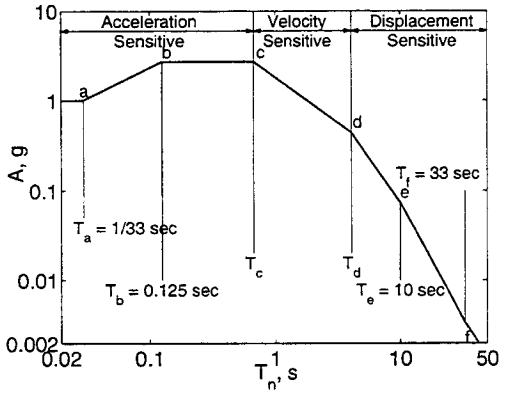

Figure 1. Newmark-Hall elastic design spectrum

Presented in Fig. 2 are the deformations determined by using three different $R_y - \mu - T_n$ equations: Newmark and Hall (1982); Krawinkler and Nassar (1992) for elastoplastic systems; and Vidic, Fajfar, and Fischinger (1994) for bilinear systems. The equations describing these relations are presented in Chopra and Goel (1999). Observe that the three recommendations lead to similar results except for $T_n < 0.3$ sec , indicating that the inelastic design spectrum is a reliable approach to estimate the earthquake-induced deformation of yielding systems, reliable in the sense that different researchers have produced similar results.

The deformation estimates by the ATC-40 method, as determined by Chopra and Goel (1999), are also included in Fig. 2. Relative to the deformation value from inelastic design spectra, the percentage discrepancy in the approximate result is plotted in Fig. 3. The approximate procedure underestimates the deformation significantly, except for very long periods ($T_n > T_f$ in Fig. 1).

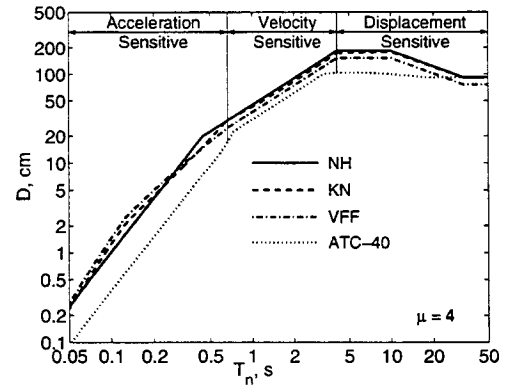

Figure 2. Deformation of inelastic systems (μ= 4) determined from inelastic design spectra using ATC-40 Procedure and three $R_y - \mu - T_n$ equations: Newmark-Hall (NH), Krawinkler-Nassar (KN), and Vidic-Fajfar-Fischinger (VFF)

In passing, note that the ATC-40 procedure is deficient relative to even the *elastic* design spectrum in the velocity-sensitive and displacement-sensitive regions $(T_n > T_c)$. For T_n in these regions, the peak deformation of an inelastic system can be estimated from the elastic design spectrum, using the well-known equal-displacement rule (Veletsos and Newmark, 1960). However, the ATC-40 procedure requires analyses of several equivalent linear systems and still produces worse results.

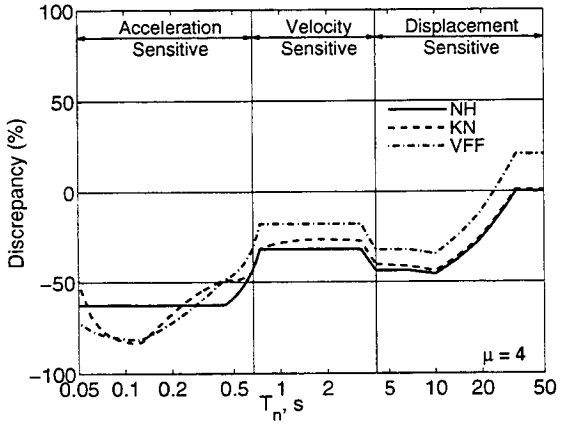

Figure 3. Discrepancy in deformations computed by ATC-40 procedure relative to three different (NH, KN, VFF) inelastic design spectra; μ = 4

IMPROVED PROCEDURES

Inelastic Design Spectrum

A constant-ductility spectrum for a bilinear hysteretic system is a plot of A_y versus T_n for selected values of μ. The pseudo-acceleration A_y is related to the yield strength f_y, by Eq. (1). The yield strength reduction factor is given by

$$R_y = \frac{f_o}{f_y} = \frac{A}{A_y} \tag{2}$$

where

$$f_o = \left(\frac{A}{g}\right) w \tag{3}$$

is the minimum yield strength required for the structure to remain elastic during the earthquake; A is the pseudo-acceleration ordinate of the elastic design spectrum at (T_n, ζ).

A constant-ductility design spectrum is established by dividing the elastic design spectrum by appropriate ductility-dependent reduction factors that depend on T_n. The earliest recommendation for the reduction factor, R_y (Eq. 2), goes back to the work of Veletsos and Newmark (1960), which is the basis for the inelastic design spectra developed by Newmark and Hall (1982). Starting with the elastic design spectrum of Fig. 1 and these $R_y - \mu$ relations for acceleration-, velocity-, and displacement-sensitive spectral regions, the inelastic design spectrum constructed by the procedure described in Chopra (1995, Section 7.10), is shown in Fig. 4a.

In recent years, several recommendations for the reduction factor have been developed (e.g., Krawinkler and Nassar, 1992; Vidic, Fajfar, and Fischinger, 1994). Based on two of these recommendations, the inelastic design spectra are also shown in Fig. 4a.

Inelastic Demand Diagram

The inelastic design spectra of Fig. 4a will be plotted in the *A-D* format to obtain the corresponding demand diagrams. The peak deformation D of the inelastic system is given by:

$$D = \mu \frac{1}{R_y} \left(\frac{T_n}{2\pi}\right)^2 A \tag{4}$$

Using Eq. (4), D is determined corresponding to the three inelastic design spectra in Fig. 4a. Such data pairs (A_y ,D) are plotted to obtain the demand diagram for inelastic systems (Fig. 4b).

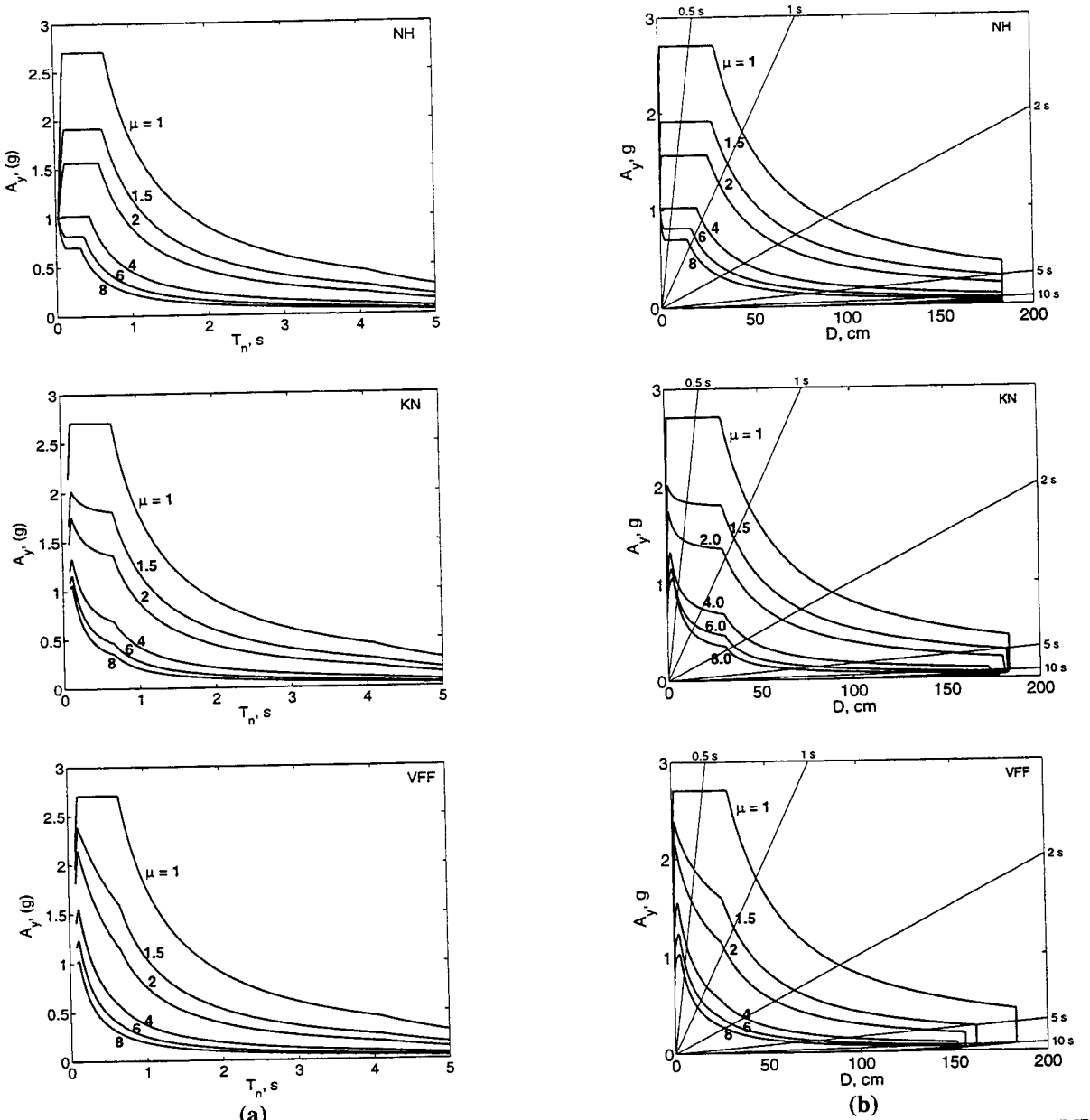

Figure 4. (a) Inelastic design spectra and (b) Inelastic demand diagrams, based on three different (NH, KN, VFF) recommendations

Improved Procedure

This procedure, which uses the demand diagram for inelastic systems (Fig. 4b), will be illustrated with reference to six elastoplastic systems defined by two values of T_n = 0.5 and 1.0 sec and three different yield strengths, given by Eq. (1) corresponding to μ = 2, 4, and 6, respectively. For systems with T_n = 0.5 sec, $f_y \div w$ = 1.5624, 0.8992, and 0.5995 for μ = 2, 4, and 6, respectively. The corresponding values for systems with T_n = 1 sec are $f_y \div w$ = 0.8992, 0.4496, and 0.2997. Superimposed on the demand diagrams are the capacity diagrams for three inelastic

systems with T_n = 0.5 sec (Fig. 5a) and T_n = 1.0 sec (Fig. 5b). The yielding branch of the capacity diagram intersects the demand diagram for several μ values. One of these intersection points, which remains to be determined, will provide the deformation demand. At the one relevant intersection point, the ductility factor calculated from the capacity diagram should match the ductility value associated with the intersecting demand curve. Determined according to this criterion, the deformation for each system is noted in Fig. 5. This result will be essentially identical to that given by Eq. (4). Implementation of this procedure is illustrated for two systems.

Examples

The yield deformation of System 1 is u_y = 3.724cm. The yielding branch of the capacity diagram intersects the demand curves for μ = 1, 2, 4, 6, and 8 at 133.93 cm, 66.96 cm, 33.48 cm, 22.3 cm, and 16.5 cm, respectively (Fig. 5a). Dividing by u_y, the corresponding ductility factors are: 133.93÷3.724=35.96 (which exceeds μ = 1 for this demand curve), 66.96÷3.724=17.98 (which exceeds μ = 2 for this demand curve), 33.48÷3.724=8.99 (which exceeds μ = 4 for this demand curve), 22.3÷3.724=6 (which matches μ = 6 for this demand curve), and 16.5÷3.724=4.43 (which is smaller than μ = 8 for this demand curve). Thus, the ductility demand is 6 and the deformation of System 1 is D = 22.3 cm.

For System 3, u_y = 9.681cm. The yielding branch of the capacity diagram intersects the demand curve for μ = 1 at 51.34 cm (Fig. 5a). The corresponding ductility factor is 51.34÷9.681=5.3, which is larger than the μ = 1 for this demand curve. The yielding branch of the capacity diagram also intersects the demand curve for μ = 2 continuously from 9.681 cm to 25.2 cm, which correspond to ductility factors of 1 to 2.6. The intersection point at 19.29 cm corresponds to ductility factor = 19.39÷9.681=2 which matches μ = 2 for this demand curve. Thus, the ductility demand is 2 and the deformation of System 3 is D = 19.39 cm.

Observe that for the presented examples, the ductility factor at the intersection point matched exactly the ductility value associated with one of the demand curves because the f_y values were chosen consistent with the same μ values for which the demand curves have been plotted. In general this is not the case, and interpolation between demand curves for two μ values would be necessary. Alternatively, the demand curves may be plotted at a finer μ interval avoiding the need for interpolation.

Comparison with ATC-40 Procedure A

The improved procedure just presented gives the deformation value consistent with the selected inelastic design spectrum, while retaining the attraction of graphical implementation of the ATC-40 Procedure A. The two procedures are similar in the sense that the desired deformation is determined at the intersection of the capacity diagram and the demand diagram. However, the two procedures differ fundamentally in an important sense; the demand diagram used is different: the constant-ductility demand diagram for inelastic systems in the improved procedure (Fig. 5) versus the elastic demand diagram in ATC-40 Procedure A for equivalent linear systems.

IMPROVED PROCEDURE: NUMERICAL VERSION

The improved procedure presented in the preceding section was implemented graphically, in part, to highlight the similarities and differences relative to the *Nonlinear Static Procedure* in the ATC-40 report. However, this graphical feature is not essential and the procedure can be implemented numerically. Such a procedure using $R_y - \mu - T_n$ equations is outlined in this section. While space limitation does not permit presentation of these equations (Chopra and Goel, 1999), they are plotted in Figures 6a and 6b. Plots of R_y versus T_n for selected values of μ are shown in Fig. 6a and of μ versus T_n for selected values of R_y in Fig. 6b. Observe the similarity among the three sets of results, indicating consensus among different researchers.

The peak deformation of systems 1 to 6 (Table) are determined using $R_y - \mu - T_n$ relations. Detailed calculations are presented in Chopra and Goel (1999: Appendix B) and the results are summarized in Table 1. Observe that the deformation values computed using $R_y - \mu - T_n$ equations are identical to those determined by the graphical procedure (Fig. 5) except for round-off differences.

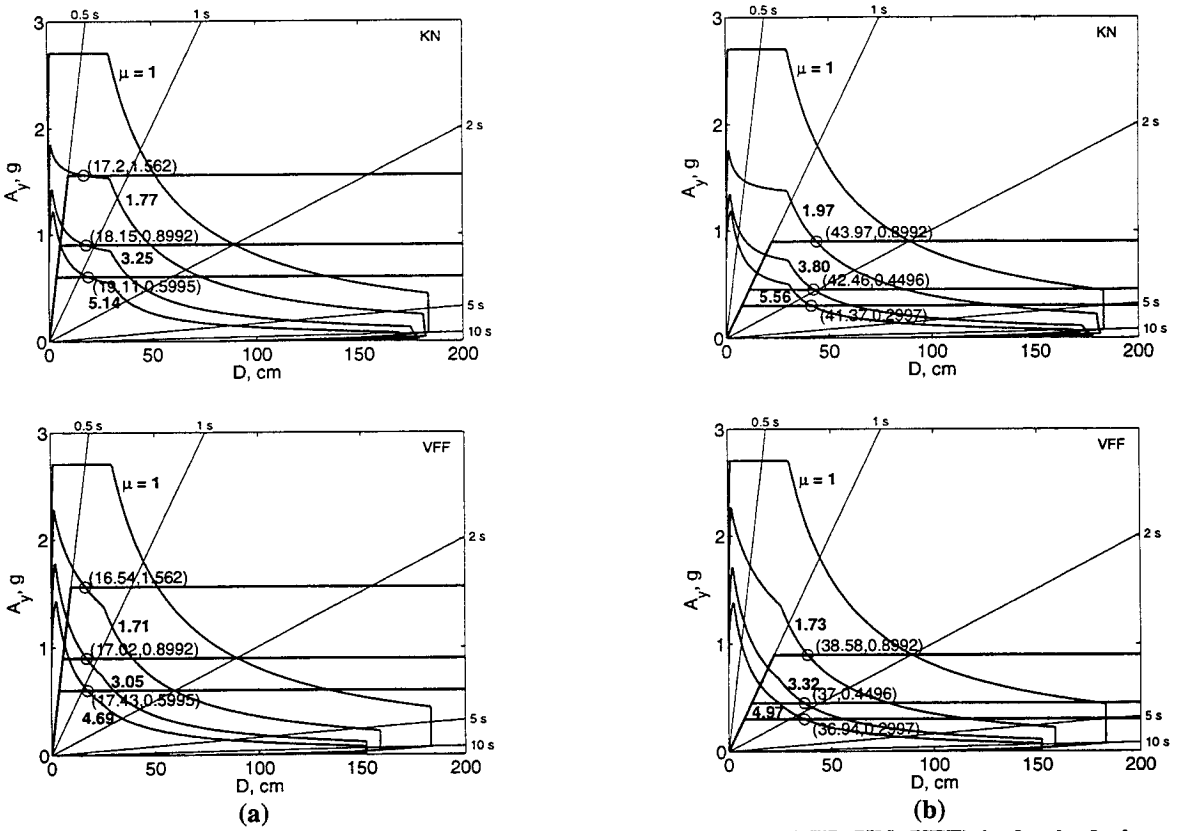

Figure 5. Application of improved procedure using three different (NH, KN, VFF) inelastic design spectra: (a) Systems 1 to 3, and (b) Systems 4 to 6.

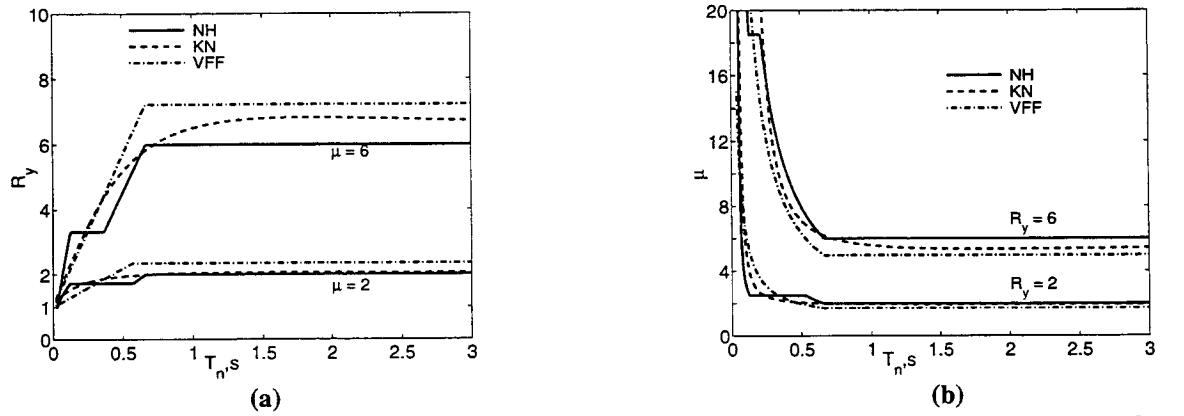

Figure 6. (a) Variation of R_y with T_n for selected ductility values , and (b) variation of μ with T_n for selected R_y values based on three different (NH, KN, VFF) recommendations

Table 1. Results from numerical implementation of improved procedure using three $R_y - \mu - T_n$ equations.

System Properties						Newmark-Hall		Krawinkler-Nassar		Vidic et al.	
System	T_n (s)	A (g)	A_y (g)	u_y (cm)	R_y	μ	D	μ	D	μ	D
1	0.5	2.7062	0.5995	3.7202	4.51	5.99	22.29	5.14	19.11	4.69	17.43
2			0.8992	5.5803	3.01	3.99	22.29	3.25	18.15	3.05	17.02
3			1.5624	9.6962	1.73	2.00	19.39	1.77	17.20	1.71	16.54
4	1	1.7984	0.2997	7.4403	6.00	6.00	44.64	5.56	41.37	4.97	36.94
5			0.4496	11.160	4.00	4.00	44.64	3.80	42.46	3.32	37.00
6			0.8992	22.321	2.00	2.00	44.64	1.97	43.97	1.73	38.58

CONCLUSIONS

This investigation of capacity-demand-diagram methods to estimate the earthquake-induced deformation of inelastic SDF systems has led to the following conclusions:

1. The ATC-40 procedure significantly underestimates the deformation of inelastic systems for a wide range of T_n and μ values compared to the value determined from the inelastic design spectrum using three different $R_y - \mu - T_n$ equations, all of which provided similar results.

2. An improved capacity-demand-diagram method that uses the well-known constant-ductility design spectrum for the demand diagram has been developed and illustrated by examples. When both capacity and demand diagrams are plotted in the *A-D* format, the yielding branch of the capacity diagram intersects the demand curves for several μ values. The deformation is given by the one intersection point where the ductility factor calculated from the capacity diagram matches the value associated with the intersecting demand curve.

3. The improved method can be conveniently implemented numerically if its graphical features are not important to the user. Such a procedure, based on equations relating R_y and μ for different T_n ranges, has been presented and illustrated by examples using three different $R_y - \mu - T_n$ relations.

ACKNOWLEDGMENT

This research investigation is funded by the National Science Foundation under Grant CMS-9812531, a part of the U.S.-Japan Cooperative Research in Urban Earthquake Disaster Mitigation. This financial support is gratefully acknowledged.

REFERENCES

Applied Technology Council. 1996. *Seismic evaluation and retrofit of concrete buildings.* Report ATC 40. November.

Bertero, V. V. 1995. Tri-service manual methods. In *Vision 2000*, Part 2, Appendix J. Sacramento, Calif.: Structural Engineers Association of California.

Chopra, A. K. 1995. *Dynamics of structures: Theory and applications to earthquake engineering*, Chapters 6, 7, and 13. Englewood Cliffs, N.J.: Prentice Hall.

Chopra, A. K., and R. K. Goel. 1999. *Capacity-demand-diagram methods for estimating seismic deformation of inelastic structures: SDF systems.* Berkeley, Calif.: Pacific Earthquake Engineering Research Center, University of California. Report No. PEER-1999/02. April.

Fajfar, P. 1999. Capacity spectrum method based on inelastic spectra. *Earthquake engineering and structural dynamics* (forthcoming).

FEMA. 1997. *NEHRP guidelines for the seismic rehabilitation of buildings,* FEMA 273; and *NEHRP commentary on the guidelines for the seismic rehabilitation of buildings*, FEMA 274. Washington, D.C.: Federal Emergency Management Agency. October.

Freeman, S. A., J. P. Nicoletti, and J. V. Tyrell. 1975. Evaluations of existing buildings for seismic risk — A case study of Puget Sound Naval Shipyard, Bremerton, Washington. *Proceedings of 1st U.S. National Conference on Earthquake Engineering*, 113–22. Berkeley, Calif.: EERI.

Krawinkler, H., and A. A. Nassar. 1992. Seismic design based on ductility and cumulative damage demands and capacities. In *Nonlinear seismic analysis and design of reinforced concrete buildings*, eds. P. Fajfar and H. Krawinkler. New York: Elsevier Applied Science.

Newmark, N. M., and W. J. Hall. 1982. *Earthquake spectra and design*. Berkeley, Calif.: Earthquake Engineering Research Institute.

Reinhorn, A. M. 1997. Inelastic analysis techniques in seismic evaluations, eds. P. Fajfar and H. Krawinkler. *Seismic design methodologies for the next generation of codes,* 277–87. Rotterdam: A.A.Balkema..

Veletsos, A. S., and N. M. Newmark. 1960. Effects of inelastic behavior on the response of simple system to earthquake motions. *Proceedings of the 2nd World Conference on Earthquake Engineering*, Japan, Vol. 2, 895–912.

Vidic, T., P. Fajfar, and M. Fischinger. 1994. Consistent inelastic design spectra: strength and displacement. *Earthquake Engineering and Structural Dynamics* 23(5): 507–21.

SESSION 3: RESPONSE OF FRAMES

Chaired by

♦ Akira Wada and James Wight ♦

PREDICTION OF EARTHQUAKE RESPONSE OF BUILDINGS USING EQUIVALENT SINGLE-DEGREE-OF-FREEDOM SYSTEM

Hiroshi KURAMOTO and Masaomi TESHIGAWARA[1]

ABSTRACT

The building standard law of Japan was largely revised in June 1998. With the revision, the adoption of the capacity spectrum method is being considered as a new seismic design procedure, which will be enforced by June 2000. In the method, a base-shear versus horizontal-displacement relation is referred to as the capacity spectrum that represents the structural performance of a building is used. The capacity spectrum is usually expressed as what represents the responses of the equivalent single-degree-of-freedom (SDOF) system for the building. Accordingly, the conversion of a building into a SDOF system should appropriately be carried out especially in estimating the seismic performance of irregular shaped buildings. This paper describes a method of the conversion. In order to examine the validity and applicable scopes of the method, the earthquake responses of the SDOF system not only for relatively regular shaped buildings but also irregular ones of various types are compared with those of the multidegree-of-freedom (MDOF) system. Three reinforced concrete buildings of 6, 10, and 19 stories and three steel buildings of 5, 10 ,and 20 stories, respectively, are analyzed. For each building, the analyses of four cases which are one regular and three irregular shaped building models, the soft first story, the stiff first story and the soft middle story types, are executed. For these 24 cases, earthquake response analyses of both SDOF and MDOF systems are executed by using an artificial earthquake wave with random phase. This paper shows that the earthquake responses of not only regular shaped buildings but also irregular ones can be predicted by using a SDOF system converted by the proposed method. For relatively highrise buildings, however, the higher mode effect should appropriately be considered to the response of SDOF system.

1. INTRODUCTION

The building standard law of Japan was largely revised in June 1998 after an interval of about 50 years. The adoption of new seismic design procedures is being considered with the revision. The likeliest procedure for adoption is the capacity spectrum method (Freeman 1978), one of the nonlinear static analysis procedures. In this method, a base shear-versus-horizontal displacement

[1] Department of Structural Engineering, Building Research Institute, Ministry of Construction, Tsukuba, Japan
Email: kura@kengen.go.jp/Teshi@kengen.go.jp

relation is used, referred to as the capacity spectrum that represents the structural performance of a building. The capacity spectrum is usually expressed as what represents the responses of the equivalent single-degree-of-freedom (SDOF) system for the building. Accordingly, the conversion of a building into a SDOF system should appropriately be carried out especially in estimating the seismic performance of irregular shaped buildings. This paper describes a method of the conversion. Through a comparison of the responses of the multidegree-of-freedom (MDOF) and SDOF systems for relatively regular shaped buildings but also irregular shaped buildings of various types, the validity and applicable scope of the converting method are also examined.

2. CONVERSION OF STRUCTURAL SYSTEM OF BUILDING INTO *SDOF* SYSTEM

The capacity spectrum method was proposed by Freeman (1978) as an approximate way of determining whether or not a building will survive an earthquake and, if it does, how damaged the building will be. This method also uses a nonlinear static analysis to estimate the seismic performance of a building. As shown in Fig. 1, the performance is estimated as the maximum earthquake response (displacement) of a building by the intersection of the capacity spectrum, which represents the whole structural performance of the building, and a reduced response spectrum (demand spectrum) for an assumed earthquake. The advantage of this method is that it estimates positively the response of a building for an assumed earthquake, in other words,

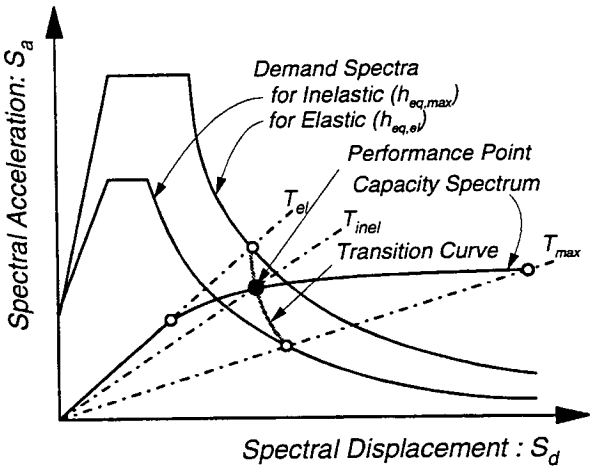

Fig. 1 Capacity and Demand Spectra

provides more information on the degree of inelastic deformation (damage) that is expected. With respect to this point, the method is largely different from the commonly used seismic design procedures using equivalent static analyses. In using this method, however, it is important how to estimate appropriately the following issues.

The first matter is how to convert the whole structural system of a building into the equivalent SDOF system. Since the demand spectrum in the capacity spectrum method is given by the response spectrum of a target earthquake, the capacity spectrum should also be of a SDOF system. Therefore, the method of the conversion and its applicable scopes should be clarified. The second consideration is the estimation of the damping characteristic of a building. The effect of the damping characteristic of a building is generally taken into account for the demand spectrum in the capacity spectrum method by assuming that the response is stationary. The effects of the inelastic behavior of a building and the foundation/soil interaction on the damping characteristic should appropriately be evaluated. The third matter is how to reduce the demand spectrum in proportion to the level of the damping characteristic of a building. Since a response spectrum with 5% damping is given beforehand as the standard spectrum for the demand spectrum, the spectrum should appropriately be reduced considering the characteristic of an assumed earthquake and the damping value at the maximum response of a building.

This paper focuses the first issue and presents a method for converting a building into a SDOF system shown below.

Considering a MDOF system for an N-story building, the maximum displacement response of the i-th story, $\delta_{i,\max}$, can generally be approximated by the following equation:

$$\delta_{i,\max} \approx \sqrt{\sum_{S=1}^{N} \left| {}_s\beta \cdot {}_s u_i \cdot {}_s\overline{M} \cdot {}_s S_a / {}_s\overline{K} \right|^2} \tag{1}$$

Similarly, the base shear at the maximum response, Q_B, can be given by

$$Q_B \approx \sqrt{\sum_{s=1}^{N} \left\{ \sum_{i=1}^{N} m_i \cdot {}_s\beta \cdot {}_s u_i \cdot {}_s S_a \right\}^2} = \sqrt{\sum_{s=1}^{N} \left\{ {}_s\overline{M} \cdot {}_s S_a \right\}^2} \tag{2}$$

in which, m_i = lumped mass in the i-th story

${}_s u_i$ = normal mode of the s-th mode in the i-th story

$_s\beta$ = participation factor of the s-th mode

$_s\overline{K}$ = equivalent stiffness corresponding to the s-th mode ($=_s\beta\{_su\}^T[K]_s\beta\{_su\}$)

$_s\overline{M}$ = equivalent mass corresponding to the s-th mode ($=_s\beta\{_su\}^T[M]_s\beta\{_su\}$)

$_sS_a$ = spectral acceleration for the s-th mode

$_sS_d$ = spectral displacement for the s-th mode

Under an assumption that the maximum response under dynamic vibration can be represented by that in static analysis, then, considering a MDOF system subjected to statically horizontal forces at each mass, of which the distribution is proportional to the first mode of vibration, Eq. (2) can be rewritten as

$$_1Q_B=_1\overline{M}\cdot_1S_a \tag{3}$$

and from Eq. (1), the displacement in each story, $\{_1\delta\}$, is given by

$$\{_1\delta\}=_1\beta\{_1u\}_1\overline{M}\cdot_1S_a/_1\overline{K}=_1\beta\{_1u\}_1Q_B/_1\overline{K} \tag{4}$$

As clarified in Eq. (4), a MDOF system can be converted to a SDOF system with the equivalent lumped mass and stiffness, $_1\overline{M}$ and $_1\overline{K}$, because the external force distribution for a MDOF system corresponds to the first mode. In this case, the horizontal displacement of a SDOF system (the representative displacement), $_1\Delta$, corresponds to the displacement at the height that the participation vector of the first mode, $_1\beta\{_1u\}$, is equal to 1.0 in MDOF system. From Eq.(4), namely, the relation between shear (the representative shear) and the representative displacement in a SDOF system is given as

$$_1\Delta=_1Q_B/_1\overline{K} \tag{5}$$

Accordingly, the representative shear corresponds to the base shear, $_1Q_B$. Then, using Eqs. (3) and (5), the representative displacement can be rewritten as

$$_1\Delta=_1S_a\cdot_1\overline{M}/_1\overline{K}=_1S_d \tag{6}$$

Eq. (6) shows that the relation between the representative shear and the displacement in SDOF system is expressed using the spectral acceleration and displacement, $_1S_a$ and $_1S_d$. Eq. (1) also gives the horizontal displacement of the *i*-th story in a MDOF system, $_1\delta_i$, as

$$ {}_1\delta_i = {}_1\beta \cdot {}_1u_i \cdot {}_1S_d = {}_1\beta \cdot {}_1u_i \cdot {}_1\Delta \tag{7} $$

Using Eqs. (2) and (7), the external force applied at the i-th story, ${}_1P_i$, is given as follows:

$$ {}_1P_i = m_i \cdot {}_1\beta \cdot {}_1u_i \cdot {}_1S_a = m_i \cdot {}_1\delta_i \cdot {}_1S_a / {}_1\Delta \tag{8} $$

and using Eqs. (3) and (8) gives the relation between ${}_1\overline{M}$ and ${}_1\delta_i$ as

$$ {}_1\overline{M} = {}_1Q_B / {}_1S_a = \sum_{i=1}^{N} {}_1P_i \Big/ {}_1S_a = \sum_{i=1}^{N} m_i \cdot {}_1\delta_i \Big/ {}_1\Delta \tag{9} $$

Similarly, using Eq.(7) forms the following relations:

$$ {}_1\overline{M} = {}_1\beta \{{}_1u\}^T [M] {}_1\beta \{{}_1u\} = \{{}_1\delta\}^T [M] \{{}_1\delta\} \Big/ {}_1\Delta^2 = \sum_{i=1}^{N} m_i \cdot {}_1\delta_i^2 \Big/ {}_1\Delta^2 \tag{10} $$

$$ {}_1\overline{K} = {}_1\beta \{{}_1u\}^T [K] {}_1\beta \{{}_1u\} = \{{}_1\delta\}^T [K] \{{}_1\delta\} \Big/ {}_1\Delta^2 = \{{}_1\delta\}^T \{{}_1P\} \Big/ {}_1\Delta^2 = \sum_{i=1}^{N} {}_1P_i \cdot {}_1\delta_i \Big/ {}_1\Delta^2 \tag{11} $$

Therefore, these relations yield the natural circular frequency or the natural period of the first mode, ${}_1\omega$ or ${}_1T$,

$$ {}_1\omega = \sqrt{\frac{{}_1\overline{K}}{{}_1\overline{M}}} = \sqrt{\frac{\sum_{i=1}^{N} {}_1P_i \cdot {}_1\delta_i}{\sum_{i=1}^{N} m_i \cdot {}_1\delta_i^2}} \qquad \left(\therefore {}_1T = 2\pi \sqrt{\frac{\sum_{i=1}^{N} m_i \cdot {}_1\delta_i^2}{\sum_{i=1}^{N} {}_1P_i \cdot {}_1\delta_i}} \right) \tag{12} $$

Also, using Eqs.(9) and (10) gives the equivalent mass of the first mode, ${}_1\overline{M}$, as

$$ {}_1\overline{M} = \frac{\left(\sum_{i=1}^{N} m_i \cdot {}_1\delta_i \right)^2}{\sum_{i=1}^{N} m_i \cdot {}_1\delta_i^2} \tag{13} $$

Namely, the spectral acceleration and displacement corresponding to the first mode, ${}_1S_a$ and ${}_1S_d$, can be given as follows using Eqs. (3) and (13), and Eqs. (6) and (12), respectively.

$$ {}_1S_a = \frac{\sum_{i=1}^{N} m_i \cdot {}_1\delta_i^2}{\left(\sum_{i=1}^{N} m_i \cdot {}_1\delta_i \right)^2} \cdot {}_1Q_B \tag{14} $$

$$ {}_1S_d = \frac{\sum_{i=1}^{N} m_i \cdot {}_1\delta_i^2}{\sum_{i=1}^{N} {}_1P_i \cdot {}_1\delta_i} \cdot {}_1S_a \tag{15} $$

By using Eqs. (14) and (15) and the information on the external forces and displacements of each

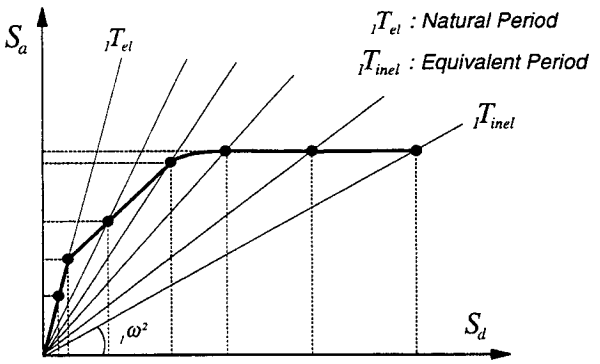

Fig. 2 Capacity Spectrum

story and the base shear in each loading step obtained from nonlinear pushover analysis with the external force distribution proportioned to the first mode, a $S_a - S_d$ curve (Capacity Spectrum) can be drawn as shown in Fig. 2.

3. COMPARISON BETWEEN RESPONSES OF *SDOF* AND *MDOF* SYSTEMS

Earthquake response analyses of both SDOF and MDOF systems for several buildings are executed to examine the validity of the conversion from the MDOF system into the SDOF system shown above and its applicable scope. For buildings for which the distribution of story strength and stiffness along the building height is extremely irregular, the predicting accuracy of the earthquake response of the SDOF system is verified by comparison with that of the MDOF system.

3.1 Modeling of Restoring Force Characteristic for Equivalent *SDOF* System

In order to execute the earthquake response analyses of a SDOF system, it is necessary to model the restoring force characteristic. In this study, converting the capacity spectrum made by the

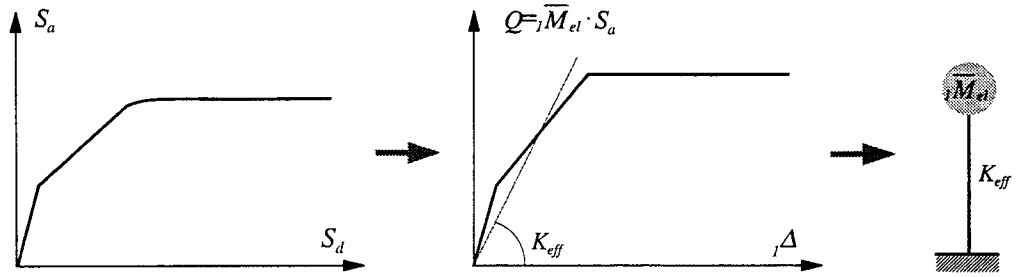

Fig. 3 Skeleton Curve for SDOF System

method, described in section 2 into the trilinear fitting curve, a skeleton curve for the $S_a - S_d$ relation is produced. As shown in Fig. 3, then, multiplying the S_a components of the skeleton curve by the equivalent mass corresponding to the first mode for elastic, ${}_1\overline{M}_{el}$, a skeleton curve for the representative shear versus representative displacement relation is obtained. The representative shear, ${}_1\overline{M}_{el} \times S_a$, does not agree with the base shear of the analyzed building when the equivalent mass, ${}_1\overline{M}$, changes after a portion of the building yields. In the analysis of a SDOF system, however, since the lumped mass is assumed to be a constant value, ${}_1\overline{M}_{el}$, the maximum response (the representative displacement) obtained is not affected. Assuming that the restoring force characteristic of a building represents that of the stories and the characteristic of a story represents that of the members, the hysteresis rules of the degrading trilinear model (Takeda model) for RC buildings and the normal tri-linear model for steel buildings are used in SDOF system.

3.2 Method of Analysis

As shown in Fig. 4, the method of analyses is as follows:

(a) Obtain the shear versus displacement relation of each story from a nonlinear pushover analysis with the external force distribution corresponding to the first mode of vibration.

(b) Make the capacity spectrum ($S_a - S_d$ curve) using Eq. (14) and (15) and the analytical results obtained from step (a), namely information on the external force and displacement of each story and base shear in each loading step.

(c) Make the skeleton curve for the base shear versus representative displacement relation by converting the $S_a - S_d$ curve into a trilinear curve and multiplying S_a by the equivalent mass

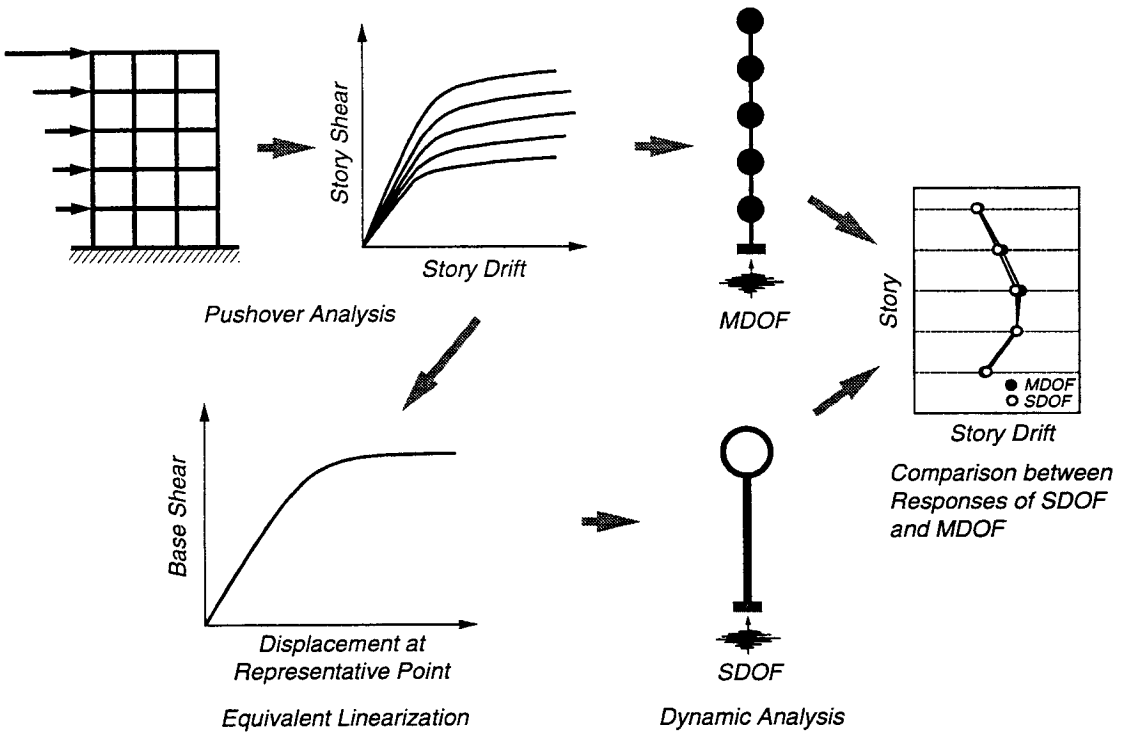

Fig. 4 Flow of Analysis

for the elastic first mode, ${}_1\overline{M}_{el}$. (see Fig. 3)

(d) Execute the earthquake response analyses for a SDOF system by using the equivalent mass for the elastic first mode, ${}_1\overline{M}_{el}$ and a restoring force characteristic with the skeleton curve made in step (c) and the assumed hysteresis rule for the structural type of analyzed buildings mentioned above.

(e) Seek a loading step on the $S_a - S_d$ curve made in step (b), which corresponds to or is nearest the maximum response of the SDOF system obtained in step (d).

(f) Seek the displacement at each story on the shear versus displacement obtained from the push-over analysis in step (a), which corresponds to the loading step obtained in step (e).

(g) Execute earthquake response analyses for a MDOF system.

(h) Compare the results of a SDOF system (step (f)) with those of a MDOF system.

3.3 Analyzed Buildings and Analytical Assumption

Analyses were carried out for three RC buildings of 6, 10, and 19 stories, and three steel

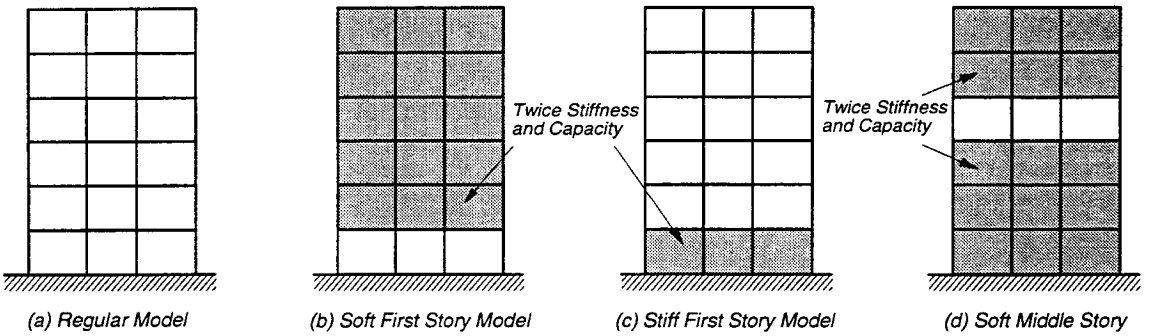

Fig. 5 Analyzed Buildings

Table 1 Characteristic of Analyzed Building

Building Type	RC			Steel		
Number of Story	6	10	19	5	10	20
Total Height (m)	17.8	30.3	61.5	19.0	38.0	80.5
Total Weight (ton)	3,710	6,510	28,638	2,800	5,300	18,325
Natural Period (sec)	0.45	0.64	1.02	0.86	1.36	2.47

buildings of 5, 10, and 20 stories, respectively. For each building, four cases including one regular and three irregular shaped building models are then analyzed as shown in Fig. 5. The irregular shaped buildings are the soft first story, the stiff first story, and the soft middle story, respectively. The regular shaped building is modeled on the design example of a real building and the restoring characteristic of each story is obtained from nonlinear pushover analysis with the frame model. In the irregular shaped buildings, Models (b) to (d) in Fig. 5, the stiffness and capacity of relatively strong stories are twice as large as those of the corresponding stories in the regular shaped building. Table 1 gives a brief outline of the analyzed buildings.

Earthquake response analyses of both a SDOF and a MDOF are executed for the above 24 cases. The earthquake wave used is an artificial one with random phase referred to as the BCJ-L2 [Kitagawa, et al. 1994], of which the maximum acceleration and velocity are 355.7 cm/s^2 and 57.4 cm/s, respectively. In the response analyses, the viscous damping of the buildings is assumed to be the transient stiffness proportioning type of 3% for RC buildings and the initial stiffness proportioning type of 2% for steel buildings.

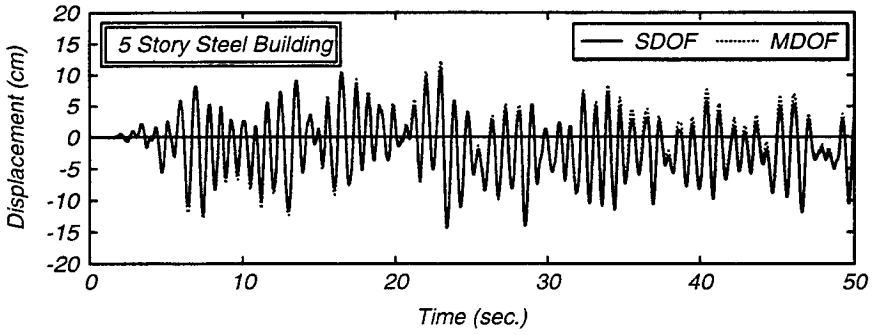

Fig. 6 Comparison between Time History of Displacement Response of SDOF and MDOF Systems for 5 Story Steel Building

3.4 Results of Analysis

For the 5-story steel buildings of the regular type, the time history of the displacement response of a SDOF system is compared with that of a MODF system in Fig. 6, in which the displacement in a MODF system corresponds to that at the equivalent height where ${}_1\beta \cdot {}_1u$ is equal to 1.0. Solid and dotted lines in the figure are for the SDOF system and MDOF system, respectively. The time history of the SDOF system shows extremely good agreement with that of the MDOF system. This result implies that the method of converting to a SDOF system and the assumed restoring force models for both the SDOF and MDOF systems were appropriate.

Figure 7 shows the story shear versus story drift relations obtained from push-over analysis for each regular shaped building. Circle and square marks in the figure are the maximum responses of each story obtained from the earthquake response analysis of SDOF and MDOF systems, respectively.

In low-rise buildings regardless of the structural types, RC or steel, the response of each story obtained from the analysis of a SDOF system shows excellent agreement with that of a MDOF system. In high-rise buildings, an increase in the displacement responses recognized as the higher mode effect is observed in the middle and/or upper stories for a MDOF system. As a result, the displacement response of each story of the SDOF system tends to be smaller than that of a MDOF system in the middle and/or upper stories because the higher mode effect can not be considered in a SDOF system. The ratio of SDOF to MDOF systems on displacement response,

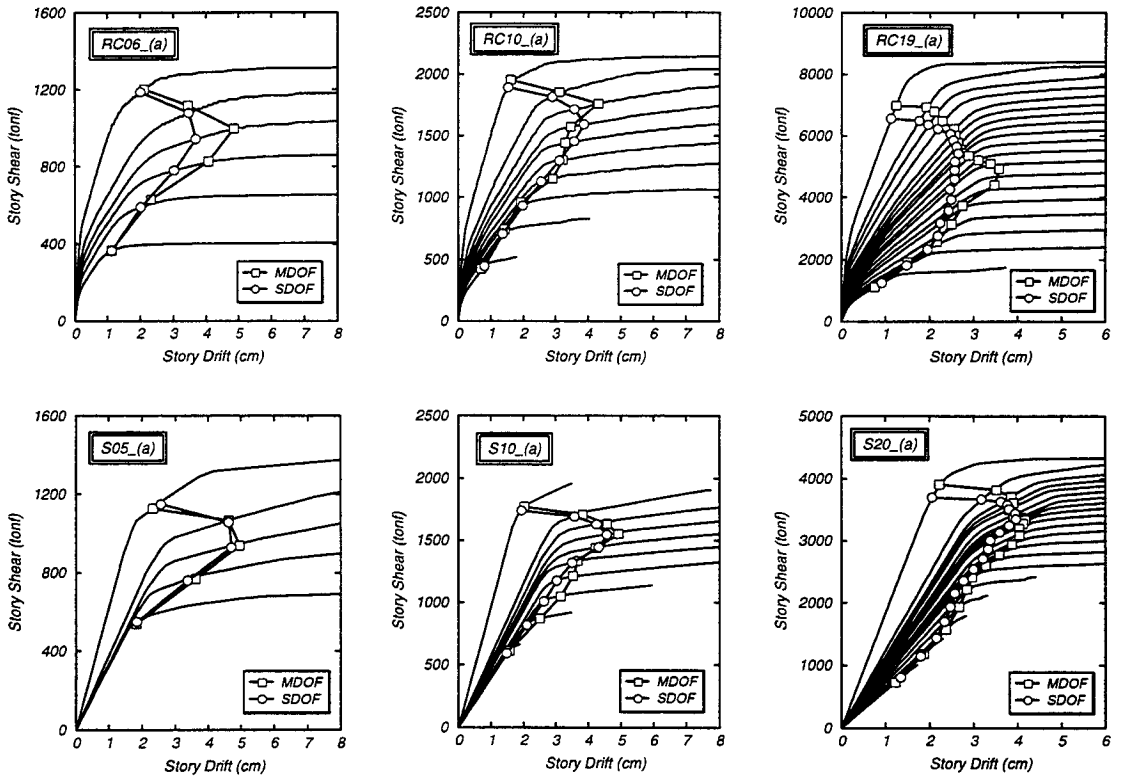

Fig. 7 Comparison between Response of SDOF and MDOF Systems for Regular Shaped Buildings

${}_s\delta/{}_m\delta$, of each story ranges from 0.8 to 1.1 in almost all models, although the ratio in the 19 story RC model ranges from 0.7 to 1.22. The ratio on shear response, ${}_sQ/{}_mQ$, of each story is between 0.9 and 1.1.

A comparison between the displacement responses of the SDOF and MDOF systems for the soft first story, the stiff first story, and the soft middle story models are shown in Figs. 8, 9, and 10, respectively.

For the soft first-story models, as shown in Fig. 8, correspondence of the responses of the SDOF system to those of the MDOF system is almost good regardless of the structural type or number of stories. In almost all models, the ratio, ${}_s\delta/{}_m\delta$, of the first story is between 0.8 and 1.2, and that of the other stories ranges from 0.7 to 1.2. The ratio, ${}_sQ/{}_mQ$, of each story ranges from 0.8 to 1.15.

The correlation between the responses of SDOF and MDOF systems for the stiff first-story models is similar to that for the regular model. In all models except the 19-story RC model, the ratio, ${}_s\delta/{}_m\delta$, of each story ranges from 0.75 to 1.15 and the ratio, ${}_sQ/{}_mQ$, is between 0.95 and 1.1. The ratios, ${}_s\delta/{}_m\delta$ and ${}_sQ/{}_mQ$, in the 19-story RC model range from 0.58 to 1.05 and from 0.58 to 1.05, respectively. Namely, predicting the accuracy of the responses of a SDOF system for the 19-story RC model is worse than that for the other models due to the higher mode effect.

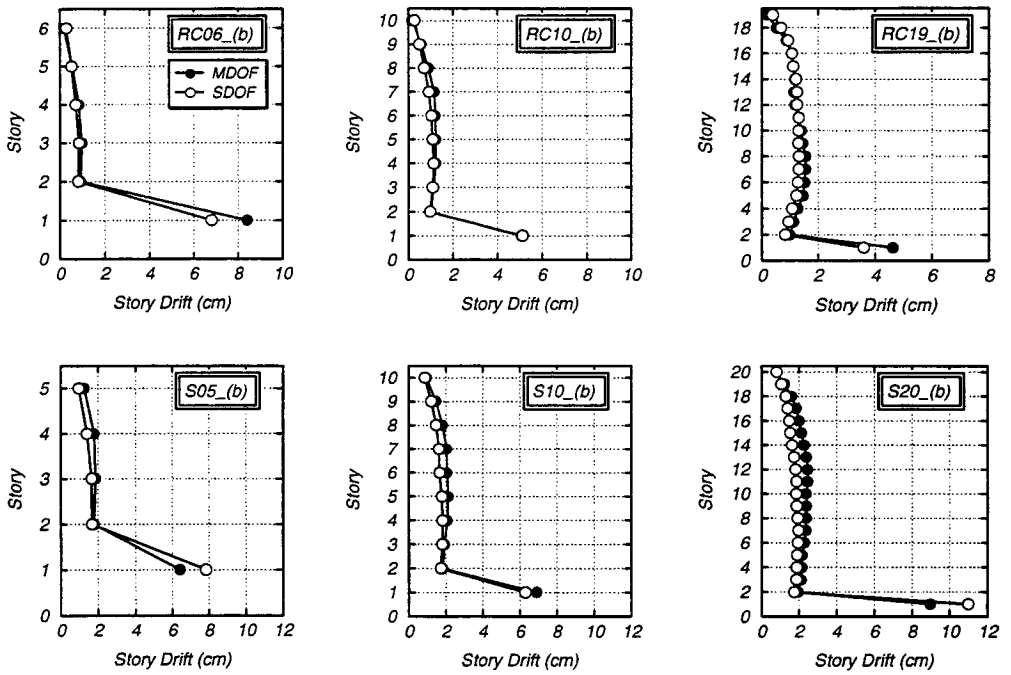

Fig. 8 Comparison between Response of SDOF and MDOF Systems for Soft First-Story Models

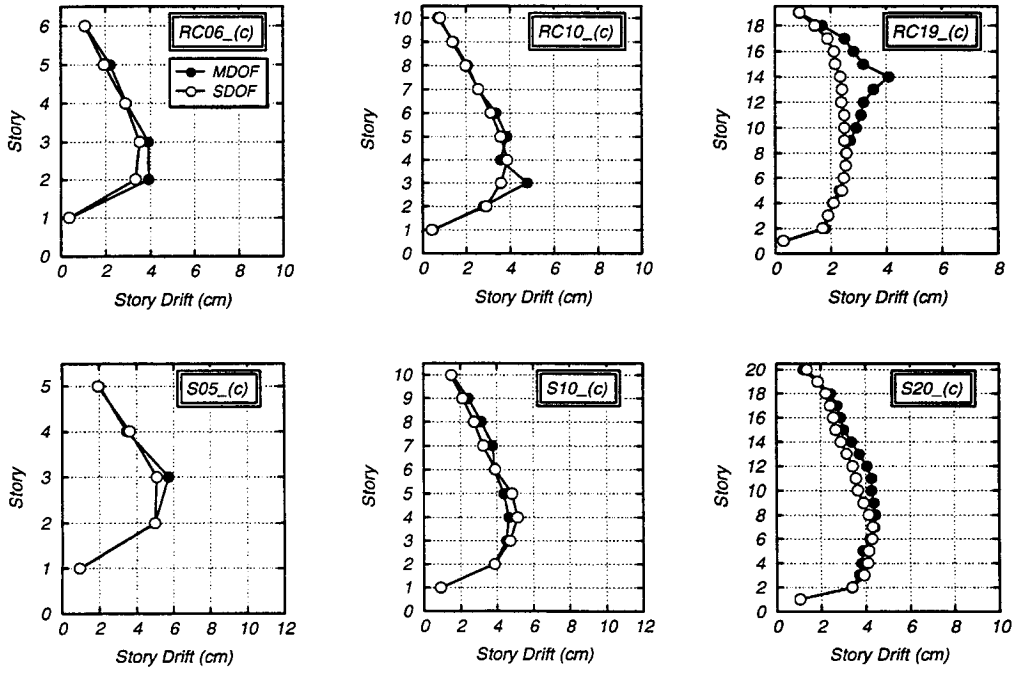

Fig. 9 Comparison between Response of SDOF and MDOF Systems for Stiff First-Story Models

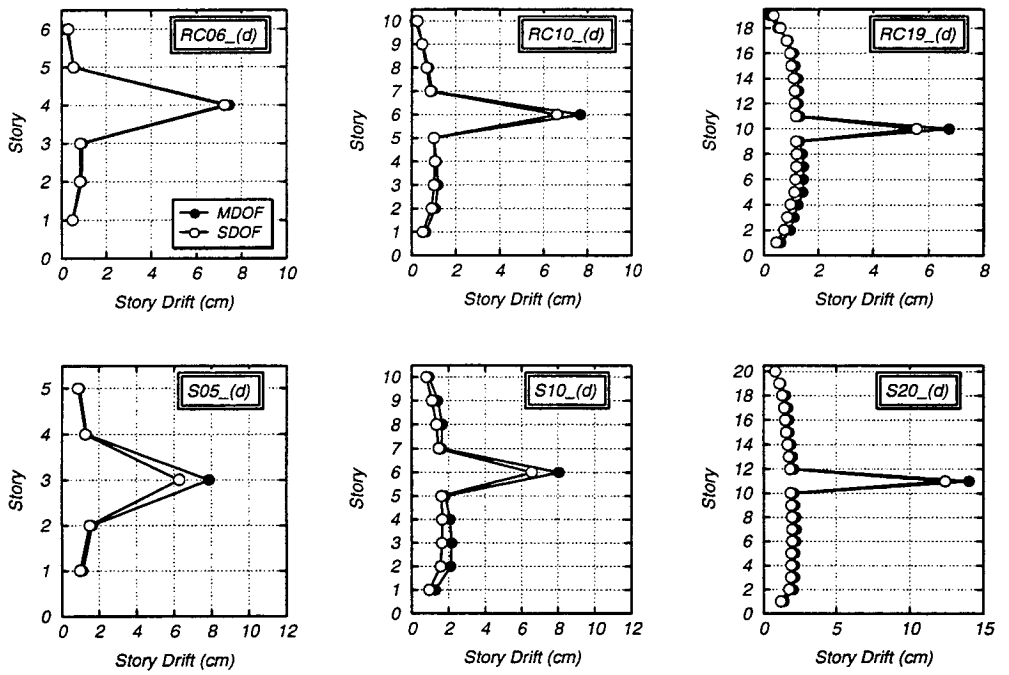

Fig. 10 Comparison between Response of SDOF and MDOF Systems for Soft Middle-Story Models

For the soft middle-story models, the correspondence of the responses of the SDOF system to those of the MDOF system is almost as good, although there is a tendency that the responses of SDOF system are a little smaller than those of MDOF system over all stories. The ratio, ${}_s\delta/{}_m\delta$, of the soft middle story ranges from 0.8 to 1.0 and that of the other stories are between 0.75 and 1.2. The ratio, ${}_sQ/{}_mQ$, of each story ranges from 0.8 to 1.2.

4. CONCLUSIONS

A method of converting the whole structural system of a building into the equivalent SDOF system was proposed in this paper. Using the method and executing earthquake response analyses of 24 cases, predicting the accuracy of the response of each story in a building obtained from the response of the equivalent SDOF system and that of the MDOF system was investigated to grasp the applicable scope of the capacity spectrum method. The conclusions obtained are

(1) In both RC and steel buildings of regular shape, good agreement was observed between the responses of the SDOF and MDOF systems regardless of the building height.

(2) For irregular shaped buildings, the responses of a SDOF system could almost simulate those of a MDOF system.

(3) In highrise buildings exceeding 10 stories, however, the displacement response of a SDOF system tended to be smaller than that of a MDOF system because of the higher mode effect in a MDOF system. Accordingly, for relatively highrise buildings, the higher mode effect should appropriately be considered in applying the capacity spectrum method.

REFERENCES

Freeman S. A. 1978. Prediction of response of concrete buildings to severe earthquake motion. *Douglas McHenry International Symposium on Concrete and Concrete Structures*, SP-55, pp. 589-605. Detroit: American Concrete Institute.

Kitagawa Y., I. Okawa, and T. Kashima. 1994. A technique for evaluation of design earthquake ground motion. *Kenchiku Kenkyu Shiryo*, No.83, Building Research Institute, Ministry of Construction. (In Japanese.)

KEYWORDS

Building Standard Law of Japan: Capacity spectrum method (CSM): Earthquake response analysis: Equivalent SDOF system: Higher mode effects: MDOF system: Prediction of Earthquake Response: Pushover analysis: Seismic design codes

SPECTRA-COMPATIBLE PUSHOVER ANALYSIS OF STRUCTURES

Sashi K. KUNNATH[1] and Balram GUPTA[2]

ABSTRACT

The reliable estimation of force and deformation demands in a structural system is crucial to the overall concept of performance-based seismic design. Nonlinear time-history methods can readily be used to accomplish this objective. However, it is likely that nonlinear static procedures, or pushover analyses, will gain more widespread use by practicing engineers. The potential drawbacks and limitations of currently available nonlinear static methods are highlighted in this paper. A new adaptive "modal" site-specific spectra-based pushover analysis is proposed, which accounts for the effect of higher modes and overcomes many of the shortcomings of traditional pushover procedures. The proposed method is able to reasonably capture important response attributes, such as interstory drift and failure mechanisms, that only a detailed nonlinear dynamic analysis could predict.

INTRODUCTION

The release of the NEHRP *Guidelines for the Seismic Rehabilitation of Buildings* (FEMA-273, 1997) marks a significant departure from traditional seismic design. A framework now exists for performance-based design of structures. Inherent in the FEMA-273 vision are three basic components: (1) definition of a performance objective, categorized in the *Guidelines* by four levels: Operational, Immediate Occupancy, Life Safety, and Collapse Prevention; (2) demand prediction using four alternative analysis procedures; and (3) acceptance criteria using force and/or deformation limits that are related to the performance objectives set forth in step (1). A reasonable estimation of seismic demand is arguably the most critical of these steps in the overall design process. Of the four analysis procedures recommended in FEMA-273 to estimate seismic demand, it would be reasonable to assume that nonlinear static procedures, or pushover analyses, will be favored by practicing engineers over nonlinear time-history methods.

[1] *Department of Civil and Environmental Engineering, University of Central Florida, Orlando, FL 32816-2450*
Email: kunnath@ucf.edu
[2] *SeniorAnalyst/Engineer, Saiful/Bouquet Consulting Structural Engineers, Pasadena, CA 91105*
Email: bgupta@sbise.com

"Pushover" analysis of structures gained prominence after its introduction in the capacity spectrum method by Freeman (1978) and later by Deierlein and Hsieh (1990). However, nonlinear static procedures have several limitations: the most significant being their inability to account for the effect of higher modes. Consequently, several attempts to refine and improve upon the original method have been proposed (Fajfar and Fischinger 1988; Eberhard and Sozen 1993; Bracci et al. 1997).

A new procedure, which derives partly from the earlier work cited above and partly from traditional response-spectrum analysis, is presented here. The explicit consideration of the input motion, in terms of its spectra, makes this approach an attractive proposition in performance-based seismic design of structures.

A NEW SPECTRA-COMPATIBLE PUSHOVER PROCEDURE

In performance-based seismic evaluation, interstory drift is an important measure that can be used for damage control. Hence, an adequate estimate (defined in the context of this paper as a value as close as possible to that predicted by nonlinear time-history analysis) of the story drift and its distribution along the height of the building should be reasonably predicted by a pushover procedure. Similarly, the identification of plastic hinge locations is another critical feature which must be simulated by an equivalent static procedure. The proposed pushover analysis procedure is an attempt to accomplish these objectives.

The primary differences between existing pushover methods and the proposed procedure are (1) the present method includes ground motion characteristics as part of the evaluation process; and (2) the applied load pattern can change from one step to the next depending on the instantaneous dynamic properties of the system. The basic steps involved in a typical analysis using the proposed procedure are as follows.

1. Create a mathematical model of the structure.
2. Specify the nonlinear force-deformation relations for various elements in the structure. In its simplest form, this entails specifying the initial stiffness, the yield moment, and the post-yield stiffness of the element. Alternatively, it is possible to define a more detailed force-

deformation envelope: for example, cracking, yielding, and P-delta softening can be used for degrading concrete structures.

3. Compute the damped (suitable damping constants, depending upon the structural system, should be used) elastic response spectrum for the site-specific ground motion to be used for evaluation. Two possible options can be pursued at this stage: use several ground motions to simulate the site-specific spectra or use a smooth NEHRP-type design spectra that characterizes the potential earthquake load at the site.
4. Perform an eigenvalue analysis of the structural model at the current stiffness state of the structure to compute periods and eigenvectors of the system. Using the story weights and the computed eigenvalues, determine the so-called modal "participation" factors:

$$\Gamma_j = \frac{1}{g}\sum_{i=1}^{i=N} W_i \phi_{ij} \qquad (1)$$

where:

Γ_j = modal participation factor for j^{th} mode

Φ_{ij} = mass normalized mode shape value at i^{th} level and j^{th} mode

W_i = Weight of i^{th} story

g = Acceleration due to gravity

N = Number of Stories

Note that the overall structural stiffness matrix is assumed to be reduced in size to *NXN* by condensing out the vertical and rotational degrees of freedom.

5. Compute the story forces at each story level for each of the n modes to be included in the analysis using the following relationship:

$$F_{ij} = \Gamma_j \Phi_{ij} W_i S_a(j) \qquad (2)$$

where:

F_{ij} = lateral story force at i^{th} level for j^{th} mode ($1<j<n$)

$S_a(j)$ = spectral acceleration corresponding to j^{th} mode

6. Compute modal base shears (V_j) and combine them using SRSS to compute the building base shear (V) as shown below:

$$V_j = \sum_{i=1}^{i=N} F_{ij} \qquad (3)$$

$$V = \sqrt{\sum_{j=1}^{N} V_j^2} \qquad (4)$$

7. The story forces computed in Step 5 are applied in small increments, which can be expressed as a fraction of the base shear given in Equation 4. If an iterative analysis procedure is used, the magnitude of the increments is not important. In a non-iterative step-by-step analysis, which applies equilibrium correction in the subsequent step, it is important to ensure that the force increments are adequately small.
8. Perform a static analysis of the structure using the scaled incremental story forces computed in the previous step corresponding to each mode independently. This means that for modes other than the fundamental mode, the structure will be pushed and pulled simultaneously.
9. Compute element forces, displacements, story drifts, member rotations, etc. by an SRSS combination of the respective modal quantities for this step and add these to the same from the previous step. For systems with closely spaced frequencies, alternative combination rules may be used.
10. At the end of every step, compare the accumulated member forces with their respective force-deformation envelopes. If any member has changed state (due to cracking, yielding or softening), re-compute the member and global stiffness matrices and return to Step 4.
11. Repeat the process until a limiting criteria, typically a specified story drift, is reached.

It is clear from the above description that the applied load pattern varies continuously based on the instantaneous dynamic characteristics of the structure. It may not be necessary to perform an eigenvalue analysis of the system for each change in member state. Alternatively, a threshold reduction in story stiffness may be used to determine when a new set of eigenvalues is needed, thereby minimizing the overall computational effort. The computation of the story forces is, at any step, identical to traditional response spectrum analysis. Since one ground motion (or one spectra) results in one pushover curve, a suite of ground motions will produce a family of curves which can be used to generate mean response parameters. However, as indicated earlier, the use of a smooth spectra can serve to substitute multiple analyses using different ground motions.

VALIDATION OF THE METHOD

The algorithm for the proposed pushover analysis procedure was incorporated into an existing computer program IDASS (Kunnath 1995). A comprehensive evaluation of the methodology was carried out on a variety of structural configurations and is summarized in the dissertation by

Gupta (1998). A sample analysis of a medium-rise building is presented in this paper. The objectives of the evaluation are to demonstrate the effectiveness of the method to reproduce the overall behavior predicted by a nonlinear time-history analysis and to highlight drawbacks of traditional pushover procedures.

A 14-story generic moment frame, whose properties were established from an existing building located in Southern California, was selected for the evaluation process. The floor plan of the building and a typical elevation of one of the moment frames are shown in Figure 1. Only the outer perimeter frames were designed to carry lateral loads. A total uniform load of 102.5 psf was used to calculate the building mass properties and axial load on columns. Element properties used for the analyses are tabulated in Table 1. A bilinear force-deformation envelope with a post-yield stiffness of 5% was assumed for all elements.

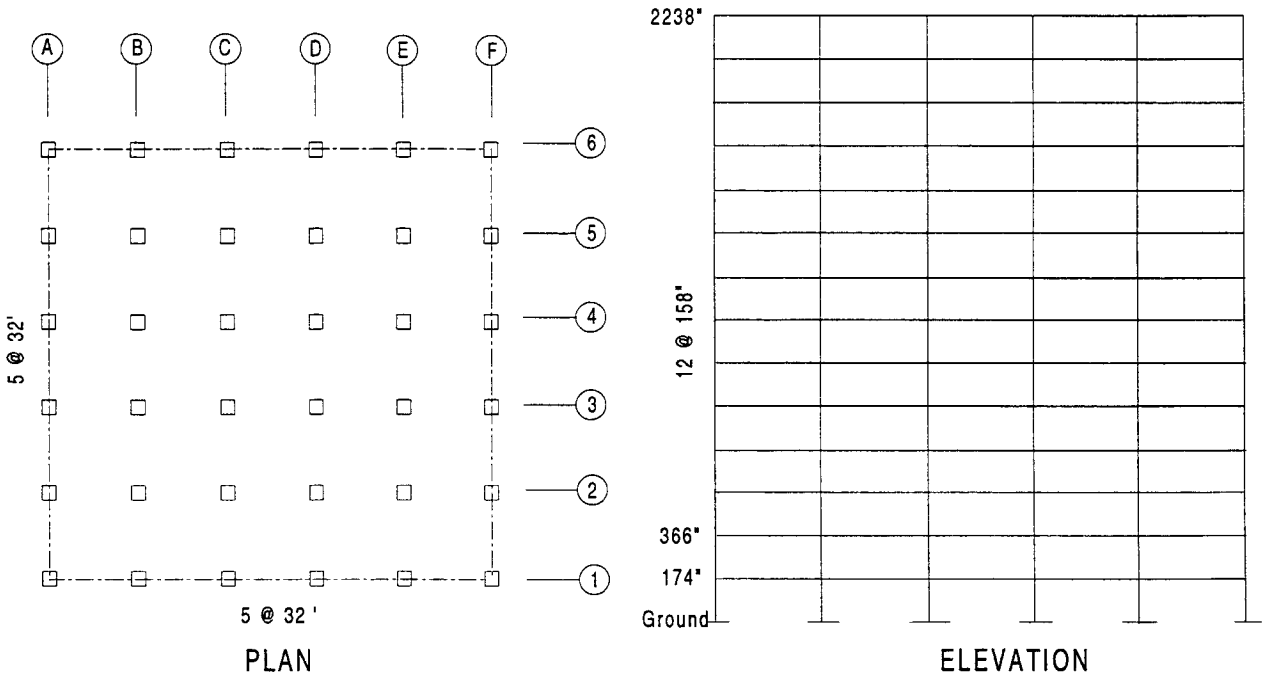

Figure 1: Plan and Elevation of Perimeter Frames

A two-dimensional model of the building was analyzed using the following methods:

(1) Nonlinear time-history analysis using a scaled (magnitude only) version of the recorded building base acceleration during the Northridge earthquake. The scaling was necessary to induce yielding in the structure.

Table 1: Element Properties Used in Evaluation Studies

STORY LEVEL	BEAMS		COLUMNS			
			EXTERIOR		INTERIOR	
	Initial Stiffness (EI, k-in^2)	Yield Moment (k-in)	Initial Stiffness (EI, k-in^2)	Yield Moment (k-in)	Initial Stiffness (EI, k-in^2)	Yield Moment (k-in)
13-14	8.27E7	9,760	4.92E7	15,350	6.21E7	17,160
11-12	17.11E7	16,600	6.51E7	21,710	9.86E7	25,680
9-10	19.46E7	18,680	7.37E7	22,825	11.14E7	27,950
7-8	21.61E7	20,560	9.21E7	24,715	12.56E7	30,520
5-6	23.66E7	22,360	10.20E7	26,950	17.40E7	40,525
3-4	23.66E7	22,360	12.26E7	29,915	19.14E7	43,815
2	43.50E7	37,720	17.18E7	39,360	23.81E7	52,430
1	35.09E8	30,680	17.18E9	393,600	23.81E9	524,300

(2) Nonlinear static procedure (NSP) using an inverted triangular distribution.

(3) NSP using a uniform load pattern.

(4) NSP using the proposed adaptive modal procedure and the actual spectra (Figure 2) of the ground motion used for the time-history analysis.

(5) NSP using the proposed adaptive modal procedure and a smooth spectra (Figure 2) which was derived from the spectra of the actual ground motion.

The nonlinear time-history analysis is assumed to be the reference or "true" response. For each nonlinear static procedure, the lateral forces were applied incrementally until the peak interstory drift (at any level) exceeded the maximum interstory drift predicted by the time-history analysis.

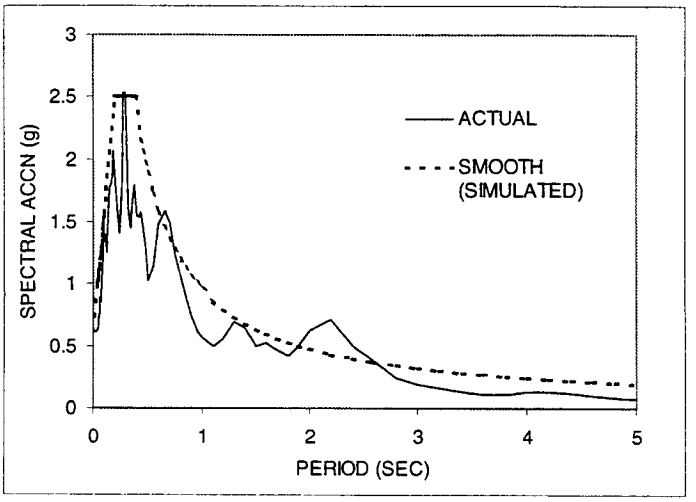

Figure 2: Actual and Simulated Smooth Spectra Used in Proposed Pushover Analysis

The first set of comparisons involves the prediction of local collapse mechanisms. Figure 2 displays the distribution of yielding in beams and columns at the end of the analysis for triangular and uniform load patterns. Figure 3 shows the final state of the structure using the proposed procedure for both the smooth and actual spectrum. In each case, the results of the nonlinear dynamic analysis are also shown. It is seen that the proposed method is significantly superior to existing methods in identifying potential yielding and the formation of local collapse mechanisms. The smooth spectra does perform well, when compared to current procedures, though it is unable to identify the column hinging in the 12^{th} story. The most important aspect of the prediction, for this structure, is the possibility of yielding in the upper stories.

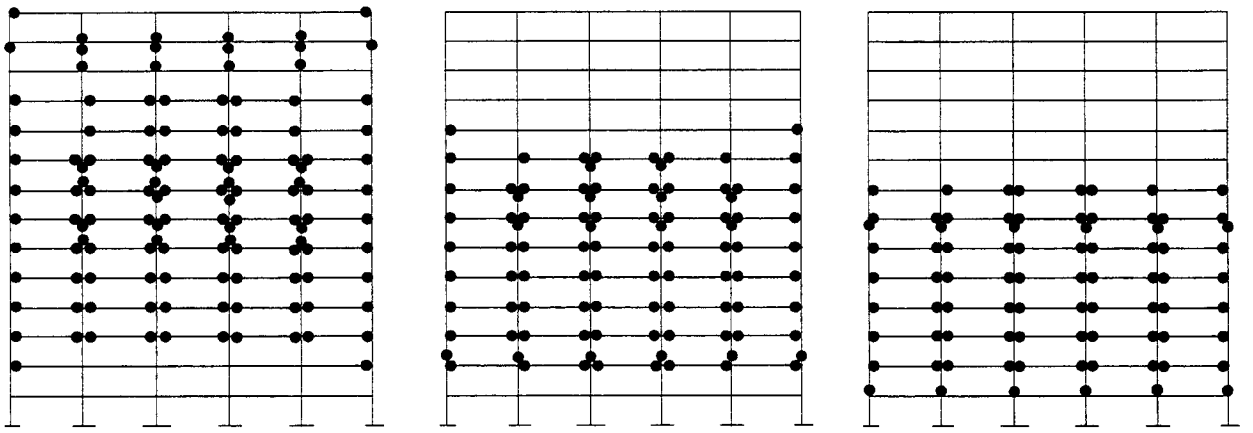

(a) Nonlinear Time-History Analysis

(b) NSP - Inverted Triangular Distribution

(c) NSP - Uniform Distribution

Figure 2: Distribution of Component Yielding Using Existing Pushover Procedures

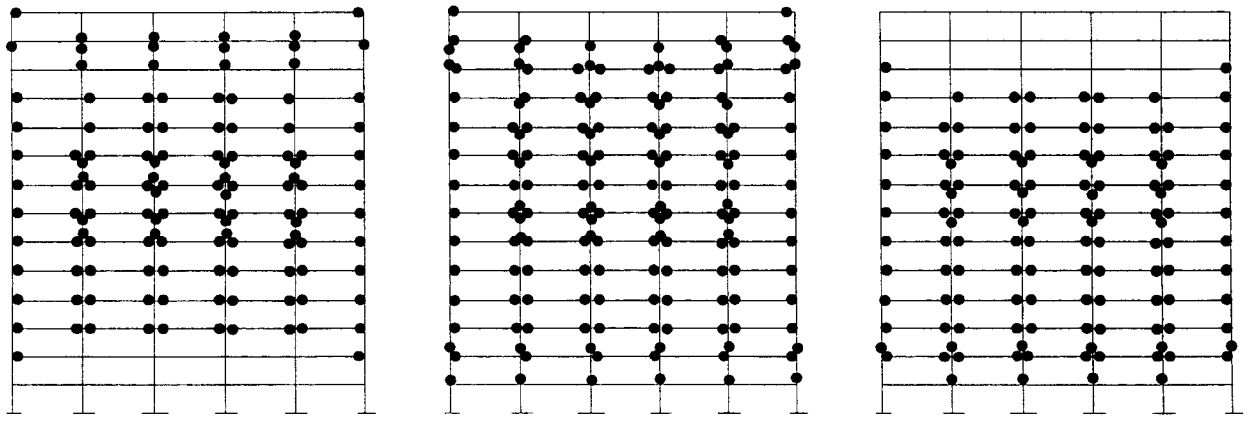

(a) Nonlinear Time-History Analysis

(b) Proposed Method - Actual Spectra

(c) Proposed Method - Smooth Spectra

Figure 3: Distribution of Component Yielding Using Proposed Pushover Procedure

Next, the ability of the various procedures to predict the interstory drift distribution is examined. Figures 4 and 5 depict the computed drift values. Again, the ability of the proposed procedure (for both the actual and smooth spectra) to capture the drift distribution is clearly evident.

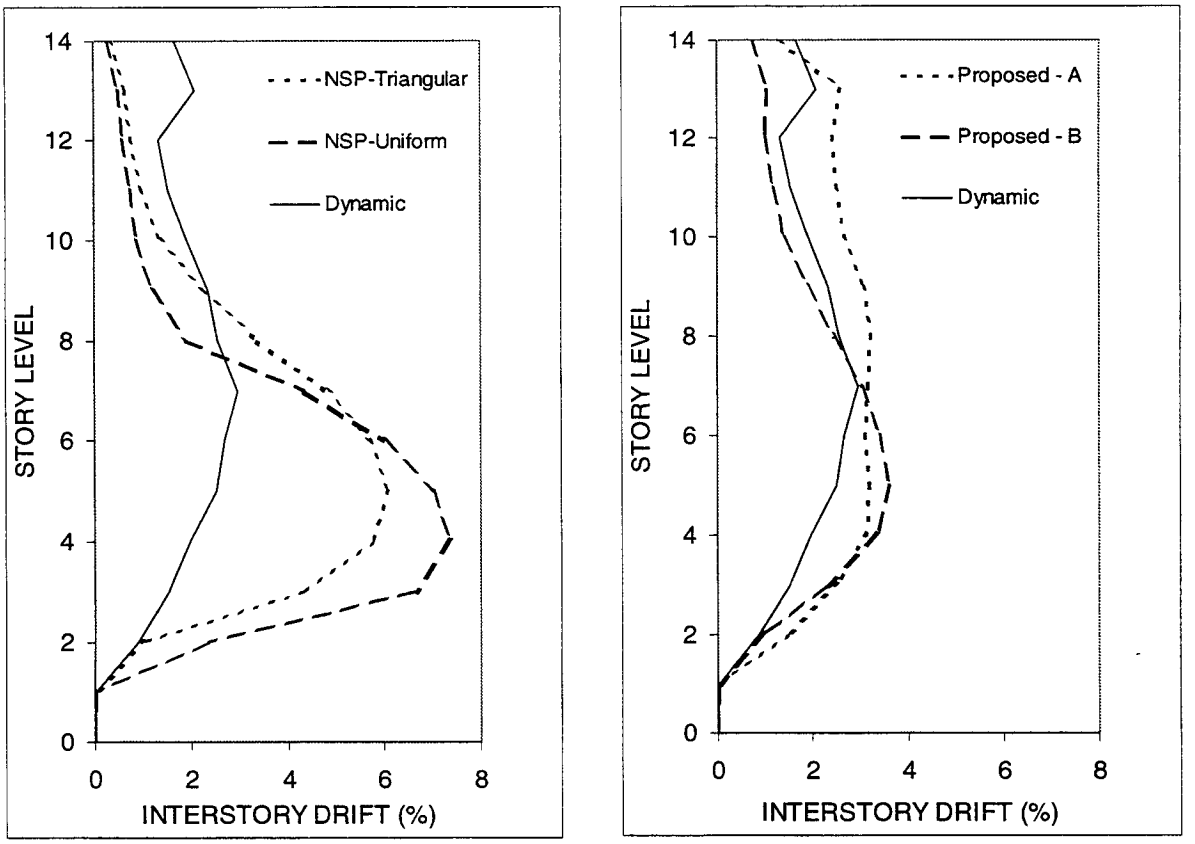

Figure 4: Estimation of Interstory Drift Using Various Procedures

CONCLUDING REMARKS

It has been demonstrated that the proposed method, which incorporates the seismic loading as part of the evaluation process, is capable of identifying both the interstory drift distribution and the formation of plastic hinges (yield distribution) with reasonable accuracy when compared to a nonlinear time-history analysis. Two different ground motion spectra were used in the analysis: (1) a spectra that represents the actual base acceleration used in the nonlinear dynamic analysis; and (2) a smooth spectra that was simulated using NEHRP (FEMA-302) provisions for an MCE event and then modified to envelop selected points on the true spectra. It was found that the

analysis is sensitive to the ground motion characteristics as evidenced by the inability of the smooth spectra to identify hinging in the 12th story of the building.

Finally, to demonstrate the sensitivity of the proposed procedure to the input loading (spectra), the computed lateral force distributions at two stages of the analysis are presented (Figures 5 and 6). The contributions of the different modes are clearly evident as the building characteristics change. Since the smooth spectra minimizes the differences in the spectral ordinates at certain critical period ranges (see period values shown in Figures 5–6 and compare these with the spectral demands shown in Figure 2), it is also apparent as to why the smooth spectra is sometimes unable to establish the correct force distribution corresponding to each mode.

Ultimately, it must be emphasized that nonlinear static procedures cannot replace nonlinear dynamic analyses. Additional effort directed towards enhancing the proposed procedure and carrying out comprehensive validation exercises are under way.

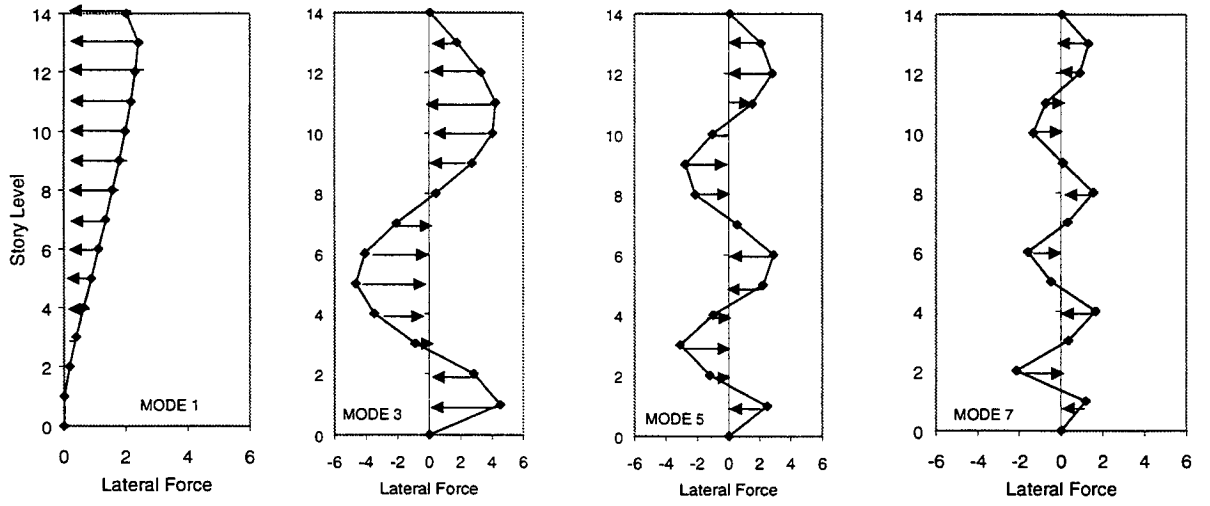

Figure 5: Applied Lateral Forces at Initial Stage of Analysis
(T_1 = 3.13 sec; T_3 = 0.67 sec; T_5 = 0.37 sec; T_7 = 0.25 sec)

REFERENCES

Bracci, J B., S. K. Kunnath, and A. M. Reinhorn. 1997. Seismic performance and retrofit evaluation of reinforced concrete structures. *ASCE Journal of Struct. Engrg.* 123: 3–10.

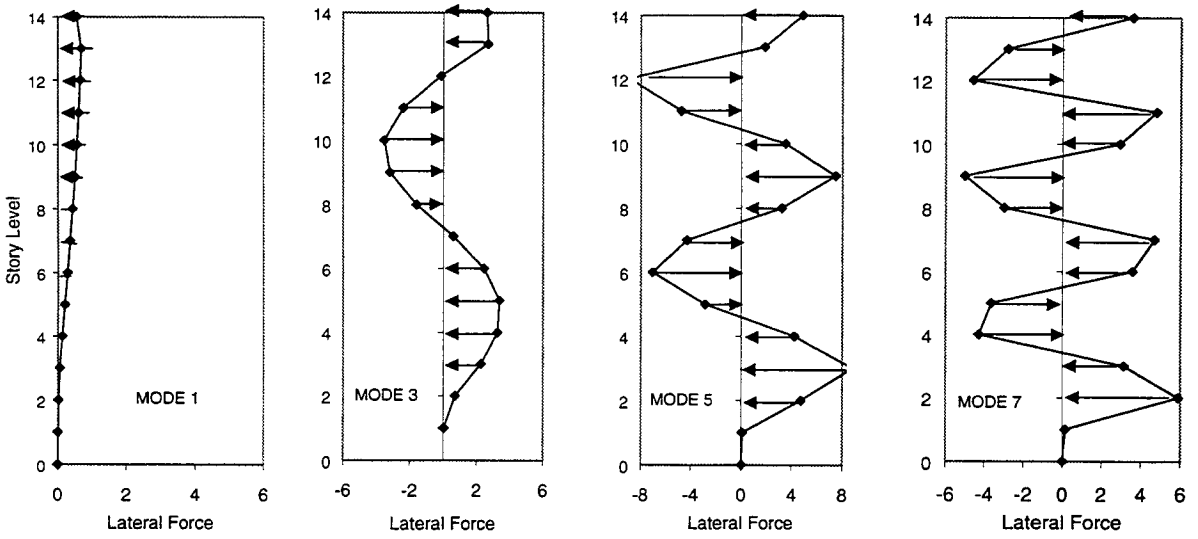

Figure 6: Applied Lateral Forces toward Final Stage of Analysis
(T_1 = 12.7 sec; T_3 = 1.68 sec; T_5 = 0.66 sec; T_7 = 0.34 sec)

Deierlein, G., and S. H. Hsieh. 1990. Seismic response of steel frames with semi-rigid connections using the capacity spectrum method. *Proc. 4th US National Conf. on Earthquake Engrg.* 2: 863–72.

Eberhard, M. O., and M. A. Sozen. 1993. Behavior-based method to determine design shear in earthquake resistant walls. *ASCE Journal of Structural Engineering* 119: 619–40.

FEMA-273. 1997. *NEHRP guidelines for the seismic rehabilitation of buildings.* Washington, D.C.: Building Seismic Safety Council.

Freeman, S. A. 1978. Prediction of response of concrete buildings to severe earthquake motion. *Douglas McHenry Int. Symp. on Concrete and Concrete Structures,* 589–605. Detroit: American Concrete Institute. ACI SP-55.

Gupta, B. 1998. Enhanced pushover procedure and inelastic demand estimation for performance-based seismic evaluation of buildings. Ph.D. Dissertation. Orlando, Fla.: University of Central Florida.

Kunnath, S. K. 1995. Enhancements to Program IDARC: *Modeling inelastic behavior of welded connections in steel moment-resisting frames.* Gaithersburg, Md.: National Institute of Standards and Technology. Report No. NIST GCR 95-673.

KEYWORDS

inelastic behavior; modal analysis; nonlinear methods; performance-based seismic design; pushover analysis; response spectra; seismic demand; transient analysis

Earthquake Member Deformation Demands in Reinforced Concrete Frame Structures

T. MATSUMORI[1], S. OTANI, H. SHIOHARA, and T. Kabeyasawa

ABSTRACT

To estimate member deformation demands in the seismic design of reinforced concrete (R/C) frame structures, the distribution of story displacements and member ductility demands along the structural height is studied by comparing the results of nonlinear earthquake response analyses and static push-over analyses. The nonlinear earthquake response analyses showed that the distribution of response displacements varies with parameters of input ground motions and structures. This paper shows that the results of two push-over analyses could reasonably estimate the distribution of girder-end ductility demands during an earthquake if the story shear distribution in the push-over analyses were taken to be the sum and the difference of the first two modes. The maximum member ductility demands obtained by the two push-over analyses give the upper bound to the earthquake ductility demands.

1. INTRODUCTION

In the final stage of a structural design, the response of a structure as designed under a given set of loads and forces must be compared with the performance objectives. A simple but effective method is highly desired to estimate realistic structural and member response, especially under earthquake environments.

A nonlinear time-history analysis of a structure under a given earthquake ground motion can provide necessary information about the maximum response of a structure and maximum stresses and strains of individual members. A major drawback of the time-history analysis is the use of a specific ground motion, which may not occur at the construction site in the future. The state of the arts is not sufficient to define a specific maximum possible ground motion at a given construction site. Therefore, it is inevitable to study the response of a structure under a set of ground motions having different characteristics to compensate uncertainties in the characteristics of ground motions as well as of the structure. A simple static analysis procedure is desired to estimate maximum structural as well as member response amplitudes under an earthquake excitation.

1 Department of Architecture, University of Tokyo, Tokyo, JAPAN
Email:Taizo.Matsumori@rcs.arch.t.u-tokyo.ac.jp

An earthquake response spectrum is often used to represent an upper bound response of a series of linearly elastic systems including the uncertainties in the characteristics of earthquake ground motions. A capacity spectrum, i.e., a plot of spectral acceleration and displacement for a series of linearly elastic single-degree-of-freedom (SDOF) systems, is proposed to represent the characteristics of a design earthquake motion (Shibata, 1976, and Dierlein, 1991).

In general, the deformation response of structural members under a given earthquake ground motion is calculated by a nonlinear response analysis of multi-degree-of-freedom (MDOF) models such as shown in Fig. 1(a). Recently, a push-over analysis, i.e., a static incremental load analysis of a structure under monotonically increasing lateral load to failure, is used to formulate the load-displacement relation of an equivalent nonlinear SDOF system as shown in Fig. 1(b). The capacity spectrum method compares the force-deformation relation of an equivalent SDOF system with the capacity spectra having different damping ratios, which correspond to the damping of a series of substitute linearly elastic systems (Shibata, 1976). The stiffness of a substitute structure is defined by secant (member) stiffness at a given displacement stage and the damping factor must be estimated for the displacement stage. The method, as shown in Fig. 1(c), to relate the response of an equivalent SDOF system to that of the original MDOF system has not been established especially when higher modes contribute to the MDOF response.

The objective of this study is to develop a general method to estimate the distribution of earthquake response deformation in a structure on the basis of nonlinear static analyses. This study emphasizes the development of a method to relate the global (structural) seismic demand to the local (member) seismic demand for framed structures designed under the capacity design concept (weak-beam strong-column type).

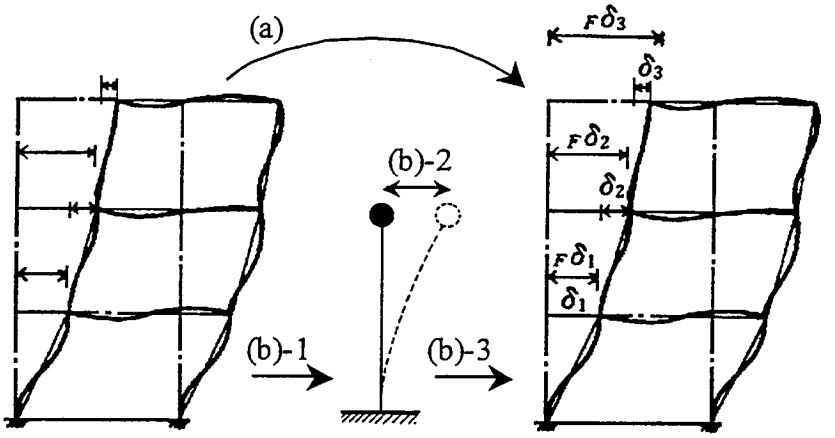

Figure 1. Calculation of response of MDOF system

2. METHOD OF STUDY

2.1 Characteristics of structural models

Five structures (two 12-story structures and three 18-story structures) were selected for study because the second mode was judged to influence the overall response in relatively tall buildings. The elastic period was varied in the model structures by changing member dimensions as shown in Table 1.

Table 1: Elastic natural periods and structural dimensions

Model	Number of stories	${}_1T$	${}_2T$	Dimensions of 1st-story column
12a	12	0.77 sec	0.28 sec	82 x 82 cm
12b		0.60 sec	0.21 sec	100 x 100 cm
18a	18	0.80 sec	0.30 sec	100 x 100 cm
18b		0.61 sec	0.22 sec	122 x 122 cm
18c		1.03 sec	0.39 sec	90 x 90 cm

The story height was uniform and 2.8 m in each story assuming the building use to be an apartment building. The dimensions of member section were reduced gradually in the upper stories; e.g., the dimensions of columns were reduced by 50 mm in every three stories. The beam depth was selected 0.95 times the column depth. The beam width was 0.75 times the beam depth. Uniform unit floor mass of 1.06 ton/m^2 was used for all structures. A moment-resisting frame structure was assumed to consist of infinitely number of uniform 5.0 m bays. Concrete strength was assumed to be 24.0 N/mm^2 for Models 12a to 18b, and 30.0 N/mm^2 in Model 18c.

Each structure was designed to form a yield mechanism of weak-beam strong-column type; i.e., flexural yield hinges were planned to form at the base of first-story columns and at the ends of all floor beams. The structure was first analyzed by a linearly elastic analysis method by using member stiffness reduced to 0.3 times the initial elastic stiffness for girders and 0.7 times for first-story columns. The yield moment at the planned yield hinges was determined as the flexural moment calculated by the linear analysis, and the yield moment at locations other than planned yield hinges was assumed to be 1.7 times the elastic moments. Shear failure was prevented in any members.

Design story shear was made same for the five structural models. The factor A_i to represent the vertical distribution of story shear coefficient C_i was determined in accordance with the Building Standard Law Enforcement Order (BCJ, 1981).

$$C_i = A_i C_B \tag{1}$$

where, C_B: base shear coefficient. The base shear coefficient was 0.30 corresponding to most ductile reinforced concrete moment resisting frame structures. Factor A_i is defined below:

$$A_i = 1 + \left(\frac{1}{\sqrt{\alpha_i}} - \alpha_i\right)\frac{2T}{1+3T} \tag{2}$$

where, T : natural period of the building; $\alpha_i = \Sigma W_i / \Sigma W_1$; and ΣW_i : total of dead and live loads above story i.

Each structure is modeled as a plane frame fixed at the base. The structural model (Fig. 2) consists of one continuous column and adjacent girders removed from a plane frame having an

infinite number of bays; the beams were cut out at their center; beam ends were supported by horizontal rollers. All inelastic rotational deformation was assumed to concentrate at the member ends. Beam-column connections were assumed to be rigid. The moment-rotation relationship of a member was idealized by a tri-linear relation with stiffness changes at flexural cracking and yielding points as shown in Fig. 3; the secant stiffness at the yield point and the post-yield stiffness were 0.3 and 0.01 times the initial elastic stiffness, respectively. The Takeda hysteresis model (Takeda, 1971) was used to represent the moment-rotation relationship at each member end under load reversals. Damping coefficient was assumed to vary proportional to instantaneous stiffness. The first-mode damping factor was assumed to be 3.0 % at the initial elastic stage.

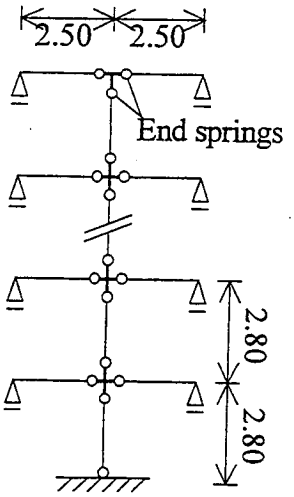

Figure 2. Analytical model of frames

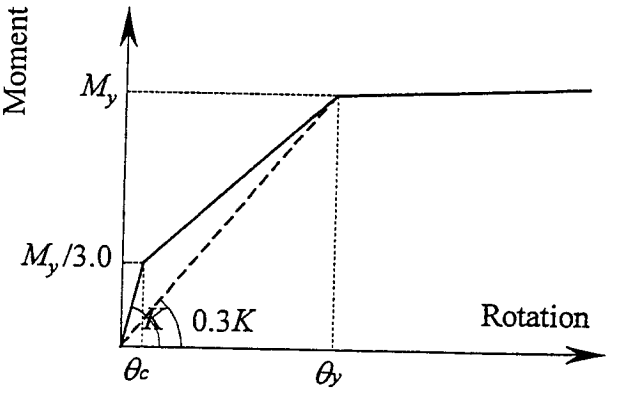

Figure 3. Moment-rotation relation at member end

2.2 Ground motions

Five earthquake ground motion records were used in nonlinear response analyses; i.e., NS component of the 1940 El Centro record (El Centro motion), EW component of the 1968 Hachinohe record (Hachinohe motion), NS component of the 1995 Kobe Marine Observatory record of Japan Meteorological Agency (Kobe Marine Observatory motion), NS component of the 1978 Tohoku University record (Tohoku University motion), and EW record of the 1952 Taft record (Taft motion). The amplitude of each motion was scaled to the maximum ground velocity of 500 mm/sec or 750 mm/sec as shown in Table 2.

Table 2: Characteristics of ground motions normalized to 500 mm/sec velocity

ID	Earthquake records	Magnification	Peak acceleration	Peak velocity
E500	El Centro NS (1940)	1.48	5.06 m/sec^2	500 mm/sec
H500	Hachinohe EW (1968)	1.40	2.56 m/sec^2	
K500	Kobe Marine Observatory NS (1995)	0.55	4.55 m/sec^2	
Ta500	Taft EW (1952)	2.83	4.98 m/sec^2	
To500	Tohoku University NS (1978)	1.38	3.41 m/sec^2	

e750~to750 are 1.5 times e500~to500.

The elastic pseudo-acceleration response spectra of these records after the normalization to the maximum ground velocity of 500 mm/sec are compared in Fig. 4. The pseudo-acceleration is

defined by multiplying spectral displacement by the square of circular frequency. The acceleration response spectrum recommended by the AIJ Load Guidelines (Architectural Institute of Japan, 1993) is also shown in the figure for comparison. The El Centro motion (E500) shows large response acceleration amplitudes between 0.20 and 0.30 seconds in structural periods, the Taft motion (Ta500) dominates between 0.20 to 0.45 seconds, and the Kobe Marine Observatory motion (K500) around 0.40 seconds. The response acceleration of the Hachinohe motion (H500) and the Tohoku University motion (To500) is relatively small in a short period range.

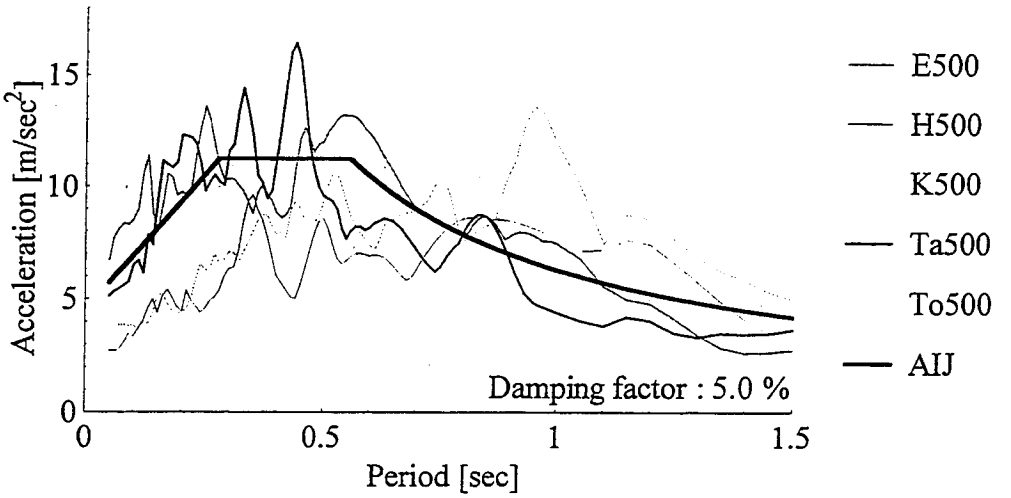

Figure 4. Acceleration response spectra of input ground motions

3. RESULTS OF NONLINEAR EARTHQUAKE RESPONSE ANALYSES

The time history earthquake response analyses were conducted to study the effect of analytical parameters on the distribution of member ductility demands. The sign of member end rotation was defined consistent with the sign of horizontal floor displacement; i.e., a positive member end rotation occurs under the positive floor displacement. The sign is important to relate the floor displacements or story drifts with member end rotations especially when the effect of higher mode response on the response amplitudes is studied.

The distribution of maximum beam-end ductility factors can be roughly classified into four patterns; (a) larger ductility demand at lower levels, (b) larger ductility demand at middle height, (c) larger ductility demand at upper levels, and (d) relatively uniform ductility demand. It is generally difficult to develop uniform girder-end ductility demand along the structural height for ground motions having different characteristics although the design procedure adopted here assumed the development of uniform ductility demand at all planned yield hinge regions under a design lateral force distribution.

3.1 Effect of intensity of ground motions

Girder-end ductility demands of twelve-story Model 12a were studied using two intensity levels of five earthquake ground motions (records E, H, K, Ta and To in Table 2); i.e., maximum

ground velocities of 500 mm/sec and 750 mm/sec. Maximum girder-end ductility demands at each floor levels are shown in Fig. 5 for positive and negative rotations. Although the same structural model was used in the analysis, the distribution pattern of ductility demands is different (a) in positive and negative directions even under the same ground motion, (b) for different ground motions of the same intensity, and (c) for the same ground motion of different intensities.

The distribution pattern of girder-end ductility demands changes drastically with the intensity of ground motions as follows;
(1) For El Centro motion, Kobe Marine Observatory motion and Taft motion, girder-end ductility demands are large at upper levels with increasing ground motion intensity. This increase in response at upper levels is attributable to the contribution of higher mode with the elongation of the natural period with structural damage associated with the fundamental mode deformation;
(2) For Tohoku University motion, ductility demands in the negative direction are significantly large in the lower levels with the ground motion intensity. In this case, the effect of elongated natural period with the increase in deformation on ductility demand was small.

The girder-end ductility demand generally increases with the intensity of ground motions, but the distribution pattern of the ductility demand along the height may significantly change for some ground motions with active contribution of higher mode response. Therefore, it is not proper to consider the sole contribution of fundamental mode response in estimating member-end ductility demand.

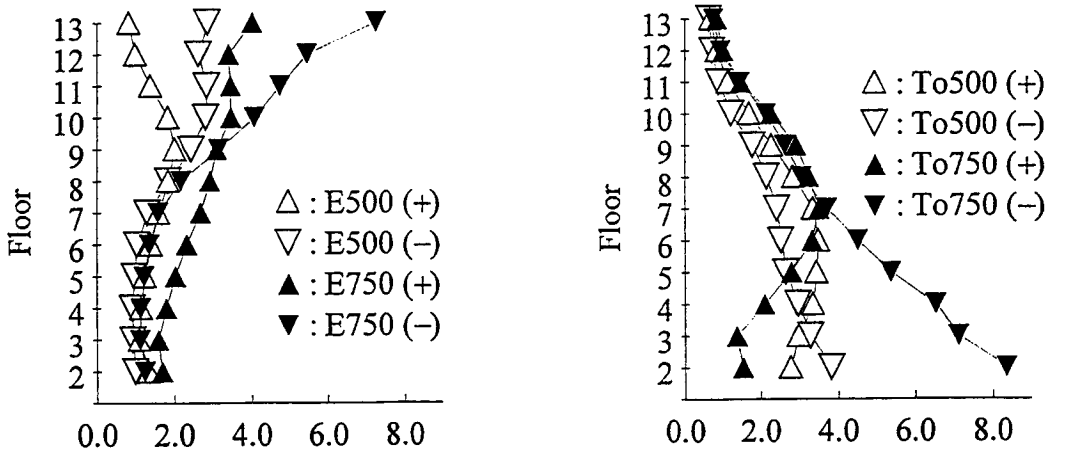

(a) Model 12a under E500, E750 (b) Model 12a under To500, To750

Figure 5: Girder-end ductility demand and ground motion intensities

3.2 Effect of natural periods and ground motion intensities

The combined effect of fundamental periods and ground motion intensities is studied on the vertical distribution of girder-end ductility demands. If the natural period of a system is varied, the response amplitude may be significantly affected by the spectral characteristics of ground motion. Therefore, the distribution of girder-end ductility demand is studied between a pair of structures subjected to different levels of ground motion. The pair of structures and ground

motion intensity levels was selected so that the first mode response displacements were comparable in the two cases. In other words, the response of Model 18a under ground motion of maximum velocity at 750 mm/sec is compared with the response of Model 18b under ground motion of maximum velocity at 500 mm/sec. The response of Model 18a under 500 mm/sec ground motion is compared with the that of Model 18c under 750 mm/sec ground motion. The vertical distribution of girder-end ductility demands is shown in Fig. 6 for the four cases.

In the response of Model 18a under 750 mm/sec ground motion shown in Fig. 6(a), large ductility demand is observed at upper level girders under El Centro motion, Kobe Marine Observatory motion and Taft motion, whereas larger ductility demand is observed at the lower level girders or uniform over the height under Hachinohe motion and Tohoku University motion. In the response of Model 18b under 500 mm/sec ground motion, shown in Fig. 6(b), large ductility demand is observed to decrease at the upper level girders and increases in the middle floor girders compared with Fig. 6(a) under El Centro motion and Taft motion, and large ductility demand is observed in the lower level girders under Kobe Marine Observatory motion, Hachinohe motion and Tohoku University motion. The comparison of Fig. 6(c) and (d) also indicates a shift of the location of large ductility demand for Models 18a and 18c. The response of Models 12a and 12b also shows a trend similar to the one observed for the response of Models 18a and frame 18b.

Therefore, the first mode response amplitude does not necessarily control the vertical distribution of girder-end ductility even for the structures of the same height.

The observed distribution of girder-end ductility demand may be summarized as follows;
(1) The distribution is relatively uniform if the first mode response is dominant; e.g. Model 18a subjected EW component of Hachinohe motion or Model 18c subjected NS component of Kobe Marine Observatory motion;
(2) In models with a shorter fundamental period, large ductility demand was observed in lower levels when the ground motion contains long period components; e.g. Model 18b subjected to EW component of Hachinohe motion or NS component of Tohoku University motion;
(3) Large ductility demand was observed in the upper levels when the ground motion contains short period components coinciding with the second mode period of a structure; e.g. Model 18a subjected to NS component of El Centro motion or Model 18c subjected to NS component of Kobe Marine Observatory motion.

3.3 Effect of vertical distribution of beam strength

In order to study the effect of vertical variation of girder strength on the distribution of ductility demand, the design lateral force distribution was varied for Model 12a. In Model 12a-t, the design story shear coefficient was increased in the upper story levels by amplifying the factor A_i by 1.1 at the eighth-story, 1.2 at the ninth story, 1.3 at the tenth story, 1.4 at the eleventh story, and 1.5 at the twelfth story. The design story shear of Model 12a-s is determined by taking the square root of the sum of squares (SRSS) of modal response story shears (AIJ, 1993); the design spectrum of ground motion was taken as recommended by the AIJ Load Guidelines (AIJ, 1993) shown in Fig. 4. The distribution of girder-end ductility demands is shown for Models 12a, 12a-s and 12a-t in Fig. 7.

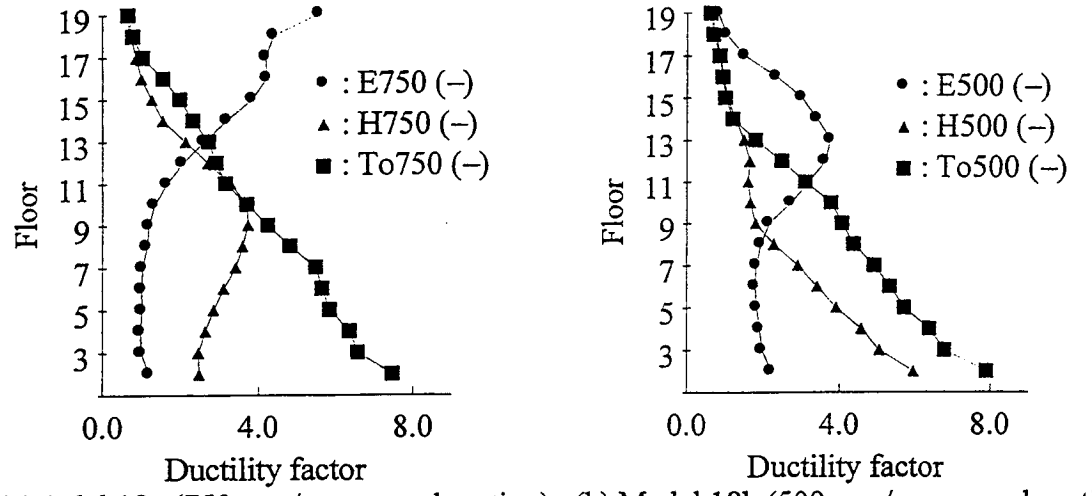

(a) Model 18a (750 mm/sec ground motion) (b) Model 18b (500 mm/sec ground motion)

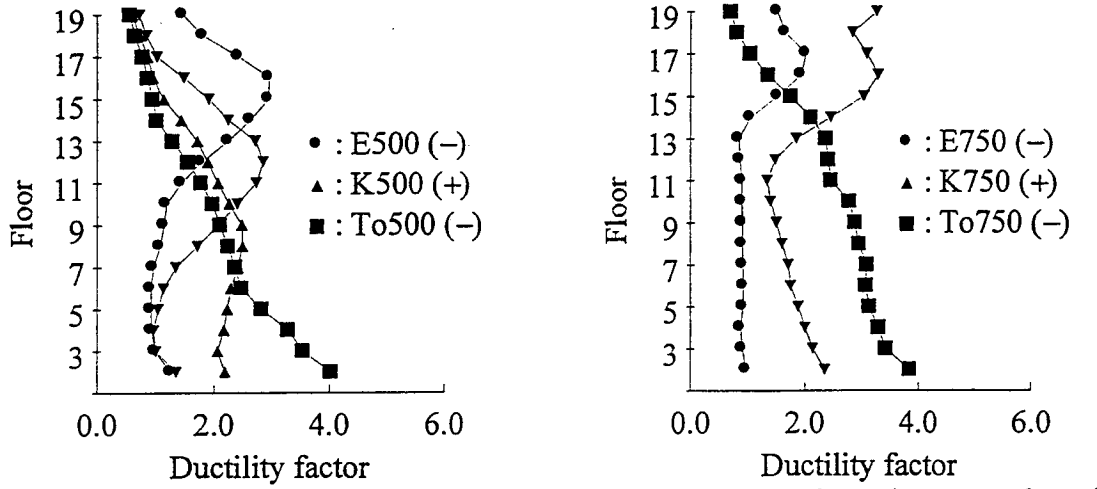

(c) Model 18a (500 mm/sec ground motion) (d) Model 18c (750 mm/sec ground motion)

Figure 6. Effect of natural periods on ductility demand

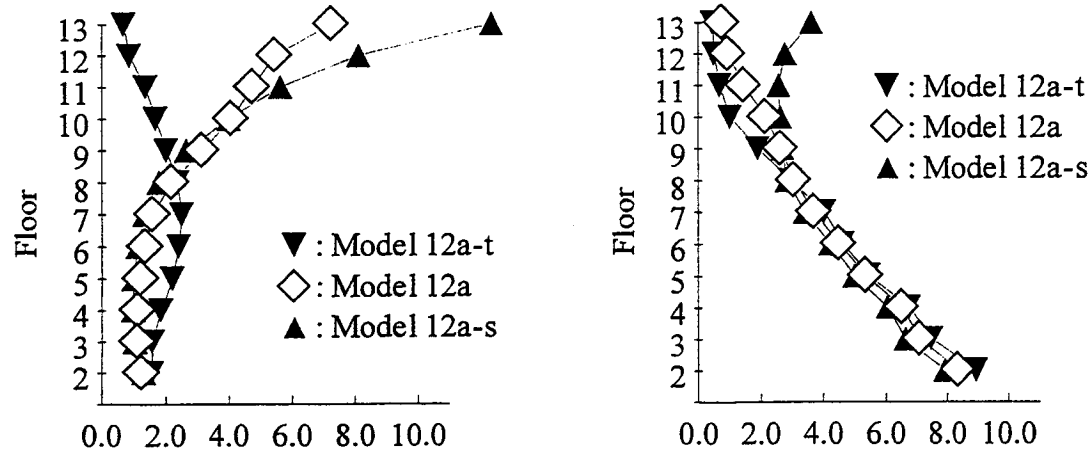

(a) Under E75 (b) Under To75

Figure 7: Effect of girder strength distribution on ductility demand

The distribution of girder-end ductility demands is significantly affected by the distribution of flexural strength along the height. The girder-end ductility demands are much larger at the upper levels in Model 12a-s than Models 12a; Model 12a-s is provided with smaller flexural resistance at upper levels. The girder-end ductility demands of Model 12a-t are very small at upper levels when the girder end flexural resistance was increased in the upper levels. If higher flexural resistance is provided in the upper level girders, no yielding takes place at the upper levels; the girder end ductility demands distribute uniformly except under the NS component of Tohoku University motion. Girder-end ductility demand of Model 12a-t increased slightly at the lower levels compared with those of Model 12a.

4. DEFORMATION DISTRIBUTION BASED ON STATIC PUSH-OVER ANALYSIS

It has been shown that the distribution of girder-end ductility demands of MDOF systems subjected to an earthquake ground motion is significantly affected by various characteristics of ground motions as well as of structures. For a given ground motion, a method to estimate the distribution and amplitude of girder-end ductility demands during an earthquake is studied.

4.1 Lateral force and story shear distributions

The results of a static push-over analysis are influenced by a choice of the distribution pattern of lateral forces. Acceleration response, and associated inertia force and story shear signals contain higher mode components and their distribution along the height varies instantaneously during an earthquake. On the other hand, the distribution of lateral forces is assumed constant in the push-over analysis. Therefore, it is difficult to estimate maximum earthquake response by a static push-over analysis; the results of two or more push-over analyses must be combined to reflect the change of lateral force distribution during an earthquake. The two patterns of story shear distribution are considered in this study; i.e., the sum of two modal story shears and the difference of two modal story shears.

For m-th mode, the ratio of i-th story shear ${}_mQ_i$ to the base shear ${}_mQ_i$ is expressed by Eq. (3);

$$\frac{{}_mQ_i}{{}_mQ_1} = \frac{\sum_{j=i}^{n} w_j \, {}_m\beta \, {}_mu_j}{\sum_{j=1}^{n} w_j \, {}_m\beta \, {}_mu_j} \tag{3}$$

where, ${}_m\beta$: m-th mode participation factor, ${}_mu_j$: m-th mode shape at j-th floor, and w_j : j-th floor weight. Therefore, the ratio of i-th story shear Q_i to base shear Q_1 for the sum and the difference of the first two modes can be expressed as

$$\frac{Q_i}{Q_1} = \frac{{}_1Q_i + {}_2Q_i}{{}_1Q_1 + {}_2Q_1} \tag{4}$$

$$\frac{Q_i}{Q_1} = \frac{{}_1Q_i - {}_2Q_i}{{}_1Q_1 - {}_2Q_1} \tag{5}$$

The ratio of m-th mode base shear ${}_mQ_1$ to the first mode base shear ${}_1Q_1$ may be assumed as follows;

$$\frac{{}_mQ_1}{{}_1Q_1} = \frac{{}_mM\,S_a({}_mT,\ {}_mh)}{{}_1M\,S_a\ ({}_1T,\ {}_1h)} \tag{6}$$

where: $S_a({}_mT,\ {}_mh)$: acceleration response spectrum ordinate at m-th mode period ${}_mT$ and for m-th mode damping factor ${}_mh$, and ${}_mM$: m-th mode equivalent mass given by the following equation:

$$\begin{aligned} {}_mM &= {}_m\beta\,\{{}_mu\}^T\,[M]\{1\} \\ &= {}_m\beta\,\{{}_mu\}^T\,[M]\,{}_m\beta\,\{{}_mu\} \end{aligned} \tag{7}$$

where ${}_m\beta$: m-th mode participation factor, $\{{}_mu\}$: m-th mode linearly elastic mode shape vector, and $[M]$: mass matrix.

The story shear coefficients, which are defined as a ratio of a story shear divided by the sum of the weights above the story, are compared for the sum and the difference of the first two modes, first mode story shear and A_i distribution in Fig. 8. The story shear coefficient for the sum of the first two modes distributes almost uniform along the height, distribution, and that for the difference of the first two modes is generally larger than any story shear coefficients.

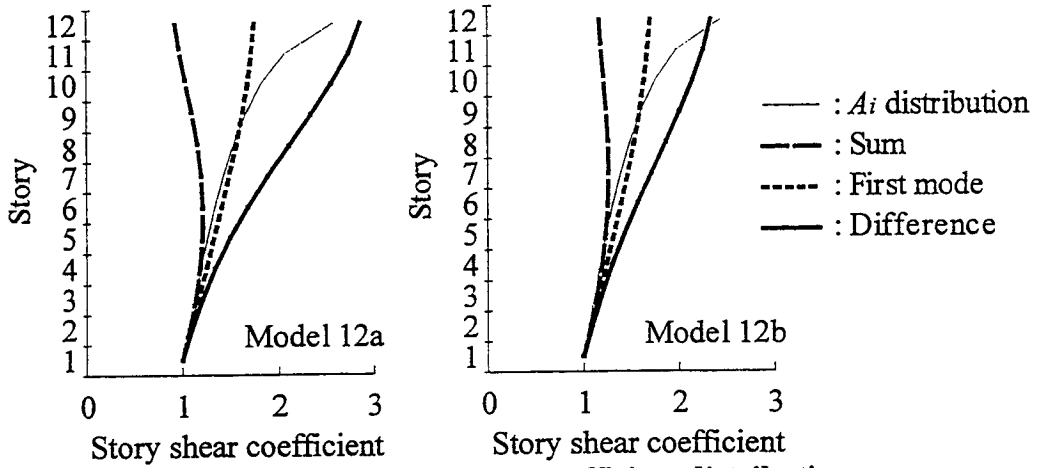

Figure 8. Story shear coefficient distribution

4.2 Story displacements under earthquake and push-over analysis

The equivalent first mode displacement ${}_1\delta$ is defined by following equation;

$${}_1\delta = \frac{{}_1\beta\,\{{}_1u\}^T\,[M]\{d\}}{{}_1M} \tag{8}$$

where ${}_1\beta$: first mode participation factor, $\{{}_1u\}$: first mode shape vector, $[M]$: mass matrix, ${}_1M$: first mode equivalent mass, and $\{d\}$: floor displacement vector. In order to compare only the deformation distribution, push-over analyses are performed up to the load step where the equivalent first mode displacement ${}_1\delta$ is equal to maximum response of ${}_1\delta$ by the earthquake response analyses.

Figure 9 compares the distribution of maximum floor displacements and story drifts obtained by an earthquake response analysis of Model 12a subjected to EW component of Taft motion and four push-over analyses at the same equivalent first mode displacement. The story shear distributions in the push-over analyses correspond to the first mode shape, the sum and the difference of the first two modes and A_i story shear coefficient distribution. The distribution of maximum positive floor displacements and story drifts may be approximately represented by the distribution pattern of the push-over analysis using the story shear distribution corresponding to the difference of the first two modes. On the other hand, the distribution of maximum negative floor displacements and story drifts may be represented by the distribution using the story shear distribution corresponding to the first mode story shear.

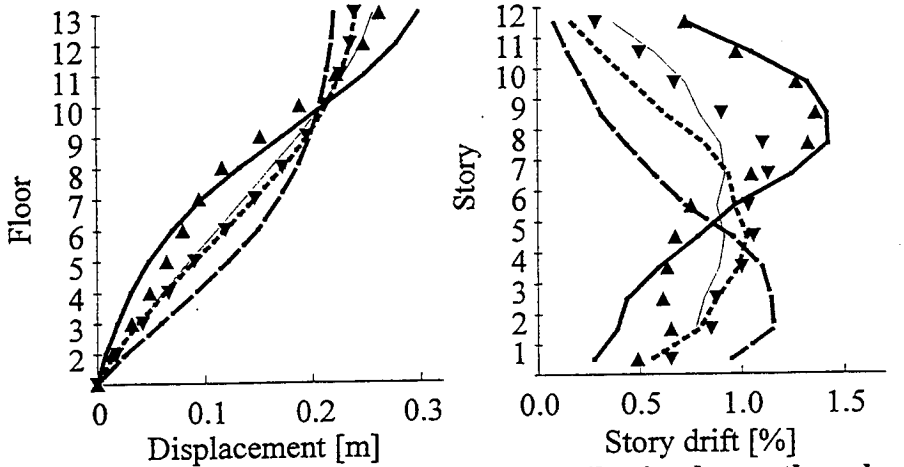

Figure 9. Floor displacement distribution by earthquake response analysis and push-over analyses

4.3 Distribution of girder-end ductility demands

Figure 10 compares the distribution of girder-end ductility demands from earthquake response analyses and four push-over analyses. Twelve-story Models 12a and 12b were subjected to Taft motion and to Hachinohe motion, respectively, both at 750 mm/sec maximum ground velocity. Models 12a-s and 12a-t were also analyzed under Kobe Marine Observatory motion and El Centro motion, respectively, both at 750 mm/sec maximum ground velocity. Models 18a and 18b were subjected to Kobe Marine Observatory motion at 750 mm/sec maximum ground velocity and to Tohoku University motion at 500 mm/sec maximum ground velocity, respectively. The story shear distributions in the push-over analyses correspond to the first mode shape, the sum and the difference of the first two modes, and A_i story shear coefficient distribution.

Models 12a, 12b, 18a, and 18b were designed using design story shear coefficient of A_i distribution. In these models, girder-end ductility demands distribute almost uniformly over the height by the push-over analysis using story shear distribution corresponding to story shear coefficient distribution A_i. On the other hand, the girder-end ductility demands by an earthquake response analysis are large either at the upper levels or at the lower levels. It is found difficult to use the results of the push-over analysis based on story shear distribution corresponding to story shear coefficient A_i in estimating the distribution of girder-end ductility demand.

If the girder-end ductility demands in an earthquake response analysis are large at the lower levels, the distribution may be approximated by the push-over analysis using the story shear distribution corresponding to the sum of the first two modes. On the other hand, if the girder-end ductility demands are large at the upper levels or in the middle levels, the distribution may be approximated by the push-over analysis using story shear distribution corresponding to the difference of the first two modes.

The push-over analysis using story shear distribution corresponding to the difference of the first two modes works reasonably well also for Models 12a-s and 12a-t, in which the design story shear was increased (Model 12a-t) or reduced (Model 12a-s). The push-over analysis using the difference of the two modes gave remarkably large girder-end ductility demands at the upper levels in Model 12a-s, and small ductility demands in Model 12a-t.

Among the push-over analyses using four story shear distributions, the result of first-mode shape distribution did not work well except in rare floor levels. Therefore, the push-over analysis using the story shear distribution corresponding to the first mode shape can be abandoned for the purpose of estimating the girder-end ductility demands over the entire height of a structure.

The girder-end ductility demands from an earthquake response analysis sometimes exceed the ductility demands obtained by the push-over analyses using the story shear distribution corresponding to the sum and difference of the first two modes. The underestimate by the push-over analyses may be attributed to the assumption of a constant ratio of the first mode shear to the second mode shear on the basis of elastic response acceleration spectra.

Figure 11 shows the girder-end ductility demands of Models 12a and 12b subjected to El Centro motion and to Hachinohe motion, respectively, both at maximum ground velocity of 500 mm/sec. The ductility demand of the push-over analysis adding the third mode contribution to the difference of the first two modes in the story shear distribution increases remarkably at the top few levels. On the hand, the ductility demand at the lower levels increases significantly by adding the third mode contribution to the sum of the first two modes in the story shear distribution.

Push-over analyses methods were examined for the following three cases;

Method 1: The results of the push-over analysis based on story shear distribution corresponding to story shear coefficient A_i is used to estimate the distribution of girder-end ductility demand.

Method 2: The envelope of the maximum girder-end ductility demands of the push-over analyses using story shear distribution corresponding to the sum and the difference of the first two modes is used to estimate the upper bound in 12-story models. In the envelope of the maximum girder-end ductility demands of the push-over analyses using story shear distribution corresponding to the first mode shape is also added to estimate the upper bound in 18-story models.

Method 3: In the story shear distribution of a push-over analysis, the story shear distribution corresponding to the third mode shear is added to the story shear corresponding to the sum and the difference of the first two modes in Method 2.

The ratios of the earthquake response ductility demands of girder ends to the ductility demands estimated by the proposed push-over analyses methods are calculated for Models 12a and 12a-t under different ground motions. Maximum ratio of entire girders in a frame is computed. Figure 12 compares the maximum ratios obtained by the three proposed methods.

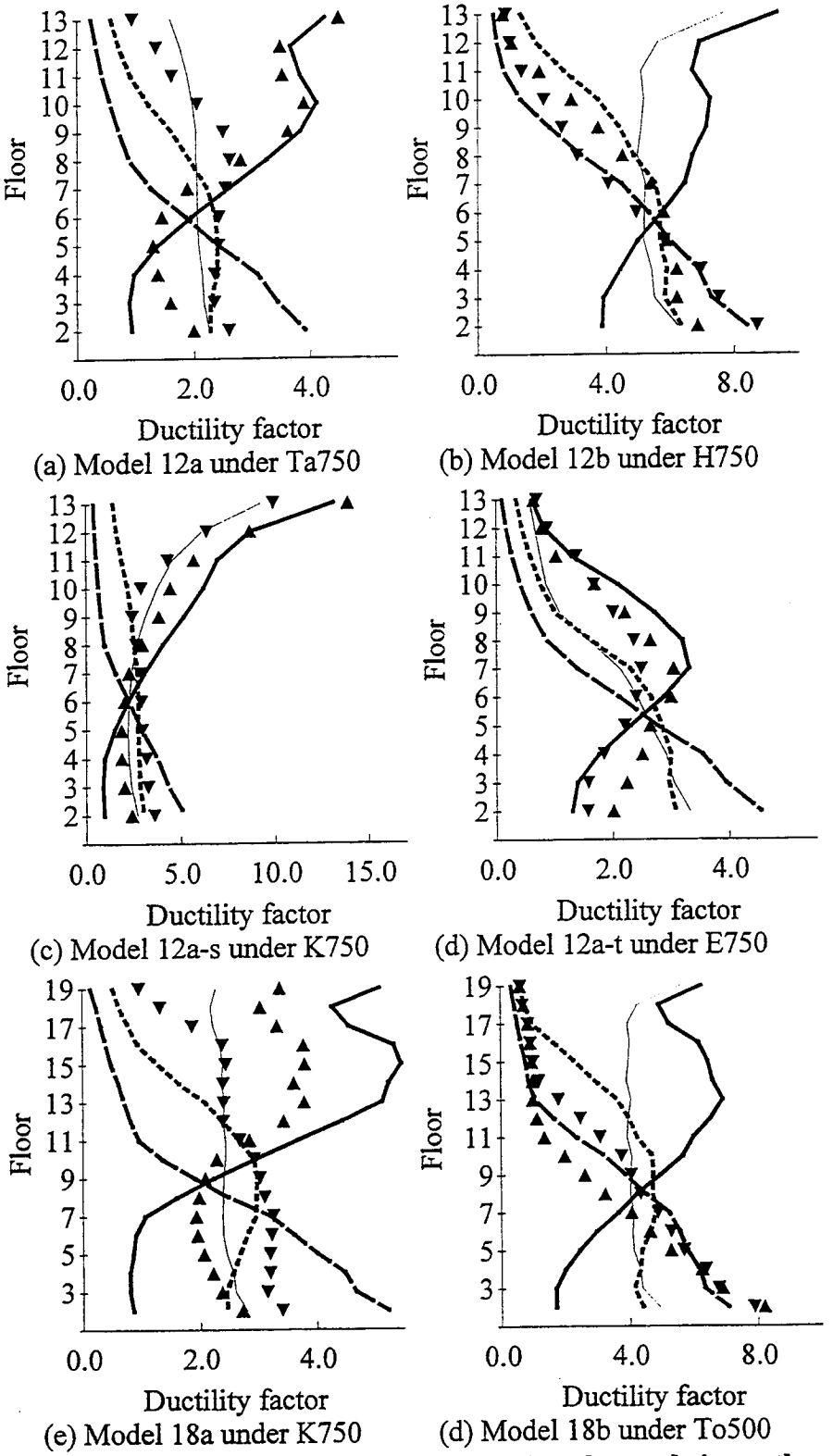

(a) Model 12a under Ta750 (b) Model 12b under H750

(c) Model 12a-s under K750 (d) Model 12a-t under E750

(e) Model 18a under K750 (d) Model 18b under To500

Figure 10. Girder-end ductility demands in earthquake response and push-over analyses

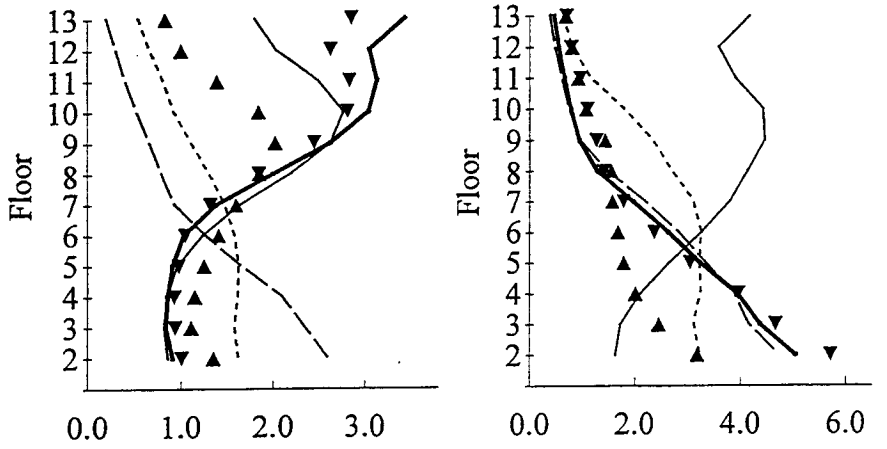

(a) Model 12a under E500 (d) Model 12b under H500

Figure 11. Girder-end ductility demand considering third mode contribution

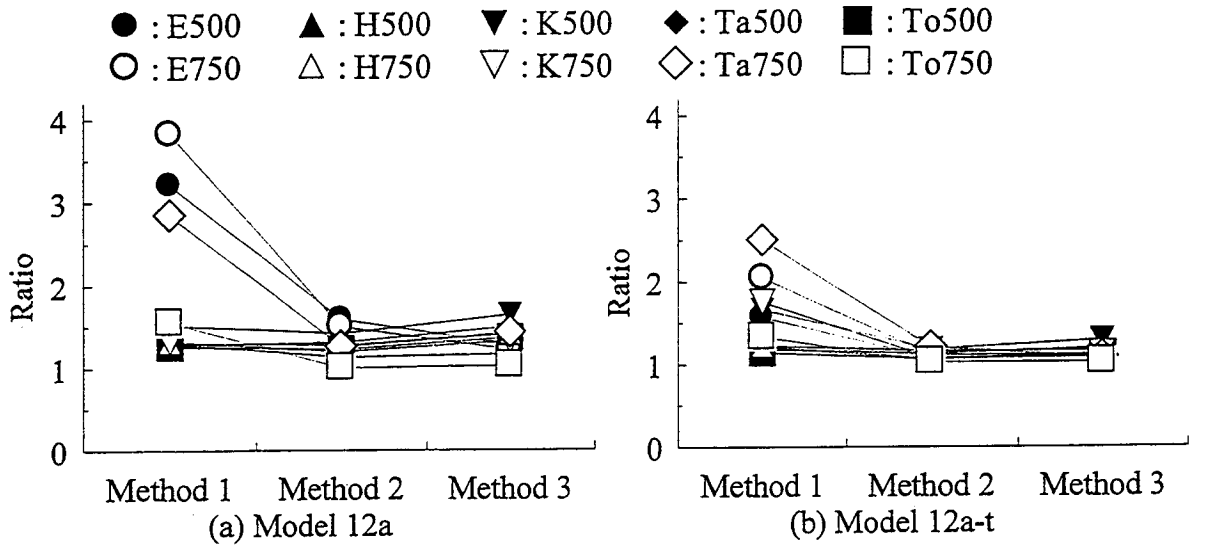

(a) Model 12a (b) Model 12a-t

Figure 12. Comparison of proposed push-over analyses methods

The ratios obtained by Method 1 reached around 4.0 in Model 12a under E500, E750, and Ta750. For Model 12a-t with relatively uniformly distributed deformation, the ratios obtained by Method 1 occasionally exceed 2.0. Method 2 most reasonably gives the upper bound values; the ratios are 2.0 or less in all the cases, and the ratios do not fall excessively below 1.0. Method 3 does not improve accuracy so much compared with Method 2.

5. CONCLUSIONS

(1) According to the earthquake response analyses of frame structures, the distribution of girder-end ductility demands during an earthquake varies significantly characteristics of ground motions and structures.

(2) Methods to estimate the girder-end ductility demands were studied using static push-over analyses. The distribution of local earthquake responses could be reasonably estimated by the results of push-over analyses using story shear distribution corresponding to the sum and the difference of the first two modes.

6. REFERENCES

Ministry of Construction of Japan (1981). *Building standard law enforcement order*. Building Center of Japan.

Architectural Institute of Japan (1993). *Recommendations for loads on buildings*. Architectural Institute of Japan.

Takeda, T., Sozen, M.A., and Nielson, N.N. (1970). "Reinforced Concrete Response to Simulated Earthquakes," *Journal of the Structural Division*, ASCE, Vol.96, pp.2557-2573.

Shibata, A. and Sozen, M. A. (1976). "Substitute Structure Method for Seismic Design in Reinforced Concrete", *Journal of the Structural Division*, ASCE, Vol. 102, pp.1-18.

ANALYSIS PLATFORM AND MEMBER MODELS FOR PERFORMANCE-BASED ENGINEERING

Filip C. Filippou[1]

ABSTRACT

The development of rational measures of global and local response for structures that undergo significant inelastic deformations play an important role in the validation of performance-based engineering concepts. A new generation of models that lend themselves more naturally to the development of rational measures of local response is the subject of this paper. These models are based on internal force interpolation functions and satisfy local equilibrium in a strict sense. Mixed force-displacement formulations are used for problems, where the interaction between element displacements and internal forces makes the exact a-priori satisfaction of internal equilibrium impossible. These models prove superior to commonly used displacement formulations for a class of problems that are of great interest in nonlinear structural analysis. The resulting smooth internal force distributions ensure excellent numerical behavior in the presence of strength softening, even though localization problems persist. These models are, therefore, ideal for failure simulation of structural models, which is an important objective of current efforts towards simulation-based design codes. The architecture of a new analysis platform that facilitates the development and deployment of material, section and element models is briefly discussed. This platform offers promise that models by many researchers will be seamlessly integrated into a powerful tool for performance-based nonlinear analysis and simulation-based design.

1. INTRODUCTION

The recent evolution of earthquake resistant design codes towards performance-based criteria makes the need for rational analytical models that can be deployed in push-over nonlinear analyses and nonlinear dynamic simulation studies of structures acute. These models should be transparent in theory and implementation, should be rational and numerically robust, should be easy to customize to specific situations, should be adaptive relative to global or local response error estimates, and should reveal limits of validity to the user. While we are presently far away from this ideal state of modeling, it is now an opportune time to develop new modeling and computational strategies that will permit us to reach this goal within a reasonable timeframe and move closer to the realization of the goal of simulation-based design codes. Recent developments in programming languages, computer and networking technologies create new opportunities for large scale simulation: object-oriented programming with its potential for modularity and

[1] *Department of Civil and Environmental Engineering, University of California, Berkeley, California*
Email: filippou@ce.berkeley.edu

teamwork, massively parallel computer architectures that promise manifold increases of computational speed in the coming years, and distributed computing with its potential for resource optimization. The development of a new nonlinear analysis platform that will take advantage of these computer developments is the objective of a new project within the Pacific Earthquake Engineering Research Center (PEER) under the leadership of Professor Fenves. Within this project, element development moves according to principles of modularity that were first realized in the structures library FEDEAS developed under the general purpose finite element analysis program FEAP ((Filippou 1996; Taylor 1996)). This library is based on the hierarchical organization of structural element, section and material: in this approach, the section response can be obtained by integration of material responses, with the widely used section force resultant model (e.g. moment-curvature relation) as special case. Similarly, the integration of section response yields the element response, with point or fixed length hinge models as special cases. The modularity of the architecture permits every element to call any section type, which in turn call any material type. Users can readily add elements, sections or materials to the library, which are accessible by all library elements, sections or materials. This approach permits a rapid validation and extension of existing code. Its porting to the object-oriented architecture of the PEER nonlinear analysis platform does not present any difficulties. Consequently, we expect the entire FEDEAS library to be functional under the PEER platform in the very near future.

2. NONLINEAR FRAME ELEMENT FORMULATION

FEDEAS is built around a new family of nonlinear frame elements. These elements use force interpolation functions and the virtual force principle to derive the nonlinear element force-deformation relation. The internal force interpolation can be written

$$\mathbf{s}(x) = \mathbf{b}(x)\,\mathbf{Q} \tag{1}$$

where $\mathbf{s}(x)$ are the internal forces, $\mathbf{b}(x)$ the force interpolation functions and $\mathbf{Q}$ the element end forces. For beam-column elements will linear geometry it is possible to use force interpolation functions that satisfy equilibrium exactly: a constant axial force and a linear bending moment distribution in the absence of element loads and higher order polynomials as particular solutions

of the beam problem under distributed element loads. With the principle of virtual forces an end deformation-force relation results that can be linearized to yield

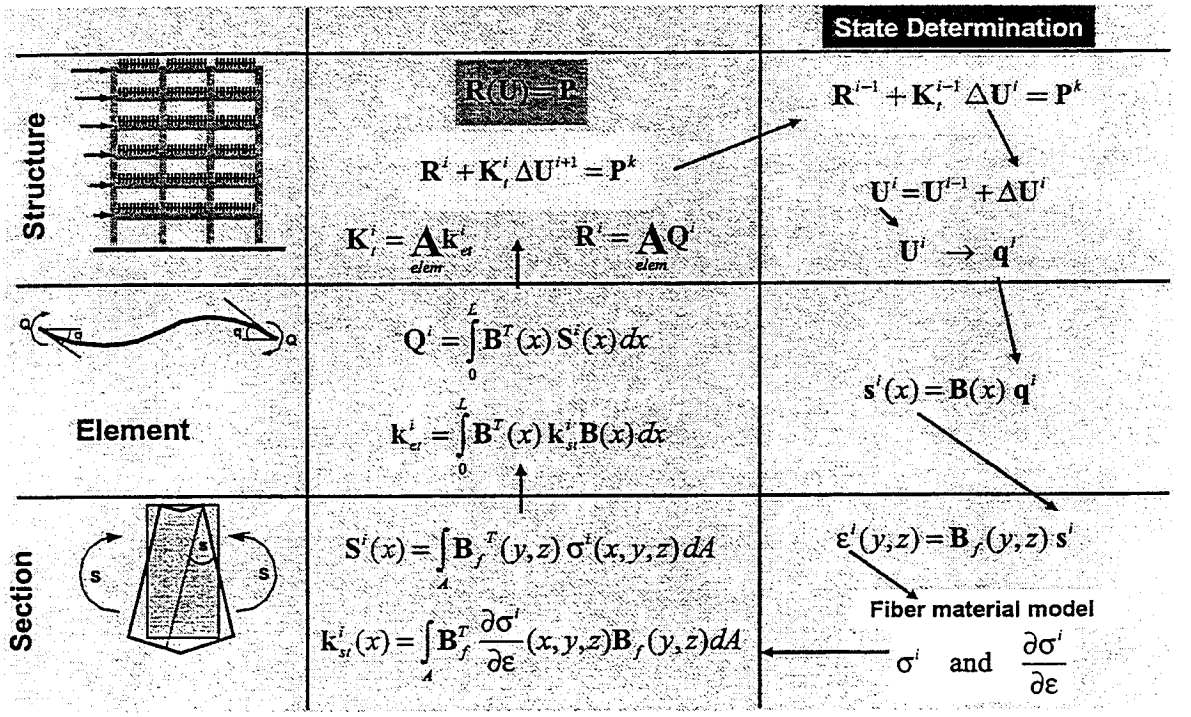

Figure 1 State Determination Process for Displacement Based Elements

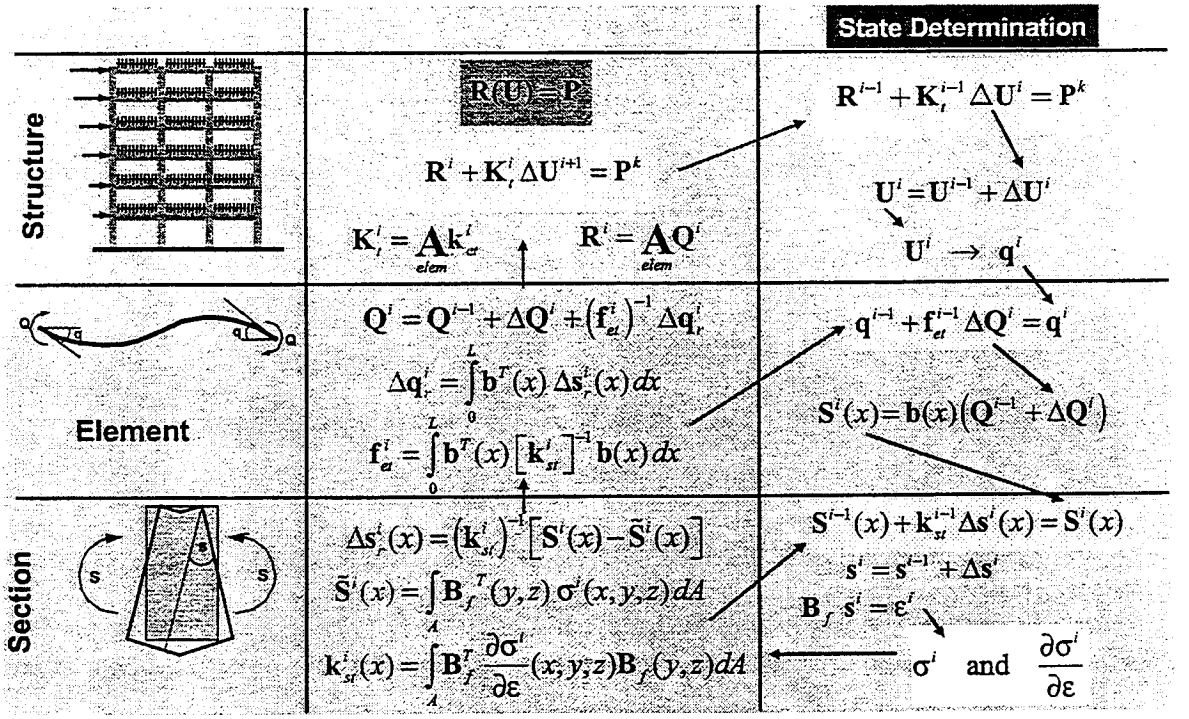

Figure 2 State Determination Process for Force Based Elements

$$\mathbf{q}^{i-1} + \mathbf{f}_{et}^{i-1} \Delta\mathbf{Q}^{i} = \mathbf{q}^{i} \qquad (2)$$

where $\mathbf{q}$ are the element end deformations and $\mathbf{f}_{et}$ is the element tangent flexibility matrix. The implementation difficulties that arise from this "inverse" form of the element force deformation relation can be illustrated with figures 1 and 2.

The structure state determination process that consists of the solution of the nonlinear structure equilibrium equations is the same in both figures, since the analysis platform is based on the direct stiffness method of analysis. In each iteration of a load step the current element end displacements $\mathbf{q}^{i}$ are passed to each element for its state determination.

This process is straightforward for elements with displacement formulations, as figure 1 shows: element displacement interpolation functions yield directly the section deformations $\mathbf{s}^{i}$ and section interpolation functions yield the strains across each section ε^{i}. Invoking the principle of virtual displacements for the section yields the section stiffness matrix $\mathbf{k}_{st}^{i}(x)$ and resisting forces $\mathbf{S}^{i}(x)$; invoking the same principle for the element yields the element stiffness matrix $\mathbf{k}_{et}^{i}$ and resisting forces $\mathbf{Q}^{i}$. The shortcoming of this approach stems from the fact that the element displacement interpolation functions are only exact for a linear elastic, prismatic beam and deviate significantly from those for a nonlinear beam element with large local inelastic deformations. In the latter case, a fine subdivision of the element into small finite elements is required for accuracy of local response. Even so, abrupt force discontinuities result at element boundaries, which can lead to numerical instabilities under softening behavior.

The element state determination process is more involved for force formulations, because the element force-deformation relation is in "inverse" form. Given the element end displacements $\mathbf{q}^{i}$ at each iteration of a load step, equation (2) needs to be solved for the unknown end force increments $\Delta\mathbf{Q}^{i}$. Since this is the linearization of a nonlinear force-deformation relation an iterative solution process is theoretically necessary. In each iteration the section forces $\mathbf{S}^{i}(x)$ are established with the force interpolation functions $\mathbf{b}(x)$. Since the section force-deformation relation is also in "inverse" form, i.e. section forces as functions of section deformations, because

of the section kinematic relation, another linearized equations needs to be solved iteratively for the section deformation increments $\Delta \mathbf{s}^i(x)$

$$\mathbf{S}^{i-1}(x) + \mathbf{k}_{st}^{i-1} \Delta \mathbf{s}^i(x) = \mathbf{S}^i(x) \tag{3}$$

Invoking the principle of virtual displacements for the section yields the new section stiffness matrix $\mathbf{k}_{st}^i(x)$ and resisting forces $\tilde{\mathbf{S}}^i(x)$. Since these do not satisfy equation (3) any longer, an iterative solution is theoretically necessary, as illustrated by the arrows that point back to equation (3) in figure 2. Consequently, three nested iteration processes result during the nonlinear solution of the structure equilibrium equations: the iteration for the global equilibrium equations, the iteration for the element end force-deformation relation and the iteration for the section force-deformation relation. This process is described in detail elsewhere (Spacone et al. 1996). It is, however, possible to bypass the internal element iterations by carrying forward the error and waiting for the next global iteration to correct. The section force error is transformed to section deformation residual $\Delta \mathbf{s}_r^i(x)$ in figure 2 and is carried forward to yield the element deformation residual $\Delta \mathbf{q}_r^i(x)$, which is transformed to an end force correction before returning the element end forces to the analysis platform. This process is only slightly more cumbersome than the element state determination for elements with displacement formulation. Significant computational savings over commonly used displacement based elements are realized, however, when comparable local response accuracy is sought: the displacement based element requires 8 to 16 finite elements in each structural member in order to yield an accurate measure of section curvature and, thus, strain, while a single element suffices for the force based formulation (Neuenhofer and Filippou 1997). Moreover, the direct state determination process is characterized by stable numerical behavior with almost quadratic numerical convergence (while the nested iteration process produces exactly quadratic numerical convergence for consistent material linearization).

3. EXAMPLES

3.1 Reinforced Concrete Column by Low/Moehle (1987)

The first example concerns the hysteretic behavior of a rectangular reinforced concrete cantilever. Specimen #5 in the test series of Low and Moehle (1987) was subjected to a rather

complex load history of biaxial bending with variable axial force intended to simulate loading conditions in structures under bi-directional acceleration input and torsional effects. The imposed tip displacement history is shown in Figure 3a and the variation of axial force in Figure 3b. The analytical model consists of a single beam element with four control sections. Each section is subdivided into material fibers for the integration of the section response. The subdivision of the section in concrete and steel fibers is advisable here on account of the variability of the axial force and the imposed biaxial displacement history.

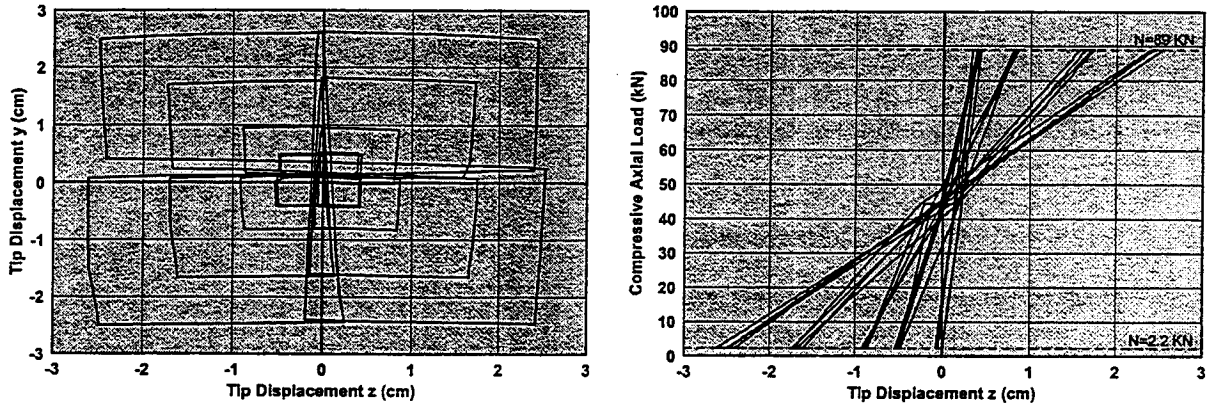

(a) (b)

Figure 3 Load History for Model of Low-Moehle Specimen #5:
(a) Imposed Tip Displacements; (b) Applied Axial Load

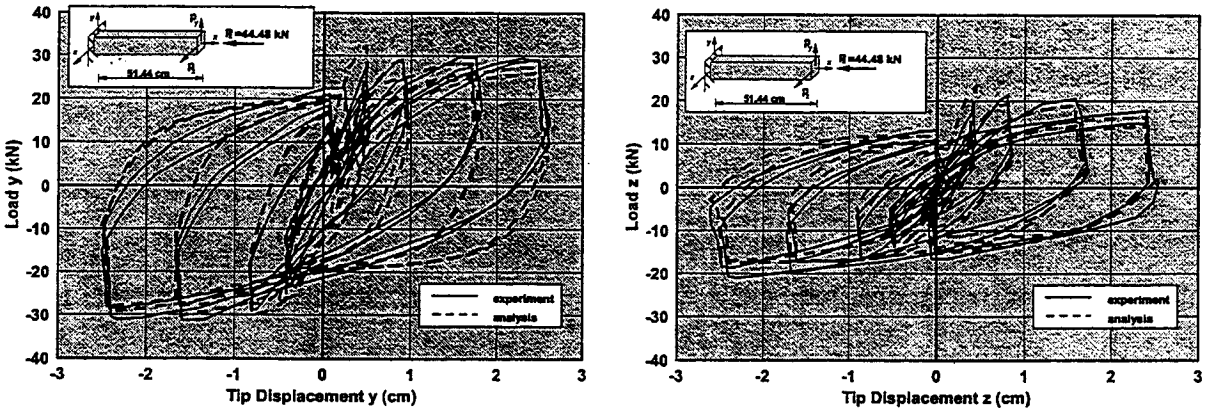

(a) (b)

Figure 4 Comparison of Analytical with Experimental Results for
Tip Load-Displacement Relation: (a) y-Direction; (b) z-direction

The model was subjected to the measured lateral displacement history and the corresponding axial force at the column tip. The agreement between experimental and analytical force-displacement relation in Figure 4 is very satisfactory, even though the discrepancy in the "pinching" behavior of the load displacement relation is noticeable. A comparison of the

measured strains at two corner reinforcing bars with calculated fiber strains in Figure 5 shows excellent qualitative agreement, but the maximum tensile strains are off by a factor of 2 or more (note the different strain scale in the side-by-side figures). It can, thus, be concluded that the effects of shear and bond-slip (pull-out) of longitudinal reinforcing steel play a significant role in the local response of reinforcing steel strains. Thus, an analytical model needs to address these effects before attaining "predictive" abilities for the failure mode of the specimen, which depends on steel and concrete strains (buckling, crushing, spalling).

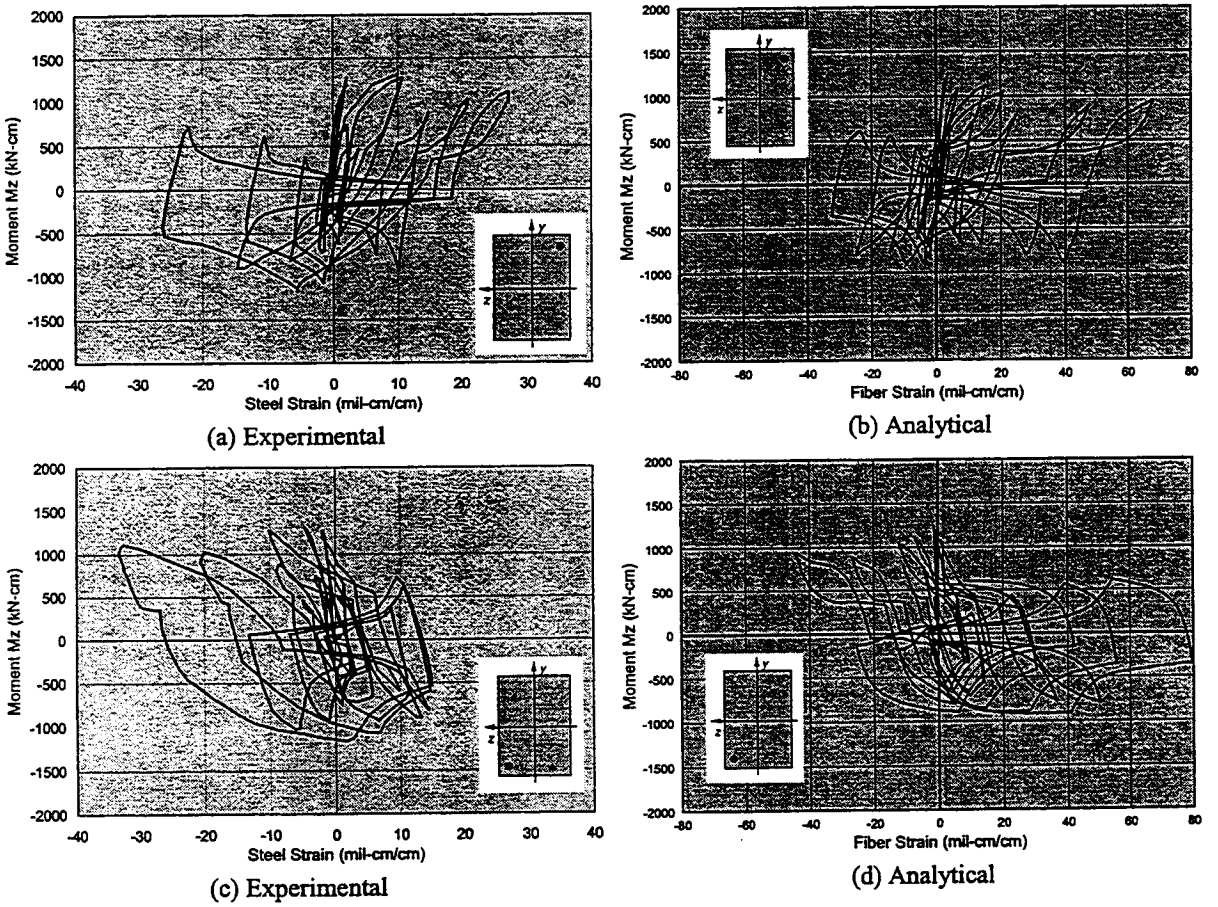

Figure 5 Strain History for Corner Reinforcing Bars of Low-Moehle Specimen #5

3.2 Reinforced Concrete Column Specimens of ISPRA (1995)

The ability of the nonlinear fiber beam-column element to simulate the hysteretic behavior of RC columns under uniaxial or biaxial flexure with constant or variable axial load is investigated by correlation of analytical results with experimental data from a test series on 0.25m square RC columns under various load paths that was conducted at Ispra ((Bousias et al. 1995)). 12 column

specimens denoted S0 through S11 were tested. All specimens had the same geometry and material properties, so that the only variable of the test series was the load path. Consequently, the data from this experimental series represent an ideal benchmark to test the capabilities of a nonlinear column element. The shear span ratio for the cantilever columns was 6, so that the effect of shear was not significant.

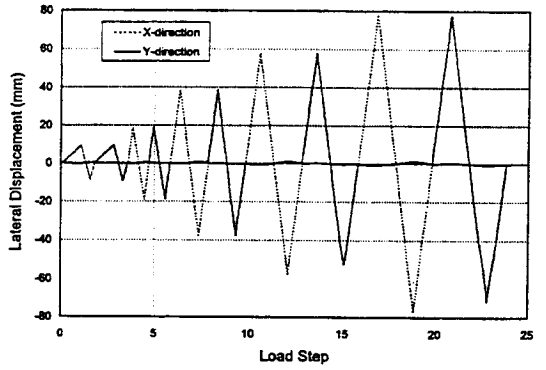

(a)Specimen S1

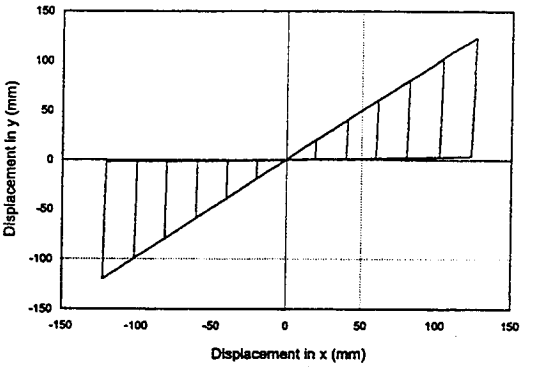

(b) Specimen S5

Figure 6 Displacement Histories for Specimens S1 and S5

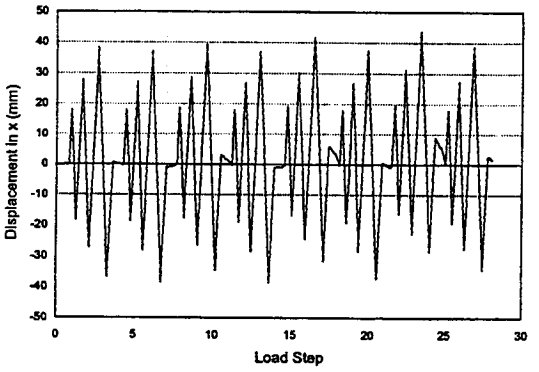

(a) Displacement History in x-direction

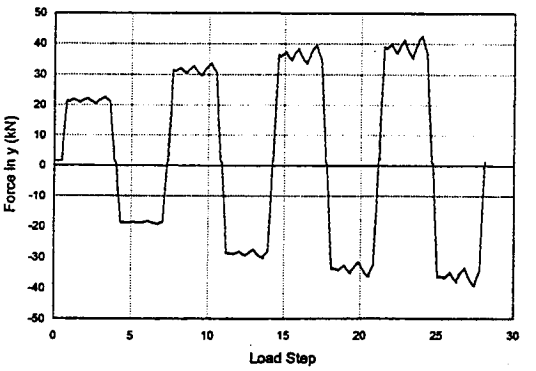

(b) Force History in y-direction

Figure 7 Displacement and Force History for Specimen S4

The analytical model consists of a single nonlinear beam-column element. Four control sections are used in the element and each control section is subdivided into 36 concrete fibers for the concrete confined by transverse reinforcement and 24 fibers for the cover concrete. In addition, 8 reinforcing steel fibers represent the 8 reinforcing steel bars of the actual specimen (3 on each face). The number of concrete fibers can be reduced significantly without affecting the accuracy of the results, but this is not pursued further in this paper. The test specimens were tested by controlling the displacements in the x- and y-direction at the tip of the cantilever or the displacement in x and the force in y. The axial force was kept constant in specimens S0 through

S8 at a compressive value between 8% and 17% of the concrete strength $A_c f_c'$ of the column. Specimen S9 experienced two levels of axial compression, while specimens S10 and S11 were subjected to a variable axial force with lateral displacement or force cycles without reversal of force or displacement. Specimens S1, S4 and S5 are used in the following correlation studies. The loading history for these specimens is summarized in Figs. 6 and 7.

Fig. 8 shows the correlation for specimen S1 under alternating uniaxial displacement cycles in the x- and y-direction. The agreement in the force-displacement hysteretic relation is satisfactory, with some discrepancy in the onset of yielding. No significant strength deterioration is observed, so that the analytical relation between lateral forces in Fig. 8(c) shows good agreement with the experiment. Good agreement is also observed in the axial displacement history, even though the change in axial displacement from one peak to the next is more pronounced in the later experimental cycles. Since the discrepancy between analysis and experiment is only evident in tension, but not in compression this might be an indication of some pull-out and reinforcing bond-slip that increases the axial extension.

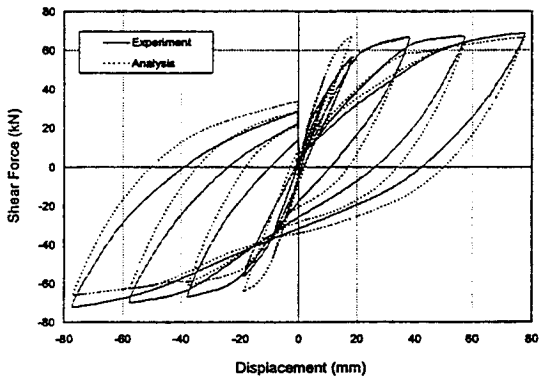

(a) Load-Displacement in x-direction

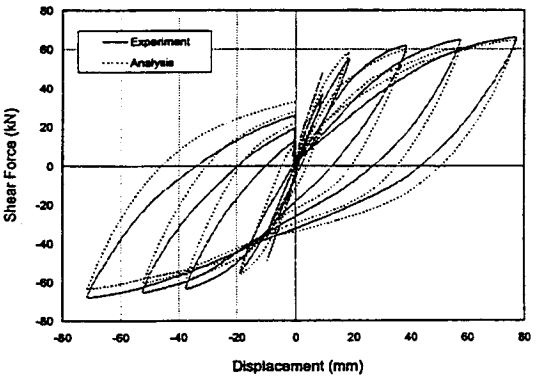

(b) Load-Displacement in y-direction

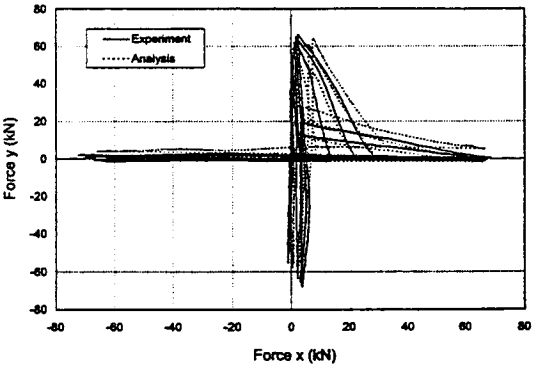

(c) Force in x-Force in y Relation

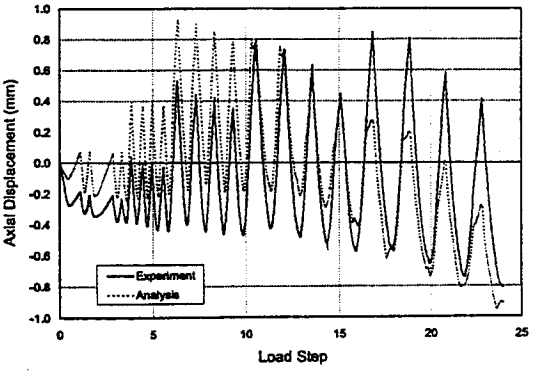

(d) Axial Displacement History

Figure 8 Experimental and Analytical Response of Specimen S1

Similarly excellent agreement is evident in Fig. 9 for the hysteretic response of specimen S4. This specimen is subjected to displacement reversals in the x-direction and force reversals in the y-direction according to the load history in Fig. 7. In this case the agreement of axial displacements between analysis and experiment is excellent. Again no strength deterioration is evident, so that the other response histories in Fig. 9 show excellent agreement, as well, with the exception of the significantly higher initial stiffness of the model in Fig. 9(a) and the consequent late onset of yielding in the x- and y-direction.

Specimen S5 was subjected to a more complex biaxial displacement load path under a constant axial compression of 12% of the concrete strength of the column. The specimen exhibits signs of strength deterioration with increasing lateral displacement, even for repeat cycles at the same displacement amplitude. This is an indication of concrete damage in compression and, possibly, the initiation of buckling of longitudinal reinforcing bars.

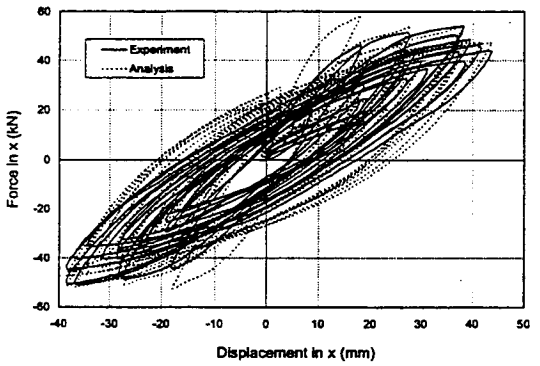

(a) Load-Displacement in x-direction

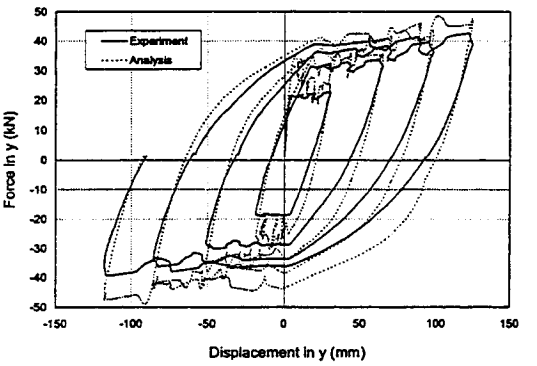

(b) Load-Displacement in y-direction

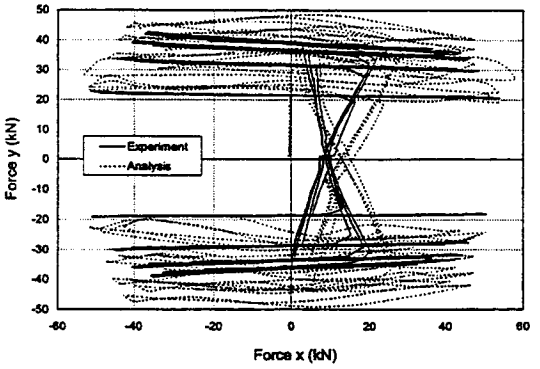

(c) Force in x-Force in y Relation

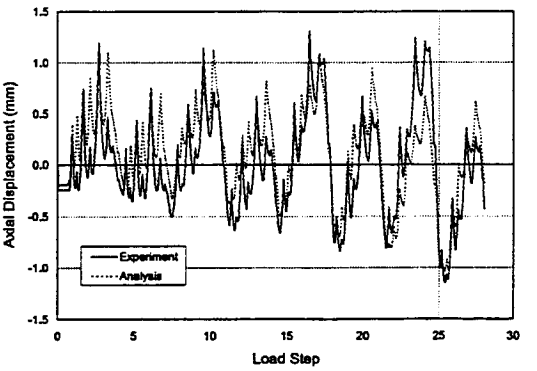

(d) Axial Displacement History

Figure 9 Experimental and Analytical Response of Ispra Specimen S4

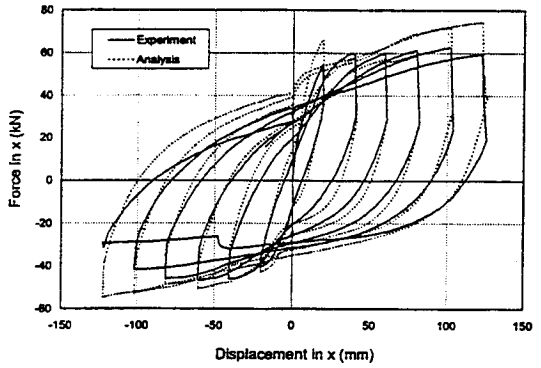

(a) Load-Displacement in x-direction

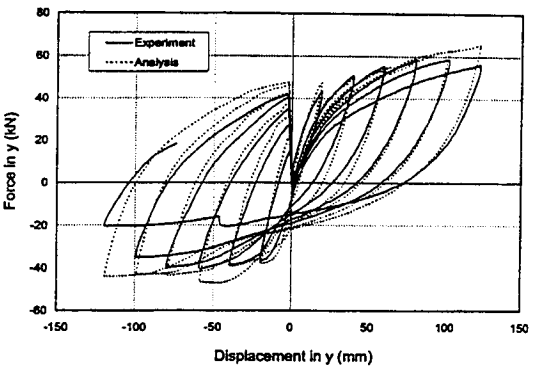

(b) Load-Displacement in y-direction

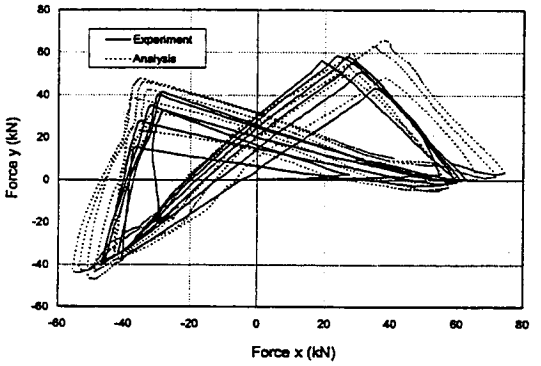

(c) Force in x-Force in y Relation

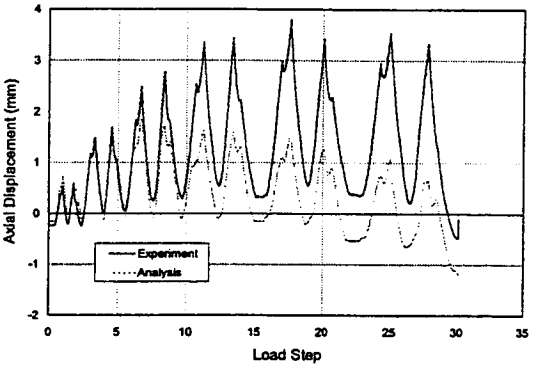

(d) Axial Displacement History

Figure 10 Experimental and Analytical Response of Specimen S5

Since neither effect is included in the fiber material models of the present study, the analytical results fail to capture this effect, as is evident in Figs. 10a and b. . Similarly, there is significant discrepancy of the axial displacement history between analysis and experiment, a clear indication that the state of damage of the specimen is not well represented by the model. This is clearly evident for the axial extension in Fig. 10d.

4. CONCLUSIONS

Force based element formulations offer significant advantages over commonly used displacement based elements: the internal force distributions satisfy equilibrium exactly and the local deformations can be accurately assessed with a single finite element for each structural member. These elements are numerically robust and stable, even under strength softening conditions. They offer excellent promise for the simulation of frame elements under complex load histories. Much work is, however, needed to include the effect of shear and bond-slip of reinforcing steel into reinforced concrete element models and the effect of local buckling and fracture in steel element

models. Moreover, better material models are also necessary. Force based models provide an excellent framework for simulation-based design of frame structures. Extensions of this formulation to two dimensional slab and wall elements hold much promise and are currently under study.

5. KEYWORDS

Nonlinear analysis; force formulation; RC column; hysteretic behavior; cyclic loading

6. REFERENCES

Bousias, S. N., Verzeletti, G., Fardis, M. N., and Gutierrez, E. (1995). "Load-Path Effects in Column Biaxial Bending and Axial Force." *Journal of Engineering Mechanics, ASCE*, 121(5), 596-605.

Filippou, F. C. "Nonlinear Static and Dynamic Analysis for Evaluation of Structures." *3rd European Conference on Structural Dynamics Eurodyn '96*, Florence, Italy, 395-402.

Neuenhofer, A., and Filippou, F. C. (1997). "Evaluation of Nonlinear Frame Finite Element Models." *Journal of Structural Engineering, ASCE*, 123(7), 958-966.

Spacone, E., Filippou, F. C., and Taucer, F. F. (1996). "Fiber Beam-Column Model for Nonlinear Analysis of RC Frames: I: Formulation." *Earthquake Engineering and Structural Dynamics*, 25(7), 711-725.

Taylor, R. L. (1996). "FEAP: A Finite Element Analysis Program, Version 5.01 Manual," , University of California, Berkeley.

SESSION 4: RESPONSE OR MODELING OF FRAMES

Chaired by

♦ Fumio Watanabe and Vitelmo Bertero ♦

RESPONSE OF IRREGULAR SLAB-COLUMN BUILDINGS

Habib L. FEGHALI and Prof. James O. JIRSA
The University of Texas at Austin

Introduction

There is growing use of nonlinear static and nonlinear dynamic (time-history) analysis procedures in design offices. These inelastic analyses yield information on the magnitude and distribution of internal forces and deformations in yielding structures but may be sensitive to assumptions and initial conditions. Confident design depends on having as accurate knowledge as possible of the response.

Flexible concrete structures have been used often in areas of low and moderate seismicity, and in some countries, are the predominant structural system. The performance of a typical flexible concrete building used in the Mediterranean basin is investigated.

A parametric study is being conducted to determine the influence of several parameters on the behavior of the structure. In this paper, the effects of infill masonry walls and the distribution of total building mass to the different vertical supporting elements are presented.

Building Description

Most of the Mediterranean basin is considered a region of low to moderate seismicity. Flexible reinforced concrete buildings are the prevailing structural system, especially on the East Coast of the Mediterranean Sea, and in seismic active areas such as Turkey, Iran, Cyprus, Greece and Lebanon. A typical eight-story reinforced concrete building was analyzed. Figure1 shows the layout of a typical floor. The lateral load- resisting system consists of a slab-column frame with concealed beams and ribbed slabs.

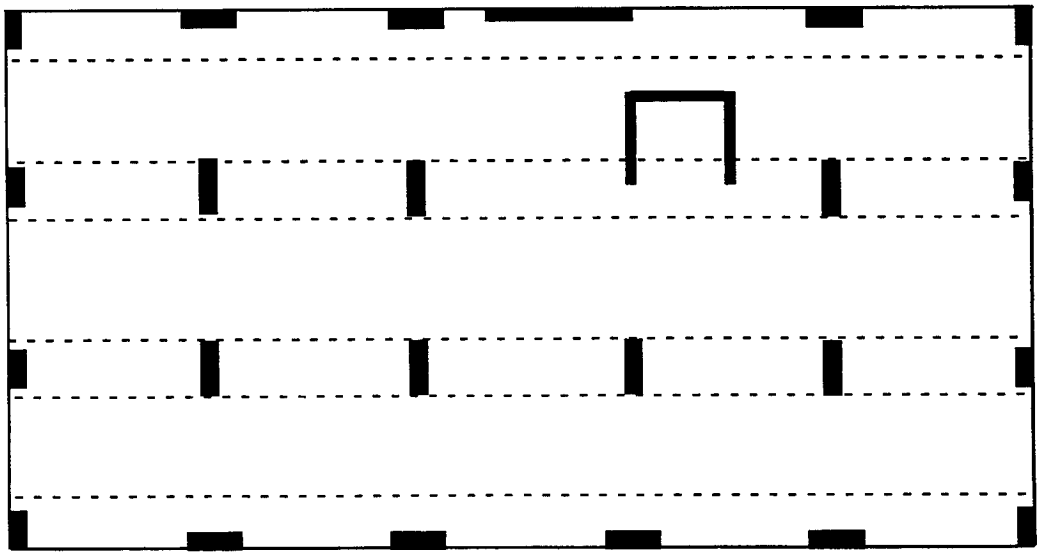

Fig. 1 Floor layout

Typically, the columns are designed with large depth to width ratio (2-5) for architectural reasons, Fig. 2.

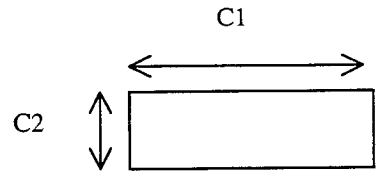

$$\frac{C_1}{C_2} \in [2;5]$$

Fig. 2 Column cross section

The slab consists of ribs separated by hollow core concrete blocks, "hourdis" in Lebanese, with beams concealed within the slab thickness. The ribs are small joists, spanning between the main beams. The beams are wide and shallow with very low deformation capacity.

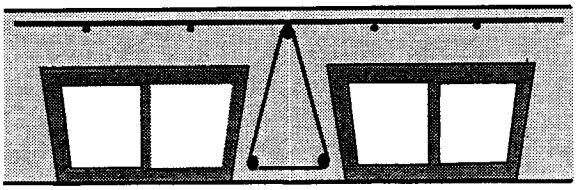

Fig.3 Slab cross section

Typically, concrete strength varies between 2Ksi and 3.5Ksi (14MPa and 24.5Mpa). Steel strength is 60Ksi (420Mpa).

Building Modeling

Drain2d[1] modified by Pincheira and Jirsa[2] was used to conduct the nonlinear analyses. Because of limitations in nonlinear analytical tools, only a planar section of the structure was analyzed. The beams were modeled using the beam element model available with Drain2d. The columns were modeled using the parallel element model suggested by Li and Jirsa[3]. The unreinforced masonry walls were modeled using the infill panel element available with Drain2d.

The beam element model consists of a linear-elastic element with bilinear rotational springs at the ends. Figure 4a shows the load-deformation characteristics for the beam element.

The parallel element model is a combination of two beam elements. One of the sub-elements changes into a truss element when a certain shear value is reached. The parallel element is intended for concrete elements susceptible to failure in shear. The formulation of the boundary conditions and the constitutive properties for the parallel element were modified so that compatibility in the plastic hinge rotations is met and the shear capacity after failure is bounded by the residual shear value specified in the formulation. Figure 4b shows the load deformation characteristics for the parallel element.

The infill panel element is intended to permit contribution of the infill masonry panels to the lateral stiffness of the structure. The element is assumed to have shear stiffness only. Figure 4c shows the load-deformation characteristics for the infill panel element.

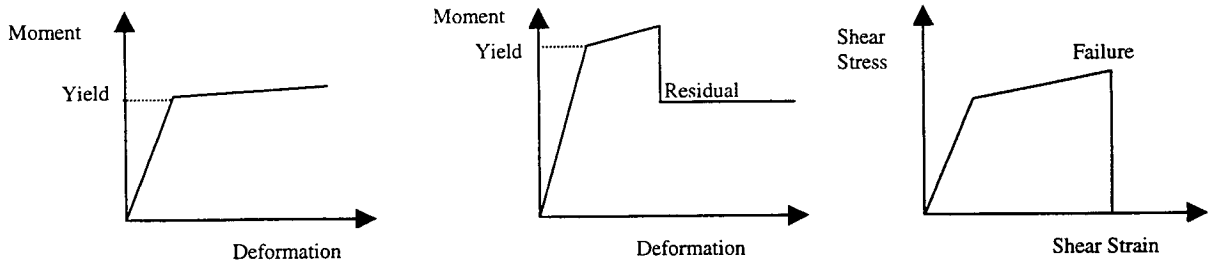

a- Beam element

b- Parallel element for columns

c- Infill panel

Fig. 4 Force-Deformation relationships

Parametric Study

The parameters being investigated include the damping ratio, material strength and properties, effective stiffness of structural elements, residual strength of failed elements, and variations in geometry and earthquake ground motions. In the present paper, only the variation of mass attributed to the analyzed section and the contribution of infill panels are discussed.

Three building models were used as shown in Fig. 5. A frame system with no infill is noted as FR. A frame building with infill panels from the second story to the roof is noted as a soft-story system, SS. And a frame building with infill panels at all levels is noted as AI. The attribution of mass to the section analyzed was not based on tributary area. Instead, the mass distributions were based on a constant mass to stiffness ratio from an elastic dynamic analysis using $0.5E_cI_g$ for beams and $0.7E_cI_g$ for columns (E_c is the modulus of elasticity for the concrete and I_g is the moment of inertia of the gross section). In a real system, the distribution of mass would be changing with time but a constant value was assumed for analyses. Hence, the frame model was assigned 15% of the total building mass, and the sections including infill panels were assigned 20% of total building mass. Models with infill panels and 15% of total building mass are discussed herein for comparison.

The building models were subjected to the ground motion (0.223 g peak acceleration) from the Ceyhan earthquake in Turkey. The magnitude of ground motions was magnified by a factor of two in order to produce failures that demonstrate the effects of the parameters under consideration.

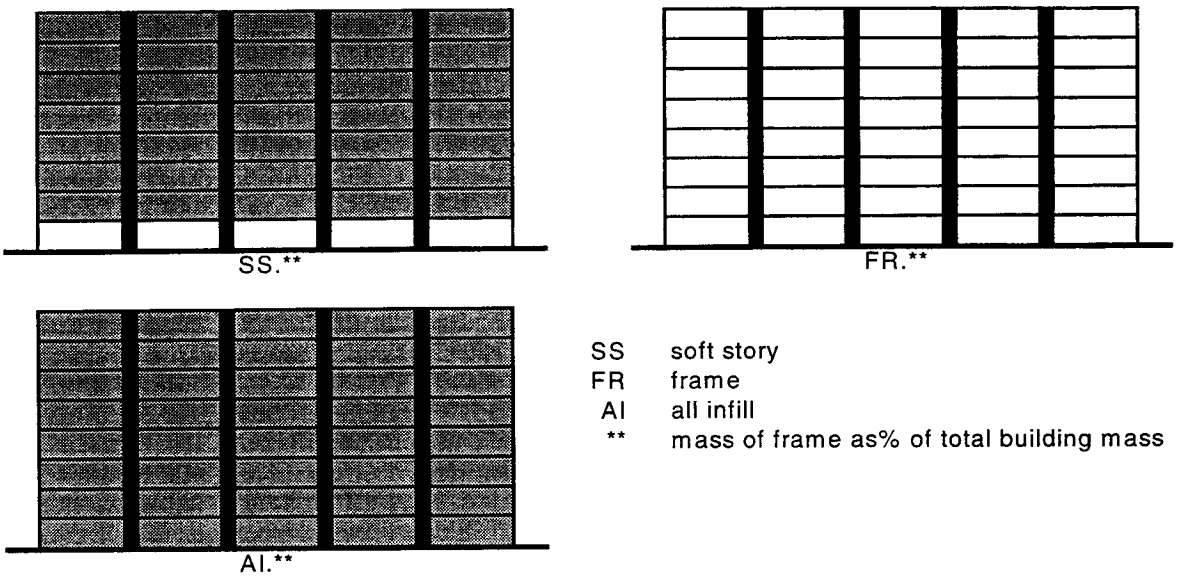

Fig. 5 Building models used in analyses

Analysis Results

The maximum story drifts, maximum interstory drifts and time-history of base shear to weight ratio were calculated for all models and are shown in Figs. 6 through 9. FR.15, which is a frame structure, shows the predominance of the first mode. In Figs.6A and 7A, the story drift for FR.15 is almost an inverted triangle. Figures 6B and 7B show that the panels have failed at the 4^{th}, 5^{th} and 6^{th} stories in SS.20, AI.15 and AI.20 and at the 4^{th} and 5^{th} stories in SS.15. Although stiffer than FR, AI and SS structures show larger deformations at upper floors after infill panels fail. At lower floors where no panel failure is occurring, AI structures are stiffer than both SS and FR systems. As expected, deformations of the first story of the SS systems are greater than FR because of the soft-story effect. Figures 6C and 7C show that SS structures reached the largest base shear to weight ratio while FR had the lowest ratios. Figures 8C and 9C show that models with a lower assigned mass had slightly higher base shear to weight ratios. With less mass, the period was smaller.

An acceptable measure of damage can be related to the drift sustained by the structure. Interstory drift provides information on the eventual failure mode of structural members. Column failure on the 6^{th} story in AI.20 was identified from the analysis. The corresponding interstory drift was the largest for AI.20 on the 6^{th} story. Column failure on the 5^{th} story in SS.15 was identified. The corresponding interstory drift was the largest for SS.15 on the 5^{th} story. AI.15 and AI.20 have the same material and physical properties except for the mass. Column failure could be identified at an interstory drift of 1.8% in AI.20, while no failure was indicated in AI.15, although a 2.6% interstory drift was calculated. The moments at the end of failing columns in AI.20 were almost equal and opposite in sign, indicating that shear reached the maximum capacity of the column before flexural yielding of the column occurred. Some columns reached the yield moment at one end, leading to large interstory drifts, however, the shear resisted by the column did not exceed the shear capacity. Thus, no failure was observed although interstory drifts were large. Figures 10 and 11 show the failure sequence in SS.15 and AI.20.

In these analyses, the distribution of total building mass to the section was an important parameter in determining the sequence of failure in a building. The base shear to weight ratio was almost unchanged for AI.15 and AI.20. There was close agreement in the shape of the story drift; however, the magnitudes of drifts were different for different assigned masses due to different sequence of failure and different inertial forces. The difficulty in assigning a mass to the analyzed section is similar to the difficulty faced when assigning a load pattern in performing a static nonlinear analysis or pushover analysis of a structure. The mode shapes of the structure vary as some elements of the structure undergo cracking, yielding or failure. Thus, assigning a constant mass for a section is expected to be accurate only if the section is perfectly isolated from the rest of the structure.

A nonlinear dynamic simulation of the response of a structure using models with load-deformation characteristics representing as many key features of the behavior of the real members as possible is expected to reproduce with acceptable accuracy the behavior of the structure. The results of the simulation depend highly on the model used especially in predicting the sequence and location of structural member failure.

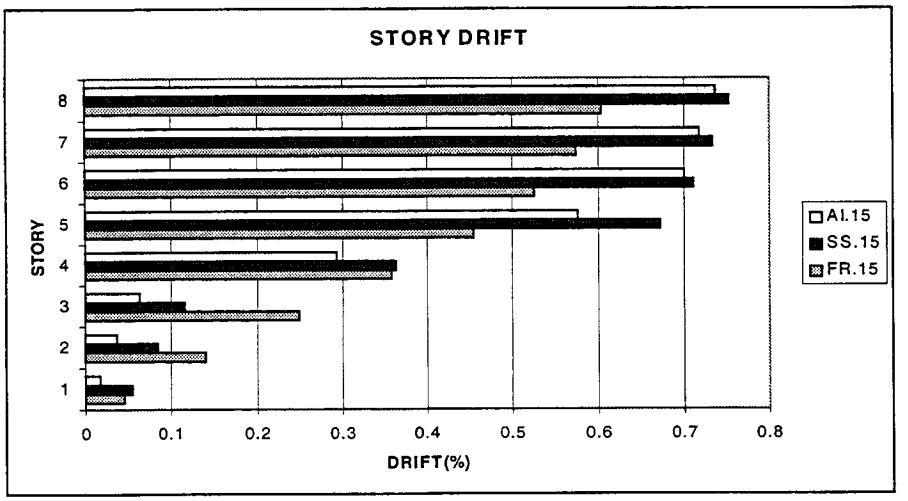

Fig. 6A Maximum story drifts for AI.15, SS.15 and FR.15

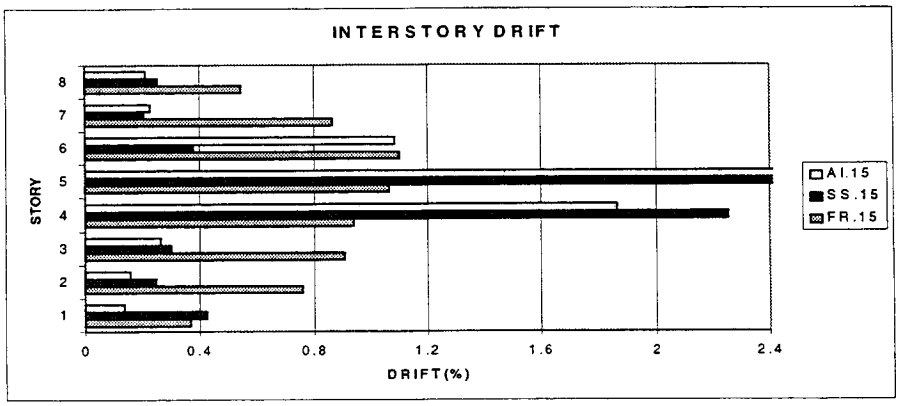

Fig. 6B Maximum interstory drifts for AI.15, SS.15 and FR.15

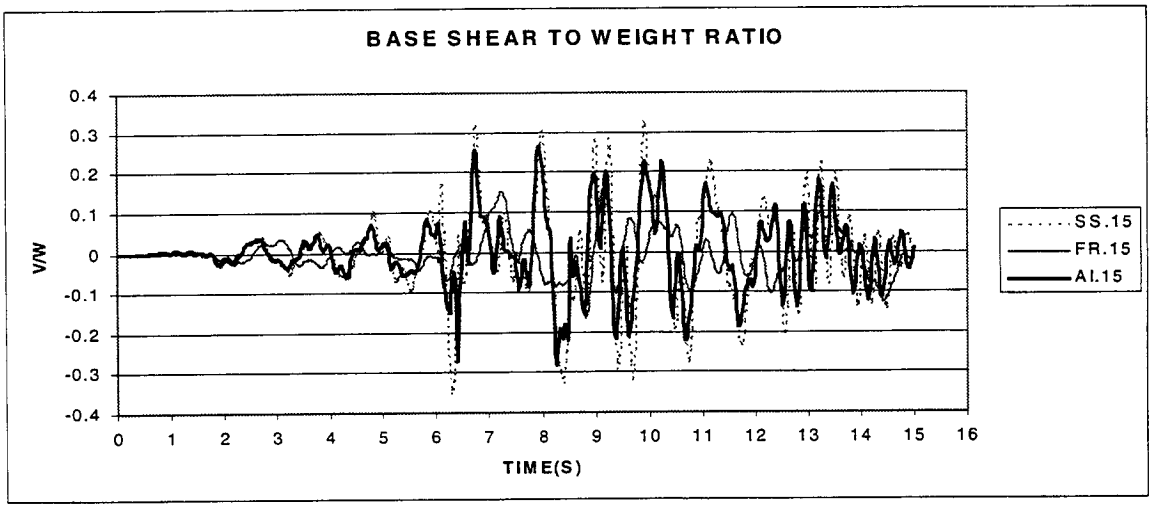

Fig. 6C Base shear to weight ratio for AI.15, SS.15 and FR.15

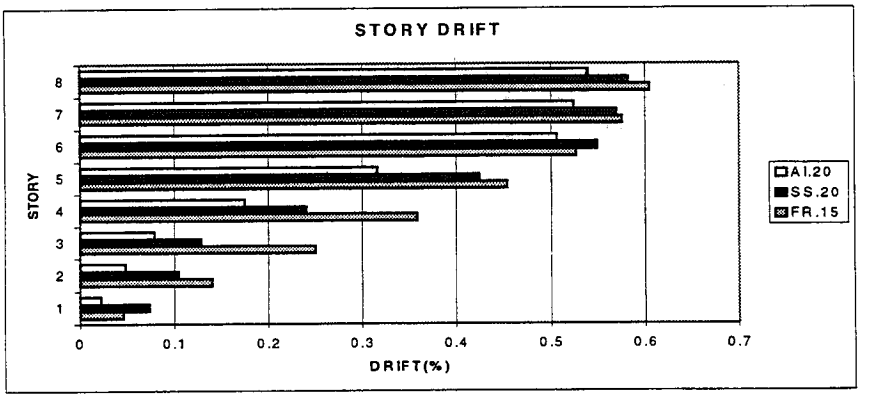

Fig. 7A Maximum story drifts for AI.20, SS.20 and FR.15

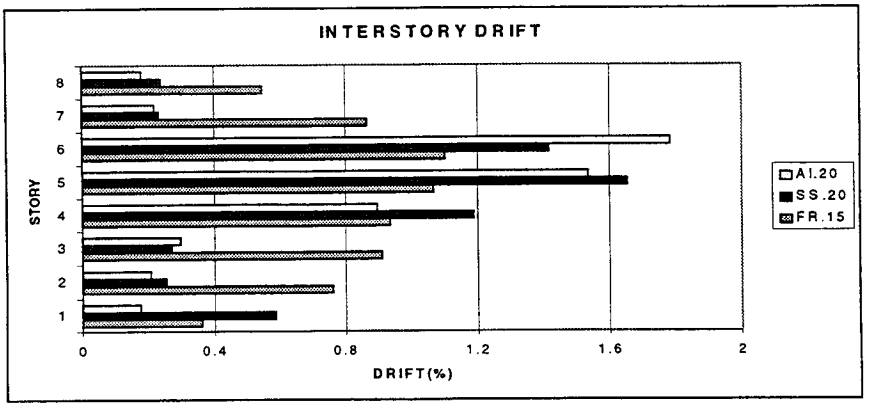

Fig. 7B Maximum interstory drifts for AI.20, SS.20 and FR.15

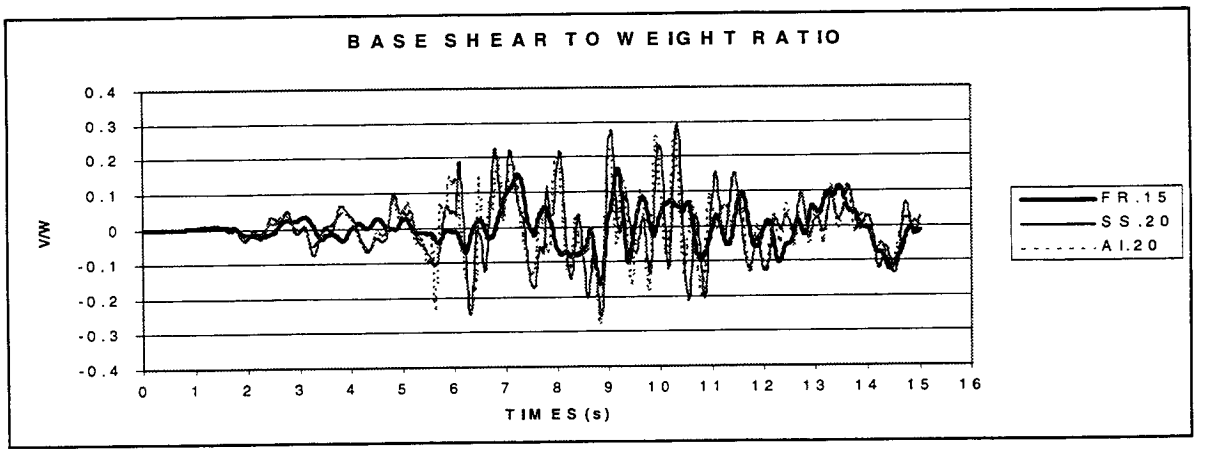

Fig. 7C Base shear to weight ratio for AI.20, SS.20 and FR.15

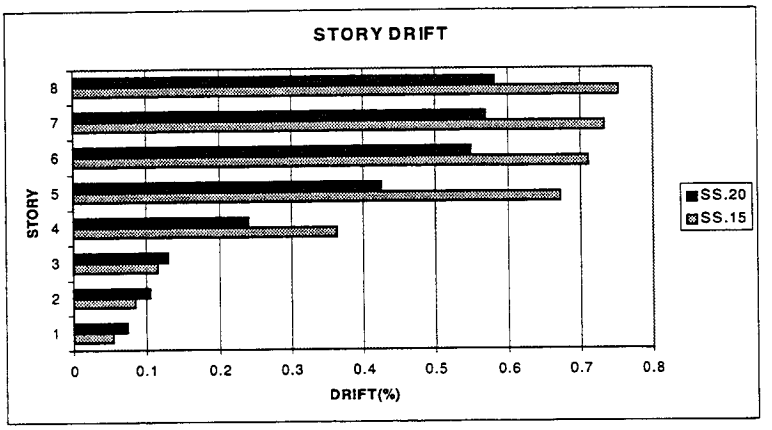

Fig. 8A Maximum story drifts for SS.15 and SS.20

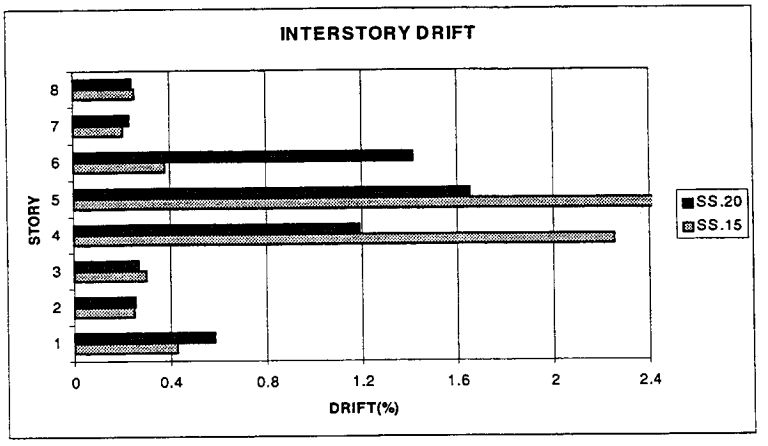

Fig. 8B Maximum interstory drifts for SS.15 and SS.20

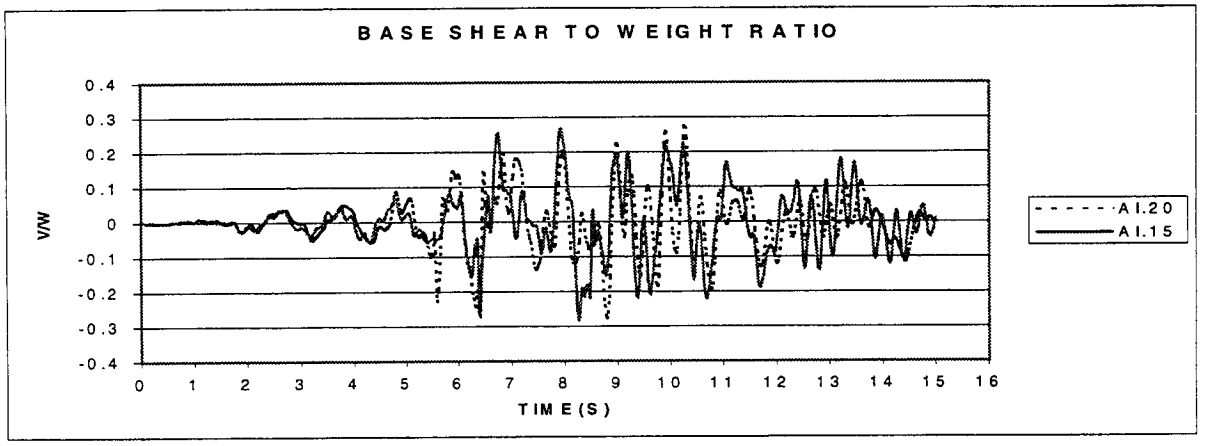

Fig. 8C Base shear to weight ratio for SS.15 and SS.20

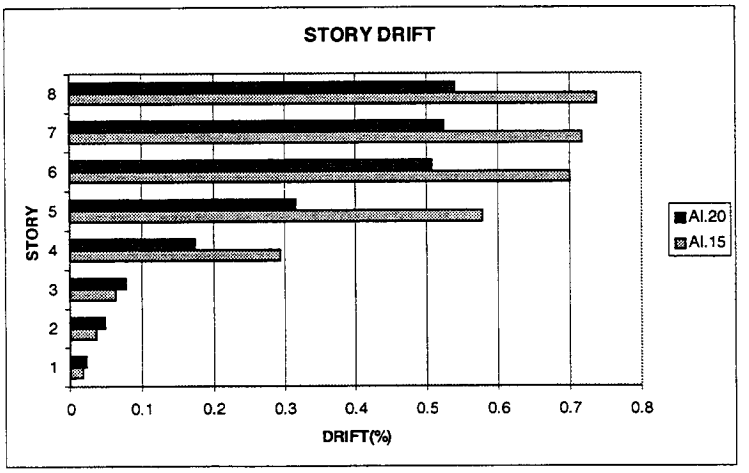

Fig. 9A Maximum story drifts for AI.15 and AI.20

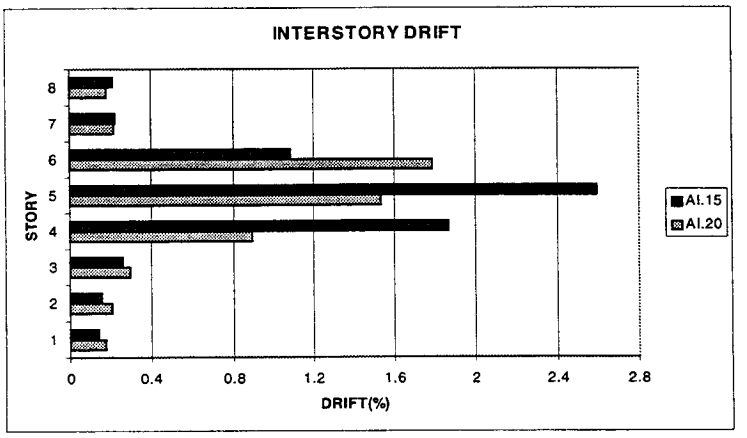

Fig. 9B Maximum interstory drifts for AI.15 and AI.20

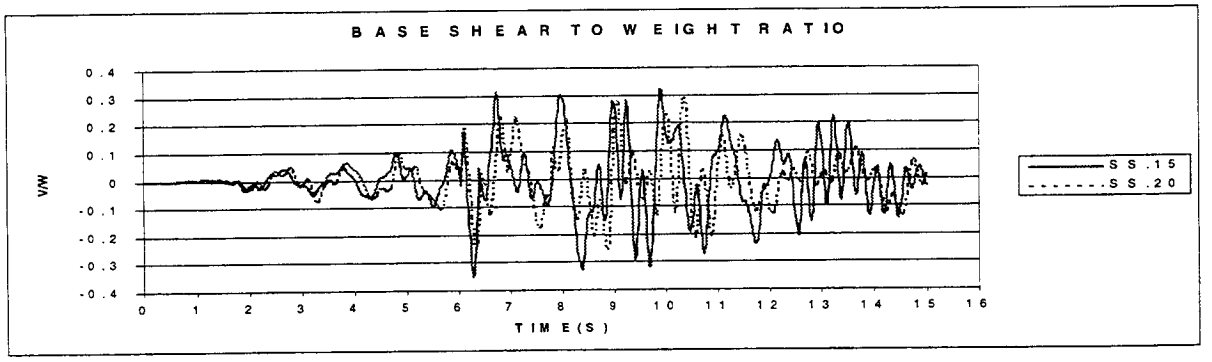

Fig. 9C Base shear to weight ratio for AI.15 and AI.20

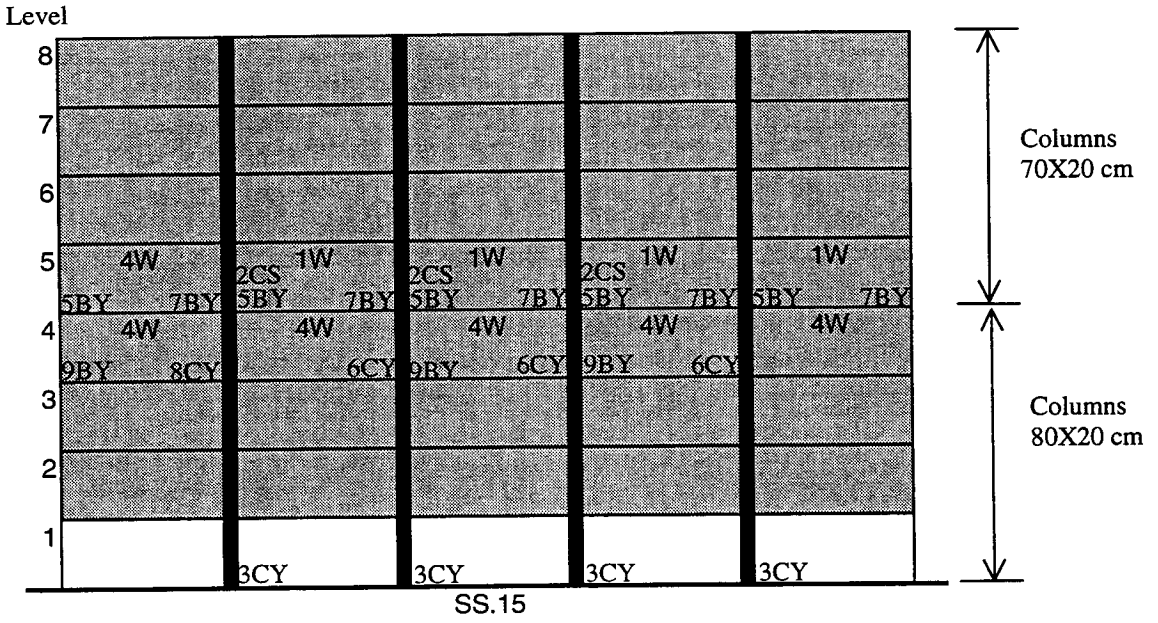

Fig. 10 Failure sequence for SS.15

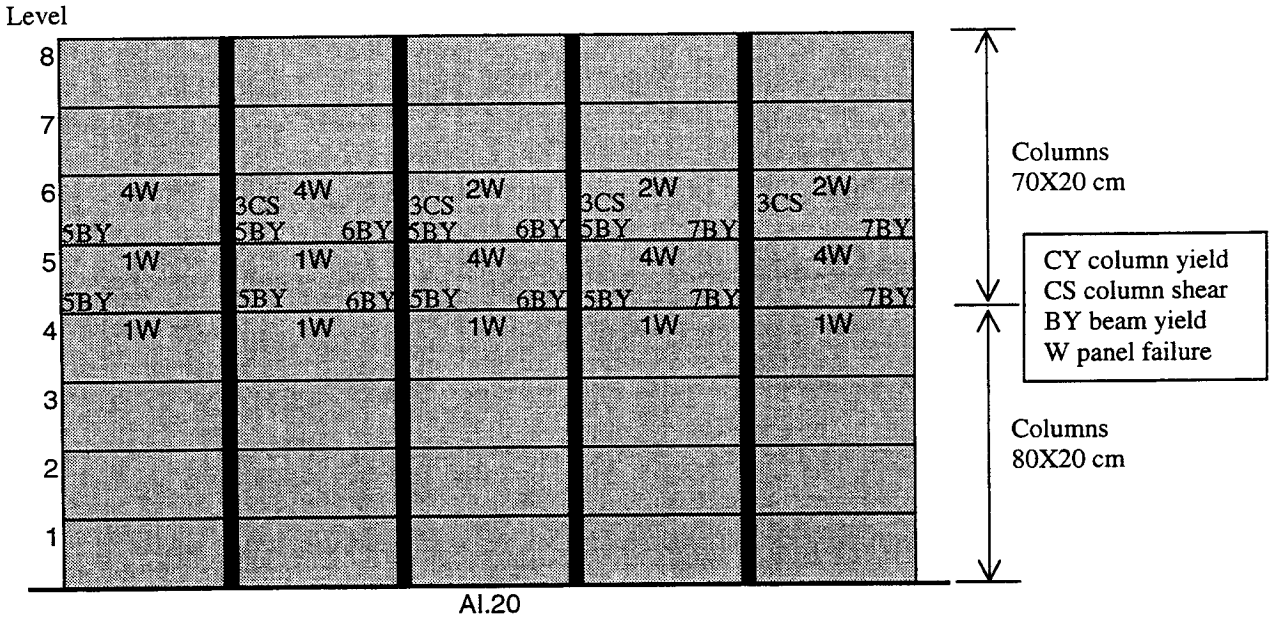

Fig. 11 Failure sequence for AI.20

Conclusion

Regardless of the sophistication of any analysis procedure, the results of an analysis can be no better than the quality of the input data. Significant uncertainties in the seismic input and the strength and deformation capacities of the various elements comprising the lateral load-resisting system continue to be vexing problems. For a given model, results may be very sensitive to parameters used for the section properties and material characteristics. A good understanding of the structural behavior and the effect of different parameters is essential in conducting a performance study of a building. The analytical results can be improved by applying engineering judgment, but field data are invaluable for calibrating analytical models and tools.

Over the past 25 years, several nonlinear time-history analysis programs have been developed. However, they remain as research tools rather than routine design tools. There is an urgent need for programs capable of 3D nonlinear analysis, larger inventory of element models, and friendly user interfaces for use in practice.

References

1. Kanaan, A. E., and G. H. Powell. 1973. *DRAIN2D: A General Purpose Program for Dynamic Analysis of Inelastic Plane Structures.* Berkeley, Calif.: University of California. Reports No. EERC 73-06 and EERC 73-22. April (Revised September 1973 and August 1975).
2. Pincheira, J. A., and J. O. Jirsa. 1992. *Seismic strengthening of reinforced concrete frames using post-tensioned bracing system.* Austin, Texas: the University of Texas. PMFSEL Report No. 92-3. December.
3. Li, Y. R., and J. O. Jirsa. 1996. *Nonlinear time history and push-over analyses for seismic design evaluation.* Ph.D. Dissertation. Austin, Texas: the University of Texas. December. 1996.

DYNAMIC RESPONSE OF TORSIONALLY UNBALANCED RC BUILDING STRUCTURES

Yoshiaki NAKANO and Koichi KUSUNOKI[1]

Yasumichi HINO[2]

ABSTRACT

In a retrofit design, a well-balanced placement of retrofit elements in a building is most essential to ensure sound seismic performance during earthquakes. For this purpose the Japanese *Guidelines for Seismic Evaluation and Retrofit* regulate that the indices representing the unbalanced distribution of lateral load-resisting members in the plan and elevation of a structure be smaller than certain criteria. However, in the case of retrofitting an RC building with steel-framed braces, their unbalanced distribution is often considered a minor problem due to stiffness lower than RC walls.

To investigate the effects of an unbalanced distribution of high-strength, low-stiffness members, torsional response analyses of RC building structures retrofitted with steel-framed braces are carried out using simplified model structures. The results show that the response is highly dependent on the unbalanced distribution of the lateral load-resisting retrofit elements rather than on their elastic stiffness. The authors also discuss the relation between the torsional response of the model structure and indices representing the unbalanced distribution of lateral load-resisting members, and conclude that an index proposed in this paper is an appropriate a candidate to estimate the maximum torsional angle during seismic excitations.

1. INTRODUCTION

In retrofitting an existing reinforced concrete (RC) building, the scheme to infill new RC walls into existing bare frames (Fig. 1(a)) has been the most conventionally applied in Japan since numerous practical experiences as well as experimental and analytical research were extensively made on this technique. Although it has been one of the most reliable strategies to retrofit a seismically vulnerable RC building, *infilling* often causes less flexibility in architectural and environmental design, and/or the increase in building weight sometimes leads to costly redesign of foundation. Steel-framed braces (Fig. 1(b)), therefore, have been more widely applied recently in Japan, particularly after the 1995 Kobe earthquake, to overcome shortcomings resulting from the conventional RC walls mentioned above.

[1] *Institute of Industrial Science, University of Tokyo, Tokyo, Japan*
Email: iisnak@cc.iis.u-tokyo.ac.jp / kusu@cc.iis.u-tokyo.ac.jp

[2] *National Institute of Industrial Safety, Ministry of Labor, Tokyo, Japan*
Email: hino@res.anken.go.jp

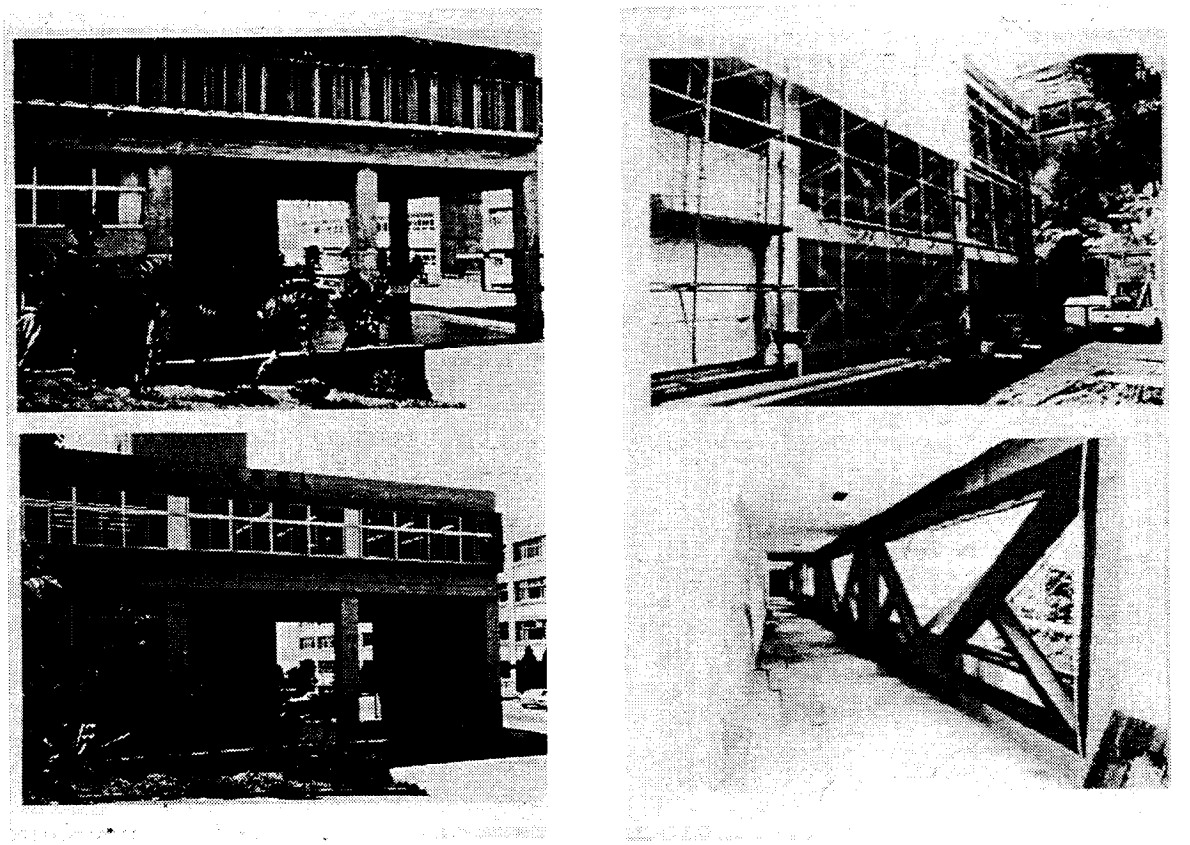

(a) Retrofit with RC walls (on the rightmost frame) (b) Retrofit with steel-framed braces

Fig. 1: Typical retrofit schemes for RC building structures in Japan

In the retrofit design, a well-balanced placement of retrofit elements in a building is most essential to ensure sound seismic performance during earthquakes. For this purpose, the *Guidelines* (JBDPA, 1990a and b) regulate that indices representing the unbalanced distribution of laterally resisting members in the plan and elevation of a structure be smaller than certain criteria. However, in the case of retrofitting an RC building with steel-framed braces, their unbalanced distribution is often considered a minor problem mainly because (1) the indices representing the unbalanced distribution of the lateral load-resisting members are calculated based on their elastic stiffness rather than on their lateral resistance, (2) the elastic stiffness of a steel-framed brace is much lower than an RC wall even if these braces are designed to have the same lateral resistance, and (3) the indices based on the elastic stiffness of a steel-framed brace are therefore often smaller than the criteria in the *Guidelines* and the unbalanced distribution is neglected in the retrofit design. However, the unbalanced distribution of lateral resistance may cause an unfavorable torsional response in a building retrofitted using high-strength but low-stiffness elements, such as steel-framed braces, when the building is subjected to a major earthquake and responds beyond the elastic range.

To investigate the effects of the unbalanced distribution of high-strength, low-stiffness members, torsional response analyses of simplified model structures retrofitted with steel-framed braces are carried out. This paper will mainly discuss the relation between the torsional response and the unbalanced distribution of lateral resistance in plan.

2. BASIC ASSUMPTIONS

2.1 Model Structures

In the numerical investigation herein, an idealized single-story building model that represents a low-rise RC building is employed as the original bare frame structure. The bare frame structure is assumed to have 3 bays in the X-direction and 2 in the Y, each span length being 4.5 m and 6.0 m, respectively. The model consists of a rigid rectangular floor slab supported on 12 lateral load resisting columns having a cross section of 60 x 60 cm. The mass is assumed to be uniformly distributed across the slab. Three sets of yield strength V_{yo} of the bare frame, i. e., $0.3W$ (30% of the total building weight W), $0.4W$, and $0.5W$ are considered to simulate a typical RC building designed in accordance with dated seismic codes in Japan.

To investigate the effects of unbalanced distribution of stiffness and strength on the torsional response of retrofitted structures, which may be dependent on the location and the amount of retrofit elements, the following parameters as shown in Table 1 are considered.

*(1) **Retrofit schemes***: Even when a frame retrofitted with steel-framed braces (referred to as SFB) is designed to have the lateral resistance equal to a frame retrofitted with post-installed RC walls (referred to as RCW), the stiffness of SFB is generally much lower than that of RCW. To investigate the effects of the fundamental properties of the retrofit elements, RCW, which has high strength and *high stiffness,* and SFB, which has high strength but *low stiffness*, are considered as the retrofit schemes investigated herein.

*(2) **Location of retrofit element***: To simulate the torsional response of a retrofitted structure, a monosymmetric and hence torsionally unbalanced (referred to as TU) building model, whose distributions of stiffness and strength are assumed to be symmetric about the transverse Y-axis but asymmetric about the longitudinal X-axis as shown in Figure 2(a), is employed. In addition, a fully symmetric and hence torsionally balanced (referred to as TB) model structure as shown in Figure 2(b) is investigated to compare with the performance of TU structural model.

*(3) **Strength increment due to retrofit***: The lateral strength increment ΔV_y due to retrofit is assumed to vary from $0.1W$ through $0.4W$ at an increment of $0.1W$, where W signifies the total building weight.

Table 1: Parameters for numerical analyses

	Vyo											
	0.3*W*				0.4*W*				0.5*W*			
ΔVy	0.1*W*	0.2*W*	0.3*W*	0.4*W*	0.1*W*	0.2*W*	0.3*W*	0.4*W*	0.1*W*	0.2*W*	0.3*W*	0.4*W*
ΔKe/Ke **	0.15	0.30	0.45	0.60	0.15	0.30	0.45	0.60	0.15	0.30	0.45	0.60
	0.45	0.90	1.35	1.80	0.45	0.90	1.35	1.80	0.45	0.90	1.35	1.80
*feκ***	0.04	0.08	0.10	0.12	0.04	0.08	0.10	0.12	0.04	0.08	0.10	0.12
	0.10	0.16	0.19	0.21	0.10	0.16	0.19	0.21	0.10	0.16	0.19	0.21
*T1***	0.46	0.45	0.44	0.43	0.46	0.45	0.44	0.43	0.46	0.45	0.44	0.43
	0.44	0.43	0.43	0.42	0.44	0.43	0.43	0.42	0.44	0.43	0.43	0.42
*T2***	0.34	0.32	0.30	0.28	0.34	0.32	0.30	0.28	0.34	0.32	0.30	0.28
	0.30	0.26	0.23	0.20	0.30	0.26	0.23	0.20	0.30	0.26	0.23	0.20

Note ΔVy : yield strength increment due to retrofit

$\Delta Ke/Ke$: (elastic stiffness increment due to retrofit) / (overall elastic stiffness of an original bare frame)

feK : $= e_K / \sqrt{B^2 + L^2}$, stiffness unbalance index defined in the Guideline [JBDPA, 1990a]

where eK : eccentricity, i.e., distance between the center of mass and the center of stiffness

B, L : width and length of a building (see also Eqs. (9) and (10) defined later)

$T1, T2$: natural period (sec.) for the first and second mode, respectively

** upper row : SFB lower row: RCW

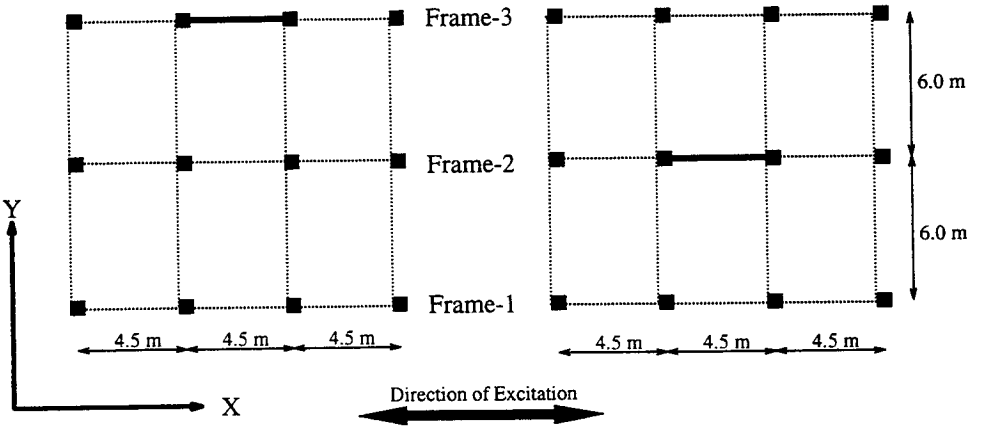

(a) Retrofitted in the exterior frame (Torsionally unbalanced (TU) structure)

(b) Retrofitted in the central frame (Torsionally balanced (TB) structure)

Fig. 2: Model structures

Considering Japanese retrofit design practices (JBDPA 1900b) and assuming that the increase in elastic stiffness of RCW is three times that of SFB, the elastic stiffness increment due to

retrofit ΔKe is determined in the following manner. When the yield strength increment ΔV_y due to retrofit is $0.1W$, ΔKe is 45% of overall stiffness of the bare frame structure for RCW, while 15% for SFB. For both retrofit elements, the stiffness increment ΔKe is assumed to be proportional to their strength increment ΔV_y.

2.2 Numerical Solution for Torsional Response Analyses

Assuming an idealized single-story structure and a rigid floor system in both the bare and retrofitted model structures described above, the fundamental equation of motion for numerical integration considering both translational and torsional response can be expressed in Eqs. (1) through (3). To simulate inelastic behaviors of model structures, the Takeda hysteretic model shown in Figure 3 is employed for both columns and retrofit elements. The yield displacement is determined from the drift angle at yielding as shown in Figure 3 and the equivalent building height, assuming that (1) the model structure represents a four-story building, (2) each story is 3.5 m high, and (3) the equivalent building height is 3/4 of the overall building height.

To simplify the subsequent discussions, a unidirectional earthquake ground motion is considered in the computation as shown in Figure 2, and the Hachinohe EW component recorded during 1968 Tokachi-oki Earthquake is used for $\ddot{x}_0$, scaling the peak ground acceleration to 0.4 g, while $\ddot{y}_0$ and $\ddot{\theta}_0$ is assumed 0.

$$m(\ddot{x}+\ddot{x}_0)+\sum_i {}_iC_x(\dot{x}+{}_il_y\dot{\theta})+\sum_i {}_iK_x(x+{}_il_y\theta)=0 \tag{1}$$

$$m(\ddot{y}+\ddot{y}_0)+\sum_i {}_iC_y(\dot{y}-{}_il_x\dot{\theta})+\sum_i {}_iK_y(y-{}_il_x\theta)=0 \tag{2}$$

$$I(\ddot{\theta}+\ddot{\theta}_0)+\sum_i {}_iC_x(\dot{x}+{}_il_y\dot{\theta})\cdot{}_il_y-\sum_i {}_iC_y(y-{}_il_x\theta)\cdot{}_il_x+\sum_i {}_iK_x(x+{}_il_y\theta)\cdot{}_il_y-\sum_i {}_iK_y(y-{}_il_x\theta)\cdot{}_il_x=0 \tag{3}$$

Where, m, I : mass and moment of inertia of model structure, respectively

x, y : response displacements at the center of mass (CM) in X- and Y-direction, respectively

θ : torsional response angle

${}_iCx$, ${}_iCy$: damping coefficient

${}_iKx$, ${}_iKy$: instantaneous stiffness of member i

$_{i}l_x$, $_{i}l_y$: distance between member i and CM

x_i, y_i : response displacement of member i ($x_i = x + {}_{i}l_x\,\theta$, $y_i = y - {}_{i}l_y\,\theta$)

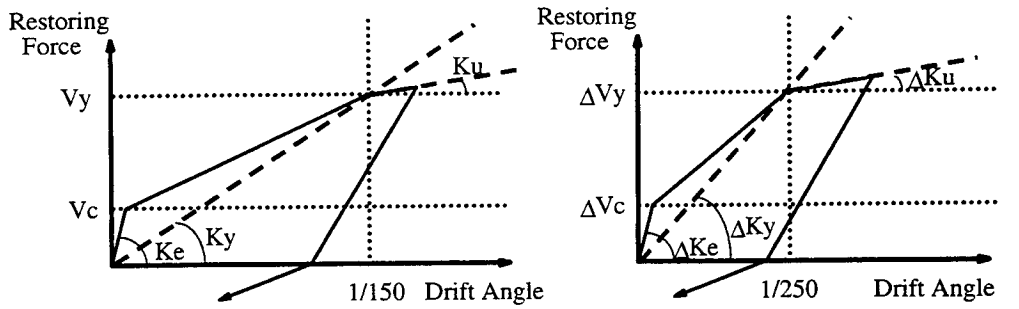

(a) Column **(b) Retrofit element (SFB and RCW)**

Note: $Vy = 3\,Vc$ $\Delta Vy = 3\,\Delta Vc$

$Ke = 4\,Ky$ ΔKe can be defined from the assumptions shown in Table 1

$Ku = Ke / 1000$ $\Delta Ku = \Delta Ke / 1000$

Drift angle at yielding is assumed 1/150 for columns and 1/250 for retrofit elements.

Fig. 3: Hysteresis models employed in the numerical analyses

3. PERFORMANCE OF RETROFITTED STRUCTURES

Based on the nonlinear response analyses, effects of (1) unbalanced distribution of stiffness and lateral resistance and (2) yield strength of a retrofitted structure on the torsional response, and the relation between torsional response and torsional moments acting on the structure are investigated in the subsequent sections.

3.1 Effects of Unbalanced Distribution of Stiffness and Lateral Resistance

Figures 4(a) and (b) show the relation between column ductility factors μ and strength increment ΔV_y of structures having original lateral strength V_{yo} equal to $0.3W$. In the figures, μ is defined as the ratio of response displacement in each frame to yield displacement when frame-1 reaches the maximum displacement. As can be seen from the figures, the ductility factors μ of both retrofit types of RCW (Fig. 4 (a)) and SFB (Fig. 4 (b)) having torsional unbalance generally decrease with increase in the lateral strength increment ΔV_y. The ductility factor of TU (torsionally unbalanced) structure is larger than that of the TB (torsionally balanced) structure in the nonretrofitted frame-1 while generally smaller in the retrofitted frame-3. However, the torsional response increases and hence the discrepancy of ductility factors μ between frames-1 and -3 becomes more significant with an increase in ΔV_y. It should be also noted that the discrepancy of ductility factors between frames-1 and -3,

which corresponds to the torsional response, is approximately the same for both retrofit types with identical ΔV_y.

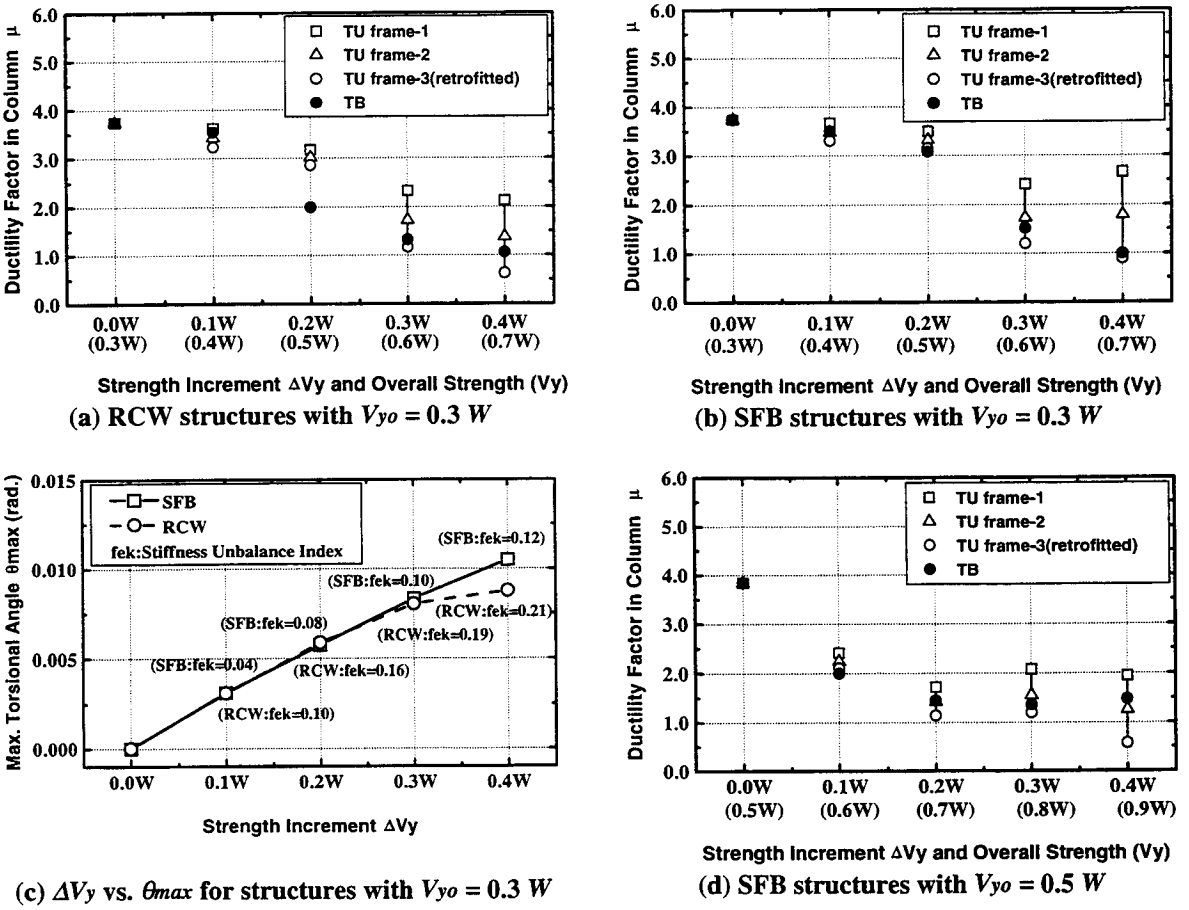

Fig. 4: Relations among strength increment ΔV_y, column ductility factor μ and maximum torsional angle θ_{max}

Figure 4(c) summarizes the relation between the strength increment ΔV_y and maximum torsional angle θ_{max}. Although RCW is assumed to have a stiffness increment ΔKe three times as much as SFB, the maximum torsional angle θ_{max} is almost identical for both retrofit types when they have identical ΔV_y. This figure clearly indicates that the strength increment rather than the elastic stiffness increment provided in the exterior frame-3 governs the torsional response of retrofitted buildings. This result demonstrates that the structural design should be more carefully done considering the unbalanced distribution of *lateral resistance* since the torsional response may not be neglected in the presence of the unbalanced distribution of lateral resistance, even when a building is retrofitted with SFB and hence the unbalanced distribution of *stiffness* is insignificant. This also suggests that indices representing structural unbalance, including the inelastic range and their criteria, need to

be developed considering unbalanced lateral resistance to ensure sound performance during a major earthquake

3.2 Effects of Yield Strength of Overall Structure

To investigate the effects of yield strength of overall structure after retrofit, torsional response of structures having different strength are compared. Figure 4(d) shows the relation between column ductility factors μ and strength increment ΔV_y of an SFB structure having $V_{yo} = 0.5W$. As can be found from Figures 4(b) and (d), column ductility factors μ for a structure with $V_{yo} = 0.5W$ are generally smaller than those for a structure with $V_{yo} = 0.3W$. It should be noted, however, that the discrepancy of ductility factors between frames-1 and -3 is similar in both structures when they have the same ΔV_y. This result implies that the torsional response is dependent on ΔV_y more significantly than V_y. Figure 5 summarizes the relation among the yield strength of overall structure V_y after retrofit, strength increment ΔV_y, and the maximum torsional angle θ_{max} of an SFB-TU structure. This figure also shows that θ_{max} is dependent on ΔV_y more significantly than V_y provided that all frames including retrofitted frame-3 respond beyond yielding to the input excitation.

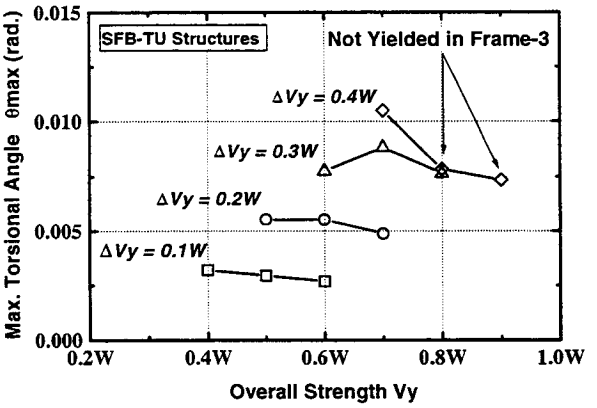

Fig. 5: Relations among V_y, ΔV_y, and θ_{max} of SFB-TU structures

3.3 Relation between Torsional Response and Torsional Moment Acting on the Structure

To understand what affects the torsional response of retrofitted structures most significantly, the relation between the torsional moment and the torsional response angle θ is investigated subsequently. Neglecting damping forces (i.e., $C_x = C_y = 0$) and the torsional component of the input motion (i.e., $\ddot{\theta}_0 = 0$) to simplify the subsequent discussions, Eq. (3) can be rewritten as Eq. (4). Considering the response shear forces in each frame and $y = 0$ for a monosymmetric structure subjected to unidirectional input motions in the X-direction, as shown in Eqs. (5) and (6), Eq. (3) leads to Eq. (7). Eq. (7) implies that the torsional response may be highly depending on the torsional moment ($\Sigma\, {}_iV_x\, {}_il_y$) acting on the structure.

$$I\ddot{\theta} + \sum_i {}_iK_x(x + {}_il_y \cdot \theta) \cdot {}_il_y - \sum_i {}_iK_y(y - {}_il_x \cdot \theta) \cdot {}_il_x = 0 \tag{4}$$

$$\sum_i {}_iK_x(x + {}_il_y \cdot \theta) \cdot {}_il_y = \sum_i {}_iV_x \cdot {}_il_y \tag{5}$$

$$\sum_i {}_iK_y(y - {}_il_x \cdot \theta) \cdot {}_il_x = -\sum_i {}_iK_y \cdot {}_il_x^2 \cdot \theta = -K_{\theta y} \cdot \theta \tag{6}$$

$$I\ddot{\theta} + K_{\theta y} \cdot \theta = -\sum_i {}_iV_x \cdot {}_il_y \tag{7}$$

where ${}_iV_x$: response shear force of member i

Figure 6 shows the time history of the torsional moment ($\Sigma\, {}_iV_x\, {}_il_y$) and the torsional response angle θ normalized by M_E and θ_{max}, respectively, for RCW-TU and SFB-TU structures having $V_{yo} = 0.3W$ and $\Delta V_y = 0.3W$. In the figure, M_E is defined as **Eq. (8)** assuming that each frame reaches the yielding strength during the excitations.

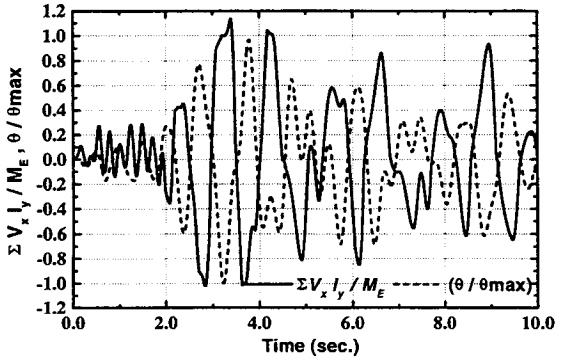

(a) RCW-TU structure

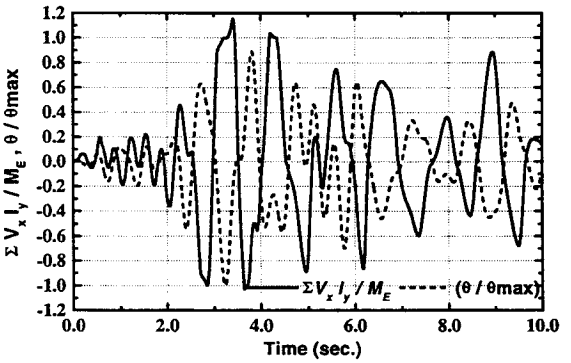

(b) SFB-TU structure

Fig. 6: Time history of ($\Sigma\, {}_iV_x\, {}_il_y / M_E$) and ($\theta / \theta_{max}$) for TU structures with V_{yo}=0.3W and ΔV_y=0.3W

$$M_E = \sum_i {}_iV_{yx} \cdot {}_i l_y \tag{8}$$

where ${}_iV_{yx}$: yield strength of member i

This figure shows that the ($\Sigma\ {}_iV_x\ {}_il_y$ / M_E) and (θ / θ_{max}) mutually correlated over the response duration for both RCW-TU and SFB-TU structures. The maximum values of ($\Sigma\ {}_iV_x\ {}_il_y$ / M_E) are approximately 1.0 for both structures because they reach the yielding strength in each frame at the same time. This result implies that the maximum value of the torsional moment $(\Sigma\ {}_iV_x\ {}_il_y)_{max}$ can be approximated by M_E defined in Eq. (8), providing that each frame of a structure reaches the yielding strength simultaneously.

Figure 7 summarizes the relations among the maximum value of torsional moment acting on the structure $(\Sigma\ {}_iV_x\ {}_il_y)_{max}$, M_E, and the maximum torsional angle θ_{max} for structures having $V_{yo} = 0.3W$. As can be seen from the figure, θ_{max} is roughly proportional to $(\Sigma\ {}_iV_x\ {}_il_y)_{max}$ and $(\Sigma\ {}_iV_x\ {}_il_y)_{max}$ can be approximated by M_E.

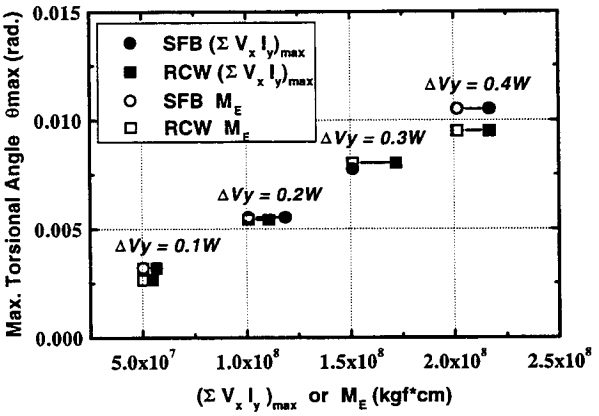

Fig. 7: Relations among $(\Sigma\ {}_iV_x\ {}_il_y)_{max}$, M_E, and θ_{max} for TU structures with $V_{yo} = 0.3W$

4. ESTIMATION OF TORSIONAL RESPONSE BY ECCENTRICITY INDICES

To obtain a better index to estimate the torsional response of TU structures, the correlation of the maximum torsional angle θ_{max} and the following three different indices, fe_K, fev', and fev are investigated.

As stated earlier, an index to represent the structural unbalance of laterally resisting members is generally based on their elastic stiffness in the conventional structural design procedures. Eq. (9) shows an example index f_{eK} based on the elastic stiffness [JBDPA, 1990a]. Figure 8(a) shows the relation between f_{eK} and θ_{max} for structures investigated in this study. As can easily be understood from the previous discussions, f_{eK} does not correlate well with θ_{max}.

$$f_{eK} = e_K \Big/ \sqrt{a^2 + b^2} \tag{9}$$

$$e_K = \sum_i {}_iK_x \cdot {}_il_y \Big/ \sum_i {}_iK_x \tag{10}$$

$$f_{eV}' = e_V \Big/ \sqrt{a^2 + b^2} \tag{11}$$

$$e_V = \sum_i {}_iV_{yx} \cdot {}_il_y \Big/ \sum_i {}_iV_{yx} \left(= M_E / V_y\right) \tag{12}$$

$$\begin{aligned} f_{eV} &= \alpha \cdot \left(\sum_i {}_iV_x \cdot {}_il_y\right)_{\max} \approx \alpha \cdot \sum_i {}_iV_{yx} \cdot {}_il_y \\ &= \alpha \cdot \left(\sum_i {}_iV_{yx} \cdot {}_il_y \Big/ \sum_i {}_iV_{yx} \right) \cdot \sum_i {}_iV_{yx} = \alpha \cdot W \cdot e_V \cdot \sum_i {}_iC_{yx} \\ &= \alpha \cdot e_V \cdot C_B \cdot W \end{aligned} \tag{13}$$

$$f_{eV} = \left(e_V \Big/ \sqrt{a^2 + b^2} \right) \cdot C_B \tag{14}$$

where e_K, e_V : eccentricity based on the *stiffness* and *strength*, respectively

a, b : building length and width

${}_iV_{yx}$, V_y : yield strength of member i and overall structure ($= \Sigma\, {}_iV_{yx}$), respectively

${}_iC_{yx}$, C_B : shear capacity coefficient of member i ($= {}_iV_{yx} / W$) and base shear coefficient ($= \Sigma\, {}_iC_{yx} = V_y / W$)

f_{eV}' in Eq. (11) is an index to incorporate the effects of the unbalanced distribution of lateral resistance, where e_K in Eq. (9) is simply replaced by e_V in Eq. (12) to define an index with analogous form to Eq. (9). Figure 8(b) shows the relation between f_{eV}' and θ_{max}. Although the correlation is better than the results in Figure 8(a), different f_{eV}' indices give similar θ_{max} and f_{eV}' is still an unsatisfactory index to estimate θ_{max}. Bearing in mind that θ_{max} is dependent on M_E as shown in Figure 7 but independent of V_y as shown in Figure 5, and that e_V in Eq. (12) can be rewritten as (M_E / V_y), one might easily understand that f_{eV}', which is a function of M_E and V_y, may not be the best index to estimate θ_{max}.

Considering the above and the results obtained from the numerical simulations as

discussed in section 3.3, i.e., "*(a) θ_{max} is roughly proportional to $(\Sigma\, {}_iV_x\, {}_ily)_{max}$,* and *(b) $(\Sigma\, {}_iV_x\, {}_ily)_{max}$ can be approximated by M_E defined in Eq. (8), if the structure responds beyond yielding in all frames,*" a new index *fev* is proposed as shown in Eqs. (13) and (14). Based on the result (a) described above, *fev* is assumed to be a linear function of $(\Sigma\, {}_iV_x\, {}_ily)_{max}$. Considering the second result (b) and $\Sigma\, {}_iV_{yx} = C_B\, W$, *fev* can be expressed by Eq. (13). Setting α in Eq. (13) equal to $1/(\sqrt{a^2+b^2}\, W)$ to obtain an analogous form with Eq. (9), *fev* can be rewritten as Eq. (14).

Figure 8(c) shows the relation between *fev* and θ_{max}. As can be found in the figure, *fev* correlates well with θ_{max} except for several cases where the retrofitted frame-3 does not yield. The reason for the above exceptions is because these cases do not meet the second result (b) described above and hence M_E overestimates $(\Sigma\, {}_iV_x\, {}_ily)_{max}$, resulting in the overestimation of *fev*. It can be concluded, however, that the proposed index *fev* can be a candidate to estimate θ_{max}, provided that all frames in a structure respond beyond the elastic range due to torsional response under seismic excitations.

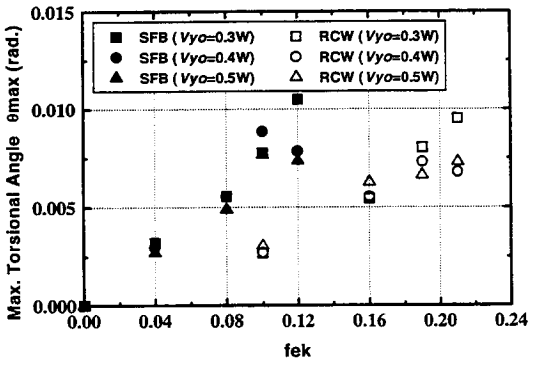

(a) *fek* - θ_{max} relation

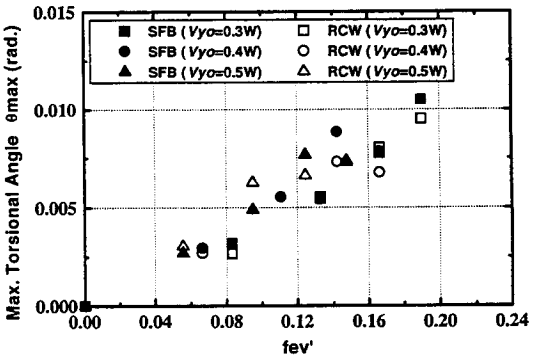

(b) *fev'* - θ_{max} relation

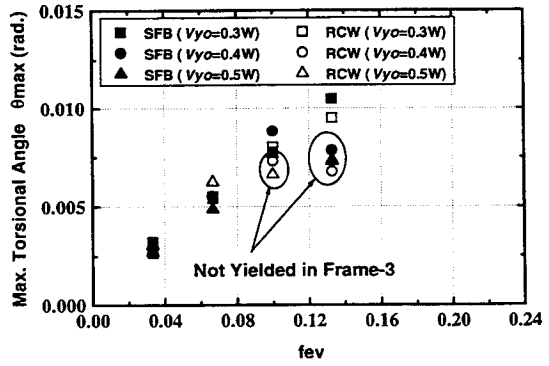

(c) *fev* - θ_{max} relation

Fig. 8: Relations among different indices representing structural unbalance and θ_{max}

5. CONCLUDING REMARKS

To investigate the effects of the unbalanced distribution of high-strength, low-stiffness members, torsional response analyses of RC building structures retrofitted with steel-framed braces were carried out using simplified model structures, and their response were compared with those retrofitted with RC walls. Although the investigated cases are limited, the major findings obtained in this study can be summarized as follows.

(1) With an increase in the strength increment ΔV_y of retrofit elements provided in frame-3, maximum response displacements of TU structures generally decreased. Because of torsional response, however, the discrepancy of the ductility factors between frames-1 and -3 became more significant.

(2) The major factor which affected the torsional response of TU structures was the unbalanced distribution of lateral resistance rather than that of elastic stiffness. This result suggested that indices representing structural unbalance including the inelastic range and their criteria need to be developed considering unbalanced lateral resistance to ensure sound performance during a major earthquake.

(3) The structural unbalance index f_{ev} based on the lateral resistance proposed in this paper could be a candidate to give a satisfactory estimation of the maximum torsional angle θ_{max} during a major earthquake, provided that all frames yielded during excitation.

REFERENCES

JBDPA/The Japan Building Disaster Prevention Association.1990a. *Guidelines for seismic capacity evaluation of existing reinforced concrete buildings.* (In Japanese.)

JBDPA/The Japan Building Disaster Prevention Association. 1990b. *Guidelines for seismic retrofit design of existing reinforced concrete buildings.* (In Japanese.)

MODELING AND SOFTWARE ISSUES FOR PUSHOVER ANALYSIS OF RC STRUCTURES

WIGHT, J. K.*, BURAK, B.†, CANBOLAT, B. A.‡, and LIANG, X.§

ABSTRACT

The implementation of performance-based design procedures for the seismic- resistant design of reinforced concrete (RC) structures requires the use of accurate and consistent analysis software. The software should be able to incorporate a variety of RC members, reinforcing details, material models and failure modes. In addition to developing a global force vs. deformation relation for the structure, the software should store information on the inelastic behavior of individual members. This paper surveys software currently available for pushover analysis of RC structures and compares their consistency, accuracy, ease of use, and range of output information. The general conclusion is that output from different software packages is not consistent and that proper use of these software packages requires well-educated users.

1. INTRODUCTION

The development of performance-based design (PBD) procedures is one of the most widely discussed topics in the international earthquake engineering community. The primary goal for the implementation of PBD is to have structural engineers make design decisions in terms of displacements (deformations) rather than forces. In order to predict the maximum lateral displacements of a structure and the corresponding deformations of individual members, an analysis tool is required. The one that is commonly selected to achieve these objectives is a pushover curve, i.e., a nonlinear lateral force vs. deformation relation for a structure.

Many software packages are currently available, or under development, for generating pushover curves for a variety of structural types. Important design decisions will be based on the output from such software, so there is a need to access the accuracy and consistency of results from each package. This paper will examine software currently available for the analysis of reinforced concrete (RC) structures. The issues to be explored are ease of use, accuracy, consistency, sensitivity to user input decisions, types of output, and ease of access to that output. Because this study is in only the initial phase, the results reported here are not complete with respect to the range of software examined and the depth of evaluation for each package.

*Professor, Dept. of Civil and Env. Eng., University of Michigan, Ann Arbor, MI 48109-2125, USA. Email: jwight@umich.edu.
†‡§Graduate Research Assistant, Dept. of Civil and Env. Eng., University of Michigan, Ann Arbor, MI 48109-2125, USA.

2. STRUCTURAL TYPES AND SOFTWARE PACKAGES

Two of the RC structures investigated in this study are shown in fig. 1a and b. The structures were selected to provide various types of members and different types of response from a pushover analysis. The first one was a three-story, three-bay slab and column frame (fig. 1a). The properties of a typical frame line were taken from a building that had been designed for only gravity loads, but was being considered for seismic rehabilitation. The second structure was a seven-story, three-bay dual system (fig. 1b) that was tested at the Building Research Institute in Japan as part of a joint U.S.-Japan research program [1]. Before this structure was analyzed it was redesigned to satisfy the seismic design requirements of UBC 97 [2] to enable a comparison between force-based and performance-based design procedures. The third structure, which was a four-story, thirteen-bay beam and column frame, was also being evaluated for seismic rehabilitation. Detailed information for this building cannot be provided in this paper due to some software and time limitations.

The following software packages were selected because of their extensive use and availability to researchers and structural engineers. The first set of software packages examined were IDARC [3] and its updated version IDASS [4]. These packages have been widely used in the U.S. because of the realistic hysteresis characteristics available for modeling RC frame and wall members. For both programs the user inputs the member section properties and appropriate material properties, then the program internally generates the inelastic moment-curvature (M-Φ) relations for use in subsequent analysis of the structure. A sample moment vs. curvature graph from the IDASS preprocessor, for both positive and negative bending of a beam section, is given in fig. 2.

The second software evaluated was DRAIN-2DX [5], which is an updated version of the DRAIN-2D software [6]. DRAIN has been used extensively for nonlinear dynamic analysis of structures, particularly in California. In this study the beam-column element, which has a bilinear plastic hinge region at the member ends, was used to model the slab and column members of structure 1. The user supplies calculated values for the yield moment and rotation, and inputs a postyield strain-hardening slope for the M-Φ relation. For this structure, the fiber member model of DRAIN-2DX was also used, where the member cross section is subdivided into fibers (layers).

The user gives material properties for the steel and concrete fibers, then the program generates M-Φ relations for the inelastic analysis of the structure.

The final software studied was the SAP2000 package [7] that contains an inelastic pushover analysis option. SAP is a widely used analysis/design package with many different elements available for modeling a variety of structural members. Due to time restrictions during this initial portion of the study, SAP2000 was used only for Study Structure 2. To generate member M-θ relations, the user may either use default material and section properties, from which the software calculates the relation, or directly enter calculated yield and ultimate points.

3. RESULTS FROM VARIOUS PUSHOVER ANALYSES

3.1 Study Structure 1

Pushover analysis results for Study Structure 1 will be used to compare IDARC, IDASS and two member models within DRAIN-2DX. Fig. 3 shows the pushover results obtained for an inverted triangular load pattern using IDASS and IDARC. The vertical axis represents the total lateral force as a fraction of the building weight. The horizontal axis represents the average story drift for the structure, i.e., roof displacement/building height. The other two vertical lines in the figure, labeled as BSE1 and BSE2, refer to Basic Safety Earthquakes 1 (10%/50yrs.) and 2(2%/50yrs.), respectively, as defined in the NEHRP Guidelines for the Seismic Rehabilitation of Buildings (FEMA 273) [8]. These displacement (drift) limits were found using the IDASS pushover analysis output and the procedure defined in FEMA 273. IDARC results are terminated at 2% average story drift due to program restrictions. On the other hand, this limit can be set by the user in IDASS, and was taken as 3% drift for this model. A force limit must also be specified, but for a pushover analysis it is normally set to a high value so that the drift limit will govern. Lateral force was applied in the recommended [9] 100 steps. IDASS results are shown for 50 and 100 steps to demonstrate convergence of the solution.

There are some significant differences in the results for IDARC and IDASS in both the elastic and postyield range. IDASS simulates the trilinear behavior of a member's moment-curvature relation, while IDARC uses a bilinear simulation. If in fig. 3 the lateral yield force is taken as

approximately 0.32 times the building weight, the cracked-elastic stiffness of the structure, as represented by IDARC, leads to a lower average building drift at yield than predicted by the IDASS model. The postyield stiffness of the building is higher for the IDARC model, even though a 2% strain-hardening slope was assumed for both programs. Because IDASS is a refinement of IDARC, it will be used as the "correct" solution for comparison with DRAIN-2DX results for Structure 1.

Two pushover curves found using DRAIN-2DX are compared to the IDASS results in fig. 4. The DRAIN member model with a plastic hinge at the member ends (Type 02) assumes a bilinear moment-rotation behavior in the plastic hinging region. One of the DRAIN models used gross section properties (I_g) for the members, and the preyield stiffness of that model matched the uncracked stiffness for the IDASS model; whereas the predicted yield drift is considerably smaller. The second DRAIN model used one-half of the gross moment of inertia ($0.5I_g$) for each member, but the resulting cracked-elastic behavior of the structure was still stiffer than the IDASS model, and thus predicted a smaller yield displacement. Because this slab-column frame structure had low reinforcement percentages, using one-third of the gross moment of inertia may have resulted in a better estimation of the yield drift. The postyield behavior is similar for all three models in fig. 4 because a strain-hardening slope of 2% was used for each model.

The locations of plastic hinging in frame members of Structure 1 were similar for IDARC, IDASS and DRAIN. However, only IDASS and DRAIN give the amount of inelastic rotation in these hinging zones, a value that can be checked against permissible values given in FEMA 273.

Comparisons of different types of member models from the DRAIN-2DX program are given in fig. 5. The results obtained using the Type 02 member model (plastic hinges at member ends, stiffness based on one-half gross moment of inertia) are compared with the results obtained using the fiber member model (Type 15). When describing the member properties for the fiber model, the length for positive and negative bending regions over the length of the member must be specified. Two ranges were selected to evaluate the sensitivity of this length on results. One model limited negative plastic-hinge behavior to end regions equal to 5% of the member length (model 05.90.05), while the other model set this length at 20% (model 20.60.20).

The results obtained with both fiber models are significantly stiffer and stronger that those obtained with either IDASS or DRAIN with member model Type 02. The reason(s) for the higher stiffness and strength in the two fiber models is not apparent at this time. The two fiber models have similar yield points, but model 20.60.20 has a larger postyield stiffness than model 05.90.05. The fiber models simulate cracking of the concrete, and thus exhibit trilinear behavior. However, this behavior is more apparent in model 20.60.20 than in model 05.90.05.

3.2 Study Structure 2

Study Structure 2 (fig. 1b) was a modified version of the large-scale RC structure tested at the Building Research Institute in 1981. Although the structural dimensions were close to full scale, the reinforcement percentages were kept relatively low so that the lateral strength of the test structure would not exceed the testing capacity of the laboratory. For this investigation the design of this building was modified to satisfy the design requirements of UBC 97. It was assumed that the structure was located on a stiff soil site in seismic zone 4. SAP2000 was used to analyze and assist in the redesign of the building. After the structure was redesigned, it was checked using the Nonlinear Static Procedure (pushover analysis) described in FEMA 273. To make this analysis approximately equivalent to the UBC 97 criteria, it was checked for the Life Safety Performance Level under the action of BSE-1.

The nonlinear pushover results obtained using an inverted triangular loading pattern for the redesigned structure are given in fig. 6. As in the previous section, the vertical axis represents the ratio of the applied lateral force to the weight of the structure and the horizontal axis represents the average story drift for the structure. The results are given for members modeled using the IDARC and IDASS programs. Both programs have wall elements, however the one in IDARC is essentially an equivalent frame element. As discussed in the pervious section, the IDARC pushover analysis limits the maximum average story drift to 2%. Also, IDARC does not give output for the magnitude of inelastic rotations in plastic hinging regions. For those reasons IDASS was the preferred software for this structure.

The average story drift limit for the IDASS pushover analysis of this structure was set to 4%. From the output, and following the procedure given in FEMA 273, the target displacement for BSE-1 was found to be an average story drift of approximately 0.65%. This value is approximately three times the average drift at "yield" for this structure. When the frame member plastic-hinge rotations were checked against the FEMA 273 limits, they were found to be acceptable. The plastic hinge rotations at the base of the shear wall could not be checked at this time because the output for this element is currently being modified [9].

The nonlinear pushover analysis of Study Structure 2 with SAP2000 has not yet been successfully completed. The SAP2000 input options are not transparent and easy to execute for RC wall members. Future analysis of this structure will use both the default option and direct user input of M-Φ relations for the wall members.

4. DISCUSSION OF RESULTS

The purpose of this study was to evaluate the use of existing software for pushover analyses of a variety of RC structures. At the conclusion of this initial investigation, a single software package will be selected for additional studies of the pushover response of several RC structures. The overall goal is to provide information leading to the development of performance-based design standards for RC structures.

The comparison of IDARC and its updated version, IDASS, indicates that IDASS has many desirable options that are not provided by IDARC. IDASS allows a pushover analysis to be taken beyond the arbitrary drift limit of 2% set in IDARC. It also gives output for inelastic rotations in member plastic hinging regions, a quantity that will be needed for checks against performance limits. IDASS also provides a realistic wall element, although the detailed output of plastic-hinge rotations for this element is still under development.

The comparison of IDASS and DRAIN-2DX for frame members indicated that strength results were consistent between these two software packages, when using the beam-column frame element (Type 02) in DRAIN. The IDASS frame member exhibits trilinear behavior compared to the bilinear behavior for DRAIN element Type 02, but this difference should not be significant

for pushover analysis that proceeds well into the postyield range of behavior. The results of this study indicate that a careful selection of the effective moment of inertia for the frame members in the DRAIN software is important. Thus, the user should consider the percentage of longitudinal reinforcement in the potential plastic hinging zone when selecting this value. The results obtained using the DRAIN fiber member model (Type 15) were not successful. Final structural response demonstrated significantly higher strength and stiffness. Adjustments in the lengths of the positive and negative bending regions along the member affected both the pre- and postyield behavior, but there is little guidance to assist the user in selecting these lengths.

At this point in the investigation the evaluation of the SAP2000 software package is incomplete. However, an updated version and corresponding manual changes will be examined for the default and user input parameters.

5. REFERENCES

1. US-Japan Technical Coordinating Committee. Interim summary report on tests of a seven story RC building. *ASCE Journal of the Structural Division*, V. 106(10): 2393–2411.

2. *Uniform Building Code* (UBC 97), Vol. 2. 1997. Whittier, Calif.: International Conference of Building Officials.

3. Kunnath, S. K., A. M. Reinhorn, and R. F. Lobo. August 1992. *IDARC version 3.0: A program for the inelastic damage analysis of reinforced concrete structures.* Buffalo, N.Y.: SUNY, and Orlando, Fla.: University of Central Florida.

4. Kunnath, S. K. 1999. *IDASS Version 3.0: Inelastic damage analysis of structural systems.* July. Orlando, Fla.: University of Central Florida.

5. Allahabadi, R. and G. H. Powell. 1988. *DRAIN-2DX user guide.* Report No. UCB/EERC-88/06. Berkeley, Calif.: University of California.

6. Kannan, A. E., and G. H. Powell. April 1973. DRAIN-2D: *A general purpose program for dynamic analysis of inelastic plane structures.* Report No. EERC 736. Berkeley, Calif.: University of California.

7. *SAP2000 Nonlinear user manuals.* Oct. 1998. Berkeley, Calif.: Computer and Structures. Inc.

8. U.S. Federal Emergency Management Agency. 1997. *NEHRP guidelines for the seismic rehabilitation of buildings* (FEMA 273). Washington, D.C.

9. Personal communication with S. K. Kunnath, developer of IDASS.

6. KEYWORDS

Performance-based design, pushover analysis, reinforced concrete structures, analysis software, member models, and plastic hinging zones.

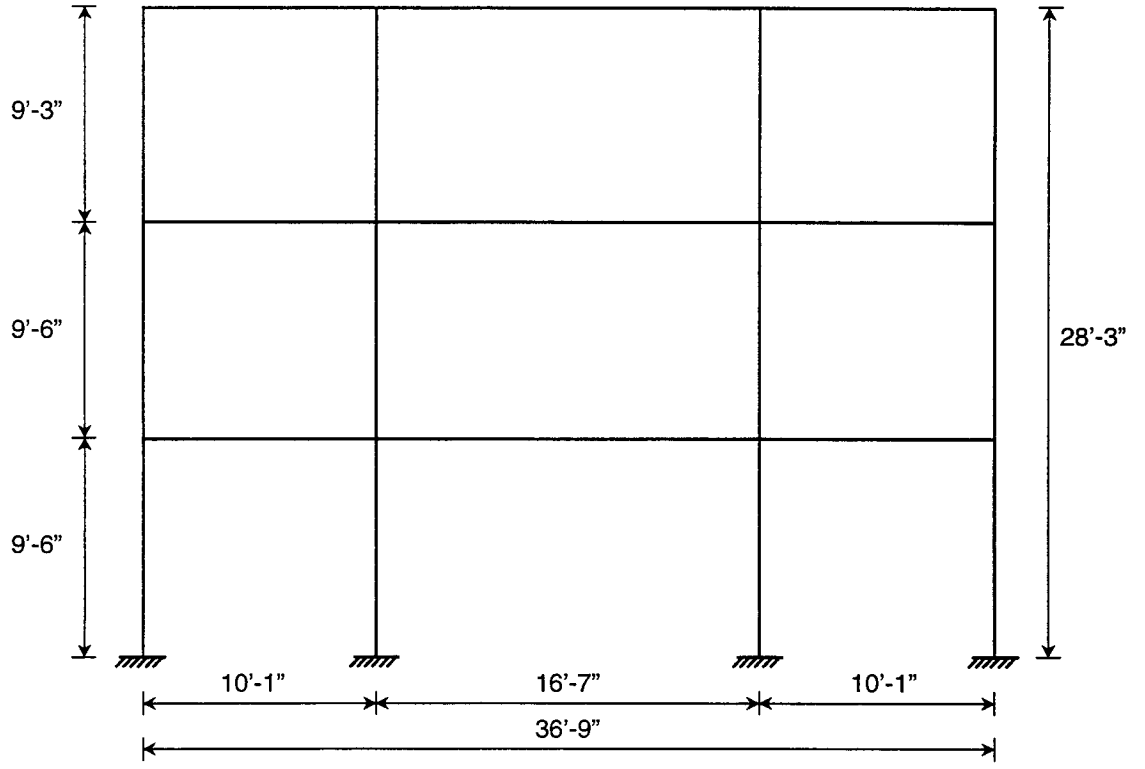

Fig. 1(a). Elevation of Study Structure 1: slab-column frame

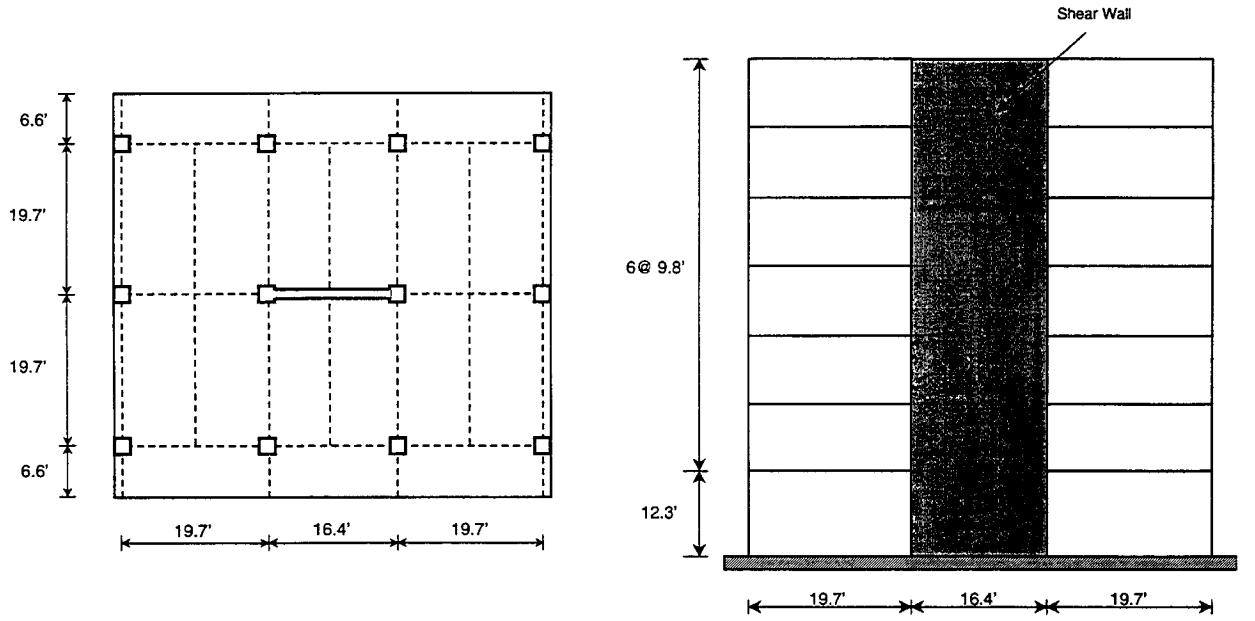

Fig. 1(b). Plan and elevation of Study Structure 2: dual system

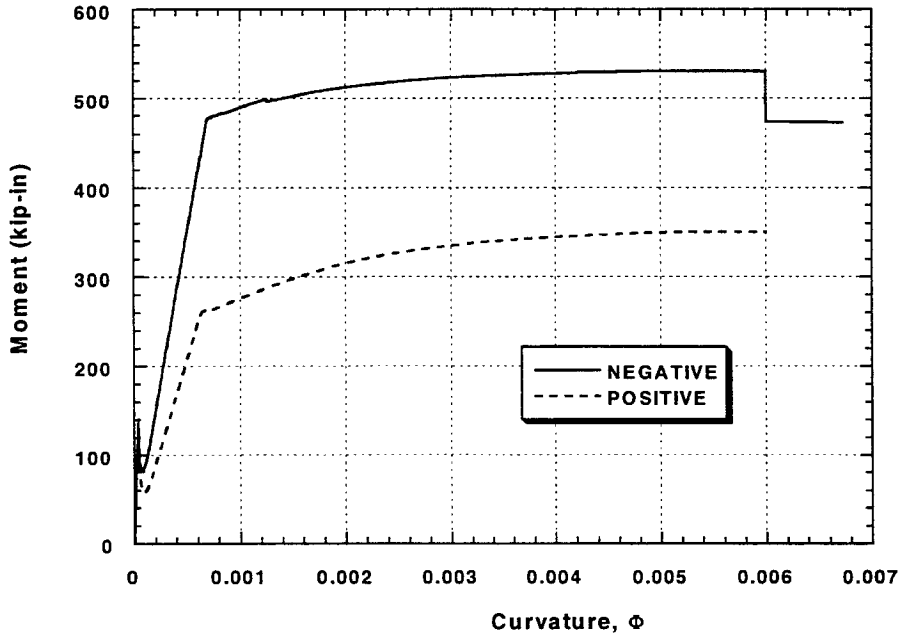

Fig. 2. Sample M-Φ output from IDASS for RC frame member

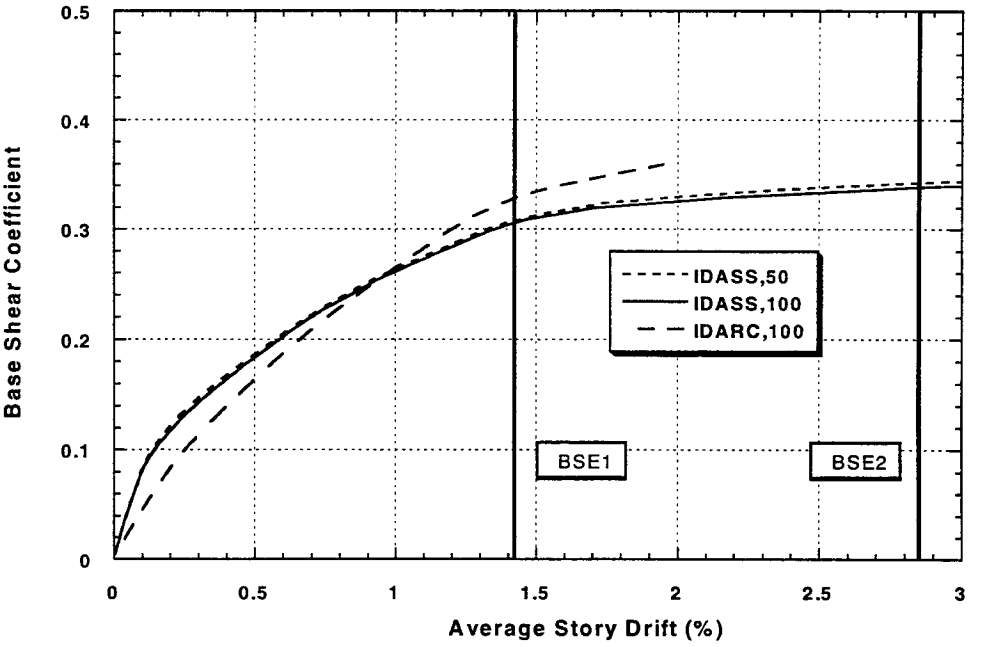

Fig. 3. Lateral pushover curves from IDARC and IDASS: Structure 1

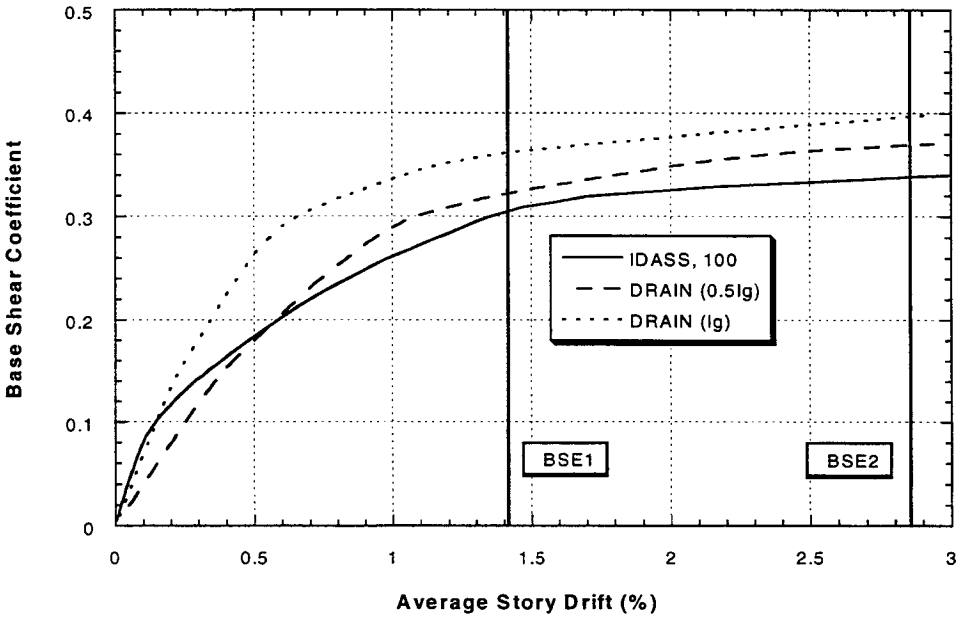

Fig. 4. Lateral pushover curves from IDASS and DRAIN (Member type 02): Structure 1

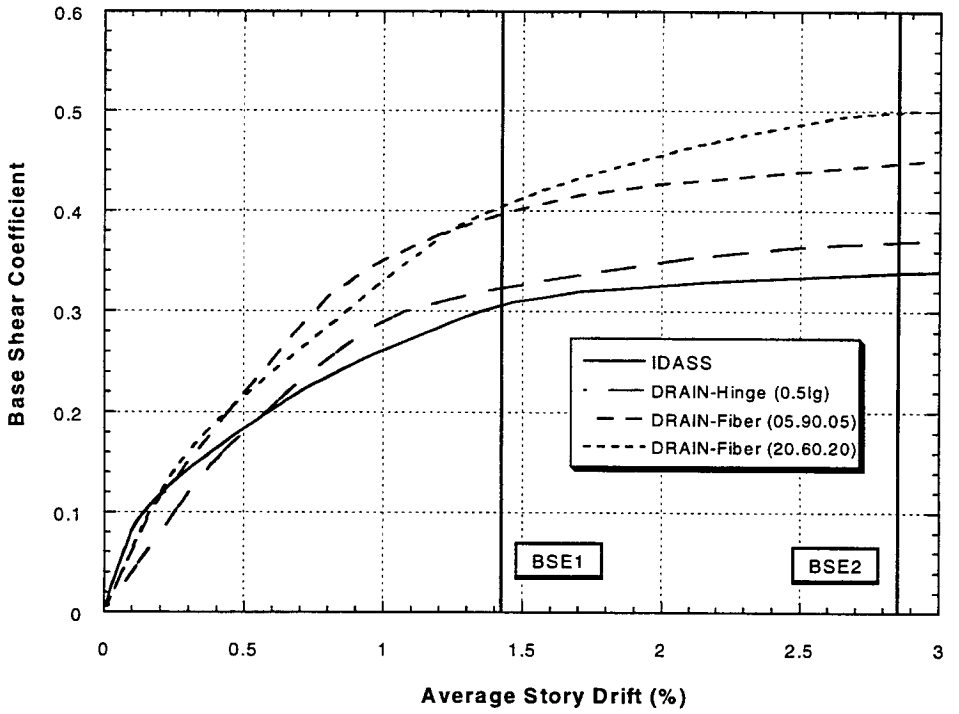

Fig. 5. Lateral pushover curves from DRAIN Member Types 02 and 15: Structure 1

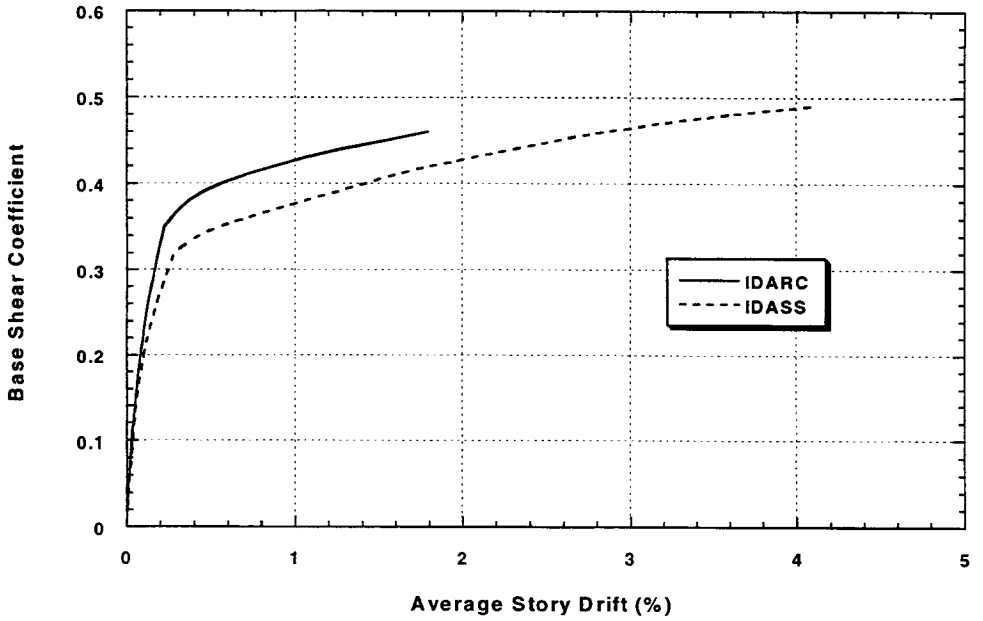

Fig. 6. Lateral pushover curves for study Structure 2 from IDARC and IDASS

PROBABILISTIC PREDICTION OF STORY DISPLACEMENT

T. Ichinose[1], N. Hanai[1], T. Umeno[1], and H. Idota[1]

ABSTRACT

A probabilistic method is proposed to predict, based on energy, the maximum story displacement of a building under seismic excitation. The input energy is subdivided into elastic and plastic components. The plastic component is assumed to be distributed over each story according to its relative strength. The proposed method is verified for story- and total-collapse modes. The proposed method may also be applicable to partial-collapse mode. The uncertainty of strength, which may be large when evaluating existing buildings, affects the maximum displacement probability density distribution, which differs significantly from a normal distribution.

1. INTRODUCTION

Since the 1994 Northridge and 1995 Kobe earthquakes, evaluating the seismic capacity of existing old buildings has been considered important. In Japan, an evaluation code was completed in 1977 and slightly revised in 1990 [*Standard* 1990]. The code is currently under review for an overall revision by committees headed by Profs. Okada and Kabeyasawa.

One of the best methods of evaluating the seismic capacity of existing old buildings would be to obtain the probability density distribution of story displacement at each story for any level of earthquake motion (from moderate to the strongest) as shown in Figure 1. On the other hand, any limit state where trouble occurs (such as when doors do not open) can be deterministically evaluated as indicated by the arrow in Figure 1. If such a distribution is evaluated, the seismic capacity of the building can be explained to the owner as shown in Table 1, where the input levels 1 through 3 shall be defined by the magnitude of the earthquake and the distance from the epicenter. The level may also be associated with return periods. In addition, such a table can be used to evaluate the insurance premium for earthquake coverage.

Housner (1959) proposed a procedure to predict the inelastic response of a single-degree-of-freedom (SDOF) system based on the principle of energy conservation. Akiyama (1985) extended Housner's idea to a multi-degree-of-freedom (MDOF) system. The objective of this study is to propose a probability-based method for evaluating the story displacement of buildings that may fail in the modes shown in Figure 2. In the present study, the proposed method is verified

1 Nagoya Institute of Technology, Gokiso, Showa, Nagoya, 466-8555, Japan. E-mail: ichinose@archi.ace.nitech.ac.jp

only for the modes shown in Figures 2a and 2c; the applicability of the method for the modes shown in Figure 2b will be discussed in the future.

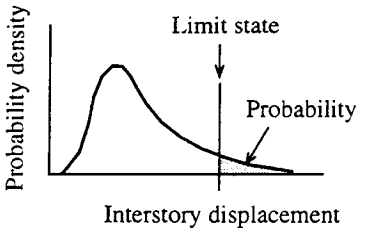

Fig. 1. Probability density distribution of story displacement

Table 1: Examples of seismic performance probability

Troubles	Story drift	Probability		
		Level 1	Level 2	Level 3
Column inclines 3 degrees (Entrance prohibited)	1/30	10^{-7}	10^{-5}	10^{-4}
Crack opens wider than 1 mm (Entrance limited)	1/80	10^{-6}	10^{-4}	0.2%
Door does not open (Evacuation difficult)	1/100	10^{-5}	0.1%	2%
Building inclines due to failure of piles (Difficult to repair)	1/100	10^{-4}	0.2%	10%
Damage to interior and/or exterior (Repair required)	1/150	0.1%	1%	20%
Elevator stops (Inconvenience)	1/200	0.2%	2%	50%

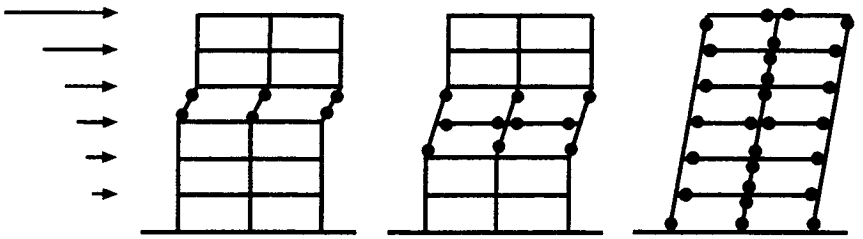

(a) Story collapse (b) Partial collapse (c) Total collapse

Fig. 2. Buildings with several collapse modes

2. TOTAL INPUT ENERGY AND EQUIVALENT VELOCITY

Newmark (1971) studied the inelastic response of a bi-linear SDOF system and found that the total input energy defined in Figure 3a is nearly constant irrespective of the yield strength of the system. In this study, "total input energy" of a MDOF system is defined as follows.

$$E_{total} = \sum_{i=1}^{N} E_i \tag{1}$$

where N is the number of stories and E_i is the input energy of each story defined in Figure 3b. In

Figure 3b δ_i is the maximum response of the i-th story displacement. "Equivalent velocity" is defined as follows.

$$V_{total} = \sqrt{\frac{2E_{total}}{M}} \tag{2}$$

where M is the total mass of the building.

Inelastic response analyses were performed for two types of buildings using the story strengths shown in Figures 4a and 4b. The story strengths in Figure 4a represent those required by Japanese building law (1981), whereas in Figure 4b the story strengths of the second and higher stories are double those required by Japanese building law (1981). The story displacements at yield strengths are assumed to be those shown in Figure 3c, where C_0 is the base shear coefficient. The displacements at cracking strengths are assumed to be one third of those at yield strengths. The cracking strengths are assumed to be one half of the yield strengths. The first and second periods of the structures are plotted in Figure 5. The damping factor is assumed to be 0.05 proportional to tangential stiffness. The Takeda model (1970) is used as the hysteresis model. The input waves are taken from the Hachinohe NS (1968 Tokachi-oki) and Takatori NS (1995 Kobe) records. The obtained equivalent velocities are plotted in Figure 6. The obtained equivalent velocities depend mostly on the earthquake motion and are insensitive to the number of stories, base shear coefficient, or strength distribution.

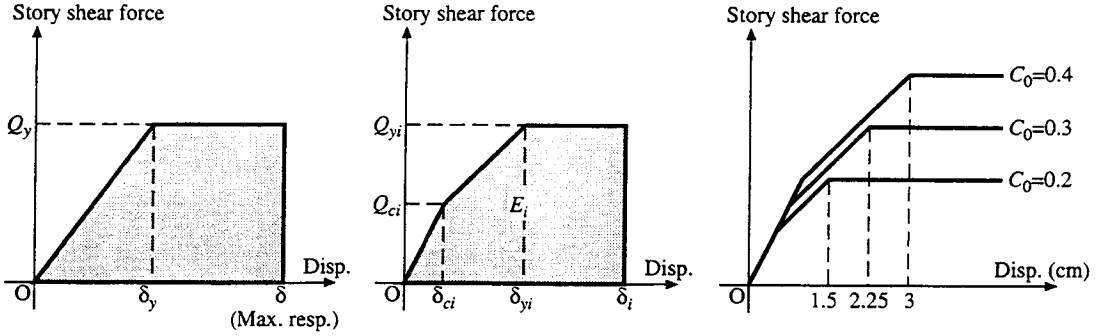

(a) Bi-linear model (b) Tri-linear model (c) Assumed model

Fig. 3. Force-displacement relationship

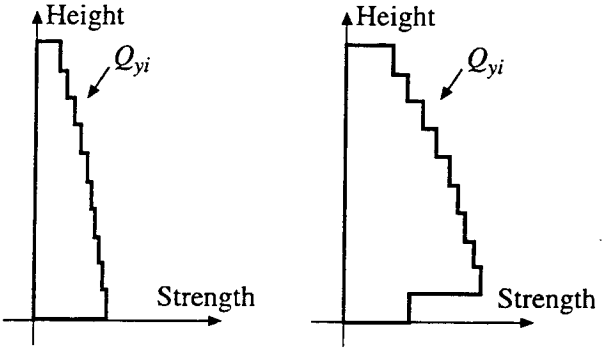

(a) Ideal strength (b) Weak first story

Fig. 4. Assumed strength distribution

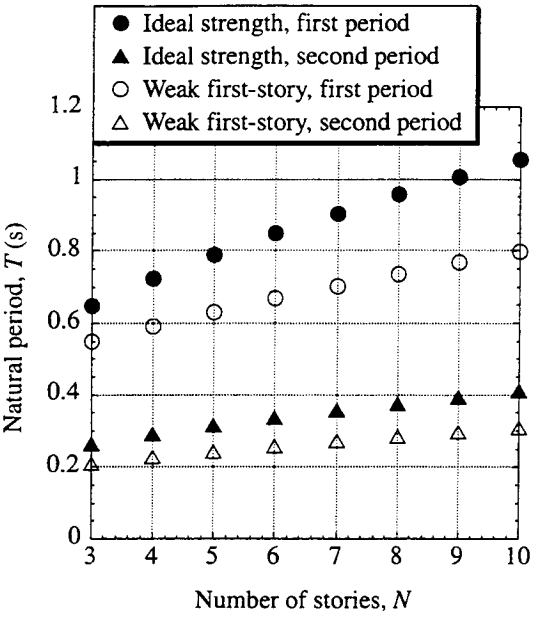

Fig. 5. First and second periods of structures

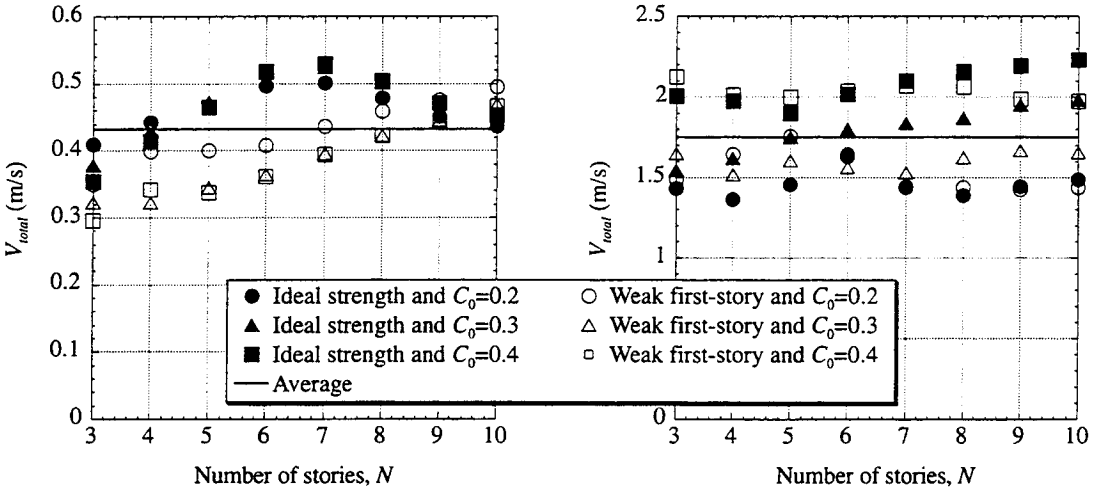

(a) Hachinohe-NS (b) Takatori-NS

Fig. 6. Equivalent velocities

3. PLASTIC ENERGY (DEFINITION AND ESTIMATION)

Denoting the maximum response of story displacement by δ_i, and the yield displacement by δ_{yi}, plastic energy E_p is defined as

$$E_p = \sum_{i=1}^{N} E_{pi} = \sum_{i=1}^{N} Q_{yi}\left(\delta_i - \delta_{yi}\right) \tag{3}$$

where the summation is performed only for the stories where inelastic deformation occurred.

To estimate the plastic energy, it is convenient to define an "ideal strength distribution, ${}_0Q_i$,"

which gives each story an equal probability of yielding under any seismic excitation. In the present study, ${}_0Q_i$ is tentatively assumed to be the strengths required by Japanese building law (1981).

The "elastic energy" of a structure E_e is defined as the energy dissipated by a structure until a collapse mode is formed under the load pattern corresponding to the ideal strength distribution. Figure 7 illustrates the case where the first story yields and the total of the shaded areas represent the elastic energy defined in the present study. The plastic energy E_p may be estimated by the following

$$E_p \approx E_{total} - E_e \tag{4}$$

Inelastic response analyses were performed using various earthquake records with various amplifications. Figure 8 shows a comparison of the observed plastic energies with those estimated by Eq. 4. As can be seen from the figure the estimated plastic energies agree well with the observed plastic energies.

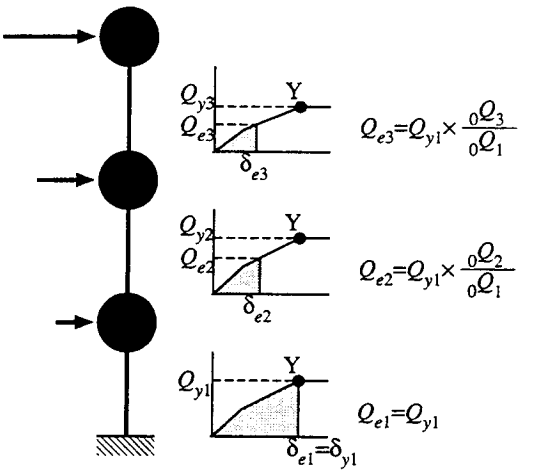

Fig. 7. Definition of elastic energy

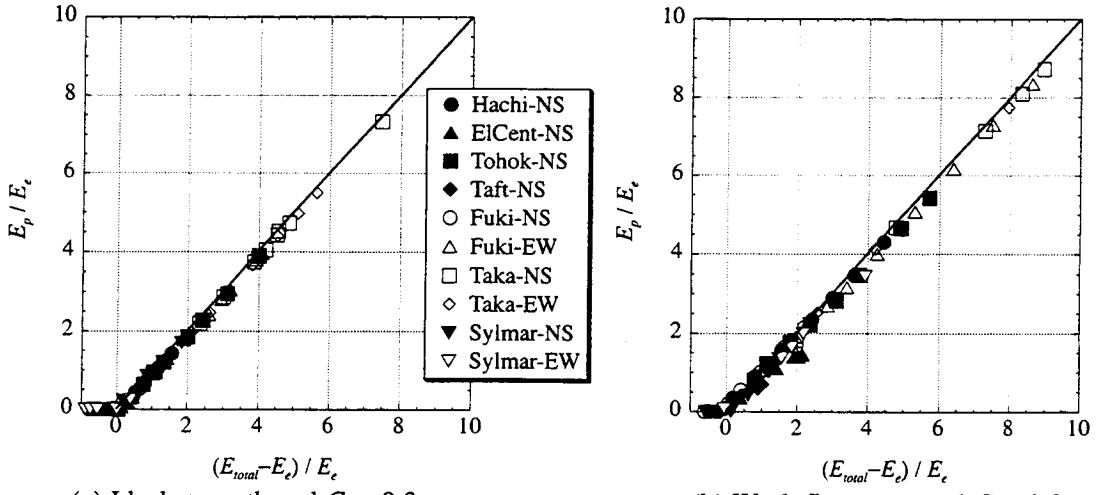

(a) Ideal strength and $C_0 = 0.3$ (b) Weak first story and $C_0 = 0.3$

Fig. 8. Comparison between plastic energy and remainder of total minus elastic energy

4. DISTRIBUTION OF PLASTIC ENERGY

How is the plastic energy allotted to each story? The relative strength of each story is the most important. Therefore, "strength factor" is defined as follows.

$$\alpha_i = \frac{Q_{yi}}{{}_0Q_i} \tag{5}$$

where ${}_0Q_i$ and Q_{yi} are the ideal strength and the actual yield strength of the i-th story, respectively. Using this factor, the following equation is provisionally assumed to estimate the plastic energy allotted to each story, E_{pi}.

$$E_{pi} = \frac{\alpha_i^{-20}}{\sum_{i=1}^{N} \alpha_i^{-20}} E_p \tag{6}$$

Note, the α_i^{-20} term means that plastic energy concentrates strongly in a weak story with smaller α_i. A similar but more complicated equation was proposed by Akiyama (1987). The story displacement can be estimated using the following:

$$\delta_i = \frac{E_{pi}}{\alpha_i \times {}_0Q_i} + \delta_{ei} \tag{6'}$$

where δ_{ei} is the story displacement when the collapse mode is formed under static analysis (see Figure 7).

To verify the above equation, a series of analyses were performed for the four kinds of 10-story buildings shown in Table 2. The second column of the table shows the strength distribution assigned by Japanese law (the distribution assumed to be ideal). The force-displacement relationship is assumed to be that of $C_0 = 0.3$ as shown in Figure 4. The input waves are amplified so that the maximum acceleration is 5.0 m/s^2. Figures 9a through 9c show the results and the prediction obtained using Eq. 6. Figures 9b and 9c indicate that plastic energy concentrates in a weak story. Figure 9d shows the results where the stiffness of the first story is increased by five times whereas the strength of each story is given by Case 3 in Table 2. This figure indicates that the stiffness distribution does not affect plastic energy concentration. To summarize the results, the average and standard deviation of E_{pi}/E_p are calculated for each group of results having an identical prediction and are compared with each prediction in Figure 10. The average agrees well with the prediction, though the standard deviation is large.

Table 2: Ideal strength distribution and assumed α_i

Story, i	$\frac{{}_0Q_i}{{}_0Q_1}$	α_i		
		Case 1	Case 2	Case 3 & 3S
10	0.24	1	2	1.2
9	0.39	1	2	1.2
8	0.52	1	2	1.2
7	0.62	1	2	1.2
6	0.72	1	1.1	1.2
5	0.80	1	1	1.2
4	0.86	1	1.1	1.2
3	0.92	1	2	1.2
2	0.97	1	2	1.2
1	1.00	1	2	1

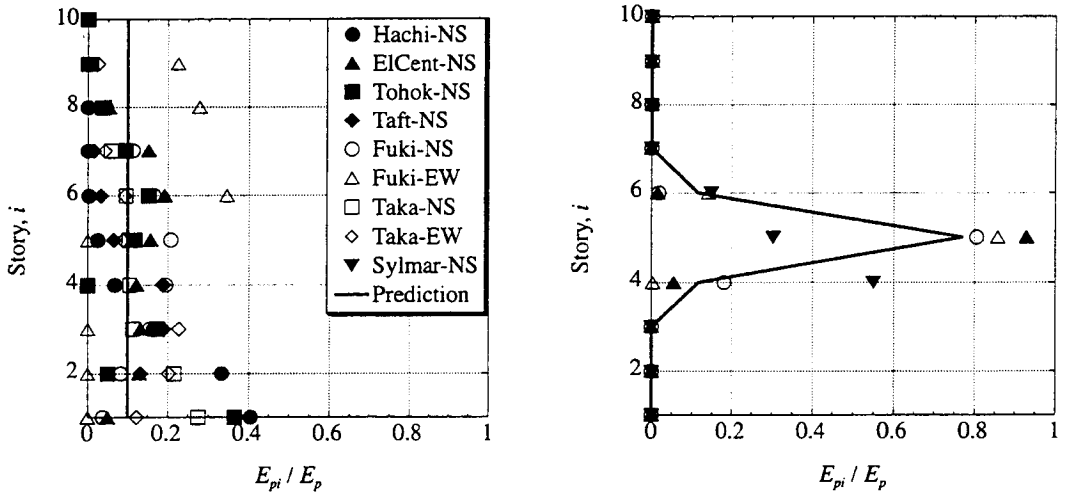

(a) Case 1 (Ideal strength distribution)

(b) Case 2 (Weak middle stories)

(c) Case 3 (Weak first story)

(d) Case 3S (Stiff and weak first story)

Fig. 9. Plastic energy dissipated in each story

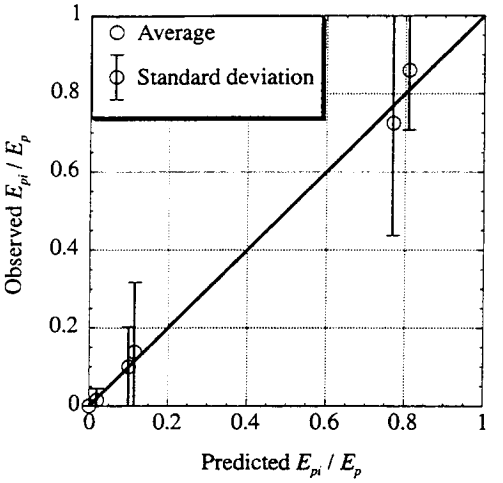

Fig. 10. Comparison between predicted and observed plastic energy

5. APPLICATION TO BEAM-COLLAPSE STRUCTURES

The RESP-F program [Kozo 1997] was used to analyze 3-, 9- and 15-story buildings each with a story height of 3 m and span length of 10 m as shown in Figure 11. The weight of each story is assumed to be 50 tons. The elastic stiffness and the crack moments of the beams and columns are calculated using the dimensions and concrete strengths shown in Table 4. The bending moments due to vertical load are neglected. The ideal strength distribution, ${}_0Q_i$, is calculated assuming that the base shear coefficient of the 3- and 9-story buildings is 0.25 and that of the 15-story building is 0.238, both of which are the minimum requirement under Japanese law. The yield moment of the column at the i-th story is given by

$$M_{cyi} = \alpha_i \times {}_0Q_i \times \frac{h}{2} \tag{7}$$

where α_i is given as shown in Figure 12 according to Umeno et al. (1999) and h is the story height. This equation indicates that the structure yields in story-collapse mode under the forces shown in Figure 11a. The yield moment of the beam at the i-th story is given by

$$M_{byi} = \frac{{}_0Q_i}{\sum_{j=2}^{N} {}_0Q_j} \times \left(h \sum_{j=1}^{N} {}_0Q_j - M_{cy1} - M_{cyN} \right) \tag{8}.$$

This equation indicates that the structure yields in total-collapse mode under the forces shown in Figure 11b. This result is because summing this equation from $i = 2$ to N and multiplying an arbitrary hinge rotation θ gives the following work equation.

$$\theta \times \left(M_{cy1} + \sum_{j=2}^{N} M_{byi} + M_{cyN} \right) = h\theta \times \sum_{j=1}^{N} {}_0Q_j \tag{9}$$

The relationship between the story shear and story displacement is plotted for each structure in Figure 13, where the open circles indicate the points when total-collapse modes are formed. The black circles in Figure 14 show the maximum response of story displacement to the Takatori NS record, whereas the open circles correspond to those in Figure 13. The maximum response agrees with the triangles in Figure 14, which show the displacement predicted by the following procedure.

First, the equivalent velocity, V_{total}, of the Takatori NS record used for the calculation is assumed to be 1.76 m/s, which is the average value of Figure 6b. This V_{total} yields the total input energy, E_{total}. Second, the elastic energy E_e is evaluated as the energy dissipated until the total-collapse mode is formed. Third, the plastic energy is evaluated using Eq. 4. Fourth, the plastic energy allotted to each collapse mode is evaluated generalizing Eq. 6 as follows.

For story collapse at the i-th story
$$E_{pi} = \frac{\alpha_i^{-20}}{\alpha_t^{-20} + \sum_{i=1}^{N} \alpha_i^{-20}} E_p \tag{10}$$

For total collapse
$$E_{pt} = \frac{\alpha_t^{-20}}{\alpha_t^{-20} + \sum_{i=1}^{N} \alpha_i^{-20}} E_p \tag{11},$$

where α_t is the ratio of the story shear force when the total-collapse mode is formed to the ideal strength distribution ${}_0Q_i$ (in this case, $\alpha_t = 1.0$). Using these energies, displacement of the i-th story is predicted as follows, where δ_{ei} is the story displacement when the collapse mode is formed under static analysis.

$$\delta_i = \frac{E_{pi}}{\alpha_i \times {}_0Q_i} + \frac{E_{pt}}{\alpha_t \times \sum_{i=1}^{N} {}_0Q_i} + \delta_{ei} \tag{12}$$

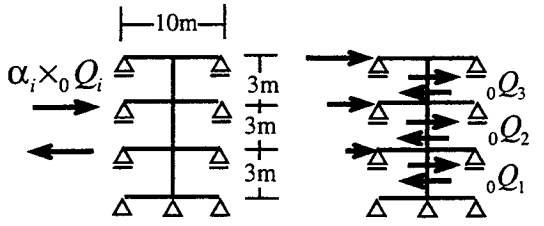

(a) Story collapse (b) Total collapse

Fig. 11. Analyzed frame and considered forces

Table 3: Assumed size and concrete strength

Model	Story	Beam (mm)		Column (mm)	Concrete Strength (MPa)
		Depth	Width		
3-story	3. 2	645	357	611	22
	1	668	392	645	26
9-story	9. 8	829	459	785	28
	7. 6	859	503	829	34
	5-1	888	548	888	41
15-story	15. 14	946	524	895	32
	13. 12	979	574	946	38
	11-1	1013	625	1013	47

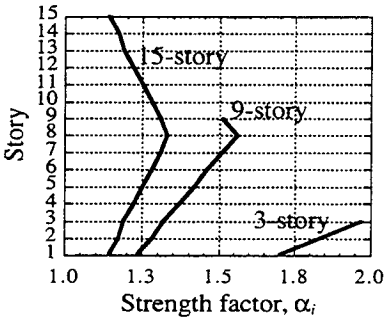

Fig. 12. Assumed α_i

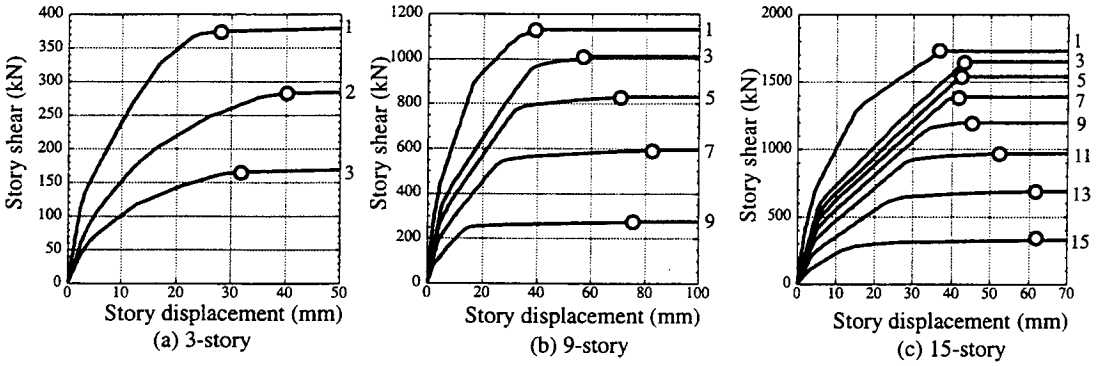

Fig. 13. Relationship between story shear and story displacement

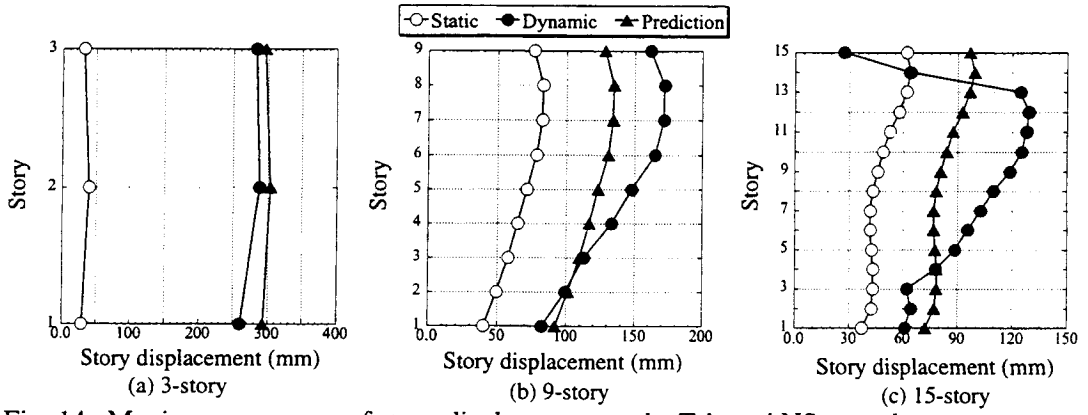

Fig. 14. Maximum response of story displacement to the Takatori NS record

6. PROBABILITY DENSITY OF STORY DISPLACEMENT

Because of the uncertainty of the properties of material and/or due to construction errors, it is necessary to consider a randomness of the strength factor α_i, which affects the distribution of plastic energy. To study the effect, a Monte-Carlo simulation is performed for the story-collapse mode of the 3- and 9-story buildings. The average of the strength factor of the first story, α_1, is assumed to be unity, whereas those of the other stories are assumed to be 1.2. The coefficient of variation (COV) of the strength factors of all the stories is assumed to be 0.1, which is probable for the evaluation of existing buildings. For the sake of reference, the cases of COV = 0 (deterministic) and 0.02 are also calculated. The uncertainty of Eq. 6 is neglected. Ten thousand sets of α_i are given to obtain each histogram of E_{pi}/E_p shown in Figure 15. In Figure 15a (3-story), it is noted that the deterministic result (COV = 0) , $E_{pi}/E_p = 0.95$, does not coincide with the peak of the distribution of COV = 0.1, $E_{pi}/E_p = 1.0$. In Figure 15b (9-story), it is also noted that the average of the distribution of COV = 0.1 does not coincide with the deterministic result. These tendencies result from the special characteristics of Eq. 6 with α_i^{-20}. The distribution for the 9-story building is flatter than that for the 3-story building because the 9-story building has eight stories which can have smaller α_i than α_1, whereas the 3-story building has only two.

Next, the probability density of story displacement is evaluated. The base shear coefficient is assumed 0.3. The strength factor of each story is assumed to be the same as the analyses in Figure 15. The equivalent velocity, V_{total}, is assumed to be 1.76 m/s, which simulates the Takatori NS record in Figure 6b. Figure 16 shows the results of the Monte-Carlo simulation. The arrow in the figure ($\delta_1 = 0.55$ m) shows the displacement obtained assuming that the total plastic energy concentrate in the first story with the average strength, $E(Q_{y1}) = 0.3\,M\,g$.

$$\delta_1 = \frac{E_p}{E(Q_{y1})} + \delta_y \tag{13}$$

The distribution decreases from around this arrow, which corresponds with $E_{pi}/E_p = 1$ in Figure 15. Figures 15a and 15b are similar to Figures 16a and 16b, respectively, except that the peaks at $E_{pi}/E_p = 1$ in Figure 15 are flattened around $\delta_1 = 0.55$ m in Figure 16.

Figure 17 shows the results when the total-collapse mode is probable. The average of the strength factor for the mode, α_t, is assumed to be 1.0 and the COV is assumed to be 0.1. The other strength factors are the same as those used previously. The distributions of Figure 17 are higher at small δ_1 than those of Figure 16 because the denominator of the second term of Eq. 12 is larger than that of the first term.

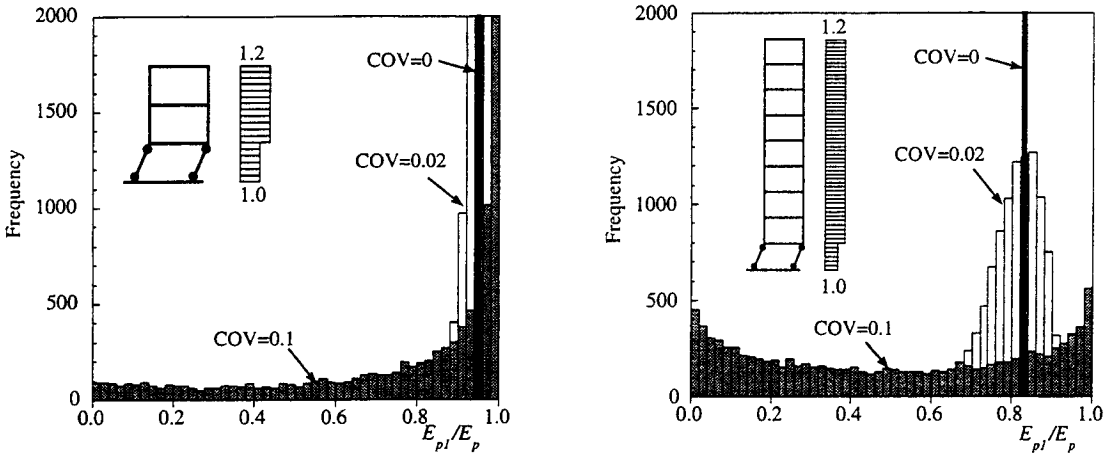

(a) 3-Story building (b) 9-story building

Fig. 15. Histogram of E_{pi}/E_p

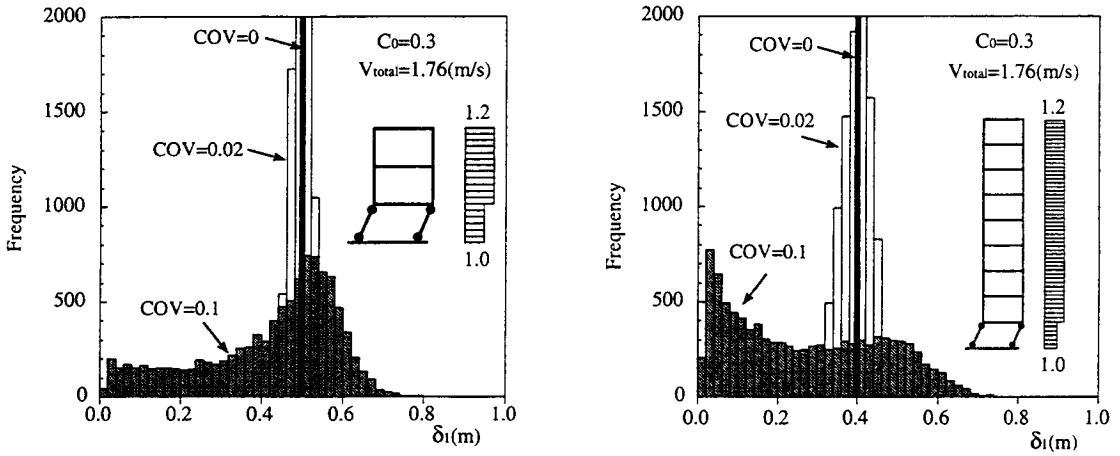

(a) 3-story building (b) 9-story building

Fig. 16. Histogram of story displacement (story-collapse type)

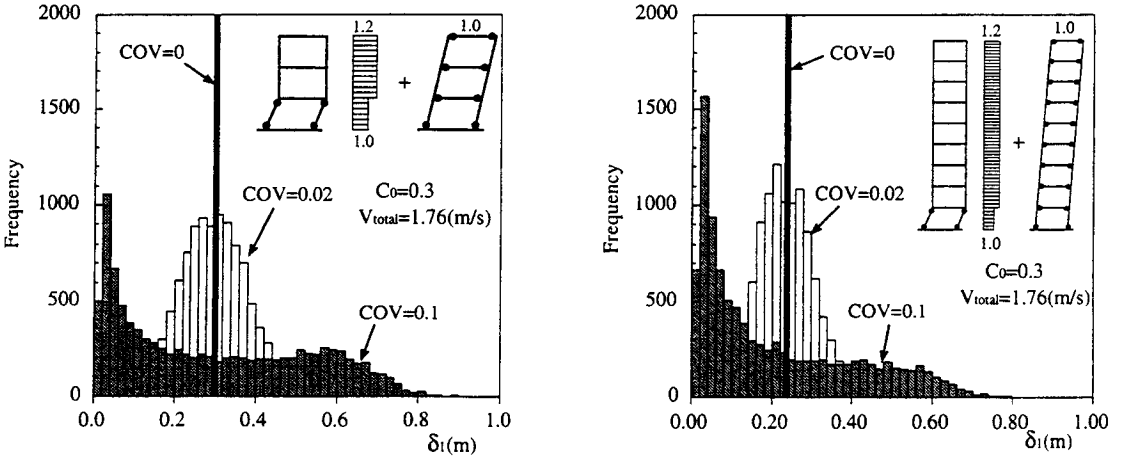

(a) 3-story building (b) 9-story building

Fig. 17. Histogram of story displacement (total-collapse type)

7. FURTHER RESEARCH NEEDS

A large amount of work is needed to complete this project. At this stage, the following eight targets require further research.

1. The effect of hysteretic model on equivalent velocity requires study. Equivalent velocity may be large for structures with slip-type hysteresis or softening.
2. The applicability of Equations 6, 10, and 11 should be verified for cases other than those presented in this study and should include structures with walls or brittle members.
3. Equations 6, 10, and 11 may be further generalized for structures with partial collapse as shown in Figure 2b.
4. The uncertainty of Equations 6, 10, and 11 requires consideration.
5. The effects of bi-axial excitation should be studied. A structure may fail in total-collapse mode in the X-Y direction and in story-collapse at 45-degree excitation.
6. Torsion effects should be included in the procedure.
7. The definition of "elastic energy" might be reexamined for taller and more flexible buildings.
8. The theoretical background of Equations 6, 10, and 11 should be clarified, if possible.

8. CONCLUSIONS

Probabilistic prediction of story displacement is possible using the following procedure.

1. Perform static analysis of the building using a set of horizontal forces that yield an "ideal strength distribution."
2. Evaluate the total input energy using $E_{total} = \frac{M \cdot V_{total}{}^2}{2}$, where M is the total mass of the building and V_{total} is given by the level of ground motion considered.
3. Evaluate the total plastic energy using $E_p = E_{total} - E_e$.
4. Evaluate the probability density distribution of story displacement using Eq. 6, 10, 11, and 12.

REFERENCES

Akiyama, H. (1985): *Earthquake resistant limit-state design for buildings*, the University of Tokyo Press, Tokyo, Japan, 384 pp.

Design Guidelines for Earthquake Resistant Reinforced Concrete Buildings Based on Inelastic Displacement Concept (1997): Architectural Institute of Japan (in Japanese)

Housner, G. W. (1959): Behavior of structures during earthquakes, *Journal of Engineering Mechanics*, ASCE, Vol. 85, No. EM4.

Kozo Keikaku Co. (1996): *RESP-M/II, Inelastic Response Analysis Program for Buildings*, Version 5.0 (in Japanese)

Kozo Keikaku Co. (1997): *RESP-F, Inelastic Response Analysis Program for Two-dimensional Buildings*, Version 8.00 (in Japanese)

Nakamura, Y., Uehan, F. and Inoue, H. (1996): Waveform and its analysis of the 1995 Hyogo-ken-nanbu earthquake (II), *JR Earthquake Information* No. 23d, Railway Technical Research Institute (in Japanese)

Newmark, N. M. and Rosenblueth, E. (1971): *Fundamentals of Earthquake Engineering*, Prentice Hall, Englewood Cliffs, N.J., 640 pp.

Paulay, T. and Priestley, M. J. N. (1992): *Seismic Design of Reinforced Concrete and Masonry Buildings*, John Wiley & Sons, Inc., New York, USA.

Standard and Commentary of Seismic Safety Evaluation of Existing R/C Buildings (1990), The Japan Building Disaster Prevention Association, Tokyo, Japan (in Japanese)

Takeda, T., Sozen, M. and Nielsen (1970): Reinforced Concrete Response to Simulated Earthquakes, *Journal of Structural Division*, ASCE, Vol. 96, No. ST12, pp. 2557-2573.

SESSION 5: SEISMIC CAPACITY OF FRAME OR MEMBERS

Chaired by

♦ Hitoshi Shiohara and John Stanton ♦

LIFECYCLE ECONOMIC LOSS ESTIMATION OF R/C FRAME STRUCTURE SUBJECTED TO MULTIPLE EARTHQUAKE LOAD SEQUENCES

Hitoshi SHIOHARA[1]

SUMMARY

The current seismic design codes for buildings are implemented such that human life should be protected from the collapse of building structures. The assumption is that the plastic energy dissipation of structural members and structural damage is inevitably accompanied by a reduction in strength demand taking hysteretic damping into consideration. After the 1994 Northridge, California, and 1995 Hyogo-ken Nanbu, Japan, earthquakes, the miscommunication between building owners, the public, and engineers about the seismic performance of buildings became apparent. Many building owners expect buildings to be fully functional without any repairs even after big, although rare, earthquakes. In order to narrow the gap between the expected and actual seismic performance of a building, performance-based engineering needs to be developed, by which building owners and structural engineers will share a common understanding of the target performance. To achieve this goal, the introduction of economic loss evaluation is essential. In economic loss evaluation, the cost necessary to repair and restore the initial performance of the building is used as a quantitative representation of capability to protect the building functions and contents from earthquake hazards. In high seismic zones, economic loss estimation is going to be more important than before because the loss due to earthquake occupies a large percentage in the life cycle maintenance cost of the building. The necessary steps to assess economic loss are identified for future works applicable to a reinforced concrete structure. The concept of the unit damage ratio and the nonuniformity factor are introduced and evaluated using a building reported as moderately damaged by the 1995 Hyogo-ken Nanbu earthquake.

1. INTRODUCTION

The current seismic design codes are implemented such that human life should be protected from the collapse of building structures. The assumption is that the plastic energy dissipation of struc-

[1] *Department of Architecture, School of Engineering, The University of Tokyo, Tokyo, Japan*
Email: shiohara@rcs.arch.t.u-tokyo.ac.jp

tural members due to irreversible deformation or damage allows a reduction in strength demand considering hysteretic damping. As a result, both rare large earthquakes as well as more frequent medium earthquakes may cause structural damage. Hence the level of damage to structures suffering from the same level of seismic input can differ depending upon differences in the structural type and design even though the structures conform to the same seismic design codes. This fact was demonstrated by many examples of damaged buildings after the 1994 Northridge and the 1995 Hyogo-ken Nanbu earthquakes. A reinforced concrete apartment building, Jeunesse Rokko, in Higashinada ward, Kobe, designed by the state-of-the-art design philosophy, the weak-beam strong-column concept, did not collapse, although it suffered widely distributed structural damage. Because it required a larger repair cost than the building owner expected, it was eventually demolished and rebuilt. The reconstructed UCLA Olive View Hospital survived the 1994 Northridge earthquake well, but was not able to function as an emergency medical station due to the loss of functioning of the plumbing and power supply systems. The important lesson from these examples is that there is a significant miscommunication about the seismic performance of buildings between building owners and engineers. Many building owners expect that a building will be fully functional without any repair even after a big, although rare, earthquake. A different structural design philosophy needs to be incorporated with a strategy to narrow the gap between the expectations of building owners and the public. This is one of the main reason to necessitate the introduction of performance-based engineering in earthquake-resistant design, so that the building owner and structural engineer can share a common understanding in normal language of the vulnerability of buildings to earthquake, and avoid the jargon that only a structural engineer can understand.

However, it is not simple to realize the new design philosophy. One of the simplest ideas to control building damage is to add a damage-control limit state to two existing criteria, i.e., the safety limit state and serviceability limit state. In the design, a specified set of limit values for structural damage, such as crack or yield, are required for structures subjected to a medium seismic force. The difficulty arises in explaining the correlation between an arbitrarily defined damage-control limit state, a chosen medium seismic force, and the true vulnerability of the building system.

An alternative idea for controlling building damage is to estimate the economic loss, or expected repair cost to the building owners. The economic loss is considered the cost required to repair and restore the original performance level of the building. It is used as a quantitative representation of the capability of protecting building functions and contents from an earthquake. The cost is meaningful to both building owners and to the public. In particular, the insurance industry, corporate administrators, and local government policymakers need this type of information to prepare for the expenditure. Additionally, the advantage of this method over the idea of the damage-control limit state is that the reliability of the evaluation method is verifiable through assessments of the actual damage to buildings and of the repair work after an earthquake.

Therefore, developing the concept of expected economic loss and implementing the evaluation method are quite important. However, the method should be carefully implemented to avoid arbitrariness and thus be reliable. All the factors affecting the result, which include (a) engineering factors, (b) economic factors, and (c) factors concerning environmental issues, need to be identified and incorporated into the formulation. Also necessary is a reliable background database that can relate the physical damage to the unit cost of repair work or to environmental issues.

In this paper, the importance of economic loss estimation is discussed, and then an example for implementing economic loss estimation for a reinforced concrete member is briefly introduced.

2. DEFINITION OF ECONOMIC LOSS ESTIMATION

The economic loss, or repair cost, is hereafter defined as all the necessary expenditure countable in economic value to recover the original performance level with respect to safety and serviceability. This economic loss is interpreted as all kinds of damage with respect to elements in one building or part of the building, using weighting factors, including (a) distribution of damage in a member (b) amount of damage, (c) unit cost of repairing work. Sometimes the definition of economic loss may include the loss to compensate the time the building does not function (Guru N. Rao et al. 1998).

The economic loss can be evaluated with respect to different levels of seismic input like a hazard function curve (Fig. 1). The economic loss usually increases as seismic input increases. The total economic loss usually consists of several parts originating from different functions of the building. It is also valuable information to building owners. The characteristics of the building may be significantly affected by the type of construction, the type of lateral force resisting system; such as ductile or strength, the use of the building; nonstructural material used for the interior and exterior; and the building site condition. The predicted economic loss can be used by the building owner to compare the total cost including initial construction, maintenance, and initial construction cost for the expected safety and serviceability.

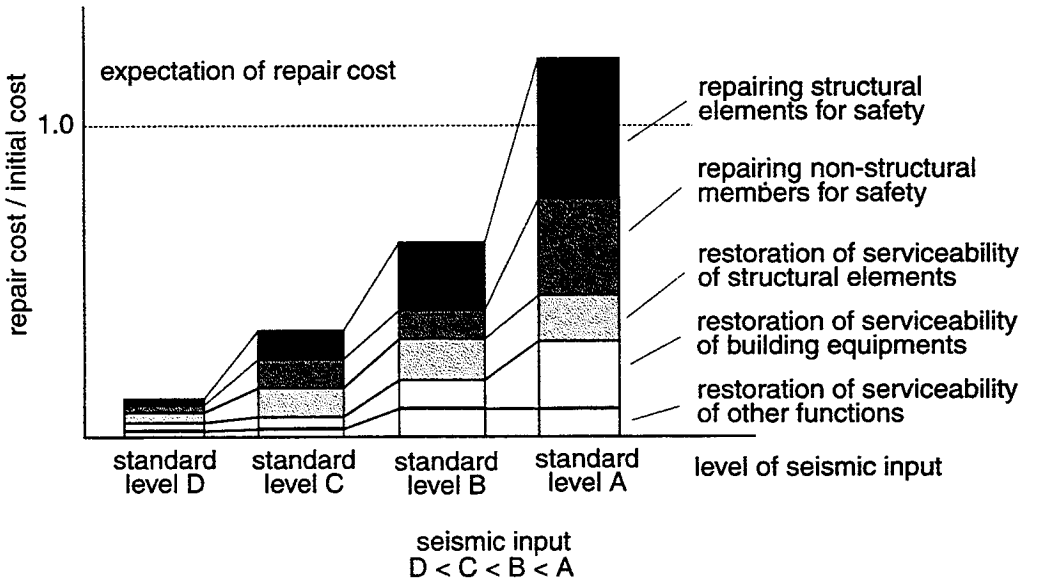

Figure 1: Concept of expectation of repair cost

3. LOSS ESTIMATION AND LIFECYCLE MANAGEMENT

In countries with high seismic zones, buildings can be subjected to medium-level earthquakes multiple times in the planned durable lifetime of the building. The total economic loss incurred by medium-level earthquakes may not be negligible in the total lifecycle cost. The expected durable period of a building in the twenty-first century is going to be longer than is currently typical. Extending the planned durable lifetime of a building and reducing new building construction are the most effective ways to mitigate the effects of construction to the environment by reducing CO_2

and by conserving energy and natural resources. Thus the importance of economic loss estimation increases in the future.

The concept of economic loss estimation in the planned durable period of a structure is shown in Fig. 2. To estimate the whole lifecycle cost, it is essential to evaluate both the effects from the action of an earthquake, including medium to large earthquakes, and the related repairs considering the damage and the reduction in durability. In particular, the statistical modeling of medium earthquakes, the modeling of damage in structural and nonstructural members, the modeling of damage to building equipment, and determining the scenario for repair and restoration work are important challenges for the future.

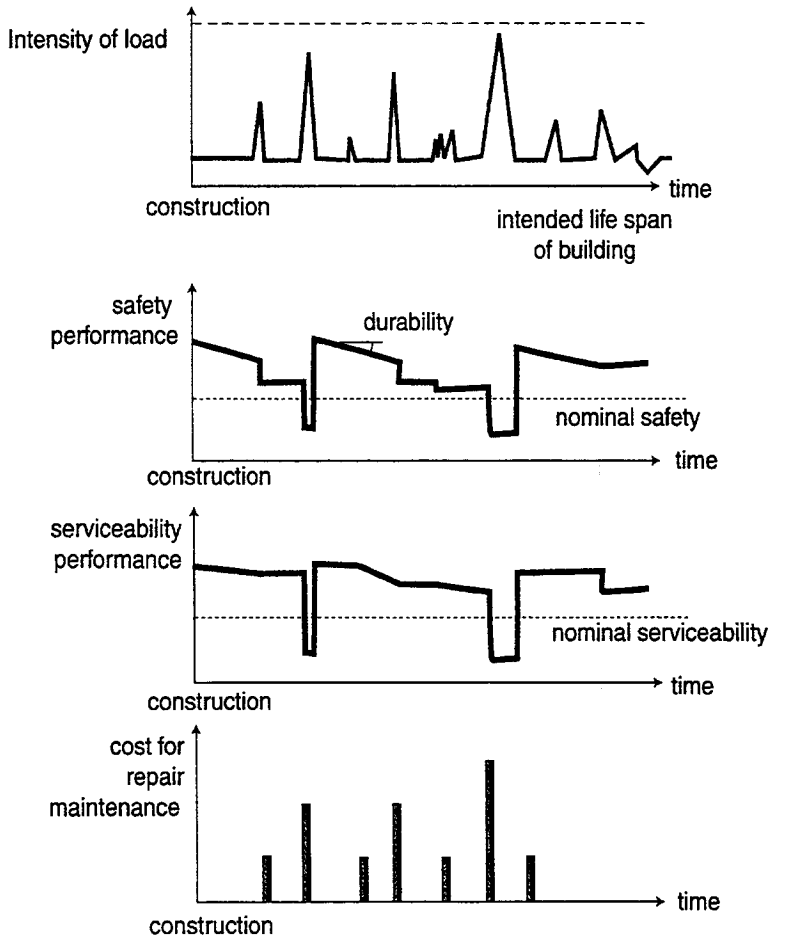

Figure 2. Typical occurrence in building life span over time

4. LOSS ESTIMATION OF R/C FRAME BUILDING STRUCTURES

The economic loss due to earthquake damage is applicable to all types of restoration process in building function, including safety and serviceability. The evaluation of the economic of a reinforced concrete structural member is considered in particular here.

The major factors affecting the total repair cost for reinforced concrete structural members include (a) the number of members requiring repair; (b) the extent and type of damage, including crack, crushing concrete, buckling of reinforcing steel; and (c) the corresponding type of repair method, e.g., epoxy resin injection, replacing spalled concrete, replacing buckled reinforcing bar, etc.; and (d) the unit cost for restoration. The steps to evaluate the economic loss may be roughly explained using Figure 3. Steps 1 and 2 are closely related to existing analytical procedures such

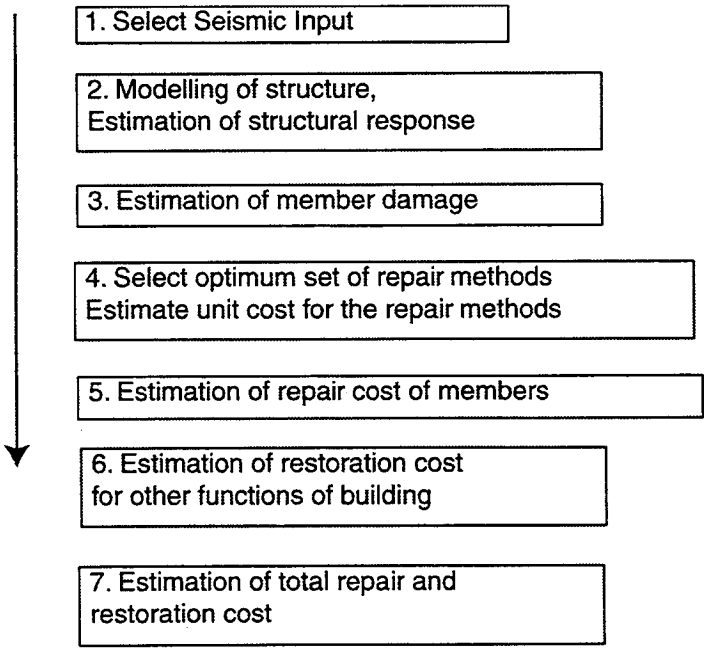

Figure 3: Necessary steps for estimation of repair cost

as displacement-based design. Steps 4 to 7 are closely connected to construction practice and its dependence on the economy. In this paper, steps 2 and step 3 were examined which need to relate the damage predicted by the response analysis of a structure and the repair cost of the members.

5. RELATION OF MEMBER DAMAGE TO REPAIR COST

The amount and type of damage such as (a) the total crack length and (b) the volume of spalled concrete or crushing concrete are more closely related to the repair cost than are more sophisticated damage indices. Thus these damage types are selected as the primary factors related to cost in this study. In order to use these indices, the correlation of these quantities to (1) the maximum response in terms of deformation, (2) the failure modes such as flexure or shear, and (3) the size of the member should be established. In nonlinear frame earthquake response analysis, the maximum deformation of members is predictable. By assuming that the amount of unit damage by volume or surface area is constant for a given attained maximum deformation and failure mode, the amount of total damage is predicted by multiplying the size of the member by the unit damage.

From existing research on the repair method for an R/C structural member, it is revealed that the mechanical properties of a reinforced concrete member can be successfully recovered in terms of strength and ductility by an epoxy resin injection of a crack for a slightly damaged member and by replacing the concrete and steel for heavily damaged members. Since the 1995 Hyogo-ken Nanbu earthquake, the epoxy resin repair method has widely been applied in Kobe. The unit cost for crack repair usually depends on the type of repair method, the amount and kind of material, and the position of the repaired member considering the difficulty of the work place. For example, the cost of an epoxy injection in a crack was estimated by assuming that the cost is proportional to the total length of crack appearing on the surface of the member, while the crack width is not sensitive to the cost. This method is generally accepted in the Japanese repair construction industry based on the experience of repair done after the 1995 Hyogo-ken Nanbu earthquake. Thus, the general formula proposed for estimating the cost is expressed follows:

$$\text{Repairing Cost of a Member} = D \times S \times U \times C \tag{1}$$

where D: unit of damage, such as total crack length, usually a function of the maximum attained deflection of the member, the geometry of the member, and the reinforcing detail; S: size of the member, such as the volume or area; U: factors considering nonuniform distribution of the dam-

age; C: unit cost for repair. This concept may be extended to express the cost for crack repair and concrete repair as shown in Table 1.

Table 1: Formulation for the estimation of repairing cost for R/C structural member

Type of damage	Definition of contributing factors, D, S, U, C
Crack repair	D: crack ratio: ratio of total crack length to surface area containing the crack in m/m^2
	S: total surface area of the member, such as beam or column, shear wall
	U: Non uniformity factors considering the distribution of cracks less than 1.0. It may be assumed depending on the failure modes, and the scale effect.
	C: repair cost for unit length of crack, not sensitive to crack width.
Concrete damage repair	D: concrete damage ratio, ratio of volume spalled off to total concrete volume of the member in m^3/m^3
	S: total volume of the member
	U: factors considering the distribution of concrete damage, less than 1.0.
	C: repair cost for unit volume of concrete replacing

6. APPLICATION EXAMPLE

To apply Eq. 1 to estimate the economic loss due to crack and concrete spalling or crushing, the unknown factors listed in Table 1 must be provided in advance as known factors. However, there is no available database to estimate the values. Thus these values are statistically investigated based on a building damage survey report.

6.1 Building

An apartment building, Jeunesse Rokko, damaged in the 1995 Hyogo-ken Nanbu earthquake is used for this investigation (Arai-Gumi Technical Research Institute 1995). The building was a nine-story reinforced concrete moment-resisting frame structure, with 6 spans of 5.5 meters in the longitudinal direction and 1 span of 6.0 meters in the transverse direction, respectively. The total height of the building was 24 meters, and the story height was 3.0 meters for the first story and 2.625 meters for other stories except the ninth story. The observed damage to the building seems to show a beam yield collapse mechanism because the flexural cracks were fully developed at the

beam ends. However, diagonal shear cracks were also seen on the columns and shear walls. The drawings of typical crack patterns are shown in Figure 2.

The factors defined in Table 1, including (a) the crack ratio, (b) the concrete damage ratio, and (c) the factors considering the nonuniform crack distribution, were calculated based on the crack drawings. The damage level of the structural members reported are summarized in Table 2. The damage levels are judged from appearance by expert judgment based on the criteria listed in Table 3. The damage level is based on the definition in Table 3 in reference (JBDPA 1991). Most of the damage level remains within II or III.

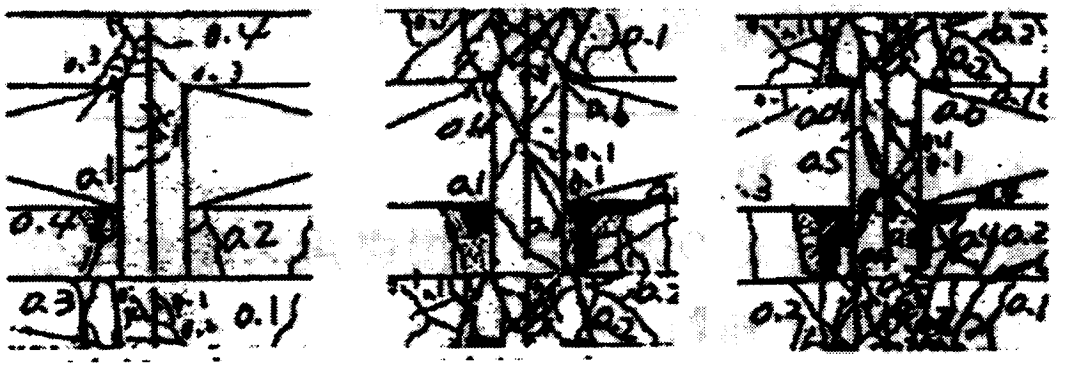

Figure 4: Examples of recorded crack patter and crack length ratio

Table 2: Damage level observed in members (Arai-Gumi Technical Research Institute 1995)

type	number of members		damage level					
	no drawing	reported with drawing	none	I	II	III	IV	V
column	1	97	4	15	43	31	4	0
beams	6	125	7	29	70	19	0	0
shear walls	0	11	0	0	7	3	1	0

6.2 Method

The total crack length was counted with respect to all the cracks drawn considering the four sides of the member. The concrete damage ratio was calculated by assuming that it is equal to the ratio of the area of the hatched part to the total surface area of the member. Then the total length of the member axis containing the crack with a width of 2.0 mm or larger is calculated. The crack concentration ratio is calculated by dividing the length by the length of the member.

Table 3: Definition of damage level of reinforced concrete beams, columns and shear walls (JBDPA 1991)

damage level	description of damage
0	no damage
I	with visible cracks but difficult to find (crack width narrower than 0.2 mm)
II	with cracks identified easily (crack width is from 0.2 mm to 1.0 mm)
III	with major crack but without concrete spalling (crack width from 1 to 2 mm)
IV	with a lot of major cracks accompanied with concrete spalled off and exposed reinforcing bar (crack width from 2 mm or wider)
V	with bent or fracture reinforcing steel, concrete inside core crush, visible inclination, settlement and their combination

6.3 Results

Table 4 and 5 show the lists of the calculated crack ratio, the concrete damage ratio, and the non-uniformity ratio of crack. The correlations of the values with the damage level, maximum response story deflection angle (Matumori and Otani 1998), and the estimated ductility response (Matumori and Otani 1998) are shown in Figure 5. The plots correspond to the members. The response analysis was based on nonlinear frame earthquake response analysis. The relation of the observed crack length ratio to the different damage indices seems to show some correlation, but the range of scattering is large in these three cases. However, these rough relations are also helpful enough to estimate the total economic loss of the building because the accumulated value is of primary concern in accomplishing this. In the Fig. 5, the white mark represents the member connected to the exterior column, whereas the black mark represents the interior member. From

Figure 5, the crack length ratio of members in the exterior frame is apparently smaller than those of the interior member. The reason for the scatterings may partly be attributed to this fact.

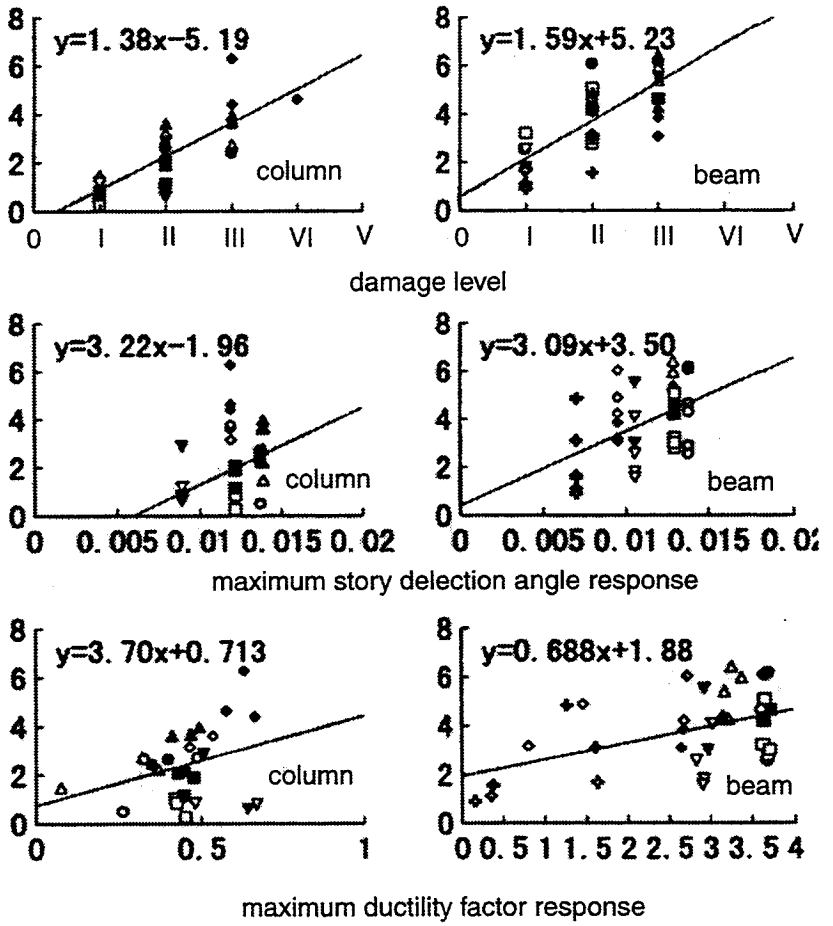

Figure 5: Correlation of crack length ratio to popular damage indices

Table 4: Average concrete damage ratio (m/m^2)

type of member	damage level				
	0	I	II	III	IV
Column	0	0	0	0	0.1
Beam	0	0	0	0.05	-
Shear walls	0	-	0	0	0.1

Table 5: Average crack length ratio (m/m^2)

type of member	damage level					Non uniformity factor of crack distribution
	0	I	II	III	IV	
Column	0	0.7	2.2	3.8	4.3	1.0
Beam	0	1.9	3.9	5.1	-	0.4
Shear walls	0	-	1.6	2.2	3.8	1.0

7. CONCLUDING REMARKS

In order to narrow the gap in understanding between engineer and building owner on the expected seismic performance of buildings performance-based engineering needs to be developed so that the building owner and structural engineer share a common understanding of performance in standard language and avoid the jargon used only by structural engineers.

In order to implement this goal, the introduction of economic loss evaluation is expected. In economic loss evaluation, the cost required to repair and recover the original performance of the building may be used as a good quantitative representation for the capability to protect building functions and contents from earthquake hazards.

Extending the durable life of the building is going to be the most important factor to the environmental issue. In highly seismic zones, economic loss estimation due to earthquake hazard is going to be more important because loss due to earthquake recovery may make up a large percentage of the cost of lifecycle maintenance.

The necessary steps to assess economic loss are identified for future works applicable to reinforced concrete structures. The concepts of the unit damage ratio and the damage nonuniformity factor are introduced and evaluated using a damage survey report of a building damaged by the 1995 Hyogo-ken Nanbu earthquake.

8. REFERENCES

Arai-Gumi Technical Research Institute. 1995. *Special issue 1995 Hyogo-ken Nanbu earthquake damage building investigation report Jeunesse Rokko*. Research Report of Arai-Gumi Construction Co. October. (In Japanese.)

Guru N. Rao, David Odeh, Javier Perez, Deepak Badoni, and Rodrigo Araya. 1998. Modeling restoration cost and time in the development of earthquake vulnerability functions. *Proceedings of 6th U.S. National Conference on Earthquake Engineering.* CD-ROM.

JBDPA/The Japan Building Disaster Prevention Association. 1991. *Standard for damage level classification of reinforced concrete buildings.* (In Japanese.)

Taizo Matsumori and Shunsuke Otani. 1998. Correlation between damage and nonlinear response analysis (case study of R/C building Jeunesse Rokko during the 1995 Hyogoken-Nanbu earthquake). *Journal of Structural and Construction Engineering* 505: 101–106. AIJ. March. (In Japanese.)

GRAVITY LOAD COLLAPSE OF REINFORCED CONCRETE FRAMES DURING EARTHQUAKES

J. MOEHLE[1], A. LYNN[2], K. ELWOOD[3], H. SEZEN[4]

ABSTRACT

Performance-based earthquake engineering methodologies generally recognize structural stability as one of the critical performance levels, yet reliable procedures for understanding and modeling collapse have not been developed. An approach is being developed to identify lateral force failure and gravity load failure criteria in individual concrete columns, and to extend those results analytically to complete building frames. The approach is intended to be applicable to older reinforced concrete building frames susceptible to column shear failures. The overall approach, failure studies of concrete columns, and planned analytical developments are described.

INTRODUCTION

Before the introduction of special requirements in the 1970s, reinforced concrete building frames constructed in zones of high seismicity in the US had details and proportions similar to frames designed primarily for gravity loads. Columns generally were not designed to have strengths exceeding beam strengths, so column failure mechanisms often prevail. Relatively wide spacing of transverse reinforcement was common, such that column failures may involve some form of shear or flexure-shear failure. As shear failure proceeds, degradation of the concrete core may lead to loss of axial load carrying capacity of the column. The

[1] Professor and Director, Pacific Earthquake Engineering Research Center, UC Berkeley
[2] Assistant Professor, California Polytechnic State University
[3] Graduate Student Researcher, PEER, UC Berkeley
[4] Graduate Student Researcher, PEER, UC Berkeley

dynamic redistribution of internal actions within the building frame may progressively lead to collapse of the building frame. This sequence is the focus of the ongoing study reported here.

Earthquakes repeatedly have shown the vulnerability of frames to column shear failures (Mexico, 1985; Guam, 1993; Northridge, 1994; Kobe, 1995; Turkey, 1999). While the vulnerability is plainly evident, the mechanisms by which collapse occurs is not. Several examples can be found of building frames having sustained shear failures of multiple columns, yet the building has stood (Figure 1). Researchers and engineers continue to debate the relation between column shear failure and building collapse.

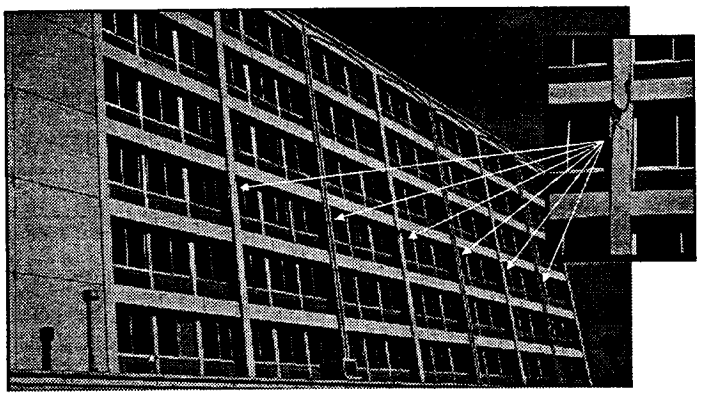

Figure 1. Building frame with column shear failures

Performance-based earthquake engineering methodologies generally recognize structural stability as one of the critical performance levels, yet reliable procedures for understanding and modeling collapse have not been developed. Component-based acceptance criteria such as those in FEMA 273 are of limited utility because structural stability is checked on the basis of individual component demands, whereas collapse is a system limit state. Application of those guidelines by several West Coast engineering offices has resulted in a plurality of cases in which the study building does not meet the collapse prevention performance objective, and no reasonable retrofitting strategy can bring it back from the brink. It is unclear whether this is the result of authentic building vulnerability, an overly simplistic and conservative criteria, or both.

Some research has defined criteria for structural collapse from a system perspective, including criteria such as total system drift, tendency of drift to increase at an increasing rate as shaking level increases, or degradation of total lateral resistance to some fraction of the peak strength. It is not clear that these approaches adequately model the component and system failure characteristics of interest for older existing concrete building frames. In the present study, an approach is being developed to identify lateral force failure and gravity load failure criteria in individual concrete columns, and to extend those results analytically to complete building frames. The overall approach, failure studies of concrete columns, and planned analytical developments are described.

REVIEW OF EXPERIMENTAL AND ANALYTICAL APPROACHES

Only limited experimental work has been done on the gravity load collapse of frames during earthquakes. Kogoma, et al. (1992) performed shaking table tests to demonstrate the rapid loss of gravity load capacity after the shear failure of non-ductile reinforced concrete columns. The test frame was restricted to a line of identical columns, all failing essentially simultaneously, such that redistribution potential of a more diverse building frame was not apparent.

Analytical studies of the collapse of frames should include strength degradation of the components and should define the collapse limit state. In the investigation of SDOF systems with stiffness and strength degrading characteristics, Song and Pincheira (1999) have defined collapse as the complete loss of lateral load resistance. A similar definition was used by Sato and Kuwamura (1996), who studied the effect of brittle steel column failures on the lateral resistance of the system. Casciati and Faravelli (1984) defined failure of a component in a reinforced concrete frame using damage indices and collapse of the system by a predetermined drift index. Unlike other studies, Casciati and Faravelli included the loss of axial capacity when failure in a column was detected.

The 50% draft of "Seismic Design Criteria for New Moment-Resisting Steel Frame Construction" prepared by the SAC steel project (SAC, 1999) defines collapse using a "dynamic pushover curve" (also known as Incremental Dynamic Analysis). The structure is analyzed with a ground motion scaled to a series of increasing spectral accelerations at the fundamental period of the structure. For each analysis the maximum interstory drift is recorded and plotted against the spectral acceleration (Figure 2). A straight line through the origin with a slope of 80% of the initial slope of the dynamic pushover curve is plotted on the figure. The drift at which the dynamic pushover curve intersects the straight line is defined as the capacity for collapse prevention.

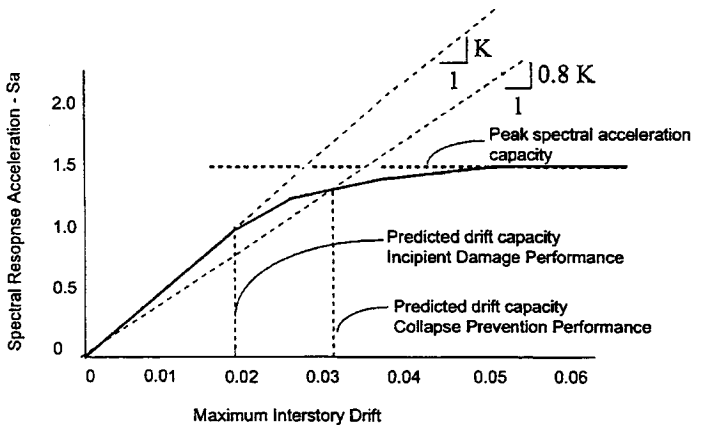

Figure 2. Dynamic pushover analysis

Collapse of reinforced concrete frames also has been defined using damage indices. Some use a weighted average of the damage indices for each component (Park and Ang, 1985), while others evaluate the index by considering the stiffness of the system before and after a nonlinear dynamic analysis (Ghobarah et al., 1998). However, most damage indices are based on models that do not consider shear failure.

The goal of the current analytical study is to identify critical failure modes that lead to the gravity load collapse of reinforced concrete frames. The current study is being conducted in two phases. The first phase will investigate the effect of column shear failures (loss of lateral capacity without loss of axial force capacity) on the lateral-load-resisting system. The second

phase will include the loss of axial force capacity. Owing to the difficulties of tracking the collapse behavior of a structure with current analysis programs, new nonlinear dynamic analysis software is being developed to conduct this study.

Shear failure of individual components is being based on the demands exceeding capacities, as determined from the test results outlined later in this paper. Flexural hinging in both beams and columns is considered, and interacts with shear failure mechanisms. Preliminary results from the first phase support a view that the sudden shear failure of a column can lead to very large drift demands at that story.

In the second phase, analyses will be conducted considering varying rates for the loss of gravity load capacity. It is believed that if the gravity load capacity of a column is lost instantaneously, then adjacent columns will experience a dynamic overshoot in additional axial load as they are forced to pick up the gravity loads from the failed column. If the loss of gravity load occurs more slowly, then the dynamic overshoot should not be as significant. The objective of the study will be to identify the effects of failure rate, inelastic response (including energy dissipation), and framing geometry on the redistribution of internal actions and the progression of collapse.

REVIEW EXPERIMENTAL COLUMN DATA

A review of the literature on experimental tests of columns representative of older existing building frames identified a large number of relevant tests. In almost all cases, however, the reported tests provided unconvincing or incomplete results. Whereas tests of nearly-full-scale columns under realistic loading and boundary conditions were sought, almost all tests were on smaller-scale columns tested as cantilevers. Furthermore, tests characteristically were discontinued after lateral load failures were observed, regardless of whether axial load capacity had been exhausted. To obtain the necessary data, new tests are being carried out. Results of these tests are supplemented by test data already existing.

Figure 3 illustrates a typical column specimen configuration. The columns were constructed at full scale. Because the focus of this project was to study only the behavior of the column, the end beams were made relatively stiff and strong. The loading routine subjected the column to nominally constant axial compression and maintained nominally zero rotation between column ends while the column was subjected to series of lateral displacements at increasing amplitude, with three cycles at each amplitude. Loading continued until axial load capacity was lost. Specific column characteristics, material properties, applied loads, and responses for tests completed as of the time of this writing are summarized in the first ten entries in Table 1.

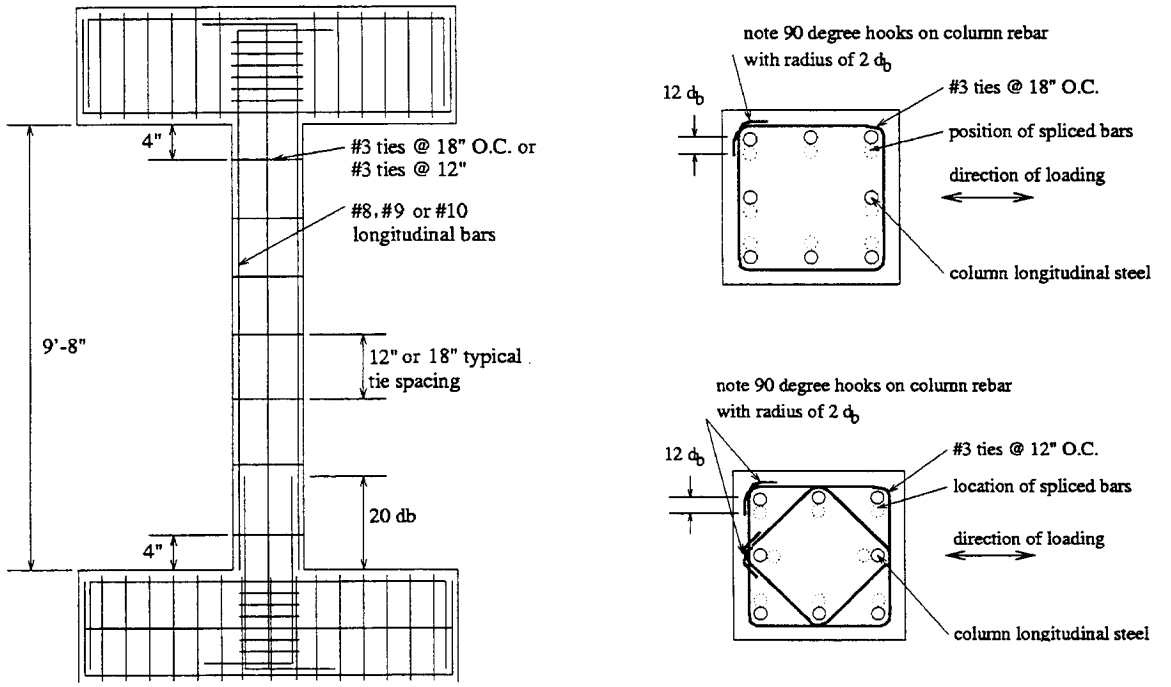

Figure 3. Typical column test specimen (Lynn, et al. 1996)

Table 1. Test specimen materials and details

Specimen	b	d	a	l_{splice}	No. bars	$\rho_{long.}$	A_{sw}	s	Tie type	f'_c	$f_{y\text{-}long.}$	$f_{y\text{-}tran.}$	P	fail. mode	V_u	δ_y	δ_u	μ_δ
	(in.)	(in.)	(in.)	(in.)	(no.)		($in.^2$)	(in.)		(ksi)	(ksi)	(ksi)	(kips)		(kips)	(in.)	(in.)	
Lynn and Moehle, 1996																		
3CLH18	18.00	15.00	58.00	none	8	0.03	0.22	18.0	r90	3.71	48	58	113	SCF	61.00	0.76	1.20	1.58
3SLH18	18.00	15.00	58.00	25	8	0.03	0.22	18.0	r90	3.71	48	58	113	SCF	60.00	0.68	1.15	1.69
2CLH18	18.00	15.00	58.00	none	8	0.02	0.22	18.0	r90	4.80	48	58	113	FSCF	54.00	0.72	3.00	4.17
2SLH18	18.00	15.00	58.00	20	8	0.02	0.22	18.0	r90	4.80	48	58	113	FSCF	52.00	0.68	1.80	2.65
2CMH18	18.00	15.00	58.00	None	8	0.02	0.22	18.0	r90	3.73	48	58	340	STF	71.00	0.31	0.60	1.94
3CMH18	18.00	15.00	58.00	None	8	0.03	0.22	18.0	r90	4.01	48	58	340	SCF	76.00	0.28	0.60	2.14
3CMD12	18.00	15.00	58.00	None	8	0.03	0.38	12.0	d90	4.01	48	58	340	SCF	80.00	0.36	0.90	2.50
3SMD12	18.00	15.00	58.00	25	8	0.03	0.38	12.0	d90	3.73	48	58	340	SCF	85.00	0.33	0.90	2.73
Sezen and Moehle, 1999																		
2CLD12	18.00	15.00	58.00	None	8	0.024	0.38	12.0	d90	3.05	64	68	150	SCF	68.00	1.00	3.00	3.00
2CHD12	18.00	15.00	58.00	None	8	0.024	0.38	12.0	d90	3.05	64	68	600	SCF	77.00	0.65	1.90	2.92
Bett, Klingner and Jirsa, 1985																		
1-1	12.00	10.38	18.00	None	8	0.02	0.20	8.0	d135	4.33	67	60	65		47.00	0.19	0.57	3.00
Ikeda, 1968																		
43	7.87	6.81	19.69	None	6	0.02	0.09	3.9	r135	2.84	63	81	18	FSCF	16.61	0.12	0.59	4.84
44	7.87	6.81	19.69	None	6	0.02	0.09	3.9	r135	2.84	63	81	18	FSCF	17.16	0.12	0.59	5.00
45	7.87	6.81	19.69	None	6	0.02	0.09	3.9	r135	2.84	63	81	35	FSCF	18.48	0.12	0.59	4.87
62	7.87	6.81	19.69	None	10	0.02	0.09	3.9	r135	2.84	50	69	18	FSCF	12.98	0.10	0.52	5.28
63	7.87	6.81	19.69	None	10	0.02	0.09	3.9	r135	2.84	50	69	35	FSCF	15.40	0.09	0.55	5.79
64	7.87	6.81	19.69	None	10	0.02	0.09	3.9	r135	2.84	50	69	35	FSCF	15.40	0.08	0.66	8.00
Umemura and Endo, 1970																		
205	7.87	7.09	23.62	None	6	0.02	0.09	3.9	r135	2.55	67	47	35	STF	16.02	0.17	0.51	3.07
207	7.87	7.09	15.75	None	6	0.02	0.09	3.9	r135	2.55	67	47	35	STF	23.80	0.13	0.25	1.88
208	7.87	7.09	15.75	None	6	0.02	0.09	3.9	r135	2.55	67	47	88	FSCF	30.36	0.10	0.31	3.20
214	7.87	7.09	23.62	None	6	0.02	0.09	7.9	r135	2.55	67	47	88	SCF	18.59	0.15	0.42	2.86
220	7.87	7.09	15.75	None	6	0.01	0.04	4.7	r135	4.77	55	94	35	FSCF	17.60	0.09	0.94	10.00
231	7.87	7.09	15.75	None	6	0.01	0.04	3.9	r135	2.14	47	76	35	FSCF	11.44	0.07	0.64	9.00
232	7.87	7.09	15.75	None	6	0.01	0.04	3.9	r135	1.90	47	76	35	FSCF	13.09	0.11	0.94	8.89
233	7.87	7.09	15.75	None	6	0.01	0.04	3.9	r135	2.02	54	76	35	FSCF	15.53	0.11	0.54	4.93
234	7.87	7.09	15.75	None	6	0.01	0.04	3.9	r135	1.90	54	76	35	FSCF	15.07	0.11	0.63	5.71
Kokusho, 1964																		
372	7.87	6.69	19.69	None	4	0.01	0.10	3.9	r135	2.88	76	51	35	FSCF	16.72	0.10	0.42	4.12
373	7.87	6.69	19.69	None	4	0.02	0.10	3.9	r135	2.96	76	51	35	FSCF	19.80	0.14	0.39	2.78
Kokusho and Fukuhara, 1965																		
452	7.87	6.69	19.69	None	4	0.03	0.10	3.9	r135	3.18	52	46	88	FSCF	24.75	0.12	0.30	2.53
454	7.87	6.69	19.69	None	4	0.04	0.10	3.9	r135	3.18	52	46	88	FSCF	24.75	0.09	0.20	2.32

Notation: A_{sw} = area of tie steel; a = shear span; b = square column dimension; d = depth to centerline of tension reinforcement; $f_{y\text{-}long}$= long. reinf. yield strength; $f_{y\text{-}tran}$ = trans. reinf. yield strength; l_s = lap splice length; P = axial load; s = hoop spacing; V_u = peak shear; δ_y = yield displacement; δ_u = displacement when 20 percent of peak shear is lost; ρ_{long} = total long. steel ratio; $\mu_\delta = \delta_u/\delta_y$. Tie types are: r90 - rect. w/ 90° hooks; r135 - rect. w/ 135° hooks; d90 - rect. and diamond w/ 90° hooks; d135 rect. and diamond w/ 135° hooks. Failure modes are: FSCF - flexural shear compression failure, several inclined cracks; SCF - shear compression failure, many inclined cracks; STF - shear tension failure, very large inclined crack.

Figure 4 plots measured relations between lateral force and lateral displacement for test columns 2CLH18, 2CLD12, and 2CHD12, illustrating three different failure modes. The data for 2CLH18 show moderate flexural ductility, followed by loss of lateral resistance due to shear failure, followed at somewhat larger displacements by axial load failure. Column 2CLD12 had low flexural ductility interrupted by loss of lateral resistance due to shear failure, but sustained vertical load capacity to relatively large displacements. Column 2CHD12 had low flexural ductility interrupted by sudden shear and gravity load failure.

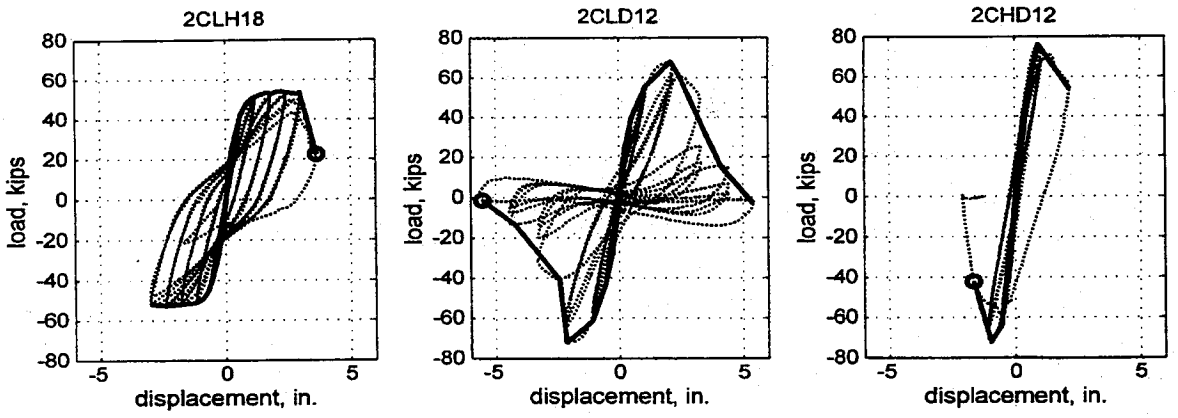

Figure 4. Measured relations between lateral load and displacement (Note: Scale approximate)

Additional data were gathered to supplement the tests of Lynn and Sezen. In selecting data, the following criteria were applied: cross sections were rectangular, with one side not less than 2/3 the dimension of the other side and minimum dimension around 8 in.; shear span ratio $2 \leq a/d \leq 4$; concrete compressive strength range 2500 psi $\leq f'_c \leq$ 6000 psi; reinforcement nominal yield stress 40 ksi $\leq f_y \leq$ 80 ksi; longitudinal reinforcement ratio $0.01 \leq \rho_l \leq 0.08$; hoop spacing $s \geq d/2$; lateral load reversed and cyclic in application; failure apparently attributable to shear distress. Although tests with contraflexure were desired, among those tests satisfying the other criteria only cantilever tests were identified. Tests reported by Bett, Klingner and Jirsa (1985), Ikeda (1968), Umemura and Endo (1970), Kokusho (1964), Kokusho and Fukuhara (1965) were added (Table 1). None of the cited works systematically reported response beyond the performance level of lateral load failure to the performance level of axial load failure.

In Table 1, all quantities were obtained from the references with the exception of the yield displacement, ultimate displacement, and resulting calculation for displacement ductility. Each of the references used a different definition of these terms. To provide uniformity among the data, the following procedure was used. A secant was defined by the origin (zero load and zero displacement) and the point where a horizontal line at 70% of the maximum applied shear intersected the envelope curve. The yield displacement was then defined by where that secant intersected a horizontal line passing through the envelope curve at the maximum applied shear. The ultimate displacement was defined as the displacement corresponding to termination of the test or where there was a loss of more than 20% of the maximum applied shear.

DEVELOPMENT OF A SHEAR STRENGTH MODEL

Performance assessments of existing concrete buildings require a shear strength model for columns. The FEMA 273 Guidelines contain the following expressions:

$$V_n = V_c + V_s \qquad \textbf{Equation 1}$$

$$V_c = 3.5\left(k + \frac{P}{2000A_g}\right)\sqrt{f_c'}bd \qquad \textbf{Equation 2}$$

$$V_s = \frac{A_{sw} f_y d}{s} \qquad \textbf{Equation 3}$$

in which V_n = nominal shear strength, V_c = contribution from concrete, V_s = contribution from hoops, k = 1 for displacement ductility less than 2, otherwise k = 0, P = axial load, A_g = gross concrete area, f_c' = concrete compressive strength (psi), b = width of section, d = effective depth, and other terms are as defined previously. In yielding regions of columns, transverse reinforcement is considered effective only if $s \leq d/2$ and hoops have hooks embedded in the core.

Figure 5 plots ratios of experimental shear strength to V_n as a function of displacement ductility achieved in the test. Values exceeding unity are cases in which the column

developed strength exceeding the strength calculated by FEMA 273. FEMA 273 tends to be excessively conservative, especially for cases in which the displacement ductility exceeds 2, because it sets V_c equal to zero.

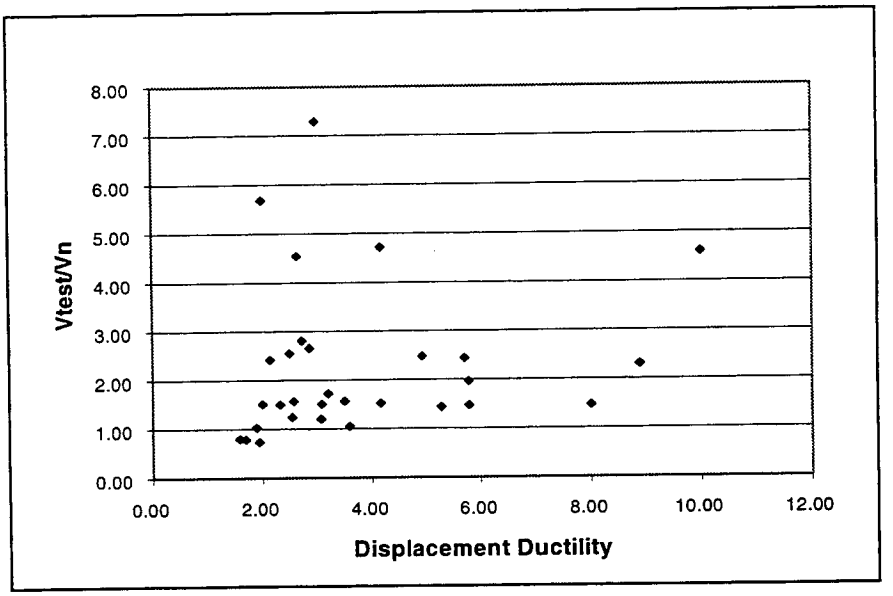

Figure 5. Comparison of FEMA 273 and measured shear strengths

An alternative shear strength model was developed. As with FEMA 273, the model assumes the strength can be represented by Equation 1. The concrete contribution was assumed to be related to the calculated nominal principal tension stress in the column. Principal tension stress capacity was set equal to $f_{tc} = 6\sqrt{f'_c}$ psi. Accordingly, the shear stress at which the principal tension stress capacity is reached is given by Equation 4.

$$\tau_{xy} = 6\sqrt{f_c'}\sqrt{1+\frac{P}{6A_g\sqrt{f_c'}}} \qquad \textbf{Equation 4}$$

In a concrete column with flexure, this shear strength is reduced because of interaction with flexural stress, and is further influenced by redistribution of internal actions as cracking occurs. This effect can be represented by introducing an aspect ratio term, a/d, where a = distance from maximum moment to inflection point. Multiplying by an effective cross-sectional area, $A_e = 0.8A_g$, results in

$$V_c = k\left(\frac{6\sqrt{f_c'}}{a/d}\sqrt{1+\frac{P}{6\sqrt{f_c'}A_g}}\right)(0.8A_g)\ \text{psi} \qquad \textbf{Equation 5}$$

The aspect ratio is limited to $2 \le a/d \le 3$.

In Equation 5, the term k is a modifier to account for strength degradation within the flexural plastic hinges. Similar terms have been introduced in other shear strength models. For this data set, k was defined as shown in Figure 6. Degradation relations proposed by other researchers [Aschheim and Moehle (1993); Priestley, Verma and Xiao (1994)], as developed from data sets including columns with higher quantities of transverse reinforcement, were found to overestimate the rate of degradation for this data set.

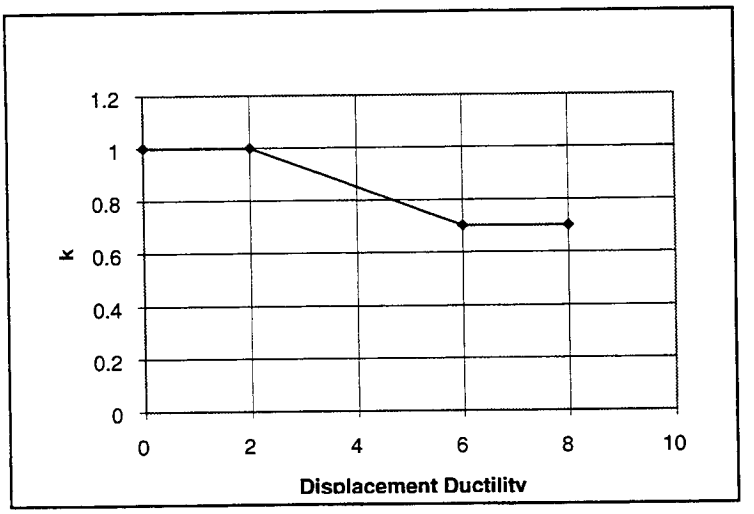

Figure 6. Parameter k

The steel contribution V_s is taken as half that given by Equation 3. Studies on the data in Table 1 showed that Equation 3 without the modifying coefficient overestimated the contribution of hoops. The coefficient 0.5 can be justified by two factors. First, the wide spacing of the hoops is such that shear cracks intersect perhaps only one or two hoop sets, and may intersect them near the cover where they are not fully anchored. Second, the low volume ratio of the transverse reinforcement may produce an under-reinforced condition in which the contribution of hoops to shear strength is not fully realized before significant degradation occurs in the concrete mechanisms.

Correlation of the shear strength model with the test data is plotted in Figure 7.

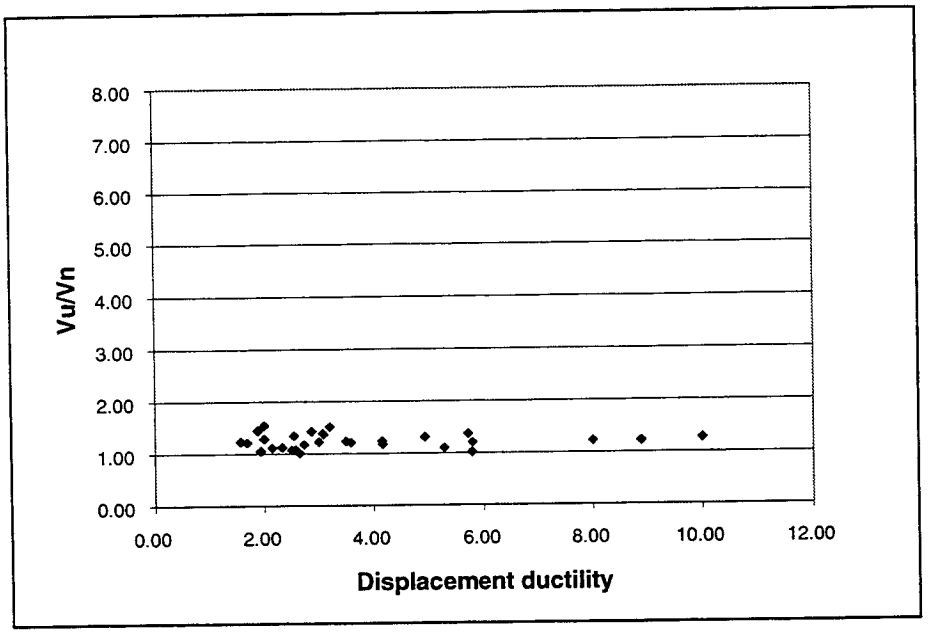

Figure 7. Comparison of shear strength model and test data

GRAVITY LOAD COLLAPSE OF CONCRETE COLUMNS

Most tests of columns have been terminated shortly after loss of lateral load capacity. This approach is sensible for columns considered as part of the lateral-force-resisting system, and also sensible from the traditional perspective of safety for new building designs — once shear failure begins, axial load collapse cannot be far behind. For existing buildings being evaluated for seismic resistance or being considered for seismic rehabilitation, a less conservative view is required by economic considerations. If a column can reliably carry gravity load after its lateral strength degradation begins, it may be possible to achieve considerable savings by considering the column as a secondary component. It was for these reasons that the tests by Lynn and by Sezen (Table 1) were conducted.

Figure 8 plots drift angles corresponding to significant events for the ten columns reported by Lynn and Sezen. For columns having lower axial loads, the tendency is for axial load failure to occur at relatively large drifts, regardless of whether shear failure had just occurred or whether shear failure had occurred at much smaller drift ratios. For columns with larger

axial loads, axial load failure tended to occur at smaller drift ratios, and might occur almost immediately after loss of lateral load capacity.

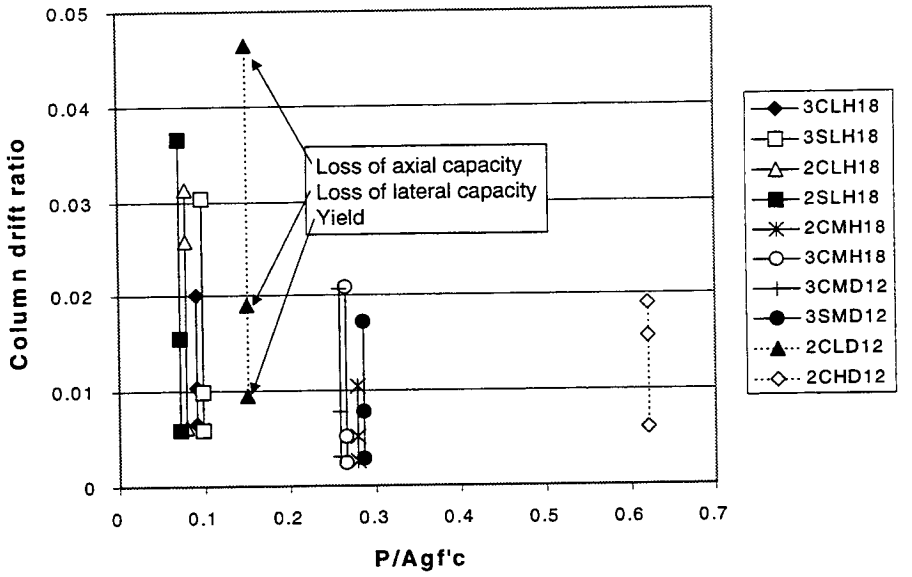

Figure 8. Plastic rotation capacity at collapse as a function of axial load

CONCLUSIONS

An ongoing effort to better understand shear failure and subsequent collapse of older existing concrete frame buildings is reported. It is concluded that current performance-based approaches to establishing the collapse limit state either are based on component acceptance criteria, thereby failing to represent collapse as a system limit state, or are based on system limit states that do not relate directly to the collapse phenomenon of concrete frames. Alternative approaches are needed.

Available data on response of lightly confined concrete columns were examined to identify an appropriate shear strength model and to identify trends in the loss of axial load capacity. A shear strength model is proposed as an improvement over the model described in FEMA 273. Trends with regard to axial load collapse are inconclusive, but suggest that

significant post-yield deformation capacities are available before loss of axial load capacity, regardless of when shear failure occurs, for lighter axial load levels. For higher axial load levels, axial load collapse can be immediate. Further studies are needed to identify specific ways to include component behaviors in system models.

ACKNOWLEDGMENT

The research reported in the paper was funded by the National Science Foundation under Grant No. BCS-9120214 and by the Pacific Earthquake Engineering Research Center (PEER). Dr. S. C. Liu was the cognizant program officer at NSF. The experimental studies by Lynn and Sezen were conducted in the research laboratories of PEER at the University of California, Berkeley.

REFERENCES

Aschheim, M. A., J. P. Moehle, and S. D. Werner. 1993. *Deformability of concrete columns.* Dames and Moore Technical Report to the California Department of Transportation. Contract 59Q122. June 1993.

Bett, B. J., R. E. Klingner, and J. O. Jirsa. *Behavior of strengthened and repaired reinforced concrete columns under cyclic deformations.* Phil M. Ferguson Structural Engineering Laboratory (PMFSEL). PMFSEL Report No. 85-3. December 1985.

Casciati, F., and L. Faravelli. 1984. Progressive failure for seismic reliability analysis. *Engineering Structures* 6 (April) 1984.

FEMA 273. 1997. *NEHRP guidelines for the seismic rehabilitation of buildings.* Washington D.C.: Federal Emergency Management Agency. October 1997.

Ghobarah, A., H. Abou-Elfath, and A. Biddah. 1998. Damage assessment of non-ductile reinforced concrete frames. *Eleventh European Conference on Earthquake Engineering.*

Hirosawa, Masaya. 1973. A list of past experimental results of reinforced concrete columns. *Building Research Institute*, Ministry of Construction 2 (March) 1973.

Ikeda, A. 1968. *Report of the Training Institute for Engineering Teachers.* Yokohama National University, Japan. March 1968.

Kogoma, I., T. Hayashida, and C. Minowa. 1992. Experimental studies on the collapse of RC columns during strong earthquake motions. *Tenth World Conf. on Earthquake Engineering, Madrid, Spain.*

Kokusho, S. 1964. *Report by Building Research Institute.* Tsukuba, Japan: Building Research Institute. March 1964.

Kokusho, S., and M. Fukuhara. 1965. *Report by Kokusho Laboratory.* Tokyo Industrial University. March 1965.

Lynn, A. C., J. P. Moehle, S. A. Mahin, W. T. Holmes. 1996. Seismic evaluation of existing reinforced concrete columns. *Earthquake Spectra* 12(4): 715–39. November 1996. Earthquake Engineering Research Institute.

Park, Y. J., and A. H.-S. Ang. 1985. Mechanistic seismic damage model for reinforced concrete. *Journal of the Structural Division* 111(4). ASCE.

Priestley, M. J. N., R. Verma, and Yan Xiao. 1994. Seismic shear strength of reinforced concrete columns. *Journal of the Structural Division* 120(ST8)(August). ASCE 1994.

SAC. 1999. *Seismic design criteria for new moment-resisting steel frame construction* (50% Draft).

Sato, Y. and H. Kuwamura. 1996. Dynamic progressive failure of multistory frames having brittle columns. *Eleventh World Conference on Earthquake Engineering, Acapulco, Mexico.*

Song, J. K., and J. A. Pincheira. 1999. *Spectral displacement demands of stiffness and strength degrading sdof systems.* Manuscript provided by authors. 1999.

Umemura, H. and T. Endo, T. 1970. *Report by Umemura Laboratory.* Tokyo University. December 1970.

RESIDUAL AXIAL CAPACITY AND RESTORABILITY OF REINFORCED CONCRETE COLUMNS DAMAGED DUE TO EARTHQUAKE

Akira TASAI [1]

ABSTRACT

The deterioration of the axial strength of a flexural column was analyzed by inelastic moment-curvature analysis of the section. In the analysis, after cyclic loading to the section, the axial strain was uniformly increased to obtain the axial strength. The analysis demonstrated significant deterioration of the axial strength before the ultimate limit state, defined as the state that the axial load capacity decreases to the level of the long-term axial load. An experimental program was executed not only to observe the phenomenon but also to study the effect of repair after the deterioration of axial strength. Column specimens about half-scale were loaded in the axial direction after cyclic lateral loading. It was found that the deterioration of axial capacity was large under a large long-term axial load or a large compressive varying axial load. Simple repair methods were applied to specimens damaged due to lateral loading; i.e., by replacing crushed cover concrete with rapid hardening type cement mortar with the same strength as the original concrete or by injecting epoxy into cracks. Both the lateral stiffness and strength of the repaired column whose axial strength had deteriorated by the original lateral loading were lower than those of the original one. Sequential moment-curvature analysis including original and post-repair loading indicated that softening of a part of the core concrete during original loading significantly influenced the performance after repair.

1. INTRODUCTION

An evaluation of the residual capacity and restorability of structures or elements at a site after a specified earthquake is important in performance-based seismic design. The ultimate state of reinforced concrete columns has often been defined by many researchers as a state of vanishing axial capacity to sustain the live and dead loads (long-term load). However, the axial capacity of a column subjected to seismic loading must gradually decrease as damage develops.

1 Department of Architecture, Faculty of Engineering, Osaka Institute of Technology, Osaka 535-8585, Japan

Email: tasai@archi.oit.ac.jp

The relation between the latent decrease of the axial capacity of columns and their restorability was investigated analytically and experimentally to contribute to performance-based seismic design.

2. PRELIMINARY ANALYSIS

The deterioration of axial capacity in a column after cyclic lateral loading was studied by applying an elementary inelastic analytical method to a section; i.e, fiber model. As is well known, by this method, after the section was divided into fiber-segments parallel to the neutral axis, assuming Bernoulli-Euler's hypothesis, the inelastic moment vs. curvature relationship was analyzed based on the assumed uniaxial stress-strain relationship of the concrete and the longitudinal reinforcement (Fujii 1973). The influence of shear and bond slip between the steel and concrete was neglected. Assumed uniaxial stress strain relationship of concrete and steel are shown in Figure 1. In the concrete model, the differences in the compressive strength and softening characteristic between the core concrete and the cover concrete were considered. In the steel model, strain hardening and the Bauschinger effect were included. After optional cyclic loading, both moment and curvature were converged to the original point, and then the strain vertical to the section were increased uniformly to obtain the maximum axial strength.

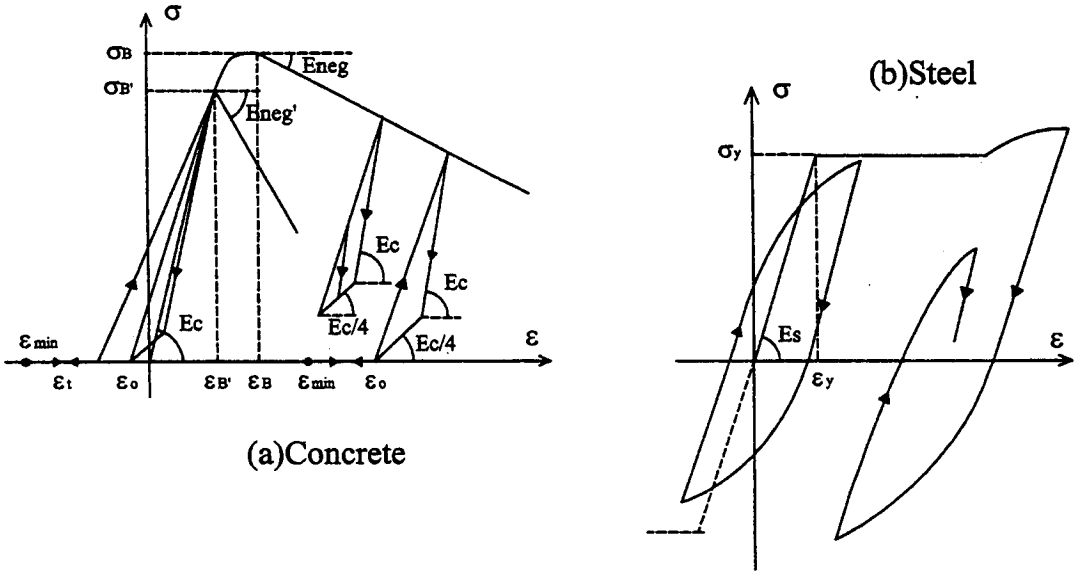

Figure 1: Uniaxial stress-strain model of materials

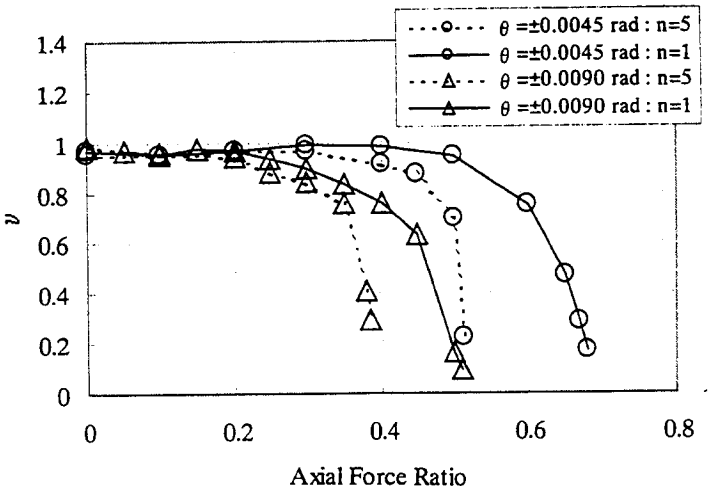

Figure 2: The ratio of residual axial strength

A column at the first story in a twelve-story office building which was designed according to the design guidelines for earthquake-resistant reinforced concrete buildings based on the ultimate strength concept of the AIJ, was chosen as an example for analysis. The deterioration of the axial strength of the column after lateral cyclic loading of constant amplitude is shown in Figure 2. The horizontal axis represents the axial force ratio, which was defined as the ratio of long-term load to the original axial strength of a column including the contribution of the longitudinal reinforcement. The vertical axis ν represents the ratio of residual axial strength, which was defined as the following equation.

$$\nu = (N_{max}' - N_L) / (N_{max} - N_L) \qquad (1)$$

Where, N_{max}: original axial strength of column,

N_{max}': axial strength of column after optional lateral loading, and

N_L: long-term axial load

When the column has lost the ability to sustain the long-term axial load, the value of ν just reaches zero, the ultimate limit state of the column. Figure 2 shows significant characteristics of residual axial strength. Under cyclic lateral loading, the axial strength deteriorated above a certain axial force ratio. The deterioration depended on the axial force ratio, the lateral deformation amplitude, and numbers of loading reversals. In the analysis, softening of a part of the core concrete strongly influenced the deterioration. The experimental program was executed

not only to observe the phenomenon but also to study the effect of repair after the deterioration of axial strength.

3. TEST OF COLUMNS

A total of eight column specimens A1–A8 were tested (Kitada 1998)(Watanabe 1999). All the specimens were designed to fail in flexure and had a uniform section of 300 x 300 mm, as shown in Figure 3. The shear span-to-depth ratio was 2.5 in specimens A1–A4 and 2.0 in specimens A5 – A8. High confinement was given to specimens A5–A8. The main parameters of the tests were

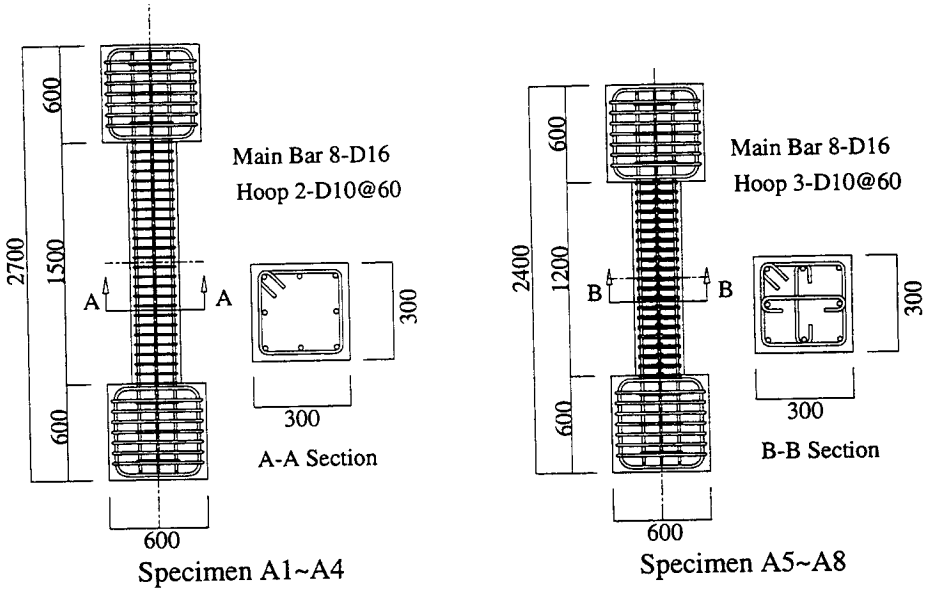

Figure 3: Outline of specimens

Table 1: Parameters of test

Specimen	Main Bar	Hoop	Pw (%)	Axial Load	Maximum Deformation Angle(rad.)		Repair Methods		Axial Loading
					Original	Post-Repair	Replacing Cover Concrete	Injecting Epoxy Resin	
A1	8-D16	2-D10 @60	0.79	$0.2\sigma_B$	1/33				Applied
A2				$0.35\sigma_B$					Applied
A3/A3R				$0.2\sigma_B$		1/33	Applied		Applied (A3R)
A4/A4R				$0.35\sigma_B$		1/33	Applied		
A5/A5R		3-D10 @60	1.19	$0.05\sigma_B$~$0.50\sigma_B$	1/33	1/100	Applied	Applied	Applied (A5R)
A6					1/100				Applied
A7/A7R				($0.25\sigma_B$)	1/100	1/100	Applied		Applied (A7R)
A8/A8R					1/100	1/33	Applied	Applied	Applied (A8R)

Pw : Shear Reinforcement Ratio σ_B : Concrete Compressive Strength by Cylinder Test

Table 2: Material properties

A1~A4

	Concrete (comp.)	Steel (yield)		Repair Mortar (comp.)
		D16	D10	
Stress (N/mm^2)	46.2	328	365	35.6

A5~A8

	Concrete (comp.)	Steel (yield)		Repair Mortar (comp.)	Epoxy Resin (comp.)
		D16	D10		
Stress (N/mm^2)	46.2	387	379	46.9	26.5

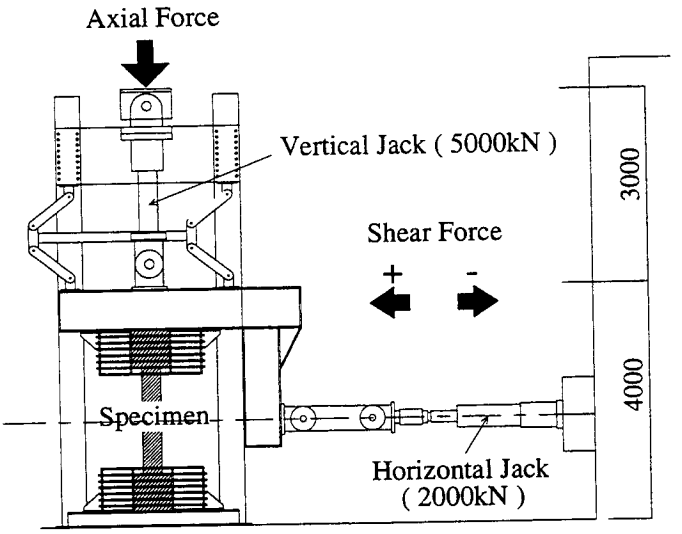

Figure 4: Loading apparatus

the damage level by controlling the axial load and maximum lateral deformation, and the repair methods as listed in Table 1. All specimens were subjected to antisymmetric bending reversals by the loading apparatus shown in Figure 4. A constant axial load of two levels was applied to specimens A1–A4, while varying axial load was applied to specimens A5–A8 as the same rule shown in Figure 5. Some specimens were loaded in the axial direction after corrected residual deformation by the original lateral loading in order to observe the deteriorated axial strength. Other specimens were repaired after the original loading by simple repair methods; i.e., replacement of the damaged cover concrete by rapid hardening type cement mortar or by injecting of epoxy resin into concrete cracks or both. Post-repaired specimens were then reloaded to investigate the restorability after deterioration of the axial strength by the original lateral loading. The constant axial load was maintained during the repair work and the curing to simulate actual repair condition. The material properties of the concrete, reinforcement, and repair materials are listed in Table 2. In addition to the column test, prism specimens with the same dimensions and materials as the column specimens were tested to obtain the uniaxial stress-strain relationship of confined and unconfined concrete.

In all specimens, cracks or crushing of the cover concrete concentrated in both ends of the column within the length of the depth, demonstrating flexural damage by the original loading. The restoring force characteristics of specimens under constant axial load A3, A3R, A4, and A4R

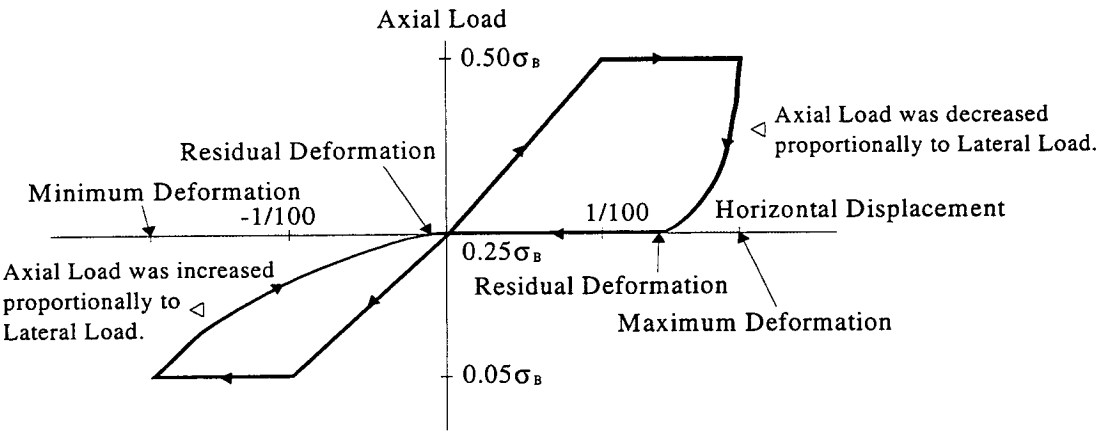

Figure 5: Rule of varying axial load

are shown in Figure 6. The P-Δ effect by the axial load was removed in the relationship. Stiffness and strength deteriorated significantly after repair in both specimens. Especially specimen A4R, that was subjected to higher axial load reached the ultimate limit state and lost the ability to sustain the constant axial load at the final loading cycle. Restoring force characteristics of specimens under varying axial load are shown in Figure 7. In these specimens, stiffness after repair deteriorated in the positive loading direction with increasing axial load. Especially, in specimen A5R in which the damage of concrete was significantly large during the original loading, the deterioration was remarkable. In negative loading direction with decreasing of axial load, the deterioration in stiffness and strength was observed to be small.

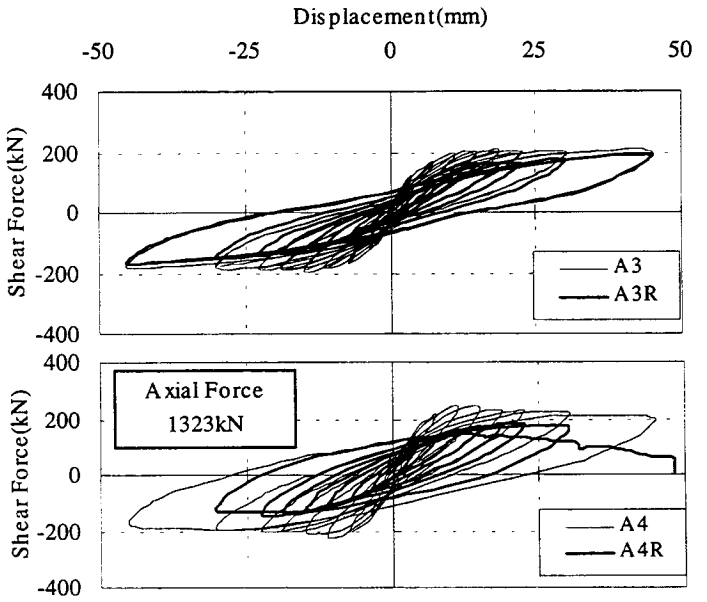

Figure 6: Observed restoring force characteristics under constant axial load

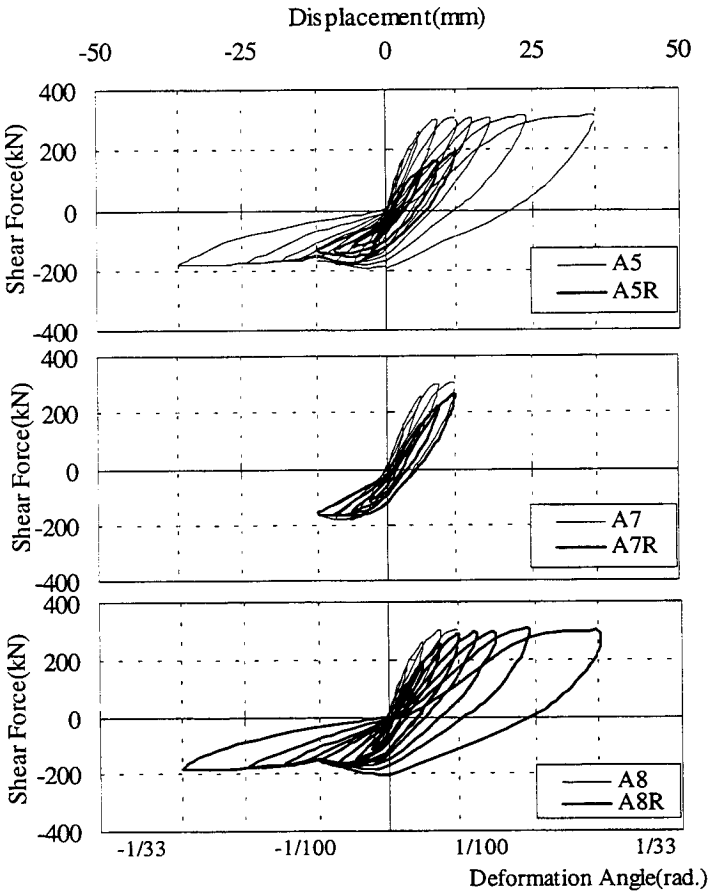

Figure 7: Observed restoring force characteristics under varying axial load

4. RESIDUAL AXIAL STRENGTH AND RESTORABILITY OF SPECIMENS

According to the procedure described in section 2, the residual axial strength of column specimens was analyzed based on the uniaxial stress-strain relationship of confined core concrete and unconfined cover concrete obtained from the uniaxial compressive test of prism specimens. An example of the uniaxial models (Nakatsuka 1989) used in the analysis is shown in Figure 8 comparing with test results of prism specimens. The curvature in the analysis was translated to the deformation of the specimen assuming that the curvature distributed uniformly along the height of the column ends within the length equivalent to the column depth. An analysis of the relationship between the axial force ratio and the ratio of residual axial strength ν for specimens A1– A4 are shown in Figure 9. The test results obtained from axial loading after lateral cyclic loading of specimens A1 and A2 are also plotted here. The decrease in the ratio of residual axial

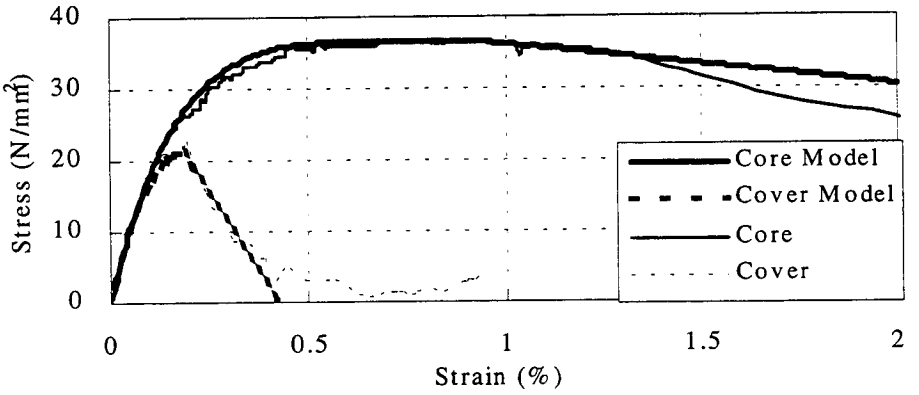

Figure 8: Uniaxial concrete model

strength was larger in the analysis than in the test result. However, the remarkable decrease under the large axial force ratio was also observed in the test. It should be noted that the ratios of residual axial strength of specimens A3 and A4 were judged to have decreased to the same levels as specimens A1 and A2 respectively and the restorability of specimen A4R was lower than that of specimen A3R. The restorability related strongly to the residual axial strength. The ratios ν of specimens A6, A5R, A7R, and A8R are plotted together with analytical result in Figure 10. The ratio decreased even with high confinement. In specimen A5, the ratio was judged to have decreased about 0.9 and to have not restored to the original level by the repair because the ratio of specimen A5R was almost equal to that of specimen A8R. Deterioration in lateral stiffness and strength was remarkable in specimen A5R.

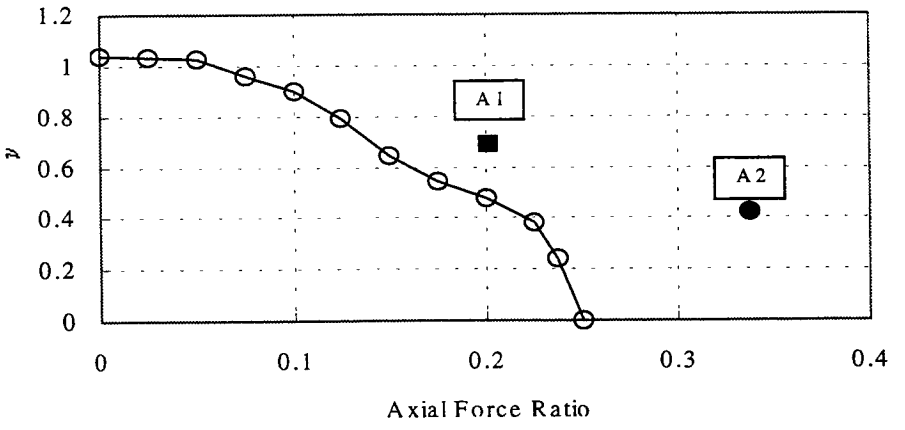

Figure 9: Residual axial strength under constant axial load

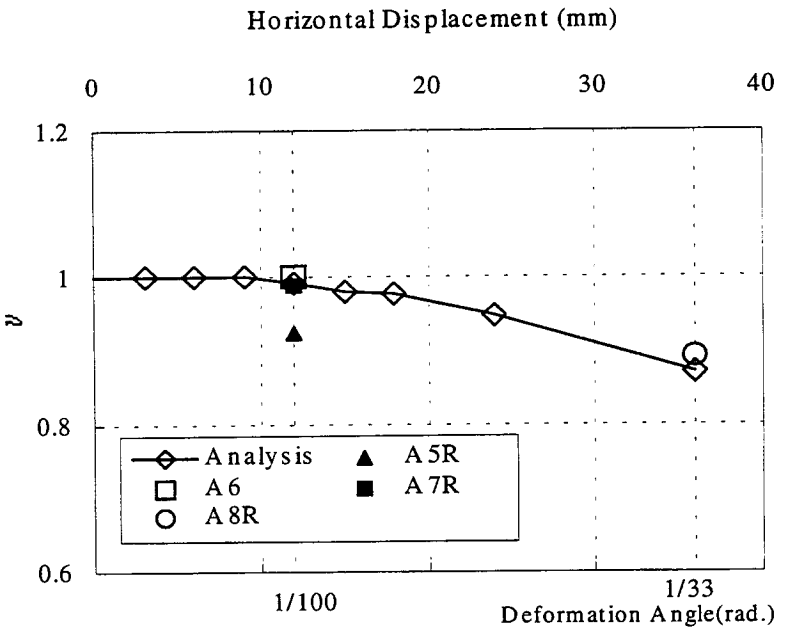

Figure 10: Residual axial strength under varying axial load

The restoring force characteristics of specimens under varying axial load was analyzed including post-repaired lateral loading by the procedure described in the section 2. The curvature in the analysis was translated to the deformation of the specimen assuming distribution of the curvature

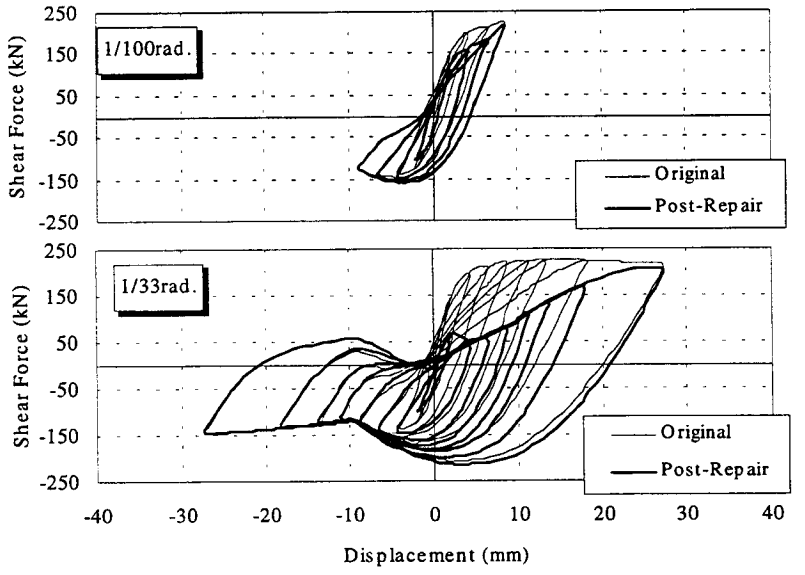

Figure 11: Analyzed restoring force characteristics

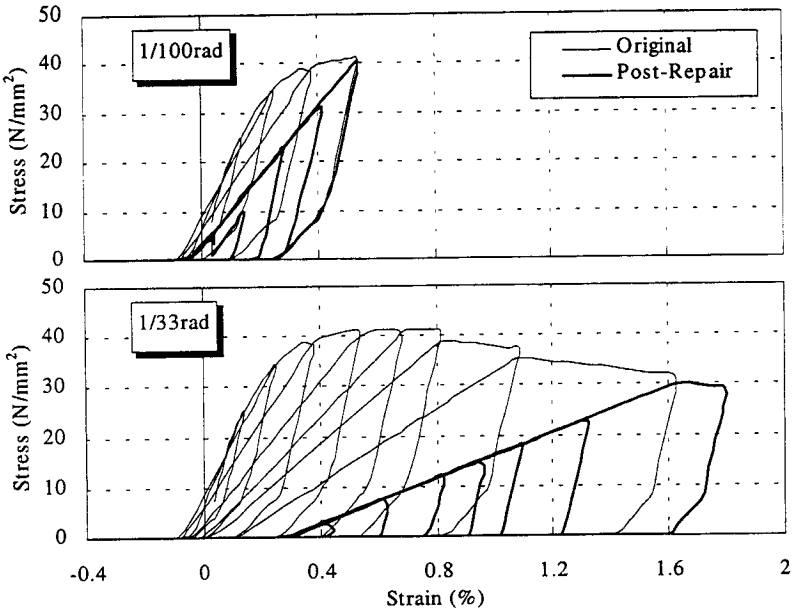

Figure 12: Response of extreme segment of core concrete

along the height. In the test, the repair work was conducted under constant axial load to the specimens. Assumption of linear distribution of strain in the section was impossible to be applied in the analysis of the post-repaired loading because of existing no axial strain in the new material formed instead of damaged cover concrete and existing axial strain corresponding to the constant axial load in the core concrete and longitudinal reinforcement at the beginning of post-repaired loading. Therefore, in the analysis of post-repaired loading, linear distribution of incremental strain was assumed after initializing the characteristics of cover concrete. Results of sequential analysis including original and post-repaired loading are shown in Figure 11. Deterioration of lateral capacity in increasing of axial load was well demonstrated especially in case of large amplitude corresponding to specimen A5R. Responses of the extreme outer segment of core concrete subjected to compression during positive loading are shown in Figure 12. Deterioration of stiffness due to original loading was observed in post-repaired loading. It should be noted that the deterioration was remarkable when the response reached the softening range during original loading. Decreasing of residual axial strength and restorability of column member was judged to be caused by the deterioration of core concrete. In order to maintain the performance to resist vertical and lateral load after earthquake, it is necessary that the response of core concrete is controlled not to reach the inelastic range.

5. CONCLUSIONS

The residual axial strength and restorability of a flexural reinforced concrete column after cyclic lateral loading were investigated analytically and experimentally. The following conclusions were obtained.

(1) Latent deterioration of the axial capacity of a reinforced concrete column subjected to seismic loading was observed experimentally even before the ultimate limit state. The ratio of the residual axial strength was smaller in cases of the larger long-term axial load. The phenomenon was well predicted by the inelastic moment-curvature analysis using a fiber model.

(2) The performance after simple repair by replacing damaged cover concrete with a new one or by injecting epoxy into cracks deteriorated proportionally to the decrease of the ratio of the residual axial capacity due to the original loading. In the case of being subjected to varying axial load, the deterioration of member stiffness was observed in compressive varying axial load even before the decrease of the ratio.

(3) The modified inelastic moment-curvature analysis clarified that the reason for the remarkable deterioration after repair was the softening of a part of the core concrete during the original loading. The response of core concrete should be controlled to not reach the inelastic range for reasonable restorability.

REFERENCES

Fujii, S., H. Aoyama, and H. Umemura. 1973. Moment-curvature relationship of reinforced concrete section obtained from material properties. *Summaries of Technical Papers of Annual Meeting AIJ*:1261–62. (In Japanese.)

Kitada, T., and A. Tasai. 1998. Study on residual axial capacity and damage restorability of flexural columns after earthquake. *Proceedings of JCI* 20(3): 433–38. (In Japanese.)

Nakatsuka, T., K. Suzuki, and M. Sugata. 1989. Mechanism of confinement and strength deformation characteristics of confined concrete with rectangular lateral reinforcement. *Proceedings of JCI* 11(2): 449–54. (In Japanese.)

Watanabe, A., and A. Tasai. 1999. Residual axial strength and damage restorability of flexural columns under varying axial load after earthquake. *Proceedings of JCI* 21(3): 619–24. (In Japanese.)

TEST AND ANALYSIS OF REINFORCED CONCRETE BEAMS UNDER AXIAL RESTRAINT

Masaki MAEDA[1], Toshimi KABEYASAWA[2], Yasushi SANADA[3]

ABSTRACT

Tests, analyses, and earthquake damage have all indicated that the shear forces in columns of yielding beams in reinforced concrete frames can be higher than calculated based on an analysis that neglects the inelastic axial elongation of the beams, which is caused by the material properties of reinforced concrete, including crack opening behavior. The effect of beam elongation has been neglected in practical design analysis, even by the most sophisticated nonlinear analytical method. The purposes of this study are to investigate experimentally the behavior of beams under axial restraint, and to establish a simple analytical model to evaluate the axial elongation and the restraint force in beams.

Four beams, with different axial restraint stiffnesses and different shear span ratios, were tested under an axial restraint force applied in proportion to the axial elongation. The effect of axial restraint stiffness on flexural strength, and the axial force in beams was investigated. The relation of flexural crack widths to beam elongation was also examined to correlate the damage level with the lateral displacement. A simple analytical model, in which the axial elongation was derived from the rotation of a rigid body and the compressive deformation of a diagonal strut, was developed to evaluate the axial elongation and the restraint force in beams.

The major findings are (1) The increase in beam elongation was nearly proportional to the lateral displacement until crushing of the concrete observed at the beam ends. The beam elongation was governed by the axial restraint stiffness, while no significant effect of the shear span ratio on the elongation was observed. (2) The axial force caused by the axial restraint raised the flexural strength in the beam. The ratio of the observed strength to strengths calculated without axial force was approximately 1.3 through 1.8 at the yielding point. The ratio was as large as 2.0 through 2.4 for the maximum shear force. (3) A fairly good agreement was obtained between the measured beam elongation and the sum of the flexural crack widths. (4) The beam axial elongation could be precisely evaluated by the proposed simplified analytical model until the maximum shear force was reached.

[1] *Associate Professor, Department of Architecture, Yokohama National Univ., Yokohama, Japan*
Email: maeda@arc.ynu.ac.jp

[2] *Professor, Earthquake Research Institute, The University of Tokyo, Dr. Eng., Tokyo, Japan*
Email: kabe@eri.u-tokyo.ac.jp

[3] *Graduate Student, Department of Architecture, The University of Tokyo, Tokyo, Japan*
Email: sanada@ eri.u-tokyo.ac.jp

1. INTRODUCTION

During severe earthquakes it is desirable that the overall structure of a reinforced concrete frame building perform like the ductile flexible collapse mechanism of the weak-beam strong-column type. In design analysis, the response of buildings, especially the shear forces in columns, should be precisely estimated to ensure the intended overall yielding beam mechanism. To this end, the actual behavior of a structure during an earthquake has been investigated considering the overstrength of the beam, dynamic magnification, or two-way action. These effects take into account the simple design formulas of recent design codes and guidelines, and the conventional and definitive design method based on equivalent static loading.

Analytical and experimental studies have revealed that the axial deformations in beams, caused by the material properties of reinforced concrete members, can significantly change column response (Takiguchi et al. 1977; Wada et al. 1990; Sanada et al. 1998). Moreover, in the recent 1994 Sanriku-Haruka-oki, and the 1995 Hyogo-ken Nanbu, Japan, earthquakes, structural damage in some buildings was centered in the first-story columns, despite predictions that these structures would perform in a ductile manner like the collapse mechanism of yielding beam type (Takeda et al. 1996 and Hori et al. 1999). In practical design analysis, the effects of the axial deformations of the beams have been neglected even by the most sophisticated nonlinear analytical method. Generally, the nodal lateral displacements in a floor are reduced to those of a representative point assuming the in-plane rigidity of the slab for the efficiency of calculation, drawback being that the beam axial deformation cannot be incorporated.

In this study, four beams, with different axial restraint stiffnesses and different shear span ratios, were tested under an axial restraint force applied in proportion to the axial elongation. The effect of the axial restraint stiffness on the flexural strength and the axial force in beams was investigated. The relation of flexural crack widths to beam elongation was also examined to correlate the damage level with the lateral displacement. Moreover, a simple analytical model, in which the axial elongation was derived from the rotation of a rigid body and the compressive deformation of a diagonal strut, was developed to evaluate the axial elongation and the restraint force in beams.

2. OUTLINE OF THE EXPERIMENT

2.1 Description of Specimens

Four one-half-scale model beam specimens were tested under anti-symmetric bending, and an axial restraint force was applied in proportion to the measured axial elongation of the beam. The properties and the reinforcing details of the specimens are shown in Table 1 and Figure 1. The dimensions of a beam section were 30 x 45 cm and the shear span-to-depth ratio was 1.0 or 2.0. Four D19 bars (nominal diameter of 1.91 cm, nominal area of 2.87 cm^2) were arranged as longitudinal reinforcement. Sufficient lateral reinforcement was provided not only to prevent brittle shear failure before flexural yielding but also to ensure adequate deformation capacity in the hinge region. The stiffness constant for the axial force was selected as 100 ton ft/cm or 400 ton ft/cm, representing the lateral restraint stiffness of the columns in the prototype frame structures. The mechanical properties of concrete and reinforcement are shown in Tables 2 and 3, respectively.

Table 1. Properties of Specimens

Specimen	B×D (cm)	L (cm)	K	Main Reinf.	σ_y (MPa)	Lateral Reinf.	pw (%)
2-400	30×45	180	400	4-D19	373	2-D10 @100	0.48
2-100			100				
1-400		90	400			4-D10 @75	1.27
1-100			100				

L:Span Length, K:Axial Restraint Stiffness (tonf/cm), σ_y:Yield Strength, pw:Lateral Reinforcement Ratio

Table 2. Mechanical Properties of Concrete

Specimen	Compressive Strength σ_B (MPa)	Strain at the Strength ε_{cu} (μ)	Elastic Modulus E_C (GPa)
2-400	33.3	2100	27.3
2-100	37.4	2270	28.2
1-400	38.9	2210	28.7
1-100	38.6	2260	27.4

Table 3. Mechanical Properties of Steel

Size	Elastic Modulus E_S (GPa)	Yield Strength σ_y (MPa)	Yield Strain ε_y (μ)	Maximum Strength σ_u (kgf/cm^2)	Maximum Strain ε_u (%)
D10	159	362	2280	513	17.8
D19	179	373	2090	561	21.1

Grade:SD345

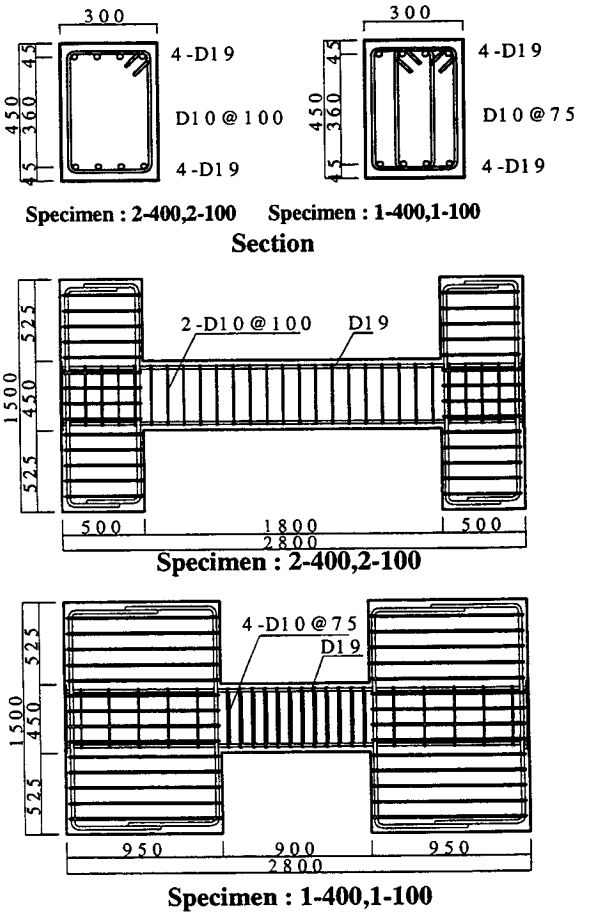

Figure 1. Reinforcing Details

2.2 Stiffness Constant for Axial Forces

The beam axial deformation, that is, the elongation that occurs during inelastic cyclic loading, even under a compressive axial force, is due to the material properties of the reinforced concrete including crack opening behavior. The restraint against beam elongation is supposedly induced by the surrounding structural members of the prototype structures, i.e., the columns, shear walls, and floor slabs, which act as a compressive axial force against the beams. However, in general, estimating the axial restraint stiffness for a beam can be complicated because it can be affected by many parameters, such as the properties of the surrounding structural members, the number of spans, and the location in the frame. To simplify the problem, a single-story multi-span frame was considered to approximate the axial restraint stiffness, K (see Figure 2). Uniform external horizontal forces P at each node and uniform axial elongation δ_{ax} in each beam were assumed. This allows estimating the stiffness constant, K_i, for the i-th beam from the left side in a n-span frame by Eq. (1).

$$K_i = \frac{N_i}{\delta_{ax}} = \frac{i(n-i+1)}{2} k_c \tag{1}$$

where, N_i: axial force in i-th beam, δ_{ax}: beam elongation, k_c: lateral stiffness of columns.

The restraint stiffnesses of 100 and 400 ton ft/cm, employed in the experiment, corresponded to those for a central beam in 6- and 12-span prototype structures, respectively, with a column section of 60 cm x 60 cm and a story height of 360 cm, in which the lateral stiffness of the column was reduced to one-third of the elastic stiffness, considering degradation due to cracking.

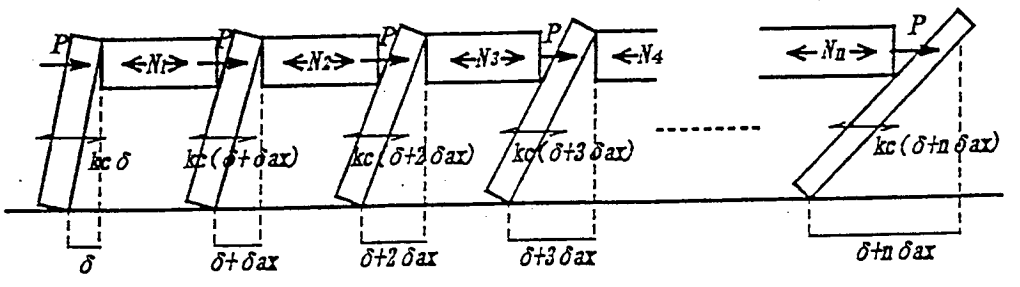

Figure 2. Beam Axial Deformation and Restraint due to Column

2.3 Method of Loading

The loading apparatus is illustrated in Figure 3. The specimens were subjected to bending and shear by horizontal jacks. The vertical jacks on both sides of the specimen kept the top and bottom stubs parallel, and the axial load was applied in proportion to the measured beam elongation. The specimens were subjected to two cycles at rotation angles of 1/200, 1/100, 1/67, 1/50, 1/33 rad after the first cycle at a rotation angle of 1/400rad.

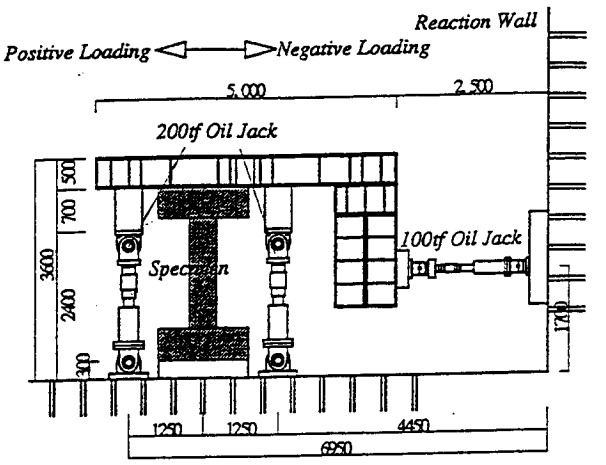

Figure 3. Loading Apparatus

3. SUMMARY OF EXPERIMENTAL RESULTS

3.1 Behavior of Specimens

Figure 4 shows the observed shear force-lateral displacement relations. In the figure, the broken lines indicate the calculated ultimate flexural strength Q_{mu} by assuming the compressive axial stress ratio η (axial stress normalized by the concrete compressive strength) of 0, 0,1, and 0,2. The experimental results are summarized in Table 4, and the crack patterns in the final cycle are shown in Figure 5. The relations of beam elongation to lateral displacement are shown in Figure 6.

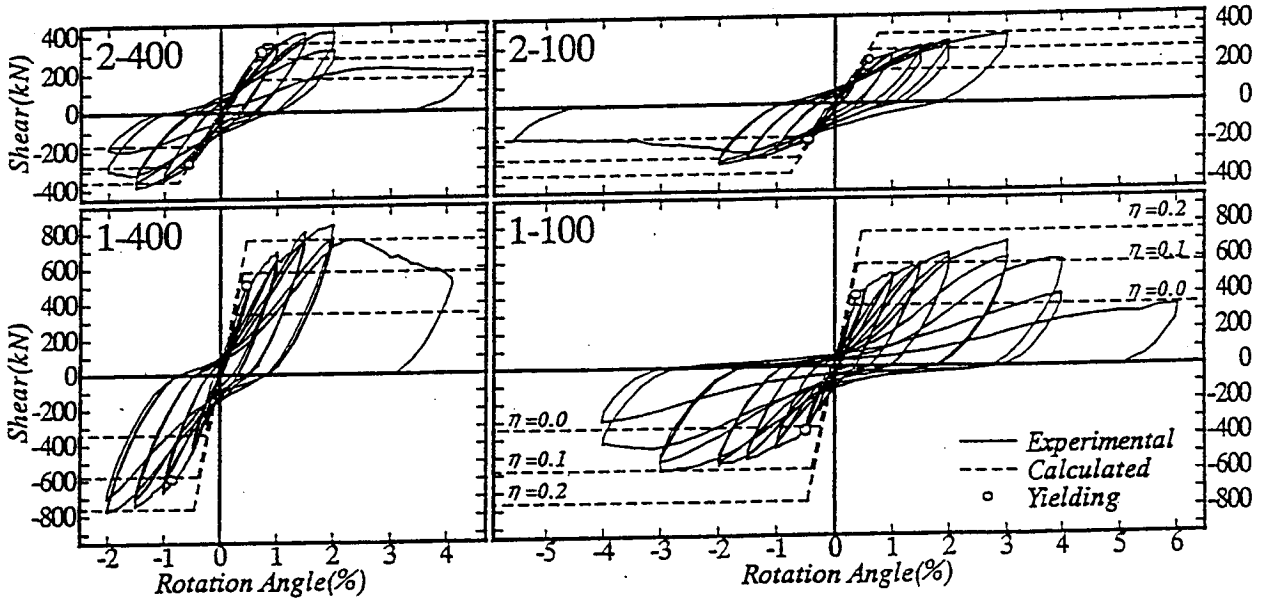

Figure 4. Shear Force-Lateral Displacement Relations

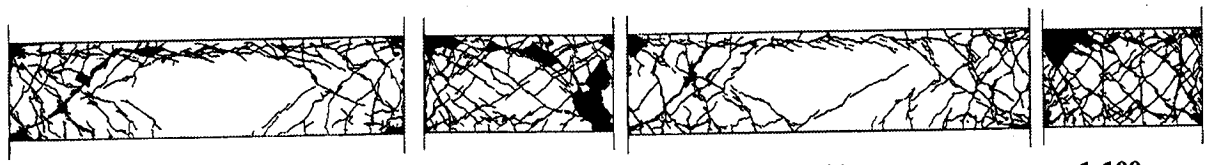

Figure 5. Crack Patterns in the Final Cycle

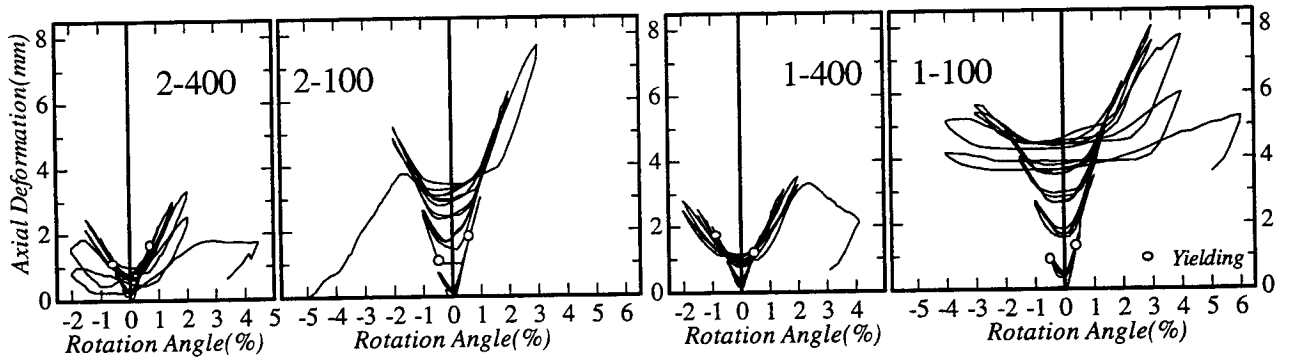

Figure 6. Beam Elongation-Lateral Displacement Relations

Table 4. Results of Experiments

Specimen	±	Q_y (kN)	Q_{max} (kN)	R_y (%)	R_u (%)	δ_{axy} (mm)	δ_{axu} (mm)	η_y	η_u
2-400	+	322	414	0.78	1.50	1.79	3.00	0.15	0.28
	–	-278	-383	-0.61	-1.50	1.17	2.47	0.10	0.23
2-100	+	225	346	0.69	2.84	2.05	7.65	0.04	0.15
	–	-198	-307	-0.50	-2.00	1.15	5.20	0.02	0.10
1-400	+	523	843	0.50	2.00	1.22	3.52	0.09	0.26
	–	-626	-770	-0.89	-2.02	1.82	2.82	0.14	0.21
1-100	+	414	703	0.42	3.01	1.33	8.01	0.03	0.15
	–	-374	-586	-0.50	-2.99	0.90	5.61	0.02	0.11

Q_y:Yield Load, Q_{max}:Maximum Load, R_y:Rotation Angle at Flexural Yielding, R_u:Rotation Angle at Maximum Load, δ_{axy}:Axial Deformation at Flexural Yielding, δ_{axu}:Axial Deformation at Maximum Load, η_y:Axial Stress Ratio at Yield Load, η_u:Axial Stress Ratio at Maximum Load

The longitudinal bars yielded in each specimen at the rotation angle of 1/200 rad after the generation of flexural and shear cracks. The process to failure was as follows: i.e., at a rotation angle of 1/100 rad, crushing of the cover concrete was observed at the beam ends. Bond splitting cracks were also observed along the tops of the longitudinal bars in specimens 2-400 and 2-100 with a shear span-to-depth ratio of 2.0. The lateral load began to decrease gradually with the decrease in the axial deformation and the axial load in cycles at 1/50rad in specimens 2-400 and 1-400 under higher axial restraint, although specimens 2-100 and 1-100 maintained the axial load until a rotation angle of 1/33 rad. Finally, bond splitting failure was observed in specimen 2-400, while specimens 1-400, 2-100, and 1-100 failed in shear.

The generation of flexural cracks induced the axial elongation in the beams, allowing the axial force to increase. As can be seen in Figure 6, the axial restraint stiffness was found to affect beam elongation. On the other hand, no significant difference in beam elongation was observed between the specimens with shear span ratios of 1.0 and 2.0, respectively, provided the axial restraint stiffnesses were the same. In the specimens under a higher axial restraint of 400 ton

ft/cm, the axial restraint force, up to an axial stress of about 0.1 times the compressive strength (η=0.1), raised the flexural yielding moments to approximately 1.8 times those calculated without axial force, as can be seen in Figure 4. The flexural yielding moments were 1.3 times, in average, those without axial force, even in the specimens under the lower axial restraint of 100 ton ft/cm, due to the axial stress ratio η of 0.03. The increase in beam elongation was nearly proportional to the lateral displacement until the lateral load decreased. The observed maximum moments were approximately 2.4 and 2.0 times the calculated strength neglecting the axial force for the specimens with the axial restraint stiffness of 400 and 100 ton ft/cm, respectively. The axial stress ratios at the maximum moment, which could increase the column shear forces in a frame, were approximately 0.1 through 0.3.

3.2 Beam Elongation and Crack Width

Figure 7 shows a comparison of beam elongation with a total crack width at the peak in each cycle and at the moment when the lateral force was unloaded. The total crack width was defined as an average of the sum of the flexural crack widths measured by the crack gage along the top and bottom surfaces of the specimen (see Fig. 8). In the specimens under a higher axial restraint, the residual beam elongation, when the lateral force was unloaded, was 40% on average that at the peak in each cycle, while the specimens under a lower axial restraint showed a larger residual elongation of 70%. It is interesting to note that fairly good agreements were found between the beam elongation and the sum of the crack widths, although this tends to be slightly larger than the measured elongation of the beams in the specimens under a higher axial restraint.

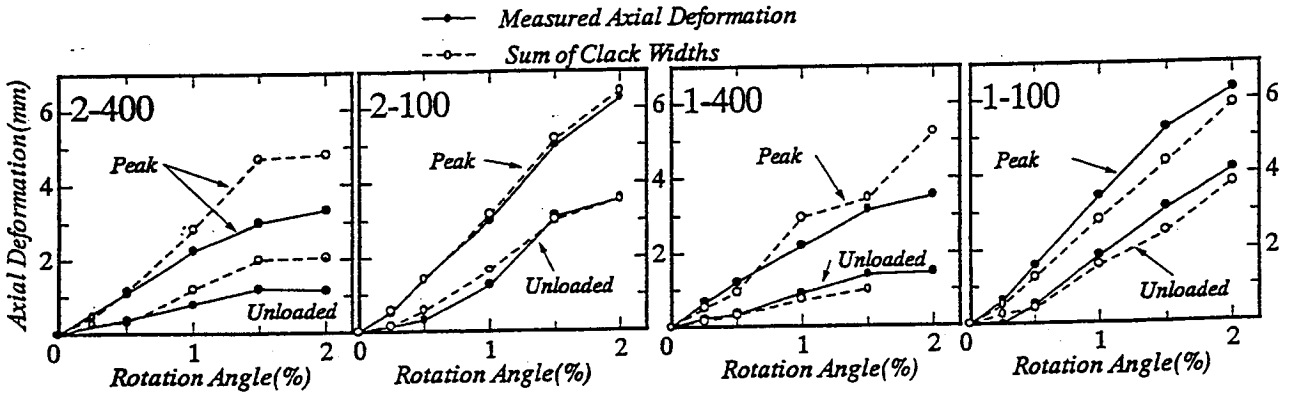

Figure 7. Comparison of Beam Elongation with Total Crack Width

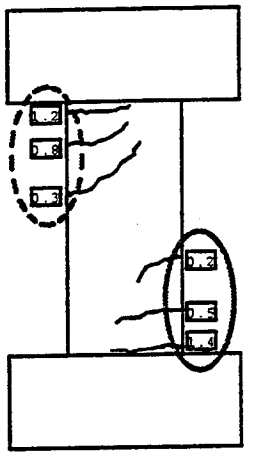

Figure 8. Measurement of Crack Widths

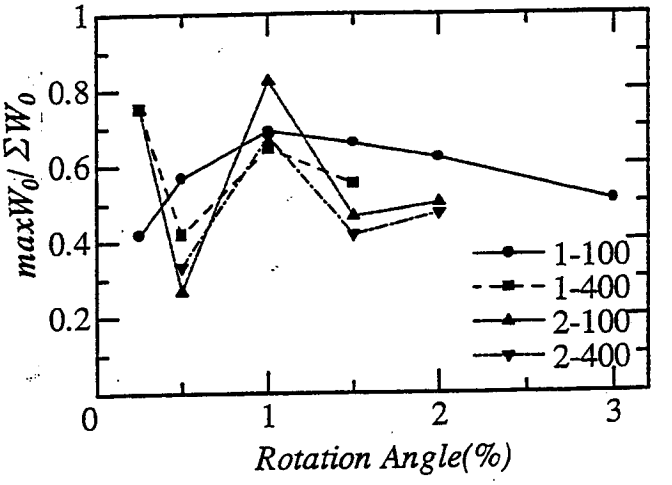

Figure 9. $_{max}w_0/\Sigma w_0$ vs. Lateral Displacement

Figure 9 shows the ratio of the maximum residual crack width, $_{max}w_0$, to the total residual crack widths, Σw_0. In each specimen, the maximum crack width was generally found at the beam end. The ratio, $_{max}w_0/\Sigma w_0$, was nearly 0.5 on average, ranging from 0.2 to 0.8. The relation between the maximum residual crack width and the lateral displacement is shown in Figure 10. The crack widths of 0.2, 1, and 2 mm correspond to the borders between the damage levels of structural members, according to the Japanese Standard for Damage Level Classification [JBDPA, 1991]. From the figure, residual crack widths were smaller than 0.2 mm, which corresponds to the "damage level 1 (slight damage)," until flexural yielding occurred in a cycle at 1/200 rad. From a performance-based design point of view, the result indicates that flexural yielding may be defined as one of the criteria for the serviceability limit state in structural members of the ductile flexural type. After flexural yielding, the maximum residual crack increased markedly with the increase in the lateral displacement, although the residual crack widths in the specimens under higher axial restraint tended to be smaller than those in the specimens under lower axial restraint.

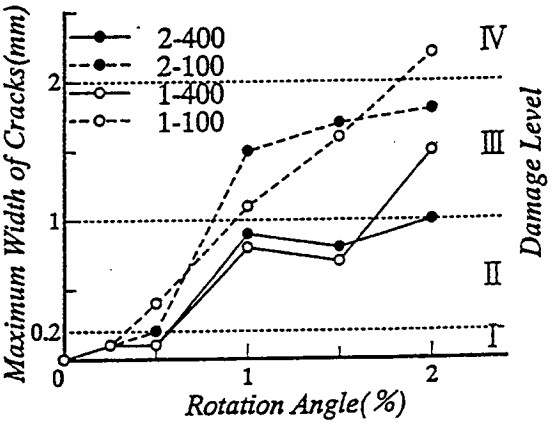

Figure 10. Maximum Residual Crack Width vs. Lateral Displacement

3.3 Curvature Distribution

Figure 11 indicates the curvature distribution along the beam axis when the longitudinal bars yielded. From the figure it can be seen that curvature was found to be concentrated in the region at the beam ends, especially after the yielding of the longitudinal bars, due to the inelastic behavior such as crack opening, inelastic bar elongation, and bar slip caused by bond deterioration.

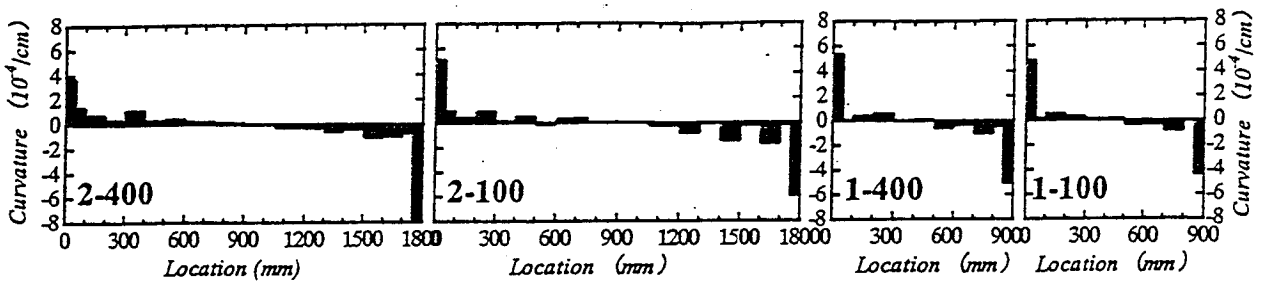

Figure 11. Distribution of Curvature along Beam Axis

4 EVALUATION OF BEAM ELONGATION BASED ON SIMPLE RIGID BODY MODEL

4.1 Description of Analytical Model

As mentioned above, the flexural deformation of the beams was mainly attributed to the rotation at the beam ends. This behavior can be represented by the rotation of a rigid body. Therefore, an analytical model, shown in Figure 12, was introduced to estimate the axial deformation in beams, in which elongation due to the rotation of a rigid body and the compressive deformation in a diagonal strut were considered. The compressive deformation in the diagonal strut δ_c was subtracted from the elongation due to the rotation of the rigid body δ_{ax0} to derive the beam elongation δ_{ax} as Eq. (2).

$$\delta_{ax} = \delta_{ax0} - \delta_c \tag{2}$$

If the beam is idealized as a rigid body, the flexural deformation of the beam can be represented by the rotation of the rigid body. This assumption gives an estimation of the axial

elongation due to the rotation of the rigid body δ_{ax0} by Eq. (3).

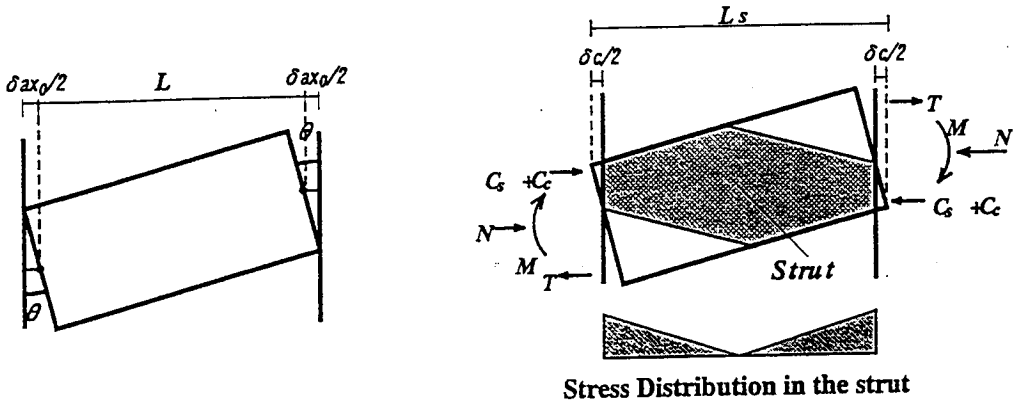

(a) Elongation due to Rotation of the Rigid Body **(b) Compressive Deformation of the Strut**

Figure 12. Analytical Model

$$\delta_{ax0} = D \cdot \theta \tag{3}$$

where, D: depth of beam, θ: rotation angle.

The compressive deformation of the strut δ_c can be evaluated from the strain at the edge of the beam end section ε_c and by assuming triangular strain distribution (see Figure 12), to derive Eq. (4).

$$\delta_c = \varepsilon_c \cdot L_s / 2 \tag{4}$$

where, L_s: length of the diagonal strut.

The restraint axial force on the beam N is given by Eq. (5).

$$N = K \cdot \delta_{ax} \tag{5}$$

The equilibrium of the axial force on the beam critical section can be expressed by Eq. (6).

$$N = C_c + C_s - T \tag{6}$$

where, C_c: compressive force in concrete, C_s: compressive force in reinforcement, T: tensile

force in reinforcement.

To make the calculation simple, C_c was assumed to be equal to T, and a simple bilinear stress-strain relation of concrete, as shown in Figure 13, was employed. These assumptions give an evaluation of beam elongation by Eq. (7a) and Eq. (7b), by solving Eq. (1) through (6).

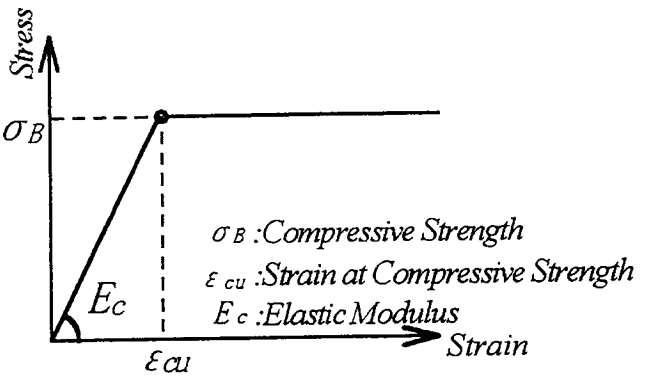

Figure 13. Stress-Strain Relation of Concrete

$$\delta_{ax} = \left(1 + 2\alpha - 2\sqrt{\alpha^2 + \alpha}\right) D \cdot \theta \quad (\theta \le \theta_u) \tag{7a}$$

$$\delta_{ax} = \left(\frac{2\beta\theta - \beta^2}{4\alpha\theta^2 + 2\beta\theta}\right) D \cdot \theta \quad (\theta > \theta_u) \tag{7b}$$

where, θ_u: beam rotation angle when concrete stress reaches compressive strength given by,

$$\theta_u = \frac{\beta}{-2\alpha + 2\sqrt{\alpha^2 + \alpha}}, \quad \alpha = \frac{L_c K}{bDE_c}, \quad \beta = \frac{\varepsilon_{cu} L_c K}{D}$$

4.2 Evaluation of Beam Elongation

The elongation calculated as above is compared with that measured experimentally in the tests, as shown in Figure 14. The solid lines represent the elongation calculated by Eq. (7a) or Eq. (7b), and the broken lines by Eq. (2). The analytical results by Eq. (7) agreed well with the experimental results until the experimental elongation began to decrease due to crushing of the concrete at the beam ends. The disagreements after the crushing of the concrete can be attributed to the simplified stress-strain relation in the analysis.

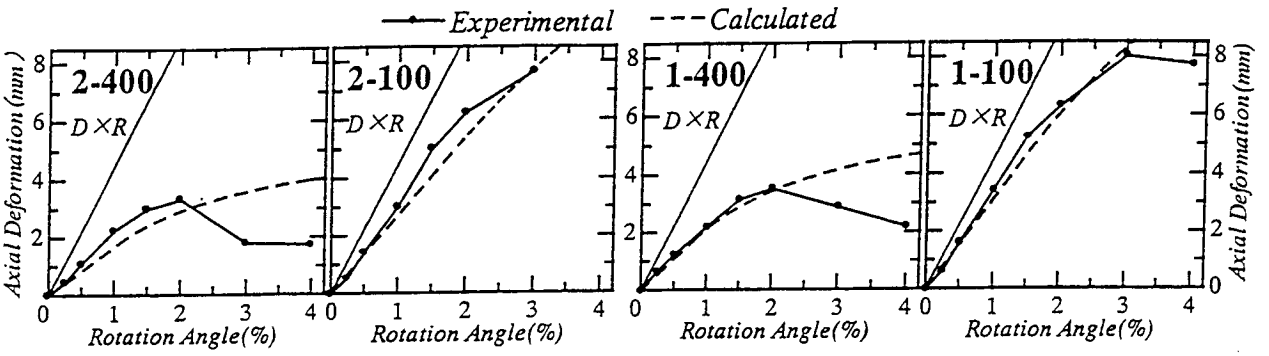

Figure 14. Comparison of Experimental and Analytical Beam Elongations

CONCLUSIONS

In this paper, four beams, with different axial restraining stiffnesses and different shear span ratios, were tested under an axial restraint force applied in proportion to the axial elongation. The effect of the axial restraint stiffness on the flexural strength and the axial force in the beams was investigated. The relation of the flexural crack widths with the beam elongation was also examined. Moreover, a simple analytical model was developed, in which the axial elongation could be derived from the rotation of a rigid body and the compressive deformation of a diagonal strut.

The major findings in this study are

(1) The increase in beam elongation was nearly proportion to the lateral displacement until crushing of the concrete was observed at the beam ends. The beam elongation was governed by the axial restraint stiffness, while no significant effect of shear span ration on the elongation was observed.

(2) The axial force caused by the axial restraint raised the flexural strength in beams. The ratio of observed strength to those calculated without axial force was approximately 1.3 through 1.8 at the yielding point. The ratio was as large as 2.0 through 2.4 at the ultimate point.

(3) A fairly good agreement was obtained between the measured beam elongation and the sum of the flexural crack widths.

(4) The beam axial elongation could be precisely evaluated by the proposed simple analytical model until the maximum shear force was reached.

ACKNOWLEDGMENTS

The beam test under axial restraint was carried out at the Structural Laboratory of Yokohama National University in 1998. The authors express their gratitude to Mr. N. Komura, Ms. A. Kimura, and Mr. M. Bunno, as well as to the Department of Architecture for their contributions in conducting the experiment.

REFERENCES

Hori, S., Maeda, M., and Nagata, M. 1999. Earthquake response analysis of a R/C school building damaged during 1994 Sanriku-haruka-oki Earthquake. (In Japanese). *Proceedings of the Japan Concrete Institute*, Vol. 21, No. 3, JCI, pp. 7–12.

JBDPA / The Japan Building Disaster Prevention Association. 1991. *Standard for damage level classification of reinforced concrete buildings*. (In Japanese).

Sanada, Y., and Kabeyasawa, T. 1998. Estimation of incremental shear force of columns due to axial deformation of beams. (In Japanese.) *Proceedings of the 10th Japan Earthquake Engineering Symposium*, pp. 2563–68.

Takeda, K., Maeda, M., and Kabeyasawa, T. 1996. Study on the damage to Hanazono Primary School of Akashi City due to 1995 Hyogo-ken Nambu Earthquake. (In Japanese.) *Proceedings of the Japan Concrete Institute*, Vol. 18, No. 2, JCI, pp. 53–58.

Takiguchi, K. and Ichinose, T. 1977. About change of axial elongation of reinforced concrete beam. (In Japanese). *Transactions of the Tokai branch of the Architectural Institute of Japan.* AIJ. February. pp. 251–254.

Wada, A., Hayashi, S., Sakata, H., and Otani, A. 1990. Experiments on reinforced concrete one-twentieth scale model frames under horizontal loading. (In Japanese.) *Journal of Structural and Construction Engineering* 417 (November): 21–29. AIJ.

APPLICATION OF PERFORMANCE-BASED ENGINEERING TO THE SEISMIC UPGRADING OF EXISTING R.C. BUILDINGS

Vitelmo V. BERTERO[1]

INTRODUCTION

One of the most pressing problems that needs to be solved in order to reduce seismic risks in our urban areas to socially and economically acceptable levels is the proper seismic upgrading of existing hazardous buildings. The inventory of seismically vulnerable buildings in urban areas located on or near active faults has increased significantly as a consequence of the lessons relearned during the significant earthquakes (EQs) that have occurred since 1989.

Earthquake Ground Motions (EQGMs) recorded during the 1989 Loma Prieta, 1992 Petrolia, 1992 Landers, and particularly the 1994 Northridge and 1995 Kobe earthquakes have clearly shown that the damage potential of EQGMs at sites near the causative faults can be significantly higher than that considered in the existing seismic building codes. The 1997 UBC has introduced Near-Source Factors (N_a, N_v) to take into account near-source effects and consequently the EQ design spectrum required by the 1997 UBC for the design of buildings near faults are significantly larger (up to 100%) than that required by the 1994 UBC. However, as is illustrated in Fig. 1, Somerville (1995) has shown that while the 1997 UBC spectra matches the average horizontal component for forward rupture directivity quite well, their values can be significantly lower than the Fault-Normal (FN) components at periods longer than 0.8 sec. Thus, many existing buildings located in U.S. urban areas on or near active faults and considered safe according to the requirements of the 1994 UBC are now seismically hazardous.

An analysis of R.C. moment-resistant frame buildings designed before 1972 shows that they have serious weaknesses for resisting significant EQGMs. Some of the weaknesses are illustrated by the amount and detailing of the reinforcement shown in the sketch (given in Fig. 2) of the girders and columns of a 15-story building designed in 1964 under the requirements of the Los Angeles City Building Code. The main weaknesses and features for this building are as follows (Sasani 1999).

- Large bay span (33′ clear) resulting in a high first-mode period (2.9 sec from the recorded response to the 1995 Northridge earthquake); thus excessive interstory drift leading to severe nonstructural damage can be expected.
- Lack of adequate anchorage of the longitudinal reinforcement at the bottom of the girders (embedment length = 6″).
- Lack of adequate amounts of top longitudinal reinforcement at midspan of the girders.
- Lack of adequate transverse reinforcement along the columns.
- Lack of transverse reinforcement at the girder-column joint.

[1] Professor Emeritus and Research Engineer, Pacific Earthquake Engineering Research Center, University of California, Berkeley

- Lack of adequate splicing of longitudinal reinforcement.
- A pushover estimated base shear capacity of 0.15W.
- The foundation consists of concrete piles (34′ deep) on a recent alluvial deposit.

Because the building is located at a distance less than 10 km from an active fault, it was decided to study how this type of R.C. building could be efficiently upgraded to resist the effects of the different types of EQGMs that can be expected at its site during its service life. The studies reported herein have the following **main objectives**: (1) to analyze the different approaches (methods) that have been suggested to carry out Performance-Based Seismic Engineering (P-B SE) and to select the one that could lead to an efficient (technically and economically) seismic upgrading of the type of R.C. building under consideration and (2) to apply such an approach in the seismic upgrading of this specific building.

SELECTION OF THE P-B SE APPROACH

ANALYSIS OF THE DIFFERENT SUGGESTED DESIGN APPROACHES. As outlined in the Vision 2000 report (SEAOC 1995), the following different approaches have been suggested for the design of new buildings:

- Comprehensive Design
- Displacement
- Energy
- General Force/Strength
- Simplified Force/Strength
- Prescriptive Approaches

The NEHRP *Guidelines for the Seismic Rehabilitation of Buildings* (FEMA 273, 1997) report recommends several simplified performance buildings. In view of the problems created by forward rupture directivity effects and because most of the simplified approaches have not yet been calibrated for this type of building and site conditions, it was decided to use the comprehensive approach.

COMPREHENSIVE APPROACH FOR P-B SE. A conceptual comprehensive methodology has been developed and proposed (R. D. Bertero et al. 1992, 1996). This conceptual methodology was developed in accordance with the comprehensive design philosophy and in compliance with worldwide accepted EQ-RD philosophy based on the use of energy concepts and fundamental principles of structural dynamics. To facilitate a proper conceptual overall design, the flow chart shown in Fig. 3 has been prepared. This chart illustrates how it is possible to implement energy concepts (through the use of an energy balance equation) using different methods (software) and different devices (hardware) which are classified under the two main groups of approaches (or methods): ***conventional and innovative.***

NEED TO CONSIDER A CUMMULATIVE DAMAGE INDEX. To satisfy the definition of P-B SE, there is a need to numerically compute different levels of structural and nonstructural damage for the different specific levels of EQ hazards that have to be considered. Structural damage during the response to EQGMs may be due to excessive deformations and/or due to accumulated damage under repeated deformation reversals. Although it cannot accurately

reproduce all possible force-deformation paths and damage mechanisms, the most widely used Damage Index (DM) is the one proposed by Park and Ang (1985)

$$(DM)_{P.A} = \frac{\delta}{\delta_{u\,mon}}\left[1 + b\frac{E_{H\mu}}{F_\gamma \delta}\right] = \frac{\delta}{\delta_{u\,mon}}\left[1 + b\gamma^2\mu\right] \tag{1}$$

where: $\gamma = \sqrt{E_{H\mu}/k\delta^2}$ defined by Fajfar (1992), which is also a good factor to identify the type of EQGMs (i.e., ***long duration of periodic strong motions*** or simply ***one or several severe pulses***); and b is a deterioration parameter.

Rewriting Eq. 1 as $(DM)_{P.A} = \frac{IDI}{\theta_{umon}}\left[1 + b\gamma^2\mu\right]$ (2)

$\left[1 + b\gamma^2\mu\right]$ can be interpreted as an amplification of the *IDI* damage due to cumulative effects, i.e., $E_{H\mu} = \gamma^2 k\delta^2$. Fig. 4 illustrates this damage amplification.

Fig. 5 illustrates the need to control not only the lateral deformations but also the ductility (μ) to limit damage (*DM*) — the larger the μ, the larger the *DM*.

NEED TO PREPARE DESIGN SPECTRA FOR LOCAL STRUCTURAL DAMAGE (DM) AND NONSTRUCTURAL DAMAGE (IDI). To use a comprehensive approach that from the beginning takes into account that the upgraded building structure is a Multi Degree of Freedom System (MDOFS) and that there can be torsional effects even under service EQGMs, the designer must prepare design spectra for local damage (*DM*) and nonstructural damage (*IDI*) like those illustrated in Fig. 6. If the use of energy dissipation devices is foreseen, these figures must be prepared by different values of damping, ξ . The *IDI* spectra can be computed using the following formula which is based on a shear beam behavior.

$$IDI(T,\mu,\xi) = \frac{2}{H}\sqrt{\sum\left[S_d(T_\eta,\mu,\xi_\eta)\right]^2}\,\beta_1\beta_2 \tag{3}$$

where H is the total height of the building; S_d is the displacement design spectra; β_1 is a coefficient to consider the *IDI* amplification due to torsional effects; and β_2 is a coefficient that quantifies the *IDI* increase due to concentration of inelastic deformation (plastic rotations in one story usually also a function of the global ductility (Hwang and Jaw 1990).

The local structural *DM* spectra can be computed rewriting Eq. 1 as follows.

$$DM(T,\mu,\xi) = \left(1 + b\gamma^2\mu\right)\beta_1\beta_2\frac{\theta}{\theta_{u\,mon}} \approx \left(1 + b\gamma^2\mu\right)\beta_1\beta_2\frac{IDI}{\theta_{u\,mon}} \tag{4}$$

where θ is the maximum rotation at the critical region during the seismic response, and $\theta_{u\,mon}$ is the ultimate monotonic rotation for the critical region. Usually in a multistory frame $\theta \approx IDI$.

Application of the above comprehensive approach to the specific R.C. building will be discussed and illustrated in the oral presentation.

REFERENCES

Bertero, R. D. and V. V. Bertero. 1992. Tall reinforced concrete buildings: conceptual earthquake-resistant design methodology.. Berkeley, Calif.: Earthquake Engineering Research Center, University of California. Report No.UCB/EERC-92/16. 1992. 243 pp.

Bertero, R. D. et al. 1996. Performance-based earthquake-resistant design based on comprehensive philosophy and energy concepts. *Proceedings, 11th World Conference on Earthquake Engineering, Acapulco, Mexico, June 23–28, 1996.* Oxford, U.K.: Elsevier Science Ltd.

Fajfar, P. 1992. Equivalent ductility factors, taking into account low cyclic fatigue. *Earthquake Engineering & Structural Dynamics* 21(10): 837–98. (October) 1992.

FEMA 273 and 274. 1997. NEHRP *guidelines for the seismic rehabilitation of buildings.* Washington, D.C.: Federal Emergency Management Agency (FEMA). (October) 1997.

Hwang, H., and J. Jaw. 1990. Statistical evaluation of deflection amplification of factors for R.C. structures. *Proceedings, 4th U.S. National Conference on Earthquake Engineering, Palm Springs, California, June 1990.*

Park, Y. J., and A. H. S. Ang. 1985. Mechanistic seismic damage model for reinforced concrete. *Journal of the Structural Division* 111 (ST4) (April) 1985. ASCE.

Sasani, M. 1999. *Seismic assessment of an old instrumented R.C. frame structure.* Berkeley, Calif.: University of California. *CE 299 Report.*1999.

SEAOC Vision 2000 Committee. 1995. *Performance-based seismic engineering.* Report prepared by Structural Engineers Association of California. Sacramento, Calif.

Somerville, P. 1995. Forward rupture directivity in the Kobe and Northridge earthquakes. *7th U.S.-Japan Workshop on the Improvement of Structural Design and Construction Practices.* Redwood City, Calif.: Applied Technology Council. 1995.

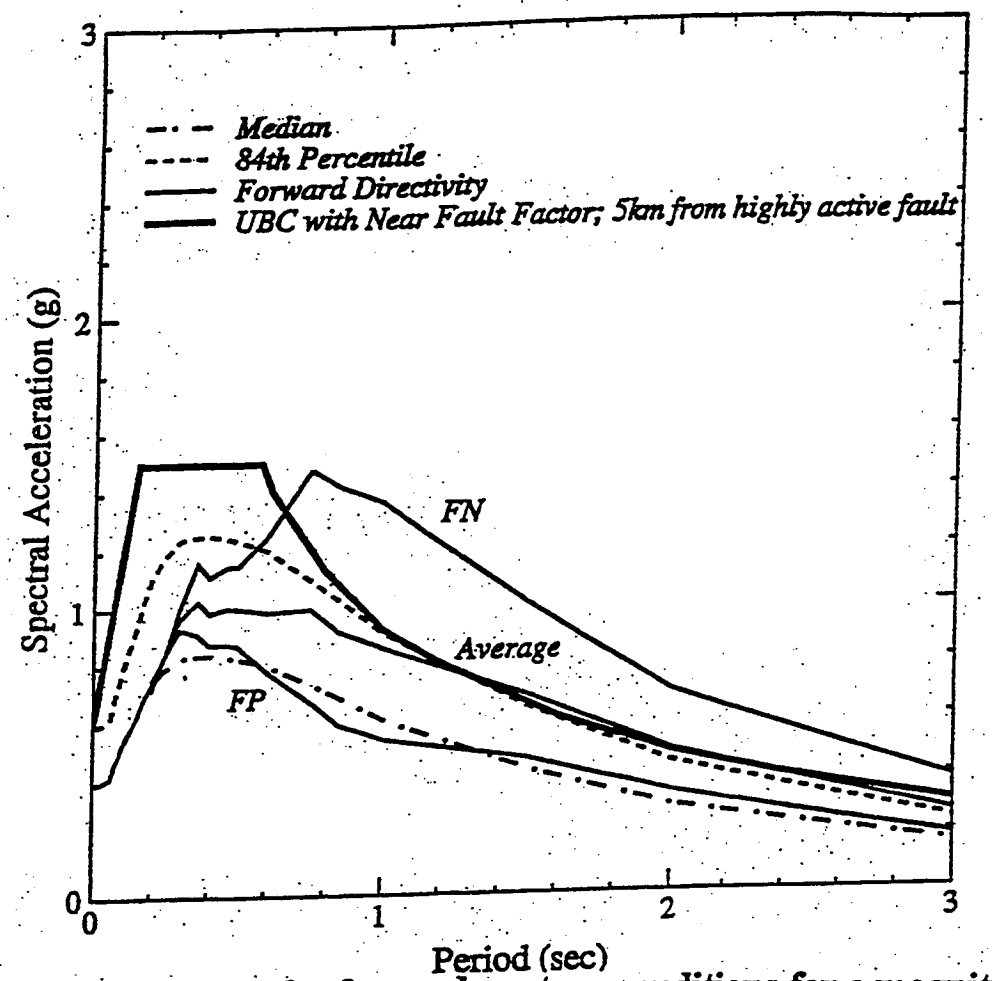

Fig. 1. Response spectra for forward rupture conditions for a magnitude 7 strike-slip earthquake at a closest distance of 6 km on soil (site category D) [Somerville 1995]

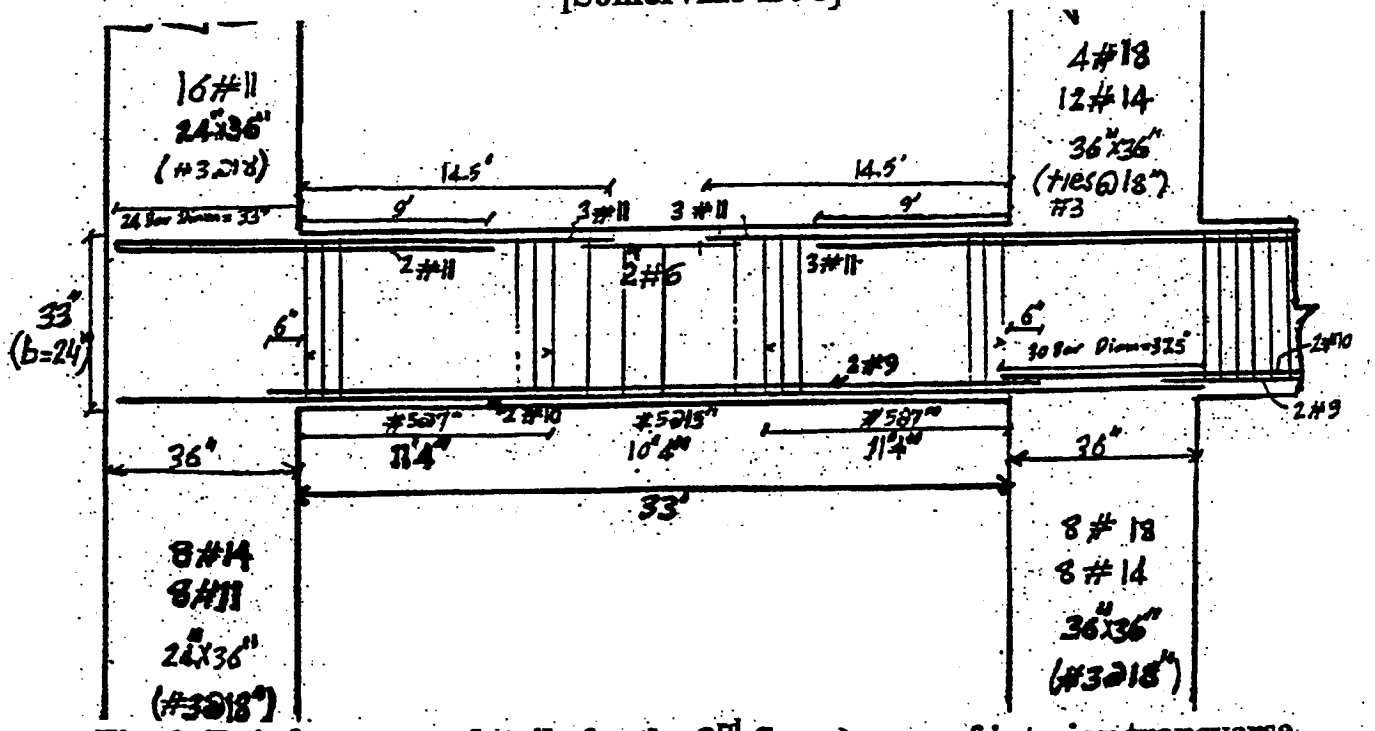

Fig. 2. Reinforcement details for the 3rd floor beams of interior transverse frames. (Similar beam reinforcement is used at the 4th and 5th floors.)

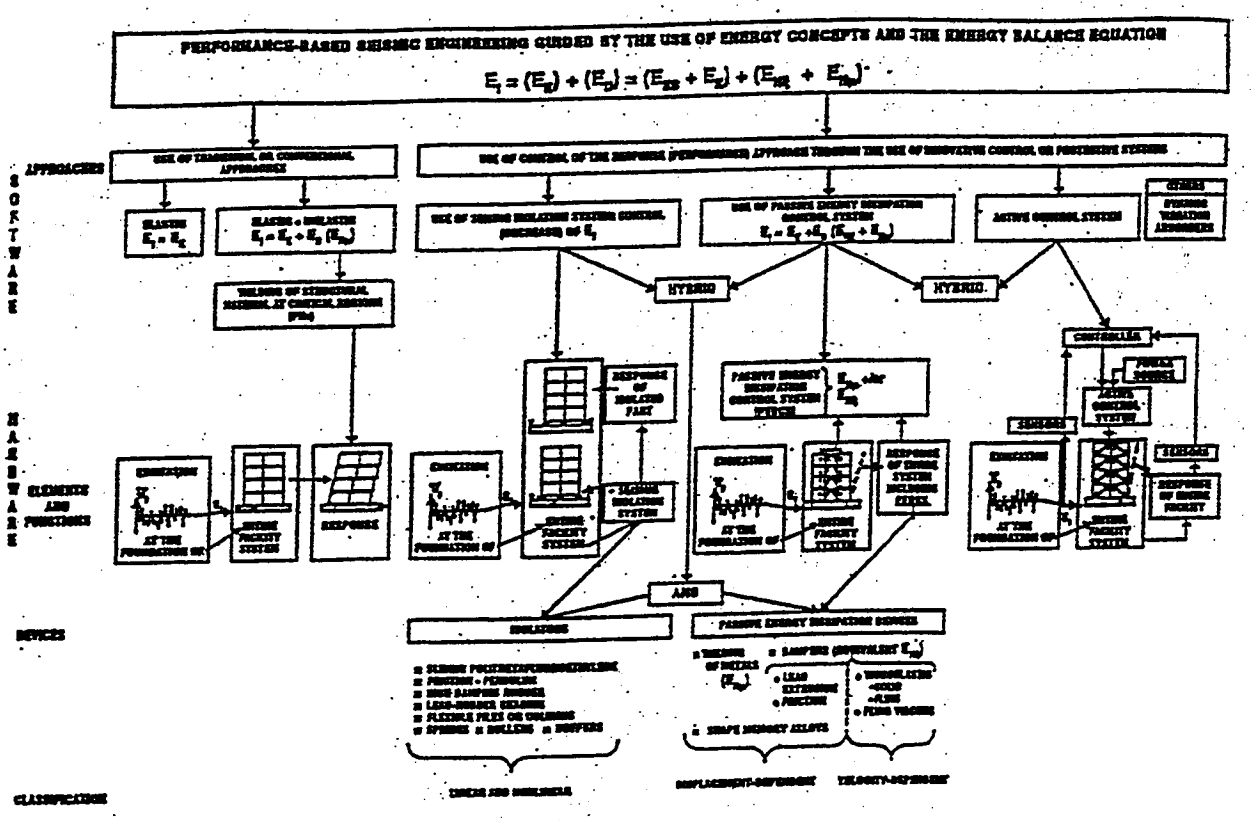

Fig. 3. Flow chart of the approaches for P-B EQ-RD

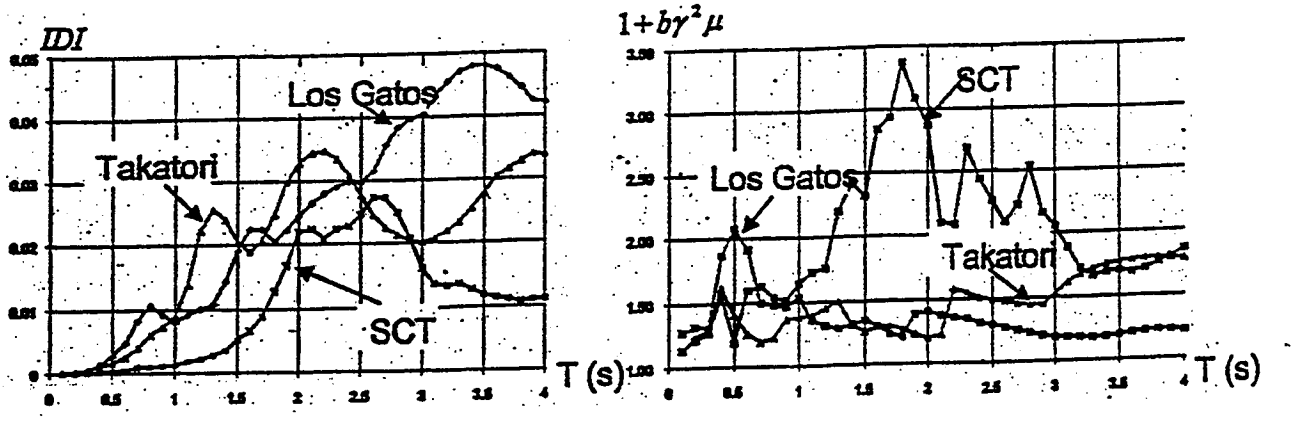

Fig. 4. Damage amplification due to cumulative effects of repeated cycles of deformation (b=0.20, ξ=0.05, and μ=3)

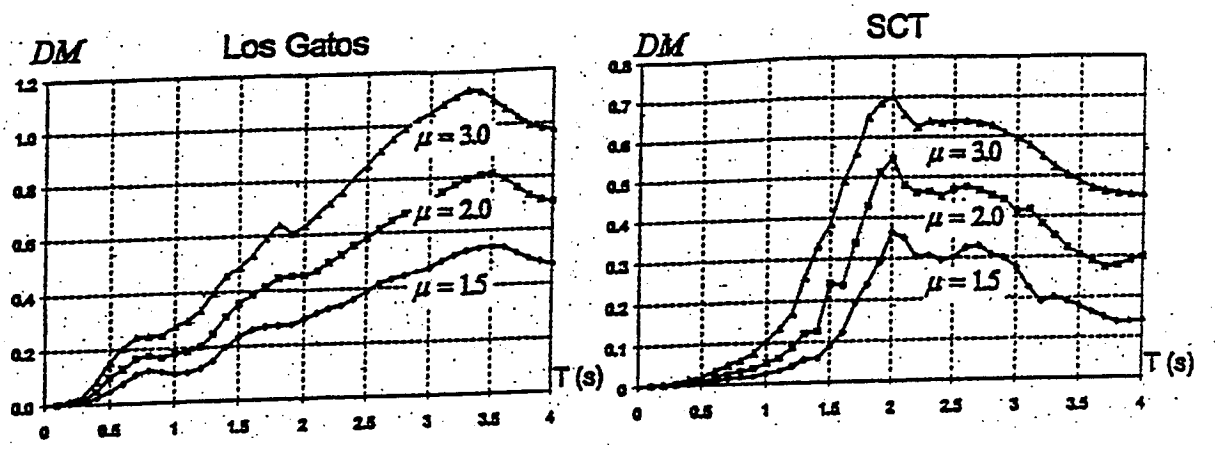

Fig. 5. Effect of the ductility on the damage index for severe pulse and periodic types of earthquake ground motions (b=0.20, ξ=0.05, and the same $\delta_{\mu\ mon}$)

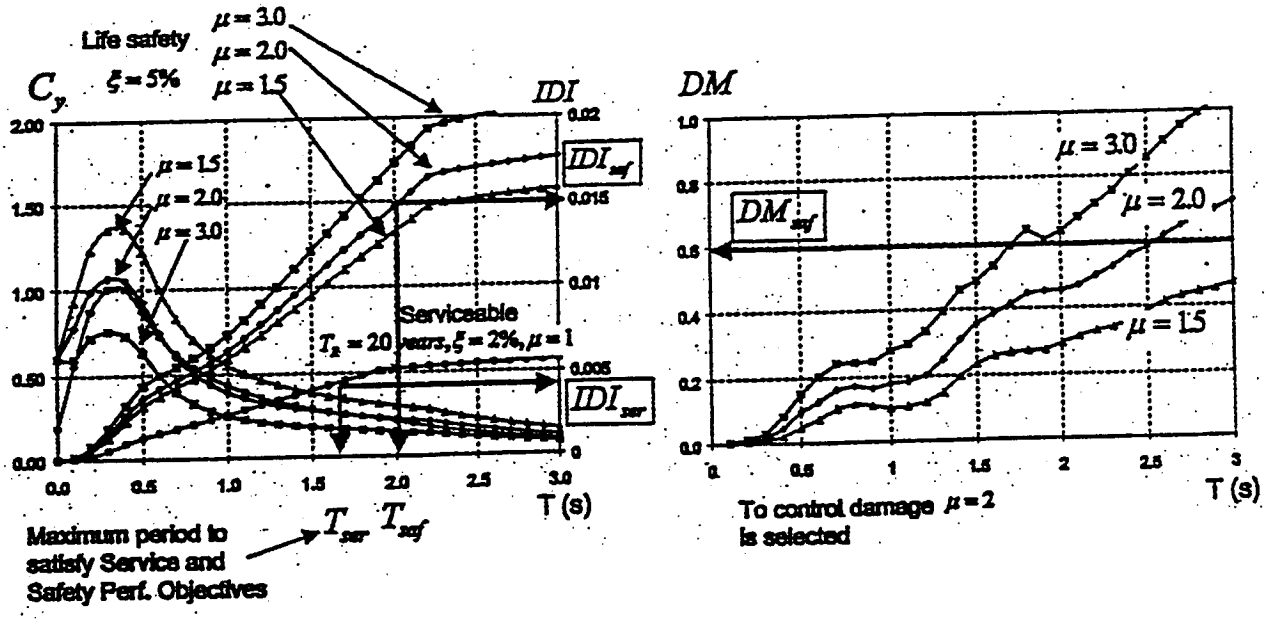

Fig. 6. Explicit selection of minimum stiffness and strength to satisfy performance objectives

ANALYTICAL METHOD FOR PREDICTING THE RESPONSE OF TIED CONCRETE COLUMNS TO SEISMIC LOADING

Fumio WATANABE — Graduate School of Engineering, Kyoto University, Sakyo-ku, Kyoto, 606-8501, Japan, e-mail:nabe@archi.kyoto-u.ac.jp

Beni ASSA — Faculty of Engineering, University of Sam Ratulamgi, Kampus Bahu, Manado 95155, Indonesia, email: bennyrc@mdo.mega.net.id

Minehiro NISHIYAMA — Graduate School of Engineering, Kyoto University, Sakyo-ku, Kyoto, 606-8501, Japan, e-mail:mn@archi.kyoto-u.ac.jp

Summary

To assure the required flexural ductility of a reinforced concrete column, it is essential to apply transverse reinforcement to the potential plastic hinge region. The compressive ductility of concrete can be improved and results in larger flexural ductility. In this research, axial loading tests were conducted on concrete cylinders laterally reinforced with spirals or circular hoops, where the concrete strength ranged from 20 to 90 MPa. The constitutive relations for concrete under axial and lateral compressive stresses were derived based on the experimental results. An analytical confinement model is applied to cross sections with various configurations of transverse reinforcement and the stress-strain curve of confined concrete was theoretically predicted. The theoretically predicted stress-strain curves showed good agreement with past experimental data. On the other hand column flexural analysis was conducted by using the proposed stress-strain idealization for confined concrete and potential plastic hinge length. The results were compared with past test data and good agreement was obtained. From this study it is concluded that the proposed stress-strain idealization for confined concrete can be used to predict the seismic response of reinforced concrete columns with various configurations of lateral reinforcement.

1. Introduction

Several stress-strain idealizations for confined concrete have been proposed and applied to the evaluation of column ductility. However these idealizations are empirical ones to a greater or lesser extent, especially for various configurations of transverse reinforcement. Therefore a more theoretical approach is needed to investigate the effects of transverse reinforcement details. This paper consists of two parts: (1) theoretical prediction of stress-strain curve of column core concrete confined with several types of transverse reinforcement configurations and (2) the application of the proposed stress-strain curve for column analysis of confined concrete.

2. Prediction of stress-strain curve for confined concrete

The stress-strain relationship of column core concrete strongly depends on the detailing of the transverse reinforcement. Several models for confined concrete have been proposed in the past. However these models are empirical ones to a greater or lesser extent. Axial loading tests on confined cylinders were first conducted to derive the constitutive law for confined concrete. Then a steel concrete interaction model was proposed, with focus placed on (a) the enhancement of strength and ductility due to lateral pressure, (b) the relationship between lateral expansion and lateral pressure at peak load, and (c) transverse reinforcement configurations.

2.1. Test program

A total of thirty-two 145x300 mm concrete cylinders were tested under monotonic concentric compression. No cover concrete was provided in all specimens. The target strength of the concrete ranged from 20 MPa to 90 MPa. The bar diameter of the continuous spirals and welded circular hoops were 6.25 mm, with nominal yield strengths of 1300 MPa and 800 MPa, respectively. The spacing of the continuous spirals or circular hoops were varied from 19 mm to 75 mm in the center. The axial deformation of the concrete cylinder was measured at the central part of the specimens with a gage length of 145 mm. The key feature in the experiments was the setup of the measurement devices. Figure 1 indicates the strain measurement system. Two reference points consisted of radial steel rods were buried in concrete, where the gage length was 145 mm (equal to section diameter). Then two external steel rings were clamped to the radial steel rods by pin contact points. This is to avoid the lateral restraint by the measuring devices due to lateral expansion of the concrete. The strain in the confining steel was measured using nine wire strain gages placed along three loops within the central measurement region. From the average value of measured strains the lateral pressure and lateral strain of concrete were calculated.

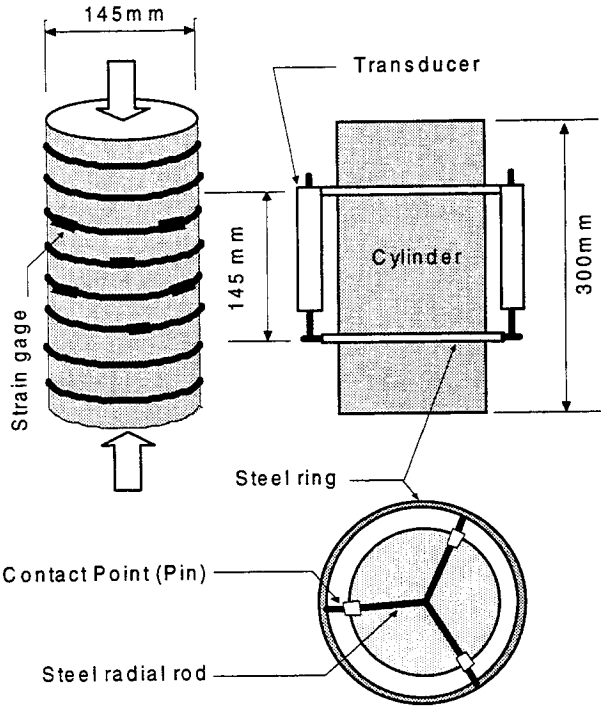

Fig. 1 Strain Measurements

2.2 Summary of test results

(1) Characteristic values on the stress-strain curve

Axial stress and axial strain of confined concrete at each characteristic point (see Fig. 2) were experimentally obtained as

$$f_{cc} = f'_c + 3.36 f_{rp} \qquad (1)$$

$$\varepsilon_{cc} = (1 + 21.5 f_{rp} / f'_c)\varepsilon_c \qquad (2)$$

$$\varepsilon_{80} = (2.74 + 32.8 f_{rp} / f'_c)\varepsilon_c \qquad (3).$$

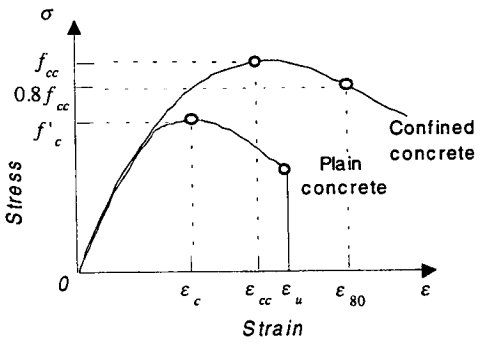

Fig. 2 Stress strain curve of concrete

(2) Lateral strain and lateral confining stress at peak load

The relationship between the lateral strain and the lateral stress at peak load was obtained by a linear curve as given by Eq. 4 regardless of the amount of transverse reinforcement. This equation is the best fit to the test results. This equation, named the peak load condition line, is a key equation in this study.

$$\varepsilon_{rp} = 0.0021 + 0.016 f_{rp} / f'_c \qquad (4)$$

where f_{cc}=strength of confined concrete, f'_c=strength of plain concrete, f_{rp}= lateral pressure at peak, ε_{cc}=strain at peak of confined concrete, ε_{80}=strain at $0.80 f_{cc}$ after peak, ε_c=strain at peak of plain concrete, ε_{rp}=lateral strain at peak.

These test results are used to predict the stress-strain curve for column core concrete confined by several types of transverse reinforcement configurations. If the lateral pressure f_r for any lateral expansion (lateral strain) ε_r is theoretically obtained for any transverse reinforcement configurations, as indicated in Fig. 3, the lateral pressure at peak load, f_{rp} , can be easily obtained at the intersection point between the peak load condition line (Eq. 4) and the f_r - ε_r line. Then the stress-strain coordinate at the peak load is obtained.

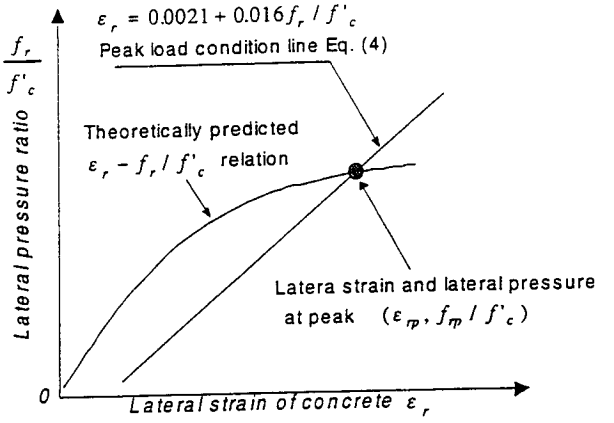

Fig. 3 Determination of lateral pressure and lateral strain at peak load

2.3 Modeling of transverse steel concrete interaction

For circular transverse reinforcement, the f_r - ε_r curve can be easily obtained and is similar in shape to the stress-strain curve of the transverse reinforcement. For other types of transverse reinforcement details, f_r - ε_r can be predicted by finite element analysis. An example of the transverse-steel concrete interaction model is indicated in Fig. 4. A perimeter hoop is divided into finite beam-column elements, which are interconnected at nodal points to satisfy the continuity. The integration points and the layering of section of a beam-column element are also indicated in Fig. 4. Internal cross-ties are modeled as a truss element. This transverse steel system is pushed out by the concrete bar element due to its lateral expansion.

The compressive stiffness of the concrete bar element is given to have the same stiffness as the corresponding triangular concrete element (see Fig. 4) where the stiffness of the concrete element in tension is assumed to be zero. This is to take into account the separation between the concrete and perimeter

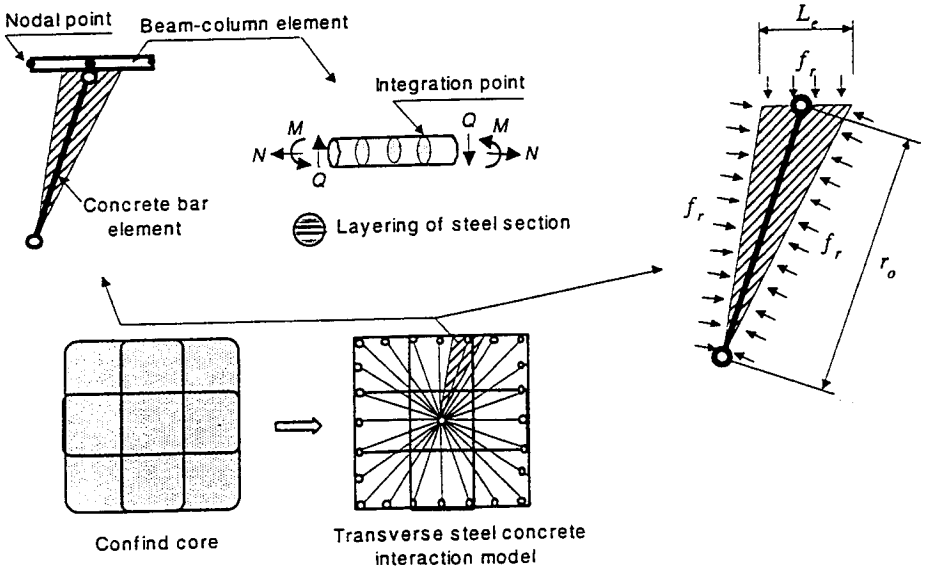

Fig. 4 Analytical Model for Transverse Steel Concrete Interaction

hoop due to bowing out of it. By giving the free elongation of the concrete bar element corresponding to the lateral strain of the concrete, ε_r, the average lateral pressure to concrete section f_r can be obtained by a numerical analysis of this steel-concrete interaction system.

Figure 5 indicates the typical examples of numerical calculation, where the volumetric ratio of the transverse reinforcement, concrete strength, and hoop spacing are assumed to be 2.15%, 34.1 Mpa, and 1300 MPa, respectively. This figure indicates that the confining efficiency of transverse reinforcement strongly depends on its detailing.

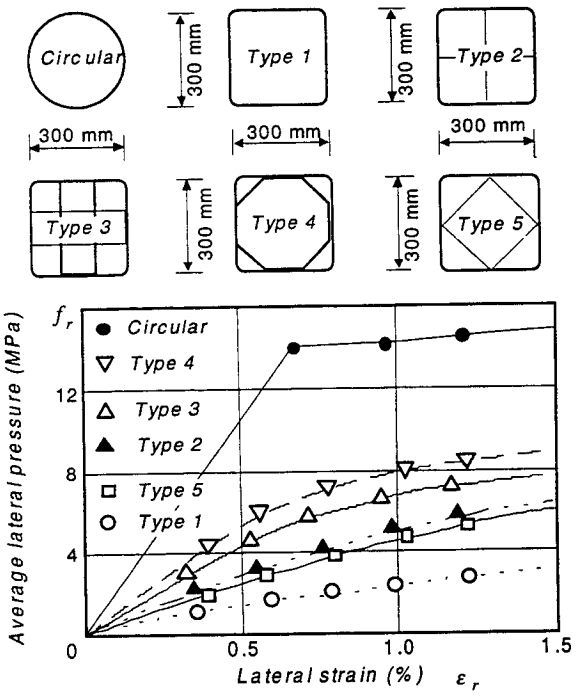

Fig. 5 Numerical calculation of lateral pressure - lateral strain relationships for various transverse steel configuration

2.4 Stress-strain curve for confined concrete

Figure 6 indicates the process to obtain the stress-strain coordinate at the peak load and the predicted stress-strain curve for Unit-2 specimen (Scott et al. 1982) with their observed one. The numerical expression of a stress-strain curve of confined concrete as proposed by Popovics is

$$\sigma = f_{cc}\frac{x\beta}{\beta - 1 + x^{\beta}} \qquad (5)$$

$$x = \varepsilon / \varepsilon_{cc} \qquad (6)$$

$$\beta = E_c / (E_c - f_{cc} / \varepsilon_{cc}) \qquad (7)$$

where E_c =initial stiffness of concrete.

3. Response of laterally confined RC columns

In this section the method to predict the load deflection relationship of RC columns is proposed based on the stress-strain models.

3.1 Stress-strain curve for plain and confined concrete

(1) Stress-strain curve for plain concrete

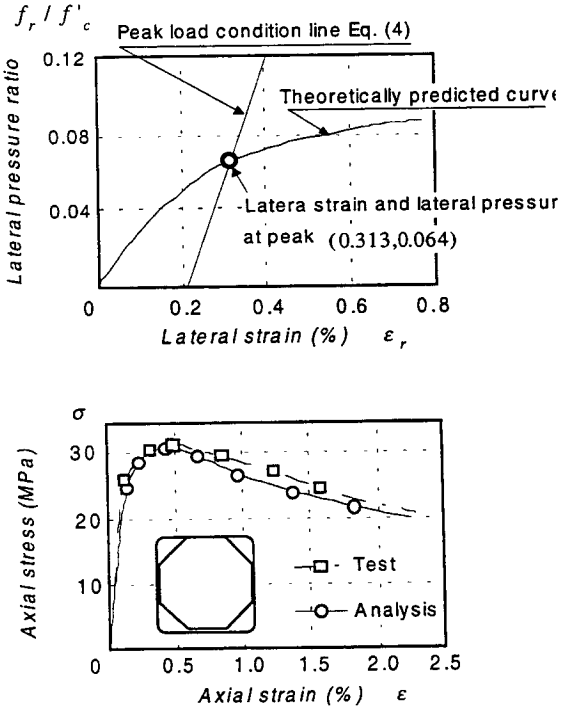

Fig. 6 Comparison between experimentally observed stress strain curve and theoretically predict-ed one

The numerical expression for a stress-strain curve for plain concrete is given by Popovics equation.

$$\sigma = f'_c \frac{x\beta}{\beta - 1 + x^{\beta}} \tag{8}$$

$$x = \varepsilon / \varepsilon_c \tag{9}$$

$$\beta = E_c / (E_c - f'_c / \varepsilon_c) \tag{10}$$

Where, the strain at peak, ε_c, and the available limit strain at extreme fiber in flexural compression, ε_u, are given for normal concrete based on the authors' tests. Beyond the strain of ε_u the cover concrete is assumed to peel off.

For $f'_c \leq 40MPa$

$$\varepsilon_c = 0.0013(1 + f'_c/100) \tag{11}$$

$$\varepsilon_u = 0.00413(1 - f'_c/200) \tag{12}$$

For $f'_c > 40MPa$

$$\varepsilon_c = (0.814k_m + 1.67)/1000 \qquad k_m \leq 1.5 \tag{13}$$

$$\varepsilon_u = (1.71 - 0.265k_m)\varepsilon_c \qquad k_m \leq 1.5 \tag{14}$$

$$\varepsilon_c = 0.0028 \qquad k_m > 1.5 \tag{15}$$

$$\varepsilon_u = 1.31\varepsilon_c \qquad k_m > 1.5 \tag{16}$$

$$k_m = (f'_c/55)(c/500)^2(w/200) \tag{17}$$

where E_c=initial stiffness of concrete, k_m=concrete mix parameter, c=cement content (kg/m^3), w=water content (kg/m^3)

(2) Hysteretic rules

Skeleton curves are given by Eq. 5 and Eq. 8 for plain and confined concrete, respectively. Hysteretic rules are given as indicated in Fig. 7. Unloading path is given by a parabola, which has a vertex on the X-axis. Residual strain ε_{res} is given by Eq. 18. The reloading curve after full unloading ($\varepsilon \leq \varepsilon_{rel}$) is given by a parabola and starts from ε_{rel}, where ε_{rel} is given by Eq. 19. This is to consider the some permanent tensile strain in concrete. When the reloading path starts between ε_{rel} and ε_{res} the reloading path and the straight line (ε_{res} - ε_{rel}) come in contact with each other at a common point.

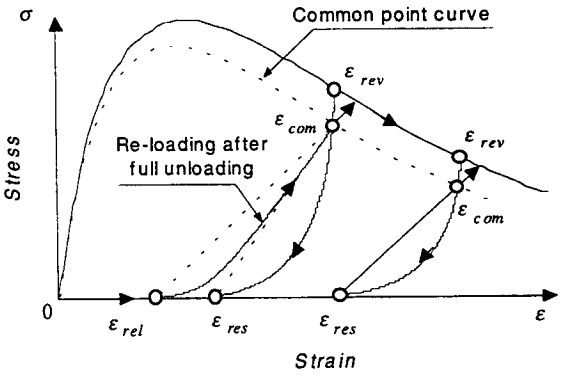

Fig. 7 Stress strain rules for cyclic loading

$$\varepsilon_{res} = 0.65\varepsilon_{rev} \tag{18}$$

$$\varepsilon_{rel} = 0.65\varepsilon_{res} \quad (19)$$

where, ε_{rev} =strain at unloading point, ε_{res} =residual strain, ε_{rel} =strain at full unloading

3.2 Stress-strain curve for longitudinal reinforcement

The stress-strain model by Yokoo and Nakamura is applied for the analysis.

$$\varepsilon - \varepsilon_{sj} = \frac{\sigma - \sigma_{sj}}{E_s}\left[1 + A^{-R}\left\{\frac{\sigma - \sigma_{sj}}{f_y}\right\}^{R-1}\right] \quad (20)$$

where, ε, σ =strain and stress of rebar, ε_{sj}, σ_{sj} =strain and stress at stress reversal, E_s =elastic modulus, A, R =strain history dependent coefficients

3.3 Modeling of column into two sub-systems

The modeling of a column is indicated in Fig. 8. A column is divided into two sub-systems. For flexural analysis, each section is divided into thin layers where the plane section before deformation is assumed to remain plane after deformation. For each layer the stress-strain laws for plain concrete (cover concrete), confined concrete (core concrete) and longitudinal reinforcement are applied. In the analysis also considered are the additional deflection due to the shear deformation of the column and slip-out of the longitudinal reinforcement from the loading stub. The shear deformation is calculated based on the 45-degree truss-model and the slippage of the longitudinal reinforcement is calculated using the finite element method based on the bond-slip model proposed in the past. Plastic hinge length, obtained by equations 21 to 23, is based on past experimental observations.

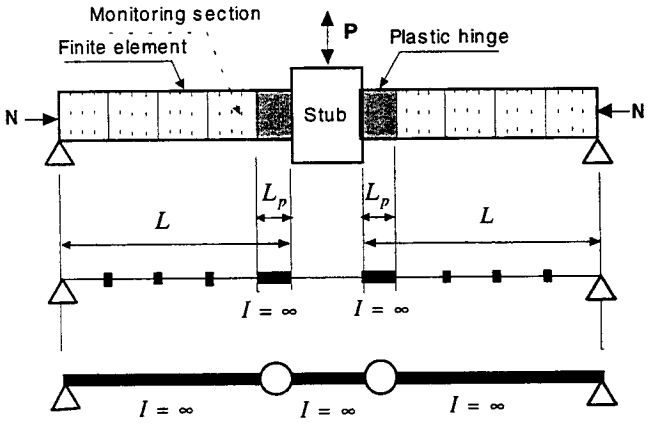

Fig. 8 Modeling of beam-column into two sub systems

$$L_p = 0.5h \quad \text{for } n = N/(bhf'_c) \le 0.2 \quad (21)$$

$$L_p = 0.75h \quad \text{for } n = N/(bhf'_c) \le 0.5 \quad (22)$$

$$L_p = 1.0h \quad \text{for } n = N/(bhf'_c) > 0.5 \quad (23).$$

3.4 Comparison between tests and analysis

Four column specimens were analyzed. These columns were tested by Park et al. in 1982. All columns have a 55 cm x 55 cm section size , a tension reinforcement ratio of 1.79% (yield strength of 375 MPa) and a clear span length L of 120cm (see Fig. 8). The yield strength of lateral reinforcement ranged from 294 to 317 MPa. The details of each specimen are indicated in Table 1.

Table 1 Details of column specimens

Spec.	ρ_s	s	*Type*	n	f'_c
Unit-1	1.5%	80mm	4	0.260	23.1MPa
Unit-2	2.3%	75mm	4	0.214	41.4MPa
Unit-3	2.0%	75mm	5	0.420	21.4MPa
Unit-4	3.5%	72mm	5	0.600	23.5MPa

$n = N/(bhf'_c)$, ρ_s, s = volumetric ratio and spacing of hoop, *Type* = Transverse reinforcement configuration (see Fig. 5)

A comparison between tests and analysis are indicated in Fig. 9. It can been seen from these figures that the proposed prediction method based on materials properties has enough accuracy for engineering purposes. However, the shape of the unloading path for the specimen with a low axial load level could not successfully be traced.

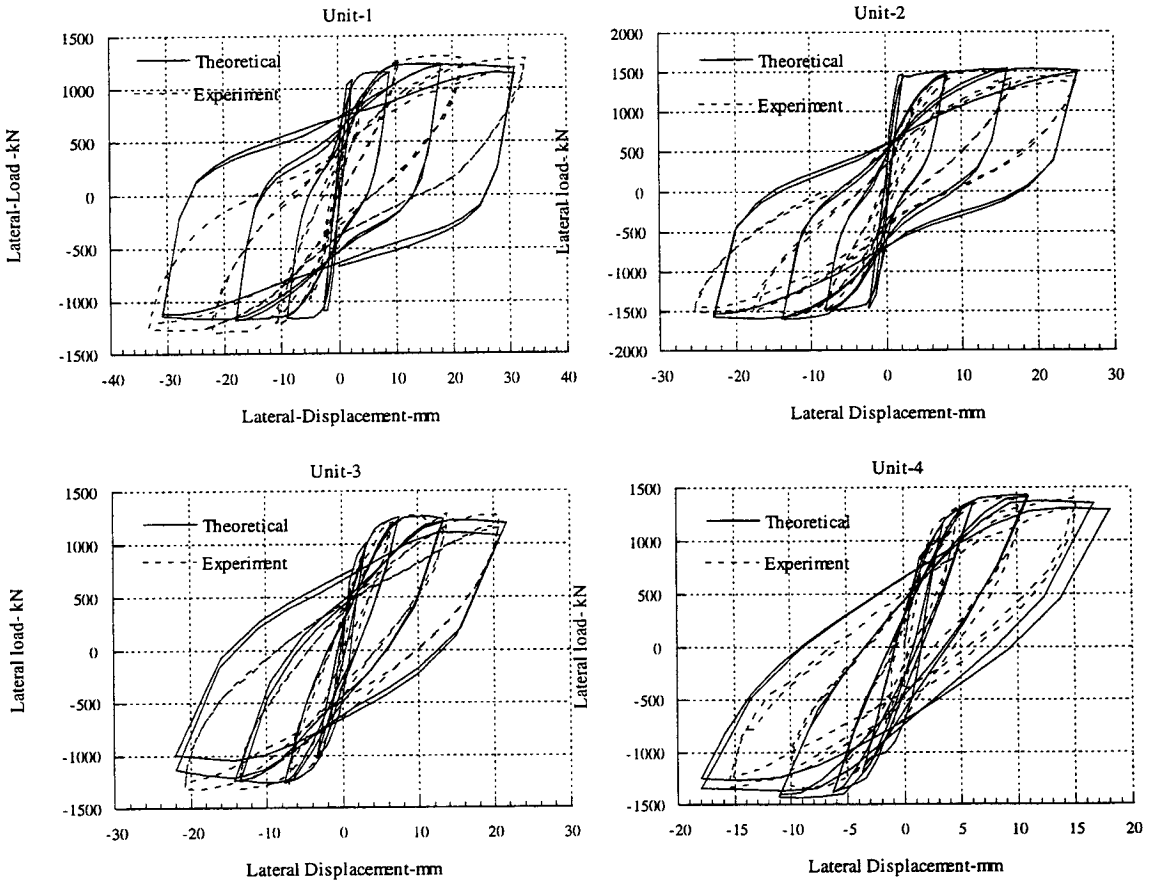

Fig 9 Comparison between tests and analysis

4. Conclusions

An analytical method for predicting the response of tied concrete columns to seismic loading is proposed based on the materials properties. The obtained results are

(1) The lateral strain and lateral pressure at the peak load of the confined concrete shows a linear relationship (P-L-C line) for a concrete compressive strength of 20 to 90 MPa.

(2) The lateral pressure and lateral expansion relationship (P-E curve) can be predicted by finite element analysis for various types of transverse reinforcement details.

(3) The intersection point of the P-L-C line and P-E curve gives the lateral pressure at a peak of stress-strain curve of confined concrete.

(4) The stress-strain curve for various configurations of transverse reinforcement can be predicted by a transverse steel-concrete interaction model.

(5) The plastic hinge length depends on the axial load level.

(6) A layered method can predict the flexural deformation of the plastic hinge region and the outside hinge region, and

(7) The deflection response of columns can be predicted considering the additional deflection due to shear deformation and re-bar slippage from the loading stub or beam-column joint.

In this research the column response and materials response were successfully linked, thereby making it possible to evaluate the damage to materials during the earthquake.

References

Richart, F. E. et al. 1928. A study of the failure of concrete under combined compressive stresses. *Engineering Experimental Station Bulletin* No. 185. University of Illinois.

Yokoo, Y. and T. Nakamura, T. 1977. Nonstationary hysteretic uniaxial stress-strain relations of wide-flange steel : Part II — Empirical formulae. *Transactions of Architectural Institute of Japan* 260 (October): 143 –49.

Popovics, S. 1973. A numerical approach to the complete stress-strain curves of concrete. *Cement and Concrete Research* 3(5)(September): 583–99.

Scott, B. D., R. Park, and M. J. N. Priestley. 1982. Stress-strain behavior of concrete confined by overlapping hoops at low and high strain rates. *ACI Journal* 79-2 (January-February): 13–27.

SESSION 6: SEISMIC DEMANDS

Chaired by

♦ Yoshiaki Nakano and William Holmes ♦

SIMPLIFICATION OF STRONG GROUND MOTIONS FOR LOADING IN PERFORMANCE-BASED SEISMIC DESIGN

Y. SAKAI, T. MINAMI, and T. KABEYASAWA[1]

ABSTRACT

The simplification of strong ground motions is proposed for performance-based design, assuming that the intensity of strong ground motions is expressed by response spectra. Strong ground motions are simplified into sine waves which are expressed by three parameters, the acceleration amplitude, period, and number of cycles such that the discrepancy of the elastic response acceleration spectra produced by strong ground motions and sine waves is minimal. This makes it possible to include factors which determine strong ground motions such as magnitude and epicentral distance and to determine the seismic design load in relation to return period which is applicable to performance-based seismic design.

1. INTRODUCTION

In performance-based seismic design, input ground motions or input seismic load have to be determined in relation to the return period. For this reason, various factors that determine strong ground motions need to be taken into account, such as (1) the source characteristics of the earthquake, (2) the path, (3) the ground surface, and (4) the interaction of structures and soil. However, it is very difficult to reproduce input strong ground motions taking into account all these factors because actual recorded strong ground motion accelerograms are very complicated. From an engineering point of view, there is no significant meaning in reproducing waveforms in fine details.

The simplification of strong ground motions into sine waves is proposed, assuming that the intensity of strong ground motions is expressed by response spectra, i.e., strong ground motions with the same response spectra are "equivalent.". Strong ground motions are simplified into sine waves which are expressed by three parameters, the acceleration amplitude, the period, and the number of cycles. This approach makes it possible to include the four factors shown above in reproducing strong ground motions and in determining the seismic design load in relation to the return period.

Lastly, as an application example is presented for rock sites more than 50km away from the epicenter considering the relationship between the three parameters of simplified sine waves and the magnitude and epicentral distance.

2. STRONG GROUND MOTIONS USED IN THE ANALYSES

Elastic and inelastic earthquake response analyses using single-degree-of-freedom (SDOF) systems were made. The input strong ground motion records used are shown in Table 1.

The FKI, KBP, and TKT records were recorded in or near areas severely damaged by the 1995 Hyogoken-Nanbu earthquake. The peak ground accelerations in these records are very high, but those even higher, as shown in many records, such as KSR, OTB, AKS, PCD, and CYC, caused little structural damage because the predominant period was short. The SCT and CDA records are those of the 1985

[1]*Earthquake Research Institute, The University of Tokyo, Tokyo, Japan*
Email: yuuki@eri.u-tokyo.ac.jp, minami@eri.u-tokyo.ac.jp, kabe@eri.u-tokyo.ac.jp

Michoacan, Mexico, earthquake which caused severe damage despite small peak ground accelerations. ELC, TFT, HAC, and THU are records often used in the earthquake-resistant design of important structures.

Response analyses were made for all the records, but to avoid confusion only the results for the 6 representative records are shown in the figures indicated by the * symbol on the shoulder of the ID. Time histories of ground acceleration for the 6 representative records are shown in Figure1. FKI and SLM are representative of the 1995 Hyogoken-Nanbu and 1994 Northridge earthquakes, respectively. Both FKI and SLM are near-field strong ground motions with high accelerations and long period pulses. KSR and OTB are representative of records that have very high peak ground accelerations but for which structural damage was not very great because of the short predominant period. The peak ground acceleration of OTB is very high, but high acceleration occurred only a few times. In contrast, high acceleration occurred many times in the KSR record. SCT is a representative record of the 1985 Michoacan, Mexico, earthquake which caused severe damage due to its long predominant period and many cyclic reversals. ELC is representative of the records often used in designing important earthquake-resistant structures.

Elastic response acceleration spectra with the damping factor of 0.05 are shown in Figure2 for all 6 representative records. FKI has a long predominant period and high acceleration responses in the more than 1.0 sec.-long period region; whereas, in the short period region of less than 0.5 sec., the response accelerations of KSR and OTB are larger than the acceleration of FKI.

3. METHOD OF SIMPLIFYING STRONG GROUND MOTIONS

Strong ground motions are simplified into sine waves such that the discrepancy between the elastic response spectra produced by strong ground motions with the damping factor of 0.05 and sine waves is minimal. In other words, the acceleration amplitude, period and number of cycles of the sine wave are determined so that the difference ratio defined in Eq.(1) is minimal.

$$R = \frac{1}{30}\sum_{N=1}^{30}\frac{\left|S(T)-S_e(T)\right|}{S(T)} \quad , \quad T = 0.1\times 1.12^{N}, \tag{1}$$

where R: the difference ratio, $S(T)$: the response spectrum produced by a strong ground motion, $S_e(T)$: the response spectrum produced by a sine wave, T: period of a system (sec).

Simplified sine waves are hereafter called "equivalent sine waves" because the elastic response acceleration spectrum produced by the sine wave is the nearest to that produced by the strong ground motion.

The elastic response acceleration spectra produced by equivalent sine waves are shown in Figure3. They are very similar to those produced by strong ground motions in Figure 2.

Acceleration amplitudes, periods and numbers of cycles of equivalent sine waves and difference ratios are shown in Table 1. The difference ratios are approximately 0.2, which means equivalent sine waves reproduce elastic response spectra with less than 20% discrepancy.

In Table 1, equivalent sine wave acceleration amplitudes are closely related to peak ground accelerations. The equivalent sine wave period is long in the case of FKI and SCT with long predominant periods and short for KSR and OTB with short predominant periods, i.e., equivalent sine wave periods adequately express the frequency characteristics of strong ground motions. The equivalent sine wave number of cycles is small for pulse waves such as FKI and SLM and large for KSR and SCT with long duration, i.e., equivalent numbers of cycles express continuity characteristics of strong ground motions to some extent. The equivalent sine wave number of cycles is 3 at most even in the case of SCT with the longest duration.

4. COMPARISON OF INELASTIC SPECTRA PRODUCED BY STRONG GROUND MOTIONS AND EQUIVALENT SINE WAVES

The seismic design load should be determined taking into account the inelastic characteristics of structures. In this study, the inelastic spectra for any hysteresis models can be calculated by using simplified equivalent sine waves as input motions instead of strong ground motion records.

Inelastic response spectra produced by strong ground motions and equivalent sine waves are compared. The required strength spectra required to produce maximum response ductility factors within constant values (called "allowable ductility factors μ_a" below) were calculated considering seismic design spectra. The bilinear and Takeda hysteresis models (Takeda 1970) were used to represent three different energy-dissipation capacities. Unloading stiffness degradation factor α values were set at 0 and 0.5 in the Takeda model. The bilinear skeleton curve was used with both models. The allowable ductility factor μ_a values were set at 2, 4, and 8.

The required strength spectra produced by strong ground motions and equivalent sine waves are shown in Figures 4 and 5, respectively. Both are very similar to each other. The difference ratios by Eq.(1) are approximately 0.2, which is approximately equal to those of elastic response acceleration spectra for any strong ground motion, hysteresis model and allowable ductility factor. This means that the required strength spectra, i.e., seismic design spectra are determined by equivalent sine waves acceleration amplitudes, periods and numbers of cycles with about 20% discrepancy.

5. AN EXAMPLE OF RELATION BETWEEN EQUIVALENT SINE WAVE PARAMETERS AND FACTORS THAT DETERMINE STRONG GROUND MOTIONS

Seismic design spectra can be determined by factors that determine strong ground motions such as (1) the source characteristics of earthquake, (2) the path, (3) the ground surface, and (4) the interaction of structures and soil, if the relationship between the three equivalent sine waves parameters (acceleration amplitudes, periods and numbers of cycles) and those factors is examined. In an application example, the relationships between the three parameters of simplified sine waves and magnitude and epicentral distance are shown for rock sites in far fields (more than 50 km away from the epicenter) where the effects of ground surface, interaction of structures, and soil and inhomogeneity of the rupture plane are small.

Strong ground motions on rock sites in far fields are shown in Table 2. The relation between the epicentral distance and the equivalent sine waves acceleration amplitudes, the periods, and the numbers of cycles are shown in Figures 6-8, respectively. The difference in magnitude is expressed by symbol density.

The equivalent sine waves acceleration amplitudes are smaller for longer epicentral distances by attenuation. Equivalent sine waves periods and numbers of cycles are respectively distributed from 0.3 to 0.7 sec and 0.5 to 2. According to previous studies (Rathje 1998; Hayashi 1997), parameters that express frequency characteristics and cycles are larger for longer epicentral distances. Such a distinct tendency was not found probably due to insufficiency of strong ground motion records. If more strong ground motion records are used and the dispersion of equivalent sine waves parameters and relation between return period and magnitude are statistically obtained, it is possible to determine the seismic design spectra in relation to the return period.

6. CONCLUSIONS

The simplification of strong ground motions into sine waves is proposed assuming that the intensity of strong ground motions is expressed by response spectra. Strong ground motions are expressed by three parameters, the acceleration amplitudes, the periods, and

the number of cycles. The strength spectra required to produce maximum response ductility factors within constant values for any hysteresis model can be calculated with about 20% discrepancy by using simplified equivalent sine waves as input motions instead of strong ground motion records. Seismic design spectra based on the return period which is applicable to loading in performance-based seismic design could be determined by examining the relation between these three parameters and the factors that determine strong ground motions.

REFERENCES

Hayashi Y., J. Miyakoshi, and K. Tamura. 1997. Intensity of strong ground motions and damage to buildings by the 1995 Hyogo-ken Nanbu earthquake. IRI Research Report 97-01(In Japanese.)

Rathje E. M., N. A. Abrahamson, and J. D. Bray. 1998. Simplified frequency content estimates of earthquake ground motions. *Journal of Geotechnical and Geoenvironmental Engineering* 124(2): 150–59. ASCE.

Takeda T., M. A. Sozen, and N. N. Nielsen. 1970. Reinforced concrete response to simulated earthquakes. *Journal of Structural Division* 96(ST12): 2557–73. ASCE.

ACKNOWLEDGMENTS

We thank the staffs of Osaka Gas Company; JR Railway Technical Research Institute; Japan Meteorological Agency; Port and Harbor Research Institute, Ministry of Transport; Building Research Institute, Ministry of Construction and the Committee on Earthquake Observation and Research in the Kansai Area; the staff of the Strong Motion Data Base at the Institute for Crustal Studies, University of California, Santa Barbara; Prof. K. Kudo the Earthquake Research Institute, University of Tokyo, and Prof. T. Sasatani the University of Hokkaido all of whom provided strong ground motion records.

KEYWORDS

simplification, strong ground motions, performance-based design, return period, required strength spectrum, sine wave, magnitude, epicentral distance

Table 1 Strong ground motions, equivalent sine waves acceleration amplitudes, periods, numbers of cycles and difference ratios

ID	Station	direction	Earthquake	PGA	Ae	Te	Ne	R
fki *	Osaka Gas Fukiai Station	NS	1995 Hyogoken-Nanbu	802	847	1.00	1.3	0.12
tkt	JR Takatori Station	NS	1995 Hyogoken-Nanbu	606	628	1.00	1.2	0.23
kbm	Kobe JMA	NS	1995 Hyogoken-Nanbu	818	816	0.73	1.1	0.19
kbp	Kobe Port 8th Bank	NS	1995 Hyogoken-Nanbu	686	875	1.53	1.2	0.18
kbu	Kobe University	NS	1995 Hyogoken-Nanbu	270	319	1.00	1.1	0.15
slm *	Sylmar	EW	1994 Northridge	827	985	0.55	1.0	0.19
trz	Tarzana	EW	1994 Northridge	1745	2037	0.40	0.8	0.14
nwh	Newhall	EW	1994 Northridge	572	603	0.81	0.7	0.26
stm	Santa-Monica	EW	1994 Northridge	866	945	0.26	1.1	0.14
otb *	Hokkaido Otobe-cho	EW	1993 Hokkaido-Nansei-oki (aftershock)	1568	1584	0.20	0.7	0.16
pcd	Pacoima Dam	EW	1971 San-Fernando	1055	1117	0.40	1.0	0.23
cyc	Coyote Lake Dam	EW	1984 Morgan Hill	1138	1335	0.40	0.5	0.23
ksr *	Kushiro JMA	EW	1993 Kushiro-oki	711	723	0.29	1.8	0.21
aks	Akkesi	NS	1994 Hokkaido-Nansei-oki	1061	1349	0.17	1.3	0.20
sct *	SCT1	EW	1985 Mexico	168	166	2.00	2.8	0.18
cda	CDAF	EW	1985 Mexico	95	102	2.70	1.9	0.17
elc *	El-Centro	NS	1940 Imperial Valley	342	450	0.65	0.7	0.18
tft	Taft	EW	1952 Arvin-Tahachapi	176	178	0.62	1.0	0.18
hac	Hachinohe	EW	1968 Tokachi-oki	182	195	0.96	1.5	0.19
thu	Tohoku University	NS	1978 Miyagiken-oki	238	255	0.94	1.6	0.16

PGA: peak ground acceleration(cm/sec.^{2}),R: difference ratio,
Ae, Te, Ne: acceleration amplitude, (cm/sec.^{2}), period (sec.) and number of cycles of equivalent sine waves

Table 2 Strong ground motions on rock sites

Station ID	Δ	Earthquake	M	PGA (EW)	PGA (NS)
MLC	51.6	1987 Whittier Narrows	6.1	53.5	63.9
MCS	152.5	1992 Landers	7.3	21.7	22.0
ANB	63.3	1994 Northridge	6.7	67.0	44.9
LRB	60.1	1994 Northridge	6.7	70.6	59.0
LV3	51.0	1994 Northridge	6.7	103.8	82.6
NBC	86.2	1994 Northridge	6.7	103.5	79.4
RDC	88.7	1994 Northridge	6.7	70.1	50.4
RHE	50.0	1994 Northridge	6.7	113.5	103.7
WJF	76.4	1994 Northridge	6.7	55.4	36.2
CPM	126.4	1994 Eureka	6.8	23.3	21.7

PGA: peak ground acceleration(cm/sec.^{2}),M: magnitude
Δ: epicentral distance (km)

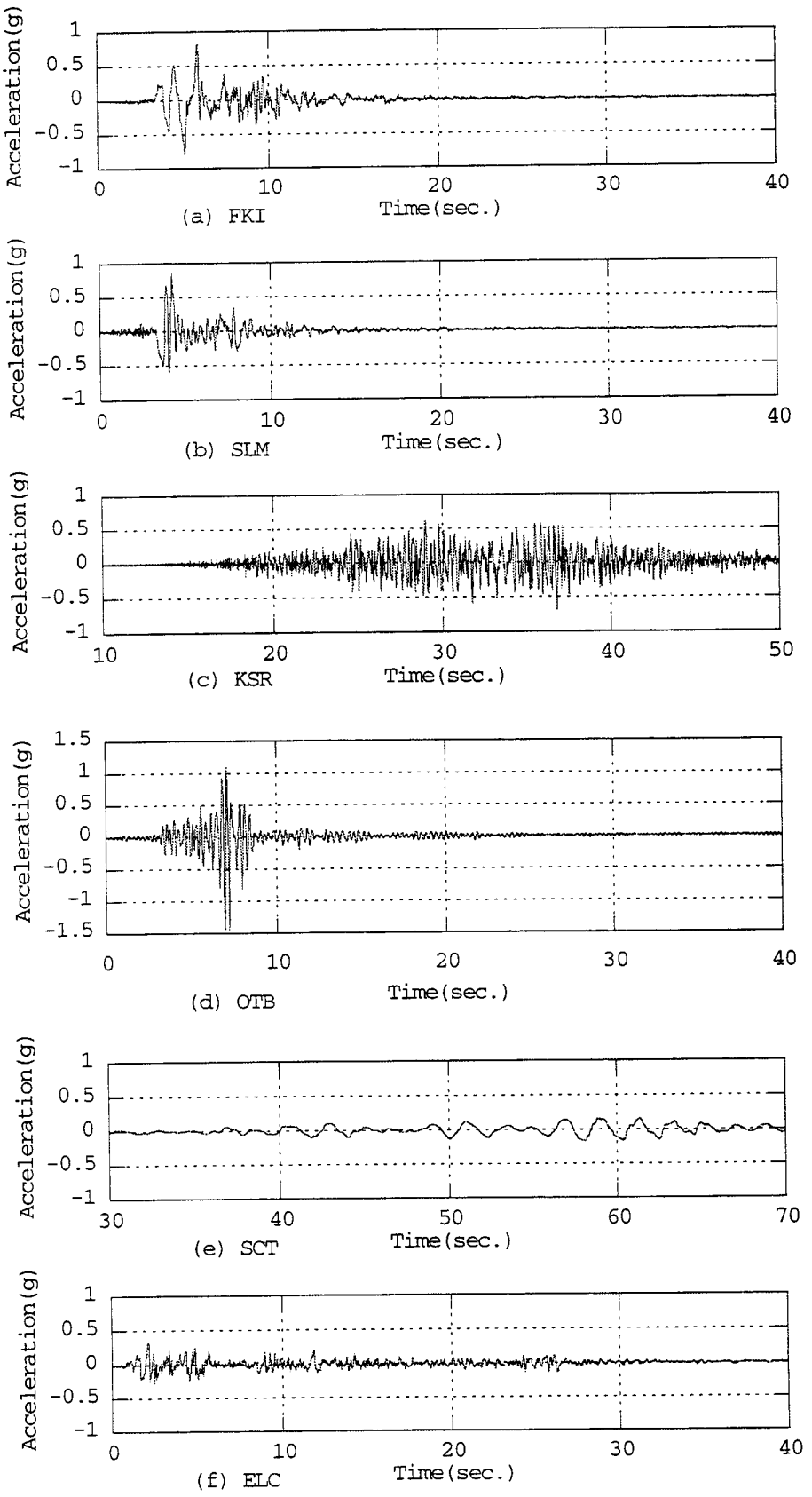

Fig.1 Time histories of ground acceleration

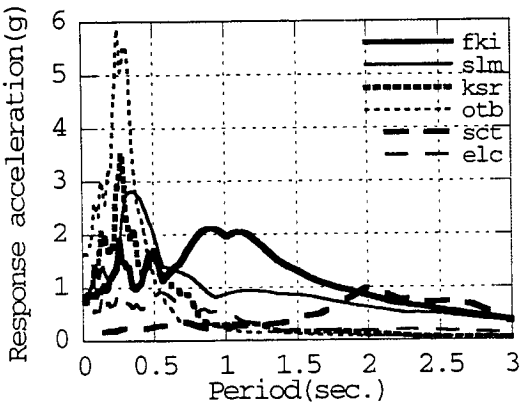

Fig.2 Elastic response acceleration spectra(h=0.05)

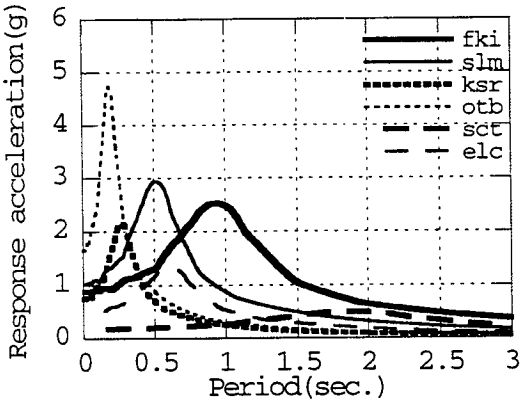

Fig.3 Elastic response acceleration spectra(h=0.05) by equivalent sine waves

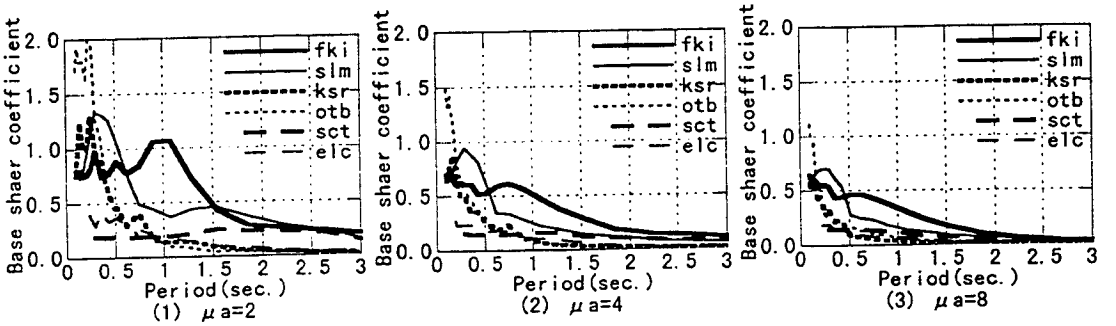

(a) Bilinear

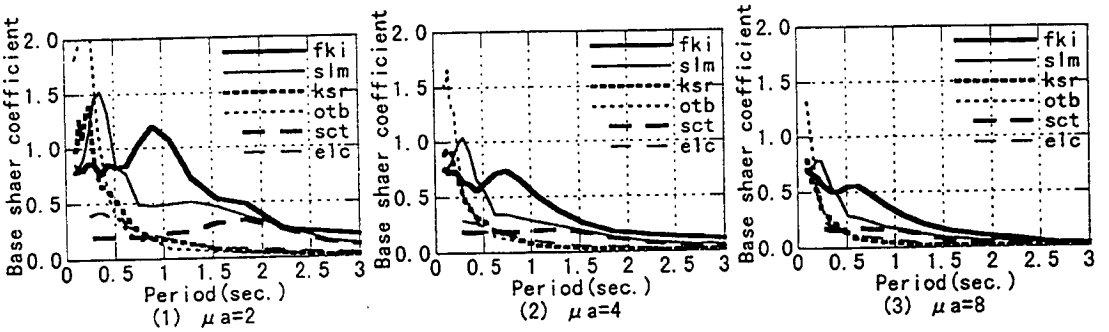

(b) Takeda (α=0)

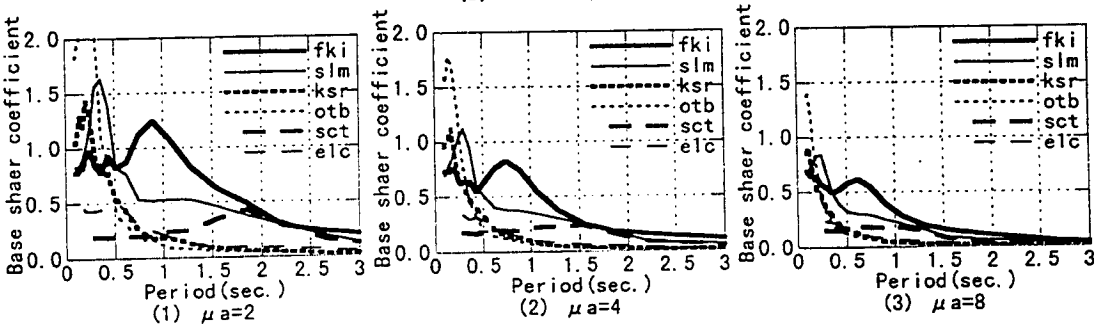

(c) Takeda (α=0.5)

Fig. 4 Required strength spectra

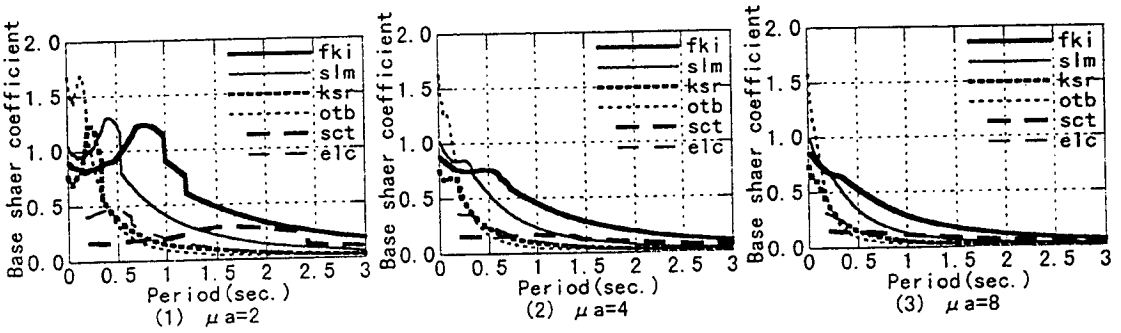

(a) Bilinear

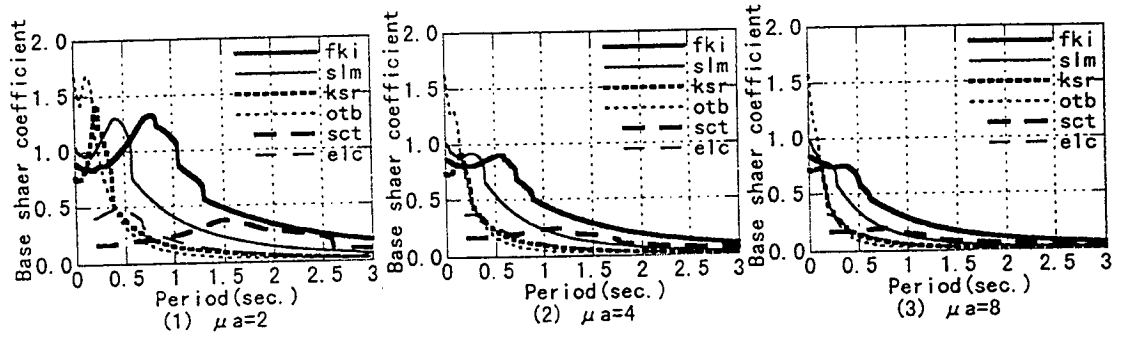

(b) Takeda(α=0)

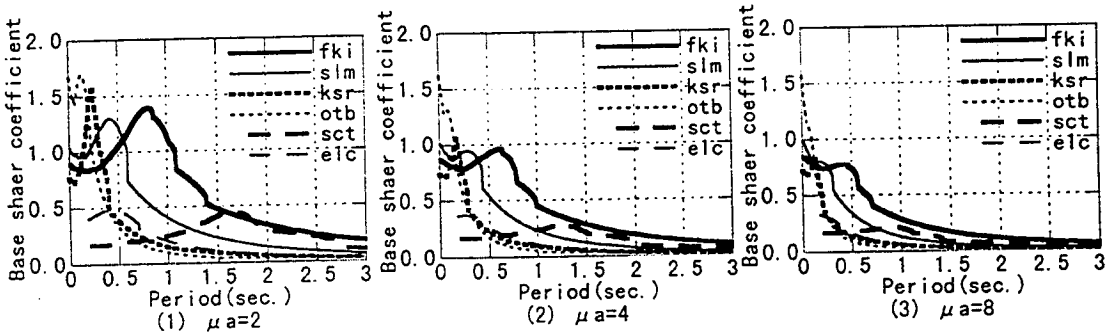

(c) Takeda(α=0.5)

Fig.5 Required strength spectra by equivalent sine waves

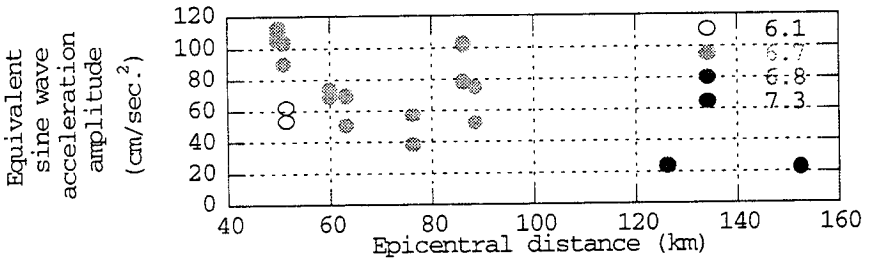

Fig.6 Relation between equivalent sine wave acceleration amplitudes and epicentral distance

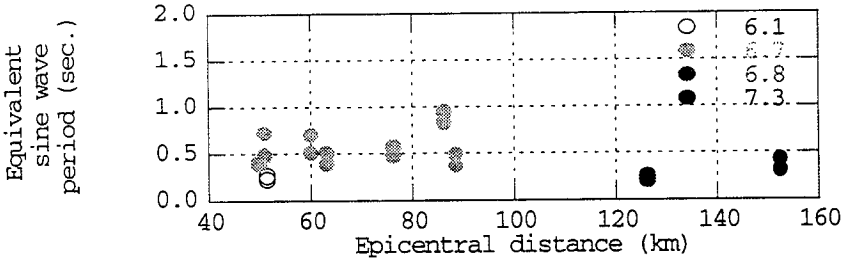

Fig.7 Relation between equivalent sine wave periods and epicentral distance

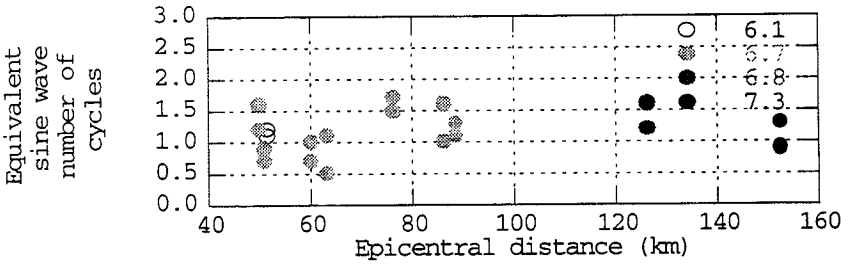

Fig.8 Relation between equivalent sine wave numbers of cycles and epicentral distance

SEISMIC DEMANDS FOR PERFORMANCE-BASED DESIGN

Helmut KRAWINKLER[1], Ricardo MEDINA[1], Manuel MIRANDA[1], Ashraf AYOUB[1]

ABSTRACT

In performance-based seismic design the need exists to establish relationships between important structural response parameters and ground motion parameters, and to assess the sensitivity of these relationships to the uncertainties inherent in ground motion and structural response prediction. This paper summarizes a few aspects of a comprehensive study on seismic demand evaluation, which focuses on the understanding and quantification of seismic demands, the identification of ground motion parameters that correlate best with seismic demands, and the assessment of relationships (and their robustness) between response and ground motion parameters.

1. A PEER PROJECT ON SEISMIC DEMAND EVALUATION

Performance-based earthquake engineering implies that the capacities provided by the structural and nonstructural systems should exceed the demands imposed by ground motions with an acceptable level of confidence and with due consideration given to important uncertainties and randomness in demand and capacity predictions. Reliability-based formulations of this demand/capacity concept are under development in professional efforts (e.g., SAC steel project) and in parallel PEER projects. These reliability-based formulations are performance evaluation procedures whose rigorous implementation may be too complex for the majority of structures. In parallel with, and in support of, the development of rigorous reliability methods for performance assessment, there must be research that will provide knowledge an engineer can implement in (a) the conceptual design process to make informed decisions, and (b) the performance evaluation process to carry out a reliability assessment with relatively simple tools.

1.1 Objectives of Study

This paper is concerned with the latter kind of research, and focuses on work in progress as part of the PEER effort on "Global Assessment/Design Methodologies." The broad objective is to establish relationships between ground motion parameters and seismic demand parameters for a comprehensive range of ground motion and structure characteristics. The selected ground motion sets are sufficiently large to permit evaluation of basic statistical values (mean [or median] and a measure of dispersion) and to address the question of whether there are systematic dependencies of demand parameters on variables such as earthquake magnitude or site-source distance. The specific objectives of the study are as follows:

- Understand and quantify seismic demands.
- Evaluate demand patterns as a function of the properties of structures and ground motion.
- Evaluate sensitivity of demands to properties of structures and ground motion.
- Evaluate sensitivity of demand predictions to analytical models and analysis methods (establish bias factors).

[1] *Department of Civil and Environmental Engineering, Stanford University, Stanford, CA 94305*
Email: krawinkler@ce.stanford.edu

- Evaluate collapse hazard for deteriorating structural systems.
- Evaluate sensitivity of demands to structure-foundation-soil interface conditions (e.g., foundation strength and stiffness, soil properties).
- Evaluate seismic demands of particular concern for nonstructural and content systems (e.g., floor accelerations, story drifts at higher performance levels).
- Utilize the acquired knowledge to formalize a procedure for conceptual seismic design that incorporates multiple performance objectives.

Ground motion variables of primary interest include magnitude, distance (R > 15 km and near-fault), rupture mechanism, and soil profile (with emphasis on NEHRP soil profile D and soft soils). Structural variables of primary interest include number of stories, fundamental period, base shear strength, strength and stiffness distribution over height, damping, P-delta, hysteresis models (with degradation), mechanism type, gravity effects, and irregularities in elevation. Figure 1 outlines the global approach to the demand evaluation research.

Frame and wall structures are being investigated with an emphasis on properties that are characteristic of reinforced concrete structures. Thus, degradation in stiffness and deterioration in strength are focal areas of this study, and will be discussed in detail later. A high performance level is investigated (incipient damage), but the emphasis is on the incipient collapse performance level with the objective of relating ground motion parameters to structural strength and deterioration properties that trigger collapse. Only 2-D structural models are investigated in this study.

1.2 Approach

The backbone of the research is response simulation by means of nonlinear time history analysis of single- and multi-degree of freedom systems. Much work in this area has been done already. Taking advantage of past work is the only way the comprehensive objective of this project can be successfully accomplished. The focus of the work is to bring together relevant information on demand predictions in order to address issues critical to advancements in PBEE. The emphasis is on an evaluation of available results, extensive parametric analysis, and the establishment of a comprehensive database that permits consistent and effective synthesis of the demand data for the purposes enumerated before.

The approach to the research consists of

- Designing a family of generic structures that cover the range of parameters of interest (see Figure 2 for the period range of frame structures under study).
- Selecting and documenting sets of ground motions that cover the range of parameters of interest.
- Developing a database management system for storage and retrieval of all the ground motion input and structure response data of interest for performance assessment.
- Developing an evaluation system through which relationships between ground motion parameters and seismic demand parameters can be established.
- Developing simple element models capable of simulating deterioration of the type seen in reinforced concrete elements and incorporating these models in available computer programs.

- Performing extensive analytical parameter studies on elastic and inelastic SDOF and MDOF structural systems, using available computer codes (DRAIN, SNAP).
- Synthesizing data and arriving at a comprehensive evaluation of seismic demands.

1.3 Why Is This Research Essential?

In concept, this research tries to address (and answer) all the questions one might want to ask on the relationships between seismic demands (at various performance levels) and ground motion parameters. It is fair to ask why this research is needed in view of the argument that the long-range objective of performance-based earthquake engineering is to perform, for each new design and for each evaluation/retrofit project, a rigorous structure-specific performance evaluation at all performance levels of interest to the owner or society. Nonlinear time history analysis appears to be the means to achieve this. If this is done in a rigorous manner, then a generic study on seismic demands appears to be superfluous. This is wishful thinking because

- most structures cannot be analyzed rigorously,
- in the analysis process many decisions have to be made on necessary modeling accuracy,
- different structures respond very dissimilarly to different ground motions,
- basic phenomena that will greatly affect the dynamic response may escape detection in a routine execution of a set of time history analyses,
- most of the important design decisions are made in the conceptual design phase in which a structure is being created and time history analysis is unfeasible.

For these and many other reasons a quantitative understanding of the relationships between ground motion and response parameters, and their "robustness", is critical. Figure 3 provides an illustration for the need for this quantitative understanding, using structural walls as an example (Seneviratna and Krawinkler, 1997). Code designs are based on a prescribed lateral load pattern (likely SRSS), which determines the story overturning moments and shear forces for design. The design overturning moment distribution may be as shown in a solid line in Figure 3(a). This moment distribution together with "conservative" shear design requirements (to avoid a shear-critical situation) are used to detail wall reinforcement. The graphs in Figure 3, which show mean response values using a set of 15 ground motions, illustrate that inelastic dynamic behavior may not be as anticipated in design. In this example the wall bending strength is kept constant over the height and is set equal to the design value at the base. Figure 3(a) shows that considerable propagation of yielding into stories above the bottom story has to be expected and that the dynamic moment envelope differs drastically from the design pattern. Figure 3(b) presents the dynamic base shear demands normalized by the design base shear. For a reasonable range of ductility (say $\mu \leq 5$) the amplification of shear demands may be very high, and likely higher than provided for in present code designs. This indicates that wall shear failure is a distinct possibility even when code design provisions to avoid shear critical situations have been followed.

2. AN ILLUSTRATIVE EXAMPLE OF DEMAND EVALUATION FOR FRAME STRUCTURES

In the demand assessment performed in this study much emphasis is placed on an evaluation of the sensitivity of response parameters to ground motion characteristics. This issue cannot be

discussed here because of space limitations. Another major aspect of the work is to close the loop between SDOF and MDOF response variables. This implies attempts to relate SDOF elastic spectral quantities to inelastic spectral quantities to MDOF global deformation parameters (e.g., roof displacement) to MDOF story drifts to local element deformation demands. Fundamental to this process are diagrams of the type shown in Figure 4.

For each ground motion and each generic structure, time history results as well as peak values for a great number of response parameters are stored in a data base. Analyses are performed for closely spaced strength values in order to permit a complete description of the dependence of response parameters on structure strength. The yield strength of the SDOF system is defined by $\eta = F_y/W$, and the base shear strength of the MDOF structure is defined by $\gamma = V_y/W$. Thus, η–$\mu_{SDOF,max}$ and γ-$\mu_{s,max}$ diagrams of the type shown in the top graphs of Figure 4 define the global response of SDOF and MDOF systems ($\mu_{s,max}$ being the maximum story ductility). A comparison between η–$\mu_{SDOF,max}$ and γ-$\mu_{s,max}$ diagrams provides one of many basic SDOF-MDOF relations.

The bottom graphs in Figure 4 focus on the MDOF maximum story ductility demand. The vertical axis on the left depicts the previously defined γ values, whereas the axis on the right represents the inverse of γ multiplied by γ_1, the base shear strength causing a maximum story ductility of unity. The ratio γ_1/γ defines the strength reduction factor R. Reading the left scale downwards corresponds to a decrease in base shear strength, and reading the right scale upwards corresponds to an increase in the ground motion intensity. Thus, the curve corresponding to the right scale (R-μ curve) is fully equivalent to the Incremental Dynamic Analysis (IDA) curve used in a recent approach to evaluate the ductility capacity at collapse (Hamburger et al., 2000).

Much can be deduced from these R-μ curves. For one, they increase at an almost constant rate at large ductilities, indicating that the ductility capacity is unlimited. This is no surprise because the element hysteresis models are bilinear and nondegrading, and P-delta effects are not considered in this case. The curve for T = 3.6 sec. shows an S-shape, which is characteristic for long period structures subjected to near-fault records (Alavi and Krawinkler, 1999). [The Northridge Rinaldi Receiving Station record is used.] The curve for T = 0.3 sec. is far below the $R = \mu$ curve, indicating that the ductility demands grow at a fast rate as the strength of the structure is reduced. The reverse is true for T = 3.6 sec., particularly at high ductility demands.

Information of the type briefly discussed here, and much additional information, is being evaluated in order to achieve a quantitative understanding of the relationships between ground motion and structural response parameters.

3. EFFECTS OF ELEMENT DETERIORATION ON COLLAPSE POTENTIAL

With the increasing emphasis on the Incremental Dynamic Analysis (IDA) for the evaluation of drift capacities associated with the limit state of collapse, it becomes a necessity to develop element hysteretic models that incorporate all important phenomena that contribute to story drift predictions as the structure approaches collapse. In earthquake engineering, collapse implies that the structural system is incapable of maintaining gravity load carrying capacity in the presence of seismic effects. Collapse may occur if vertical load carrying elements fail in compression, or if

shear transfer is lost between horizontal and vertical elements (e.g., shear failure between a flat slab and a column), or if an individual story displaces sufficiently so that the second order P-delta effects fully offset the first-order story shear resistance and instability occurs.

In either case replication of collapse necessitates the modeling of deterioration characteristics of structural elements. The literature on this subject is extensive, but few if any simple deterioration models exist, and little systematic research on the effects of element deterioration on the collapse potential has been performed. Rigorous evaluation of collapse safety will not be feasible unless such research is carried out. A conceptual tool for safety evaluation has recently been developed (Hamburger et al., 2000), but its utilization is feasible only if modeling of deterioration is incorporated in the response prediction.

This research project addresses the deterioration issue in great detail. The research utilizes bilinear (or trilinear) hysteresis skeletons and is based on a relatively simple deterioration model (Rahnama and Krawinkler, 1993) defined by a single deterioration parameter of the type

$$\beta_i = \left(\frac{E_i}{E_t - \sum_{j=1}^{i} E_j} \right)^c \tag{1}$$

in which
- β_i = parameter defining the deterioration in excursion i
- E_i = hysteretic energy dissipated in excursion i
- E_t = hysteretic energy dissipation capacity = $\gamma F_y \delta_y$
- $\sum E_j$ = hysteretic energy dissipated in all previous excursions
- c = exponent defining the rate of deterioration

Hysteretic response is defined by the following characteristics (see Figure 5, which illustrates, in three columns, basic models in the top row with deteriorating models of various complexities below):

- A skeleton that is either bilinear (or trilinear)
- Basic restoring force characteristics that are of one of the following types (row 1 of Figure 5):
  - Bilinear (or trilinear)
  - Peak oriented (Clough model)
  - Pinching model with a given residual strength
- Capping of monotonic hardening at a specified deformation, to be followed by a degraded stiffness that may be positive or negative (row 2)
- Strength deterioration (row 3) defined by

$$F_i = (1 - \beta_i) F_{i-1} = \beta_s F_{i-1} \tag{2}$$

  in which
  - F_i = deteriorated yield strength after excursion i
  - F_{i-1} = deteriorated yield strength before excursion i
  - β_s = $(1 - \beta_i) > 0$, with the value of β_i given by Eq. 1, using the appropriate γ value to model strength deterioration.
- Strength deterioration with capping (row 4)

- Unloading stiffness degradation (row 5) defined by
$$K_{u,i} = (1-\beta_i)K_{u,i-1} = \beta_u K_{u,i-1} \quad (3)$$
(each term is defined in the manner presented for Eq. 2)
- Accelerated reloading stiffness degradation (row 6), defined by moving the target deformation for the Clough and pinching model by
$$\delta_{t,i} = (1+\beta_i)\delta_{t,i-1} = \beta_k \delta_{t,i-1} \quad (4)$$

This model was investigated for different loading histories (symmetric, Figure 5, and asymmetric, Figure 6), and was tested on load-deformation data obtained from experiments on steel, reinforced concrete, and wood components (Figure 7). The variables to adjust are the skeleton strength and stiffnesses, the capping deformation, and the deterioration rates described by γ, a multiple of $F_y\delta_y$. The values of γ may differ between models and modes of deterioration. For the results shown in Figures 5 and 6 the γ values are 100 for all deterioration modes of the bilinear and Clough models, and 50 for all deterioration modes of the pinching model.

It is believed that the deteriorating hysteresis models summarized here are relatively simple but sufficiently versatile to model all basic deterioration modes in structures of different material. They are being used to perform IDAs for SDOF systems and generic MDOF structures. The results of this part of the study are expected to provide insight in the effects of deteriorating element characteristics on the collapse safety of structural systems.

SUMMARY

The work summarized here will result in a comprehensive database that relates structural response parameters to ground motion parameters. Major effort is devoted to selecting comprehensive sets of representative ground motions and structural systems, identifying all ground motion and response parameters that may be of interest, and developing a database management system that will make it feasible to extract all relevant relationships between parameters and to assess the robustness of these relationships.

REFERENCES

Alavi, B., and H. Krawinkler. 1999. Effects of near-fault ground motions on the response of frame structures. *Proceedings of the 1999 Structures Congress*, SEI, ASCE, New Orleans.

Hamburger, R. O., D. A. Foutch, and C. A. Cornell. 2000. Performance basis of guidelines for evaluation, upgrade and design of moment-resisting steel frames. *Proceedings of the 12th World Conference on Earthquake Engineering*, Auckland, New Zealand.

Rahnama, M., and H. Krawinkler. 1993. *Effects of soft soils and hysteresis model on seismic demands.* John A. Blume Earthquake Engineering Center Report No. 108, Department 110 of Civil Engineering, Stanford University.

Seneviratna, G. D. P. K., and H. Krawinkler. H. 1997. *Evaluation of inelastic MDOF effects for seismic design.* John A. Blume Earthquake Engineering Center Report No. 120, Department of Civil Engineering, Stanford University.

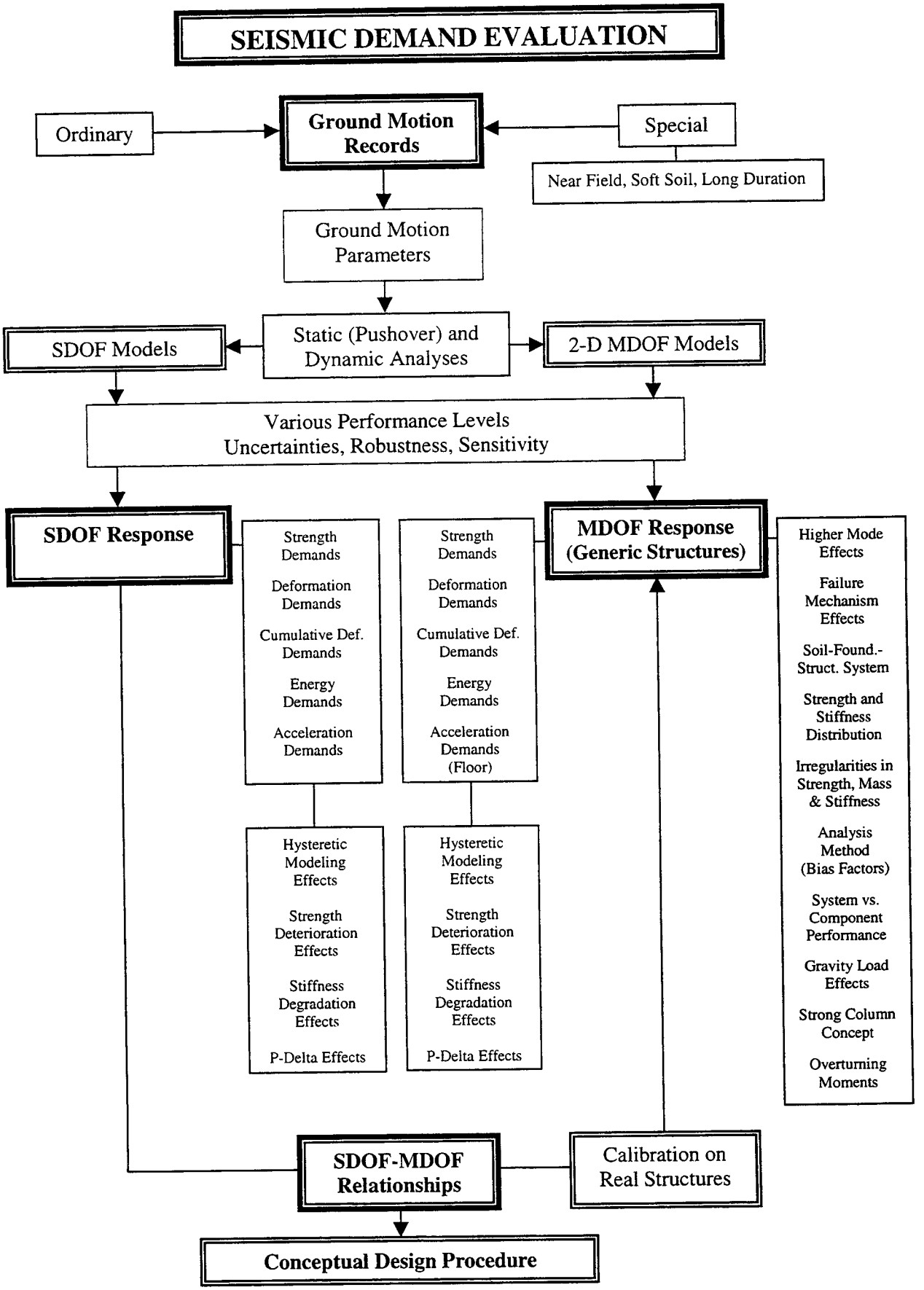

Figure 1. Seismic Demand Evaluation Process

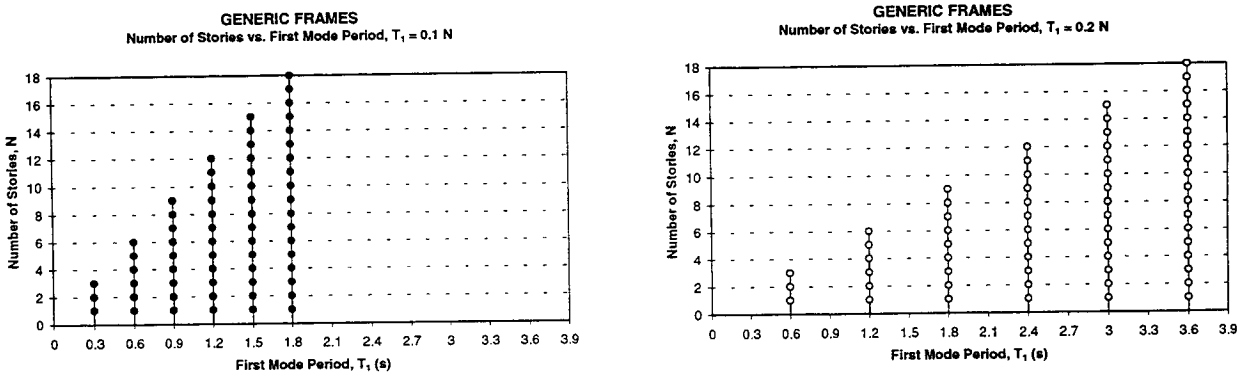

Figure 2. Periods and Number of Stories for Generic Structures

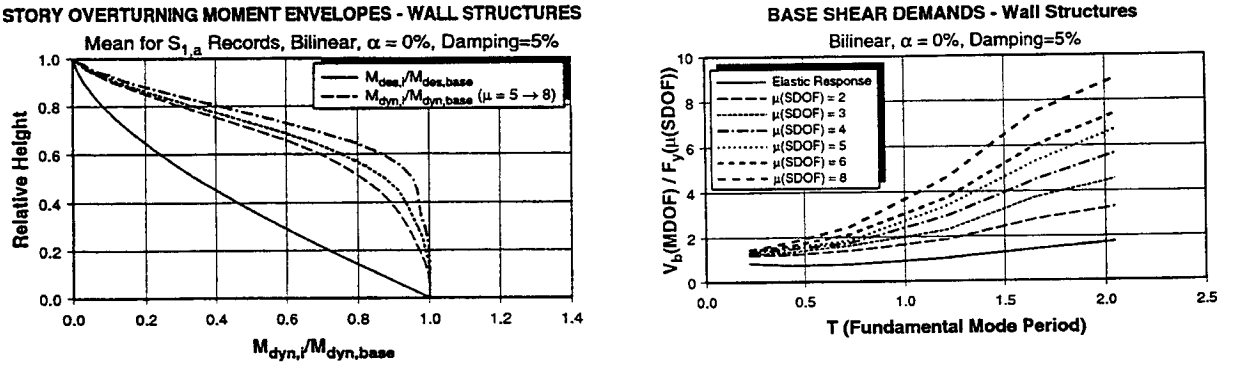

Figure 3. Seismic Demands for Wall Structures; (a) OTM Demands for T = 1.22 sec., (b) Amplification of Base Shear Demands as Function of T and Ductility (Seneviratna, 1997)

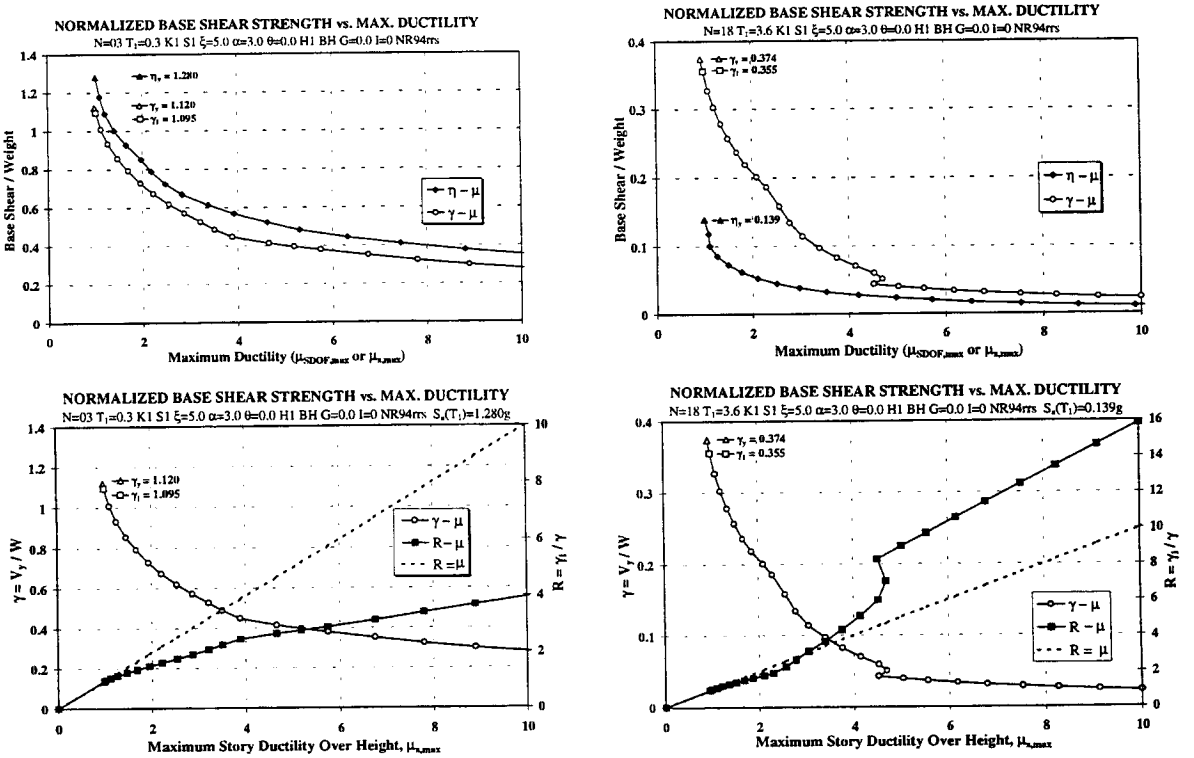

Figure 4. Strength-Ductility Diagrams for SDOF & MDOF Systems, T = 0.3 and 3.6 sec.

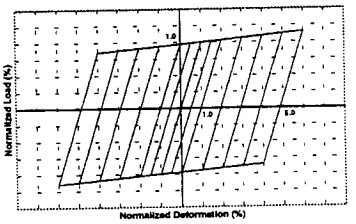

Bilinear, no deterioration

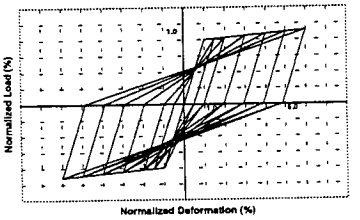

Clough, no deterioration

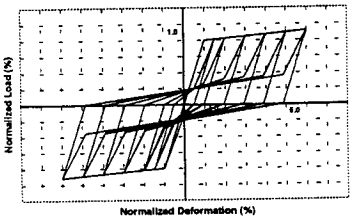

Pinching, no deterioration

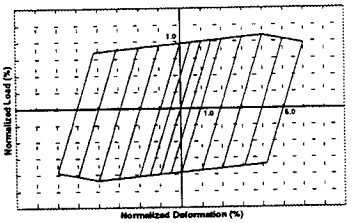

Bilinear, with cap, no cyclic det.

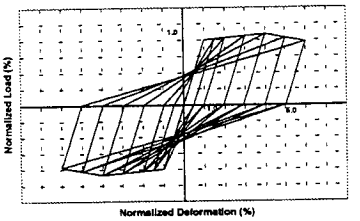

Clough, with cap, no cyclic det.

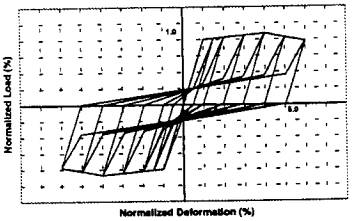

Pinching, with cap, no cyclic det.

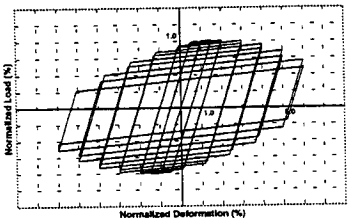

Bilinear, strength det., no cap,

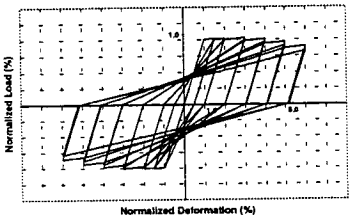

Clough, strength det., no cap,

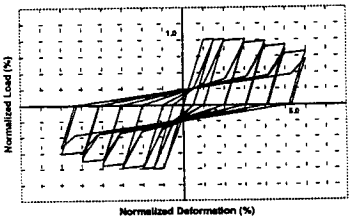

Pinching, strength det., no cap

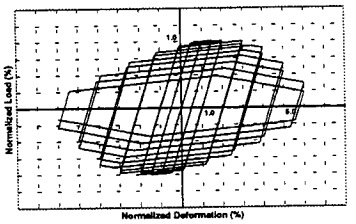

Bilinear, strength det. with cap,

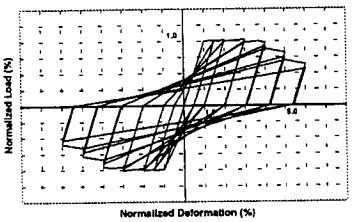

Clough, strength det. with cap,

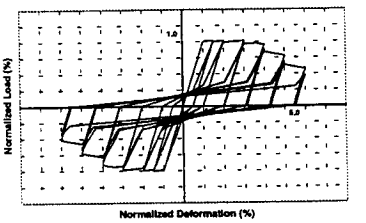

Pinching, strength det., with cap

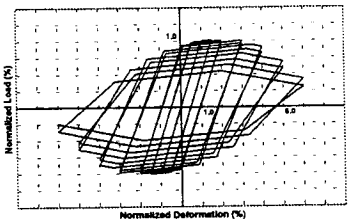

Bilinear, strength & stiff. det. & cap

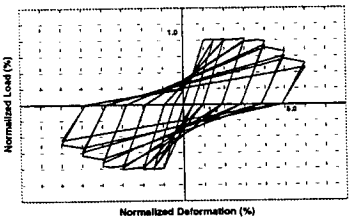

Clough, strength & stiff. det. & cap

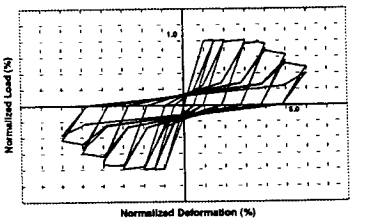

Pinching, strength & stiff. det. & cap

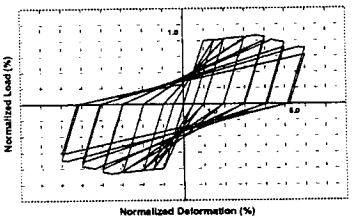

Clough, accel. reldg stiff. degr. + cap

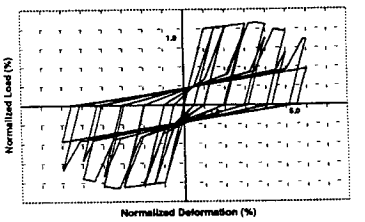

Pinchg, accel. reldg stiff. degr. + cap.

Figure 5. Hysteresis Models without and with Deterioration; Symmetric Histories

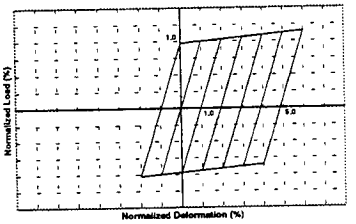

Bilinear, no deterioration

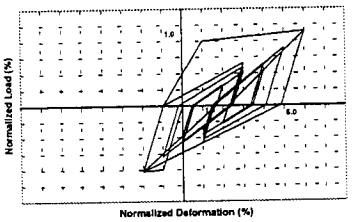

Clough, no deterioration

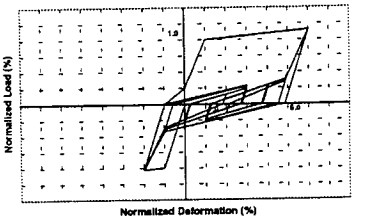

Pinching, no deterioration

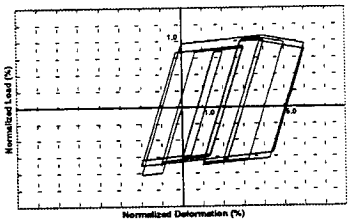

Bilinear, strength det. with cap

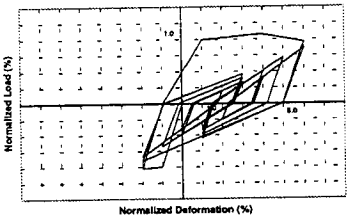

Clough, strength det. with cap

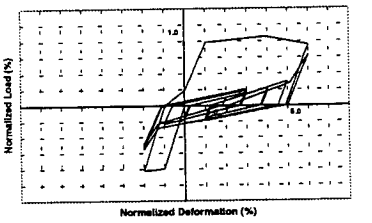

Pinching, strength det. with cap

Figure 6. Hysteresis Models without and with Deterioration; Asymmetric Histories

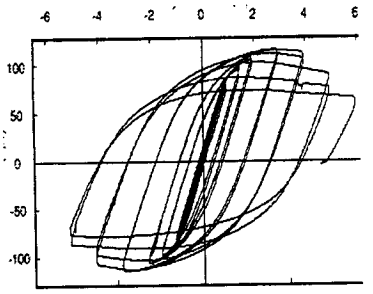

Steel Beam – Test

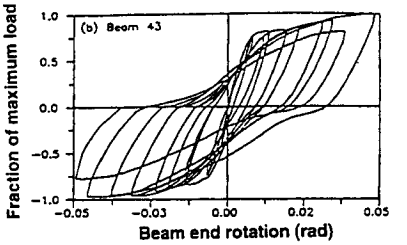

Reinf. Concrete Beam – Test

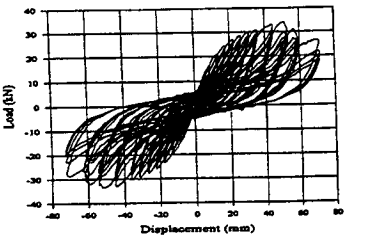

Plywood Wall - Test

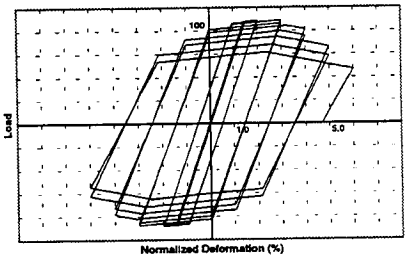

Steel Beam – Simulation

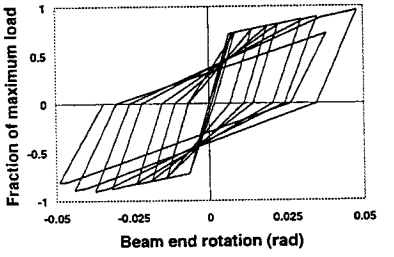

Reinf. Concrete Beam – Simulation

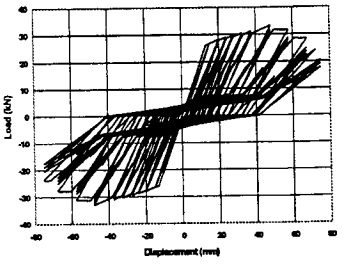

Plywood Wall - Simulation

Figure 7. Experimentally Obtained and Simulated Hysteretic Responses

THE EFFECT OF VERTICAL EXCITATION ON SEISMIC RESPONSE CHARACTERISTICS OF STRUCTURES

Koichi KUSUNOKI[1] and Yoshiaki NAKANO[1]

Tsuneo OKADA[2]

ABSTRACT

Under an earthquake excitation, structures might vibrate not only horizontally but also vertically due to vertical excitation. In general, however, the effect of the vertical excitation is currently not considered directly or with scientific justification in Japan. The effect of vertical excitation must be studied to improve the seismic capacity of structures under earthquakes. In this paper, nonlinear dynamic response analyses of a 2-span-12-story R/C structure are carried out to investigate the effect of vertical excitation on both the horizontal and vertical response displacements of structures, and on earthquake-induced axial forces in columns. Furthermore, a new flexural design method for columns is proposed to ensure a total yield hinge mechanism of the beam-yield type.

1. INTRODUCTION

Under an earthquake excitation, the vertical excitation can cause structures to vibrate not only horizontally but also vertically. In general, however, the effect of vertical excitation, is currently not considered directly or with scientific justification in Japan. The effect of vertical excitation must be studied to improve the seismic capacity of structures under earthquakes. Especially corresponding to the capacity design concept, it is important to make a structure form a total yield mechanism of the beam-yield type. The three-dimensional dynamic characteristics of structures under three-dimensional ground motion, (the effect of vertical excitation on columns, and the vertical vibration of slabs and beams, for example), must be verified to make a structure form a total yield mechanism at an ultimate state under real earthquakes.

In this paper, the effect of vertical excitation on columns is investigated. It can be predicted from the interaction of the axial and bending restoring force that a column designed without respect to vertical excitation can yield caused by additional axial load due to this excitation. The main purposes of this paper are to examine nonlinear dynamic response analyses with a plain R/C frame under horizontal and vertical excitations, to discuss the effect of vertical excitation on columns, and to propose a new flexural design method for columns.

1 Institute of Industrial Science, University of Tokyo, Tokyo, Japan
E-mail kusu@cc.iis.u-tokyo.ac.jp
2 Shibaura Institute of Technology, Tokyo, Japan
E-mail okada@sic.shibaura-it.ac.jp

2. NONLINEAR DYNAMIC RESPONSE ANALYSES

One component model, shown in Figure 1, is applied to all members so that the interaction of the axial and bending restoring force can be taken into account. In this model, it is assumed that flexural failure can occur at both ends of a member. Nonlinear axial and shear springs are arranged at the center of a member, and in two multi-spring models at both ends. The multi-spring model consists of nonlinear axial spring elements with real lengths that represent the nonlinear characteristics of concrete and steel materials. The multi-spring model can directly. represent the effect of the axial and bending restoring force interaction. The length of the spring element is determined as D/4 in this paper (D represents depth of member).

The investigated frame is a 2-span-12-story R/C structure with a span length is 6.0 m and story height of 3.0 m in which a total yield mechanism forms in which the yield hinges are developed at the ends of all beams and at the bottom of the first-story columns under lateral seismic loads.

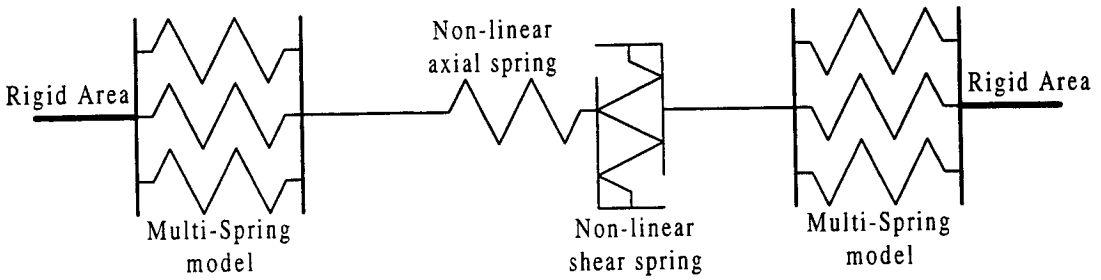

Fig. 1. One component model

Table. 1. Parameter of analysis

Case	Peak Ground Acceleration (g)	
	Horizontal	Vertical
No.1	0.700	0.000
No.2	0.700	0.413
No.3	0.700	0.700

Ten seconds of the Taft EW and UD components recorded during the 1952 Kern County, California, earthquake, including peak records are applied to the input motions, scaling the peak ground acceleration of the horizontal component up to 0.700G to make the structure form a total yield mechanism. The parameter of analysis is the level of vertical excitation, as shown in Table. 1. There is no vertical excitation in case 1; the ratio of the peak ground acceleration of the vertical component to that of the horizontal (0.59 (= 0.413/0.7)) is the same as that of the original records in case 2, and the peak ground acceleration of the vertical component is amplified to 0.7 g which is the same as that of the horizontal in case 3.

In the results of the modal analysis, the first vibration mode of the structure is the first mode of horizontal vibration, and its natural period is 0.798 sec. The second vibration mode is the second mode of the horizontal vibration and its natural period is 0.287 sec. And the fifth vibration mode is the first mode of vertical vibration, and its natural period is 0.084 sec. In the Rayleigh damping model, a 1.0% damping factor for the first and fifth vibration modes is assumed in the subsequent nonlinear analyses.

The results of the analyses are discussed as follows. The distributions of the maximum horizontal response displacements are shown in Figure 2, and those of the vertical are shown in Figure 3. It can be seen that vertical excitation does not affect the maximum horizontal response displacements, while it does affect the maximum vertical response displacements significantly, especially those of interior columns when additional axial force due to vertical excitation causes tensile forces in columns. The locations of the yield hinges are shown in Fig. 4. Case 1 (no vertical input) forms a total yield mechanism as planned. But in case 2 (the ratio of peak vertical ground acceleration to that of horizontal is same as the ratio of the original records), more yield hinges are develop, especially in interior columns at lower stories. This tendency can be founded more clearly in case 3 (the peak ground acceleration of vertical component is the same value as that of the horizontal). This result is mainly because the varied axial force on the interior columns due to the overturning moment caused by horizontal vibration is negligibly small, and no varied axial force is therefore taken into account for interior columns under lateral seismic loads in seismic design. On the other hand, the varied axial force due to vertical excitation in the interior columns is generally larger than that in the exterior columns considering the first vertical vibration mode and larger mass supported by the interior columns than by the exterior columns.

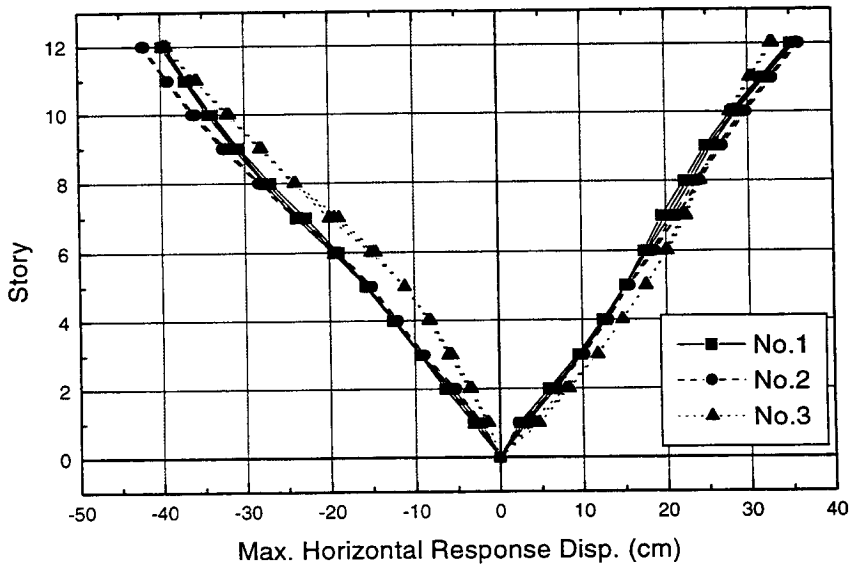

Fig. 2. Distributions of maximum horizontal response displacements

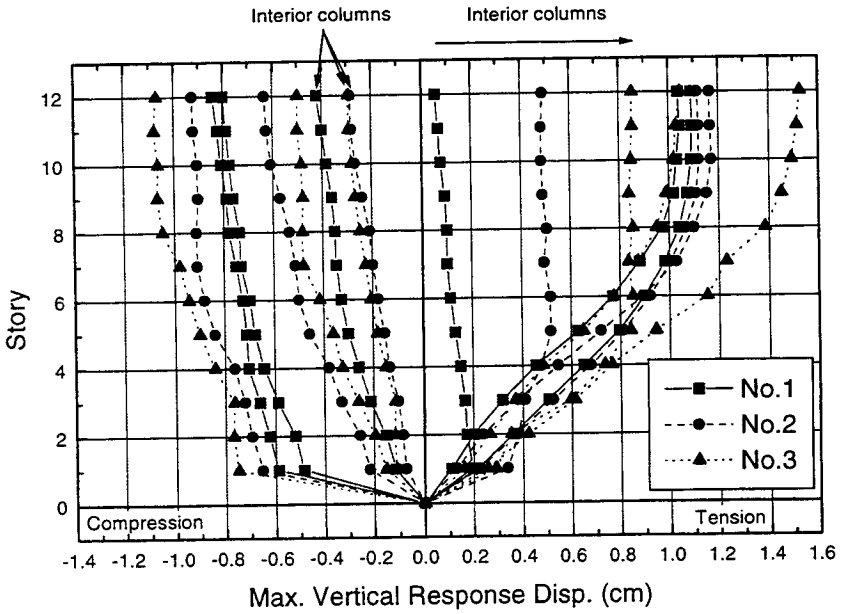

Fig. 3. Distributions of maximum vertical response displacements

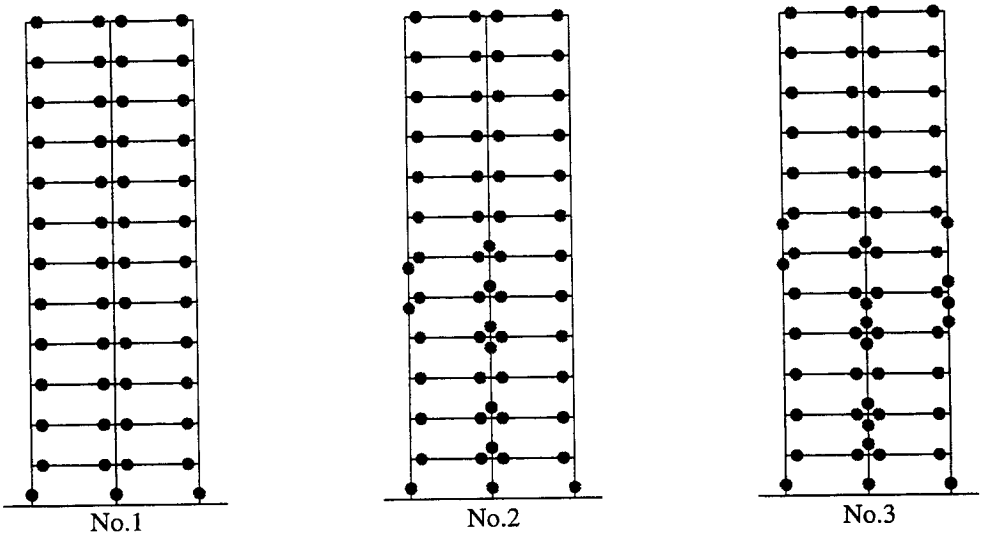

Fig. 4. Locations of yield hinges

3. NEW FLEXURAL DESIGN METHOD OF COLUMNS CONSIDERING THE EFFECT OF VERTICAL EXCITATION

In this chapter, a new flexural design method for columns is proposed considering additional varied axial force due to vertical excitation to ensure a total yield mechanism of the yield-beam type. It is difficult to define the vertical peak ground motion that a structure might experience, as well as to define the horizontal peak ground motion. Furthermore, the lateral and vertical seismic loads should be defined not individually but interrelatedly because the horizontal and vertical excitations are interrelated. The concept of proposed design method is not to define the vertical seismic load directly but to define the ratio of the vertical to horizontal seismic loads. Procedures for calculating a vertical seismic load in relation to this

concept are proposed as follows.

1. assume the horizontal response acceleration spectrum S_{ah}^{*} as lateral seismic load
2. assume the ratio spectrum of vertical response acceleration to horizontal, $R_{\frac{V}{H}}$
3. calculate the vertical response acceleration spectrum S_{av} as S_{ah}^{*} times $R_{\frac{V}{H}}$
4. calculate the vertical seismic load of single-degree-of-freedom system from S_{av}, and vertical seismic loads of each column according to its first mode shape of vertical vibration

3.1 Procedure I: the horizontal response acceleration spectra S_{ah}^{*}

The horizontal response acceleration spectra used in general seismic design in Japan are shown in Fig. 5. These spectra are based on the Rt (response characteristic factor function) curve of which the maximum response accelerations are 1.0 g, while the response accelerations in the shorter natural period region are reduced, as shown in Equation (1).

$$S_{ah}^{*}(G)=\begin{cases}0.4+1.2\dfrac{T}{Tc} & (T < Tc/2)\\ 1.0 & (Tc/2 \le T < Tc)\\ 1-0.2\left(\dfrac{T}{Tc}-1\right)^{2} & (Tc \le T < 2Tc)\\ \dfrac{1.6Tc}{T} & (2Tc \le T)\end{cases} \qquad (1)$$

In this Equation, T represents the natural period of the structure and Tc represents the upper bound of the natural period to have a constant response acceleration of 1.0 g.

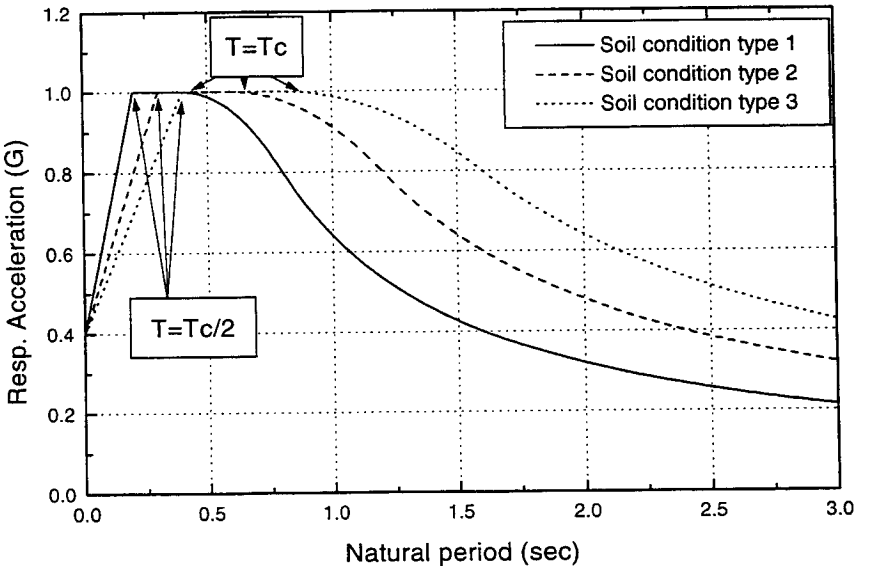

Fig. 5. Horizontal response acceleration spectrum for seismic design

3.2 Procedure II: ratio spectrum of vertical response acceleration to horizontal $R_{\frac{V}{H}}$

The horizontal and vertical natural periods of a structure are generally quite different. This difference must be considered to predict the ratio of the vertical response acceleration of the structure to the horizontal. The ratio of the horizontal natural period (referred to as T_H subsequently) to the vertical (referred to as T_V subsequently) is formulated as Equation (4) with six assumptions as follows.

Assumptions

(1) There is no interrelation between the horizontal and vertical stiffness of a structure to each other.

(2) The slab of each floor is rigid.

(3) The dimensions of the columns and the span length of a structure are the same throughout the whole structure.

(4) An inflection point of a column places at the center of height.

(5) No axial and shear deformation occur in a column.

(6) The section of a column is rectangular.

The equations of motion in the horizontal and vertical directions without damping are formulated as Equation (2).

$$\begin{aligned}\left(-\omega_H{}^2[M]+[K_H]\right)\{u_H\}&=0\\ \left(-\omega_V{}^2[M]+[K_V]\right)\{u_V\}&=0\end{aligned} \qquad (2)$$

The horizontal and vertical natural frequencies (referred to as ω_H and ω_V subsequently) then lead to Equation (3) from Equation (2) and the six assumptions mentioned above.

$$\begin{aligned}&\left(-\omega_V{}^2[M]+[K_V]\right)\{u\}=0\\ &\therefore \omega_V=\sqrt{a}\,\omega_H\end{aligned} \qquad (3)$$

"a" in Equation (3) represents the ratio of vertical stiffness matrix to horizontal so that $[K_V]=a[K_H]$.

The ratio T_H /T_V (referred to as the ratio of period subsequently) then can be obtained as Equation (4) from Equation (3).

$$\frac{T_H}{T_V}=\sqrt{\frac{K_V}{K_H}}=\sqrt{\frac{\frac{EA}{H}}{\frac{12EI}{H^3}}}=\sqrt{\frac{AH^2}{12I}}=\sqrt{\frac{bDH^2}{12\frac{bD^3}{12}}}=\frac{H}{D} \qquad (4)$$

H, D, b, E, I, and A represent the story height, column depth, column width, Young's modulus, moment of inertia, and cross sectional area of the column in Eq. (4), respectively.

Twelve sets of ground motion records are used to define the ratio spectrum of the vertical response acceleration to the horizontal $R_{\frac{V}{H}}$. The records were obtained from the Chiba experimental station of the Institute of Industrial Science, University of Tokyo, during the 1987 Chiba-Ken-Toho-Oki earthquake, the Taft records,, the El Centro records, the Hachinohe records, 7 sets of records obtained from 7 JMA stations during the 1995 Hyogo-Ken-Nanbu earthquake (referred to as Kobe 1~7 subsequently) and records obtained from Kobe Port Island (an artificial island) during the same earthquake (referred to as KPI subsequently). These sets of records have two horizontal components and one vertical component. One horizontal component having a peak acceleration larger than the other is chosen to define $R_{\frac{V}{H}}$. The soil condition type 1 (hard soil) is used to define $R_{\frac{V}{H}}$ in this paper, and the horizontal components of each record set are normalized so that these peak response velocities correspond to that of S_{ah}^{*}. The vertical components are then normalized so that the ratio of the peak ground acceleration of the vertical to the horizontal component is the same as that of the original record sets. The ratio spectrum of the vertical response acceleration to S_{ah}^{*}, $R_{\frac{V}{H}}$, considering the ratio of the period (Eq. (4)) is shown in Fig. 6. Five percent damping factor and H/D=6.0 are assumed. The ratio spectra of 12 record sets are roughly enveloped by the curve of Equation (5). This curve (referred to as the ratio spectrum model subsequently) means the ratio of the required vertical seismic capacity to the horizontal.

$$R_{\frac{V}{H}} = \begin{cases} 0.625T_h^2 + 0.4 & (0 \le T_h \le 2.0) \\ 3.0 & (2.0 \le T_h) \end{cases} \tag{5}$$

3.3 Procedure III: Vertical response acceleration spectrum S_{av}

The vertical response acceleration spectrum S_{av} for design is obtained as S_{ah}^{*} (Equation (1) times $R_{\frac{V}{H}}$ (Equation (5)). S_{av} is shown in Fig. 7, and the response acceleration spectra of the vertical components of 12 record sets, which are normalized as mentioned above, are also superimposed in Fig. 7 for comparison.

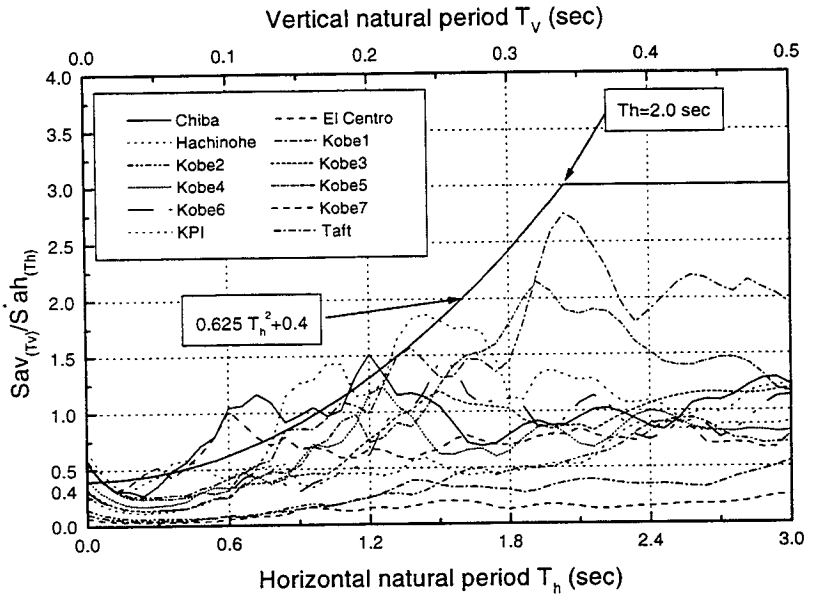

Fig. 6. Ratio spectrum of vertical response acceleration to horizontal $\frac{R_V}{H}$

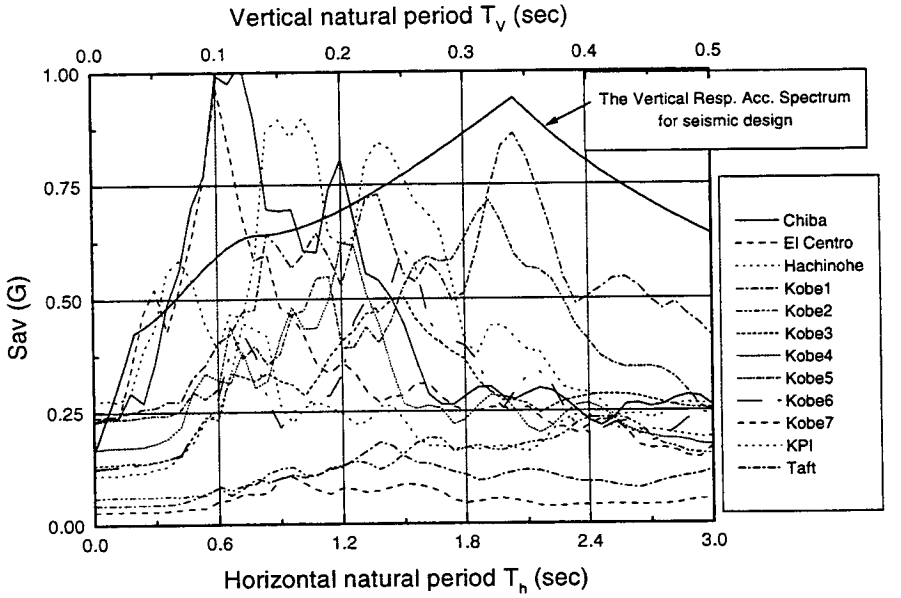

Fig. 7. Response vertical acceleration spectrum

3.4 Procedure IV: Vertical earthquake loads of each node

The vertical seismic loads of a SDF system can be obtained from the horizontal natural period of the structure and Figure 7. The vertical seismic loads of each column are calculated from Equation (6) according to its first mode shape of vertical vibration.

$$\{N_i\} = S_{av} \cdot {}_1\beta \cdot \{{}_1u_i\} \tag{6}$$

S_{av} represents the vertical seismic loads of SDF system, $\{N_i\}$ represents the nodal force vector of the vertical seismic loads, ${}_1\beta$ represents the modal participation function of the first mode,

and $\{_1u_i\}$ the modal vector of the first mode, respectively.

When columns under lateral seismic loads are subjected to high compressive axial forces, vertical excitation can generate additional compressive axial forces that can have an unfavorable effect upon the columns.

On the other hand, the low compressive or tensile forces acting on columns under lateral seismic load can also have an unfavorable influence on such columns. The negative effects of additional axial forces, compressive or tensile, due to vertical excitation must be considered in the seismic design of columns.

4. NONLINEAR ANALYSIS OF RE-DESIGNED PLANE FRAME WITH PROPOSED DESIGN METHOD

To estimate the validity of the proposed flexural design method for columns considering the effect of vertical excitation, a plane frame analyzed in section 2 is re-designed with the method and analyzed again under horizontal and vertical excitations. The input motions for analysis, parameters, modeling of the structure, and the damping coefficient value are the same as used in section 2. The locations of the yield hinges are shown in Figure 8. It is eliminated to develop yield hinges at the interior columns in the lower stories compared with Figure 4, and a total yield mechanism of the yield-beam type is formed as planned in case 2 (the ratio of peak vertical ground acceleration to horizontal is the same as the ratio that in the original records). The number of columns, which develop yield hinges, are successfully reduced in case 3 (the peak ground acceleration of the vertical component is the same value as that of the horizontal), though yield hinges are developed at the base of 5^{th} story exterior columns. As the result, it can be said that the proposed design method is valid for improving the seismic capacity under horizontal and vertical ground motions.

5. CONCLUDING REMARKS

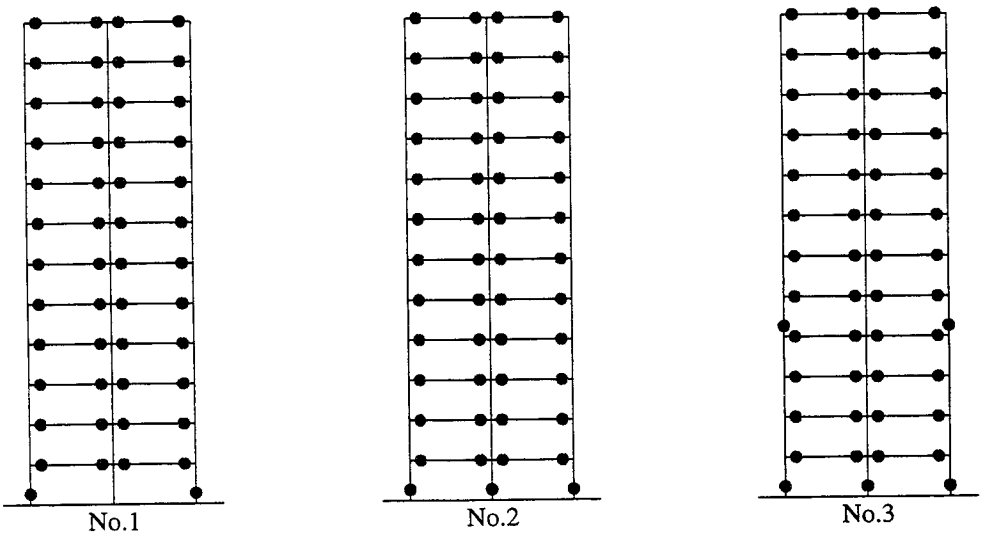

Fig. 8. Locations of yield hinges

Nonlinear dynamic analyses under horizontal and vertical excitations were carried out to investigate the effect of vertical excitation on the dynamic response characteristics of structures, and a flexural design method was proposed for columns considering the effect of vertical excitation. The results obtained from the investigations can be summarized as follows.

(1) Vertical excitation affected the vertical response displacements of the structure significantly, while it did not affect the horizontal response.

(2) Damage concentrated in interior columns which had varied axial force due to vertical excitation relatively larger than those of the exterior columns, because the varied axial force due to the overturning moment caused by horizontal vibration is negligibly small on interior columns, but the varied axial force due to vertical excitation in the interior columns is generally larger than that in the exterior column.

(3) A design spectrum of vertical excitation was proposed considering the ratio of the required vertical seismic capacity to horizontal.

(4) A new flexural design method was proposed for columns considering the effect of vertical excitation, and a structure re-designed according to the proposed method could perform as successfully as desired.

REFERENCES

AIJ / Architectural Institute of Japan. 1991. *Standard for structural calculation of reinforced concrete structures.*

AIJ. 1990. *Structural design guidelines for reinforced concrete buildings.*

AIJ.1986. Recommendation for detailing and placing of concrete reinforcement.

Kusunoki, Koichi. 1997. "The effect of vertical excitation on the dynamic response of structures." Doctoral thesis, University of Tokyo.

AIJ. 1993. *Recommendations for loads on buildings.*

Committee of Earthquake Observation and Research in the Kansai Area (Chairman: Prof. K. Toki)

Yoshimura, Koji, and Kenji Kikuchi. 1984. Effect of vertical component of ground motions on seismic elastic behavior of R/C frame-wall structures. *Transactions of the Architectural Institute of Japan* 344.

IMPROVEMENTS TO THE FEMA 273 LINEAR STATIC PROCEDURE

J. A. HEINTZ[1], C. D. POLAND[2], W. A. LOW[3]

ABSTRACT

The FEMA 273 Linear Static Procedure is appropriate for evaluation of simple, regular structures. Results of case studies, however, have shown that the procedure appears to be overly conservative, and predicts poor performance in buildings that would otherwise be expected to perform satisfactorily. This paper addresses potential sources of conservatism in the LSP including the calculation of building response based on an empirical formula for period, the use of 100% of total building weight without regard for higher mode mass participation effects, the calculation of pseudo lateral forces based on the initial elastic stiffness of the structure, and the acceptance criteria that are inconsistent with assumptions about degradation. The results reported on a database of recent projects show that conservatism in the LSP can be reduced with a few improvements to the procedure.

1. INTRODUCTION

The *NEHRP Guidelines for the Seismic Rehabilitation of Buildings,* FEMA 273, is a recently published comprehensive reference for performance-based engineering of the seismic rehabilitation of buildings. FEMA 273 outlines four analysis tools: the Linear Static Procedure (LSP), Nonlinear Static Procedure (NSP), Linear Dynamic Procedure (LDP), and Nonlinear Dynamic Procedure (NDP), each with different strengths and different limitations in applicability.

The purpose of this paper is to study the potential sources of conservatism in the LSP in an effort to improve correlation with expected results based on the historic performance of buildings and more advanced analysis techniques. Potential sources of conservatism addressed in this study include the calculation of building response based on an empirical formula for period, the use of 100% of total building weight without regard for higher mode mass participation effects, the calculation of pseudo-lateral forces based on the initial elastic stiffness of the structure, and the acceptance criteria that are inconsistent with assumptions about degradation. Data presented in this report are based on results from 25 of the most recent Degenkolb performance-based

[1] *Associate, Degenkolb Engineers, San Francisco, California, USA. Email:* jheintz@degenklb@degenkolb.com
[2] *President, Degenkolb Engineers, San Francisco, California, USA. Email:* cpoland@degenklb@degenkolb.com
[3] *Design Engineer, Degenkolb Engineers, San Francisco, California, USA. Email:* wlow@degenklb@degenkolb.com

engineering projects to date, and studies of similar issues published in the literature. The intent of this study is to identify trends observed in data available at this time and to suggest changes that would reduce the conservatism and improve the effectiveness of the LSP for use in situations when linear static procedures are appropriate.

2. FEMA 273 LINEAR STATIC PROCEDURE

Current code procedures rely on elastic analyses for design, with the understanding that in an actual earthquake, structures will be loaded beyond their elastic limits. The difference between actual demands and code design forces is rationalized on the basis of ductility, overstrength and energy dissipation. In FEMA 273, performance-based design is achieved through the explicit evaluation of these parameters on a component basis. In the nonlinear range of response, small changes in force demand correspond to large changes in displacement demand and correspondingly large differences in structural damage. For this reason, displacement-based design procedures are considered the best measures of performance, and the explicit calculation of displacement demands using nonlinear analysis techniques are considered the best tools for the performance-based design of structures.

Nonlinear analyses, however, can be difficult and time consuming to perform. For simple, regular buildings, this level of effort may not be practical, and it can be appropriate to use simplified yet conservative linear procedures to evaluate building performance. The LSP is one such displacement-based approach. Based on the theory of equal displacements, pseudo lateral forces calculated using the LSP are those forces that would push the elastic structure to approximately the same displacements as those expected in the actual inelastic response of the structure subjected to the design earthquake. This relationship is shown graphically in Figure 1. In the LSP, displacement-based concepts have been translated back to force-based calculations for reasons of simplicity and familiarity. This is accomplished with Equation (1), which consists of the building weight (W), the spectral acceleration (S_a), and a series of coefficients (C_1, C_2, C_3) that modify the calculated displacements to account for inelastic activity, pinched hysteric behavior, and P-delta effects respectively. The coefficients C_1, C_2, and C_3 vary with period so the resulting lateral force will vary with period even if the building response is on the plateau of the spectrum.

$$V = C_1 C_2 C_3 S_a W \quad (1)$$

A logical consequence of simplification is conservatism. In compensation for less precise information, a procedure can be made more conservative. The key to producing reasonable results with a simplified procedure, however, is installing an appropriate level of conservatism. Since the publication of FEMA 273 in 1997, the LSP has been implemented in practice, and has been the subject of verification case studies. In many cases, results using the procedure appear to be overly conservative, and predict poor performance in buildings that would otherwise be expected to perform satisfactorily based on historic earthquake performance.

3. EMPIRICAL FORMULAS FOR PERIOD

FEMA 273 offers three methods for the calculation of building period. Method 1, calculation of period using eigenvalue analysis of the structure, is the most accurate and preferred method. Method 2 uses a formula based on code empirical equations for period. Method 3 is a special case for single-story, flexible diaphragm systems.

When using force-based, elastic methods of analysis, a conservative estimate of base shear is obtained by using periods that are shorter than actual periods. Code empirical equations were developed with the intent of underestimating the actual period by 10-20% (Goel and Chopra 1997). Using data recorded from instrumented buildings during the 1989 Loma Prieta, and the 1994 Northridge, California, earthquakes, it was shown that empirical equations underestimate measured periods for frame structures on the order of 20-40% (Goel and Chopra 1997), and had very poor correlation with measured periods for shear wall buildings (Goel and Chopra 1998). These results are supported by results on recent Degenkolb projects shown in Table 1. Using data from more recent earthquakes to supplement the data used in the ATC3-06 project, empirical equations can be improved to better correlate with measured building response (Goel and Chopra 1997, 1998). Equations (2), (3), and (4) are best the fit equations proposed by Goel and Chopra for steel frame, concrete frame and concrete shear wall buildings respectively, where H is the building height in feet and $\overline{A_e}$ is a ratio based on the shear wall area defined in the paper.

$$T = 0.035\ H^{0.80} \quad (2)$$

$$T = 0.018\ H^{0.90} \quad (3)$$

$$T = 0.023\ H / (\overline{A_e})^{0.50} \quad (4)$$

Analytically, the best estimate of period comes from an eigenvalue analysis. Empirical equations that more closely approximate eigenvalue periods could help reduce the conservatism in the LSP, even when the building response period is on the plateau of the spectrum. Figure 2 compares empirical equations with eigenvalue periods when the proposed formulas were tested on recent Degenkolb projects. The results were somewhat scattered, showing poor correlation between periods for concrete buildings, and pier spandrel buildings in particular. For steel moment-frame buildings, the proposed formulas generally showed improved correlation with eigenvalue periods. Formulas were not available for braced frame systems. Figure 3 compares base shears calculated using different periods, normalized to the base shear resulting from the eigenvalue period. While the results are also scattered, this figure demonstrates that a significant reduction could be achieved if empirical equations could be better correlated with eigenvalue periods. The data suggest that this reduction is on the order of 30% on average across building types, and improved correlation of empirical equations is suggested for future research.

4. HIGHER MODE MASS PARTICIPATION EFFECTS

The LSP, like code-based equivalent lateral force procedures, calculates base shear using 100% of the total building weight. This is contrary to the general results of the dynamic analyses of multidegree-of-freedom (MDOF) systems in which the effective weight can be less than the total weight due to higher mode mass participation effects. In the acceleration-controlled region of the spectrum, base shears determined by response spectrum analyses are less than static base shears based on the total building weight because the effective weight is always less than 100% (Chopra and Cruz 1986). In the velocity- and displacement-controlled regions, higher mode effects can be significant enough that the response may be increased (Chopra and Cruz 1986). These results are dependent upon period as well as the distribution of mass and stiffness within the building, and any potential reductions resulting from these higher mode effects have been explicitly ignored in the development of the LSP (BSSC 1997b).

Dynamic analyses on recent Degenkolb projects show that response spectrum base shears are always less than static base shears using 100% of total building weight. The data suggest that the effect increases with increasing number of stories, and is closely related to the first mode effective mass. Figure 4 shows the ratio of LDP to LSP base shears as compared to the first mode effective mass. Because the periods for most buildings in this study are on the spectral plateau this result was expected, however, it was also true for taller steel moment-frame buildings with periods significantly beyond the plateau.

An adjustment for mass participation effects could be incorporated into the LSP by considering only the effective weight of the building in calculating base shear. This could be done with a matrix of factors, such as that shown in Table 2, developed based on the data in Table 1. The data suggest that mass participation effects could be used to reduce the conservatism in the procedure up to 30%, depending on the building type and number of stories, as indicated in Table 2.

5. INITIAL VERSUS EFFECTIVE STIFFNESS

The pseudo lateral forces of the LSP are those forces that would push the elastic structure to approximately the same displacements as those expected in the actual inelastic response of the structure. The resulting forces are therefore dependent upon an appropriate representation of the elastic stiffness of the structure. One example is the line with slope K_i in Figure 1. In nonlinear analyses, target displacements are calculated using an effective stiffness shown as the line with slope K_e in Figure 1. However, even in elastic analyses, some level of nonlinearity has been traditionally considered in the calculation of the elastic stiffness when the overall response is better characterized by some effective stiffness. In the case of concrete, the use of cracked section properties is common practice.

Analogous to using cracked section properties for concrete elements, it was thought that if the effective response of a structure is more appropriately represented by an effective stiffness K_e, then the use of K_i as a basis for pseudo lateral forces may be a source of over-conservatism in the LSP. This hypothesis is not supported by data from recent nonlinear analysis projects. The ratio

of K_e/K_i is dependent upon the shape of the pushover curve and is shown in Table 1. For most buildings in this study, the ratio of K_e/K_i was nearly equal to 1.0, indicating little or no difference between effective and initial stiffness. Since period, and therefore spectral acceleration, varies with the inverse square root of stiffness, small changes in stiffness would result in even smaller changes in calculated pseudo lateral forces and no significant impact on conservatism in the LSP. As a result, no improvements related to effective stiffness are proposed at this time.

6. ACCEPTANCE CRITERIA AND DEGRADATION

The Collapse Prevention Performance Level is defined as substantial damage, including significant degradation, on the verge of partial or total collapse (BSSC 1997a). The Life Safety Performance Level is defined as significant but repairable damage, with some margin against collapse remaining (BSSC 1997a). In determining demands, the C_2 coefficient is used to account for increased displacements resulting from poor cyclic behavior or pinched hysteresis loops. Pinching of hysteresis loops is a manifestation of structural damage. A smaller degree of nonlinear response results in a smaller degree of pinching (BSSC 1997b). Thus demands multiplied by the C_2 factor are amplified under the presumption that the primary elements of the structure will experience degradation.

FEMA 273 acceptance criteria are set based on generalized component behavior curves corresponding to ductile, limited ductile or nonductile behavior. These curves, reproduced from FEMA 273, are shown in Figure 5. They are characterized by an elastic range, followed by a plastic range (with or without strain hardening), and finally a strength-degraded range. For ductile behavior the strength-degraded range includes significant residual strength. Nonductile behavior has no plastic range and little residual strength.

Using the curves in Figure 5, the acceptance criteria for primary elements is set at point 2 for the Collapse Prevention Performance Level, and 75% of point 2 for the Life Safety Performance Level. As defined, the acceptance criteria limit the acceptable response of each component to the elastic or plastic regions of the idealized backbone curves. The primary lateral force-resisting elements are not permitted to experience demands in the strength-degraded range. A building will fail the acceptance criteria as soon as the worst case primary element begins to

degrade, which means that the overall structure is never permitted to experience degradation. This is not consistent with demands calculated presuming the presence of degradation, and not consistent with the descriptions of damage used to distinguish between performance levels.

To establish an appropriate level of conservatism, this "double counting" should be eliminated. If demands are to be calculated presuming the components will degrade, the acceptance criteria should be consistently set permitting some level of degradation. The validity of this approach can be seen when considering the global behavior of a structure. Consider a four-story concrete shear wall structure with the pushover curve depicted in Figure 6. The curve was developed using components modeled with the full degrading backbone curves. The individual components were allowed to exceed collapse prevention acceptance criteria and slip into the degraded range of response. As can be seen by the curve, even as individual elements degrade, the overall structure maintains a stable level of resistance. The performance limit of the building is not reached until a significant number of components have had a chance to degrade.

The acceptance criteria, as currently defined, are not pushing buildings to the limits of performance. Limiting the response of individual components within elastic or plastic behavior results in a much more conservative result when the components are combined in the overall structural system. To reduce the level of conservatism in the LSP, the acceptance criteria shown in Figure 5 should be adjusted so that life safety occurs at the limit of plastic response, point 2, and collapse prevention occurs at the limit of residual strength, point 3 on the behavior curves. This will allow components to respond at extreme limits of performance to better calibrate the resulting global behavior, and will result in potential reductions in conservatism of up to 33%, depending on component *m* factors.

7. CONCLUSIONS

The results of case studies have shown that the LSP appears to be overly conservative and predicts poor performance in buildings that would otherwise be expected to behave satisfactorily. The potential conservatism in the LSP can be reduced in three ways. Empirical equations for period can be improved to better correlate with actual periods, reducing pseudo lateral forces by an average of 30%, even when the response is on the spectral plateau. A matrix of effective

weight factors can be developed to take into account higher mode mass participation effects to reduce pseudo lateral forces up to 30%, depending on building type. The component acceptance criteria can be adjusted to permit degradation of the individual components reducing conservatism by up to 33%, depending on component *m* factors. Results show that the presence of some component degradation can still result in acceptable overall building performance.

8. REFERENCES

BSSC (1997a). *NEHRP guidelines for the seismic rehabilitation of buildings, FEMA 273.* Washington, D.C. Developed by ATC for FEMA.

BSSC (1997b). *NEHRP commentary on the guidelines for the seismic rehabilitation of buildings, FEMA 274.* Washington, D.C. Developed by ATC for FEMA.

Chopra, A. K., and E. F. Cruz. 1986. Evaluation of building code formulas for earthquake forces. *Journal of Structural Engineering* 112(8): 1881–99. ASCE.

Cruz, E. F., and A. K Chopra. 1990. Improved code-type earthquake analysis procedure for buildings. *Journal of Structural Engineering* 116(3): 679–99. ASCE.

Goel, R. K. and A. K Chopra. 1997. Period formulas for moment-resisting frame buildings. *Journal of Structural Engineering*. 123(11): 1454–61. ASCE.

Goel, R. K., and A. K. Chopra. 1998. Period formulas for concrete shear wall buildings. *Journal of Structural Engineering* 124(4): 426–33. ASCE.

9. KEYWORDS

FEMA 273, LSP, Linear Static Procedure, empirical, period, mass participation, effective stiffness, acceptance criteria, degradation.

Table 1: Building Data

Building		LSP			LSP			LSP			LDP			NSP	
		Method 1 Period (Eigenvalue)			Method 2 Period (Empirical)			Best Fit Period (Empirical)							
System	Stories n	Period T_1 (sec)	Base Shear V_1 (k)	Roof Displ d_1 (in)	Period T_2 (sec)	Base Shear V_2 (k)	Roof Disp d_2 (in)	Period T_{BF} (sec)	Base Shear V_{BF} (k)	Roof Disp d_{BF} (in)	Base Shear V_{LDP} (k)	Roof Disp d_{LDP} (in)	Effect Mass 1st Mode	Stiffness ratio Ke/Ki	Target Disp d_T (in)
1. CMRF	3	0.78	9325	18.93	0.74	9439	19.16	1.08	8533	17.32	8949	18.17	96%	1.00	24.33
2. CMRF	6	0.97	5652	7.60	0.65	8443	11.35	0.72	7615	10.23	5006	6.73	87%	1.00	6.33
3. CSW	4	0.44	26447	4.56	0.42	26447	4.56	0.68	23040	3.97	19900	3.52	80%	1.00	3.50
4. CSW	4	0.55	21424	6.70	0.38	27260	8.52	0.25	28190	8.81	n/a	5.13	77%	0.86	6.38
5. CSW	6	0.40	20455	3.56	0.50	19214	3.34	0.43	20361	3.54	14578	2.54	68%	0.99	3.85
6. CSW	6	0.45	19900	4.44	0.50	19214	4.29	0.49	19371	4.32	13363	2.98	64%	0.91	3.89
7. Conc P/S	1	0.48	1743	5.06	0.25	1743	5.06	0.37	1845	5.36	1699	4.93	95%	1.00	4.89
8. Conc P/S	3	0.27	3195	1.37	0.38	2413	1.04	0.07	4300	1.84	1983	0.85	67%	1.00	1.31
9. Conc P/S	4	0.32	59652	3.35	0.47	59652	3.35	0.16	59652	3.35	35826	1.94	84%	0.43	6.11
10. Conc P/S	4	0.40	25600	5.44	0.45	24000	5.10	0.13	40900	8.69	19210	4.08	71%	0.78	7.00
11. Conc P/S	5	0.23	86306	2.86	0.39	75659	2.51	0.15	78226	2.60	80630	2.67	66%	0.87	2.67
12. Conc P/S	5	0.39	81559	7.56	0.39	81550	7.56	0.19	93106	8.63	n/a	8.58	83%	0.85	4.99
13. Conc P/S	5	0.37	21700	3.59	0.39	20945	3.46	0.43	20523	3.39	16580	2.74	75%	1.00	2.90
14. Conc P/S	10	0.80	12225	15.85	0.79	12332	15.99	1.47	2750	3.57	8449	10.95	66%	1.00	13.77
15. Conc P/S	10	0.79	12753	15.14	0.79	12547	14.90	1.47	2777	3.30	10613	12.60	73%	1.00	13.19
16. SMRF	2	0.47	692	3.27	0.43	718	3.40	0.50	671	3.17	645	3.05	93%	1.00	2.63
17. SMRF	4	1.82	340	19.17	0.66	936	52.77	0.81	768	43.29	316	17.81	90%	1.00	15.29
18. SMRF	4	1.42	430	15.13	0.64	963	33.88	0.78	789	27.76	392	13.79	87%	1.00	12.30
19. SMRF	4	1.55	400	17.38	0.66	936	40.67	0.81	768	33.37	356	15.47	84%	1.00	13.38
20. SMRF	4	1.24	499	14.22	0.64	963	27.44	0.78	789	22.48	422	12.02	80%	1.00	10.78
21. SMRF	6	2.42	2861	26.07	0.96	7201	65.61	1.19	5810	52.94	2522	22.98	83%	1.00	20.34
22. SMRF	6	1.12	6656	13.05	0.96	7770	15.24	1.19	6311	12.37	5245	10.28	71%	1.00	9.58
23. CBF	2	0.31	5898	1.79	0.28	6379	1.94	n/a	n/a	n/a	4933.00	1.78	84%	1.00	1.90
24. CBF	4	0.84	37290	14.55	0.47	40246	15.70	n/a	n/a	n/a	n/a	n/a	51%	1.00	27.00
25. EBF	8	1.49	2146	11.58	1.07	2993	16.15	n/a	n/a	n/a	1836	9.91	74%	1.00	8.13

Table 2: Proposed Factors for Effective Weight

Stories	CMRF	CSW	Conc P/S	SMRF	CBF	EBF
1-2	1.00	1.00	1.00	1.00	1.00	1.00
3-4	1.00	0.80	0.80	0.90	0.90	n/a
5-7	0.90	0.70	0.80	0.90	n/a	n/a
8-10	n/a	n/a	0.80	n/a	n/a	0.90

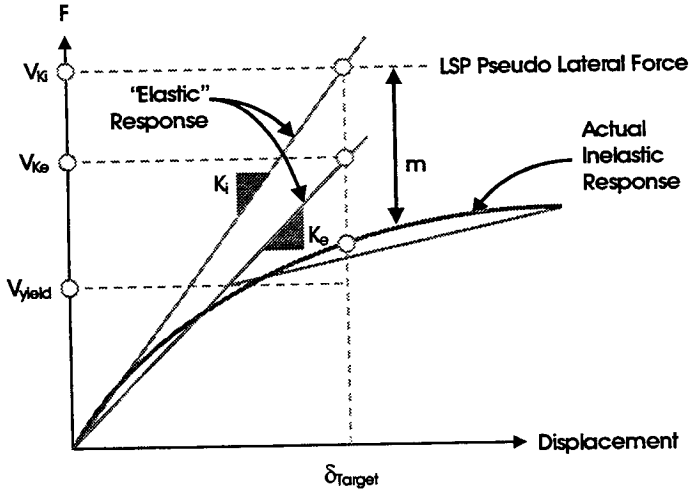

Figure 1:
Graphical Representation of the LSP

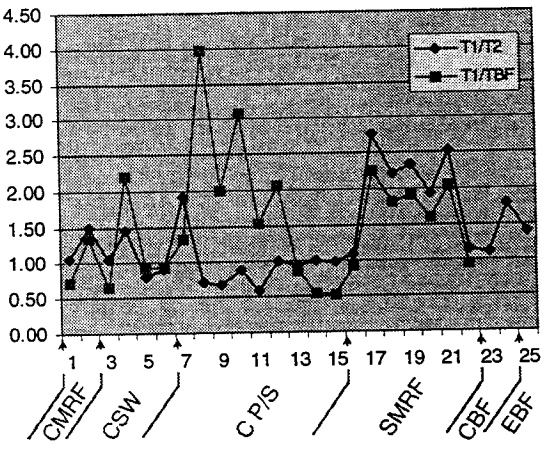

Figure 2: Comparison Between Empirical and Eigenvalue Periods

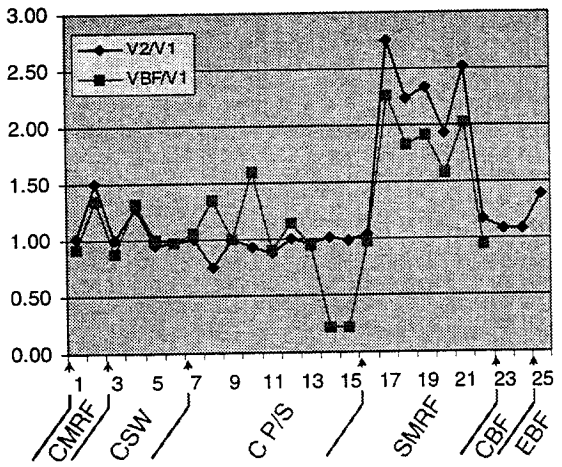

Figure 3: Base Shear Comparison

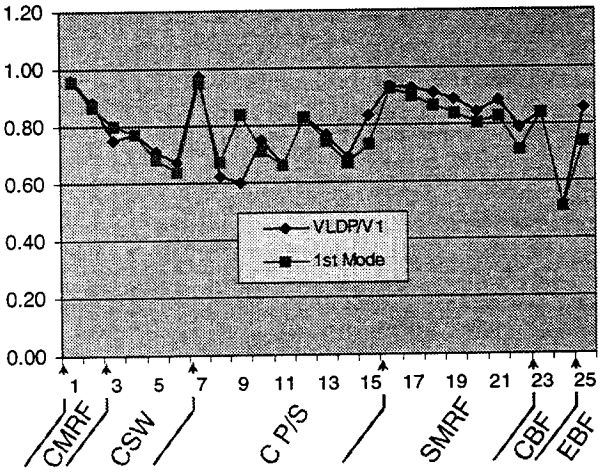

Figure 4: Ratio of LDP to LSP Base Shear and Comparison to First Mode Effective Mass

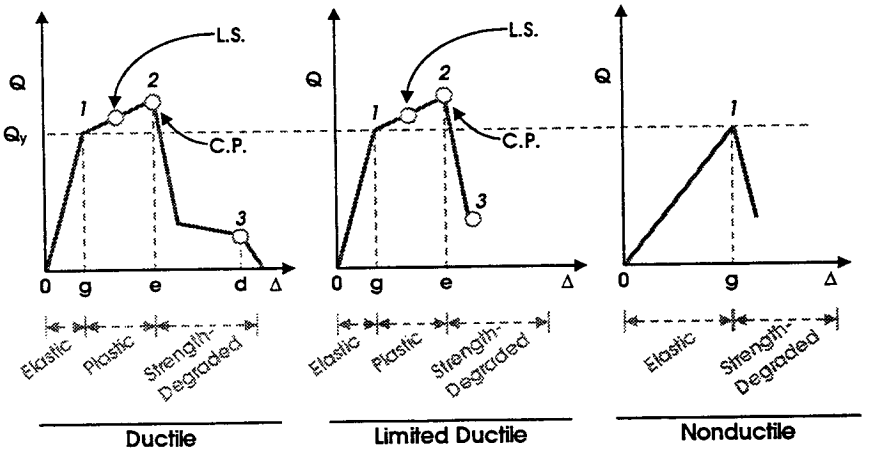

Figure 5:
General Component Behavior Curves

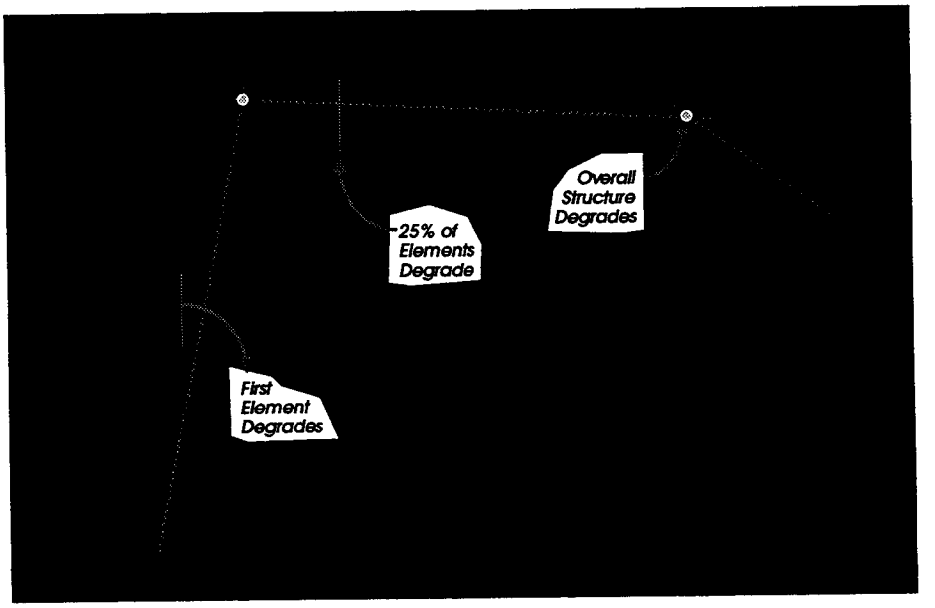

Figure 6: Pushover Curve, Four-Story Shear Wall (Building 9)

SESSION 7: DESIGN PHILOSOPHY

Chaired by

♦ Daisuke Kato and James Jirsa ♦

DAMAGE-CONTROLLED STRUCTURES IN JAPAN

Akira WADA[1] and Yi-Hua HUANG[2]

ABSTRACT

Since the concept of "damage-controlled structures" was proposed in Japan 1992, it has been widely applied to the design and construction of new building projects. The development of various new materials, especially high-strength steels and high-damping material, has greatly contributed to the realization of damage-controlled structures. The philosophy behind the damage-controlled structure views the global structure as two independent parts: the first being the elastic primary structure that is designed to support the vertical service load, the second being the damping system designed to resist the lateral earthquake load. The damage caused by the earthquake is artificially controlled by the damping system. The elastic primary structure can remain elastic even during an extreme event. This paper reviews the concept and philosophy of the damage-controlled structure, which was proposed before the 1994 Northridge, California, and 1995 Hyogoken-Nanbu, Japan, earthquakes. Some results are presented for static cyclic loading tests of a modeled damage-controlled steel frame with hysteretic dampers (unbonded brace). A number of actual example building projects are presented that were designed based on the concept of a damage-controlled structure and that exemplify the current seismic design trend in Japan.

1. INTRODUCTION

The concept of a "damage tolerant" structure was proposed in Japan about ten years ago (Wada et al. 1992). Damage tolerant means that the acceptable damage due to an earthquake occurs in specific structural components such as braces, shear walls, or supplemental dampers. These damaged components are called the "sacrifice members" and function somewhat like a fuse to protect the primary structure from severe damage. Since the Northridge and the Hyogoken-Nanbu earthquakes, this kind of structure has received increasing attention by researchers and structural engineers in both the U.S. and Japan.

Since these earthquake-resistant buildings installed with a damping system have also widely increased in both countries as evidenced by the literature (Soong, et al. 1994, 1997; Constantinou et al. 1998; Housner et al. 1997; Whittaker, etc. 1997); (Wada et al. 1992, 1995, 1997). On the cover of the *Engineering News-Record* (ENR 1997), the word "sacrifice" was used in the short explanatory notes that appeared together with a conceptual picture of a damped structure. These notes explained that the energy absorption that occurred from the axial yielding of the damping brace became the sacrifice through which highrise building structures were saved even during a large earthquake. For framed steel structures without braces, the sacrifice becomes the flange welded part of the beam ends. Little energy

[1] *Professor, Structural Engineering Research Center, Tokyo Institute of Technology, Japan, Email: wada@serc.titech.ac.jp*

absorption can be expected from the plastic deformation of the beam ends during an earthquake, as was clearly demonstrated during the Northridge and the Hyogoken-Nanbu earthquakes, because the plastic deformation of the beam ends is equivalent to the method of mounting elasto-plastic dampers in series in a part of an elastic frame, leading to large deformation of the whole frame after it becomes plastic.

This paper reviews the concept of the damage-controlled structure, which was proposed before the Northridge and Hyogoken-Nanbu earthquakes. Test results are presented for a series of dynamic loadings of a modeled damage-controlled steel frame with hysteretic dampers. A number of actual example projects are reviewed that exemplify the current seismic design trend in Japan.

2. PHILOSOPHY OF DAMAGE-CONTROLLED STRUCTURES

Japanese seismic design standards define two levels of earthquake ground motions and allowable damage for each. For level 1, medium and small earthquake ground motions, only minor damage such as cracks in walls and beams are allowed, while human life and the building structure are secured. For level 2, the largest earthquake ground motions, a building structure is allowed to be damaged as far as human life is guaranteed. Current seismic design and research in Japan are based on this consensus. However, since the buildings have recently increased in scale and value, due to the need to accommodate expensive computer and communication equipment, the traditional design consensus should be reviewed. The lessons learned from the Northridge and Hyogoken-Nanbu earthquakes was that damage to the primary structure could cause both great loss of human life and economic activities. It is obvious that overly large plastic deformation of a building should not be allowed for large earthquakes, yet construction activities requiring the production of cement and steel raise new concerns about environmental problems, such as depleting rain forests and increasing CO_2. These problems can be largely addressed by lengthening a building's life span, but to be meaningful such solutions must also provide that large buildings remain functional after an extreme event.

The deformation of a frame consisting of a beam and column with a brace placed at 45 degrees is considered (see Figure 1). Compared with the shear deformation Δ occurring in the frame, the expansion and contraction of the brace becomes $\Delta/\sqrt{2}$. Because the brace length is $\sqrt{2}$ times the column length L, the axial strain in the brace becomes 1/2 of the shear deformation angle of the frame. Taking into account that the joints at the brace ends are of high rigidity and strength and are thus not

[2] *Assistant professor, Structural Engineering Research Center, Tokyo Institute of Technology, Japan, Email: yihua@yhb.att.ne.jp*

made plastic, the findings are as follows. After converting the yield strain of the steel member to be a little higher than 0.1%, it is found that the story deformation angle is as small as 1/500 when the brace yields.

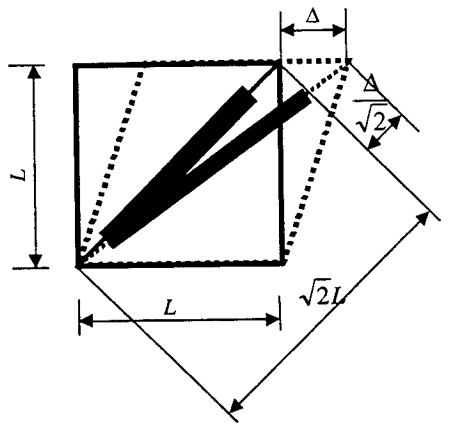

Fig. 1. Axial deformations of brace and shear deformation of frame

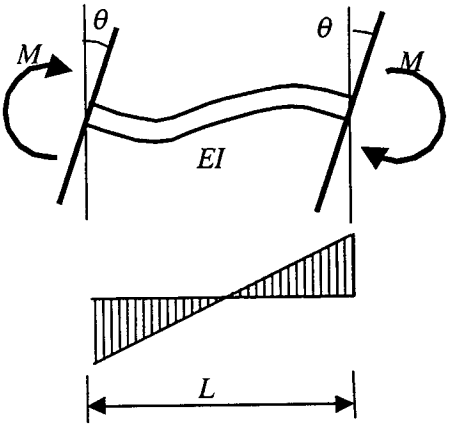

Fig. 2. Deformation angle at beam ends of a rigid frame

For a steel plate shear wall, since the yield shear stress is $1/\sqrt{3}$ times the yield normal stress and the shear elastic modulus is 1/2.6 times Young's modulus, the shear yield strain is then about 1.5 (= 2.6/1.732) times the axial yield strain. Therefore the story deformation angle becomes about 1/667 when the steel plate shear wall begins to yield, and it is made plastic at almost the same level as the small story deformation angle for the brace. It is possible to make the story deformation angle at the beginning of plastic deformation smaller for the brace and steel plate wall by using ultra-low yield steel to locally concentrate the plastic-deforming part.

The yield deformation angle of a rigid joint frame comprising columns and beams that receive an asymmetric bending moment is considered (Figure 2). For the steel structure frame, discussion is focused on the rotational distortion occurring at the beam ends because the bending deflection in the beam comprises nearly half of the structure deformation. Let the span and the depth of the beam be L and D, respectively. Then, the deformation angle for the stress of the flange at the beam ends to reach the yield point σ_y becomes $(\sigma_y/3E)(L/D)$. The span L of the frame is predetermined and Young's modulus E is a constant. Therefore, it is found that the deformation at the yield point of the frame can be increased by using steel having a high yield point σ_y and members having a smaller depth D than conventional ones. In other words, the elastic deformation capacity of a frame can be increased using a slender flexible frame manufactured by high-strength steels. In conclusion, the yield deformation of the

moment-resistant frame can be easily determined by selecting the materials and the cross sections of the structural members; whereas the yield deformations of the damping components such as braces and shear walls are determined from the overall configuration and the material selection. Thus, yield deformation cannot be changed by adjusting the plate thickness and the local configuration. When the damping materials are combined with the moment-resisting frame, neglecting problems such as brace buckling, shear failure of shear wall, etc., the following difficulties occur. Deformation where strength takes effect comes earlier than that in a moment resisting frame, so strength deterioration occurs thereafter. Therefore, it is difficult to rationally add both of the resistant strengths. In recent years, the development of new materials, such as high-performance steels and high damping materials, made the concept of a damage-controlled structure easily put into practice.

The technology of damage-controlled structures is theoretically based on the performance-based design (Connor et al. 1992, 1996). This concept suggests that a rational design can be achieved if each design parameter individually corresponds to each design requirement. The design strategy of damage-controlled structures is composed of two independent requirements. One is to design the primary structure resisting only the vertical service load; the other is to design the damping system resisting the lateral earthquake load.

3. EXPERIMENTAL STUDY OF DAMAGE-CONTROLLED STRUCTURES

In damage-controlled structures, much of the input energy of the earthquake is absorbed and thus controlled by specific members. In order to verify experimentally the difference between conventional steel frame and damage-controlled steel frames, a series of static cyclic loading and dynamic loading tests were carried out (Wada et al. 1996; Iwata 1995; Onishi et al. 1997). Experimental studies confirmed that in energy-dissipation capacity a damage-controlled structure is much better than a conventional steel structure. Based on the weight calculation of the specimens shown in Table 1, the damage-controlled structure (MRF2) can be made lighter than the conventional steel frame (MRF1) to achieve the same strength.

As an example of the experimental study of a damage-controlled structure, Figures 3(a) and (b) illustrate two types of tested steel frame. Specimen MRF1 is designed as a conventional steel frame without a damper, and MRF2 is designed based on the concept of a damage-controlled structure with a hysteretic damper (unbonded brace). Two different strength steels HT590 (high-strength steels) and SM490A (mild strength steel) were used for the different test specimens. The sectional size and the

weight ratio of the two specimens are shown in Table 1. For comparison, two test specimens were designed with the same ultimate strength. Owing to the contribution of the damper to the frame stiffness, the sectional size of specimen MRF2 can be made smaller than that of MRF1 so that the weight of MRF2 is less than that of MRF1. The weight w_2 does not include the weight of the brace.

Table 1. Sectional size and weight ratio of the tested specimens

Steel	Frame type	Beam(length=200cm)	Column(length=245cm)	Weight(kN)	W_1/W_2
SM490A	MRF1	H-380×200×9×12	H-320×300×19×22	W_1=4694	1.52
	MRF2+brace	H-300×170×9×12	H-260×260×12×16	W_2=3097	
HT590	MRF1	H-380×160×6×9	H-320×300×19×22	W_1=4234	1.58
	MRF2+brace	H-300×130×6×9	H-260×260×12×16	W_2=2685	

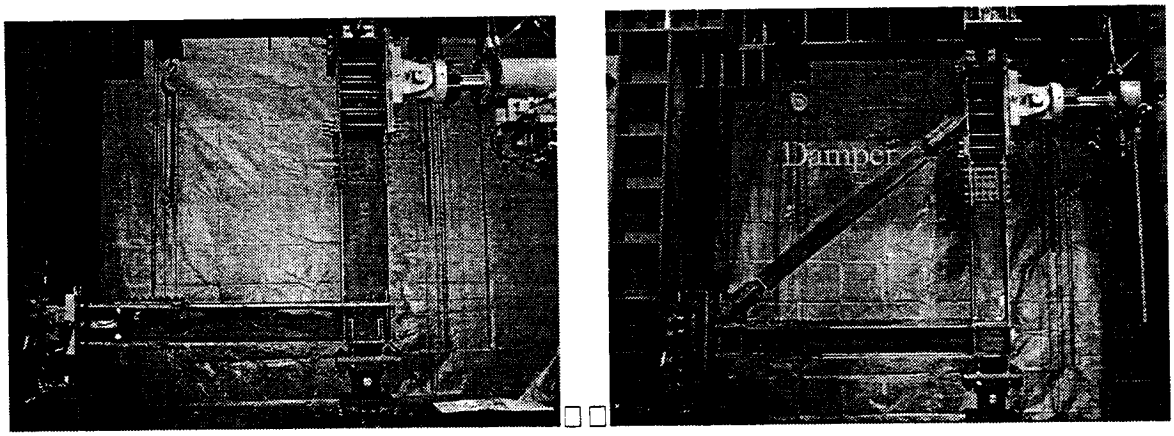

(a) MRF1 (Moment-resistant frame) (b) Slender MRF2 with unbonded brace

Fig. 3. Two types of test specimens

During the cyclic static loading program, after the first 2 cycles under 5 mm amplitude, 5 cycles for each amplitude were applied until the amplitude reaches 40 mm, that is equal to an interstory angle of 1/50. After that, cyclic static loading was continuously applied until the ultimate load decreased to 90% of the maximum load.

Figures 4(a) and (b) and 5(a) and (b) show the relations between load and deformation of the specimens made of medium-strength steel SM490 and high-strength steels HT590 under a static cyclic loading test. Figures (a) and (b) of Figures 4 and 5 show the results of specimens MRF1 without a damper and those of MRF2 with a hysteretic damper (unbonded brace). Compared to the plastic extent of MRF1, MRF2 (seen in the central loops of Figures 4(b) and 5(b)) remained almost elastic even when the displacement reached 40 mm, equal to 1/50 of the interstory deformation angle. On the contrary, it is obvious that the energy-dissipation capacity of MRF2 with a damper is much larger than that of

MRF1. In fact, the displacement response of the MRF2 frame will be much smaller than that of the MRF1 frame because the damping system in MRF2 will dissipate much more energy than that of MRF1. It can be concluded that the seismic performance of MRF2 is much better than that of MRF1.

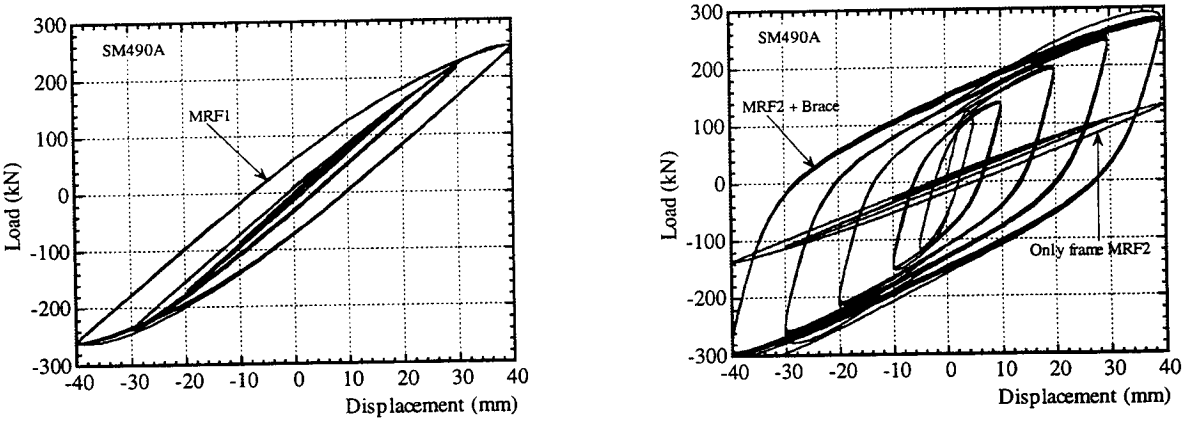

(a) MRF1 specimen (b) MRF2 specimen

Fig. 4 Relation between load and deformation (SM490)

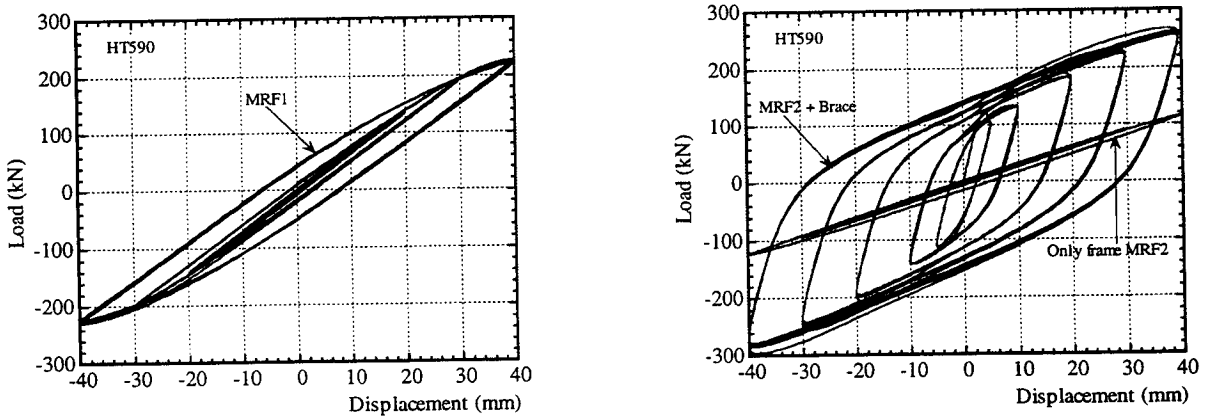

(a) MRF1 specimen (b) MRF2 specimen

Fig. 5. Relation between load and deformation (HT590)

4. TYPICAL PROJECTS OF DAMAGE-CONTROLLED STRUCTURES

Since the Hyogoken-Nanbu earthquake, many building projects that were designed based on the concept of damage-controlled structures have been examined by the Japan Building Center. Some have already been constructed. Table 2 lists some typical projects.

Table 2. Tall steel buildings designed based on the same concept of DCS in recent years

Year	Project name	Location	Usage	Height (m)	Structure type	Dampers	Ductility ratio
995.6	International Congress	Osaka	Congress	104	S_F	HD_B	0.95
1995.7	Todai Hospital	Tokyo	Hospital	82	S_F	VD_S	0.93
1995.7	Tohokudai Hospital	Sendai	Hospital	80	S_F	VD_S	0.97
1995.8	Central Government	Tokyo	Office	100	S_F	HD_B + VD_S	0.78
1995.10	Harumi 1 Chome	Tokyo	Office, Shop	175	S_F	HD_B	0.88
1996.2	Toranomon 2 Chome	Tokyo	Office, Shop	94	S_F	VD_S	0.94
1996.3	Passage Garden	Tokyo	Office	61	S_F	HD_B	0.88
1996.4	Shiba 3 Chome	Tokyo	Office	152	S_F	HD_B	0.97
1996.6	Art Hotel	Sapporo	Hotel	96	S_F	HD_BD	0.85
1996.8	Kanto Post Office	Saitama	Office	130	S_F	VD_S	0.87
1996.10	Nakano Urban	Tokyo	Office, Shop	96	S_F	VD_S	0.68
1997.7	DoCoMo Tokyo	Tokyo	Communication ,etc.	240	S_F	VD_S	0.79
1997.10	Minato Future	Yokohama	Hotel, Shop, Office	99	S_F	HD_BD	0.98
1997.11	Nishiguchi Shintoshin	Yamagata	Office, Hotel, etc.	110	S_F	HD_B	1.00
1998.2	DoCoMo Nagano	Nagano	Communication	75	S_F	VD_S	0.89
1998.4	East Osaka City	East Osaka	Office	120	S_F	HD_S	1.00
1998.5	Kouraku Mori	Tokyo	Office, Shop	82	S_F	HD_B	1.00
1998.7	Harumi 1 Chome	Tokyo	Office, Shop, etc.	88	RC_F	HD_B	1.00
1998.11	Adago 2 Chome	Tokyo	Office, Shop	187	S_F	VD_B	0.71
1998.11	Gunyama Station	Fukushima	Shop, School, etc.	128	S_F	HD_B + VD_S	0.98

In Table 2 HD_B stands for brace-type hysteretic dampers. The following introduces a few of typical examples of these projects.

4.1 Central Government Building

The Central Government Building (Figure 6) located in Chiyoda-ku, Tokyo, is a typical damage-controlled structure combining hysteretic and viscous fluid dampers. This building was designed by the Architecture Department of the Ministry of Construction and Kume Sekkei Co., Ltd. The total height is 144.5 m, including a 55 m antenna tower on the roof. The superstructure above the ground level is a moment-resistant steel frame installed with various damper systems, while the underground structure is

a steel reinforced concrete frame with reinforced concrete shear walls. The columns and beams of the primary structure used SN490B steel (maximum strength is 490MPa). This critical building is the headquarters of the Government Police Board. The primary structure is designed to behave elastically even under a large intensity earthquake whose maximum velocity is 50 cm/s. Most of the earthquake energy is designed to be absorbed by the damping system. The hysteretic dampers (HDs) are steel walls made of extra-low yield point steel (yield point is 100 MPa). The yield shear force level of the hysteretic damper system at the first floor location is assumed to be 5% of the total building weight. The distribution of yield shear force throughout the height of the building is assumed to be proportional to the distribution of the yield shear force of the primary structure. On the other hand, the viscous dampers consist of two movable steel plates and three fixed steel plates. The space between the movable steel plates and the fixed steel plates is filled with viscous liquid like silicone oil.

4.2. Passage Garden Building in Shibuya, Tokyo

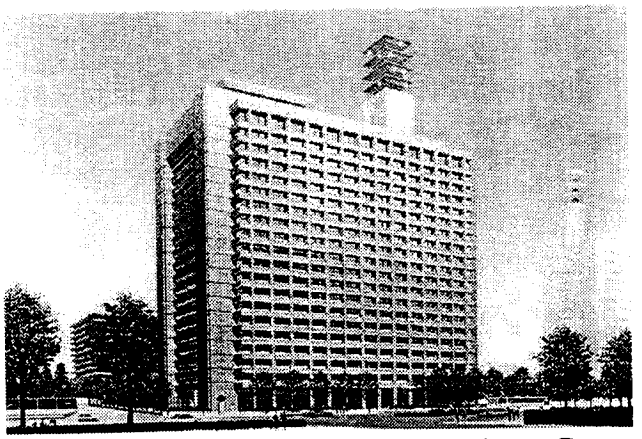

Fig. 6. Central government building (with HD+Viscous Damper)
(Courtesy of Kume Sekkei Co. Ltd.)

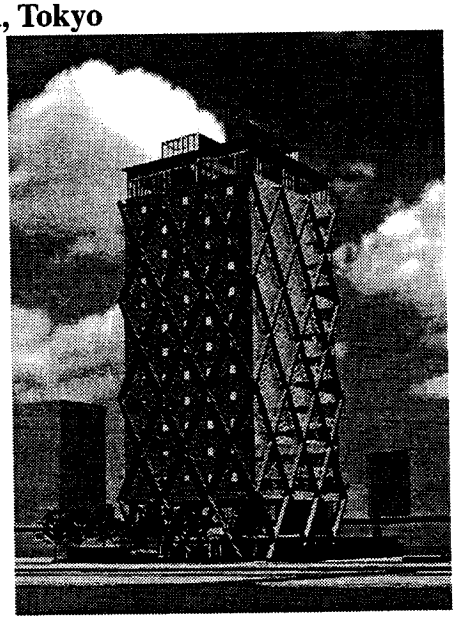

Fig. 7. Passage Garden in Shibuya (with HD)
(Courtesy of Nippon Steel Corporation)

The Passage Garden Building, located in Shibuya, Tokyo (Figure 7) was designed by Plantec Design Office (structural design was by Alpha Structural Design Office and Nippon Steel Corporation). The structural system of this office building has no vertical columns. The vertical and lateral loads are supported by the inclined column system. This building is 61.4 m high with 14 stories. The entire structural system is composed of two independent structural systems; an elastic column system and an unbonded member system. The unbonded member system has an equivalent damping coefficient of

about 8%. Since the entire structural system is divided into two independent systems, damage to the building in the case of an extremely large earthquake would be confined to the unbonded members that are designed to be easily replaceable.

4.3 Art Hotel in Sapporo

The Art Hotel in Sapporo (Figure 8), designed and constructed by Kumagai Corporation, is another damage-controlled building. This building is 96 m high and has 26 stories above the ground. The primary structure is a moment-resisting steel frame that is designed to support only the vertical service load. Two thousands slit steel dampers (SSD), whose shape is shown in Figure 9, made of medium-strength steel (SN490B) were installed in the building. When the SSD subjects the shear force through the top and bottom bolts, each slender bar experiences bending deformation and yields quickly, even under small shear deformation at the end parts of the bar, because the cross section of each bar is very small. However, since the yielding parts of this kind of damper are easily concentrated on the small end parts of the slender bars, the slits should be manufactured very carefully to avoid excessive local strain concentration.

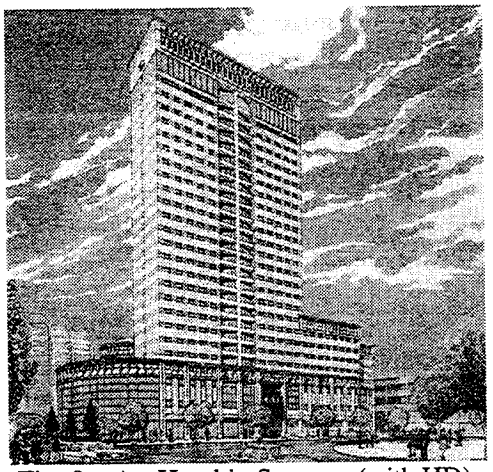

Fig. 8. Art Hotel in Sapporo (with HD)
(Courtesy of Kumagai Corporation)

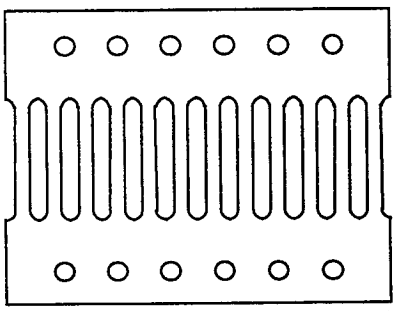

Fig. 9. Details of the Steel Slit Damper (SSD)

4.4 DoCoMo Tokyo Building

The building shown in Figure 10 is located in metropolitan Tokyo. The structural design was made by NTT Power and Building Facilities, Inc. This building has two parts. The lower part has 27 stories and is mainly used for the office; the upper part is the antenna that has 23 stories used for mobile communication. There are also three stories underground. The total height of the building is 240 m. The office building part is a steel frame structure with 76 viscous damping walls in both X and Y directions.

The supplemental viscous damping wall system has the same energy dissipation capacity of 5% equivalent viscous damping in both directions. The antenna is a steel frame structure with steel braces. The viscous damping wall is a kind of high quality highly stable damping system and has been used in more than 10 tall building projects since it was first used in a seismic-resistant building in 1988. Owing to the use of an additional viscous damping wall, the primary steel structure is designed within the elastic region even under the level II strong earthquake load (maximum velocity is 50 cm/s).

Fig. 10. DoCoMo Tokyo Building (with Viscous Dampers)
(Courtesy of NTT Power and Building Facilities Inc.)

5. CONCLUSIONS

In Japan, the current trend for seismically designed building structures is based on the concept of a damage-controlled structure instead of the conventional strong-column weak-beam system. The philosophy behind a damage-controlled structure views the global structure as divided into two independent parts: the elastic primary structure that is designed to support the vertical service load, and the damping system designed to resist the lateral earthquake load. The damage caused by the earthquake is artificially controlled by the damping system. The primary structure remains in the elastic region even during an extremely large earthquake. In this paper, the concept and philosophy of the damage-controlled structure were first reviewed. The results of some static cyclic loading tests of a modeled damage-controlled steel frame were presented, and a number of actual building projects were reviewed that were designed based on this concept.

6. REFERENCES

Kenneth L. Carper. 1998. Lessons learned from the 1994 Northridge earthquake: Performance of steel moment frames. *J. of Performance of Constructed Facilities* 12(4): 171. ASCE.

Connor J. J., Wada A., et al. 1992. Performance-based design methodology for structures. *International Workshop on Recent Development in Base-Isolation Techniques for Buildings, Tokyo*, 57–70.

Connor J. J., and B. S. A. Klink. 1996. *Introduction to motion based design.* Southampton, U.K.: Computational Mechanics Publications.

Constantinou M. C., T. T. Soong, and G. F. Dargush. 1998. *Passive energy dissipation systems for structural design and retrofit.* Monograph Series. [Buffalo, N.Y.]: Multidisciplinary Center for Earthquake Engineering Research, A National Center of Excellence in Advanced Technology Applications.

Engelhardt, M. D., and T. A. Sabol. 1995. Lessons learned from the Northridge earthquake: Steel moment frame performance. *Proceedings of Symposium on a New Direction in Seismic Design,* 1–14. Tokyo: AIJ.

ENR. 1997. Seismic survival. *The construction weekly Engineering News-Record.* July 21.

Housner G. W., L. A. Bergman, T. K. Caughey, A. G. Chassiakos, R. O. Claus, S. F. Masri, R. E. Skelton, T. T. Soong, B. F. Spencer, and J. T. P. Yao. 1997. Structural control: Past, present and future. *J. of Engineering Mechanics* 123(9): 897–971. ASCE.

Iwata M. 1995. Applications of various structural steels to seismic design, *Proceedings of Symposium on A New Direction in Seismic Design,*171–94. Tokyo: AIJ.

Krawinkler, H. 1994. Preliminary observations and thoughts on building damage in the January 17, 1994 Northridge earthquake. *Flash of the investigation on the disaster of Northridge earthquake in 1994,* 73–82. AIJ.

Mahin S. A., R. O. Hamburger, and J. O. Malley. 1998. National program to improve seismic performance of steel frame buildings. *J. of Performance of Constructed Facilities* 12(4): 172–79. ASCE.

Onishi, Y., K. Hayashi, Y. H. Huang, M., Iwata, A. Wada. 1997. Cyclic behaviors of welded beam-column connections used in the damage tolerant structures. *J. of Structure and Construction Engineering* 501: 143–50. AIJ.

Soong, T. T., and M. C. Constantinou. 1994. *Passive and active structural vibration control in civil engineering.* New York: Springer-Verlag, Inc.

Soong T. T., and G. F. Dargush.. 1997. *Passive energy dissipation systems in structural engineering.* Chichester, N.Y.: John Wiley & Sons.

Wada A., J. J. Connor, H. Kawai, M. Iwata, and A. Watanabe. 1992. Damage tolerant structures. *Fifth US-Japan Workshop on the Improvement of Building Structural Design and Construction Practices,* Sept. 8–9, 1992, *Mission Valley Hilton, San Diego, California,* 1–12. Redwood, City, Calif.: ATC.

Wada A., and Y. H. Huang. 1995. Preliminary seismic design of damage tolerant tall building structures. *Proceedings of Symposium on A New Direction in Seismic Design,* 77–93. Tokyo: AIJ.

Wada A., Y. H. Huang, Y. Onishi, and M. Iwata. 1996. *Cyclic behaviors of high-strength steels with welded connections used in the damage tolerant structures,* 385–90. Hong Kong.

Wada, A., M. Iwata, and Y. H. Huang. 1997. Seismic design trend of tall steel buildings after the Kobe earthquake. *International Post-SMiRT Conference Seminar on Seismic Isolation, Passive Energy Dissipation and Control of Vibrations of Structures, Taormina, Italy.* 251–69.

Whittaker, A., M. Constantinou, C. Kircher C. 1997. Development of analysis procedures and design guidelines for supplemental damping. *International Post-SMiRT Conference Seminar on Seismic Isolation, Passive Energy Dissipation and Control of Vibrations of Structures, Taormina, Italy,* 189–96.

ANALYTICAL NEEDS FOR PERFORMANCE-BASED DESIGN OF CONCRETE

William T. HOLMES[1]

ABSTRACT

Performance-based design has great promise to assist in earthquake risk mitigation. For many, performance-based design is primarily associated with changes in the building code, but it also offers many advantages to other aspects of earthquake engineering. Performance-based earthquake engineering has the potential to provide a common description of performance, and a common method of prediction and measurement of performance that could tie together several aspects of earthquake engineering that are now unrelated due to differing methodologies. To maximize usefulness, any prediction of performance must be able to quantify likely significant losses including casualties and economic losses from repair costs and loss of building use. However, current consensus would seem to indicate that we are now unable to predict damage to concrete buildings with sufficient specificity to allow translation of the analytical results into these measurable loss categories. The possibility of realizing the full potential of performance-based engineering is thus unclear.

INTRODUCTION

Performance-based earthquake engineering, for the purposes of this paper, encompasses the full range of engineering functions—design, evaluation, loss estimation, code-writing, post-earthquake reconnaissance and data gathering, and research—and is based on the principle that the performance of a given structure, for a given ground motion can be predicted with acceptable accuracy and known reliability. Performance-based earthquake engineering is intended to be more general than *performance-based codes*—which are only one product of performance-based earthquake engineering, or *performance-based design*—which only covers a narrow design function.

In the last ten years, particularly due to damage from the 1989 Loma Prieta, and Northridge, California, and 1995 Kobe, Japan, earthquakes, interest has grown worldwide in performance-based earthquake engineering techniques. Unfortunately, owing to a lack of uniform definitions and standards, the work in various countries is

[1] Structural Engineer, Vice President, Rutherford & Chekene, San Francisco, CA; wholmes@ruthchek.com

not coordinated and seldom transportable, despite bilateral workshops and other cooperative efforts (e.g., Fajfar 1997 and Shimazu 1999). Despite the great interest in performance-based earthquake engineering, the powerful and wide-ranging effects that such a system would have once fully developed is underappreciated

The most development has occurred in the area of performance-based codes, where a history of conceptual development exists by other disciplines. However, this work has never been considered in a systematic context within the rich and varied field of earthquake engineering. There is also a common misunderstanding that a performance-based code consists merely of the provisions of various performance standards that can be chosen by an owner, rather than of a systematic application of performance-based earthquake engineering at several different levels in code development and application.

PERFORMANCE-BASED BUILDING CODES

A common misconception is that performance-based earthquake engineering begins and ends with a performance-based building code. This focus has created a high level of interest and a large body of development work in this area. However, the proper integration of performance-based provisions into seismic codes is also commonly misunderstood as simply replacing the traditional prescriptive single-performance-level code with a code that offers multiple performance levels. Instead, code development within performance-based earthquake engineering should follow the procedures developed over many decades for more generic performance-based codes.

The conceptual development of performance-based codes began early in the twentieth century and has resulted in several generic performance-based codes including those in England, New Zealand, and Australia. These generic performance-based codes create a process that can be applied to any aspect of building design. To date, much of the use of these performance-based "shells" has been in the area of fire safety. Currently, a renewed interest in performance-based codes, including performance-based seismic codes, may extend this use to many other areas of building design. The process that has been developed includes methods for defining *Performance Objectives*, *Performance Requirements*, and *Acceptability Criteria.* The performance-based code design methodology will normally not replace the traditional

prescriptive methods but will parallel them as an acceptable alternative. Most buildings will continue to be designed using the simpler, prescriptive approaches.

Previous work in generic performance-based codes includes a description of the steps necessary for a fully functional code in a specific design area. These steps are shown in figure 1. The key characteristics to be noted are the flow from top to bottom and the need to develop overall verification criteria first, before prescriptive-type code provisions are developed—so that the prescriptive provisions can be validated by the verification criteria. Furthermore, the true performance-based verification criteria become available to form a clear and acceptable alternative to strict prescriptive code design procedures.

.

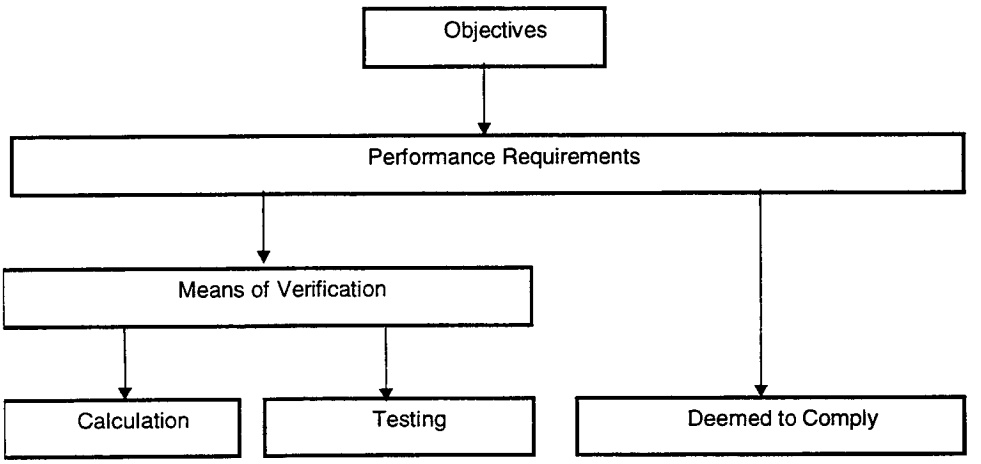

Figure 1. The Basic Performance-Based Code Process

Related specifically to earthquake engineering, the process shown in figure 1 can be made more specific, as shown in figure 2. Note that a credible verification procedure will enable the development of codes to suit a desirable performance level, and, more importantly, for the first time, will enable policymakers in each region or country to set appropriate goals for normal, special, and emergency buildings in their local code. Traditional, relatively prescriptive requirements can be developed for code use, and checked for appropriate performance using the verification procedure. For specific building types, completely prescriptive and relatively foolproof simplified provisions can be developed with confidence that they are equivalent to the primary code. Examples of such simplified and highly prescriptive codes that are not now checked for equivalency include the Conventional Construction provisions for small wood buildings in the U.S. and the stand-alone codes for certain simple building types used in China

(Ministry 1994). As shown in figure 2, the general verification procedure can be used directly for design purposes for special or unusual buildings that have unique seismic requirements.

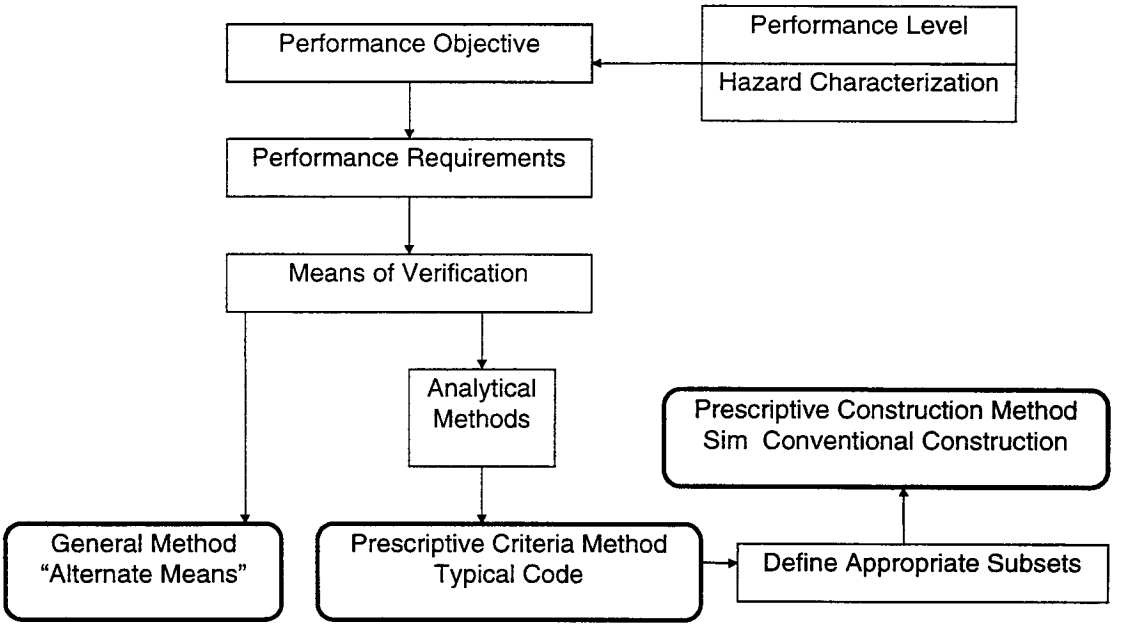

Figure 2. The Performance-Based Code Process Applied to Seismic Design (Hamburger, 1998)

OTHER APPLICATIONS OF PERFORMANCE-BASED EARTHQUAKE ENGINEERING

It is envisioned that performance-based earthquake engineering, using a common and interchangeable platform of performance descriptions and prediction, can be applied

- to improve evaluation and retrofit of existing buildings,
- to improve and refine regional loss estimation,
- to provide a rational method for economic analysis (PML),
- to improve the applicability of postearthquake reconnaissance, and
- to improve the efficiency of earthquake engineering research.

THE VERIFICATION PROCEDURE

Clearly, the missing link currently for development of performance-based codes is the lack of a reliable and acceptable "means of verification." For performance-based earthquake design purposes, this key element would consist of an analytical procedure, supplemented by testing as

necessary, that could reliably predict performance of a structure for various ground motions. In order to take full advantage of the potential, the verification procedure

- must predict performance for any ground motion, including those representing both statistically determined design criteria and individual events;
- must account for the duration of ground motion and the structural degradation; a damage index similar to Park and Ang (Park 1984) may be needed to yield sufficient information for loss determination;
- must be able to model ductile and brittle elements;
- must have outputs that include risk of casualties, damage translatable to repair costs, and damage translatable to building downtime;
- must include the reliability of explicitly stated outputs;
- must include formal or informal consensus for all procedures in order to gain acceptability for all of the uses described.

LIMITATIONS OF CURRENT ANALYSIS PROCEDURES FOR CONCRETE BUILDINGS

An excellent status report for current analytical capabilities for concrete buildings is found from the results of a 1997 workshop organized by the American Concrete Institute and funded by the National Science Foundation (NSF) (Jirsa 1997). The objective of the workshop was to assess the capabilities of analyzing the earthquake response of reinforced concrete structures through several detailed studies of a structure that was damaged by earthquake. The studies concentrated on the response of the Van Nuys Holiday Inn—an instrumented structure that was damaged in the 1971 San Fernando, California, earthquake and again in the 1994 Northridge event. The analysis was performed by a structural designer experienced in analysis techniques, and teams from Purdue University, the University of Texas at Austin, and the University of California, Berkeley.

After presentations of the results from the four analyses, the workshop broke into three groups. A summary of conclusions of the groups follows:

Group 1

- There is confidence in nonlinear analysis, although the results are extremely sensitive to choice of initial stiffness.
- Based on experimental data, it is difficult to assess the sensitivity of columns to shear failures.
- Three members of the group placed the performance of the structure at *collapse prevention* and two at a *life safety* level.
- It is difficult for current analysis procedures to predict failure and local damage, but a reasonable representation can be obtained of displacement and shear response for a structure

Group 2

- It was possible to analyze nonlinear response if reasonable assumptions were made with regard to initial stiffness and stiffness degradation.
- Slab-column framing poses special problems.
- Current analytical methods can adequately estimate maximum displacements and interstory drifts, but are most reliable for predicting collapse or near-collapse performance levels.
- The failure of reinforcement anchorage is difficult to predict.
- Pushover analysis can give a lower bound estimate of base shear capacity and can identify weak links, but there can be significant "misses" of behavior.

Group 3

- Nonlinear analysis is a valuable tool for understanding building behavior.
- Higher mode effects can be important to understand building flaws.
- Effective section properties and material properties should be modeled using all contributing areas.
- More information is needed on concrete acceptance criteria for various performance levels.
- The group was divided on whether the analyses of the Holiday Inn indicate a *collapse prevention* or a *life safety* performance state.
- There was no agreement on whether pushover or time history analysis offers a clear advantage over the other.

The results above indicate general agreement that analysis is best at predicting the extremes of nonlinear behavior—the elastic limit and the brink of collapse—as shown in figure 3.

However, for a specific instrumented building for which actual damage records had been had been extensively analyzed, there was little agreement as to the appropriate damage state (performance level) that should be assigned.

Although of interest in performance-based earthquake engineering, knowledge of the points of elastic limit and brink of collapse are far from adequate. As shown in figure 3, the important loss parameters of repair cost, casualty rate, and building downtime are of interest primarily between these limit states.

Skeletons of performance-based codes can be developed, and the advantages of a common platform for all of earthquake engineering can be detailed, but significant advancement in performance-based earthquake engineering cannot take place until far more sophisticated damage-prediction techniques are developed than are currently available.

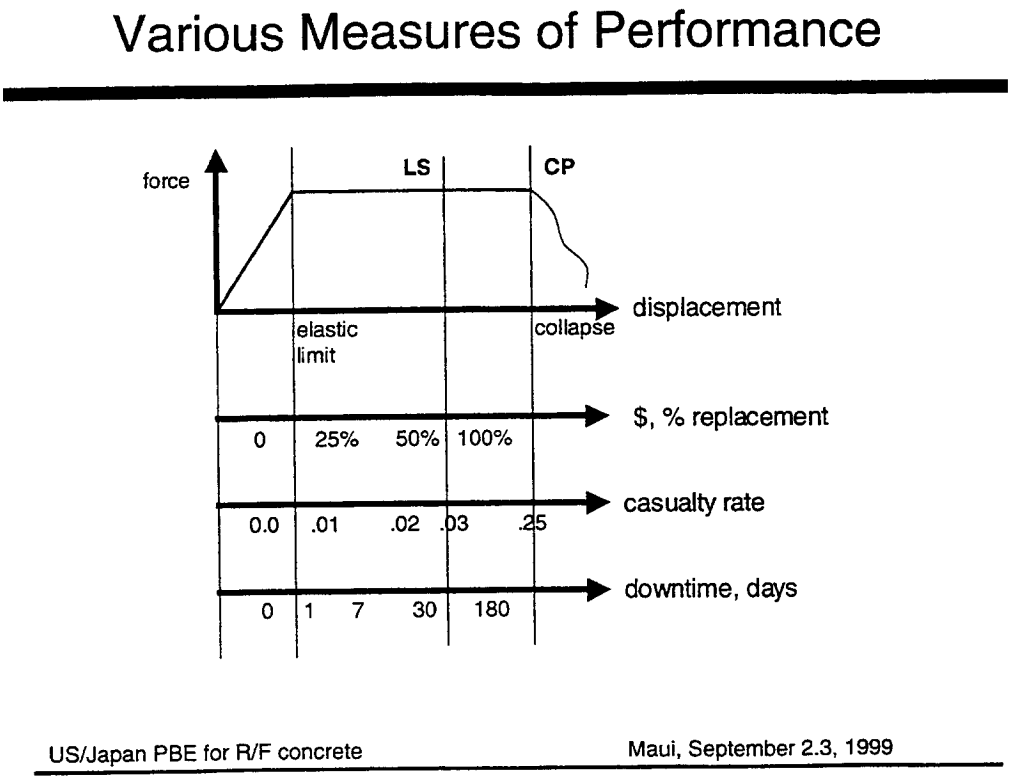

Figure 3. Various Measures of Performance

REFERENCES

Fajfar, P. and Krawinkler, H., eds. 1997. *Seismic design methodologies for the next generation of codes*. Rotterdam: A. A. Balkema.

Hamburger, R. O. and Holmes, W. T. 1998. *Vision statement: EERI/FEMA Performance-based Seismic Engineering Project*, Background Document for the EERI/FEMA Action Plan. Oakland, Calif.: Earthquake Engineering Research Institute.

Jirsa, James O. and Zia, Paul. 1997. Seismic analysis of instrumented reinforced concrete buildings. Draft Report on a Workshop supported by NSF Award 9525972, Salt Lake City, Utah, March 7 and 8, 1997.

Ministry of Construction of the P.R. China. (1994. *Code for seismic design of buildings*. GBJ 11-89. Beijing: New World Press..

Park, Y.J., and A. H. S. Ang. 1984. Mechanistic seismic damage model for reinforced concrete. *ASCE Journal* 113 (ST8). New York.

Shimazu, Takayuki, Yayong Wang, and M. J. Nigel Priestley. 1999. Overall program and its implementation among the three countries, Japan-U.S.-China International Joint Study on the Mitigation of Earthquake Hazards. *ASCE Structures Congress, April 19–21, 1999, New Orleans*, Louisiana. Washington, D.C.: ASCE.

KEYWORDS

Concrete structures, performance-based engineering, seismic codes, verification, and analysis.

SESSION 8: DESIGN OF ELEMENTS OR CODE REQUIREMENTS

Chaired by

♦ Tsuneo Okada and Helmut Krawinkler ♦

SATISFYING PERFORMANCE CRITERIA FOR RC FRAMES BASED ON ALLOWABLE DRIFT

JoAnn BROWNING[1]

ABSTRACT

A simple procedure is used to proportion earthquake-resistant reinforced concrete (RC) frames for two levels of performance objectives. The performance objective is based on a maximum allowable total building drift and the assumption that adequate detailing is provided to allow the building to deform to that drift without brittle failure of any element. Drift is limited using a maximum-period criterion and a simplified representation of the expected displacement demand spectrum. This paper evaluates the proportioning procedure using a set of five analytical reinforced concrete frames and a maximum allowable drift equal to 1.5% and 1.0% of the total building heights. The maximum responses of the frames were estimated using nonlinear dynamic analyses and a suite of ten scaled ground motions. The structural dimensions that are required to satisfy the maximum-period criterion influence the selection of an appropriate structural configuration for economic and architectural considerations. The results of the study showed that the period criterion was an effective tool to limit drift and to indicate the relative performance expected for a structure with adequate detailing.

1. INTRODUCTION

The focus of this paper is the application of a simple period criterion to provide different levels of expected structural performance during a design-level earthquake event. A simple method was developed to proportion earthquake-resistant reinforced concrete (RC) building frames that requires only the original structural configuration and a simplified displacement response spectrum for the level of expected demand (Browning, 1998). The method is attractive because it separates ideas of stiffness requirements for resisting lateral loads from strength requirements for resisting gravity loads. By selecting the appropriate structural dimensions to satisfy a period criterion, the maximum drift is limited and the amount of expected damage is reduced. The procedure is a simple way to limit drift so that more emphasis can be provided for proper detailing of all elements to reach the target deformations without brittle failure.

A previously-developed method (Browning, 1998) is used as a design tool to provide an expected level of performance for a given displacement demand. If the expected performance of a structure is defined in terms of allowable drift, then satisfying the performance criteria can be accomplished by providing appropriate stiffness in combination with proper detailing for a

[1] Department of Civil and Environmental Engineering, University of Kansas, U.S.A., jpbrown@ukans.edu

ductile response. This paper highlights some implications of using the proposed proportioning procedure to define a level of expected performance for reinforced concrete frames for a region of high seismicity. A series of analytical frames were proportioned using the proposed method for two levels of performance, both aimed at preventing structural damage but differing in the expected level of non-structural damage. Once proportioned, an estimate of the displacement response was calculated using a suite of scaled ground motions.

2. PROPORTIONING METHOD

A brief description of the proposed proportioning method is given to provide a basis for evaluating the relative performance of a series of analytical frames. A detailed description of the formulation and analytical evaluation of the method can be found in Browning (1998).

The basis for the proportioning method is derived from work completed by Shimazaki (1988) and Lepage (1997). Shimazaki showed that an upper-bound level of drift for a reinforced concrete system could be estimated using a smooth displacement response spectrum and a modified system period equal to the fundamental period of vibration of the system multiplied by $\sqrt{2}$. This method worked well for systems with initial periods exceeding the characteristic period of the ground motion (T_g, the period at the intersection of the nearly constant acceleration range of response and the nearly constant velocity range of response). Strength was found to be

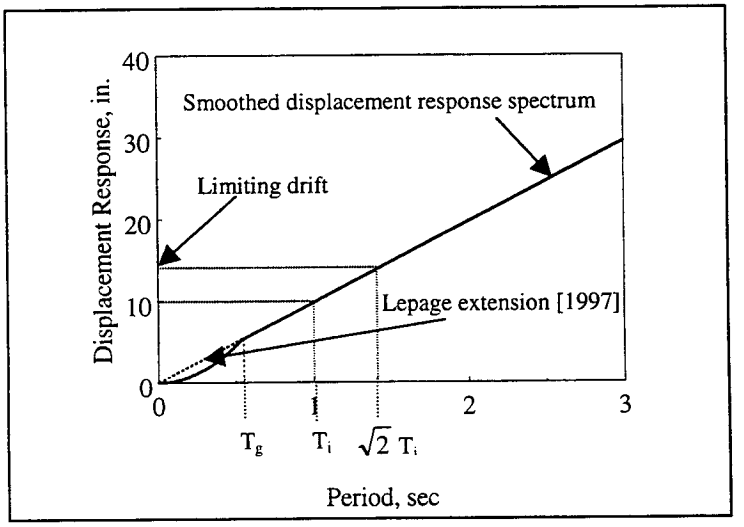

Fig. 1 Upper-Bound Estimate for Maximum Drift

an important parameter for estimating an upper-bound level of drift for the responses of systems with initial periods less than T_g. In later research, Lepage (1997) found that if a simplified displacement response spectrum was used, one that remained linear following the slope of the nearly constant velocity region of response through the nearly constant acceleration region of response to the origin (Fig. 1), then an upper bound for displacement response could be determined using the simple method provided by Shimazaki.

A method for proportioning reinforced concrete frame buildings was developed using the ideas presented by Shimazaki (1988) and Lepage (1997). The maximum expected drift of a reinforced concrete frame for a given event was limited by satisfying a maximum allowable period criterion (target-period criterion). Following the form of the simplified spectrum defined by Lepage, a reasonable estimate of displacement demand was selected as D = 10T for a region of high seismicity (Fig. 1), where D is the displacement demand in inches and T is the modified period of the system in seconds. Using this estimate for the displacement demand, the target-period criterion can be represented by Eq. 1:

$$T_i \leq \frac{R_L \cdot H}{10 \cdot \sqrt{2} \cdot F_p} \tag{1}$$

where R_L is the limiting maximum drift ratio (ratio of total drift to total building height), T_i is the initial period of the system (sec), H is the total height (in.), and F_p is the participation factor for the mode considered.

3. EXAMPLE FRAMES

The procedure described above can be used to proportion frames for a general performance objective that is defined by a maximum allowable drift. A series of five reinforced concrete frames were proportioned using two maximum drift criteria to illustrate possible design scenarios. Once the target drift criterion is satisfied, adequate reinforcement for shear and bond considerations must be provided so that the target drift can be obtained without brittle failure occurring in any element.

The selected frame configurations had three square bays with dimensions of 30 ft. and ranged from 5 to 13 stories in two-story increments. The story heights were regular with dimensions of

10 ft. The concrete was assumed to have a compressive strength (f'_c) of 4000 psi with an average modulus of elasticity of 4000 ksi. The reinforcing steel was assumed to have a yield stress of 60 ksi. The total girder depths were selected as one-twelfth the span length with average reinforcement ratios of 0.75%. Square column dimensions were selected to satisfy the target-period criterion using a loading considered effective on the building during response to strong ground motion of 200 psf.

To illustrate the effectiveness of the proposed method for a general performance criteria, a maximum allowable drift equal to 1.5% of the total building height was specified. A building with proper detailing at this level of response would represent a performance category without structural damage and with a limited amount of non-structural damage.

The column proportions were selected to satisfy the criterion defined by Eq. 1 with a maximum allowable mean-drift ratio of 1.5%. The resulting square column dimensions are shown in Table 1 and range from 30-in. square columns for a 5-story frame, to 36-in. square columns for a 13-story frame. The frame periods were found to be consistent with periods estimated for existing reinforced concrete building frames in a region of high seismicity (Goel and Chopra, 1997).

Table 1 Column Dimensions to Satisfy R_L = 1.5% Criterion

Number of Stories	Target Frame Period (sec)	Initial Frame Period (sec)	Square Column Dimension (in.)
5	0.51	0.52	30
7	0.71	0.73	30
9	0.92	0.95	30
11	1.12	1.13	32
13	1.32	1.28	36

It is of interest to estimate a level of response for the proportioned frames when subjected to the prescribed displacement demand, D = 10T in. To accomplish this task, a suite of ground motions was used to calculate the nonlinear dynamic responses of the proportioned frames. The ground motions were previously selected and scaled so that the calculated displacement response spectra would fill the displacement demand curve for a range of building periods up to 3.0 sec (Browning, 1998). The displacement response spectra for the scaled motions are shown in Fig. 2. It is noted that in the period range around 1.0 sec, the displacement demand exceeds the target

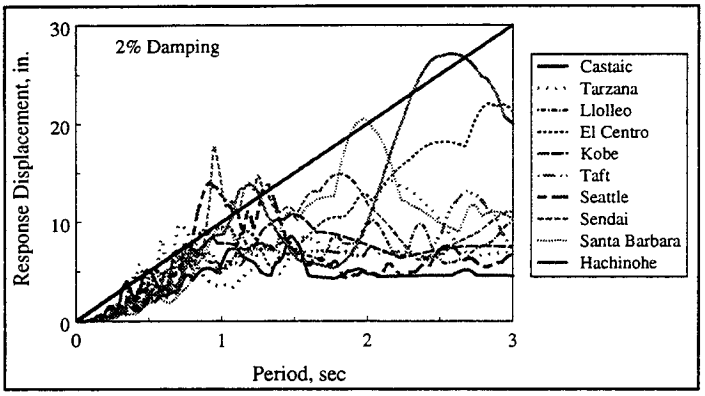

Fig. 2 Displacement Response Spectra for Scaled Ground Motions

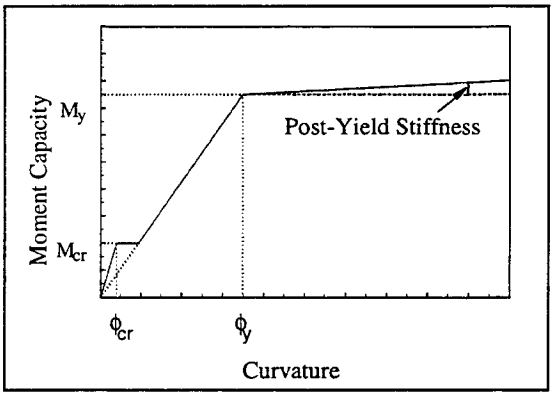

Fig. 3 Moment-Curvature Relationship for Analyses

demand curve. This was necessary to fill the range of building response periods (from 0 to 3 sec) with representative displacement demand.

A nonlinear dynamic analysis program developed by Otani (1974) and later modified by Saiidi (1979a, 1979b) and Lopez (1988) was used to calculate the responses of the frames to the scaled ground motions. Previous studies that used the program to calculate responses of experimental and existing reinforced concrete structures to strong ground motion have demonstrated good results (Saiidi, 1979b; Eberhard, 1989; Lopez, 1988; Lepage, 1997; Browning et al., 1997). Deformations for all members were defined for the program using the tri-linear moment-curvature relationship shown in Fig. 3 that includes points associated with cracking and yield, and has a 0.1% post-yield stiffness. Initial stiffnesses for all members were determined using gross sectional properties with girder stiffnesses calculated considering the stiffness contribution of the slab. The moment capacity at yield was equivalent to the nominal moment capacity calculated using a stress-strain relationship for the concrete defined by Hognestad (1951) with a maximum compressive strain of 0.004. Hysteresis in the elements was defined using the rules specified by Takeda (1970) with an unloading slope coefficient of 0.4. A reinforcement ratio of 1.0% was selected for all columns.

Additional deformations due to slip of the reinforcement and second-order effects (P-Δ) were included in the analysis routine (Saiidi, 1979a, 1979b). The slip rotation at yield of the reinforcement was estimated for developing the full yield stress in the steel with a uniform bond

stress of $6\sqrt{f'_c}$. A damping coefficient of 2.0% of critical damping was assumed in the analyses.

The results of the analyses are represented by the solid symbols and lines in Figures 4 and 5. The maximum mean-drift ratios calculated for all input ground motions, shown in Figure 4, were less than the target limit of 1.5%. The frames with 5 and 7 stories had maximum total drifts that were close to the limit, but the maximum drift decreased for the frames with increasing number of stories. This trend was the result of the periods of the systems exceeding the largest displacement demand region of response.

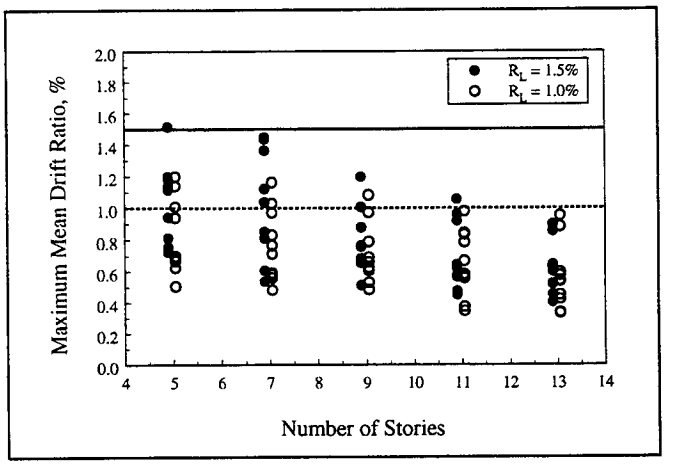

Fig. 4 Maximum Calculated Mean-Drift Ratios

Figure 5 shows the maximum story-drift ratios that were calculated for each story during the response to all ground motions. The solid vertical line in the figures represents the maximum calculated mean-drift ratio for all input ground motions. The performance of the frames satisfied the intended objective with maximum total drifts that were less than 1.5% of the total height of the structures and having maximum story-drifts that were approximately 2.0% of the total story heights. It is interesting to note that although the mean-drift ratio decreased with increasing number of stories, the maximum story-drift ratio reached 2.0% for every frame. The point to be made from this analysis is that the proportioned building frames had typical member dimensions and initial building periods and represented response characteristics that satisfied a general performance criterion of 1.5% maximum mean-drift ratio.

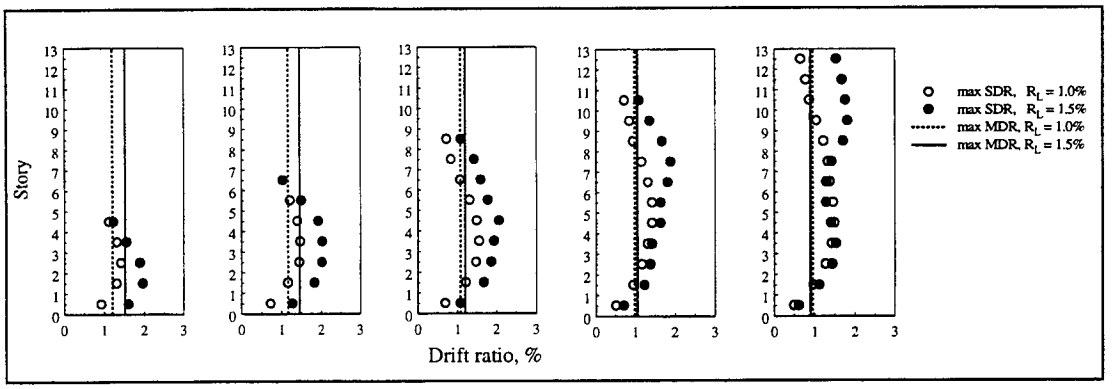

Fig. 5 Maximum Story-Drift Ratios (All Earthquakes) with Maximum Mean-Drift Ratio

4. ALTERNATIVE PERFORMANCE OBJECTIVES

A more stringent performance criterion was considered by limiting the maximum allowable drift to 1.0% of the total height of the structure. The new limitation would decrease the maximum distortion and the expected amount of damage. At this level of drift, the frames would likely have nonlinear response and proper detailing for a ductile response must be provided in order to protect the integrity of the structure.

The columns of the frames described in the previous section were re-proportioned according to the criteria defined by Eq. 1 with R_L=1.0%. The resulting target periods, initial periods, and square-column dimensions are listed in Table 2. It is interesting to note that the target periods calculated for this performance objective are identical to the target periods for a performance objective with a maximum mean-drift ratio of 1.5% and a displacement demand defined by D = 15T in. The resulting square column dimensions ranged from 56-in. for the 5-story frame to 70-in. for the 13-story frame. Clearly, the dimensions required to limit the maximum expected drift

Table 2 Column Dimensions to Satisfy R_L = 1.0% Criterion

Number of Stories	Target Frame Period (sec)	Girder Depth = Span / 12		Girder Depth = Span / 10	
		Initial Period (sec)	Column Width (in.)	Initial Period (sec)	Column Width (in.)
5	0.34	0.34	56	0.34	40
7	0.48	0.47	60	0.47	42
9	0.61	0.60	64	0.61	42
11	0.75	0.75	66	0.75	44
13	0.88	0.87	70	0.88	44

to 1.0% of the total height of the structure are not economically feasible. The resulting structural configuration is more like a building with slender walls than a frame.

One solution to satisfy the target-period criterion with reasonable column dimensions is to increase the total girder depths to one-tenth the span length. The required square-column dimensions to satisfy the target-period criterion were reduced dramatically (Table 2). These column dimensions, although larger than the original frames described in Table 1, represent a possible solution for the higher-performance criterion.

The nonlinear response of the frames with column dimensions listed in Table 2 and girder-depths of one-tenth the span length were calculated using the scaled ground motions to test the hypothesis that limiting the initial period of the frame will limit the drift in a predictable manner. The results of the analyses are shown in Figure 4 and Figure 5 as the hollow symbols and dotted lines. The responses of 46 out of the 50 analyses remained within the prescribed maximum mean-drift ratio limit of 1.0%. Because the initial periods of the frames were less than 1.0 sec, all of the frames experienced the high drift demands indicated in Figure 2 around the one-second period range. As a result, all of the frames had maximum mean-drift ratios that were close in value or exceeded the 1.0% limit. The four analyses with maximum mean-drift ratios that exceeded the 1.0% limit were calculated using the Kobe, Seattle, and Sendai records, all of which had calculated displacement response spectral values that exceeded the design spectrum in the short-period range.

Perhaps a better indication of the improved performance of the re-proportioned frames are the calculated story-drift ratios (Fig.5). The maximum story-drift ratios that were calculated for all frames subjected to the ten ground motions did not exceed 1.5%. The larger girder and column proportions promoted a decrease in the distortion in the bottom-half of the frames with 5 and 7 stories, whereas the top-half of the frames with more than 7 stories experienced less distortion than the original frames.

By using the target-period criterion to proportion frames for a maximum mean-drift ratio of 1.0%, it can be shown that alternative structural systems may prove to be a better economic and/or performance solution. A structural system that includes walls could satisfy the period

criterion without requiring excessive member proportions. Special control or damping devices also could be provided to limit drift. The advantage of using these special devices is that the period of the systems could remain outside the range of response where acceleration response and drift demands were critical for the motions considered in the analyses. For either alternative, the target-period criterion is a simple tool to determine the feasibility of limiting drift using traditional framing systems.

5. CONCLUSIONS

A simple target-period criterion was used to proportion earthquake-resistant reinforced concrete frames for various levels of intended performance based on drift limitations and proper detailing. For average performance levels, such as a maximum expected drift of 1.5% of the total height of the structure, the required column dimensions to satisfy the criterion are similar to the dimensions of existing reinforced concrete columns in regions of high seismicity. Larger member proportions were necessary to limit the maximum expected drift to 1.0% of the total building height. The calculated responses of the proportioned frames with increased girder and column proportions remained mostly within the prescribed limit. The target-period criterion was found to be a useful tool for assessing the feasibility of using traditional framing systems to limit drift.

6. REFERENCES

Browning, J. 1998. *Proportioning of earthquake-resistant reinforced concrete building structures.* Thesis submitted in partial fulfillment of the requirements for the degree of Ph.D. in Civil Engineering. West Lafayette, Ind.: Purdue University.

Browning, J., Y. R. Li, A. Lynn, and J. P. Moehle. 1997. Performance assessment for a reinforced concrete frame building. *Proceedings of the International Workshop on Seismic Design Methodologies for the Next Generation of Codes.* Bled, Slovenia, June 24–27, 265–76.

Eberhard, M. O. and M. A. Sozen. 1989. Experiments and analyses to study the seismic response of reinforced concrete frame-wall structures with yielding columns. Structural Research Series No. 548. Civil Engineering Studies. Urbana, Ill.: University of Illinois.

Goel, R. K., and A. K. Chopra. 1997. Period formulas for moment-resisting frame buildings. *Journal of Structural Engineering* 123(11): 1454–461. ASCE

Hognestad, E. 1951. a study of combined bending and axial load in reinforced concrete members. Bulletin Series No. 399. Urbana, Ill.: University of Illinois Engineering Experiment Station

Lepage, Andres. 1997. *A method for drift-control in earthquake-resistant design of reinforced concrete building structures.* Thesis submitted in partial fulfillment of the requirements for the degree of Ph.D. in Civil Engineering. Urbana, Ill.: University of Illinois at Urbana-Champaign.

Lopez, R. R. 1988. *Numerical model for nonlinear response of r/c frame-wall structures.* Ph.D. Thesis Submitted to the Graduate College. Urbana, Ill.: University of Illinois.

Otani, S. 1974. *SAKE: A computer program for inelastic response of R/C frames to earthquakes.* Structural Research Series No. 413. Civil Engineering Studies. Urbana, Ill.: University of Illinois.

Saiidi, M. and M. A. Sozen. 1979a. *Simple and complex models for nonlinear seismic response of reinforced concrete structures.* Structural Research Series No. 465. Civil Engineering Studies. Urbana, Ill.: University of Illinois.

Saiidi, M. and M. A. Sozen. 1979b. *User's manual for the LARZ family: Computer programs for nonlinear seismic analysis of reinforced concrete planar structures.* Structural Research Series No. 466. Civil Engineering Studies. Urbana, Ill.: University of Illinois.

Shimazaki, K. 1988. Strong Ground Motion Drift and Base Shear Strength Coefficient for R/C Structures. *Proceedings, Ninth World Conference on Earthquake Engineering.* Tokyo and Kyoto, Japan. Vol 5: 165–70.

Takeda, T. M., M. A. Sozen, and N. N. Nielsen. 1970. Reinforced concrete response to simulated earthquakes. *Journal of the Structural Division* 96 ST12: 2557–73. ASCE.

Keywords: performance, proportioning, reinforced concrete, building structures, frame structures, drift limits, dynamic analyses

STRENGTH AND DEFORMATION CAPACITY OF CANTILEVER STRUCTURAL WALLS WITH OPENINGS

Daisuke KATO[1], Hiroshi NODA[2], and Yoichi SUGISHITA[3]

ABSTRACT

The main objectives of this study were to examine the effects of wall openings on the strength and deformation capacities of cantilever shear walls. Six reinforced concrete cantilever shear wall specimens with openings, which were designed to fail in flexure, were tested under static reversal load. Variables in the six specimens were the peripheral ratios of the wall panel (0.3, 0.4 and 0.5), the locations of the openings, and the reinforcement of the side walls beside the opening. The test results indicated that if the shear force could be resisted by a side wall in compression only, the flexural strength and deformation capacity of the wall could be obtained just like a wall without an opening. However, if the shear force could be resisted by both side walls, the flexural strength and deformation capacity must be reduced by the effects of the opening.

1. INTRODUCTION

Shear walls with an opening in Japan have been designed according to the standard for structural calculation of reinforced concrete structures(Architectural Institute of Japan (AIJ), 1985) using the allowable stresses of materials. In this AIJ standard methods to calculate the reduction factors γ by openings for strength and elastic stiffness and the amount of the peripheral reinforcement according to the peripheral ratio of the opening are shown based on the elastic theory or a quite simplified equilibrium assumption, which means these methods cannot be applied to the design approach based on the ultimate strength concept. The reduction factor for shear strength γ is defined as follows;

$$\gamma = 1 - \max\left((ho\ lo/h\ l)^{0.5},\ lo/l\right) \qquad (1)$$

where, ho and lo are the height and width of the opening and h and l are the story height and span length.

In order to develop a design method for shear walls with openings based on the ultimate strength concept, tests of first story shear walls with an opening have been conducted (Kato 1988). These tests were mainly conducted in order to get the shear strength of walls with a variety of openings. Figure 1 shows the strut and tie models for structural walls with openings and shows the main findings from these tests. Figure 1(a) shows the original strut and tie model. The test results indicated that the diagonal strut of the concrete of side walls beside the opening could not be formed due to the lack of horizontal tie reaction to balance the strut force. And the model shown in Figure1(b) was found to be more practical to calculate the shear strength. In this case the

[1] *Department of Architecture, Faculty of Engineering, Niigata University, Niigata, Japan*
Email: dkato@eng.niigata-u.ac.jp
[2] *Tokyo Electronic Power Company, Japan*
[3] *Nishimatsu Construction Company, Japan*

reaction of the diagonal strut of the concrete can be balanced by longitudinal reinforcement of the beam. So the main conclusion of these tests was that in order to get the shear strength of the wall by summing the strength of both side walls, the shear resisting mechanism of each side wall should be modeled as shown in Figure1(b). The evaluation of the height for the equation of the shear strength of a side wall should be noted.

Using these findings a method of earthquake-resistant design of cantilever structural walls with openings was proposed(Kato 1995) based on the AIJ's ultimate strength concept (AIJ 1994). According to this method structural walls with openings could be designed as ductile walls failing in flexure. However the effects of wall openings on the flexural strength and deformation capacities of structural walls have not been studied widely enough to verify the design method. Especially lacking are tests of multistory walls failing in flexure. From this viewpoint tests of two-story structural walls with openings were conducted in order to examine the effects of openings on the strength and deformation capacities of cantilever structural walls with openings.

2. OUTLINE OF TESTS

2.1 Specimens

Six reinforced concrete cantilever structural wall specimens with openings were tested (Noda 1997 and Ootani 1998). Two specimens reported in 1997 are called the WNO-series, and others reported in 1998 are called WSO-series in this study. All specimens were two-story single-bay walls, but the top girders were intentionally made very stiff and strong in order to apply uniform loads to the wall panels as well as to simulate the confining effect of multistory shear walls. The sections and reinforcement of the wall panels, boundary columns, and beams are shown in Tables 1(a)(b)(c), respectively.

Figure 2 shows the variations of specimens. The main variables were the size of the openings and their locations. The size of the opening was expressed as the currently used reduction factor of γ, which varied from 0.5 to 0.7. Another important variable was the location of the opening. The central window opening type specimens, the central door opening type specimen and the eccentric door opening type specimen were tested. Only one specimen was tested as an eccentric door type specimen but its behavior was quite different between positive loading and negative loading due to the anti-symmetrical proportion. In this sense the behavior of this specimen is discussed separately according to the loading direction in this paper. That in the positive loading direction is called Specimen WSO4(P) and that in the negative is called Specimen WSO4(N). The diagonal lines in Figure 2 represent diagonal reinforcement to enhance their shear strength.

The dimensions and reinforcement of the specimens are shown in Fig. 3. Specimen WNO1 with a peripheral ratio of 0.3 had conventional peripheral reinforcement around the opening, arranged according to the AIJ standard (AIJ 1985). However note that the peripheral reinforcing bars in the horizontal direction of specimen WN01 were extended to boundary columns, which were assumed to be effective shear resistance of the side wall. In specimen WNO2 with a peripheral ratio of 0.4, which was the maximum value to design as a wall in the current design method (AIJ 1985), the traditional peripheral reinforcement was replaced by twelve diagonal D6 (deformed and 6 mm diameter) bars, arranged bidirectionally in the side walls of the left and right sides of

the opening to enhance the shear strength. Note that these diagonal bars were not anchored into the footing base not to contribute their flexural strength.

Specimen WSO1 with a peripheral ratio of 0.4 had a conventional peripheral reinforcement around the opening. However note that the peripheral reinforcing bars in the horizontal direction of specimen WSO1 were not extended to boundary columns, unlike specimen WNO1. In specimen WSO2 with a peripheral ratio of 0.5, which was larger than the maximum value to design as a wall in the current design method, in addition to the traditional peripheral reinforcement of four D6 bars eight D6 bars were arranged diagonally in the side walls of the left and right sides of the opening to enhance the shear strength.

Specimen WSO3 had door openings with a peripheral ratio of 0.4 at the center of the span width. Specimen WSO4 had eccentric door openings at the edge of the wall panels, which made one of the boundary columns isolated from the wall panels. In these two specimens conventional traditional peripheral reinforcement was arranged according to the AIJ standard (AIJ 1985). However note that the vertical peripheral reinforcement was anchored into the footing beam, which contributed to the flexural strength.

All specimens were designed to fail in flexure and the first story of the wall was assumed to be a hinge region. The side walls and beams were designed to resist shear force and flexural force calculated by the design load. Table 2 shows the characteristics of the reinforcement and concrete.

2.2 Loading Method and Measurement

Figure 4 shows the loading set-up. The specimens were subjected to a total constant axial load of 150kN by two vertical jacks. Lateral load reversals were applied at the end of the girder. The height of the lateral loading point from the wall base was 1900 mm. The lateral load was reversed at drift angles R equal to approximately 1/400, 1/200, 1/100, 1/67, 1/50, and 1/25. Measurements included the horizontal displacement and the flexural rotation determined by the rotation of the beam of each floor. Strains in the column and wall reinforcement were also measured.

3. OUTLINE OF TEST RESULTS

In the first loading cycle at the top drift angle of 0.25% of all specimens, flexural cracks appeared at the column base and shear cracks in the side walls from the corners of the opening. In the third cycle at the top drift angle of 0.5%, a large number of flexural cracks were observed at the bottom of the walls, and yielding was observed in the main bars of all specimens. In the same cycle the cover concrete of the bottom of the columns spalled off in all specimens.

After the 9-th cycle at the top drift angle of 2% kinking actions of the vertical reinforcement of the wall were observed in specimens WNO1,2 and WSO1,2. In these specimens the restoring force degraded with the compressive failure of the concrete at the bottom of the wall and the rupture of the vertical reinforcement of the wall. In specimen WSO3, with door openings at the center of the span, shear failure was dominant at the upper zone of the first floor of the side wall. On the other hand in specimen WSO4, with eccentric door openings shear failure at the lower

zone of the first floor side wall was dominant in the positive direction in which the isolated column was subjected to compression.

Figure 5 shows the examples of relations between the lateral load and flexural rotation, and relations between the lateral load and lateral deflection angle by shear deformation at the loading point. The flexural rotation was defined as the rotation of the loading beam and the shear deformation was obtained by subtracting the flexural contribution from the total deformation.

Each specimen showed ductile behavior up to the top drift angle of 1%, and the pinching-type behavior was observed in the hysteresis loop for further loading exceeding 1%. In specimen WNO1 the restoring force degraded rapidly in the first cycle toward the drift angle of 3%. On the other hand, in specimen WNO2 the restoring force degraded gradually in the repeating cycle of the drift angle of 2%. The behavior of specimen WSO1 without diagonal reinforcement was similar to that of specimen WNO1 without diagonal reinforcement, and the behavior of specimen WSO2 with diagonal reinforcement was similar to specimen WNO2 with diagonal reinforcement. The ratio of flexural deformation to total deformation of these four specimens with window openings was approximately 80-90%. On the other hand, the ratio of the shear deformation of specimen WSO3 with center door openings was larger than specimens with window openings.

The behavior of specimen WSO4 with eccentric door openings was different from other specimens due to the anti-symmetric proportion. In the negative loading direction where the isolated column was subjected to tensile axial force, favorable ductile behavior was observed. However in the positive loading direction where the isolated column was subjected to compressive axial force, the maximum strength was higher than that of negative loading, but the restoring force degraded rapidly after the maximum strength point. Also the shear component of specimen was large in the positive direction in which the isolated column was subjected to compression.

4. DEFORMATION CAPACITY AND MAXIMUM STRENGTH

The AIJ guidelines (AIJ 1994) showed that the deformation capacity of a shear wall without openings could be calculated using the effectiveness factor of concrete to make the shear strength equal to flexural strength. In order to evaluate the deformation capacities of walls with openings the same method as used for walls without openings was applied. Namely, the design equation for the ultimate point are assumed to be expressed as a function of the effectiveness factors of concrete, which are chosen to match the shear strength with its flexural strength. In this section the relation between the observed deformation capacities and the effectiveness factors of concrete is discussed.

The ultimate point in this study was defined as the point where the restoring force degraded to 80% of the maximum strength, which is a method popularly referred to in Japan. The circles in Figure 5 indicate these ultimate points. Note that the smaller value of two drift angles in the positive and negative loading directions was chosen as a value of each specimen except for specimen WSO4, in which both positive and negative values were chosen due to the anti-symmetric elevation. For practical design the flexural rotation of the first floor is the most important one. From this viewpoint the deformation capacities are expressed as the flexural

rotation of the first floor in this study.

Figure 6 shows the relations between the observed deformation capacities of specimens and the effectiveness factors of concrete used to obtain the same shear strength as flexural strength. The flexural rotation of the first floor beam at the ultimate point (when the restoring force degraded to 80% of the maximum load) was chosen as a deformation capacity of each specimen. Solid lines in these figures represent the design relation proposed by AIJ (AIJ 1994).

Figure 6(a) shows the relation using the currently used shear equation with the reduction factor of γ. This figure shows almost no correlation, which means that this method can not explain the test results. Figures 6(b) shows the same relation using the method proposed in the previous paper (Kato 1995), in which the shear strength of a wall with an opening can be obtained as the summation of the strength of both side walls. A better correlation comparing to Fig. 6(a) can be seen. However there are still two data under the design equation in Fig. 6(b). These two specimens are those with diagonal reinforcement and with eccentric door openings in positive loading, which means that the isolated column is subjected to compression.

Strut and tie models have been recognized as effective tools to investigate the effects of openings on the behavior of structural walls (Paulay 1992 and Taylor 1998). In this study simplified strut and tie models shown in Figs. 7(a) were introduced in order to discuss this problem. Figure 7(a1) shows the strut and tie model for a wall without an opening. In this model the shear force is carried by one diagonal strut of the wall. And the flexural strength *Py* is defined as the strength when the tensile longitudinal tie reaches yielding force *Ty*. On the other hand, Fig. 7(a2) shows the simplified strut and tie model for a wall with an opening. For simplification only a first-story opening is considered. In this model the shear force is carried by two diagonal struts of both side walls. And there are two points to be discussed in this model comparing to the model without opening shown in Fig. 7(a1).

The first point is about the strength. The flexural strength *Py* can not be attained in this model due to the existence of the compressive reaction C1. C1 is a part of compressive reaction and travels from the column center to inside the wall panel as shown in this figure, reducing the moment resistance. The second point is about the deformation mechanism; i.e., is sway deformation occurs in this model. The effects of these problems depend on the proportion of the shear force resisted by two side walls. From this viewpoint two extreme cases of this original model shown in Figures 7(b) are helpful to understand these points. In the model shown in Figure 7(b1) the shear force is resisted by one side wall subjected to compressive axial force only. In this study this type of wall is called type F wall, which means flexural type. And in the model shown in Figure 7(b2) the shear force is resisted by the right side side wall only, which is subjected to mainly tensile axial force. This type of wall is called type FS wall, which means flexural shear type. These two models are statically determined structures. So the flexural strength and mechanism of the deformation at the yielding of the tensile tie can be obtained easily.

Figures 7(c) show the flexural strength and mechanism of the deformation of two types after yielding. In case of type F walls (Fig. 7(c1)) the same flexural strength and mechanism of deformation as walls without openings can be obtained. However in case of type FS walls, the flexural rotation and flexural strength are reduced as shown in Fig. 7(c2). It depends on α and β, which are determined by the size and location of the opening. From these two figures two

important suppositions can be obtained. The first supposition is that in order to design walls with openings just like walls without openings, the walls should be designed as type F walls, which means the shear force must be resisted by one side wall only subjected to compression. The second supposition is that if it is impossible to design walls as type F walls and they are still required to be designed as ductile walls, the flexural strength and deformation capacity should be reduced according to these equations shown in Fig.7(c).

Figure 6(c) shows the relations between the effectiveness factors of concrete and the deformation capacities of test specimens. In this figure the strength of only one side wall in compression was taken in account, which means that specimens with the value of the vertical axis of less than 1 are classified into type F walls. In this figure a good correlation in this relation can be seen and there is no data under the design equation, which indicates that this equation is conservative. Note that six specimens are classified as type F walls, which means shear is resisted by one side wall in compression. And one specimen is classified into a non-type-F wall, for which ductile behavior can not be expected by this method. This is the specimen with eccentric door openings in the positive loading direction, which means that the isolated column is subjected to compressive axial force. If this wall is still required to be designed as a ductile structural wall, this wall must be designed as a type FS wall.

In order to design this wall as a type FS wall the calculated deformation capacity must be reduced according to the method shown in Fig. 7(c2). Figure 8 shows the same relation as Figure 6(b) using specimen WSO4(P) only, in which the shear strength of both side walls are taken in account. Dashed line represents the original design equation. And as already seen in Fig. 6(b), this specimen was located under this original line. But the solid line which is reduced by a design equation for type FS wall shows that the plot is just on the line and that the proposed method for deformation capacities of type FS walls is useful.

The flexural strength should be also reduced according to the method shown in Fig.7 (c2) in order to design specimen WSO4(P) as a type FS wall. Figure 9(a) shows the relation between tests of maximum strength and calculated flexural strength. The calculated flexural strength was obtained by assuming that the plane remains plane after bending at the bottom of the wall. The calculated flexural strength of specimen WSO4(P) before reduction was as same as the test result and the ratio of the calculated strength to the test result was lower than other type F specimens. On the other hand the calculated strength moves to a conservative point by this reduction as shown in Fig. 9(a). But Fig. 9(b) showing the lateral load-drift angle relations of this specimen indicates that this reduced flexural strength represents the average flexural strength of the specimen, which means it is not so conservative and is useful to predict the flexural strength of type FS walls.

5. DESIGN METHOD OF ISOLATED COLUMN

In practical design shear resistance is not always necessary for the isolated column of type FS walls but it is deformed under high axial force. So it must be designed for axial force. Two points should be discussed. Firstly what is the design axial force and secondly what is the design deformation. However this discussion is omitted in this paper (it was discussed in another paper (Kato 1999)).

6. CONCLUSIONS

(1) All six specimens, which were designed to fail in flexure, showed ductile behavior.

(2) If the shear force can be resisted by a side wall in compression only (this is called type F wall), the flexural strength can be obtained by the yielding moment of the base. On the other hand, if the shear force can be resisted by both side walls, (this is called type FS wall), the flexural strength must be reduced by the effects of the opening. Other walls are classified into Type S walls failing in shear.

(3) If the wall is a type F wall, the deformation capacity can be obtained by the effectiveness factor of concrete with the proposed design equation for shear using a side wall in compression only. If the wall is a type FS wall, the deformation capacity can be obtained by the effectiveness factor of concrete using the summation of both side walls and this deformation capacity must be reduced by the effects of the opening. It must be noted that the ductility design of the isolated column of type FS wall is required for axial force.

REFERENCES

Architectural Institute of Japan. 1985. *AIJ standard for structural calculation of reinforced concrete structures* (Revised in 1985).

Architectural Institute of Japan. 1994. *AIJ structural design guidelines for reinforced concrete buildings.*

Kato, D., and M. Ishizuka. 1988.. Shear reinforcement of R/C shear walls with an opening. *Transactions of the Japan Concrete Institute* 10: 313–20.

Kato, D., T. Kabeyasawa, S. Otani, H. Aoyama. 1995. Earthquake resistant design of shear walls with an opening. *ACI Structural Journal* 92(4) July–August.

Kato, D., and Y. Sugishita. 1999. Design method of reinforced concrete cantilever walls with openings. *Proceedings of the Japan Concrete Institute* 1.21(3): 721–26 (in Japanese).

Noda, H., Y. Sugisita, and D. Kato. 1997. Tests of reinforced concrete cantilever walls with openings. *Transactions of the Japan Concrete Institute* 19.

Ootani, H., et al. 1998. Tests of reinforced concrete cantilever walls with openings. *summaries of technical papers of annual meeting.* Architectural Institute of Japan, (in Japanese).

Paulay, T., and M. J. N. Priestley. 1992. *Seismic design of reinforced concrete and masonry buildings.* A Wiley Interscience Publication. New York: John Wiley & Sons.

Taylor, C. P., P. A. Cote, and J. W. Wallace. 1998. Design of slender reinforced concrete walls with openings. *ACI Structural Journal* 95(4) July–August.

Table 1 Structural properties of specimens

(a)Dimension and detail of column

Specimen	Section	Main bar	Ratio of main bar	Hoop (1st floor)	Hoop ratio	Hoop (2nd floor)	Hoop ratio
Common	150mmX150mm	4-D10	0.0127	2-D6-@50	0.0142	2-D6-@50	0.0085

(b)Dimension and detail of wall

Spesimen	Peripheral ratio of opening	Wall thickness	Wall reinforcement	Ratio of wall reinforcement	Peripheral reinforcement (1st floor)	Peripheral reinforcement (2nd floor)
WNO1	0.3	75mm	2-R4-@50	0.0069	4-D10 # type	
WNO2	0.4				12-D6 X type (60 degree)	4-D10 # type
WSO1	0.4				4-D10 # type	
					4-D6 # type	
WSO2	0.5				8-D6 X type (68 degree)	
					4-D6 # type	
WSO3	0.4				3-D13 # type	
WSO4	0.4				2-D13 # type	

(c)Dimension and detail of beam

Spesimen	Section	Main bar	Ratio of main bar	Stirrup	Stirrup ratio
Common	150mm×150mm	4-D10	0.0127	2-D6-@50	0.0142

Table 2 Characteristics of materials

(a1)Characteristics of reinforcement (WNO1,WNO2)

Reinforcement		R4	D6	D10
Sectional area	(mm2)	12.6	32	71
Yield stress	(MPa)	530	317	330
Maximum stress	(MPa)	560	478	469

(a2)Characteristics of reinforcement (WSO1,WSO2,WSO3,WSO4)

Reinforcement		R4	D6	D10	D13
Sectional area	(mm2)	12.6	32	71	127
Yield stress	(MPa)	521	331	348	354
Maximum stress	(MPa)	629	482	492	648
Young's modulus	(×10000MPa)	2.09	1.76	1.86	1.72

(b)Characteristics of concrete

Specimen		WNO1	WNO2	WSO1	WSO2	WSO3	WSO4
Compressive strength	(MPa)	24.9	27.2	31.2	30.4	31.3	32.9
Strain at compressive strength (ppm)		2187	2417	2588	2575	2591	2646
Young's modulus	(×10000MPa)	2.23	2.34	2.39	2.38	2.39	2.42

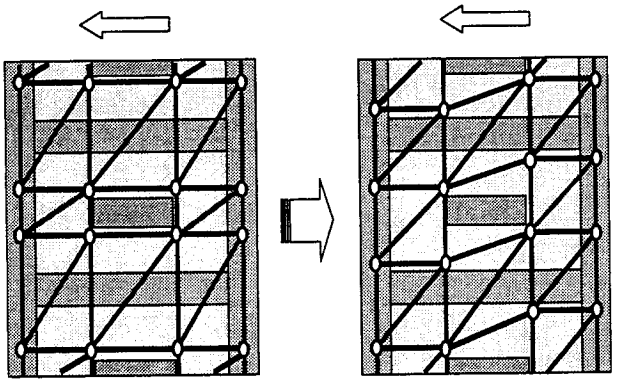

(a) original model (b) revised model

Figure 1 Models for walls with openings

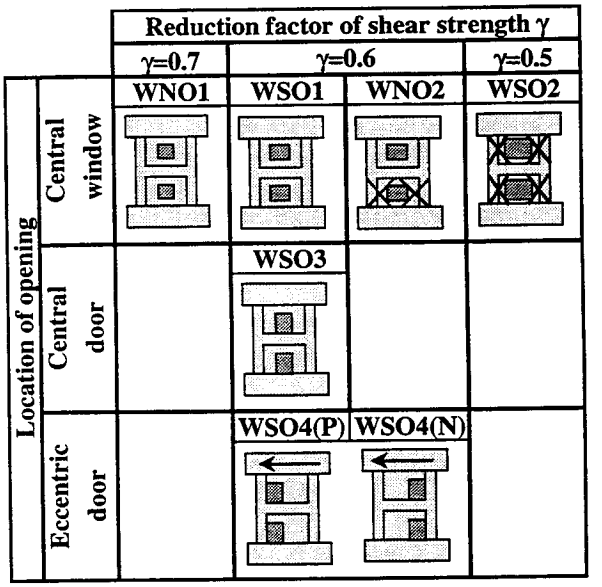

Figure 2 Variations of specimens

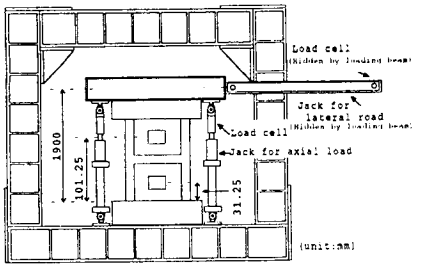

Figure 4 Loading set-up

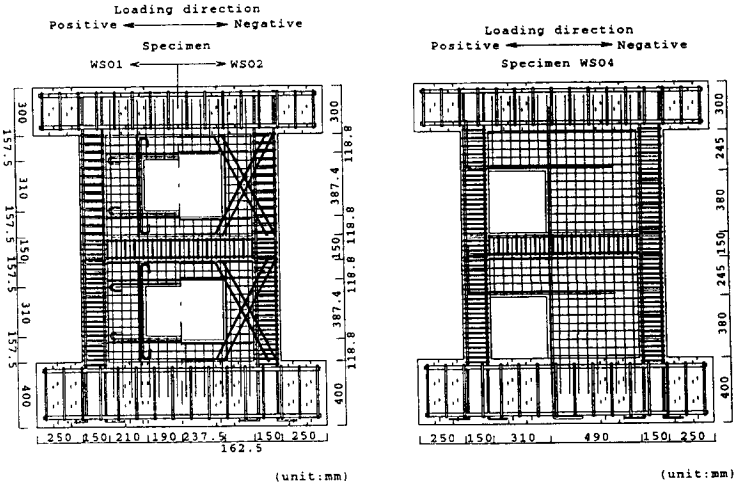

Figure 3 Reinforcement of specimen(WSO1,2 and 4)

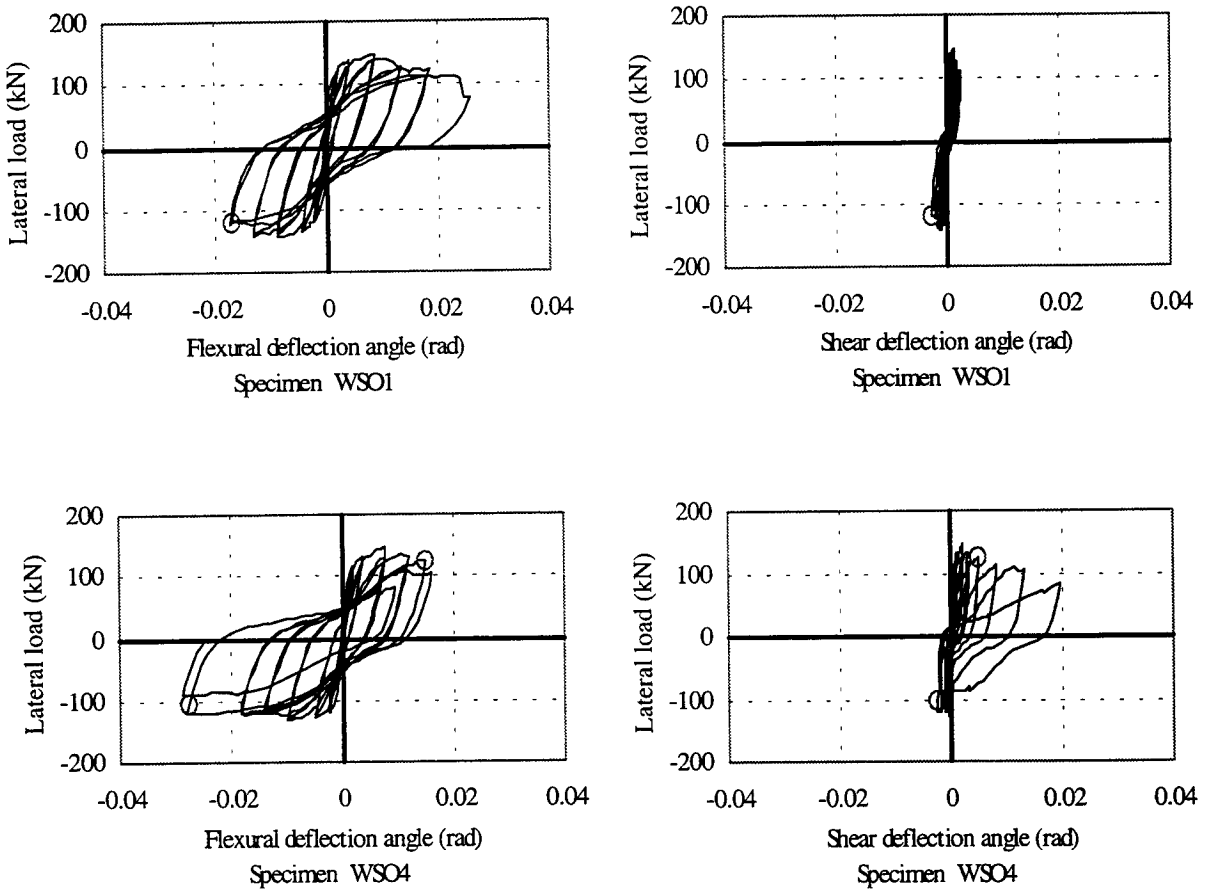

Figure 5 Lateral load-deflection angle by flexure (left) and shear (right) at the loading point (Specimen WSO1 (top) and WSO4 (bottom))

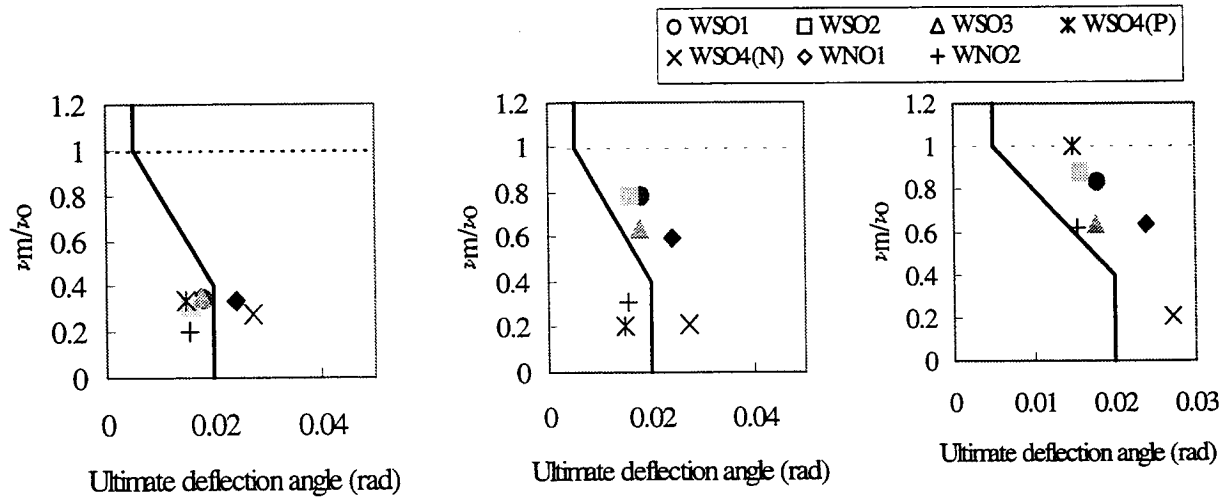

(a) using reduction factor by opening (b) using shear equation with summing both sidewalls (c) using shear equation with a side wall in compression only

Figure 6 Relation between ultimate flexural rotation of first floor and effective factor of concrete to match the shear strength as the flexural strength

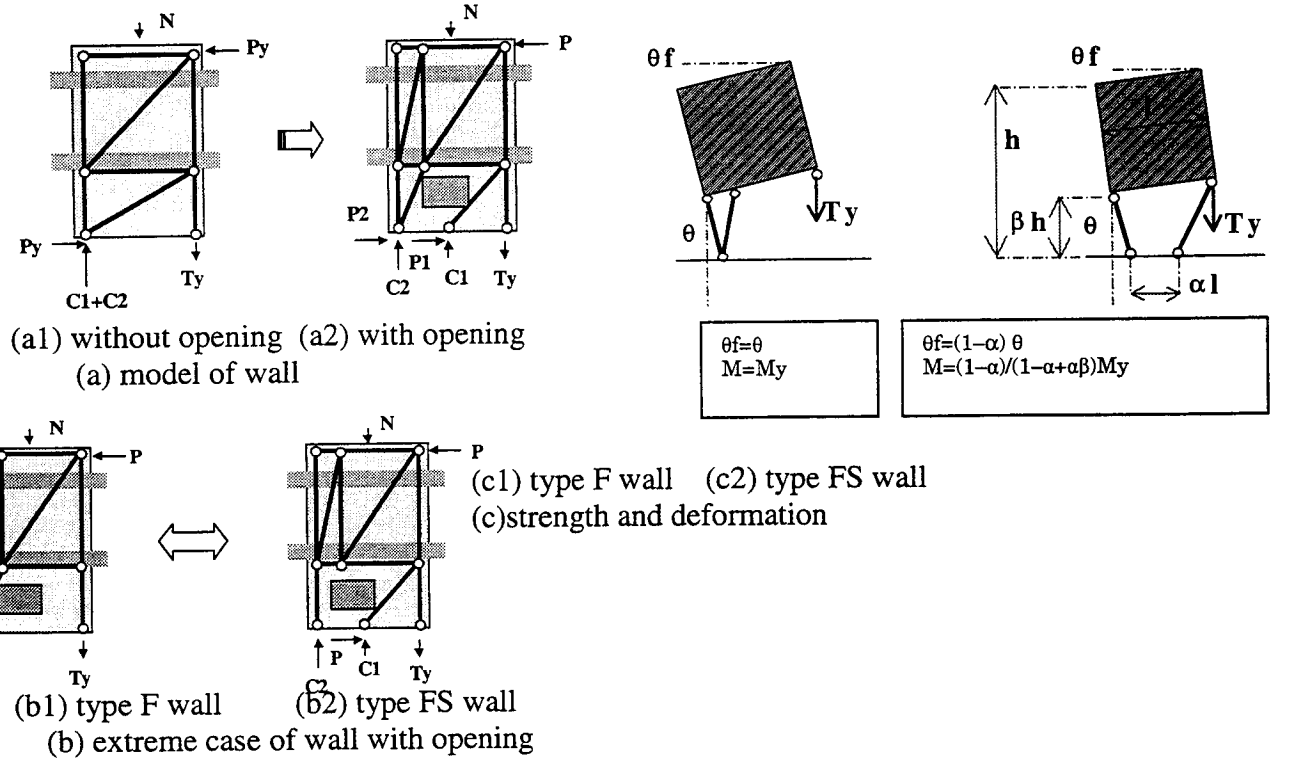

Figure 7 Simplified strut and tie models for walls with openings

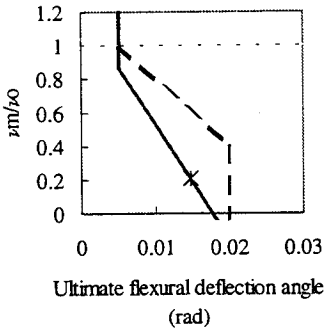

θf = (1−α) θ
α = 0.41 (WSO4(P))

Figure 8 Relation between ultimate deformation and effective factor of concrete to match the shear strength as the flexural strength of specimen WSO4(P) (using proposed shear equation with summing both side walls)

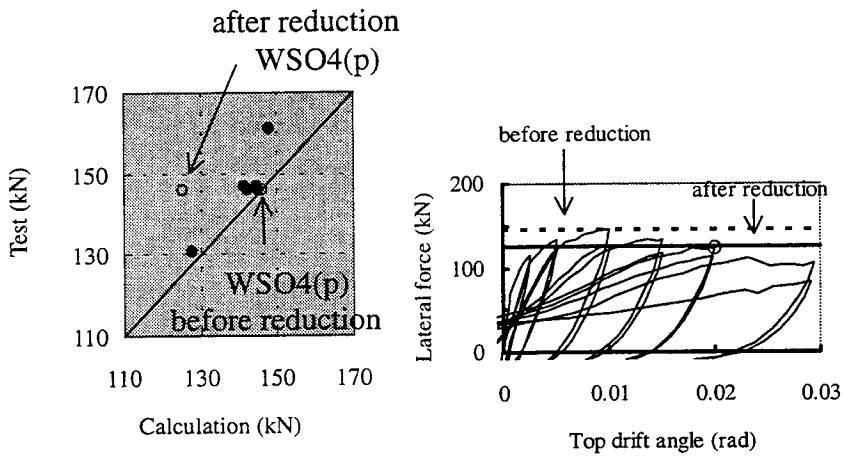

(a)Comparison of flexural strength (b)Behavior of Specimen WSI4(P)

Figure 9 Comparison of flexural strength between test and calculation

IMPROVING THE CYCLIC RESPONSE OF SLENDER STRUCTURAL WALLS BY CHANGING THE ORIENTATION OF THE WEB REINFORCEMENT

Chadchart SITTIPUNT[1] and **Sharon L. WOOD**[2]

ABSTRACT

A series of four reinforced concrete walls were tested to failure to evaluate the influence of diagonal web reinforcement on the hysteretic response. Two walls contained conventional horizontal and vertical web reinforcement and two walls contained inclined reinforcement. The reinforcement details were representative of construction practice in regions of low to moderate seismic risk. A single layer of web reinforcement was used and the transverse reinforcement in the boundary elements did not confine the concrete core.

Both walls with conventional web reinforcement failed due to web crushing. Pinched shapes characterized the hysteresis curves for top displacement and shear distortion near the base. In contrast, the walls with diagonal reinforcement displayed rounded hysteresis curves, and failed due to crushing of the boundary elements. The choice of web reinforcement did not have a significant influence on the maximum lateral load resisted by the walls, but measured crack widths were less, and more energy was dissipated by the walls with diagonal reinforcement during loading cycles to comparable levels of displacement.

INTRODUCTION

Fundamental studies of the behavior of slender reinforced concrete structural walls were conducted during the 1970s at the Portland Cement Association (Oesterle et al. 1976, 1979). The results from these tests provide a wealth of information about the influence of longitudinal, web, and confinement reinforcement on the strength and displacement capacity of typical walls. Subsequent analytical studies of these walls (Sittipunt and Wood 1995) indicated that the hysteretic response of specimens that failed in shear could be improved if diagonal reinforcement had been used in the web. Diagonal web reinforcement provides a more effective mechanism for transferring lateral forces from the wall into the foundation and reduces the shear strains near the base of the wall, thereby improving the energy-dissipation characteristics.

Experience during the 1989 Loma Prieta and 1994 Northridge earthquakes has shown that economic losses can be significant in buildings that satisfied the life safety design criteria inherent to current building codes. In order to reduce these losses from future earthquakes,

[1] *Department of Civil Engineering, Chulalongkorn University, Bangkok, Thailand Email: fcecst@kankrow.eng.chula.ac.th*
[2] *Ferguson Laboratory, University of Texas, Austin, Texas, USA Email: swood@mail.utexas.edu*

procedures are currently being developed that consider the post-earthquake condition of a building when establishing design limit states. Diagonal web reinforcement in structural walls appears to be one way to control structural damage using conventional methods of construction. The results of an experimental investigation comparing the hysteretic response of walls with conventional and diagonal web reinforcement are described in this paper.

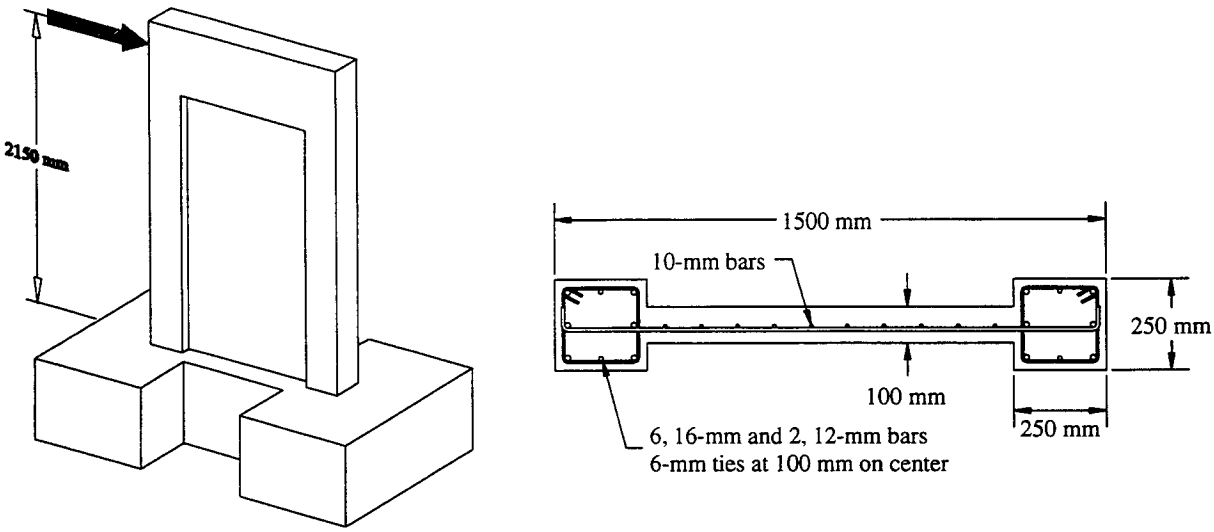

(a) Overview of Test Setup (b) Cross-Sectional Dimensions

Figure 1: Dimensions of Test Specimens

EXPERIMENTAL PROGRAM

Four reinforced concrete wall specimens were constructed and tested at Chulalongkorn University to investigate the influence of diagonal web reinforcement on the hysteric response of structural walls. The dimensions of the specimens are shown in Figure 1. All walls had a barbell-shaped cross section with a web thickness of 100 mm and 250 by 250-mm boundary elements. The overall length of the cross section was 1500 mm. Vertical reinforcement was anchored in a 600-mm thick base girder that was bolted to the laboratory floor. A 250-mm-wide by 500-mm-deep beam was cast on top of the wall panel, and a hydraulic actuator was attached to the specimen at mid-depth of the beam. Lateral loads were applied 2150 mm above the base of the wall.

The primary experimental parameters were the amount and orientation of the web reinforcement. The longitudinal and transverse reinforcement in the boundary elements was the same in all four

specimens. The transverse reinforcement in the boundary elements was not intended to provide confinement of the concrete core. The amount of transverse reinforcement in the boundary elements was consistent with current practice in Thailand and was approximately one-fifth that required in the U.S. in regions of high seismic risk. A single layer of web reinforcement was used in all walls. Specimens W1 and W2 were reinforced with conventional horizontal and vertical web reinforcement, while diagonal web reinforcement was used in specimens W3 and W4 (Fig. 2).

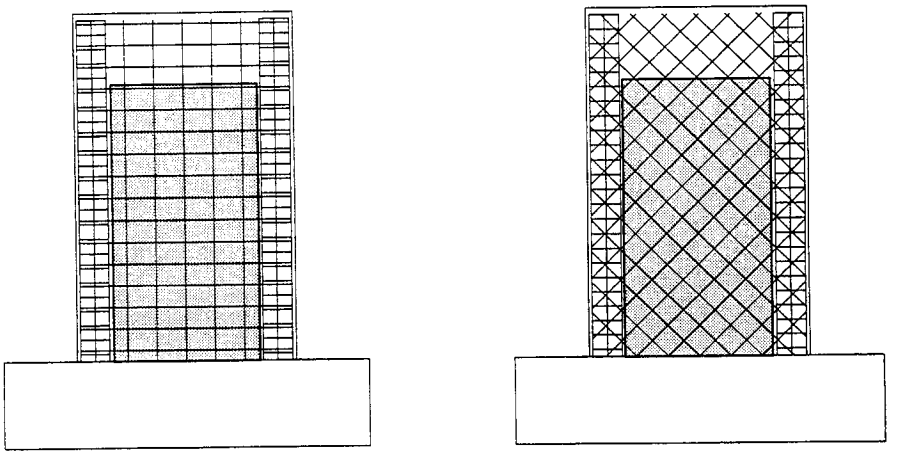

(a) Wall W1 (b) Wall W3

Figure 2: Layout of Longitudinal and Web Reinforcement in Two of the Specimens

The design procedures in the American Concrete Institute Building Code (ACI 318, 1995) for regions of low and moderate seismic risk were used to proportion the walls. During design, the concrete compressive strength was assumed to be 29 MPa and the yield stress of the reinforcement was assumed to be 390 MPa. The measured strengths of the materials used to construct the walls exceeded these values and are summarized in Table 1.

The reinforcement in specimen W1 was selected such that the nominal shear and flexural strengths of the wall were the same. The horizontal web reinforcement was spaced at 150 mm on center, and the vertical web reinforcement was spaced at 200 mm on center for specimen W1. Bar spacings were decreased to 100 mm for the horizontal reinforcement and 150 mm for the vertical reinforcement in specimen W2. This change in spacing had a negligible influence on the calculated flexural capacity but increased the nominal shear strength by 25% relative to

specimen W1. The spacing of the web reinforcement in specimens W3 and W4 was the same as the spacing of the horizontal web reinforcement in specimens W1 and W2, respectively (Table 1). However, the web reinforcement in specimens W3 and W4 was rotated 45 degrees with respect to the longitudinal axis of the wall. The nominal strengths of specimens W1 and W3 and specimens W2 and W4 were essentially the same. Nominal capacities calculated using the measured material properties are listed in Table 2.

Table 1: Material Properties and Reinforcement Ratios

	W1	W2	W3	W4
Concrete Compressive Strength, MPa	36.6	35.8	37.8	36.3
Horizontal Web Reinforcement*				
Spacing, mm	150	100	—	—
Reinforcement ratio, %	0.52	0.79	—	—
Vertical Web Reinforcement*				
Spacing, mm	200	150	—	—
Reinforcement ratio, %	0.39	0.52	—	—
Diagonal Web Reinforcement*				
Spacing, mm	—	—	150	100
Reinforcement ratio, %	—	—	0.52	0.79
Longitudinal Reinforcement in Boundary Elements†				
Area, mm^2	1430	1430	1430	1430
Reinforcement ratio, %	2.29	2.29	2.29	2.29
Transverse Reinforcement in Boundary Elements‡				
Spacing, mm	100	100	100	100

Notes:

* Single layer of 10-mm deformed bars, f_y = 450 MPa

† Six, 16-mm deformed bars, f_y = 473 MPa and two, 12-mm deformed bars, f_y = 425 MPa

‡ Single tie, 6-mm plain bars, f_y = 444 MPa

Table 2: Calculated and Measured Capacity of Specimens

Specimen	Calculated per ACI 318-95		Observed Response		
	Flexural Capacity	Shear Capacity	Maximum Load	Load at Web Crushing	Mode of Failure
	kN	kN	kN	kN	
W1	496	482	491	351	Web Crushing
W2	515	621	608	350	
W3	518	485	569	—	Crushing of Boundary Element
W4	545	622	618	—	

MEASURED RESPONSE

The cyclic loading history used to test the specimens may be divided into six discrete stages, each comprising three complete cycles to a specified force or displacement level. During the first stage, the walls were pushed with a maximum force of ±200 kN, which corresponded to the nominal cracking load. In subsequent stages, the specimens were pushed to integer multiples of the observed yield displacement, beginning with a displacement ductility of 1 in the second stage (Fig. 3).

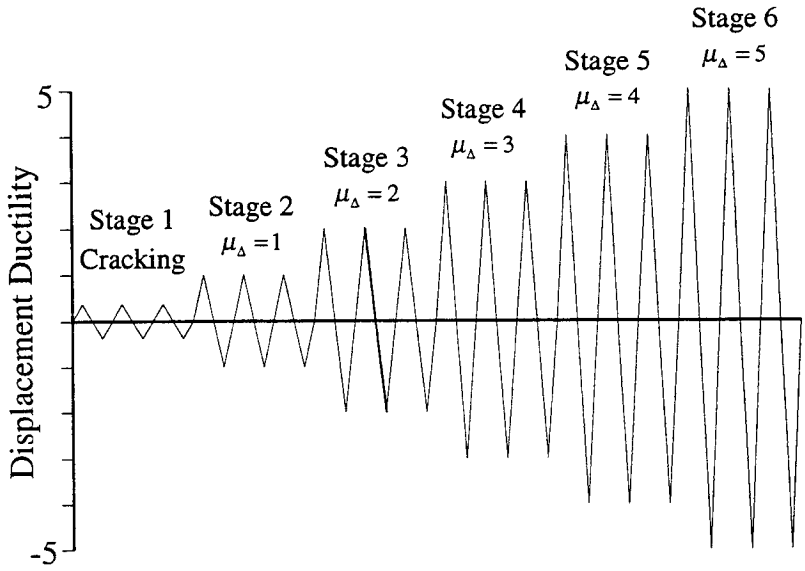

Figure 3: Loading History

The maximum positive displacement resisted by each wall during the first five stages of loading is shown in Figure 4. Slight differences may be observed in the maximum displacements sustained by each wall during the first four stages of loading. Differences among the test specimens may be attributed to variations in the observed displacement at yield. Variations within a given loading stage for an individual wall may be attributed to problems with the algorithms used to control the hydraulic actuators. These variations increased in amplitude during subsequent loading stages. Testing continued until the lateral load capacity of each specimen was reduced by the abrupt failure of the web or boundary elements. Three of the four specimens were able to withstand three complete cycles to a displacement ductility of 4 before failure, while specimen W3 failed during the second cycle to this displacement level.

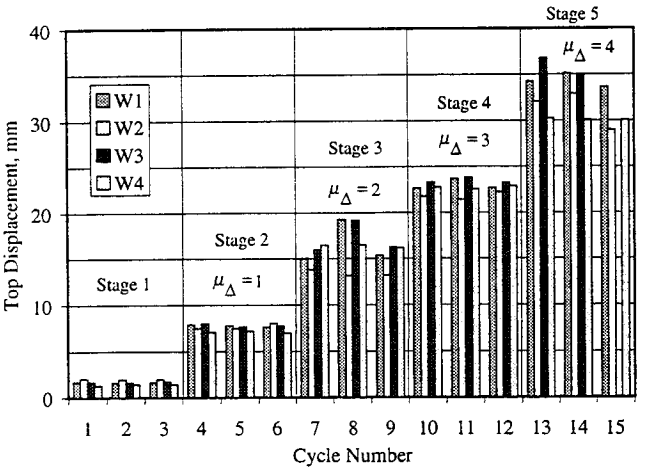

Figure 4: Maximum Positive Displacement Sustained during the First Five Stages of Loading

Continuous plots of load versus top displacement are shown in Figure 5. Significant differences may be observed between the hysteretic response of the walls with conventional web reinforcement (W1 and W2) and the walls with diagonal web reinforcement (W3 and W4). A pinched shape characterized the hysteresis curves for walls W1 and W2. Cracks in the lower portion of the wall did not close when the applied load was reduced to zero, leading to a large reduction in the stiffness of the wall at low levels of applied load. In contrast, the hysteresis curves for walls W3 and W4 exhibited a rounded shape and the effective stiffness did not depend on the magnitude of the applied load during an individual loading cycle.

Hysteresis curves for shear distortion in the lower 900 mm of the web are plotted in Figure 6. These data also indicate appreciable improvements in the response due to the diagonal reinforcement.

All four specimens sustained maximum loads that exceeded the calculated nominal capacities (Table 2). The walls with diagonal web reinforcement resisted higher loads than the companion walls with conventional reinforcement; however, the increase in strength was not significant for the walls with higher web reinforcement ratios.

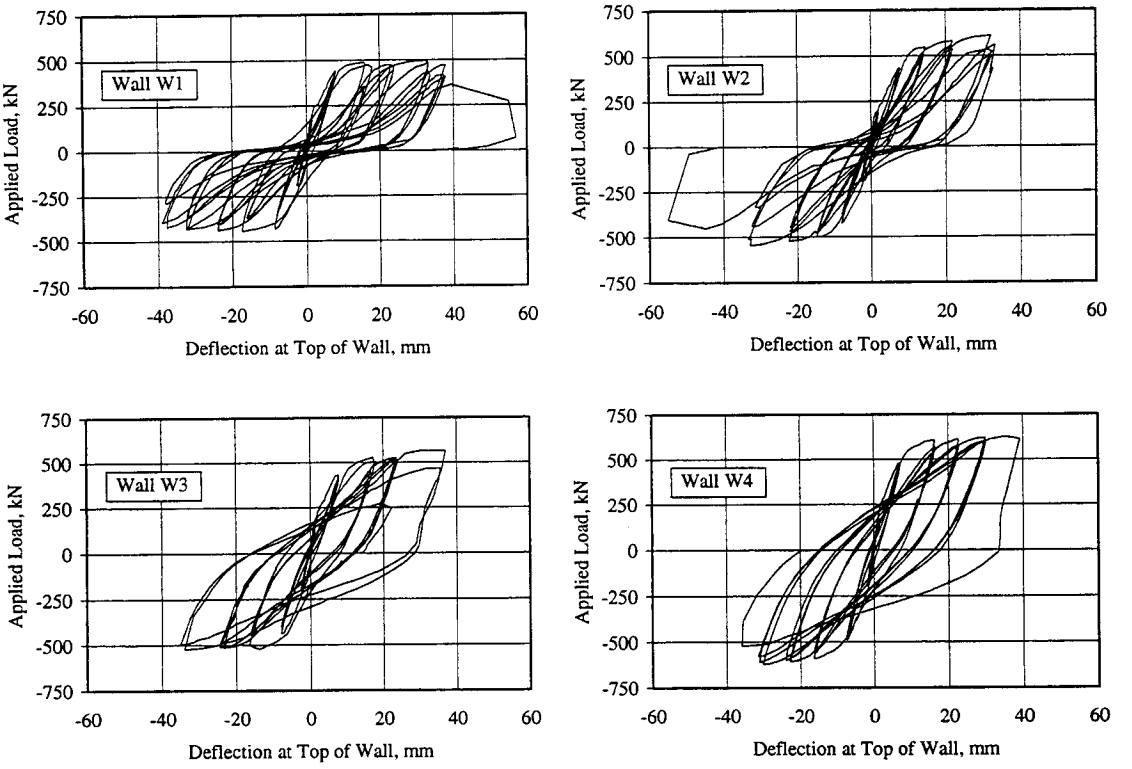

Figure 5: Load vs. Top Displacement

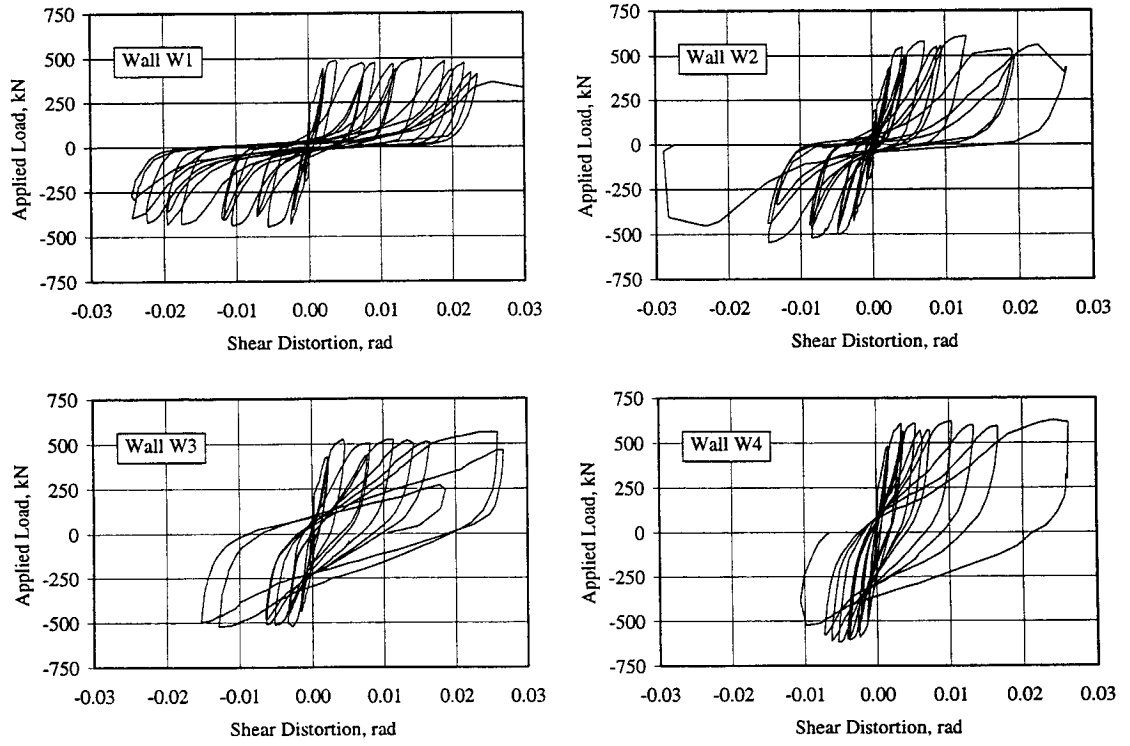

Figure 6: Load vs. Shear Distortion at the Base of the Web

Walls W1 and W2 failed abruptly due to web crushing. The applied load at the onset of web crushing was approximately the same for the two specimens. This load was slightly more than 70% of the maximum load resisted by wall W1 and slightly less than 60% of the load resisted by wall W2. Similar reductions in shear strength with cycling have been observed in previous experimental investigations (Wolschlag 1993).

Walls W3 and W4 failed when the concrete in the boundary elements crushed. This mode of failure was not unexpected, given the modest amount of transverse reinforcement in the boundary elements. Significant increases in the displacement capacities of walls were observed in previous tests when the amount of confinement reinforcement in the boundary elements was increased (Oesterle et al. 1976).

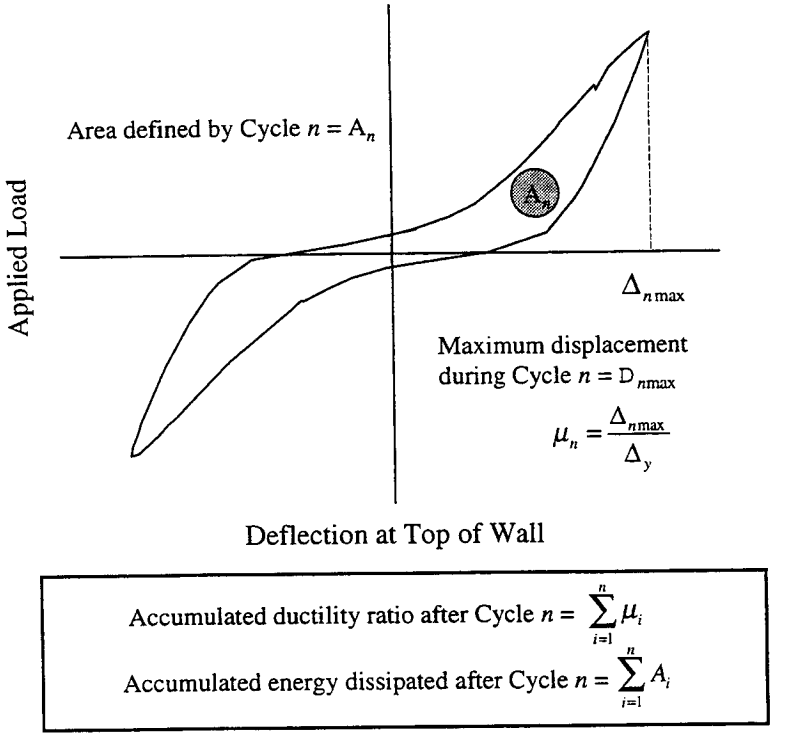

Figure 7: Definition of Accumulated Ductility and Energy

Because the amplitudes of the imposed displacements were not the same for corresponding loading cycles for the four walls, normalized parameters were used to compare the energy dissipation characteristics of the walls. For each loading cycle, the maximum ductility ratio and the area enclosed by the overall hysteresis curves were calculated (Fig. 7). The accumulated

ductility ratio was then defined as the maximum ductility ratio for a given cycle plus the sum of the maximum ductility ratios in all previous cycles. Similarly, the accumulated energy was a sum of the area enclosed by the hysteresis loops. These data are plotted in Figure 8 for loading stages 1 through 5. Accumulated energy increased nearly linearly with the accumulated ductility ratio for the four walls. The rate of increase was considerably higher for the walls with diagonal web reinforcement, indicating their ability to dissipate more energy at a given level of distortion. This confirms the qualitative observations based on the shape of the hysteresis curves.

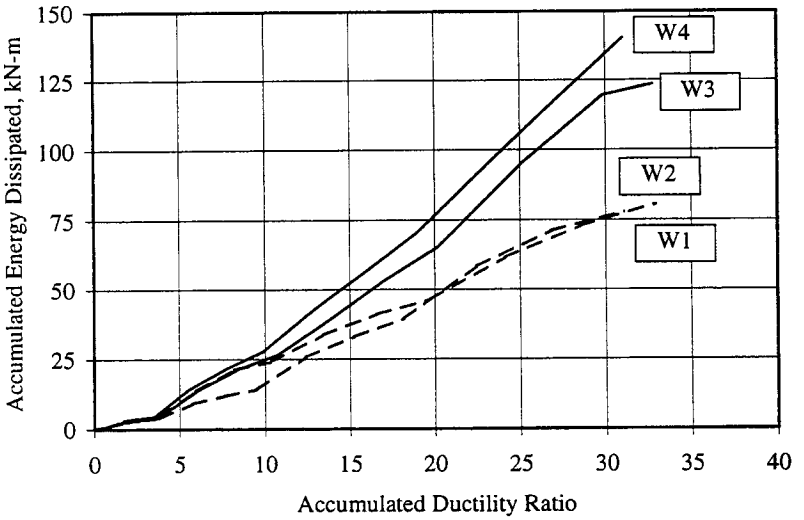

Figure 8: Energy Dissipated during the First Five Loading Cycles

CONCLUSION

The results of this experimental investigation have demonstrated that distributed diagonal web reinforcement is an effective means of improving the hysteretic response of structural walls. Because the diagonal web reinforcement crosses the paths of the cracks nearly perpendicularly, the reinforcement resists the applied loads in tension. In contrast, conventionally reinforced walls must rely on dowel action by the vertical steel and compressive struts in the concrete to transfer the applied loads into the foundation. The strength and stiffness of both of these mechanisms degrade with cycling, and these walls are susceptible to web crushing, a brittle mode of failure. While the capacities of walls W3 and W4 were also limited by the compressive strength of the concrete, previous research has shown that the response can be improved with additional confinement reinforcement in the boundary elements.

As engineers adopt performance-based design philosophies, new techniques must be developed to control structural damage reliably during earthquakes. Diagonal web reinforcement is one such approach. For loading cycles to a specified lateral displacement, walls with diagonal web reinforcement exhibit smaller crack widths and dissipate more energy than conventionally reinforced walls. In addition, with appropriate confinement of the boundary elements, brittle modes of failure can be avoided. These advantages in performance offset the difficulties associated with placement of diagonal bars during construction.

ACKNOWLEDGMENT

The Thailand Research Fund provided funding for this project through a senior research scholar grant to Professor Panitan Lukkunaprasit at Chulalongkorn University. Opinions and findings do not necessarily represent those of the sponsor. P. Pattararattanakul, a former graduate student at Chulalongkorn University, was responsible for construction and testing of the walls.

REFERENCES

ACI Committee 318. 1995. *Building code requirements for structural concrete.* Farmington Hills, Mich.: American Concrete Institute.

Oesterle, R.G., A. E. Fiorato, L. S. Johal, J. E. Carpenter, H. G. Russell, and W. G. Corley. 1976. *Earthquake resistant structural walls —tests of isolated walls.* Skokie, Ill.: Portland Cement Association.

Oesterle, R. G., J. D. Aristizabal-Ochoa, A. E. Fiorato, H.G. Russell, and W. G Corley. 1979. *Earthquake resistant structural walls —tests of isolated walls — Phase II.* Skokie, Ill.: Portland Cement Association.

Sittipunt, C., and S. L. Wood. 1995. Influence of web reinforcement on the cyclic response of structural walls. *ACI Structural Journal* 92(6): 745–67.

Wolschlag, C. J. 1993. *Experimental Investigation of the Response of R/C Structural Walls Subjected to Static and Dynamic Loading.* Ph.D. Dissertation. Urbana, Ill.: Department of Civil Engineering, University of Illinois.

NEW REQUIREMENTS FOR BOND, ANCHORAGE, AND LAP SPLICES IN AIJ STANDARD FOR STRUCTURAL CALCULATION OF REINFORCED CONCRETE STRUCTURES

Shigeru FUJII [1]

ABSTRACT

In 1999, an overall revision was made to the bond and anchorage requirements of the *AIJ Standard*. The dual requirements for the flexural local bond and the anchorage bond were repealed and a method for the development length was adopted based on calculation of the average bond. The allowable average bond stresses were evaluated based on previous research on splitting bond failure in beams and columns. Even for continuous longitudinal bars the clear span length of the member is examined to prevent the premature bond-shear failure. For bent bar anchorage, a configuration of a standard hook is defined and the requirement of the projected development length is specified. Two kinds of projected development lengths are specified depending on different anchorage failure modes. The minimum side cover on the hook portion is specified for the combinations of concrete strength and steel grade. The main points of the new requirements and issues needing future investigation are discussed.

1. INTRODUCTION

The *AIJ* (Architectural Institute of Japan) *Standard for Structural Calculation of Reinforced Concrete Buildings* (AIJ Standard) was revised in 1999. This standard was first published in 1933 and has been revised several times by adding new information based on progress made in research and on lessons learned as the result of several earthquakes. In Japanese structural design practice, the *AIJ Standard* is the technical document referred to in the first step of calculating (allowable stress design calculation) for every RC building. The major points for this latest revision are (1) an extension of the available specified concrete strength up to 60 MPa, (2) changes in the bond and anchorage requirements, (3) the development of the requirement of shear stress in the beam-column joints, and (4) the change to the SI Unit. This paper introduces the summary of the new requirements on the bond and anchorage of reinforcement. Recent research findings on bond and anchorage are reviewed, and issues needing future clarification are pointed out.

2. SPLITTING BOND-SHEAR FAILURE IN BEAMS AND COLUMNS

2.1 Failure Mode

The bond-shear failure mode was first acknowledged in seismic loading tests of short columns in a Japanese national research project conducted after the 1968 Tokachioki earthquake. Figure 1 shows the typical bond-shear failure pattern. The characteristic behaviors are the significant progress of stitched cracks along the longitudinal bars, and the

[1] *Department of Global Environment Engineering, Graduate School of Engineering, Kyoto University, JAPAN, (E-mail:fujii@archi.kyoto-u.ac.jp)*

decrease in shear strength and the energy-dissipation capacity due to bond slip. This type of bond deterioration (splitting bond failure) results from the wedging action of bars deformed under high bond stress (see Figure 2). Columns and beams with a larger longitudinal reinforcement ratio, a smaller concrete cover or bar spacing and a smaller transverse reinforcement ratio tend to fail in this mode. It is thus necessary to check the bond stress in the continuous reinforcement along the entire span length.

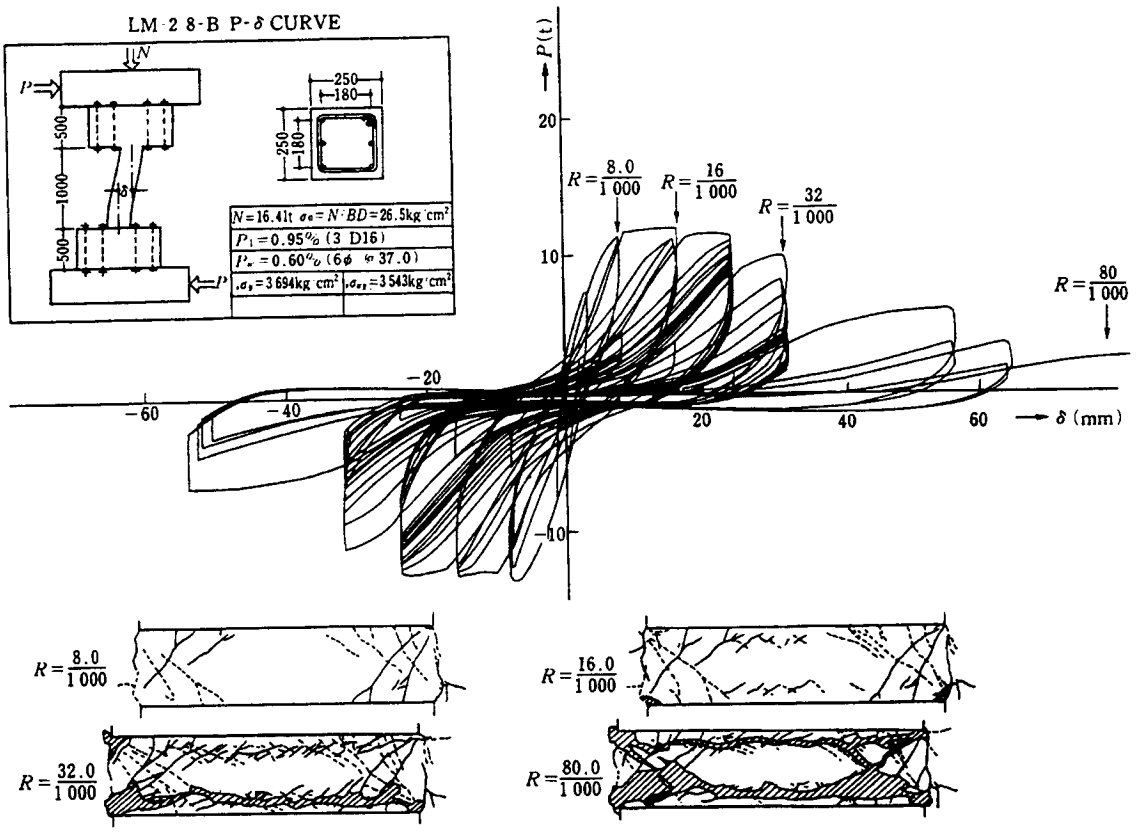

Fig. 1. Bond-shear failure of columns (AIJ Standard 1991)

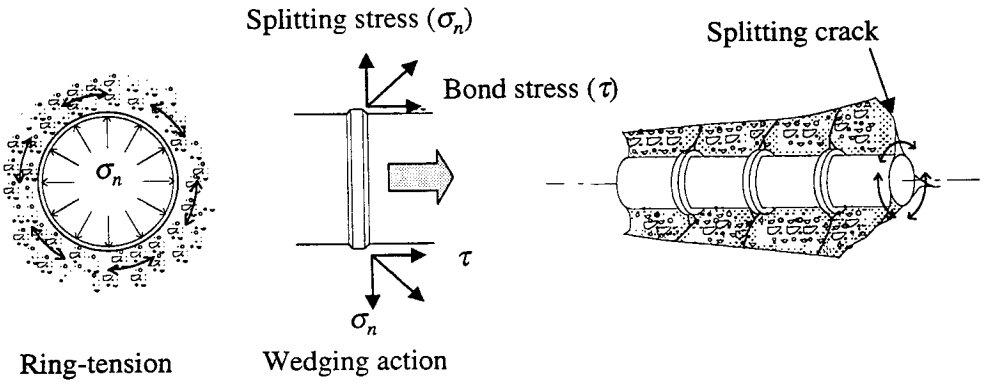

Fig. 2. Wedging action and bond splitting cracks in deformed bars

2.2 Splitting Bond Strength Equation

Splitting bond strength has been investigated experimentally and several strength equations have been proposed in Japan. The strength equation proposed by Morita et al. (1982) was adopted as the basis of the design equation in the *AIJ Standard,* shown in Table 1. In the equation, the effect of the concrete cover and bar spacing is evaluated by factor b_i, the average splitting concrete width to bar diameter ratio considering the three types of splitting patterns shown in Figure 3. The yield strength of the transverse reinforcement is not included in the equation based on the test result that the high-strength transverse reinforcement did not contribute to improving the bond strength. The research findings of the advantageous effects of multiple stirrup legs and the case of a short bond length were ignored.

Table 1 Splitting Bond Strength Equation Proposed by Morita et al. (1982)[2]

For top cast bars: $\tau_{bu} = \tau_{co} + \tau_{st}$ (1) $\tau_{co} = (0.307 b_i + 0.427)\sqrt{\sigma_B}$ (in kgf/cm^2) $\tau_{st} = 24.9 \cdot \frac{k \cdot A_{st}}{s \cdot N \cdot d_b}\sqrt{\sigma_B}$ $\left(\leq 0.87\sqrt{\sigma_B}\right)$ $b_i = min[b_{vi}, b_{ci}, b_{si}]$ $b_{vi} = \sqrt{3} \cdot \left(\frac{2 \cdot C_{min}}{d_b} + 1\right)$ $b_{ci} = \sqrt{2} \cdot \left(\frac{C_s + C_b}{d_b} + 1\right) - 1$ $b_{si} = \frac{b}{N d_b} - 1$ k $b_i=b_{vi}$ $k=0$ $b_i=b_{ci}$ $k=\sqrt{2}$ $(N=2)$ $b_i=b_{si}$ $k=1$ For bottom cast bars the coefficient of 1.22 is multiplied.	Where τ_{bu} =bond strength in kgf/cm^2 τ_{co} =bond strength without transverse reinf. τ_{st} =bond strength increase by transverse reinf. b_I =factor for cover and bar spacing effect C_s =side cover C_b =bottom or top cover, d_b =bar diameter b =member width s =spacing of transverse reinforcement. C_{min} =minimum cover (cm) A_{st} =total sectional area of a set of transverse reinforcement (cm^2) N =number of bars in splitting plane σ_B =concrete strength (kgf/cm^2) k =coefficient depending on splitting patterns

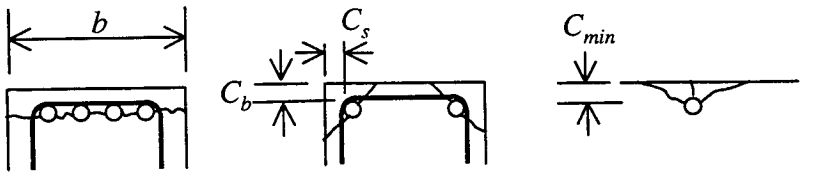

(a) Side-Split (b) Corner Split (c)V-notch Split

Fig. 3. Splitting patterns

By simplifying the original equation, the bond strength evaluation for the *AIJ Standard* was obtained by applying a reduction factor of 0.8. For bottom-cast bars, the allowable bond strength τ_{bu}^* for short term loadings is as follows:

$$\tau_{bu}{}^{*} = 0.8 \cdot 1.22 \cdot \left(0.307 b_i + 0.427 + 24.9 \cdot \frac{k \cdot A_{st}}{s \cdot N \cdot d_b} \right) \sqrt{\sigma_B}$$

$$\approx \left(\frac{0.30 \cdot (C + 80 \cdot \frac{A_{st}}{s \cdot N})}{d_b} + 0.417 \right) \cdot \sqrt{F_c}$$

$$\approx \left(0.3 \cdot (\frac{C+W}{d_b}) + 0.4 \right) \cdot (0.025 F_c + 9) \quad (\text{in kgf / cm}^2)$$

$$\approx \left(0.3 \cdot (\frac{C+W}{d_b}) + 0.4 \right) \cdot (\frac{F_c}{40} + 0.9) \qquad (\text{in N / mm}^2) \tag{2}$$

Where, F_c is the specified concrete strength.

The contribution of the concrete cover and bar spacing is evaluated by the factor C, which is given by the smaller between the clear bar spacing and three times the minimum of the concrete cover. The effect of transverse reinforcement is given by the factor W that has the dimension of length (see Figure 4). The notations of other factors are listed in Table 1.

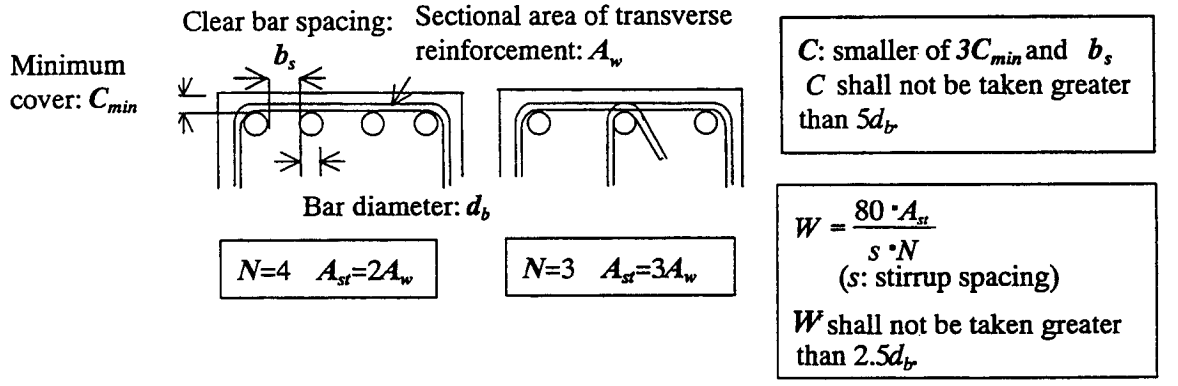

Fig. 4. Definition of factors N, A_{st}, C, and W

2.3 Requirement on Development Length in Member Span Region

The tension calculated for the reinforcement at critical sections in the structural concrete members shall be developed so that the *effective embedment length* l_d (defined in Sec. 2.4) satisfies the following equation. Considering the behavior brought about by an increase in tension stress at the member ends due to diagonal cracking, the effective member depth d must be added to the *required development length* l_{db}. When it is ascertained that diagonal shear crack does not occur, the term d need not to be added in the required development length in Eq.(3).

$$l_d \geq l_{db} + d \tag{3}$$

$$l_{db} = \frac{\sigma_t \cdot A_s}{K \cdot f_b \cdot \psi} \tag{4}$$

Where,

σ_t: the design tensile stress at the critical section. If the standard hook was applied at the end in the span region, two thirds can be multiplied.

A_s: the sectional area of a bar

ψ: nominal perimeter of a bar

f_b: $\frac{F_c}{40}+0.9$ for bottom cast horizontal bars and vertical bars in the ultimate loading condition, $\frac{2}{3}(\frac{F_c}{40}+0.9)$ in the service load condition

Coefficient 0.8 shall be multiplied to f_b for top cast bars. Coefficient 0.6 shall be further multiplied for the inner bars of multiple layers' bar arrangement.

d: beam or column effective depth

K: modification factor for concrete cover and bar spacing

For service load condition: $K = 0.3\frac{C}{d_b}+0.4$ (5)

For ultimate load condition: $K = 0.3\left(\frac{C+W}{d_b}\right)+0.4$ (6)

Where,

C: the smaller of clear bar spacing and three times the minimum of the concrete cover, which shall not be larger than five times of the bar diameter

W: coefficient given by Eq.(7), which shall not exceed 2.5 times the bar diameter

$$W = 80 \cdot \frac{A_{st}}{s \cdot N} \quad (7)$$

Where,

A_{st}: total sectional area of one set of transverse reinforcement that cross the splitting crack

s: spacing of a set of transverse reinforcement

N: number of longitudinal bars at the splitting crack line

d_b: bar diameter

For a multiple-layered bar arrangement, the strength reduction coefficient 0.6 is applied to Eq.(4), which is based on the experimental evidence. The splitting bond strength of inner-layered bars is decreased by the shear stress originating from the bond stress in the outer-layered bars. The design criteria were formulated to prevent splitting cracks under the service load condition and bond failure under the ultimate load condition. Under the service load condition, the conservative evaluation was made ignoring the contribution of the transverse reinforcement.

2.4 Effective Embedment Length l_d

The critical sections for developing reinforcement in members are at the points of maximum stress and where adjacent cut-off bars are no longer required to resist flexure in the calculation for the remaining bars. The effective embedment length l_d is given as the length from the critical section to the terminated reinforcement end. The reinforcement shall extend the point at which it is no longer required to resist flexure for a distance equal to the effective depth d of the member. In continuous members, at least one-third the total positive and negative reinforcement shall extend through the whole span. Figure 5 shows the case of the

continuous reinforcement running to the opposite support face of member. The effective embedment length is specified corresponding to the member types whether yield hinge is planned at one end or at both ends.

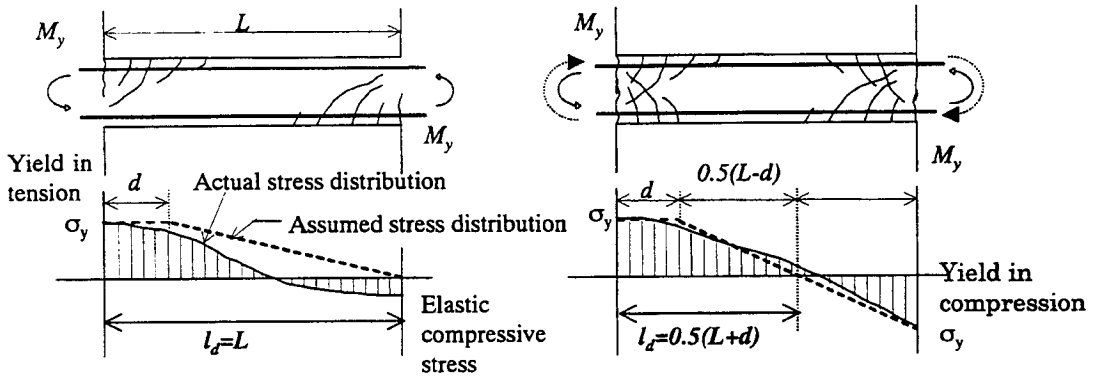

(a) Member with yield hinge formation at one end

(b) Member with yield hinge formation at both ends

Fig. 5. Effective embedment length for continuous reinforcement

2.5 Interaction between Bond and Shear Actions

The above development length requirement in the *AIJ Standard* is for the induced tensile stress in the longitudinal reinforcement originating from the bending moment. In the *AIJ Design Guidelines for Earthquake Resistant Reinforced Concrete Building Based on Ultimate Strength Concept* (1988), the other bond requirement is provided from the viewpoint of the shear transfer capacity by the truss action. The shear strength of the beams and columns in the *Guidelines* is the following:

$$V_{cal} = b \cdot j_t \cdot p_w \cdot \sigma_{wy} \cdot \cot\phi + \frac{\tan\theta \cdot (1-\beta) \cdot b \cdot D \cdot \nu\sigma_B}{2} \tag{8}$$

Where $\tan\theta = \sqrt{(\frac{L}{D})^2 + 1} - \frac{L}{D}$ (9)

$$\beta = \frac{(1+\cot^2\phi) \cdot p_w \cdot \sigma_{wy}}{\nu\sigma_B} \tag{10}$$

b, D: width and overall depth of the section,

j_t: distance between the top and bottom bars,

L: clear span of the member, σ_B: specified compressive strength of concrete,

σ_{wy}: strength of the shear reinforcement, p_w: shear reinforcement ratio,

$\nu = 0.7 - \frac{\sigma_B}{200}$ (in N/mm^2): effective concrete compressive strength,

ϕ: angle of the compressive strut in the truss mechanism,

$\cot\phi$: minimum of $(2.0, \frac{j_t}{D \cdot \tan\theta}, \sqrt{\frac{\nu\sigma_B}{p_w \cdot \sigma_{wy}} - 1})$

Figure 6 illustrates the truss and strut actions on which the equation is based. The shear strength governed by the splitting bond failure can be calculated by limiting the first term of Eq.(8) (a contribution of truss action) as listed in Figure 6(c). For the ultimate load condition,

it is recommended that the bond stress necessary for shear transfer should be smaller than the splitting bond strength τ_{bu}^{*} given by Eq.(2).

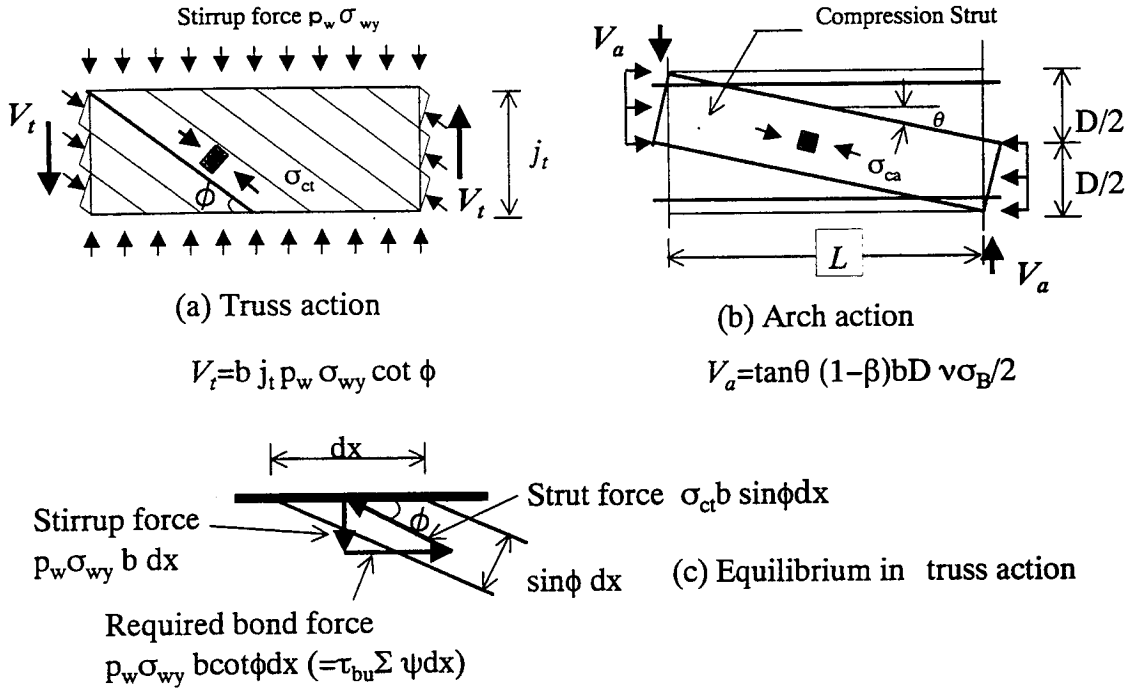

Fig. 6. Concept of applied shear strength equation (*AIJ Design Guidelines*)

2.6 Required Lap Splice Length

The length of the lap for the tension of the lap splices is calculated by the same equation for the development length (Eq.(4)), where the stress of the spliced bars σ_t shall be the factored yield strength (actual yield strength) in every case. In the calculation, the bar spacing for non-contact lap splices should be taken as the same value as for the case of the contact lap splices. The factor N is taken as the number of set of spliced bars in Eq.(7). Splices of all bars are permitted in the same section as elastic members when the special requirement on additional transverse reinforcement is provided, and in the plastic hinge region for the beams by taking a somewhat longer lap length further. This treatment is based on the *AIJ Design Guidelines of Lap Splices for Splicing All Bars at the Same Section (Draft)*(1996).

3. ANCHORAGE REQUIREMENT FOR BENT BARS

3.1 Anchorage Failure of Bent Bars in Beam-Column Joints

Based on several experimental research projects, the anchorage failure of bent bars is classified according to two failure modes, shown in Figure 7. The splitting failure of the side of the concrete cover is due to high bearing stress at the inside of the bend. For this failure mode, the important factors for anchorage strength are (1) the side cover to the bent portion, (2) the projected development length l_{dh}, (3) the transverse reinforcement crossing the bent portion, and (4) the condition of the stress in the surrounding concrete at the hook portion (which was expressed by the ratio of l_{dh} to whole column depth and the ratio of l_{dh} to beam depth in previous research (Fujii et al. 1991). On the other hand, the raking-out failure of the front concrete can be considered as one of the joint shear failure modes. The anchorage capacity is proportional to the projected development length and the amount of shear reinforcement crossing the failure plane.

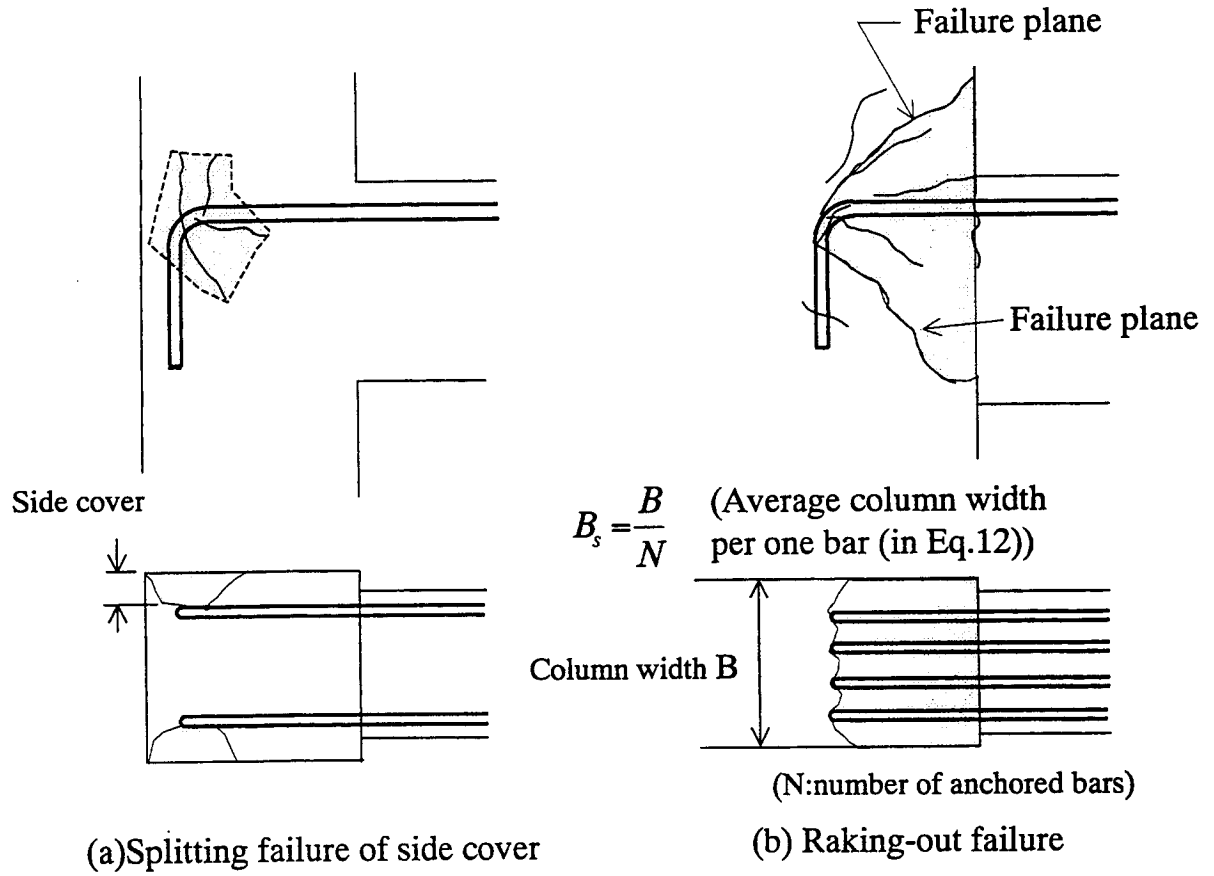

Fig. 7. Failure modes of bent bar anchorage

3.2 Design Criteria and Requirement of Bent Bar Anchorage

For beam or column reinforcement anchored in beam-column joints, Eq.(11) specifies the required projected development length. When the bar is anchored in the joint core region

enclosed by transverse reinforcement, the coefficient 0.8 can be multiplied to the calculated. However, l_{dh} shall not be less than 8 d_b nor less than 300 mm.

$$l_{dh} \geq \frac{S \cdot \sigma_t \cdot d_b}{8 \cdot (\frac{F_c}{40} + 0.9)} \tag{11}$$

Where,

d_b bar diameter

σ_t : the design tensile stress at the critical section (The specified yield strength f_y should be taken in principle.)

S : modification factor for effect of side cover (normal to plane of hook) listed in Table 2

Table 2 Factor S in Eq.(11)

Side cover not less than	5.5 d_b	4.5 d_b	3.5 d_b	2.5 d_b	others
S	0.6	0.7	0.8	0.9	1.0

Figure 8 shows the supplementary requirement of anchorage length in beam-column joints. For beam or column bars anchored in beam-column joints, the ratio of the projected development length to the whole depth of the member in which the bar is anchored should not be less than 0.75, or the bend portion shall be started over the center of the member depth. Raking-out failure can be excluded by this requirement and the requirement on shear stress in beam-column joints. A poor performance in strength and deformation for bent-down anchorage of beam bottom bars is widely recognized, so that the bent-up bar arrangement or U-shape bent anchorage is recommended.

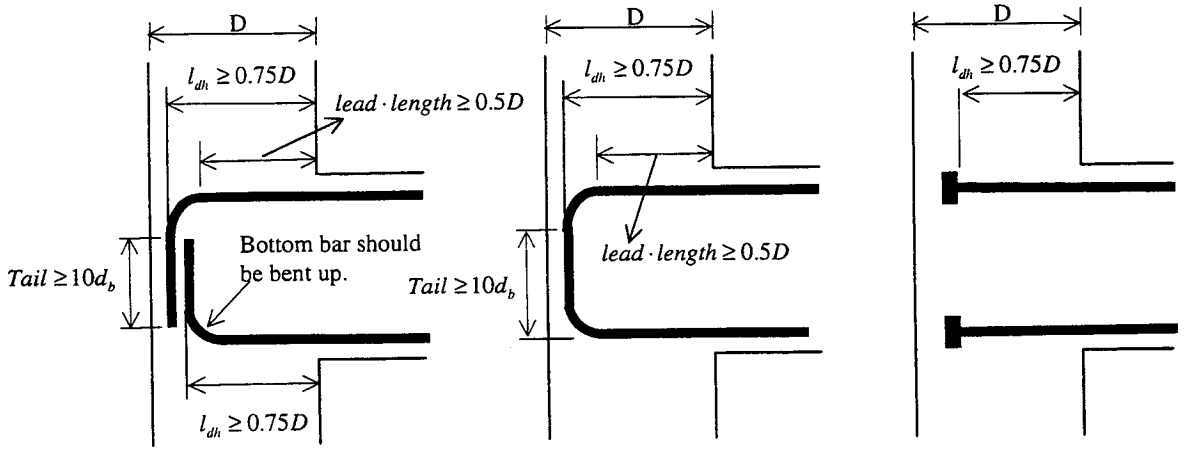

Fig. 8. Projected development length requirement

Previous test results indicate that there is a limit to improving the anchorage strength by taking larger l_{dh} (Fujii et al. 1991). It means that larger confinement of the hook portion is essential for anchorage in these cases. Based on this standpoint the minimum side cover to the hook portion is specified depending on the combination of concrete strength and the grade of reinforcement, listed in Table 3.

Table 3 Minimum Side Cover to Hook

F_c(N/mm^2)	Grade of Reinforcement (Specified yield strength f_y (N/mm^2))		
	SD295	SD345	SD390
18, 21	4.5 (2.5) d_b	5.5 (4) d_b	not in use
24, 27	3.5 (1.5) d_b	4.5 (3) d_b	5.5 (4) d_b
30	2.5 (1.5) d_b	4 (2) d_b	5 (3.5) d_b
36	2 (1.5) d_b	3.5 (1.5) d_b	4 (2.5) d_b
42	2 (1.5) d_b	2.5 (1.5) d_b	3.5 (1.5) d_b
48	2 (1.5) d_b	2 (1.5) d_b	3 (1.5) d_b
54, 60	2 (1.5) d_b	2 (1.5) d_b	2.5 (1.5) d_b

Number in parenthesis is for the case of anchorage in confined joint core region

In general, for cases other than beam or column bars anchored in beam-column joints, such as bar anchorage in basement, and wall and slab reinforcement anchored in adjacent members, etc., an inspection against the raking-out failure is required. The required projected development length for these cases is calculated by changing the definition of the factor S in Eq.(11) to that given by the following Eq.(12).

$$S = \frac{4 \cdot d_b}{B_s} \tag{12}$$

Where, B_s is the average member width per one anchored bar, which shall not be larger than $5d_b$. This evaluation is obtained by simplifying the strength equation for raking-out failure (Joh et al. 1993).

3.3 Standard Hook

Figure 9 shows the configuration (inside the diameter of the bend and the tail extension) of the standard hook for flexural reinforcement. The specified standard inside the bend diameter and the $10d_b$ tail extension are based on previous test results on which the adopted anchorage strength equation is based. To avoid the difficulty of bar arrangement in beam-column joints, the use of a smaller bend diameter, of $2d_b$ at maximum, is permitted when (a) the hook portion is covered by a transverse member, or (b) an additional transverse bar in the normal direction of the hook plane, whose diameter is not less than the anchored bar, is placed inside the bend, or (c) two sets of additional transverse ties were placed at the bend portion. For other cases, 1.1 and 1.2 should be multiplied to the calculated l_{dh} for the reduced bend diameter by $1d_b$ and $2d_b$, respectively.

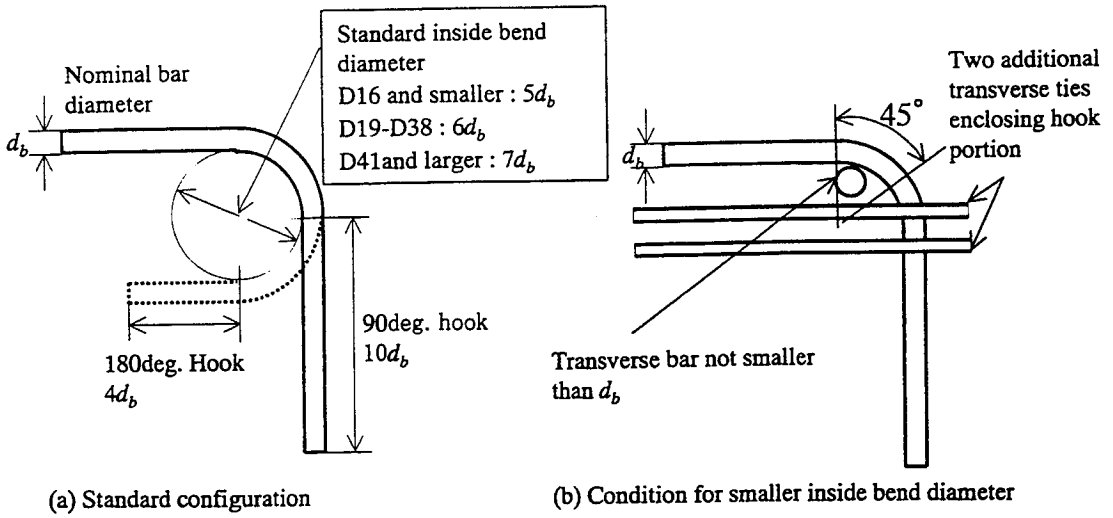

Fig. 9. Standard hook

3.4 Mechanical Anchorage

Most of the previous test results on mechanical anchorages showed that similar failure modes and equivalent anchorage capacities to the 90-degree hooked bar anchorage. In the *AIJ Standard,* the same development length equation is permitted for anchored bars terminated with the appropriate mechanical anchorage device in beam-column joints. The projected development length is defined as the length to the front face of the end-bearing plate as shown in Figure 8.

3.5 Anchorage Requirement of Knee-Joints

Previous test results show that satisfying only the projected development length requirement is not enough for top beam bars in knee-joints (Figure 10). Top bars shall be anchored with a 90-degree hook and its tail extension shall be as long as that calculated by Eq.(4). The mechanical anchorage and 180-degree hook anchorage should not be used for top beam bars in knee-joints unless the effective additional reinforcement was arranged.

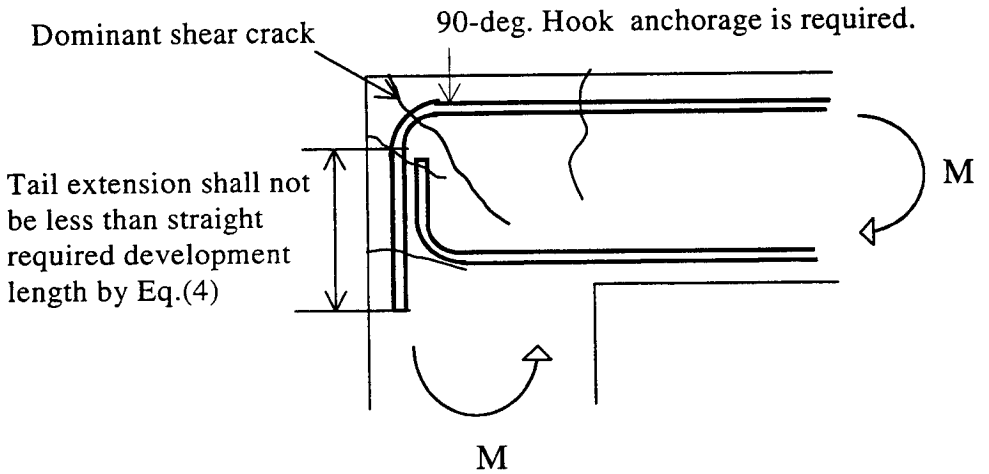

Fig. 10. Top bar anchorage in knee-joint

4. BOND REQUIREMENT FOR BEAM BARS PASSING THROUGH INTERIOR COLUMN-BEAM JOINTS

To prevent premature bond deterioration in the beam bars passing through the joint, the following requirement is provided in the *AIJ Design Guidelines for Earthquake Resistant R/C Buildings Based on Inelastic Displacement Concept* (1997).

$$\frac{d_b}{D} \le \frac{7.5}{1+\gamma} \cdot (1+\frac{\sigma_0}{\sigma_B}) \cdot \frac{0.46 \cdot \sigma_B^{2/3}}{\sigma_{yu}} \quad (\text{in kgf/cm}^2) \tag{13}$$

Where,

D: Column depth, d_b: beam bar diameter,

γ: ratio of bottom to top beam longitudinal reinforcement amount,

σ_0 : column axial compressive stress, σ_B: specified concrete compressive strength,

σ_{yu} : reinforcement strength to estimate the upper bound strength (1.3 f_y for SD295 and 1.25 f_y for SD345 and SD390, where f_y is specified (nominal) yield strength)

In the *Guidelines*, the following alternative method is permitted considering the effect of degraded hysteretic energy absorption on earthquake responses.

$$\frac{d_b}{D} \le \frac{\mu_i \cdot \sigma_B^{2/3}}{\sigma_{yu}} \quad (\text{in kgf/cm}^2) \tag{14}$$

Where, μ_i =3.6 for structures with the elastic fundamental period of less than 0.4 sec., and μ_i = 5.0 for others.

Considering that the *AIJ Standard* is used for all kinds of RC buildings, the following simplified requirement is specified. The calculated minimum column depth is listed in Table 3.

$$\frac{d_b}{D} \le \frac{3.6 \cdot (15+0.1F_c)}{f_y} \tag{15}$$

Table 3 Minimum Column Depth to Prevent Bond Deterioration

F_c(N/mm^2)	Grade of Reinforcement (Specified yield strength f_y (N/mm^2))		
	SD295	SD345	SD390
18	25 d_b	30 d_b	33 d_b
21	23 d_b	27 d_b	31 d_b
24	22 d_b	25 d_b	28 d_b
27	20 d_b	23 d_b	26 d_b
30	19 d_b	22 d_b	25 d_b
36	17 d_b	19 d_b	22 d_b
42	15 d_b	17 d_b	20 d_b
48	14 d_b	16 d_b	18 d_b
54	12 d_b	14 d_b	16 d_b
60	11 d_b	13 d_b	15 d_b

5. CONCLUSIONS

The 1999 revision to the AIJ Standard introduced more rational design requirements for bond, anchorage, and splices. However, more than a few specifications are based on the limited experimental findings obtained from the element test specimens for bond and anchorage. The bond and anchorage abilities in actual members are highly dependent on the surrounding stress conditions of the concrete and the cracking behavior. It is important to consider the behavior of the members or the behavior of a structure after the bond has deteriorated. For anchorage and splices, full-strength (factored yield strength) development and transfer should be the criterion. On the other hand, the influence of bond deterioration on member performances considering shear, flexure, and axial loads should be examined for the design criteria of the bond requirement.

Based on the foregoing discussion, further research effort seems to be required on the following:
(1) Splitting bond deterioration behavior in beam and column bars under reversed cyclic seismic loadings;
(2) The role of bond capability in the performance of a member considering shear, flexure, and axial loadings;
(3) The differences of bond behaviors in anchorage, lap splices, and cut-off bars;
(4) The interactions between anchorage failure and shear failure in beam-column joints;
(5) Joint shear capacity and the capability of the vertical load support, depending on the anchorage details in the exterior and corner column-beam joints, and
(6) The size dependence of the bond and anchorage properties.

Acknowledgments

The members of the committee for the revision of the *AIJ Standard* (Chairman: Prof. Shizuo Hayashi, Tokyo Institute of Technology) are gratefully acknowledged.

References

Architectural Institute of Japan. 1997. *Design guidelines for earthquake resistant reinforced concrete buildings based on inelastic displacement concept (draft).* Tokyo: AIJ.

Architectural Institute of Japan. 1996. *AIJ design guidelines of lap splices for splicing all bars at the same section (draft).* Tokyo: AIJ.

Architectural Institute of Japan. 1991. *AIJ standard for structural calculation of reinforced concrete structures.* Tokyo: AIJ. (English version published 1985.)

Architectural Institute of Japan. 1990. *Design guidelines of earthquake resistant reinforced concrete buildings based on ultimate strength concept.* Tokyo: AIJ. (English version was published in 1994.)

Fujii S., Morita S., Kawakami S., and Yamada T. 1991. Re-evaluation of test data on 90 degree bent bar anchorage. *J. of Structural and Construction Engineering (Transactions of AIJ)* 429 (November 1991): 65–75 (In Japanese.)

Joh O., Goto Y., and Shibata T. 1993. Anchorage failure mode and performance of 90-degree hooked beam bars anchored to R/C beam-column joints. *Proceedings of Japan Concrete Institute*, Vol.15, No. 2, 159–164 (In Japanese.) (References 5 and 6 are reviewed in Fujii S., Noguchi, H., and Morita, S. Bond and anchorage of reinforcement in high strength concrete. *ACI SP*-176, 23–43, 1998

Morita, S. and Fujii, S. 1982. Bond capacity of deformed bars due to splitting of surrounding concrete. *Bond in Concrete,* P. Bartos, ed., 331–41. London: Applied Science Publishers.

Keywords

Bond, anchorage, lap splice, development length, standard hook, beam-column joint, shear, splitting bond failure, projected development length, slip

GLOBAL VERSUS ELEMENTAL RETROFIT SCHEMES IN PERFORMANCE-BASED DESIGNS

John D. HOOPER[1]

ABSTRACT

This paper compares global versus elemental retrofit schemes for a generic two-story concrete frame building. The process of establishing the retrofit schemes, including a description of the evaluation procedure and definition of performance objectives, is also presented. Especially for enhanced seismic performing global retrofit schemes are generally selected due to cost, the limited area of the building that is affected, and construction constraints especially in occupied buildings.

1. PROCESS FOR ESTABLISHING RETROFIT SCHEMES

1.1 Introduction

The process for establishing a retrofit scheme commences with a detailed evaluation of the existing building. Once the building deficiencies are identified, generally on an element-by-element basis, and the damage (limit) states predicted, the retrofit scheme can be determined. Detailed evaluation guidelines have been developed which assist in establishing these limit states. A brief discussion of these guidelines is presented below.

1.2 Detailed Evaluation Guidelines

Numerous guideline documents are available that are used in establishing the damage states of the elements and the likely performance of the overall system. The most commonly used guideline documents include the following:

- FEMA 178 *Handbook for the Seismic Evaluation of Existing Buildings*
- FEMA 273 *Guidelines for Seismic Rehabilitation of Buildings*
- ATC 40 *Methodology for Evaluation and Retrofit of Reinforced Concrete Structures*

[1] *Skilling Ward Magnusson Barkshire Inc., Seattle, Washington*
Email: jdh@skilling.com

Typically, these guidelines are utilized as a framework for identifying element damage states. Important information regarding analysis techniques is also presented but, once again, generally serve as guidance only—engineering judgment, especially for those experienced in the evaluation and retrofit of existing buildings, is exercised regularly in practical applications.

1.3. Establishing Damage States

As discussed above, the process in establishing an appropriate retrofit scheme for an existing concrete building begins with a detailed evaluation to ascertain the damage states of its elements. Identification of damage states for both the "primary" lateral load-resisting system and the "secondary" gravity load-resisting system is required, especially when utilizing FEMA 273 as the basis for the evaluation. Many times, the retrofit scheme selected is governed by the performance of secondary system elements.

For concrete buildings, the primary and secondary elements comprise the following:

- Columns
- Beams and slab-beams
- Beam-column joints
- Foundations

The analysis method selected generally determines the method for establishing the damage states for the elements. For example, linear procedures utilize element demand-to-capacity ratios, based on the shear, moment, and axial acting of the element. For the more sophisticated nonlinear approaches, maximum element rotations or interstory drift indices are determined and compared to the their respective capacities.

It is important to establish the global displacement or interstory drift when the elements first reach yield as well as at structural collapse. This is necessary for identifying the performance of the building at multiple performance levels. Nonlinear static procedures are particularly useful in this regard.

1.4. Establishing the Performance Objective for the Retrofit

The initial step when selecting an appropriate retrofit is establishing the anticipated performance. This involves selecting performance level(s) for given seismic hazard(s). The selection of both establishes the performance objective for the retrofit. For instance, two basic performance objectives are defined in FEMA 273, (1) Basic Safety Objective and (2) Enhanced Objective. Other guideline documents present different, yet similar, definitions for performance. With these documents supplying the basic definitions, the design team (architect and engineer) can present these performance objectives to owners for selection and implementation.

The Basic Safety Objective (BSO) is selected for the retrofit of most buildings. The BSO is generally considered equivalent to the design intent for new buildings. A common alternate name for the BSO is Life Safety, which actually represents the typical structural performance level that is evaluated using this objective. The Enhanced Objective (EO) provides performance that exceeds the BSO. The EO is selected for buildings that house police stations, hospitals, or other essential facilities that are needed following a major earthquake. This objective is also commonly referred to as Immediate Occupancy, which, as Life Safety is to the BSO, represents the structural performance level that is typically evaluated.

2. ELEMENTAL AND GLOBAL RETROFIT SCHEMES FOR CONCRETE BUILDINGS

2.1. Background

Retrofit schemes can generally be categorized into one of three of the following:

1. Elemental improvements to enhance the capacity of the identified deficient members.
2. Global improvements to reduce the demand on existing **elements** found to be deficient, generally by reducing global drifts or by reducing energy dissipation in existing building elements.

3. A combination of elemental and global improvements, with the major emphasis, typically, on a global scheme.

The following sections describe, in more detail, both element and global retrofit schemes for a typical concrete frame building.

2.2. Elemental Retrofit Schemes

Elemental retrofit schemes are defined as those that strengthen or upgrade the deficient elements identified in the detailed evaluation process. Examples of elements that are typically upgraded in concrete frame buildings are presented below.

2.2.1. Columns

Due to the reinforcement detailing practice that was used in most columns prior to the mid-1970s, there are several conditions that generally require upgrading.

- Column confinement at flexural hinges
- Column bar splices, especially those that occur just above the floor line
- Column shear capacity, especially in columns reinforced with ties, in lieu of spirals
- Column axial capacity, especially at the ends of frames and walls

Upgrade techniques to mitigate these conditions include

- Wrapping the columns using steel, carbon or fiberglass to improve the confinement at potential flexural hinge and splice locations. These wraps can also be used to improve the column's flexural and shear capacity.
- Adding a layer of concrete to improve the axial, flexural and shear capacity of the column.

2.2.2. Beams

Inadequate detailing, relative to today's standards, results in the following conditions that generally require improvement.

- Beam confinement at flexural hinges
- Bottom steel termination at face of column
- Lack of shear reinforcement, especially in slab-beams and beams reinforced with bent bars
- Deep, perimeter spandrel beam configuration

Upgrade techniques to mitigate these conditions include

- Augmenting the beams using steel, carbon or fiberglass to improve the confinement at the potential flexural hinge, which can also be used to improve the beam's flexural and shear capacity
- Splicing reinforcing steel through the column to enhance beam continuity
- Adding a partial concrete cover or steel rods to improve the shear capacity of the beam
- Weakening the spandrel beam by slotting the beam adjacent to the column to reduce the force transfer into the column

2.2.3. Beam-Column Joints

The beam-column joints are deficient in the majority of concrete frame buildings constructed prior to the mid-1970s. Little regard was given to the force transfer mechanism that occurs as the beams deliver the shear force into the joint, resulting in beam-column joints with little or no reinforcement. Techniques to improve the capacity include wrapping the joint with carbon fiber or steel, or by adding steel rods through the joints.

2.3. Global Retrofit Schemes

Global retrofit schemes are those that upgrade the entire building by adding strength, stiffness, or damping. The selected system is sized to reduce the demand on the deficient elements to acceptable levels. The new elements that comprise the global retrofit scheme should be designed and, more importantly, detailed to meet the requirements of the latest building code. Three examples of global retrofit schemes are presented below.

2.3.1. Concrete Shear Walls

Perhaps the most cost-effective global retrofit scheme, especially for concrete frame buildings, consists of adding concrete shear walls. The concrete shear walls are typically doweled into the existing columns as are the wall ends to aid in overturning resistance. The walls are generally connected to the diaphragm by coring the concrete slab and adding reinforcing bars that connect the walls and floors. Depending on the wall layout and diaphragm capacity, collector elements are added to transfer the loads into the walls. The foundation connection is also an important load transfer mechanism that is required to complete the load path.

Unless located around the elevator or stair cores, the concrete shear walls typically have a major impact on the building's architecture. Foundation improvements, through the addition of piles, grade beams, or footings are also often required.

2.3.2. Steel Braced Frames

Steel braced frames provide a reasonable, cost-effective alternative to adding concrete shear walls. The challenging aspect of adding steel braced frames is in transferring the earthquake load into the new braces. This force transfer is generally accomplished by attaching new steel members, including columns, beams, and collector, to the existing concrete elements using epoxy bolts.

As with the concrete shear walls, steel braced frames can have a significant impact on the building's architecture. Improvements to the building's foundation are also generally affected, resulting in the addition of new footings or piles under the braced frame columns.

2.3.3. Steel Braced Frames with Added Damping

Interstory drift demands, especially for an Enhanced Objective, can be achieved through added damping. These devices generally consist of one of the following types:

- Friction
- Viscous

- Visco-elastic
- Material yielding

Drift demands can be reduced by up to a factor of 2 or 3, depending on the building's strength and stiffness, thus minimizing the demands on the existing elements. Steel braced frames are generally the most cost-effective way to introduce added damping into a building. The steel braced frames are usually connected to the existing concrete elements as described above.

3. COMPARISON OF ELEMENTAL AND GLOBAL RETROFIT SCHEMES

3.1. Pros and Cons of Elemental and Global Retrofit Schemes

Although every existing building presents its own unique deficiencies and, hence, affects the selection of the appropriate retrofit scheme, the issues regarding elemental and global retrofit schemes are generally similar. The table 1 highlights the typical pros and cons of the two retrofit scheme approaches.

Table Typical Pros and Cons

Elemental Retrofit Schemes		**Global Retrofit Schemes**	
Pros	**Cons**	**Pros**	**Cons**
Keeps architecture relatively unchanged	Disrupts area around all strengthened elements	Limits disruption to limited areas	Affects building architecture, sometimes significantly
Usable square footage relatively unchanged	Difficult to perform in occupied buildings	Feasible in occupied buildings	Can reduce usable square footage in area of retrofit
Extremely redundant and reliable: all deficient elements retrofitted	Costs are usually high and can affect other services	Costs are usually reasonable, if foundation work is limited	Foundation retrofits are often required

Specific comparisons for a generic concrete frame building are presented in Section 3.2.

3.2. Examples of Retrofit Schemes

Four example retrofit schemes are presented in figures 1 through 4 below, along with their specific pros and cons. These retrofit schemes have been prepared for a generic, two-story concrete frame structure constructed in the 1950-1960s. The frame exhibits the following deficiencies based on the detailed evaluation.

- Column confinement at potential flexural hinges
- Column bar splices, especially those that occur just above the floor line
- Column shear capacity, especially in columns reinforced with ties, in lieu of spirals
- Deep, perimeter spandrel beam configuration

The building is partially occupied by a data center that operates 24 hours a day, 7 days a week. This area of the building requires extreme care in implementing the retrofit. Due to the operational requirements of the remaining tenants, an Enhanced Objective has been selected by the owner.

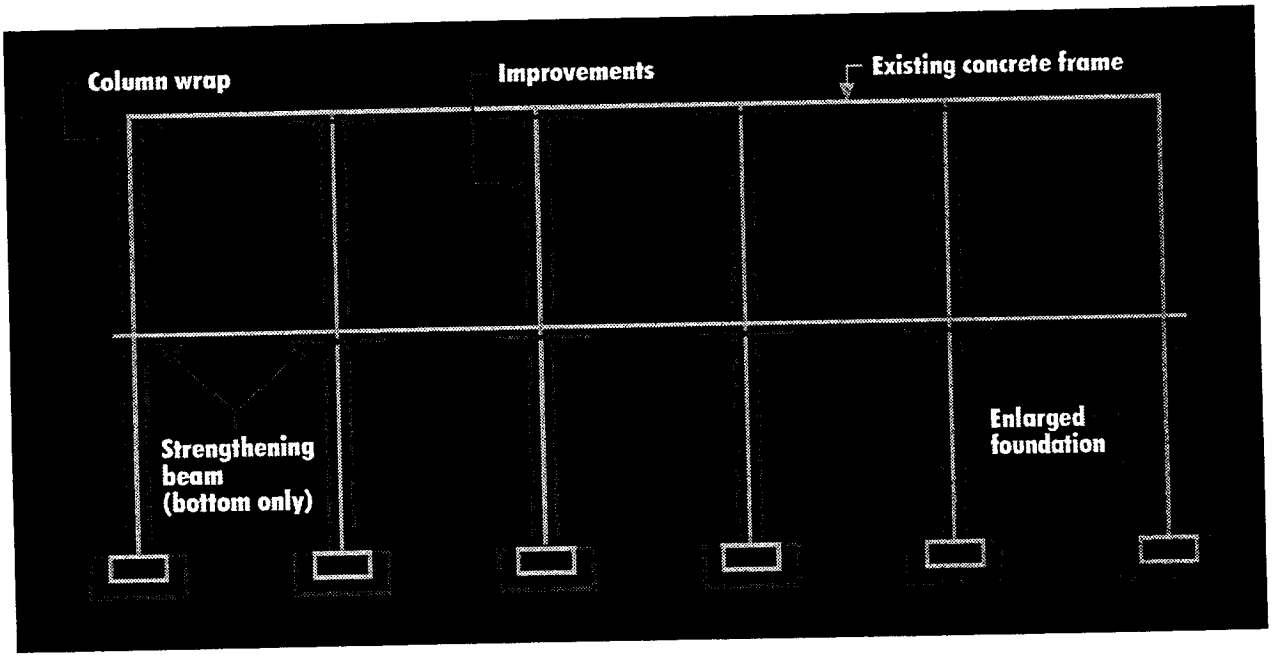

Pros
- Architecture relatively unchanged
- Usable square feet relatively unchanged
- Extremely redundant and reliable; all elements retrofitted

Cons
- Disrupts area around all strengthened elements, especially at exterior
- Difficult to perform in occupied buildings
- Costs usually fairly high

Figure 1. Elemental Improvements

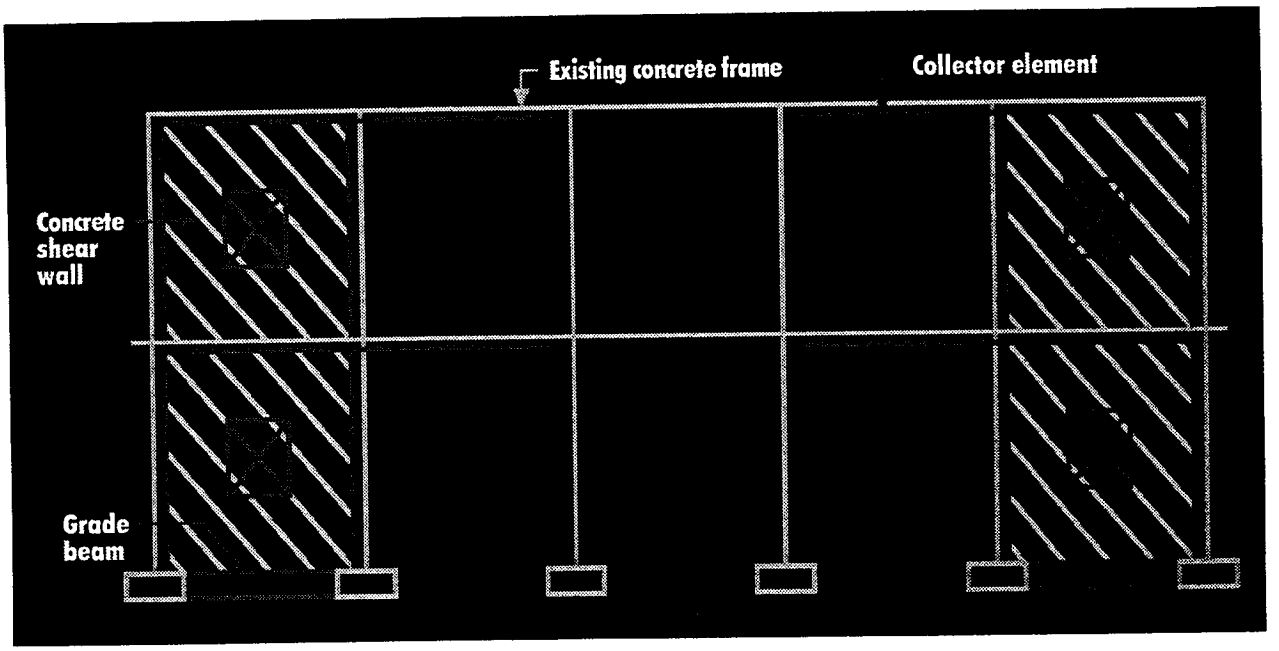

Pros
- Limits disruption to select areas
- Feasible for occupied buildings
- Costs usually reasonable

Cons
- Affects architecture, sometimes significantly
- Can reduce usable square feet
- Limited system redundancy

Figure 2. Global Improvements—Concrete Shear Walls

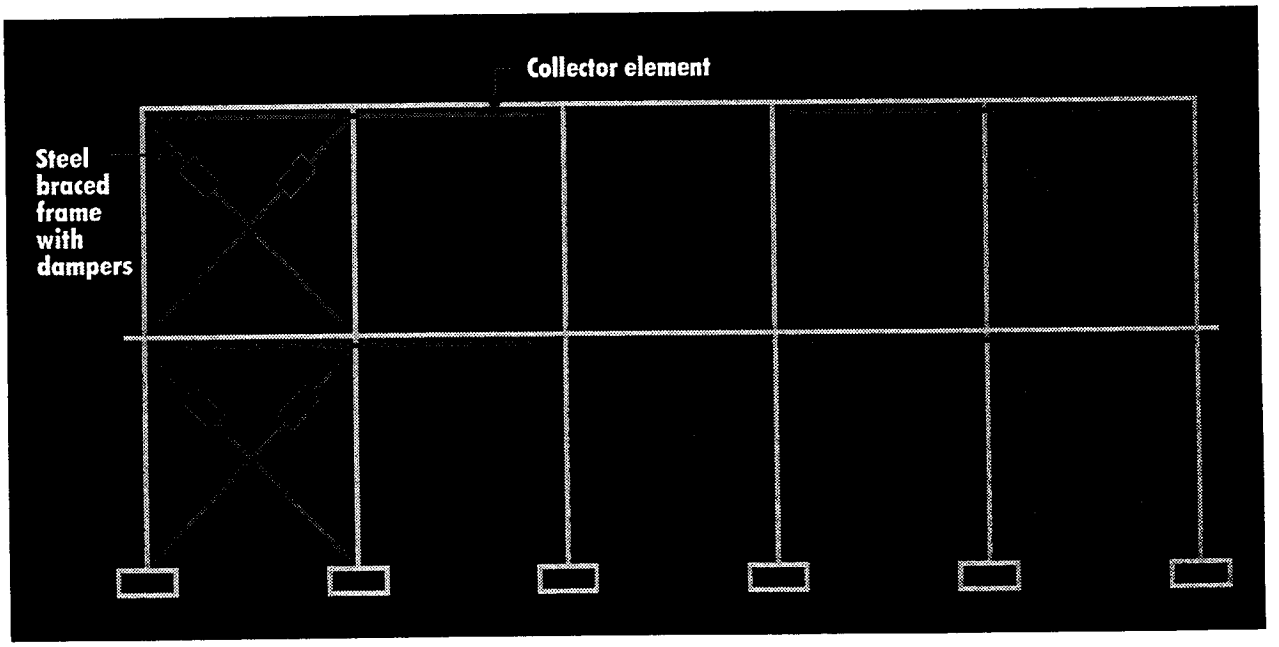

Pros
- Limits disruption to select areas
- Feasible for occupied buildings
- Costs usually reasonable
- System reliability enhanced with dampers
- Can help eliminate foundation improvements

Cons
- Affects architecture, sometimes significantly
- Can reduce usable square feet

Figure 3. Global Improvements—Steel Braced Frames with Dampers

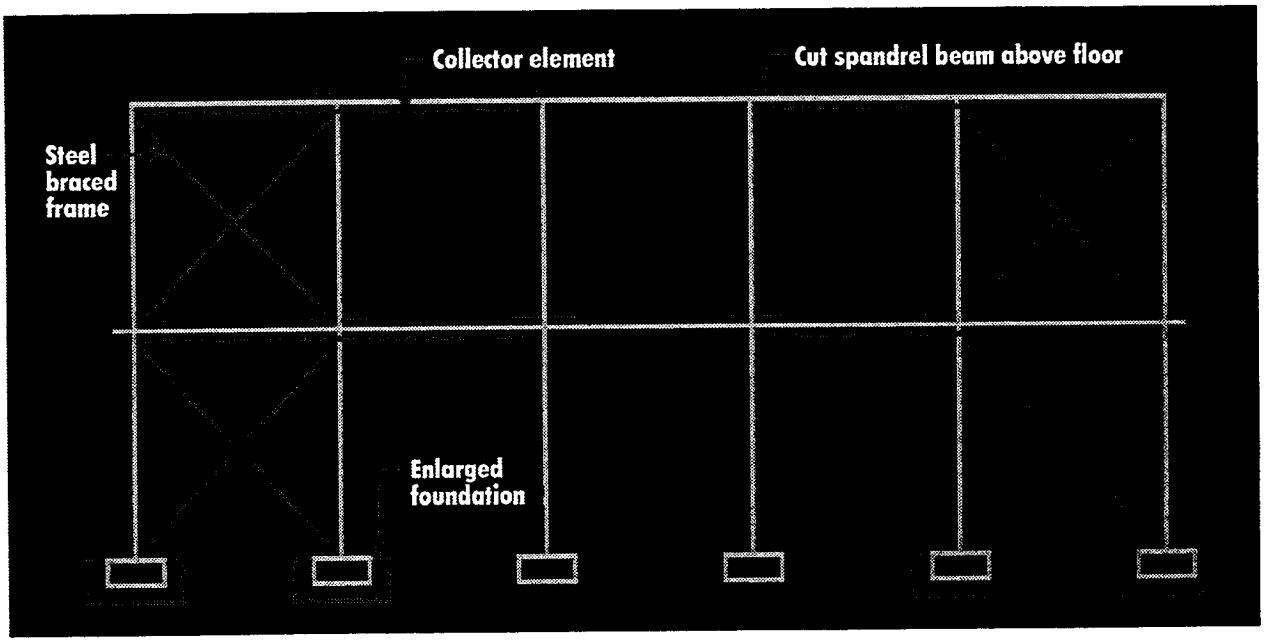

Pros
- Limits disruption to select areas
- Feasible in occupied buildings
- Costs usually reasonable, if foundation work is limited

Cons
- Affects architecture
- Can reduce usable square feet
- Limited system redundancy

Figure 4. Combined Elemental/Global Improvements—Steel Braced Frame with Select Elemental Improvements

4. SUMMARY

Global and elemental retrofit schemes in performance-based designs have been presented. The steps necessary to select the appropriate retrofit schemes are summarized below.

- A detailed evaluation must be performed and the deficiencies identified.
- The performance objective needs to be selected.
- Retrofit schemes need to be developed that satisfy the selected performance objective.
- Select the retrofit scheme that meets the overall goals of the project.

The pros and cons for the two approaches, elemental and global, have been presented. The effects on the existing structure are quite different, including costs and impact on architecture, and need to be considered on a case-by-case basis.

Global retrofit schemes are generally selected for Enhanced Objectives due to cost, the limited area of the building that is affected, and the construction constraints in an occupied building. Utilizing combined retrofit schemes, adding a global system while strengthening existing, deficient elements, is generally required; it is rare when global retrofits alone mitigate all the identified deficiencies.

KEYWORDS: Performance-Based Design, Seismic Retrofit, Concrete Structure, Global, Elemental Scheme, Evaluation Process

NEW FRAMEWORK OF SEISMIC AND STRUCTURAL PROVISIONS IN JAPAN

Masaomi TESHIGAWARA[1], Hisahiro HIRAISHI, Hiroshi KURAMOTO

Mitsumasa MIDORIKAWA, Wataru GOJO, Izuru OKAWA

ABSTRACT

The Japanese Building Code related to the structural engineering will be drastically revised from the prescriptive type of the provisions to the performance-based one. There are two kinds of performance requirements for the seismic provisions in the new code : human life safety and damage control of a building corresponding two earthquake motion levels. The return periods of this two earthquake motion levels are approximately 500 years and approximately 50 years, respectively. The earthquake motion is defined as the design acceleration response spectrum in the code which is specified at the engineering bedrock in order to take the soil condition and soil-structure interaction effect into consideration as properly as possible. Here, the engineering bedrock is defined based on shear wave velocity of the soil at a site. The ordinate of the design response spectrum is determined by considering historical seismicity data, seismo-tectonic zones and active faults of the region.

The response values of structures are estimated based on this design response spectrum. They should be less than the limit values such as deformation capacity of structural members.

1. INTRODUCTION

Japanese Building Standard Law was revised in 1998. The highlight related to the structural engineering is the drastic revision from the prescriptive type of the provisions to the performance-based one. The detailed specification is now under development and new code related to structural engineering will be enforced by June 2000. In the proposal developed under the revised Law, the precise definitions for performance requirements and verification method based on accurate response and limit values are specified so that the code should be applicable to any kind of materials and any type of structures such as seismic isolation systems as long as the material property is clear and the structural behavior of a building is appropriately estimated.

This paper presents the framework and concepts of the proposal developed by Building Research Institute for the new performance-based structural provisions, focusing on earthquake engineering.

2. CONCEPTUAL FRAMEWORK OF PERFORMANCE-BASED STRUCTURAL CODE

The conceptual framework of performance-based structural code proposed by BRI is shown in Figure 1. Following the principles of structural requirement, the evaluation procedures to be used for the estimation of structure's conformity with the required performance level are roughly classified as: Proposed route, Conventional route, Small building route and Others.

1 Building Research Institute, Ministry of Construction, Tsukuba, Japan
E-mail: teshi@kenken.go.jp

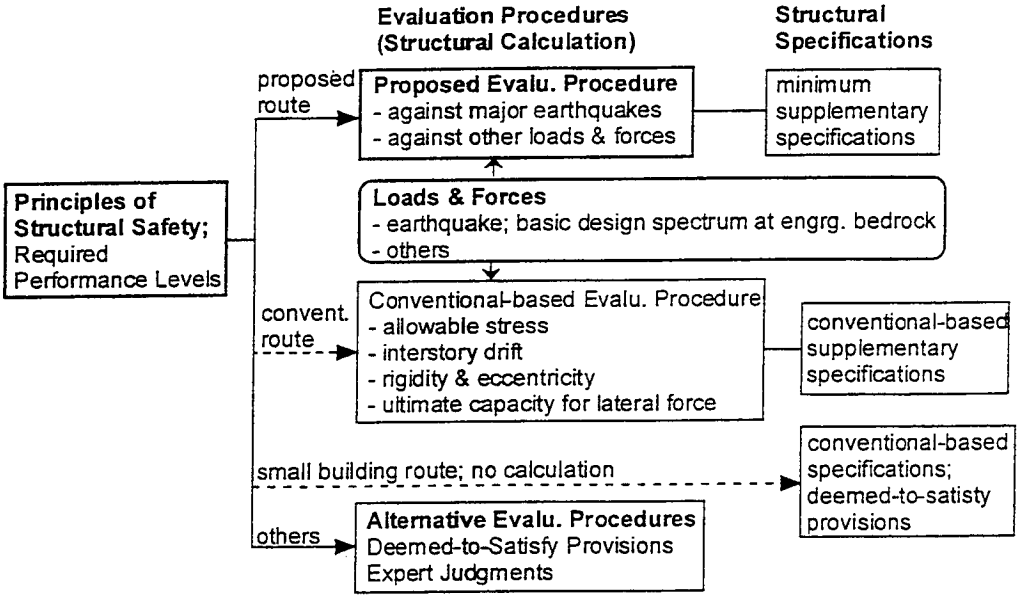

Figure 1: Conceptual framework of proposed performance-based structural provisions

The proposed route represents a new evaluation procedure to be used as well as the current one. The current one is based on the calculation of allowable stress and estimation of ultimate capacity for lateral load. It considers the major earthquakes as well as other forces and loads. The other effects, which are not considered in the structural calculations, such as construction quality, durability, quality of construction materials, and nonstructural elements, are covered by structural specifications. In essence, by using this procedure it is possible to evaluate and verify the structural performance possessed by a designed structure, regardless of the design method used. It is just an evaluation procedure that verifies whether or not the prescribed performance objectives are met.

The second route represents the conventional evaluation procedure now in use, adopted as the standard structural calculation method. It can be supplemented with additional provisions in addition to those of the first route described above. However, if the principles of performance-based provisions are to be followed, it should be noticed that the obviously unnecessary parts to be considered by structural calculations are eliminated. To this extent, this route can be considered as a kind of deemed-to-satisfy evaluation procedure.

The third route is applied to small buildings. This route does not require structural calculations and is considered to be deemed-to-satisfy provisions. It prescribes only conventional-based structural specifications.

In the fourth route are included all other alternative evaluation procedures and deemed-to-satisfy provisions, such as those developed and certified by private institutions as well as those requiring expert judgments.

The types of loads and forces considered in the newly proposed evaluation procedure remain almost the same with those currently in use. However, for the case of seismic effects, new earthquake motion provisions are prepared to replace the current earthquake force provisions.

In a definite proposal, the earthquake motion response spectra at the engineering bedrock,

assumed to be the stratum having shear wave velocity in the range of several hundreds m/s, is considered as the basic design spectra. On the basis of this conception for the earthquake input motion, it is possible that earthquake effects is not only accounted rationally through the incorporation of influence of local soil conditions on ground motion characteristics at the free surface but also conveniently incorporated in the newly developed design procedures of seismically isolated and response controlled structures. Furthermore, it is anticipated that the future proposals expected for the evaluation and design procedures are suitably implemented.

3. REQUIRED SEISMIC PERFORMANCE LEVEL'S FOR BUILDING STRUCTURES

An outline of requirements for building structures and earthquake motion levels is shown in Table 1. In the vertical column on the left hand side of the table are shown the requirements for building structures, while in the rest of the table are shown the earthquake motions to be considered and their corresponding levels for each of the requirements assigned for building structures.

As it is shown in Table 1, the requirements for building structures are classified in two categories, which are described below.

Table 1: Seismic performance requirements for building structures and earthquake motion levels illustrating representative response/limit values

<table>
<tr><th>Requirement</th><th colspan="3">Earthquake</th></tr>
<tr><td rowspan="2">(a) Life Safety
(to prevent failure of stories in structural frames)</td><td rowspan="2">Maximum Earthquake to be considered (earthq. records, seismic and geologic tectonic structures, active faults, etc.)</td><td>Response Value</td><td>Maximum Internal Force/Displacement</td></tr>
<tr><td>Limit Value</td><td>Limit Strength/Displacement *1</td></tr>
<tr><td rowspan="2">(b) Damage Limitation
(to prevent damage to structural frames, members, interior and exterior finishing materials in order to avoid the conditions not satisfying the requirement (a) and others)</td><td rowspan="2">Once-in-a-lifetime Event (return period: 30-50 years)</td><td>Response Value</td><td>Internal Force/Displacement taking place at each structural element</td></tr>
<tr><td>Limit Value</td><td>Limit Strength/Displacement *2</td></tr>
</table>

Notes:

*1 - Repeating cycles effect at plastic region of response to be taken into account.

*2 - The whole building structure behaves roughly within elastic range.

1) The limit values corresponding to Maximum Event Level are determined based on the condition that equilibrium of forces and displacement compatibility in the structural system are guaranteed.

2) Displacement and acceleration related limit values, determined on the basis of the requirements for architectural, mechanical and electrical elements permanently attached to building structures, are thought to be considered in certain cases.

3) The deterioration of materials during the lifetime of a structure should be considered.

3.1 Life Safety

The essential purpose of this requirement is the safety of human life. It should be expected that under the action of earthquake motions taken into consideration, not only the building as a whole but also any story of the building should not experience any story collapse.

3.2 Damage Limitation

The aim of this requirement is damage limitation. Under this provision, it is required first that after the action of earthquake motions taken into consideration, no structural damage which could threaten the structural safety of the building will take place. In other words, the structural safety performance required for life safety should be preserved even after the earthquake considered. Furthermore, it is required that no other kind of damage causing in the building structure a situation which does not comply with other requirements of the Building Standard Law, concerning fire safety should be experienced.

3.3 Maximum Earthquake Motion Level

This level of earthquake motions corresponds to the category of requirements for life safety for building structures and is assumed to produce the maximum possible effects on the structural safety of a building to be constructed at a given site. The maximum possible earthquake motion level is determined on the basis of historical earthquake data, recorded strong ground motions in the past, seismic and geologic tectonic structures, active faults, and others. This earthquake motion level corresponds nearly to that of highest earthquake forces used in the current seismic design practice, representing the horizontal earthquake forces induced in the building structures in case of major seismic events.

3.4 Once-in-a-Lifetime Event Level

This level of earthquake motions corresponds to the category of requirements for damage limitation for building structures and is assumed to be experienced more than once during the lifetime of the building. A return period interval of 30-50 years is supposed to cover these events. This level of earthquake motion corresponds nearly to the middle level earthquake forces used in the current seismic design practice, representing the horizontal earthquake forces induced in the building structures in case of moderate earthquakes.

4. Design Earthquake Motion

The design seismic force currently in use specifies the story shear force without apparent prescription of the ground motion. Therefore, this method is so easy to pursue the design procedure. However, a contradiction exists in this method that the derived earthquake ground motions are not equal even within the class, since the design force is derived from the response values of the building itself and the design force is prescribed uniformly with a class of buildings. Considering these situations, it is concluded that the seismic design should start with the defining the input earthquake ground motion. This also coincides with the idea of performance-based structural design aiming at more flexible design.

4.1 Design Response Spectrum at Engineering Bedrock

The ground motion is represented with its acceleration response spectrum in the new

provisions. The basic ground motion is firstly defined at the engineering bedrock corresponding to the seismicity of the area. The engineering bedrock is defined herein as follows. The engineering bedrock is underlain in the underground within the area. The geotechnical data is mostly obtained in the investigations conducted within the area. And also the considerable number of strong motion data is obtained and the characteristics are evaluated with the recordings at the depths. This upper face of the soil layer is defined as engineering bedrock. This definition of engineering bedrock gives the idea of layers with shear velocity larger than approx. 400m/s. The amplification characteristics of the surface soil layers are to be evaluated with the geological data of the site.
The design earthquake ground motion is represented in the following equation.

$$S_A(T) = Z \cdot G_s(T) \cdot S_0(T) \qquad (1)$$

Where,

$S_A(T)$= design earthquake ground motion,
Z = regional seismicity coefficient,
$G_s(T)$=amplification of surface soil,
$S_0(T)$= basic spectrum at exposed engineering bedrock, and
T = period in second.

The basic spectrum is set up to be very basic. It consists of two parts, i.e., a uniform acceleration portion in shorter periods, and a uniform velocity portion in longer periods. The two intensities of uniform levels are determined with expected peak values and response factors for acceleration and velocity. The intensity level of the design motion is based on the design force for the intermediate soil class specified in the current Building Standard Law of Japan. In addition, the relationship between the story shear force and the input motion is also taken into consideration.

The resultant design ground motion for capacity design is defined as 0.8G for the 5% damping acceleration response spectrum and as 80cm/s for the 5% damping velocity response spectrum at the exposed engineering bedrock. For the periods shorter than 1/4 of the intersection of the uniform acceleration and the velocity, the spectral values are reduced so that the acceleration amplitude at zero period equals to the peak acceleration of the input motion. The peak acceleration is set to 1/2.5 of the uniform acceleration level. The design spectrum thus defined is shown in Figure 2.

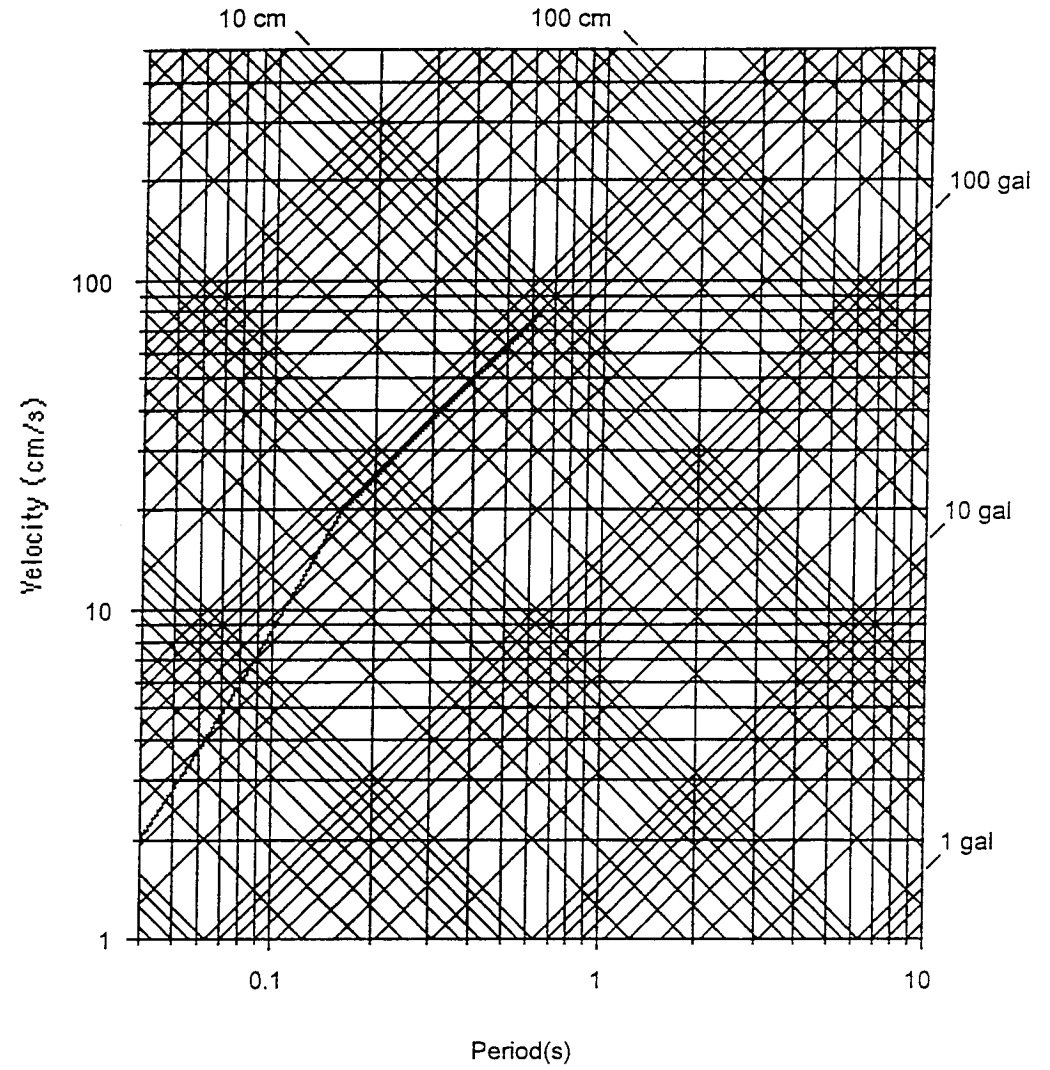

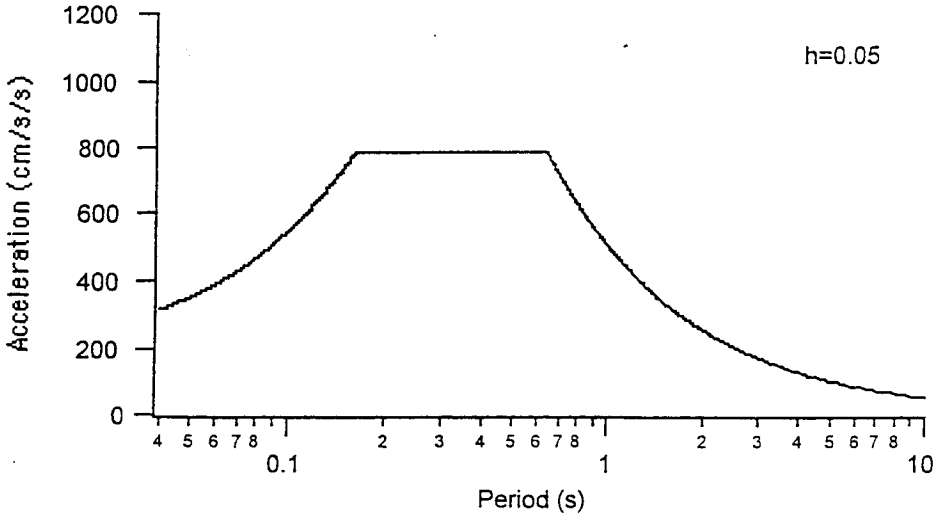

Figure 2: Design response spectrum of major earthquake motion at the exposed engineering bedrock

4.2 The Regional Seismicity Coefficient

The research on the seismic hazard map on which the coefficient is based has been continued from the pioneering work by Dr. Kawasumi [Kawasumi,1951]. The advances in the prediction methodology of strong ground motion with the collection of strong motion records for near source region in this decades have become a thrust to upgrade the site-specific design earthquake motion to date. The regional seismicity coefficient is evaluated as relative factors representing the difference in the expected ground motion parameters such as peak ground acceleration or peak ground velocity with regions for both of large and intermediate earthquake motions. In addition, since the frequency content presumably differs in the expected values, the coefficients are to be defined with separately for acceleration and velocity, respectively. Therefore, as results, the four types of coefficients are proposed reflecting the intensity levels and the frequency contents.

To prepare the regional maps, the following two ground motion levels are defined.

1) Large earthquake motion which is represented by the largest annual maximum in 500 years.
2) Intermediate earthquake motion which is represented with the 10^{th} largest annual maximum in 500 years.

The data used in this study are as follows.
1) Earthquakes occurring during 1496-1984 selected from the Usami's Engineering Catalogue.
2) Earthquake data issued from the Japan Meteorological Agency (JMA) during 1985-1995.
3) Fault parameters which have been proposed for major past earthquakes.

The following two empirical formulae (attenuation formulae) were used to estimate the peak amplitudes for the earthquakes. These formulae are applicable to the near source area such as Kobe during the 1995 Hyogo-ken Nambu Earthquake.

1) Peak ground acceleration (A) for the diluvial soil class [Fukushima,Tanaka,1992]

$$\log A = 0.51M - \log[R + 0.006 \cdot 10^{0.51M}] - 0.0033R + 0.59 \qquad (2)$$

Where,

A= peak ground acceleration (cm/s^2),
M= earthquake magnitude, and
R= the closest distance to the fault plane in kilometer.

2) Peak ground velocity (V) for the engineering bedrock level [Midorikawa,1993]

$$\log V = -0.22M^2 + 3.94M - \log[R + 0.01 \cdot 10^{0.43M}] - 0.002R - 11.9 - 0.71 \cdot \log Vs \qquad (3)$$

Where,

V= peak ground velocity (cm/s),
M_w = moment magnitude,
R = the distance to the fault rupture zone (km), and
Vs = average shear wave velocity for upper 30m surface soil deposit (m/s).

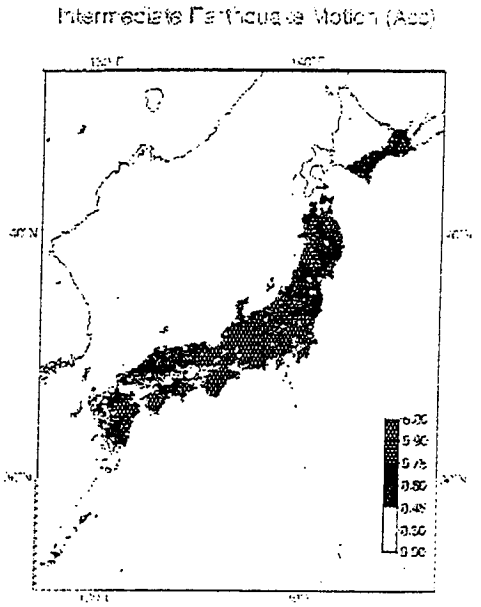

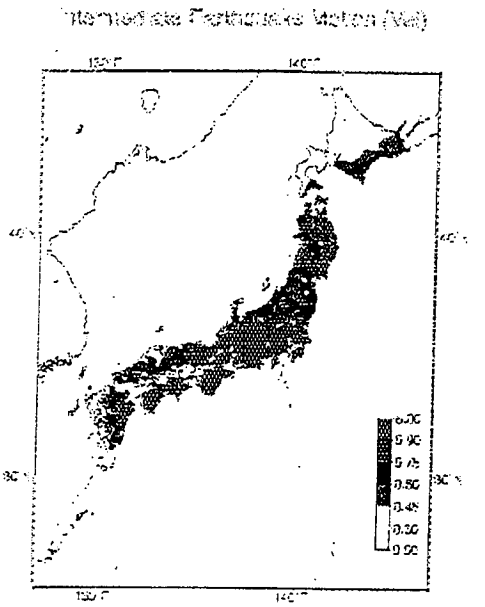

Figure 3(a): Distribution of PGA at engineering bedrock expected in 50 years (normalized with 0.064G)

Figure 3(b): Distribution of PGV at engineering bedrock expected in 50 years (normalized with 8cm/s)

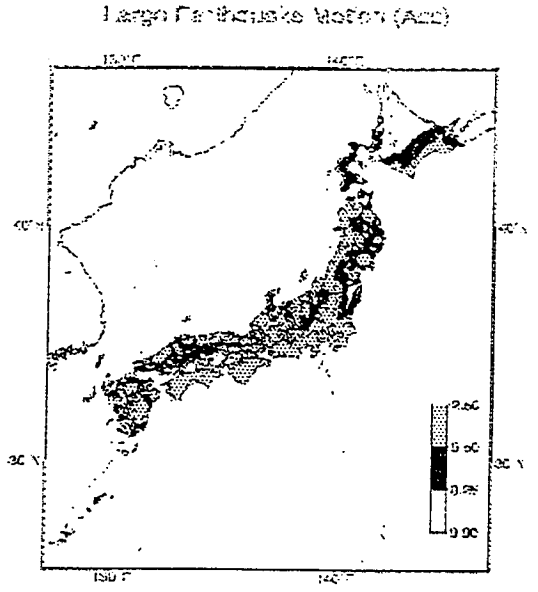

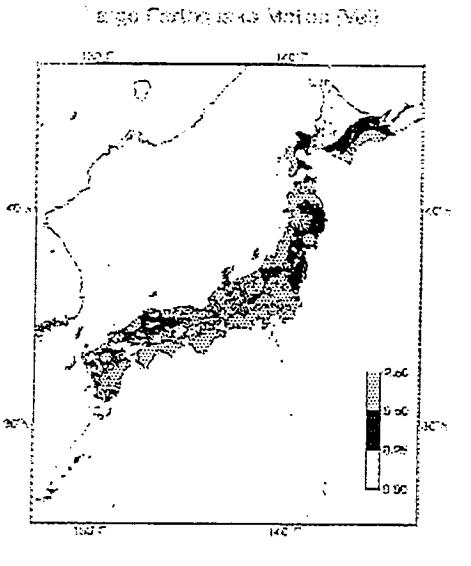

Figure 3(c): Distribution of PGA at engineering bedrock expected in 500 years (normalized with 0.32 G)

Figure 3(d) : Distribution of PGV at engineering bedrock expected in 500 years (normalized with 40 cm/s)

For peak ground velocity, the JMA magnitude is used in place of moment magnitude, since both are approximately equal in values for the scope of our study. The shear wave velocity 600 m/s was used for computation, although this does not affect the result as far as the relative regional difference is concerned.

Using these formulae, the expected peak values for each location were calculated. Regional maps were drawn based on the computed vales normalized by 0.32G and 40cm/s for large earthquake motion, and 0.064G and 8cm/s for intermediate earthquake motion, respectively. The maps are shown in Figure3a-3d. It is seen that larger expected values are found corresponding the epicentral locations of bigger earthquakes. For large earthquake, most locations show the ratio below 2.5 in comparison of the previously mentioned engineering bedrock intensity levels for acceleration, and below 2.5 for velocity levels. The expected intensity levels estimated with the data in 500 years are comparable with or slightly larger than the level of seismic force currently in use for the second class of soil condition.

The maps shown herein are examples of evaluation using the sets of proposed empirical formulae and generally available data. Therefore, a more extensive study including applying other methodologies or referring other proposals will be necessary to establish the regional seismicity coefficient maps to be specified in the building code or provisions.

4.3 Evaluation Procedure of Acceleration Response Spectrum at Ground Surface

To evaluate the acceleration response spectrum at the ground surface, the amplification of surface soil deposits on the engineering bedrock is estimated. An evaluation procedure by using the equivalent linearization technique considering nonlinear soil properties is expressed in the followings. The simplified analytical method in this procedure is proposed and examined in detail elsewhere [Miura et al., 2000].

(1) *Transformation of response spectrum defined at outcrop engineering bedrock*: The earthquake motion defined at the outcrop engineering bedrock is given as an acceleration response spectrum with 5% damping ratio, $S_A(T, \xi=0.05)$. $S_A(T, \xi=0)$, a velocity response spectrum, $S_v(T, \xi=0)$, and a Fourier spectrum of acceleration, $F_A(T)$, have the approximate relations as follows.

$$F_A(T) \approx S_v(T, \xi = 0) \approx (T / 2\pi) S_A(T, \xi = 0) \tag{4}$$

(2) *Eigen value analysis of soil profile*: Subdividing the soil profile, a shear model of n degrees of freedom is formed. The natural period, T_i, the vibration mode, U_i (normalized by the value at the surface), and the modal damping ratio, ξ_i, are obtained through the eigen value analysis.

(3) *Equivalent shear wave velocity and impedance*: The surface soil layers are replaced to an uniform stratum with an equivalent shear wave velocity, V_{se}, and an equivalent mass density, ρ_e, and an equivalent damping ratio, ξ_1, which are calculated from the properties of each soil layer.

$$V_{se} = \frac{1}{H} \sum_{i=1}^{n-1} V_{si} d_i \tag{5}$$

$$\rho_e = \frac{1}{H} \sum_{i=1}^{n-1} \rho_i d_i \tag{6}$$

Where, $V_{si} = \sqrt{(G_i / \rho_i)}$, H: the total thickness of the surface soil layers, and, G_i, ρ_i and d_i are shear modulus, mass density, layer height, and damping ratio at the i-th layer from the

surface, respectively. The impedance of a wave motion, ρ_i, between the equivalent surface soil layer and the engineering bedrock is expressed as follows.

$$\alpha = (\rho_e \cdot V_{se})/(\rho_b \cdot V_{sb}) \tag{5}$$

Where, V_{sb}: shear wave velocity at the engineering bedrock, and ρ_b : mass density at the engineering bedrock.

(4) *Amplification of surface ground*: The amplification of the uniform surface soil layer to the outcrop engineering bedrock is obtained by using the one-dimensional wave propagation in frequency domain. The transfer function of the surface soil layer and the engineering bedrock to the outcrop one are expressed as follows: a) surface/outcrop engineering bedrock; $G_s(T,\xi_1,\alpha)$, and b) engineering bedrock /outcrop engineering bedrock; $G_b(T,\xi_1,\alpha)$. An equivalent shear modulus G_{ei}, and an equivalent damping ratio, h_{ei}, of each soil layer are calculated through the G-γ, h-γ relationships of soil properties considering the nonlinear characteristics of the surface soil layers.

(5) *Acceleration response spectra at ground surface and engineering bedrock*: They are evaluated as follows.

$$S_{As}(T,\xi=0) \approx F_A(T)G_s(T,\xi_1,\alpha)/(T/2\pi) \tag{6}$$

$$S_{Ab}(T,\xi=0) \approx F_A(T)G_b(T,\xi_1,\alpha)/(T/2\pi) \tag{7}$$

(6) *Modification of acceleration response spectrum at ground surface*: To estimate the acceleration response spectrum conservatively at the ground surface, the spectrum is modified by connecting the two peak points, by a straight line, of the acceleration response spectrum corresponding to the first and second modes of the surface soil layer, in order to avoid excessive reduction between these peaks.

4.4 Examples of Evaluation of Acceleration Response Spectrum at Ground Surface

Figure 4 shows shear wave velocities, V_s, in several soil deposits to be evaluated. The shear wave velocities are measured by the PS logging method. The soil layer of V_s of more than 400 m/s is selected as the engineering bedrock. The nonlinear characteristics of the surface soil layers are modeled according to the other publication [Ohsaki et al., 1978]. The mass density of the soils is around 1.6 to 2.0.

The amplification factors (transfer functions) of the ground surface to the outcrop engineering bedrock are shown in Fig. 5. The figure includes the results from three analytical methods in the following.

1) Transfer functions in case of multi-layers with V_s by the linear analysis (indicated by "Linear"),
2) Ratios of acceleration response spectrum at the ground surface to that at the outcrop engineering bedrock, that are calculated by the computer program Shake [Schnabel et al., 1972] (indicated by "Equivalent"), and
3) Transfer functions obtained by the proposed method (indicated by "Proposed").

The predominant periods of the surface soil layers subjected to severe earthquake motions are longer by 1.3 to 2.0 times than those to moderate earthquake motions because of the nonlinear behavior of soils. There are some differences between the predominant periods of the proposed method and Shake at Sites 3 and 4. The amplification factors at Sites 3 and 4 by

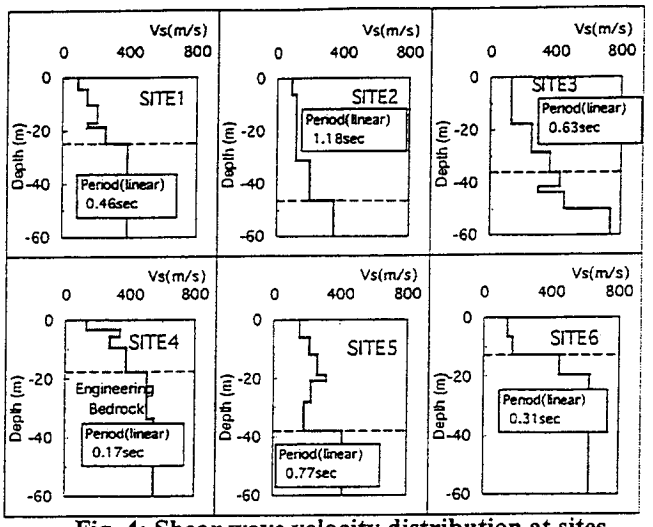

Fig. 4: Shear wave velocity distribution at sites

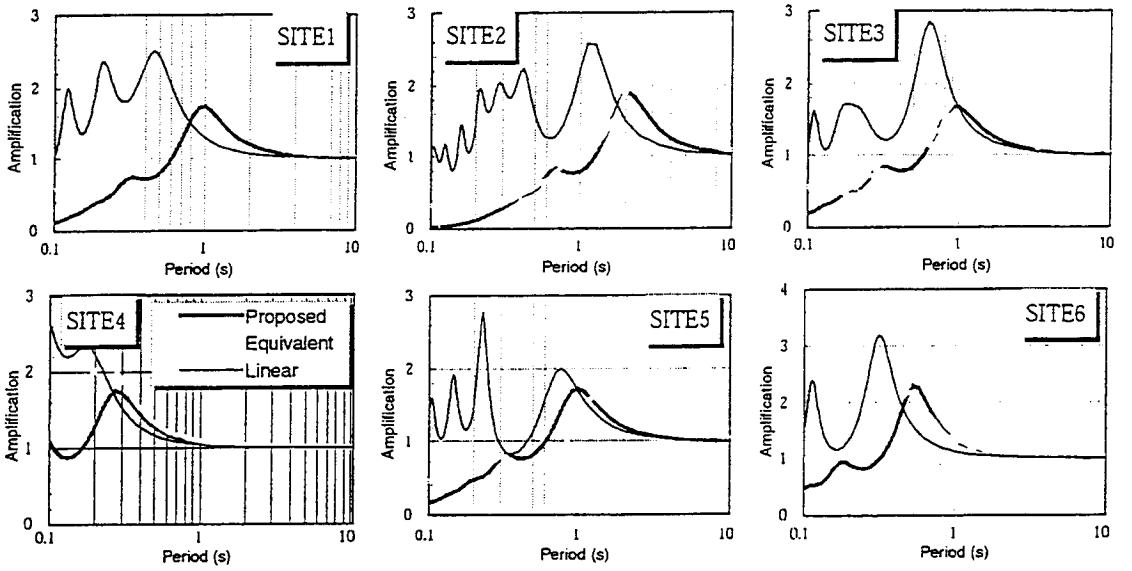

Figure 5: Transfer functions of ground surface to engineering bedrock

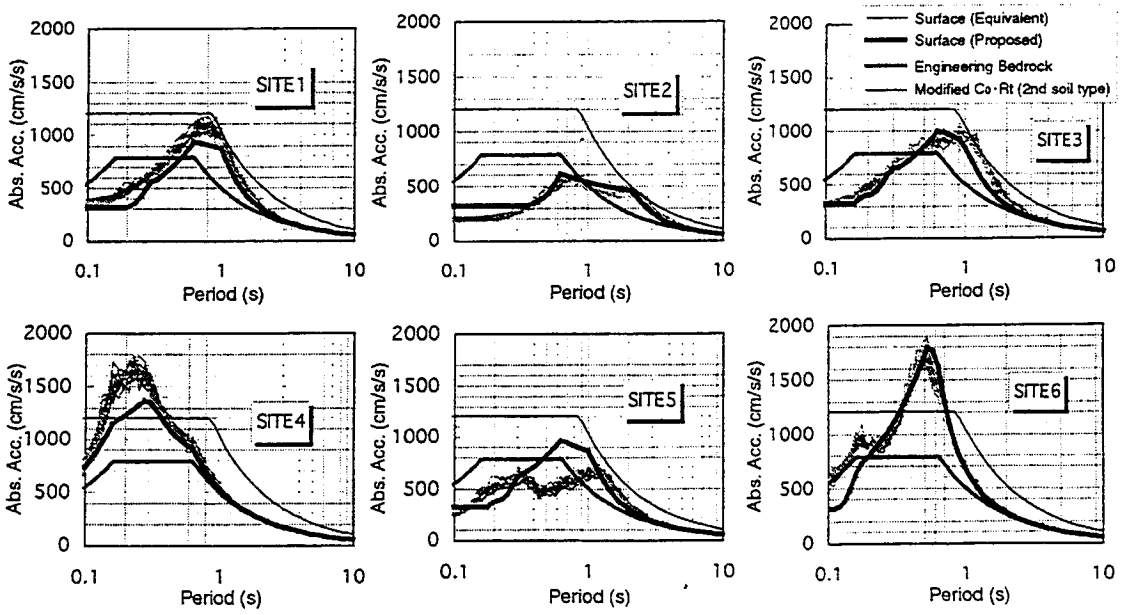

Figure 6: Acceleration response spectra at ground surface (h = 5%)

the proposed method are a little less than those by Shake. Figure 6 shows the acceleration response spectra at the surface, which are obtained by the proposed method and Shake. "Modified $C_0 \cdot R_t$" also indicates the acceleration response spectrum converted from the base shear coefficient of buildings for medium soil deposits prescribed in the Building Standard Law of Japan. The response spectra by the proposed method have good agreement with those by Shake.

5. PROPOSED EVALUATION PROCEDURES FOR MAJOR EARTHQUAKES

Various response and limit values are considered for use in the performance evaluation procedures in accordance with each of the requirements prescribed for building structures. A representative example of this arrangement is shown in Table 1. The principle of evaluation procedures is that the predicted response values due to the action of earthquake motions on building structures should not exceed the estimated limit values. In case of major earthquakes, the maximum response values of strength and displacement of a structure should be smaller than the ultimate capacity for strength and displacement.

Hereafter the focus is put on the proposed evaluation procedures for major earthquakes. The analytical method to be used for predicting the structural response applies the equivalent linearization technique using an ESDOF system and the response spectrum analysis. A flow chart of the procedures is shown in Fig. 7.

According to the procedures, the steps to be followed are:
(1) Confirm the scope of application of the evaluation procedures and the mechanical characteristics of materials and/or members to be used in a structure.
(2) Determine the response spectra to be used in the evaluation procedures.
a) For a given basic design spectrum at the engineering bedrock level, draw up the free-field site-dependent acceleration (S_a) and displacement response spectra (S_d) for different damping levels.
b) In the estimation of free-field site-dependent acceleration and displacement response (step a) above), consider the strain-dependent soil deposit characteristics.
c) In case of need, present graphically the relation of S_a-S_d for different damping levels (see Fig. 7c).
(3) Determine the hysteretic characteristic, equivalent stiffness and equivalent damping ratio of the structure.
a) Model the structure as an ESDOF system and establish its force-displacement relationships (see Fig. 7a).
b) Determine the limit strength and displacement of the structure corresponding to the ESDOF system.
c) The soil-structure interaction effects should basically be considered.
d) In case of need, determine the equivalent stiffness in accordance with the limit values.
e) Determine the equivalent damping ratio on the basis of viscous damping ratio, hysteretic dissipation energy and elastic strain energy of the structure (see Fig. 7b).
f) In case that the torsional vibration effects are predominant in the structure, these effects should be considered when establishing the force-displacement relationship of the ESDOF system.
(4) Examine the safety of the structure. In this final step, it is verified whether the response values predicted on the basis of the response spectra determined according to step 2 satisfy the condition of being smaller than the limit values estimated on the basis of step 3 (see Fig. 7c).

In order to determine the limit strength and displacement of the structure, a specific displaced mode is necessary to be assumed in advance for its inelastic response (see Fig. 7a). Basically, any predominant or possible to be experienced displaced mode of the structure subjected to earthquake motions can be applied. This implies any of the failure modes observed during major earthquakes such as beam failure, story failure or any other definite failure modes.

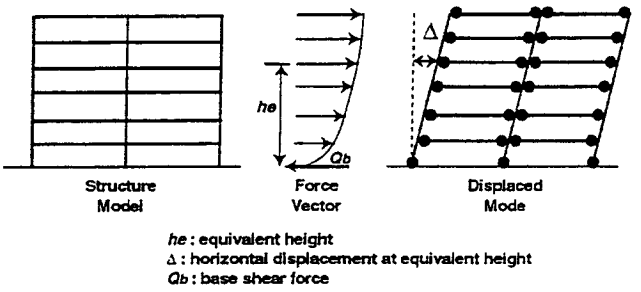

(a) Structure model and inelastic

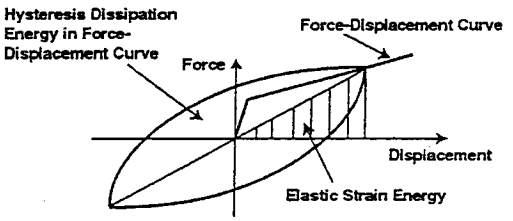

(b) Energy for equivalent damping

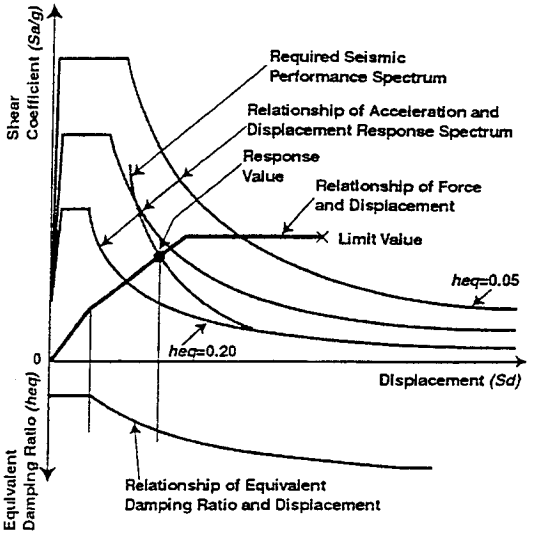

(c) Comparison of expected

Figure 7: Illustration of proposed evaluation procedures for major seismic events

6. HYSTERETIC CHARACTERISTICS AND EQUIVALENT DAMPING RATIO OF STRUCTURES

A multi-story building structure is reduced to an ESDOF system as shown in Fig. 8. The reduction to ESDOF system is based on the result of a push-over static analysis by applying horizontal forces at each floor level. The force-displacement relationship of the ESDOF system is given when the force corresponds to the base shear (Q_b), and its displacement ($_1\Delta$) corresponds to the displacement at the height (h_e) where the natural modal participation function is equal to 1.0 ($\beta_1\{u\}_1$=1.0). The details of this procedure is discussed elsewhere [Kuramoto et al., 2000].

The equivalent damping ratio is defined by the viscous damping ratio, hysteretic dissipation energy, elastic strain energy of structure, and the radiation effects of the ground. The effects of the soil-structure interaction are considered if necessary. The equivalent damping ratio of a SDOF system, h_{eq}, is given by the following equation (see Fig. 8).

$$h_{eq} = (1/4\pi)(\Delta W/W) \quad (10)$$

where, ΔW = Dissipation energy of SDOF system, and W = Potential energy of SDOF system ($=Q_b \cdot {}_1\Delta/2$).

Here, the dissipation energy of a stationary hysteretic loop at the assumed maximum response of a structure can be obtained by calculating the area of the enclosed cyclic loop of the structure in a static push-over analysis, or based on the total damping ratios of all the

members and joints considered.

7. PREDICTION OF MAXIMUM RESPONSE

One of typical analysis methods for predicting the maximum earthquake response of an inelastic system is the response spectrum analysis using equivalent linearization techniques. In this procedure, as shown in Fig. 7(c), the intersection of the force-displacement curve of ESDOF system and the required seismic performance spectrum is the maximum response point. In general, the maximum response obtained by using the equivalent damping ratio, h_{eq}, of Eq. (10) is theoretically valid in stationary vibration. In non-stationary vibration caused by earthquakes, h_{eq} based on the assumed maximum response has to be reduced appropriately for appropriately predicting the maximum response. The factor for reducing h_{eq} can be estimated through examination using recorded and synthesized earthquake motions, and some hysteresis curves consisting of bi-linear or tri-linear skeleton curves such as normal bi-linear model and Takeda model [Takeda et al., 1970]. Figure 8 illustrates an example of the results on bi-linear skeleton curves shown in Fig. 9(a). The four input earthquake motions consist of a synthesized earthquake motion by the Building Center of Japan (BCJ) and three recorded earthquake motions; 1995 Kobe NS, 1968 Hachinohe EW and 1940 El Centro NS. Analytical parameters include the natural period, yield stiffness and yield strength. The damping ratio of 2% except for the hysteretic energy dissipation is included. The estimated equivalent damping ratio is reduced to 70 percent of h_{eq}. The responses obtained from the equivalent linearization analysis compare well with the time history responses, although differences are observed to a certain extent as the ductility becomes larger.

Takeda model is used to simulate the response of reinforced concrete structures. The equivalent damping ratio for Takeda model is expressed in the following equation.

$$h_{eq} = \frac{1}{\pi}\left\{1 - \frac{1 + d_c / d_y}{1 + p_c / p_y}\mu^{\gamma}\frac{1 - \alpha + \alpha\mu}{\mu}\right\} \tag{11}$$

Where, d_c = displacement at crack point, d_y = yield displacement, p_c = strength at crack point, p_y = yield strength,

μ = maximum displacement divided by yield displacement, γ = decrease factor of stiffness on unloading, and

α = stiffness after yielding divided by initial stiffness.

By arranging the parameters given in Fig. 9(b), Equation (11) can be expressed as follows.

$$h_{eq} = 0.3\{1 - (0.82 + 0.01\mu)/\sqrt{\mu}\} \tag{12}$$

The comparison of the results between the equivalent linearization and time history analyses is shown in Figs. 10,11. Here, the natural period, T, calculated using the initial stiffness, is equal to 0.3 s. The yield shear coefficient, $Q_y/(mg)$ (Q_y: yield strength, m: mass, g: acceleration of gravity), is changed from 0.2 to 0.5 by an increment of 0.1. The figure shows that the equivalent damping ratio reduced to 70 percent of h_{eq} is suitable for the design purpose.

8. CONCLUSIONS

There are two kinds of performance requirements: human life safety and damage control of a building for the seismic provisions. There are corresponding two earthquake motion levels. The earthquake motions are defined as the design acceleration response spectrum which is specified at the engineering bedrock in order to take the soil condition and soil-structure interaction effect into consideration as properly as possible. The ordinate of the design response spectrum is determined by considering historical seismicity data, sieismo-tectonic zones and active faults of the region. Here, the engineering bedrock is defined based on shear wave velocity of the soil at a site. The return periods of the earthquake motion of approximately 500 years and approximately 50 years are used to evaluate life-safety level and damage control level, respectively. The required performance shall be verified by comparing the response values with the limit values. The evaluation procedures of structural seismic performance presented are in essence a blend of ESDOF modeling of building structures with the site-dependent response spectrum concept, which make possible the prediction of maximum structural response for major earthquakes without using time history analyses.

The validity of the proposed evaluation procedures is examined in the paper, focusing on the following items:

1) Simplified analytical method of site-dependant response from surface geotechnical data with the equivalent single surface soil layer considering the nonlinear behavior of soft soils.
2) Estimation of equivalent damping ratios for various hysteretic characteristics such as bi-linear and degrading tri-linear hysteresis models.
3) Applicability of the equivalent linearization technique.

The results show that the proposed evaluation procedures are appropriate to practical seismic design. The proposed evaluation procedures make it realistic and simple to predict the maximum structural response for major earthquakes as well as to confirm whether the predicted response values are smaller than the limit ones.

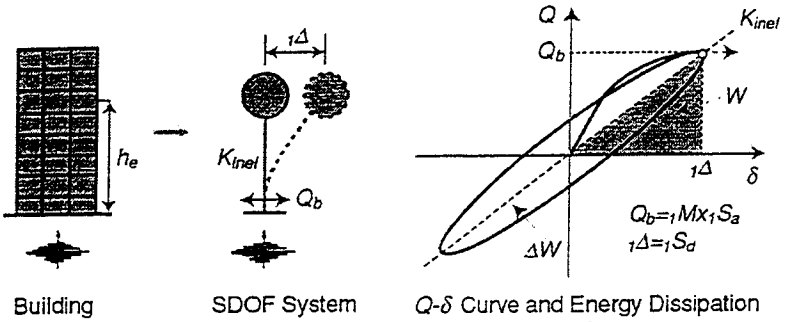

Figure 8: Reduction to single-degree-of-freedom system

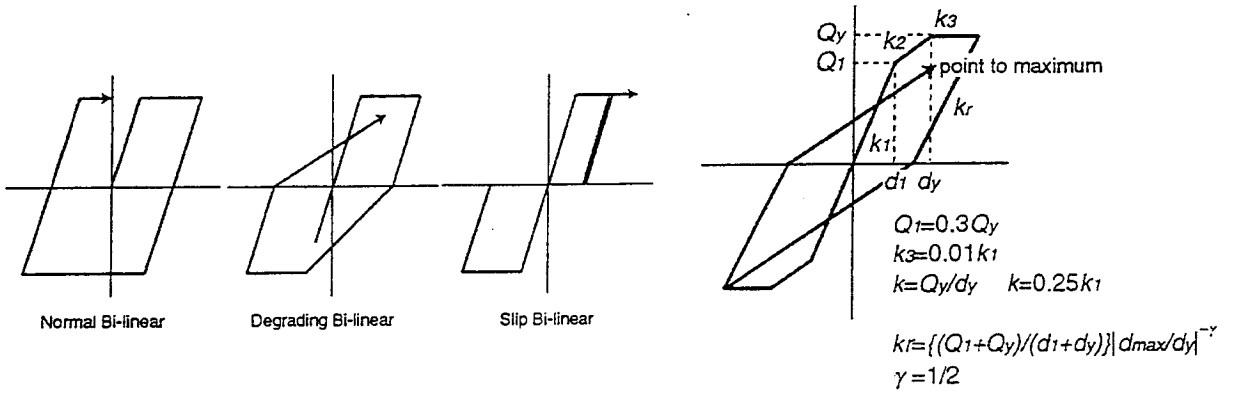

(a) Bi-linear hysteresis models **(b) Parameters of Takeda model**

Figure 9: Analytical hysteresis models

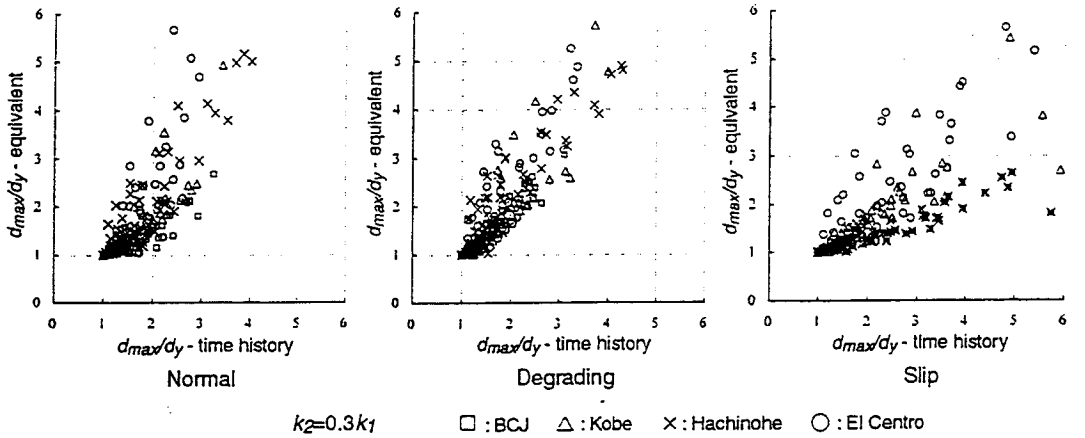

Figure 10: Comparison of maximum response displacements between equivalent linearization and time history analyses

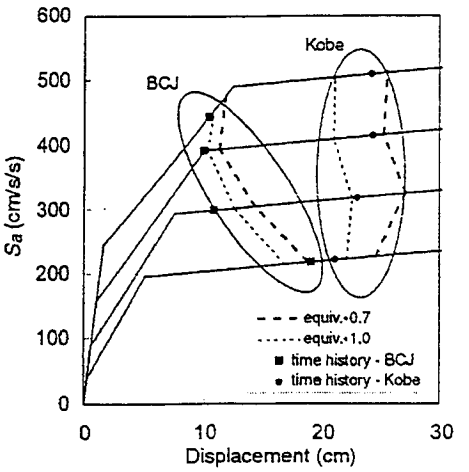

Figure 11: Comparison of equivalent linearization and time history analyses

ACKNOWLEDGMENT

This manuscript was stimulated by the BRI "Task Committee to Draft Performance-based Building Provisions" chaired by H. Hiraishi, where all the members in the committee have shared their opinions with other members. Authors would like to express their gratitude towards all of them.

REFFERENCES

AIJ (1989), *Recommendation for the Design of Base Isolated Buildings*, Architectural Institute of Japan (in Japanese).

AIJ (1992), *Seismic Loading - Strong Motion Prediction and Building Response*, Architectural Institute of Japan, Tokyo (in Japanese).

ATC-40 (1996), *Seismic Evaluation and Retrofit of Concrete Buildings*, Report No. SSC 96-01, Applied Technology Council.

Freeman, S. A. (1978), "Prediction of response of concrete buildings to severe earthquake motion", *Douglas McHenry International Symposium on Concrete and Concrete Structures*, SP-55, ACI, pp. 589-605.

Fukushima, Y. and Tanaka, T. (1992), "*Revised Attenuation Relation of Peak Horizontal Acceleration By Using A New Data Base*", Progr. Abstr. Seismol. Soc. Jpn., 2, 116 (in Japanese).

Hiraishi, H. and et al. (1999), "Seismic evaluation of buildings by acceleration spectrum at engineering bedrock (Part 1-Part 13)", Structures II, *Summaries of Technical Papers of Annual Meeting*, AIJ (in Japanese).

Hiraishi, H., Midorikawa, M., Teshigawara, M., Gojo, W. and Okawa, I. (2000), "Development of performance-based building code of Japan -framework of seismic and structural provisions-", *Proceedings 12th World Conference on Earthquake Engineering.*

Kawasumi, H. (1951), "Measures of Earthquake Danger and Expectancy of Maximum Intensity Throughout Japan as Inffered from the Seismic Activity in Historical Times", Bulletin of Earthquake Research Institute, 29, pp.469-481.

Kuramoto, H., Teshigawara, M., Okuzono, T., Koshika, N., Takayama, M. and Hori, T. (2000), "Predicting the earthquake response of buildings using equivalent single degree of freedom system", *Proceedings 12th World Conference on Earthquake Engineering.*

3) Midorikawa, S. (1993), "*Preliminary Analysis for Attenuation of Peak Ground Velocity on Stiff Site*", Proceedings of the International Workshop on Strong Motion Data, 2, pp.39-48.

Miura, K., Koyamada, K. and Iiba, M. (2000), "Response spectrum method for evaluating nonlinear amplification of surface strata", *Proceedings 12th World Conference on Earthquake Engineering.*

Ohsaki, Y., Hara, A. and Kiyota, Y. (1978), "Stress-strain model of soils for seismic analysis", *Proceedings 5th Japanese Earthquake Engineering Symposium*, pp. 679-704 (in Japanese).

Shibata, A. and Sozen, M. A. (1976), "Substitute structure method for seismic design in R/C", *Journal of the Structural Div.*, ASCE, 102, ST1, pp. 1-18.

Schnabel, P. B., Lysmer, J. and Seed, H. B. (1972), "SHAKE: A computer program for earthquake response analysis of horizontally layered sites", *Report No. UCB/EERC-72/12*, Univ. of California, Berkeley, Calif.

Takeda, T., Sozen, M. A. and Nielsen, N. N. (1970), "Reinforced concrete response to simulated earthquakes", *Journal of the Structural Division*, ASCE, 96, 12, pp. 2557-2573.

SESSION 9: GENERAL DISCUSSION AND RESOLUTIONS

Chaired by

♦ Toshimi Kabeyasawa and Jack Moehle ♦

RESOLUTIONS

Recent urban earthquakes have caused significant fatalities, injuries, and economic losses in both the U.S. and Japan. This was evident in the U.S. during the 1994 Northridge earthquake, and in Japan during the 1995 Hyogo-ken Nanbu earthquake. These and other earthquakes, such as the recent earthquake in Turkey, point out the need for effective and practical methods for

- evaluating and rehabilitating existing hazardous buildings and
- for designing new buildings for more reliable and improved performance.

While great progress has previously been made in engineering for earthquake resistance, suggested frameworks for performance-based earthquake engineering will accelerate progress by focusing efforts and bridging gaps. This will lead to a future of earthquake engineering that will include increased emphasis on quantitative measures of performance over qualitative measures, precision over approximation, reliability over uncertainty, and intelligent engineering and life-cycle cost design over minimum capital cost design.

The papers presented at the *First US-Japan Workshop on Performance-Based Earthquake Engineering Methodology for Reinforced Concrete Building Structures* demonstrate progress being made in performance-based earthquake engineering. The papers covered earthquake ground motion effects on structures, performance of structural components, seismic assessment and design, philosophy of performance-based earthquake engineering, and future needs. Discussion of the presented papers enhanced understanding and advanced the state of the art in performance-based earthquake engineering. Important outcomes of the Workshop include

(a) better understanding of the present state of knowledge and practice of performance-based earthquake engineering in the U.S. and Japan, which speeds progress and implementation in both countries;
(b) improved understanding of the use and limitations of analysis methods for performance-based earthquake engineering of reinforced concrete buildings;
(c) identification of common areas of concern and areas of needed advancement, both in practice and research, in performance-based earthquake engineering; and
(d) identification of areas that would benefit from joint study.

The topic of performance-based earthquake engineering is a particularly effective one for workshop discussion because it brings together and promotes a common focus of experts in ground motion, analysis, and design. Understanding of the work of individuals with different expertise was achieved in ways that would not be possible without meeting in this format.

The Workshop was a successful continuation of progress made over two decades of cooperative U.S.-Japan research in earthquake engineering. The success of this Workshop suggests that the two countries will benefit from continued cooperation.

Reasons for continued cooperation include

(a) the two countries have a shared need to develop improved methods for seismic design and evaluation;

(b) in both countries, there is a need for integrated analytical and experimental approaches, which is promoted in this meeting format; and

(c) each side brings unique experience, knowledge, facilities, the sharing of which benefits all.

These discussions are best accomplished through face-to-face meetings of extended duration such as occurs in a workshop format.

Therefore, the following recommendations are offered:

(1) Because of the rapid rate at which new information and applications are being achieved, the importance of advances to Japan and the U.S., and the success of the first Workshop, the participants recommend that the "Second US-Japan Workshop on Performance-Based Seismic Design Methodology for Reinforced Concrete Building Structures" be organized by the Japan side in about one year.

(2) At future workshops, several topics for focused discussion should be considered. A reduced number of these should be the focus of the second Workshop:

(a) the new Japanese seismic code;
(b) simplified and rigorous methods for predicting seismic demands;
(c) validation of performance-based earthquake engineering methods;
(d) use of probabilistic bases for PBE;
(e) procedures for gauging system performance as opposed to component performance;
(f) nonstructural and structural component and system behavior;
(g) definitions and measures of performance; and
(h) practical application of advanced analysis methods.

(3) At the second Workshop, the following format should be considered:

(a) focus on three or four topics, emphasizing presentation of papers on those topics coupled with working group sessions to examine topics in greater detail; and

(b) participation of professional engineers, representatives of code-writing organizations, representatives of national organizations responsible for construction, as well as academic researchers.

(4) Cooperative activities between individual participants from the U.S. and Japan are encouraged to address problems of mutual concern. As a start, efforts should be undertaken to facilitate exchange of personnel, including students, faculty, and professional researchers and practitioners, as well as of information on technical issues and applications. Funding agencies are encouraged to support these activities.

PEER REPORTS

PEER reports are available from the National Information Service for Earthquake Engineering (NISEE). To order PEER reports, please contact the Pacific Earthquake Engineering Research Center, 1301 South 46th Street, Richmond, California 94804-4698. Tel.: (510) 231-9468; Fax: (510) 231-9461.

PEER 2000/03 *Framing Earthquake Retrofitting Decisions: The Case of Hillside Homes in Los Angeles.* Detlof von Winterfeldt, Nels Roselund, and Alicia Kitsuse. March 2000. $13.00

PEER 2000/01 *Further Studies on Seismic Interaction in Interconnected Electrical Substation Equipment.* Armen Der Kiureghian, Kee-Jeung Hong, and Jerome L. Sackman. November 1999. $20.00

PEER 1999/14 *Seismic Evaluation and Retrofit of 230-kV Porcelain Transformer Bushings.* Amir S. Gilani, Andrew S. Whittaker, Gregory L. Fenves, and Eric Fujisaki. December 1999. $26.00

PEER 1999/12 *Rehabilitation of Nonductile RC Frame Building Using Encasement Plates and Energy-Dissipating Devices.* Mehrdad Sasani, Vitelmo V. Bertero, James C. Anderson. December 1999. $26.00

PEER 1999/11 *Performance Evaluation Database for Concrete Bridge Components and Systems under Simulated Seismic Loads.* Yael D. Hose and Frieder Seible. November 1999. $20.00

PEER 1999/10 *U.S.-Japan Workshop on Performance-Based Earthquake Engineering Methodology for Reinforced Concrete Building Structures.* December 1999. $33.00

PEER 1999/09 *Performance Improvement of Long Period Building Structures Subjected to Severe Pulse-Type Ground Motions.* James C. Anderson, Vitelmo V. Bertero, and Raul Bertero. October 1999. $26.00

PEER 1999/08 *Envelopes for Seismic Response Vectors.* Charles Menun and Armen Der Kiureghian. July 1999. $26.00

PEER 1999/07 *Documentation of Strengths and Weaknesses of Current Computer Analysis Methods for Seismic Performance of Reinforced Concrete Members.* William F. Cofer. November 1999. $15.00

PEER 1999/06 *Rocking Response and Overturning of Anchored Equipment under Seismic Excitations.* Nicos Makris and Jian Zhang. November 1999. $15.00

PEER 1999/05 *Seismic Evaluation of 550 kV Porcelain Transformer Bushings.* Amir S. Gilani, Andrew S. Whittaker, Gregory L. Fenves, and Eric Fujisaki. October 1999. $15.00

PEER 1999/04 *Adoption and Enforcement of Earthquake Risk-Reduction Measures.* Peter J. May, Raymond J. Burby, T. Jens Feeley, and Robert Wood. $15.00

PEER 1999/03 *Task 3 Characterization of Site Response General Site Categories.* Adrian Rodriguez-Marek, Jonathan D. Bray, and Norman Abrahamson. February 1999. $20.00

PEER 1999/02 *Capacity-Demand-Diagram Methods for Estimating Seismic Deformation of Inelastic Structures: SDF Systems.* Anil K. Chopra and Rakesh Goel. April 1999. $15.00

PEER 1999/01 *Interaction in Interconnected Electrical Substation Equipment Subjected to Earthquake Ground Motions.* Armen Der Kiureghian, Jerome L. Sackman, and Kee-Jeung Hong. February 1999. $20.00

PEER 1998/08 *Behavior and Failure Analysis of a Multiple-Frame Highway Bridge in the 1994 Northridge Earthquake.* Gregory L. Fenves and Michael Ellery. December 1998. $20.00

PEER 1998/07 *Empirical Evaluation of Inertial Soil-Structure Interaction Effects.* Jonathan P. Stewart, Raymond B. Seed, and Gregory L. Fenves. November 1998. $26.00

PEER 1998/06 *Effect of Damping Mechanisms on the Response of Seismic Isolated Structures.* Nicos Makris and Shih-Po Chang. November 1998. $15.00

PEER 1998/05 *Rocking Response and Overturning of Equipment under Horizontal Pulse-Type Motions.* Nicos Makris and Yiannis Roussos. October 1998. $15.00

PEER 1998/04 *Pacific Earthquake Engineering Research Invitational Workshop Proceedings, May 14–15, 1998: Defining the Links between Planning, Policy Analysis, Economics and Earthquake Engineering.* Mary Comerio and Peter Gordon. September 1998. $15.00

PEER 1998/03 *Repair/Upgrade Procedures for Welded Beam to Column Connections.* James C. Anderson and Xiaojing Duan. May 1998. $33.00

PEER 1998/02 *Seismic Evaluation of 196 kV Porcelain Transformer Bushings.* Amir S. Gilani, Juan W. Chavez, Gregory L. Fenves, and Andrew S. Whittaker. May 1998. $20.00

PEER 1998/01 Unassigned.